This work is protected by copyright and other intellectual property rights and duplication or sale of all or part is not permitted, except that material may be duplicated by you for research, private study, criticism/review or educational purposes. Electronic or print copies are for your own personal, non-commercial use and shall not be passed to any other individual. No quotation may be published without proper acknowledgement. For any other use, or to quote extensively from the work, permission must be obtained from the copyright holder/s.

Proteomics-based identification and characterisation of spinal muscular atrophy disease pathways

Darija Šoltić

Submitted for the degree of Doctorate of Philosophy

July 2020

Keele University

Table of contents

Abstract

Spinal muscular atrophy (SMA) is a debilitating genetic disorder, characterised by homozygous loss of the survival of motor neuron 1 (*SMN1*) gene, resulting in insufficient levels of ubiquitously expressed survival of motor neuron (SMN) protein. The traditional picture of SMA as a neuromuscular disease is slowly being changed by the findings of systemic pathology in SMA patients. This is also one of the reasons why therapeutic strategies aimed at increasing the levels of functional SMN protein are not completely effective, since they would often target neuromuscular pathology only. Here, the research was focused on identifying and characterising new disease pathways in SMA that could potentially be used as therapeutic targets in SMA. In the first results chapter, six proteins, lamin A/C, UBA1, ANXA2, GAPDH, NCAM and GAP43, identified previously in a multi-study comparison as having consistent direction of differential expression across three proteomic studies of SMA, were investigated in SMA tissues and cells using western blotting. Of these, lamin A/C, UBA1, ANXA2 and GAPDH showed widespread dysregulation across a range of tissues from severe Taiwanese mouse model of SMA and in fibroblast cells from SMA patients, suggesting that each one of these proteins might have a role in SMA disease pathways. Selection of drugs that can target these proteins proved to be very challenging, and further efforts are needed to identify appropriate therapeutic strategies. In the second results chapter, the potential role for lamin A/C in SMA disease pathways was further highlighted by findings of mechanistic link between lamin A/C and UBA1, a known SMA modifier. Lamin A/C dysregulation might be especially relevant in the context of heart pathology, where increased levels of lamin A/C would likely stiffen the cardiomyocytes and impair normal heart function. In the third results chapter, multi-study comparison of published proteomic studies of amyotrophic lateral sclerosis (ALS) identified core protein changes in ALS tissues and cells, and biochemical investigation of two proteins,

ALDOA and GAPDH, highlighted defects in cell metabolism as an important disease mechanism in ALS. Of these, fifteen proteins were also differentially expressed across at least two proteomic studies of SMA, however, when investigated biochemically in SMA and ALS mouse spinal cords, these proteins showed very little evidence that two diseases converge on the same molecular mechanisms. When taken together, results presented here show that published proteomic studies contain a wealth of information that often get overlooked when examined in isolation. These datasets were exploited here to identify core proteins and molecular mechanisms that drive disease pathogenesis in SMA and ALS. Knowledge of general disease mechanisms may allow development of therapies that can systemically target peripheral pathology in SMA. For example, systemic restoration of lamin A/C levels might prove useful for correcting defects in a range of tissues, with an emphasis on stiff tissues like the heart and muscles, and when combined with an SMN-targeted approach, it might bring greater therapeutic benefit to SMA patients compared to SMN-targeted approach alone. In conclusion, several proteins identified in a multi-study comparison, including lamin A/C, GAPDH and ALDOA, were linked to different SMA and ALS disease pathways, providing evidence that multi-study comparison has the power to identify core disease-related protein changes. This thesis also opened a range of new questions that need to be addressed in the future work, including the selection of drugs that can restore defects in the expression or activity or target proteins. Many other proteins, identified in multi-study comparisons, could not be investigated here in more detail. These proteins may help to further expand the knowledge of SMA and ALS disease pathways and therefore demand further experimental attention.

List of figures

List of tables

Abbreviations

53BP1	TP53-binding protein 1
α-COP	Coatomer subunit alpha
ABC	Active β-catenin
AChR	Acetylcholine receptor
ADSMA	Autosomal dominant proximal spinal muscular atrophy
ALDOA	Aldolase fructose-bisphosphate A
ALS	Amyotrophic lateral sclerosis
AMPA	Alpha-amino-3-hydroxy-5-methylisoxazole-4-propionate
ANXA2	Annexin A2
ASO	Antisense oligonucleotide
ATP	Adenosine triphosphate
Bad	Bcl2-associated agonist of cell death
BMD	Bone mineral density
BP	Biological process
C1QB	Complement c1q b chain
Ca^{2+}	Calcium ion
CALD1	Caldesmon 1
CALR	Calreticulin
CBs	Cajal bodies, coiled bodies
Cdc42	CDC42 small effector protein 1
CC	Cellular component
Cdc5l	Cell division cycle 5-like protein
CDKN1A	Cyclin dependent kinase inhibitor 1A

cDNA	Complementary DNA
CHODL	Chondrolectin
CMT2D	Charcot-Marie-Tooth disease Type 2D
CNS	Central nervous system
COL1A1	Collagen type I alpha 1 chain
COL6A1	Collagen type VI alpha 1 chain
COL6A3	Collagen type VI alpha 3 chain
COPI	Coat protein complex I
CSF	Cerebrospinal fluid
Ct	Cycle threshold
CTR	Control
CysC	Cystatin C
DAVID	Database for Annotation, Visualization and Integrated Discovery
DSBs	Double-strand breaks
DCM	Dilated cardiomyopathy
DCX	Doublecortin
DNA	Deoxyribonucleic acid
DRG	Dorsal root ganglia
DSMAs	Distal SMAs
DT	Doubling time
EAAT2	Excitatory amino acid transporter 2
ECG	Electrocardiogram
ECL	Enhanced chemiluminescence
ECM	Extracellular matrix

EDMD	Emery-Dreifuss muscular dystrophy
ELISA	Indirect enzyme-linked immunosorbent assay
ER	Endoplasmic reticulum
ERAD	ER-associated degradation
ESEs	Exonic splicing enhancers
ESSs	Exonic splicing silencers
fALS	Familial amyotrophic lateral sclerosis
FasL	Fas ligand
FC	Fold change
FDA	The Food and Drug Administration
FDR	False discovery rate
FUS	Fused-in-sarcoma
GAP43	Neuromodulin
GAPDH	Glyceraldehyde 3-phosphate dehydrogenase
GARS	Glycine-tRNA ligase
GEMs	Gemini of the coiled bodies
GFAP	Glial fibrillary acidic protein
GMG	GM2 gangliosidosis
GO	Gene ontology
GOT2	Glutamic-oxaloacetic transaminase 2
H2AX	H2A.X Variant Histone
HBA1	Hemoglobin Subunit Alpha 1
HBB	Hemoglobin subunit beta
HDACi	Histone deacetylase inhibitor

HEK	Human embryonic kidney
HFL-1	Human foetal lung fibroblasts
HFMSE	Hammersmith Functional Motor Scale– Expanded
HGPS	Hutchinson-Gilford progeria syndrome
hnRNPs	Nuclear ribonucleoproteins
HP	Haptoglobin
HSP90AA1	Heat shock protein HSP 90-alpha
HSP90B1	Heat shock protein 90 beta family member 1
HSPD1	60 kDa heat shock protein, mitochondrial
IBD	Inflammatory bowel disease
IDH	Isocitrate dehydrogenase
IFNγ	Interferon gamma 1
IGF-1	Insulin-like growth factor-1
IGFBP-3	IGF-1 binding protein 3
IKK	I-kappa-B kinase
IL-1β	Interleukin 1 beta
IL-6	Interleukin 6
IL-8	Interleukin 8
IMF	Immunofluorescence
iNOS	Nitric oxide synthase
IPA	Ingenuity Pathway Analysis
iPSC	Induced pluripotent stem cell
ISEs	Intronic splicing enhancers
ISSs	Intronic splicing silencers

iTRAQ	Isobaric tags for relative and absolute quantification
KD	Knockdown
KO	Knockout
LAL	Levator auris longus
LCHAD	Long-chain L-3-hydroxyacyl-CoA dehydrogenase
LGMD1B	Limb-girdle muscular dystrophy 1B
LMNA	Lamin A/C
MC	Migrated cells
MEFs	Mouse embryonic fibroblast cells
MF	Molecular function
miR	MicroRNA
MR	Magnetic resonance
mRNA	Messenger RNA
MSCs	Mesenchymal stem cells
mTOR	Mammalian target of rapamycin
Myf5	Myogenic factor 5
MyoD	Myoblast determination protein
NADH	Nicotinamide adenine dinucleotide
NCALD	Neurocalcin-delta
NCAM	Neural cell adhesion molecule 1
NCBI	National Center for Biotechnology Information
NF	Neurofilament
NF-L	Neurofilament light
NKT	Natural killer T

NMDA	N-methyl-d-aspartic acid
NMJ	Neuromuscular junction
NO	Nitric oxide
NOS	Nitric oxide synthase
NOX	NADPH oxidase
OD	Optical density
ORM1	Alpha-1-acid glycoprotein 1
P	Postnatal day
p	P-value
Pax7	Paired box protein Pax7
PBMC	Patient blood mononuclear cells
PCR	Polymerase chain reaction
PDGF-BB	Platelet-derived growth factor-BB
PGK1	Phosphoglycerate kinase 1
PI3K	Phosphoinositide 3-kinase
PLS3	Plastin 3
PMOs	Phosphorodiamidate morpholino oligonucleotides
POLR2J	RNA Polymerase II Subunit J
PSPEP	Proteomics System Performance Evaluation Pipeline
PTEN	Phosphatase and tensin homolog
PTH	Parathyroid hormone
R^2	R-squared
Rab1	Ras-related protein Rab 1A
Rac1	Ras-related C3 botulinum toxin substrate 1

RBC	Red blood cells
RhoA	Transforming protein RhoA
RNA	Ribonucleic acid
ROCK	Rho-associated protein kinase 1
ROS	Reactive oxygen species
RT	Room temperature
RT-qPCR	Quantitative reverse transcription polymerase chain reaction
sALS	Sporadic amyotrophic lateral sclerosis
SAHA	Suberoylanilide hydroxamic acid
SBMA	Spinal and bulbar muscular atrophy
scAAV9	Self-complimentary adeno-associated virus serotype-9
SCHAD	L-3-hydroxyacyl-CoA dehydrogenase
SD	Standard deviation
SDS	Sodium dodecylsulfate
SDS-PAGE	Sodium dodecylsulfate -polyacrylamide gel electrophoresis
shRNA	Short hairpin ribonucleic acid
Sm	Smith
SMA	Spinal muscular atrophy
SMA-LED1	Spinal muscular atrophy, lower extremity predominant
SMA-LED2	Spinal muscular atrophy, lower extremity predominant 2
SMA-MDS	Spinal muscular atrophy with mitochondrial DNA depletion syndrome
SMA-PCH	Spinal muscular atrophy with pontocerebellar hypoplasia
SMA-PME	Spinal muscular atrophy with progressive myoclonic epilepsy
SMAX2	X-linked infantile spinal muscular atrophy

SETX	Senataxin
SMN	Survival of motor neuron
SMN1	Survival of motor neuron 1
SMN2	Survival of motor neuron 2
SMNΔ7	SMN transcripts lacking exon seven
snRNAs	Small nuclear ribonucleic acids
snRNPs	Small nuclear ribonucleoproteins
SOD1	Superoxide dismutase 1
SPF	Specific-pathogen-free
SR	Serine-arginine-rich
STRING	Search Tool for the Retrieval of Interacting Genes/Proteins
SUN2	SUN domain-containing protein 2
SV2	Synaptic vesicle protein 2
TBP	TATA-Box binding protein
TC	Transfected cells
TDP-43	TAR DNA Binding protein-43
TF	Transferrin
TNFα	Tumor necrosis factor alpha
TSA	Trichostatin A
UBA1	Ubiquitin-like modifier activating enzyme 1
UDG	Uracil-DNA glycosylase
Unrip	Unr interacting protein
UPP	Ubiquitin proteasome pathway
UPR	Unfolded protein response

VPA	Valproic acid
WB	Western blot
WT	Wild type
ZMPSTE24	zinc metallopeptidase STE24

Dissemination

Publications:

Soltic D. and Fuller H.R. (2020) Molecular crosstalk between non-SMN-related and SMN-related spinal muscular atrophy. *Neuroscience Insights*; 15: 1–3. doi: 10.1177/2633105520914301

Soltic D., Shorrock H.K., Allardyce H., Wilson E.L., Holt 1., Synowsky S.A., Shirran S.L., Parson S.H., Gillingwater T.H., Fuller, H.R. (2019) Lamin A/C dysregulation contributes to cardiac pathology in a mouse model of severe spinal muscular atrophy. *Hum Mol Genet*.; 28 (21): 3515–3527. doi: 10.1093/hmg/ddz195.

Soltic D., Bowerman M., Stock J., Shorrock H.K., Gillingwater T.H. and Fuller H.R. (2018) Multi-study proteomic and bioinformatic identification of molecular overlap between ALS and SMA. *Brain Sci.*; 8 (12): E212. doi: 10.3390/brainsci8120212.

Podium presentations:

1. **Cure SMA Annual Research Conference on Spinal Muscular Atrophy (California, USA 2019):** Lamin A is Dysregulated in Spinal Muscular Atrophy.
2. **Robert Jones and Agnes Hunt Orthopaedic Hospital Research Day (Oswestry, UK 2019):** Lamin A is dysregulated in spinal muscular atrophy.
3. **Robert Jones and Agnes Hunt Orthopaedic Hospital Research Day (Oswestry, UK 2019):** Identification of Core Molecular overlap between Spinal Muscular Atrophy (SMA) and Amyotrophic Lateral Sclerosis (ALS).
4. **UK SMA Research Day (Keele University, UK 2019):** Lamin A is dysregulated in SMA: implications for mechanically burdened tissues.

5. **ISTM Postgraduate Symposium (Keele University, UK 2018**)- three minutes thesis competition: Big data analytics identifies potential therapeutic target for childhood motor neuron disease.
6. **Robert Jones and Agnes Hunt Orthopaedic Hospital Research Day (Oswestry, UK 2018):** The intermediate filament protein, lamin A/C, is dysregulated in spinal muscular atrophy.

Poster presentations

1. **ISTM Postgraduate Symposium (Keele University, UK 2018):** Finding a new therapy for childhood motor neuron disease.
2. **Institute of Liberal Arts and Sciences Postgraduate Conference (Keele University, UK 2018):** Finding a new therapy for childhood motor neuron disease.
3. **UK SMA Research Day (Sheffield, UK 2018):** The intermediate filament protein, lamin A/C, is dysregulated in spinal muscular atrophy.
4. **SMA Europe International Scientific Congress on Spinal Muscular Atrophy (Krakow, Poland, 2018):** The intermediate filament protein, lamin A/C, is dysregulated in spinal muscular atrophy.
5. **ISTM Postgraduate Symposium (Keele University, UK 2017):** Lost in translation? Multi-study transcriptome analysis reveals new insights into conserved mechanisms in spinal muscular atrophy.
6. **Robert Jones and Agnes Hunt Orthopaedic Hospital Research Day (Oswestry, UK 2017):** Lost in translation? Multi-study transcriptome analysis reveals new insights into conserved mechanisms in spinal muscular atrophy.

Acknowledgments

I would like to express my sincere thanks to all the members of the neuromuscular group at the Robert Jones and Agnes Hunt Orthopaedic Hospital for their support over the three years. In particular, I would like to express my gratitude to my supervisors Dr Heidi Fuller and Dr Emma Wilson for their guidance and mentoring. I would also like to thank Dr Hannah K. Shorrock and Prof. Thomas H. Gillingwater (University of Edinburgh) for kindly providing UBA1 KD and wild type HEK293 cells and tissues from a mouse model of SMA, Dr Melissa Bowerman (Keele University) for providing tissues from a mouse model of ALS, and Prof. Colin L Stewart (Institute of Medical Biology, Singapore) for providing wild type and LMNA KO mouse embryonic fibroblasts.

Ovaj doktorski rad posvećujem svojim roditeljima u znak zahvalnosti za svu potporu koju su mi pružili u toku mog studiranja

I would like to dedicate this thesis to my parents for their constant support and encouragement during my studies

CHAPTER 1: Introduction

1.1. Spinal muscular atrophy

Spinal muscular atrophy (SMA) is debilitating neuromuscular disorder, genetically characterised by functional loss of the survival of motor neuron 1 (*SMN1)* gene (Wirth *et al.*, 1999), and the most common genetic cause of infantile death that shows the autosomal recessive mode of inheritance (Wirth, Brichta and Hahnen, 2006; D'Ydewalle and Sumner, 2015). SMA is characterised by the loss of alpha motor neurons in anterior horn of the lumbar spinal cord, leading to progressive weakening and atrophy of voluntary muscles of the limbs and trunk (Monani, 2005). With an incidence of 1:6000 to 1:10000 births, and a carrier frequency between 1:35 to 1:60, SMA is one of the most frequent autosomal recessive disorders (Ogino *et al.*, 2002; Prior, 2010). Homozygous functional loss of *SMN1* gene is SMA determining factor (Lefebvre *et al.*, 1995), however, disease severity is modulated by the number of copies of survival of motor neuron 2 (*SMN2*) gene (Feldkötter *et al.*, 2002; Wirth *et al.*, 2006).

The most significant clinical symptoms in SMA are tremor of fingers and hands, absence of deep tendon reflex, hyporeflexia, fasciculation of the tongue muscle, hypotonia and symmetrical muscle weakening (Simic, 2008). Weakness is usually first expressed in proximal voluntary muscles of limbs. Distal voluntary muscles of limbs and eventually the entire trunk gets affected during disease progression, while the diaphragm and extraocular muscles remain spared until the late stages of disease (Simic, 2008). Patients are usually divided into four groups (SMA I-IV) based on age of disease onset and motor function (Dubowitz, 1995; Zerres, Klaus; Rudnik-Schöneborn, 1995). There is one additional group, the most severe type (SMA 0) (Dubowitz, 1999), with disease onset at neonatal stage. Movement impairments in those patients can be detected even in prenatal stage, and if untreated, do not survive beyond first month (Mercuri, Bertini and Iannaccone, 2012; D'Ydewalle and Sumner, 2015).

Approximately 50% of the patients have severe type I SMA (Werdnig-Hoffmann disease) (Wirth, Brichta and Hahnen, 2006; Lunn and Wang, 2008). In the natural history of disease progression, symptom onset is usually before 6 months and death around the age of 2. The term “floppy infant” is often used for clinical description of these children because of generalized muscle weakness and hypotonia (Wirth, Brichta and Hahnen, 2006). Children are never able to sit or walk, have problems with breathing (paradoxical breathing) and feeding. Airway impairment increases incidence of respiratory infections, an important cause of death in type I SMA patients (Wirth, Brichta and Hahnen, 2006; Lunn and Wang, 2008). In type II SMA (intermediate form), the first symptoms appear between 6-18 months (Lunn and Wang, 2008; Mercuri, Bertini and Iannaccone, 2012). Children can sit but are never able to walk, often develop kyphoscoliosis and tremors, and have problems with swallowing and breathing. In the natural history of disease progression death usually occurs in adolescence or early adulthood due to respiratory failure (Lunn and Wang, 2008; Mercuri, Bertini and Iannaccone, 2012). In SMA III (Kugelberg-Welander disease) lifespan is not reduced (Wirth, Brichta and Hahnen, 2006). All patients can sit and walk, but motor function capabilities differ between two subgroups (IIIa and IIIb). In SMA type IIIa symptom onset is before the age of 3, and less than 50% of the patients can still walk at the age of 20. In SMA type IIIb symptom onset is after the age of 3, and around 90% of the patients can still walk at the same age (Wirth, Brichta and Hahnen, 2006). Type IV SMA (adult form) has later onset, around the age of 30. Patients express mild motor problems, but retain ability to walk and do not have reduced lifespan (Lunn and Wang, 2008).

1. 2. SMA determining gene: survival of motor neuron (SMN)

In 1990, the location of the SMA determining gene was linked to chromosome 5 by two separate groups, Gilliam's (Gilliam *et al.*, 1990) in New York and Melki's (Melki *et al.*, 1990) in Paris. Five years later, an inverted duplication in 5q13 was identified, leading to isolation and characterization of *SMN* gene (Lefebvre *et al.*, 1995; Bürglen *et al.*, 1996). The *SMN* gene is highly conserved across species, however, duplication of about 500 kb long sequence containing *SMN* gene is specific for primates, where humans only developed two different *SMN* copies (*SMN1* and *SMN2*) (Rochette, Gilbert and Simard, 2001). While *SMN1* gene (SMN^T) is present in one copy and located at the telomeric part of the sequence, the number of copies of centromeric *SMN2* (SMN^C) gene varies (Wirth, Garbes and Riessland, 2013). *SMN* genes are highly homologous, contain ten exons and code for the same 294 amino acid protein (Lefebvre *et al.*, 1995; Bürglen *et al.*, 1996). Several point mutations have been identified in *SMN2* gene that distinguish it from *SMN1* gene (Singh and Singh, 2018), however, only C to T substitution at the position six in exon seven is in the coding region of the gene (Lorson *et al.*, 1999). Although the mutation is translationally silent, it leads to splicing defects and production of SMN transcripts lacking exon seven (SMNΔ7) (Lunn and Wang, 2008). Consequently, protein products are truncated, non-functional and prone to fast degradation. Only 10% of the spliced SMN2 transcripts code for the full-length functional SMN protein (Lunn and Wang, 2008) (Figure 1.1A).

In healthy individuals, contribution of the *SMN2* gene in protein production is minor, however, when *SMN1* is depleted low levels of functional SMN protein become essential for prenatal development and regulation of disease severity (Taylor *et al.*, 1998). An inverse correlation between the number of *SMN2* copies and disease severity is usually observed (Feldkötter *et*

al., 2002; Wirth *et al.*, 2006). Thus, patients with neonatal onset SMA (SMA 0) carry one *SMN2* copy, type I SMA patients usually carry two copies, type II SMA patients three copies, type III SMA patients three or four copies and type IV SMA patients four to six copies of *SMN2* (Wirth, Garbes and Riessland, 2013) (Figure 1.1B).

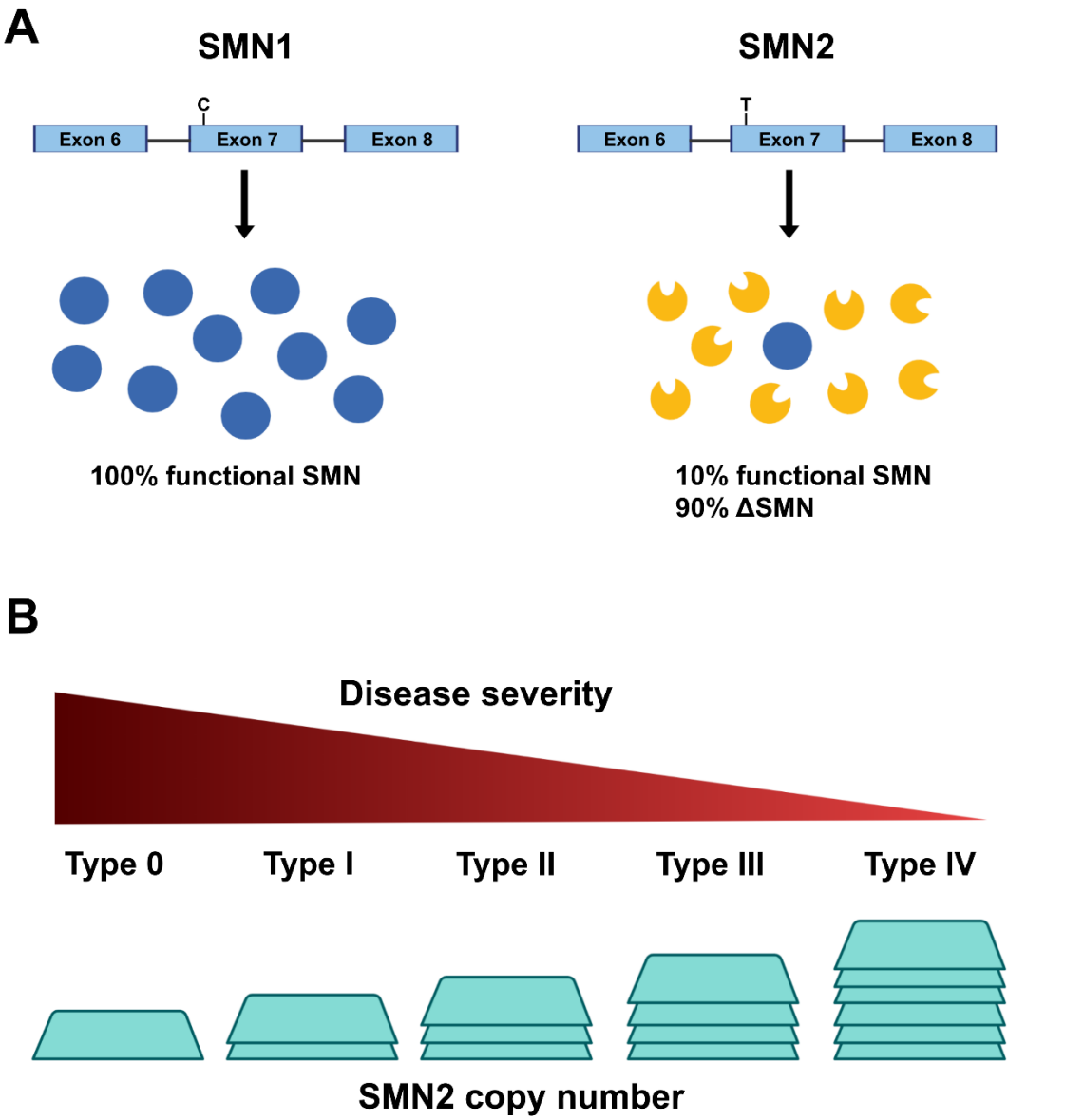

Figure 1. 1. Genomic structure of SMN genes and genome-phenotype correlation. (A) C to T mutation in exon seven of the SMN2 gene causes alternative splicing of the pre-mRNA and skipping of exon 7. Truncated SMNΔ7 proteins are unstable, non-functional and prone to degradation. **(B)** SMN2 copy number inversely correlates with disease severity in SMA. Image created with BioRender.com.

1.2.1. Splicing mechanism in SMN transcripts

Correct splicing of SMN transcript is regulated by a large number of specific transcript sequences (cis elements), that can be stimulating, exonic splicing enhancers (ESEs) and intronic splicing enhancers (ISEs), and inhibitory, exonic splicing silencers (ESSs) and intronic splicing silencers (ISSs) (Wirth, Brichta and Hahnen, 2006). Cis elements get recognised by splicing factors (trans elements), including the serine-arginine-rich (SR) proteins and heterogeneous nuclear ribonucleoproteins (hnRNPs). SR protein SF2/ASF, for example, recognises SE1, an important ESE that is localized at the 5' end of SMN exon seven (Wirth, Brichta and Hahnen, 2006). An early study, using ESE motif-prediction tools, proposed that the C to T mutation in SMN2 exon seven is located within the heptamer sequence of the SE1, which disrupts binding of the SF2/ASF splicing factor to ES1 (Cartegni and Krainer, 2002). Consequently, exon seven is not recognised by the splicing machinery which results in generation of SMNΔ7 transcripts (Cartegni and Krainer, 2002). Soon after that, it has become clear that SF2/ASF is not responsible, at least not solely, for SMN2 exon seven skipping. For example, depletion of SF2/ASF splicing factor in DT40-ASF cells had no effect on exon 7 splicing in either SMN1 or SMN2 transcripts (Kashima and Manley, 2003). The same study proposed the idea that C to T mutation in SMN2 exon seven generates specific ESS for hnRNP1 A1, a strong splicing inhibitor, that is responsible for SMN2 exon seven skipping (Kashima and Manley, 2003). Indeed, incubation of Hela nuclear extracts with purified 5’ half RNA fragments of SMN1 and SMN2 exon 7 resulted in selective binding of hnRNP A1 to the exon seven of the SMN2 transcript (Kashima and Manley, 2003). In addition, inhibition of hnRNP A1, hnRNP A2 and hnRNP A1/A2 in combination enhanced inclusion of SMN2 exon seven into messenger ribonucleic acid (mRNA) in Hela cells, but did not affect splicing efficiency of SMN1 exon seven (Kashima and Manley, 2003). Further studies identified several hnRNP A1/A2 binding sites that

have a role in SMN2 exon 7 splicing, including one in intron 6 (between nucleotide 41 to 55) (Hua *et al.*, 2008) and one in intron seven (between nucleotide 10 and 24) named ISS-N1 (Singh *et al.*, 2006; Hua *et al.*, 2008). For example, deletion of ISS-N1 region in Neuro-2a, NSC-34, SK-N-SH, P-19 and HEK293 cell lines induced SMN2 exon seven inclusion in mRNA (Singh *et al.*, 2006). In addition, simultaneous deletion of ISS-N1 and abrogation of one of the stimulatory cis elements, including intronic element 2, Tra2-ESE, Conserved tract and a critical guanosine residue at the first position of exon 7, promoted SMN2 exon seven inclusion into mRNA, thus showing the critical role for ISS-N1 in SMN2 exon seven splicing defects (Singh *et al.*, 2006). In line with this, antisense oligonucleotide against ISS-N1 increased SMN2 exon seven inclusion into mRNA (Singh *et al.*, 2006), which is also the mechanism of action of an approved antisense oligonucleotide drug nusinersen (described in more detail in section 1.5.1.1) (Ottesen, 2017). Other SMN2 splicing regulators have been described including, for example, splicing inhibitor Sam68 that was shown to bind the C to T mutation site in exon seven in HEK293T cells (Pedrotti *et al.*, 2010). Indeed, mutations that affect RNA binding activity of Sam68 induced SMN2 exon seven inclusion into mRNA in HEK293T cells and SMA patient fibroblasts, and SMN protein production in SMA patient fibroblasts (Pedrotti *et al.*, 2010). In addition, positive splicing factors, Htra2-β1 (Hofmann *et al.*, 2000) and hnRNP M (Cho *et al.*, 2014), were shown to promote SMN2 exon seven inclusion by binding to the ESE region in SMN exon seven. Other positive splicing factor, including hnRNP G, TDP-43 and SRp30c were shown to promote SMN2 exon seven inclusion by direct interaction with other factors like Htra2-β1 (Hofmann and Wirth, 2002; Young *et al.*, 2002; Bose *et al.*, 2008). A schematic diagram, showing SMN exon seven splicing regulation, is presented in Figure 1.2.

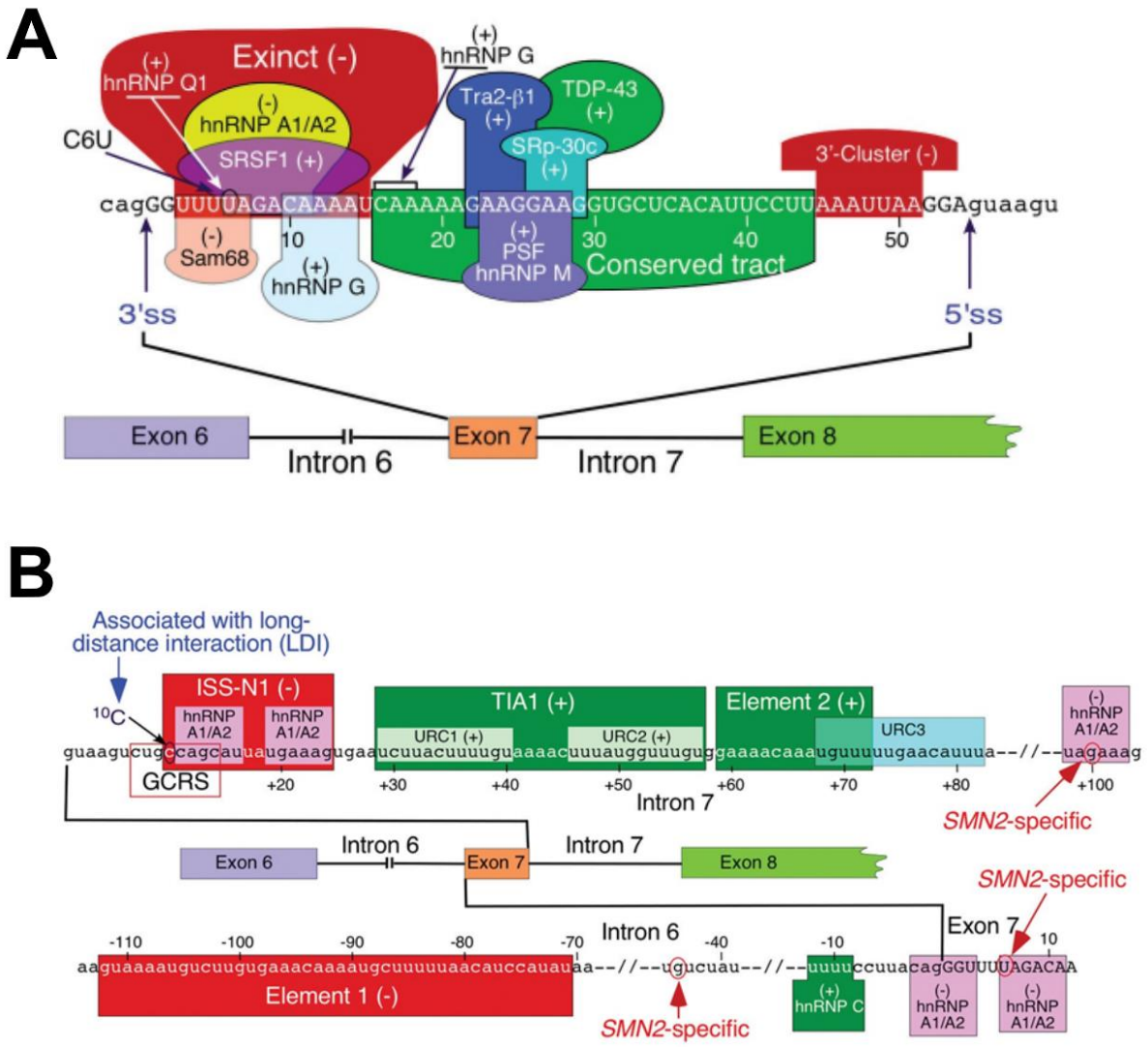

Figure 1. 2. SMN2 exon 7 splicing regulation. Schematic diagram showing known cis and trans splicing factors, within **(A)** exon seven and **(B)** introns six and seven, that modulate SMN2 exon 7 splicing. Positive (+) and negative (-) splicing elements are indicated, together with exonic (upper case) and intronic (lower case) sequences. C to T (C to U) mutation at position six of exon seven is indicated by black arrow. Additional SMN2-specific single nucleotide substitutions are indicated by red arrow (Singh and Singh, 2018).

1.2.2. Functions of the SMN protein

SMN controls different aspects of RNA metabolism including transcription, pre-mRNA splicing, snRNP assembly, mRNA trafficking, telomerase activity and translation [reviewed in (Singh *et al.*, 2017)].

1.2.2.1. SnRNP assembly

SMN has well established function in assembly of small nuclear ribonucleoproteins (snRNPs) that are involved in splicing of pre-mRNA (Morris, 2008). SnRNAs are synthesised in the nucleus and transported to the cytoplasm where they interact with SMN complex. SMN complex is comprised of SMN, gemin proteins (2-8) and unr interacting protein (unrip) (Baccon *et al.*, 2002; Carissimi *et al.*, 2006; Battle *et al.*, 2007). In an adenosine triphosphate (ATP)-dependent manner, SMN complex attaches snRNA to heptameric ring of Smith (Sm) proteins to assemble the snRNPs (Raker *et al.*, 1999). After assembly, SMN complex transports snRNPs to the nucleus, where they get released into the Cajal bodies (CB, coiled bodies) for further modification (Narayanan *et al.*, 2004). The interaction between coilin, an essential protein of CBs, and SMN complex seems to be involved in snRNP release into the CB, and consequent release and recycling of the SMN complex to the cytoplasm (Hebert *et al.*, 2001).

The efficiency of SnRNP assembly strongly correlates with disease severity and survival in SMA mice, where spinal cords from the most severe mice showed the lowest capacity for snRNP assembly compared to less severe SMA mice or healthy controls (Workman *et al.*, 2009). Dysregulation of snRNP assembly caused splicing defects in a range of tissues including spinal cord, brain and kidney from SMA mice (Gabanella *et al.*, 2007; Zhang *et al.*, 2008, 2013; Bäumer *et al.*, 2009; Huo *et al.*, 2014). In addition, these changes seem to be tissue/cell type

specific (Zhang *et al.*, 2008, 2013), and correlate with disease severity (Gabanella *et al.*, 2007; Bäumer *et al.*, 2009). For example, motor neurons and glial cells from SMA mice both showed widespread dysregulation of mRNA levels, however, very few dysregulated transcripts were common to both cell types (Zhang *et al.*, 2013).

Defective snRNP assembly was proposed as one of the explanations for selective lower motor neuron vulnerability. It was suggested that motor neurons are more sensitive to defects in snRNP assembly, and consequent pre-mRNA splicing, because of their size and higher energy demands (Battaglia *et al.*, 1997). However, other large, high energy demanding cells, like cortical motor neurons and sensory neurons, do not show the same vulnerability, which makes this theory questionable (Monani, 2005). Tissue specific splicing changes, especially in the minor spliceosome snRNAs, may thus provide an alternative view of how defects in SMN housekeeping role can lead to specific motor neuron pathology. It has been suggested that motor neurons may preferentially use minor spliceosomes in a greater manner then other cells, which would make them more vulnerable in an environment of decreased SMN (Tu *et al.*, 2017). Indeed, reduction of minor spliceosome snRNAs, including U11, U12, and U4atac, was identified in the brain, spinal cord and heart tissue from SMA mice, while in skeletal muscles and kidneys, the same snRNAs stayed unaffected (Zhang *et al.*, 2008).

1.2.2.2. Axonal specific role of SMN

Other studies, showing SMN expression in neurites, growth cones, and filopodia-like structures in neuronal and glial cells, proposed a motor neuron specific function for SMN (Sharma *et al.*, 2005). Zhang et *al*. demonstrated cytoskeleton-dependent bidirectional transport of SMN granules in neurites and axonal processes of rat spinal cord and chick

forebrain cultured neurons, and showed colocalization of SMN and ribosomal RNAs in growth cones of rat spinal cord cultured neurons (Zhang *et al.*, 2003). A number of RNA-binding proteins were shown to interact with SMN, all of which have a known role in transport of axonal mRNAs (Rossoll *et al.*, 2003; Akten *et al.*, 2011; Fallini *et al.*, 2011; Hubers *et al.*, 2011). Correct localization and rapid translation of axonal mRNAs is necessary for regulation of axon growth and function. For example, a role for heterogeneous nuclear ribonucleoproteins R (hnRNP R) in the regulation of β-actin dynamics was identified in PC12 cells, where hnRNP R overexpression resulted in accumulation of β-actin mRNA in the growth cones of PC12 cells, whereas β-actin mRNA localization to growth cones was completely abolished in PC12 cells expressing mutant hnRNP R (Rossoll *et al.*, 2003). In addition, reduced accumulation of both hnRNP R and β-actin was identified in motor neurons from a mouse model of SMA, suggesting that interaction between SMN and hnRNP R might be necessary for the transport and localization of β-actin mRNA to growth cones (Rossoll *et al.*, 2003). Indeed, overexpression of SMN and hnRNP R lead to substantial accumulation of β-actin mRNA in growth cones of PC12 cells and increase in neurite growth (Rossoll *et al.*, 2003). Other RNA-binding proteins, including HuD, have shown direct interaction with SMN in mouse motor neurons and motor neuron-derived MN1-cells (Akten *et al.*, 2011; Fallini *et al.*, 2011; Hubers *et al.*, 2011). HuD protein and poly(A) mRNA were both reduced in axonal compartment of mouse motor neurons following SMN knockdown (Fallini *et al.*, 2011). Cpg15 mRNA, for example, was shown to interact directly with both SMN and HuD in mouse cortical neurons (Akten *et al.*, 2011). Reduction of cpg15 mRNA was identified in SMN-deficient mouse cortical neurons, and overexpression of cpg15 partially rescued axonal growth defects in zebrafish model of SMA (Akten *et al.*, 2011). All the evidence suggests that SMN might be involved in axonal mRNA trafficking by regulating assembly and transport of axonal RNPs. Although this proposed

function strongly correlates with a function in snRNP assembly, an essential snRNP component, Sm ring, is not present in axonal SMN granules, thus indicating that nucleus-specific and axon-specific functions of SMN are independent (Fallini, Bassell and Rossoll, 2012).

1.3. Clinical manifestation of SMA

1.3.1. Neuromuscular pathology

Neuromuscular pathology in SMA has been associated with intrinsic muscle and motor neuron defects. For example, axonal terminals from SMNΔ7 mouse model of SMA failed to develop proper terminal branching, and appeared swollen with accumulation of neurofilament (NF) from a pre-symptomatic stage of the disease (Kariya *et al.*, 2008). In addition, defects in acetylcholine receptor (AChR) clustering have been identified in diaphragm from embryonic SMNΔ7 mice, suggesting neuromuscular junction (NMJ) maturation defects (Kariya *et al.*, 2008). Similar defects were observed in a zebrafish model of SMA, where animals presented with shorter axons that had abnormal branching (Mcwhorter *et al.*, 2003). A reduction in synaptic vesicle protein 2 (SV2), which is found in presynaptic vesicles, was observed in SMA zebrafish, suggesting that SMN reduction also affects synaptic transmission (Boon *et al.*, 2009). Restoration of SMN protein levels rescued motor axon and NMJ defects (Boon *et al.*, 2009; Hao *et al.*, 2013), and increased zebrafish survival when introduced early during development (Hao *et al.*, 2013). Kariya et *al.* generated transgenic mouse model of SMA (*SMN2;CreER;Smn*$^{F7/-}$) carrying floxed *SMN* allele (*Smn*^{F7}) that can be inactivated following Cre-mediated recombination (Kariya *et al.*, 2014). This was done to examine the consequences of SMN depletion in different timepoints of mouse postnatal development (Kariya *et al.*, 2014). Early SMN depletion induced severe SMA phenotype and NMJ defects, whereas SMN

depletion in adult animals delayed SMA pathology, thus replicating disease spectra in SMA patients. In addition, SMA pathology in adult mice was further ameliorated following focal NMJ injury (Kariya *et al.*, 2014). These observations indicate that high levels of SMN protein during early postnatal development are necessary for NMJ maturation, after which requirements for SMN drastically decreases, and in adulthood SMN is necessary for the maintenance and repair of NMJs (Kariya *et al.*, 2014). Interestingly, tissue specific reduction of SMN levels results in different phenotypes in mouse models (Frugier *et al.*, 2000; Cifuentes-Diaz *et al.*, 2001). For example, motor neuron specific depletion of SMN levels resulted in both motor neuron degeneration and muscle atrophy (Frugier *et al.*, 2000). Depletion of SMN levels specifically in skeletal muscles resulted in severe muscle dystrophy phenotype, evidenced by necrotic muscle fibers and infiltration of connective tissue with mononuclear cells, however, no evidence of motor neuron pathology was observed in these mice (Cifuentes-Diaz *et al.*, 2001). This suggests that muscle atrophy is not purely a product of motor neuron degeneration, and intrinsic muscle defects contribute to impairment of motor functions in SMA (Cifuentes-Diaz *et al.*, 2001).

1.3.2. Systemic pathology

Although SMA is traditionally classified as neuromuscular disorder, it is becoming more evident that SMN depletion influences a variety of different cells and tissue types (Shababi, Lorson and Rudnik-Schöneborn, 2014). Indeed, a review study, looking at the health insurance claims from SMA patents, confirmed that many SMA patients experience non-neuromuscular problems, in cardiovascular, gastrointestinal, metabolic, reproductive and skeletal system, even before the symptom onset (Lipnickid *et al.*, 2019). SMA-associated pathologies are presented in Figure 1.3.

1.3.2.1. Pathological changes in the brain and non-motor neuron cells

Brain

SMN was highly expressed in the developing foetal brain (Briese *et al.*, 2006), rat spinal cord and chick forebrain during embryonic development (Zhang *et al.*, 2003), so it would seem logical that other parts of nervous system, besides motor neurons, should be affected by its depletion. Indeed, morphological changes in brain regions that express high levels of SMN, including hippocampus and hippocampal dentate gyrus, have been identified from pre-symptomatic stage of the disease in severe mouse model of SMA (Wishart *et al.*, 2010). The size of hippocampus and hippocampal dentate gyrus was significantly reduced in SMA mice compared to controls (Wishart *et al.*, 2010). Decreased size of SMA mice hippocampus was associated with lower number of proliferating cells (Wishart *et al.*, 2010). This was also confirmed by quantitative proteomics, showing dysregulation of proteins connected to cell proliferation, migration and development in the hippocampus from late-symptomatic SMA mice (Wishart *et al.*, 2010). Furthermore, degeneration of thalamus was observed by magnetic resonance (MR) imaging in severe SMA patient (Ito *et al.*, 2003), and by neuropathological examination in five type I SMA patients (Harding *et al.*, 2015).

Sensory neurons

Degenerative changes were also reported in sensory neurons from type I SMA patients (Harding *et al.*, 2015), and reduction in the number of proprioceptive-motor neuron synapses was identified in SMA mouse spinal cords from an early stage of the disease (Ling *et al.*, 2010; Mentis *et al.*, 2011). At the molecular level, defects in sensory-motor neuron connectivity have been connected to the ubiquitin-like modifier activating enzyme 1 (UBA1)- glycine-tRNA ligase (GARS) pathway (Shorrock *et al.*, 2018). Reduced levels of UBA1 were previously identified in

zebrafish and mouse models of SMA, and in induced pluripotent stem cell (iPSC)-derived motor neurons from patients with type I SMA (Wishart *et al.*, 2014; Powis *et al.*, 2016), and pharmacological or genetic suppression of UBA1 was sufficient to induce an SMA-like phenotype in zebrafish, thus demonstrating that UBA1 directly contributes to SMA disease pathways (Wishart *et al.*, 2014). In a study by Shorrock et *al*., upregulation of GARS levels was identified in spinal cord tissues from a severe mouse model of SMA (Shorrock *et al.*, 2018). Interestingly, upregulation of GARS levels was restricted to dorsal root ganglia (DRG) that contain sensory neuron bodies (Shorrock *et al.*, 2018), and mutations in *GARS* are known to cause Charcot-Marie-Tooth disease Type 2D (CMT2D) that is typically characterised by sensory impairment (Antonellis *et al.*, 2003). Quantitative analysis of mouse spinal cord sections revealed reduction in the number of sensory neurons in DRG from SMA mice, and overexpression of UBA1 was sufficient to restore GARS levels in DRGs and correct sensory neuron defects in SMA mice (Shorrock *et al.*, 2018). It was proposed that dysregulation of UBA1/GARS pathways is responsible, at least in part, for disrupted sensory neuron fate and altered sensory-motor connectivity in SMA mice (Shorrock *et al.*, 2018).

Schwann cells

An increased number of unmyelinated intercostal nerves, and intercostal nerves with thinner myelin sheet was identified in 'severe' (*Smn*$^{-/-}$; *SMN2*$^{tg/tg}$) and Taiwanese (Smn$^{-/-}$; SMN2$^{tg/0}$) mouse models of SMA, and this morphology was evident at early symptomatic stage of the disease in Taiwanese mice (Hunter *et al.*, 2014). In addition, immature Schwann cells from SMA mice failed to respond to differentiating clues *in vitro* (Hunter *et al.*, 2014). Myelination defects were corrected *in vitro* in murine Schwann cells (Hunter *et al.*, 2014), and *in vivo* in a mouse model of SMA (Hunter *et al.*, 2016) by overexpression of wild type SMN. Mass

spectrometry analysis revealed widespread defects in the proteome of Schwann cells derived from SMA mice, with a number of dysregulated proteins being linked to ubiquitination pathways (Aghamaleky Sarvestany *et al.*, 2014). For example, reduction of UBA1 levels was confirmed by immunostaining in cultured Schwann cells from SMA mice, and pharmacological inhibition of UBA1 in murine Schwann cells was sufficient to disrupt the expression of myelin protein zero (MPZ), an important regulator of myelination process (Aghamaleky Sarvestany *et al.*, 2014).

Astrocytes

Astrocytes are specialised glial cells that regulate central nervous system (CNS) blood flow, provide nutrient and oxygen supply for neurons, participate in the maintenance of synapses and modulate synaptic transmission. Astrocytes too have been implicated in SMA pathogenesis. For example, restoration of SMN levels specifically in astrocytes improved survival and motor functions in severe (SMNΔ7) and intermediate (smn^{2B-}) mouse models of SMA (Rindt *et al.*, 2015). Interestingly, an increased number of fully innervated NMJs and improved sensory-motor neuron connectivity were identified in SMA mice following restoration of SMN levels, however, the total number of spinal cord motor neurons did not change (Rindt *et al.*, 2015). This suggested that restoration of SMN levels in astrocytes acts by stabilising functions of remaining motor neurons rather than stopping motor neuron death (Rindt *et al.*, 2015).

Activated astrocytes were identified in spinal cord from SMA patients (Rindt *et al.*, 2015) and SMNΔ7 mouse model of SMA (Rindt *et al.*, 2015; Ohuchi *et al.*, 2019), indicating that SMN-deficient astrocytes might contribute to SMA pathogenesis by promoting inflammation. Indeed, increased expression of proinflammatory cytokines, including interleukin 1 beta (IL-

1β), interleukin 6 (IL-6) and tumor necrosis factor alpha (TNFα), was identified in the spinal cord from SMA patients and SMNΔ7 mouse model of SMA, (Rindt *et al.*, 2015), and restoration of SMN levels specifically in astrocytes decreased the expression of both IL-1β and IL-6 in SMA mouse spinal cord (Rindt *et al.*, 2015). Consistent with this finding, increased expression and secretion of another modulator of immune response, microRNA (miR)-146a, was detected in iPSC-derived astrocytes from type I SMA patients and in spinal cord from SMNΔ7 mice (Sison *et al.*, 2017). Treatment of healthy iPSC-derived motor neurons with synthetic miR-146 or conditioned medium from SMA patient iPSC-derived astrocytes was sufficient to induce motor neuron loss, which was blocked by addition of miR-146a inhibitor (Sison *et al.*, 2017).

1.3.2.2. Skeletal system abnormalities

Skeletal problems such as the scoliosis, pelvic obliquity and hip dislocation were commonly reported among type I-III SMA patients (Bach, 2007; Fujak *et al.*, 2013). In addition, a high frequency of bone fractures was reported in SMA patients (Fujak *et al.*, 2010; Vai *et al.*, 2015; Wasserman *et al.*, 2017), which coincided with decreased bone mineral density (BMD) (Khatri *et al.*, 2008; Vai *et al.*, 2015; Wasserman *et al.*, 2017). Indeed, negative regression observed between two bone metabolism markers, where 25-OH vitamin D showed decreased and parathyroid hormone (PTH) increased levels, confirmed these findings (Vai *et al.*, 2015). Decreased levels of 25-OH vitamin D negatively influence bone metabolism by increasing the expression of PTH, which in turn increases bone resorption (Vai *et al.*, 2015). In addition, increased levels of bone resorption marker CTx were identified in type II and III SMA patients in two separate studies (Vai *et al.*, 2015; Baranello *et al.*, 2019), and increased osteoclast activity and bone resorption, and decreased osteoblast differentiation were identified in vertebrae from a severe mouse model of SMA (Shanmugarajan *et al.*, 2009). These studies

suggest that SMA patients are at higher risk of osteopenia, osteoporosis and fractures, and further studies are clearly warranted to elucidate the precise molecular mechanism of bone metabolism dysregulation in SMA. This would allow identification of novel therapeutic targets and better management of bone fragility in SMA (Baranello *et al.*, 2019).

1.3.2.3. Cardiovascular defects

A systematic review of the literature in 2017 found 58 studies that reported on a total of 264 SMA patients with cardiac abnormalities (Wijngaarde *et al.*, 2017). Common findings among the 77 patients with the most severe type of SMA were structural pathology, observed mainly in the septum and/or cardiac outflow tract, and electrocardiogram (ECG) abnormalities, the most common of which was bradycardia (Wijngaarde *et al.*, 2017). All of the 63 type II SMA patients identified in the literature search had ECG abnormalities, while the 124 patients with Type III SMA had cardiac rhythm disorders and/or structural abnormalities. Structural heart abnormalities have also been identified in severe and intermediate mouse models of SMA, including thinning of ventricle walls and interventricular septum (Shababi *et al.*, 2010; Maxwell *et al.*, 2018) and dilation of ventricles (Heier *et al.*, 2010; Bogdanik *et al.*, 2015; Maxwell *et al.*, 2018). In addition, cardiac fibrosis was frequently reported in SMA patients and mouse models of SMA (Wijngaarde *et al.*, 2017), and it was detected at a pre-symptomatic stage of the disease in severe and intermediate mouse models of SMA (Shababi *et al.*, 2010; Cobb *et al.*, 2013). All of these defects mimic dilated cardiomyopathy, the functional consequence of which is systolic heart failure where the heart cannot pump blood properly (Maxwell *et al.*, 2018). This would be evidenced by decreased ejection fraction and blood pooling in ventricles, both of which were identified in SMA mice (Heier *et al.*, 2010; Shababi *et al.*, 2012; Bogdanik

et al., 2015; Maxwell *et al.*, 2018) and SMA patients (Yasuma, Kuru and Konagaya, 2004; Roos *et al.*, 2009; Iwahara *et al.*, 2015).

At the cellular level, cardiomyocytes from SMA mice were highly disorganised, meaning they failed to develop typical spiral organization of the middle heart muscle layer that is necessary for transduction of electrical impulse and ventricle contraction (Maxwell *et al.*, 2018). In addition, trabeculae, that form during embryonic development to increase surface area for nutrient uptake, failed to compact in the SMA heart which is necessary to increases the mass of the heart muscle (Maxwell *et al.*, 2018). Disorganisation of cardiomyocytes was connected to defects in the basement membrane, evident by decreased and non-uniform collagen IV staining (Maxwell *et al.*, 2018). In addition, increased oxidative stress, identified at pre- and early-symptomatic stages of the disease in two severe mouse models of SMA (Shababi *et al.*, 2010; Maxwell *et al.*, 2018), was connected to cardiomyocyte apoptosis, that was observed at early symptomatic stage of the disease in the heart from severe Taiwanese mice (Maxwell *et al.*, 2018). Another factor that is likely contributing to cardiomyocyte death in SMA hearts is decreased microvasculature that was evident at early-symptomatic stage of the disease in Taiwanese SMA mice (Maxwell *et al.*, 2018).

Another group observed vascular defects in proximal skeletal muscles and spinal cord in two severe mouse models (Taiwanese and SMNΔ7), and in proximal skeletal muscles of SMA I and SMA II patients (Somers *et al.*, 2016). The rate of vascularization increases with age in unaffected control muscles, however, SMA muscles do not show the same developmental pattern. For example, patient muscles showed a 10-fold decrease in the rate of vascularization at the age of three compared to their respective controls, and a 50% decrease in

vascularization was observed in muscles from two severe mouse models of SMA at late-symptomatic stage of the disease (Somers *et al.*, 2016). The same developmental defects in vascularization were observed in spinal cords from two severe mouse models of SMA, and vascular defects, accompanied by hypoxia, were detected at an early symptomatic stage of the disease in Taiwanese SMA mice (Somers *et al.*, 2016). In addition, impaired vasculature is thought to be responsible for necrosis of the fingers and toes in severe type I SMA patients (Rudnik-Schöneborn *et al.*, 2010).

1.3.2.4. Altered metabolism

A progressive decrease in the number of insulin producing β cells and a parallel increase in the number of glucagon producing α cells was reported in the pancreas of *Smn*$^{2B/-}$ mouse model of SMA, starting from pre-symptomatic stage of the disease (Bowerman *et al.*, 2012). Similar findings were observed in type I SMA patients, where pancreatic islets contained predominantly glucagon producing α cells (Bowerman *et al.*, 2012). In addition, hyperglycemia and hyperglucagonemia were identified at pre- and early symptomatic stages of the disease in *Smn*$^{2B/-}$ mouse model, which by the end stage of the disease resulted in glucose intolerance, suggesting developmental problems in the pancreas (Bowerman *et al.*, 2012).

Abnormal fatty acid metabolism was observed in severe SMA patients (Tein *et al.*, 1995; Crawford *et al.*, 1999; Deguise *et al.*, 2019) and in a mouse model of SMA (Deguise *et al.*, 2019). The increased levels of abnormal fatty acid metabolites, identified in type I and II SMA patient plasma and urine (Tein *et al.*, 1995; Crawford *et al.*, 1999), were associated with compromised activity of several enzymes involved in fatty acid metabolism, including L-3-hydroxyacyl-CoA dehydrogenase (SCHAD), long-chain L-3-hydroxyacyl-CoA dehydrogenase

(LCHAD), acetoacetyl-CoA thiolase and 3-ketoacyl-CoA thiolase (Tein *et al.*, 1995). In addition, accumulation of fat in the liver (steatosis) was identified in type I SMA patients and in SMNΔ7 and *Smn*$^{2B/-}$ mouse models of SMA (Deguise *et al.*, 2019). Morphological examination of the liver from Taiwanese SMA mice showed disorganisation of sinusoids, accumulation of immature red blood cells (RBC) within the sinusoids and iron deposition, all of which indicate developmental liver problems (Szunyogova *et al.*, 2016). In addition, an increased number of megakaryocytes was identified in the liver from SMA mice, which resulted in accumulation and clumping of platelets in the liver (Szunyogova *et al.*, 2016). All evidence suggest that SMN is required for normal liver development, since SMN depletion resulted in abnormal fatty acid metabolism and persistent haematopoiesis, which is typical for embryonic liver (Szunyogova *et al.*, 2016).

1.3.2.5. Compromised renal function

Pathological changes were detected in kidney tissue from type I SMA patients, including tubular injury, calcifications and fibrosis, and calcifications were accompanied by T-cell and macrophage accumulations, indicating inflammatory response (Nery *et al.*, 2019). In addition, type I SMA patients showed decreased serum creatinine, cystatin C (CysC) and sodium levels, high glucose and calcium levels, and granular casts and amorphous crystals in the urine, all of which indicate renal tubular dysfunction (Nery *et al.*, 2019). Renal abnormalities, including decreased circulating creatinine, blood urea nitrogen, albumin, calcium and chloride, were also observed in *Smn*$^{2B/-}$ mice at a symptomatic stage of the disease, thus showing that renal dysfunction in conserved pathology in SMA (Nery *et al.*, 2019).

1.3.2.6. Immune system dysregulation

Compromised spleen development was identified in severe (Taiwanese and $SMN^{-/-}$; SMN2) and intermediate (Smn^{2B-}) mouse models of SMA, as evidenced by the failure of the spleen to grow and develop mature morphology (Deguise *et al.*, 2017; Khairallah *et al.*, 2017; Thomson *et al.*, 2017). During normal postnatal development, homogenous spleen tissue differentiates into distinct red and white pulp, and the spleen develops defined capsule and trabeculae (Thomson *et al.*, 2017). In contrast, spleens from SMA mice maintained homogenous morphology throughout development, with no segregation between red and white pulp (Deguise *et al.*, 2017; Khairallah *et al.*, 2017; Thomson *et al.*, 2017), and failed to develop defined capsule and trabeculae (Thomson *et al.*, 2017). Pathological changes in the spleen were also confirmed in approximately 50% of type I SMA patients (Thomson *et al.*, 2017). Morphological abnormalities in the thymus have been observed in the symptomatic stage of the disease in severe ($SMN^{-/-}$; SMN2) and intermediate (Smn^{2B-}) mouse models of SMA, including decreased size, thinner cortex, reduced cell content, and increased number of apoptotic bodies and tangible body macrophages (Deguise *et al.*, 2017). Molecular analyses revealed reduced numbers and altered localization of B- lymphocytes in the spleen from intermediate *$Smn^{2B/-}$* (Deguise *et al.*, 2017) and severe Taiwanese (Thomson *et al.*, 2017) mouse models of SMA, and a general reduction in the number of circulating lymphocytes was identified in the blood from severe SMA mice (Thomson *et al.*, 2017). Diffuse distribution and expression pattern of T cells was also evident in the spleen from *$Smn^{2B/-}$* mice (Deguise *et al.*, 2017).

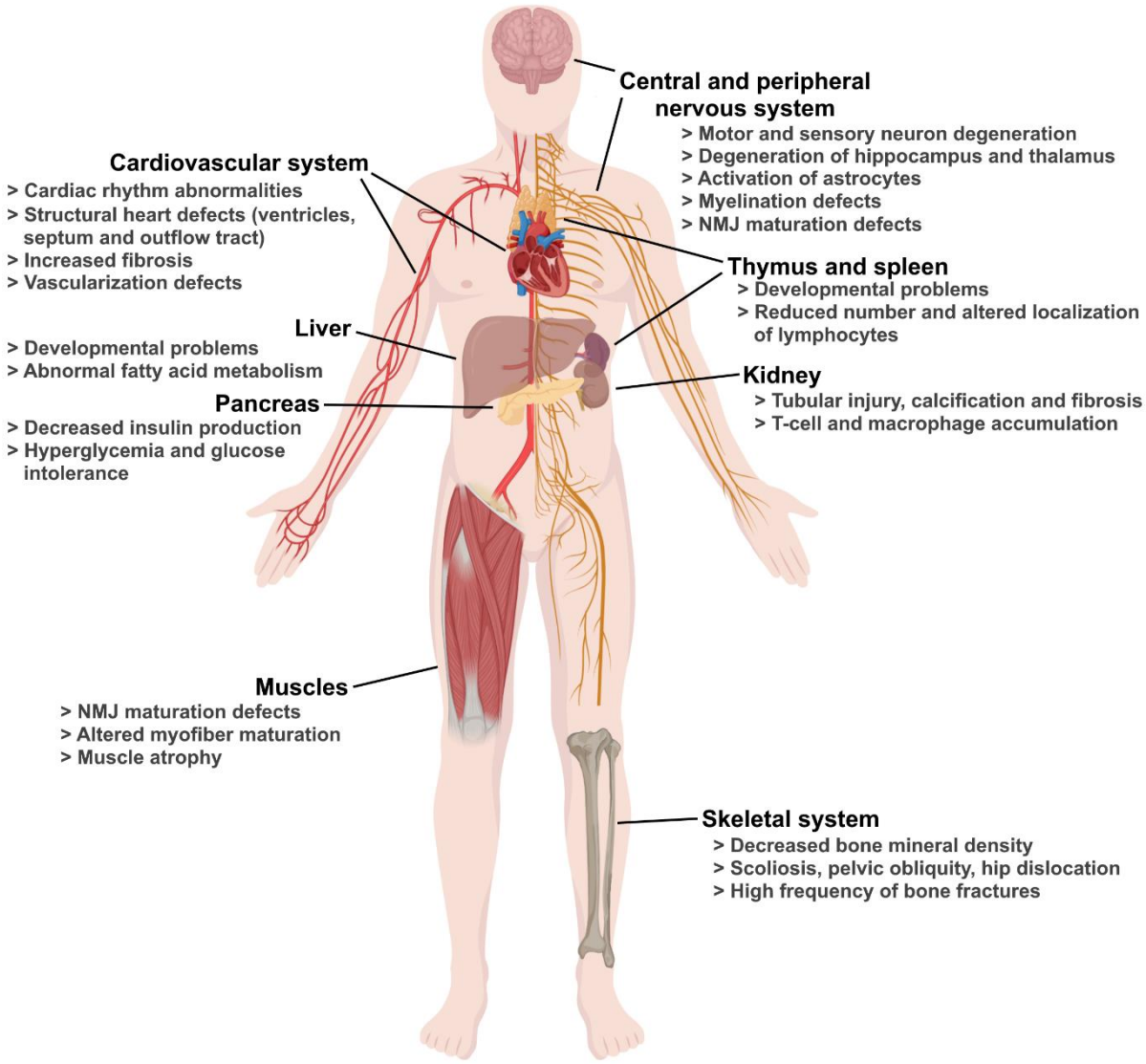

Figure 1. 3. Systemic SMA pathology. Depletion of SMN causes structural and functional defects in a range of organs and organ systems. Image created with BioRender.com.

1.4. SMA models

Several animal models have been used in SMA research, including *Caenorhabditis elegans, Drosophila melanogaster,* zebrafish*,* mice (Edens *et al.*, 2015) and pigs (Holm, Alstrup and Luo, 2016).

1.4.1. Caenorhabditis elegans

The nematode, *Caenorhabditis elegans,* carries one *SMN* gene, *SMN-1*, whose protein product shows 36% homology with the human *SMN* ortholog (Bertrandy *et al.*, 1999). A nematode model of SMA was created by deletion of *SMN-1* allele (ok355), where an otherwise lethal mutation is rescued by the presence of maternal *SMN-1* protein (Briese *et al.*, 2009). Mutant nematodes develop up to late larval stage when maternal SMN-1 protein levels decrease below critical levels, leading to developmental arrest, motoric defects and early death at late larval stage (Briese *et al.*, 2009). Created mutants cannot completely mimic the SMA phenotype, but they can be used to study the response of different tissues to decreased SMN-1 levels, or as a platform for drug screening studies (Briese *et al.*, 2009). Sleight et *al.*, for example, created a less severe nematode model of SMA by introducing a point mutation in exon 2 of the *SMN-1* gene (Sleigh *et al.*, 2011). The *SMN-1 (cb131)* mutant nematodes presented with the same pathology, however, disease progression was slower and resulted in longer survival (Sleigh *et al.*, 2011). This model was then used to screen 1040 chemical compounds as potential drugs for SMA, six of which were chosen for further validation studies. Three drugs, including 4-aminopyridine, gaboxadol hydrochloride and N-acetylneuraminic acid rescued at least one aspect of *SMN-1* phenotypic dysfunction, including increase in the lifespan (Sleigh *et al.*, 2011), thus showing that nematode model is a good platform for big drug screening studies.

1.4.2. Drosophila melanogaster

D. melanogaster has one *SMN* gene whose protein product shows 41% homology with the human ortholog (Miguel-Aliaga *et al.*, 2000). Like *C. elegans,* maternal SMN protein is expressed during early embryogenesis, and is responsible for the rescue and early development of the *Drosophila* mutants carrying lethal *SMN* alleles, SMN^{73Ao} and SMN^{B} (Chan *et al.*, 2003). As maternal Smn protein decreases, motor abnormalities start to develop, resulting in paralysis and death in late larval stage; a phenotype that can be completely rescued by delivery of the wild type Smn protein to both neurons and muscles (Chan *et al.*, 2003). Both mutants showed defects in NMJs (Chan *et al.*, 2003), confirming findings previously observed in a mouse model of SMA (Cifuentes-Diaz *et al.*, 2002). Short life cycle and easy genetic manipulation make *Drosophila* a valuable research tool (Muqit and Feany, 2002). Indeed, *Drosophila* has been used in genetic screening for identification of SMN modifiers (Chang *et al.*, 2008; Dimitriadi *et al.*, 2010; Sen *et al.*, 2013).

1.4.3. Danio rerio

Zebrafish (*Danio rerio*) has numerous advantages that make it an excellent model organism for neuromuscular research (Edens *et al.*, 2015). It has relatively simple, but conserved and well-characterized organization of the nervous system. Transparency of the zebrafish embryos allows easy *in vivo* manipulation and imaging of motor neurons. In addition, easy manipulation of the genome allows creation of transgenic animals, making it a desirable model in SMA research (Edens *et al.*, 2015). The zebrafish *SMN* gene encodes for the protein that shows 52% homology with the human ortholog (Bertrandy *et al.*, 1999). Consistent with previously described models, early development of the zebrafish *SMN* mutants is rescued by maternal SMN, with the death occurring at larval stage (Boon *et al.*, 2009). Motor neuron defects,

including axonal truncation and abnormal branching have been described in several zebrafish models of SMA (Mcwhorter *et al.*, 2003; Winkler *et al.*, 2005; McWhorter *et al.*, 2008; Hao *et al.*, 2013), together with abnormal NMJs (Boon *et al.*, 2009), thus proving that zebrafish is a good model to study motor neuron defects in SMA.

1.4.4. Mus musculus

The mouse *SMN* gene shows 83% homology with the human ortholog (Bertrandy *et al.*, 1999). Contrary to previously described models, mouse embryos do not have maternal *SMN*, and so homozygous deletion of *SMN* gene is embryonically lethal (Schrank *et al.*, 1997). Easy genetic manipulation and higher physiological similarity to humans (compared to previously described models) make mice models preferable for exploring SMA pathogenesis (Sleigh, Gillingwater and Talbot, 2011). The first severe mouse model of SMA was created by introduction of human *SMN2* gene into mouse *SMN* knockdown ($Smn^{-/-}$; SMN2) (Hsieh-Li *et al.*, 2000; Monani *et al.*, 2000). *$Smn^{-/-}$;SMN2* mice, carrying low number of *SMN2*, showed remarkable phenotypical resemblance to type I SMA patients. They were indistinguishable from control animals in the first two days after birth, after which motoric function defects developed, leading to death before postnatal day 7 (P7) (Hsieh-Li *et al.*, 2000; Monani *et al.*, 2000). Growth defects, decreased movement, decreased or lack of suckling, laboured breathing, tremors in the limbs and motor neuron degeneration, starting from P3, are all consistent with SMA I phenotype (Monani *et al.*, 2000). Moreover, high copy number *$Smn^{-/-}$;SMN2* mice did not show any symptoms, thus mimicking less severe SMA phenotype (Hsieh-Li *et al.*, 2000; Monani *et al.*, 2000). Introduction of human *SMN* cDNA lacking exon 7, *SMNΔ7* transgene, into severe mouse model resulted in creation of severe *SMNΔ7* model (*$Smn^{-/-}$/SMN2/SMNΔ7*) (Le *et al.*, 2005). It was initially created to assess SMNΔ7 toxicity, but instead was shown to increase lifespan from

6 to 13 days. Improvement of the phenotype is thought to be due to the complex formation between SMN and SMNΔ7 proteins which stabilizes SMNΔ7 turnover (Le *et al.*, 2005). Introduction of other *SMN1* transgenes, containing point mutations A2G (Monani *et al.*, 2003) or A111G (Workman *et al.*, 2009), into severe mouse model of SMA (*Smn*$^{-/-}$*/SMN2*) resulted in further increase of the lifespan. It was proposed that A2G transgene is able to form partially functional SMN complexes in the presence of low levels of full length SMN, which results in a mouse model with mild SMA (*SMN A2G;SMN2;Smn*$^{-/-}$) that mimics SMA type III (Monani *et al.*, 2003). SMN (A111G) transgene, on the other hand, rescued the SMA phenotype, which was associated with the ability of the A111G allele to participate in snRNP assembly (Workman *et al.*, 2009). The intermediate SMA mouse model (*Smn*$^{2B/-}$) carries a three nucleotide substitution in ESE sequence of exon 7 (Didonato *et al.*, 2001). Mimicking SMN2 splicing defects, this change results in production of Δ7SMN transcripts, leading to death by the age of 1 month (Didonato *et al.*, 2001).

1.4.5. Sus scrofa

Lorson et *al.* started developing a porcine model of SMA in 2011, by first creating heterozygous *SMN* knockout animals (SMN$^{+/-}$) (Lorson *et al.*, 2011). Pigs, out of all animal models, show most similarities with humans, and creation of a porcine model of SMA may thus provide a valuable platform for evaluation of drug efficiency and toxicity (Lorson *et al.*, 2011). In 2016, Holm et *al.* reported that splicing pig model of SMA (*Smn*$^{+/-}$*/SMN2*) has been successfully created and is being evaluated for the use in drug studies (Holm, Alstrup and Luo, 2016). Another pig model of SMA was developed by intrathecal administration of self-complimentary adeno-associated virus serotype-9- short hairpin RNA (scAAV9-shRNA) vector into five day old piglets (Duque *et al.*, 2015). Knockdown of SMN expression in motor neurons resulted in SMA-like phenotype,

including motor neuron loss and progressive muscle weakness (Duque *et al.*, 2015). Neuromuscular pathology was rescued by introduction of scAAV9-SMN 24 hours after the knockdown (Duque *et al.*, 2015).

Animal models of SMA generated valuable knowledge on molecular mechanisms underlying SMA pathology and have been extensively used in SMA therapy design (Foust *et al.*, 2010; Hua *et al.*, 2011; Ling *et al.*, 2012), however, translation of these findings into clinics was often shown to be challenging. For example, treatment with the histone deacetylase inhibitor (HDACi) valproic acid (VPA) improved neuromuscular pathology and motor functions in intermediate mouse model of SMA, however, type II and III SMA patients treated with VPA showed little or no improvement in motor functions (Swoboda *et al.*, 2010; Darbar *et al.*, 2011; Kissel *et al.*, 2011, 2014). Although SMN has a highly conserved function in RNA metabolism (Bertrandy *et al.*, 1999), homology differences in SMN gene exist between species (Bertrandy *et al.*, 1999) and could explain some discrepancies between animal and clinical studies. In addition, the *SMN2* gene is specific to primates only (Lefebvre *et al.*, 1995), while some species like *Caenorhabditis, Drosophila* and zebrafish have maternal *SMN* that can rescue early embryonic development (Chan *et al.*, 2003; Boon *et al.*, 2009; Briese *et al.*, 2009). Although pigs show most similarities to humans, development of porcine transgenic animal models is expensive and time-consuming (Prather *et al.*, 2013). All these problems raise a need for a simpler and genetically similar model system that would complement research utilising animal models of SMA.

1.4.6. *In vitro* models of SMA

Human skin fibroblasts are easily accessible, and easy to grow and maintain in cell culture (Ebert and Svendsen, 2010), and SMA patient fibroblasts showed reduced levels of SMN at the protein and mRNA level (Wadman *et al.*, 2016). A correlation between SMN protein levels and *SMN2* copy number was observed in fibroblast cells from SMA patients, which makes them a desirable *in vitro* model for the study of SMA disease mechanisms (Wadman *et al.*, 2016). For example, Custer and Androphy have reported accumulation of early autophagosomes, and protein p62, which is degraded exclusively by autophagy, in SMA patient fibroblasts and motor NSC-34 cells, indicating that autophagy is dysregulated in SMN-deficient cells (Custer and Androphy, 2014). Fibroblasts have also been used extensively as a platform for testing and optimization of potential therapeutics (Mohseni *et al.*, 2016; Woll *et al.*, 2016). For example, increased expression of SMN mRNA and protein levels was identified in SMA patient fibroblasts after the treatment with HDACis, suberoylanilide hydroxamic acid (SAHA) and Dacinostat (Mohseni *et al.*, 2016), thus showing that patient fibroblasts can serve as a good platform for *in vitro* drug screening studies.

Another useful *in vitro* model for SMA research are induced pluripotent stem cells (iPSCs) that are reprogrammed from adult somatic cells by viral transduction (Takahashi *et al.*, 2007) or episomal plasmid (Sareen *et al.*, 2012). Pluripotency of generated iPSCs allows generation of any human cell type that can be studied *in vitro,* which in the case of SMA means motor neurons to study their selective vulnerability (Fuller *et al.*, 2016). Indeed, iPSC-derived motor neurons have been successfully generated from SMA patient fibroblasts (Corti *et al.*, 2012; Sareen *et al.*, 2012; Fuller *et al.*, 2016). They showed selective death compared to control cells, thus mimicking *in vivo* motor neuron degeneration (Corti *et al.*, 2012; Sareen *et al.*, 2012), and

widespread dysregulation of the proteome compared to control cells (Fuller *et al.*, 2016). In addition, Yoshida et *al.* successfully co-cultured SMA patient iPSC-derived motor neurons with murine myoblasts to study NMJs *in vitro*, and found neurofilament (NF) accumulation in axon terminals and AChR clustering defects that were previously observed in animal models (Yoshida *et al.*, 2015). This model was also used to assess therapeutic potential of two drugs that increase SMN expression: valproic acid (VPA) and phosphorodiamidate morpholino oligonucleotides (PMOs). For example, VPA rescued AChR defect but did affect NF accumulation, while PMOs improved both AChR clustering and NF accumulation, implicating that *in vitro* models using patient cells are a useful system for evaluation of therapeutic efficiency (Yoshida *et al.*, 2015).

1.5. SMA therapies

There is no cure for SMA, but the last few years have seen significant progress in the development of therapies aimed at alleviating symptoms by raising full-length SMN protein levels (Sumner and Crawford, 2018). Nusinersen (Spinraza™), an antisense oligonucleotide drug, is now widely available for children and young adults with SMA, and most recently, Zolgensma™ (previously known as AVXS-101), an adeno-associated virus-based gene replacement therapy, was given approval by The Food and Drug Administration (FDA) for the treatment of SMA children under 2 years of age (Sumner and Crawford, 2018). Other therapeutic approaches, employing both SMN-dependent and SMN-independent strategies, have been developed over the years, and are summarised below and in Figure 1.4.

1.5.1. SMN-targeted therapies:

SMN-targeted therapies employ one of the two approaches to raise the levels of full length SMN protein: a) by promoting SMN2 expression (Brichta *et al.*, 2003; Andreassi *et al.*, 2004; Riessland *et al.*, 2006, 2010; Avila *et al.*, 2007; Garbes *et al.*, 2009; Schreml *et al.*, 2012; d'Ydewalle *et al.*, 2017) or correct splicing (Finkel *et al.*, 2017; Mercuri *et al.*, 2018), and b) by replacing the defective SMN1 gene (Mendell *et al.*, 2017).

1.5.1.1. Increasing the efficiency of SMN2 splicing

Nusinersen (Spinraza™)

Nusinersen, an antisense oligonucleotide (ASO) therapy, was approved by the FDA in December 2016 as the first available treatment for SMA (Hensel, Kubinski and Claus, 2020). Nusinersen in administrated intrathecally, four times within the first three months (12 mg on day 0, 14, 28 and 63), after which the treatment is repeated every four months (Finkel *et al.*, 2016). Nusinersen targets the intronic splicing silencer (ISS)-N1 to promote SMN2 exon 7 inclusion into the transcript and production of full length SMN protein (Ottesen, 2017). Indeed, a phase two clinical study on type I SMA patients identified increased SMN levels in spinal cord and brain tissue following nusinersen treatment (Finkel *et al.*, 2016). Nusinersen improved motor milestones in 51% of patients with the most severe type of SMA, 22% of which achieved full head control, 10% were able to roll over, 8% were able to sit and 1% were able to stand (Finkel *et al.*, 2017). The treatment also improved event-free survival, meaning it reduced the risk of death or the use of permanent assisted ventilation in SMA patients by 47% compared to untreated group (Finkel *et al.*, 2017). In the group of type II and III SMA patients, nusinersen treatment improved motor milestones in 57% of patients, measured as an increase of at least three points from the baseline in the Hammersmith Functional Motor

Scale– Expanded (HFMSE) score (Mercuri *et al.*, 2018). In both studies younger patients showed greater improvement in motor functions, however, some patients, especially those with a more advanced stage of the disease, showed no or little change in motor functions or even a decline with disease duration (Finkel *et al.*, 2017; Mercuri *et al.*, 2018). This shows the existence of a critical "time window" when SMN-targeted therapies can bring maximal benefit to SMA patients (Chiriboga *et al.*, 2016; Finkel *et al.*, 2016). Indeed, all patients enrolled in these trials were symptomatic, and so it is possible that treatment was delivered too late in some patients (Chiriboga *et al.*, 2016; Finkel *et al.*, 2016). Clinical trial on pre-symptomatic type I and II SMA patients confirmed these findings, since all 25 patients were able to sit without support after 2.9 years of the treatment, 92% were able to walk with assistance and 88% were able to walking independently (De Vivo *et al.*, 2019). The delivery route is another consideration to think about when treating older SMA patients, since a growing body of evidence suggests the involvement of other organs in SMA pathogenesis (summarised in section 1.3.2), and so nervous system specific delivery of SMN may not be sufficient to completely rescue SMA phenotype.

Branaplam (LMI070) and Risdiplam (RG7916)

Branaplam and risdiplam are orally administrated small drugs that increase the efficiency of SMN2 exon7 inclusion into the transcript (Poirier *et al.*, 2018). For example, ten daily doses of risdiplam increased the levels of full length SMN protein in the brain, spinal cord, muscle, heart, skin and blood from SMA mice, thus showing that orally administrated drug can systemically rescue SMN levels (Poirier *et al.*, 2018). In a phase I clinical trial on 25 healthy subjects, a single oral dose of risdiplam (0.6- 18 mg) was safe and well tolerated, which was prerequisite for phase II and III clinical trials on type I, II and III SMA patients (currently under

investigation) (Sturm *et al.*, 2019). Preliminary data from FIREFISH study indicate that type 1 SMA infants treated with risdiplam achieve better motoric milestones compared to the natural history of disease development [1], and risdiplam is currently under review by the FDA as a treatment for all types of SMA[2].

A daily dose of Branaplam improved body weight and survival in SMNΔ7 mouse model of SMA, which was accompanied by increased levels of the full length SMN protein in the brain (Palacino *et al.*, 2015). A phase I clinical trial on 13 type I SMA patients was conducted initially over the course of 13 weeks, with weekly dosage of branaplam, to assess safety and tolerability of the drug, and was then extended to 13 months (Charnas *et al.*, 2017). Adverse effects were mild but manageable, and some SMA patients showed improvement in motor functions (Charnas *et al.*, 2017).

1.5.1.2. Regulation of *SMN2* gene expression

Several histone deacetylase inhibitors (HDACi), including valproic acid (VPA) (Brichta *et al.*, 2003), phenylbutyrate (Andreassi *et al.*, 2004), suberoylanilide hydroxamic acid (SAHA) (Riessland *et al.*, 2010), trichostatin A (TSA) (Avila *et al.*, 2007), benzamide M344 (Riessland *et al.*, 2006), hydroxamic acid LBH589 (Garbes *et al.*, 2009) and Dacinostat (Mohseni *et al.*, 2016) were shown to increase SMN mRNA and protein levels in *in vitro* an *in vivo* models of SMA. HDAC inhibitors promote expression of *SMN2* gene by blocking the activity of HDACs, known suppressors of gene expression (Mohseni, Zabidi-Hussin and Sasongko, 2013). Some of these,

[1] https://www.prnewswire.com/news-releases/risdiplam-rg7916-pivotal-firefish-study-demonstrated-statistically-significant-improvement-in-infants-with-type-1-spinal-muscular-atrophy-300991624.html
[2] https://smanewstoday.com/2019/11/25/risdiplam-potential-oral-therapy-all-sma-types-under-fda-priority-review/

like SAHA (Riessland *et al.*, 2010) and TSA (Avila *et al.*, 2007), improved NMJ defects and motor functions, and increased survival of severe mouse models of SMA, however, only two HDACi were tested in clinical trials. For example, oral daily doses of phenylbutyrate over the course of a week increased the levels of full length SMN transcript in the blood of six type II and III SMA patients, and improved motor functions and muscle strength (Brahe *et al.*, 2005). However, a larger study on 103 type II SMA patients, where phenylbutyrate was taken orally for 13 weeks by using an intermittent schedule (7 days on/7 days off), found no difference in motor functions between the phenylbutyrate and placebo treated group (Mercuri *et al.*, 2007). Another clinical study on type I and II SMA patients has been completed, however, it is not clear whether phenylbutyrate treatment improved motor functions is those SMA patients[3]. The first VPA clinical trial on type I, II and III SMA patients showed good safety and tolerability, however, increased body weight, identified in some SMA patients, was associated with the decline in motor functions (Swoboda *et al.*, 2009). VPA was administrated orally, every day for 12 months. The majority of SMA patients that showed improvement in motor functions were under the age of 5, thus indicating that VPA treatment might not be appropriate for all SMA patients (Swoboda *et al.*, 2009). Indeed, subsequent clinical studies, using similar experimental design, showed that VPA does not improve muscle strength and motor function in older SMA patients, while some improvement can be observed in younger population of SMA patients (Swoboda *et al.*, 2010; Darbar *et al.*, 2011; Kissel *et al.*, 2011, 2014). Once again, the critical 'time window' for effectiveness of SMN-targeted therapies was emphasised here, suggesting that alternative approaches are necessary for older SMA patients.

[3] https://clinicaltrials.gov/ct2/show/results/NCT00528268?term=phenylbutyrate&cond=spinal+muscular+atrophy&draw=2&rank=1

1.5.1.3. Replacement of the defective *SMN1* gene

Zolgensma™ (Onasemnogene Abeparvovec)

Zolgensma, a single dose gene therapy that relies on self-complementary adeno-associated virus 9 (scAAV9) delivery of functional *SMN* gene, was approved by the FDA in 2019 for the treatment of SMA children under the age of 2 (Hensel, Kubinski and Claus, 2020). The scAAV9 vector carrying *SMN* gene does not integrate into the genome, which greatly reduces the risk of insertional mutagenesis, and it crosses the blood-brain barrier thus allowing systemic drug delivery (Al-Zaidy and Mendell, 2019). Only one study to date, a phase I clinical trial, has been published and included 15 infants with type I SMA (Mendell *et al.*, 2017). All patients, enrolled in low dose (n = 3) or high dose cohort (n = 12), were alive at the age of 20 months, did not require permanent ventilation and showed improvement in motor milestones, which is in stark contrast with the natural history of disease development. Of the 12 patients who had received the high dose of gene therapy, 11 achieved head control, 11 were able to sit unassisted, 9 were able to roll over, 11 were able to speak and swallow independently, and 2 were able to crawl, stand and walk independently (Mendell *et al.*, 2017). Four patients had increased levels of liver enzymes that were attenuated by prednisolone treatment (Mendell *et al.*, 2017). Similar to nusinersen treatment, SMA children treated at a younger age achieved better motor milestones (Mendell *et al.*, 2017). There are no published studies on older SMA patients, however, a study on type I SMA patients (Mendell *et al.*, 2017), and previous experiences with nusinersen (Finkel *et al.*, 2017; Mercuri *et al.*, 2018) and valproic acid (Swoboda *et al.*, 2009, 2010; Darbar *et al.*, 2011; Kissel *et al.*, 2011, 2014) suggest that the beneficial effect of gene therapy is likely to be reduced in older SMA patients.

Though undoubtedly an enormous step forward, none of the two strategies (i.e. nusinersen and zolgensma) that have been approved for the treatment of SMA show complete efficiency (Finkel *et al.*, 2017; Mendell *et al.*, 2017; Mercuri *et al.*, 2018; Sumner and Crawford, 2018). Coupled with uncertainties around long-term effectiveness and the extremely high price of both strategies, there is keen interest to find alternative therapeutic strategies that could, in combination with SMN-targeted therapy, offer maximal therapeutic benefit to all SMA patients (Bowerman, 2019).

1.5.2. Non-SMN-targeted therapies

Molecular pathways downstream of SMN (reviewed below) have been identified as crucial in the regulation of SMA pathogenesis, and as such present attractive targets that can complement SMN-targeted therapies.

1.5.2.1. Neuroprotection

Regulation of mitochondrial stability

Olesoxime is small cholesterol–oxime that binds to the components of the mitochondrial permeability pore and stops excessive permeability under stress conditions, and it showed neuroprotective effect *in vitro* and *in vivo* models (Bordet *et al.*, 2010). For example, Olesoxime treatment delayed cell death in rat embryonic cortical neurons treated with a deoxyribonucleic acid (DNA) damaging agent Camptothecin (Gouarné *et al.*, 2013), and reduced astrogliosis, microglial activation, and motor neuron death in $SOD1^{G93A}$ mouse model of ALS (Sunyach *et al.*, 2012). The efficiency of Olesoxime was assessed in type II and III SMA patients, where patients received daily oral doses of Olesoxime for 24 months (Bertini *et al.*, 2017). Treatment was safe and well tolerated, and motor functions stayed preserved in

Olesoxime-treated group, which is in contrast with a natural decline in motor functions observed in placebo-treated group (Bertini *et al.*, 2017). However, another study, looking at the long-term effectiveness and safety of Olesoxime in type II and III SMA patients, showed deterioration of motor functions after 18 months of treatment, and so development of Olesoxime was stopped at this point [4].

Activation of PI3K-Akt-mTOR pathway

The phosphoinositide 3-kinase/protein kinase B/mammalian target of rapamycin (PI3K-Akt-mTOR) pathway controls different aspects of cellular function including, for example, cell signalling, apoptosis, neuronal polarity, proliferation and cytoskeletal protein expression (Godena and Ning, 2017). Downregulation of phosphatase and tensin homolog (PTEN), a negative regulators of PI3K-Akt-mTOR pathway, improved axonal growth and cell survival in SMN-deficient and healthy mouse motor neurons (Ning *et al.*, 2010). This phenotype was associated with increased phosphorylation of the proteins involved in PI3K-Akt-mTOR pathway, including Akt, I-kappa-B kinase (IKK) and Bcl2-associated agonist of cell death (Bad), and with restoration of β-actin protein levels (Ning *et al.*, 2010). Depletion of PTEN levels in levator auris longus (LAL) muscle at postnatal day one increased the number of functional NMJs in SMNΔ7 mouse model of SMA, and systemic depletion of PTEN levels increased the survival rate of SMNΔ7 mice by three-fold and improved their motor functions (Little *et al.*, 2015). Another inhibitor of PI3K-Akt-mTOR pathway, a specific microRNA, miR-183, was found upregulated in SMN-knockdown neurons, patient-derived fibroblasts, and spinal cord and sciatic nerve from SMNΔ7 mice (Kye *et al.*, 2014). Binding of miR-183 to mTOR mRNA was

[4] https://www.curesma.org/roche-releases-community-statement-on-olesoxime-program/

shown to be directly responsible for decreased translation of mTOR in SMN-deficient neuron cultures, which was restored upon miR-183 knockdown (Kye *et al.*, 2014). Knockdown of miR-183 improved axonal growth defects in SMN-depleted neuron cultures, and spinal motor neuron-specific depletion of miR-183 levels in SMNΔ7 mice resulted in a modest improvement of motor functions and survival (Kye *et al.*, 2014). All studies indicate that modulation of PI3K-Akt-mTOR pathway may have important implications in neuroprotection.

Restoration of actin dynamics

Neuronal growth is dependent on dynamic rearrangements of the actin cytoskeleton, which is controlled by different proteins including Rho GTP-ases, transforming protein RhoA (RhoA), CDC42 small effector protein 1 (Cdc42) and Ras-related C3 botulinum toxin substrate 1 (Rac1) (Bowerman, Shafey and Kothary, 2007). Of these, when in an active state, RhoA-GTP has an inhibitory effect on neuronal outgrowth and differentiation, while both Cdc42-GTP and Rac1-GTP were shown to induce neuronal outgrowth and differentiation (Bowerman, Shafey and Kothary, 2007). Perturbations in actin cytoskeleton were identified in SMN-deficient PC12 cells, including mis-localization of F-actin and dysregulation of GTP-ases. For example, total RhoA and RhoA-GTP levels were increased in SMN-knockdown PC-12 cell line, while the levels of Cdc42-GTP decreased compared to control cells (Bowerman, Shafey and Kothary, 2007). In the $Smn^{2B/-}$ mouse model of SMA, total RhoA protein levels stayed unchanged, however, RhoA-GTP levels were significantly increased in spinal cord tissue at pre-symptomatic stage of the disease (Bowerman *et al.*, 2010). Activated RhoA activates its downstream effector Rho-associated protein kinase 1 (ROCK), and subsequent activation of other members of the RhoA pathway results in inhibition of neuronal growth and differentiation (Bowerman, Shafey and Kothary, 2007). Indeed, pharmacological inhibition of ROCK increased muscle fiber size,

improved NMJ defects and survival of $Smn^{2B/-}$ mice, thus showing that activation of RhoA pathways and defective actin cytoskeleton play important role in motor neuron defects in SMA (Bowerman *et al.*, 2010). In addition, profilin IIa, a known regulator of actin dynamics and ROCK binding partner, was upregulated at the mRNA and protein level, suggesting that increased formation of RhoA-ROCK-profilin IIa might be driving neuronal growth defects (Bowerman *et al.*, 2010).

PLS3 (plastin 3) is an another protein involved in actin filament organization and actin stabilization (Bowerman *et al.*, 2009). It was found highly expressed in the human foetal brain and adult spinal cord, and is significantly increased during neuronal differentiation in rat PC12 cells (Oprea *et al.*, 2008). PLS3 was reduced in the spinal cord and brain tissue from $Smn^{2B/-}$ mice, and this pattern of expression was directly linked to dysregulation of profilin IIa levels, since knockdown of profilin II in $Smn^{2B/-}$ mice increased PLS3 levels (Bowerman *et al.*, 2009). PLS3 was identified as a key protective modifier in asymptomatic female patients carrying homozygous deletion of SMN1 gene (Oprea *et al.*, 2008). In addition, higher expression of PLS3 was identified in some SMA I and III patients, and in this group of patients, a milder phenotype was observed only in female patients, suggesting that PLS3 protective effect may be gender-specific (Oprea *et al.*, 2008). Since PLS3 has a role in actin filament organization, the relationship between monomeric G-actin and filamentous F-actin was examined. Increased levels of PLS3 in asymptomatic females, and type I and III SMA patients correlated with upregulation of F-actin level, suggesting that protective effect of PLS3 is exacerbated through stabilization of actin filament organization and axonal growth (Oprea *et al.*, 2008). Indeed, knockdown of PLS3 in PC12 cells impaired neurite growth, while overexpression of PLS3 in PLS3-knockdown zebrafish and severe mouse model of SMA rescued neurite growth defects,

increased muscle fiber size and axon number per endplate, improved maturation of NMJs and improved survival (Oprea *et al.*, 2008; Ackermann *et al.*, 2013). In addition, upregulation of PLS3 levels, in combination with SMN-targeted therapy (SMN-ASO), increased the survival rate of severe SMNΔ7 mouse model of SMA compared to SMN-ASO treatment alone, thus showing that combinatorial approach may bring greater therapeutic benefit to SMA patient (Kaifer *et al.*, 2017).

Regulation of endocytosis

Neurocalcin-delta (NCALD) overexpression in primary olfactory neuron cultures previously demonstrated a negative effect on axonal growth (Yamatani *et al.*, 2010), and interestingly, decreased NCALD levels were identified in asymptomatic individuals carrying homozygous deletion of SMN1 gene, indicating that low levels of NCALD might have a neuroprotective action in SMA (Riessland *et al.*, 2017). Indeed, retinoic acid-induced differentiation of NSC34 cells led to a steady reduction of NCALD levels over time, and NCALD knockdown was sufficient to induce motor neuron differentiation and axonal growth in NSC34 cells (Riessland *et al.*, 2017). In addition, NCALD knockdown rescued axonal growth defects in cultured motor neurons from SMA mice, and ameliorated neuromuscular defects in a zebrafish, *C. elegans* and mouse models of SMA (Riessland *et al.*, 2017; Torres-Benito *et al.*, 2019). Dysregulation of endocytosis was proposed as a mechanism of NCALD action in SMA, where NCALD binds to clathrin, an important pre-synaptic vesicle protein, and inhibits vesicle recycling at the NMJs (Riessland *et al.*, 2017). Indeed, endocytosis was impaired in SMA patient fibroblasts, SMN-deficient NSC34 cells and in NMJs from a mouse model of SMA, and knockdown of NCLAD levels rescued endocytosis defects in NSC34 cells and SMA mice (Riessland *et al.*, 2017). In addition, ASO directed against NCALD, in combination with an SMN-targeted therapy, at a pre-

symptomatic stage of the disease ameliorated neuromuscular pathology in Taiwanese SMA mice (Torres-Benito *et al.*, 2019). Improvement in neuromuscular pathology using a combinatorial approach was greater compared to SMN-ASO treatment alone, suggesting once again that additional therapies, in combination with SMN approach, are necessary to preserve motor neuron health in SMA (Torres-Benito *et al.*, 2019).

1.5.2.2. Muscle-enhancing strategies

Therapies aimed at improving muscle size and fatigue are also being developed in SMA and include compounds like Reldesemtiv and SRK-015 (Shorrock, Gillingwater and Groen, 2018). Reldesemtiv (CK-2127107) is fast skeletal muscle troponin binding protein that slows calcium release, and leads to increased force output following motor neuron stimulation in animals and humans (Hwee *et al.*, 2015). A phase II clinical trial evaluated safety, tolerability and effectiveness of daily oral administration of Reldesemtiv in 70 patients with type II, III and IV SMA. At the half point (four weeks) and completion of the study (eight weeks), SMA patients in both treatment groups (150 and 450 mg dose) showed improvement in muscle fatigue (measured by Six Minute Walk Distance test) and increased strength of respiratory muscles compared to placebo group, and the drug was safe and well tolerated[5]. This drug showed promising results for preserving muscle strength in SMA patients, and other studies, possibly in combination with SMN strategy, are anticipated in the near future.

In a recent study using the SMNΔ7 mouse model of SMA, SRK-015P, a monoclonal antibody which specifically inhibits myostatin, a negative regulator of muscle mass, showed promising results in combination with SMN2 splicing modifier (Long *et al.*, 2019). When compared to

[5] https://www.curesma.org/cytokinetics-presents-data-from-the-phase-2-clinical-trial-of-reldesemtiv-ck-2127107-in-patients-with-sma-at-the-2018-annual-sma-conference/

SMN-targeted therapy alone, the combinatorial approach increased body and skeletal muscle weight, increased the percentage of large muscle fibers, and improved motor functions in SMA mice (Long *et al.*, 2019). An optimised variant of SRK-015P, SRK-015, is currently being evaluated in a phase II clinical study, to assess safety, tolerability and efficiency of the treatment in type II and III SMA patients [6].

1.5.2.3. Other therapeutic approaches

Systemic restoration of IGF levels

IGF-1 (insulin-like growth factor-1), hormone that regulates cellular growth, proliferation, differentiation and survival, has been studied as a potential therapeutic approach in SMA (Murdocca *et al.*, 2012; Tsai *et al.*, 2012, 2014). Reduced levels of endogenous IGF-1 were identified in the blood from SMNΔ7 mice (Murdocca *et al.*, 2012). Nervous system targeted delivery of human IGF-1 reduced motor neuron death in intermediate mouse model of SMA, but did not rescue NMJ defects or improve motor functions (Tsai *et al.*, 2012). Perinatal treatment of SMNΔ7 mice with IPLEX (IGF-1/IGFBP-3 complex), where IGFBP-3 (IGF-1 binding protein 3) increases half-life of circulating IGF-1, had mild effect on motor neuron degeneration and motor function improvement, but did not improve survival or body weight of SMA mice (Murdocca *et al.*, 2012). On the other hand, systemic administration of AAV1-IGF-1 on P1 in severe mouse model of SMA increased IGF-1 protein levels in spinal cord, brain, muscles and heart (Tsai *et al.*, 2014). Treated animals showed a decrease in motor neuron degeneration and NMJ defects, decreased muscle and heart atrophy and improved motor functions and lifespan, once again showing the necessity for systemic approach in SMA

[6] https://clinicaltrials.gov/ct2/show/NCT03921528?term=SRK-015&cond=Spinal+Muscular+Atrophy&draw=2&rank=1

therapy design (Tsai *et al.*, 2014). However, type II and III SMA patients treated with daily doses of somatotropin, growth hormone that induces IGF-1 expression, for three months showed no significant change in motor functions compared to untreated patients (Kirschner *et al.*, 2014).

Restoration of the proteasomal pathway

Ubiquitin-like modifier activating enzyme 1 (UBA1) is the first member of the ubiquitin proteasome pathway (UPP) which has a well-established role in regulation of protein homeostasis by control of their degradation (Lecker, Goldberg and Mitch, 2006). Mutations in the *UBA1* gene cause X-linked infantile SMA (SMAX2) (Ramser *et al.*, 2008), and in SMN-dependent SMA, decreased UBA1 expression was identified across a range of tissues in severe and Taiwanese mouse models of SMA, including spinal cord, skeletal muscles, heart, liver, lung and kidney (Wishart *et al.*, 2014; Powis *et al.*, 2016), in zebrafish embryos, and in iPSC-derived motor neurons from type I SMA patients (Fuller *et al.*, 2016; Powis *et al.*, 2016). In addition, UBA1 was completely absent from motor neuron cytoplasm of Taiwanese SMA mice at early symptomatic stage of the disease, indicating defects in subcellular distribution of the UBA1 (Wishart *et al.*, 2014). A direct role for UBA1 in SMN-dependent disease pathways was established in zebrafish embryos, where genetic and pharmacological suppression of UBA1 levels resulted in axonal branching defects, thus mimicking motor neuron defects previously observed in SMN-deficient zebrafish (Wishart *et al.*, 2014). Restoration of UBA1 levels increased motor performance in zebrafish and mouse models of SMA, as well as increased survival and improved systemic pathology in SMA mice (Powis *et al.*, 2016). The efficiency of UBA1- directed approach remains to be investigated in clinical settings.

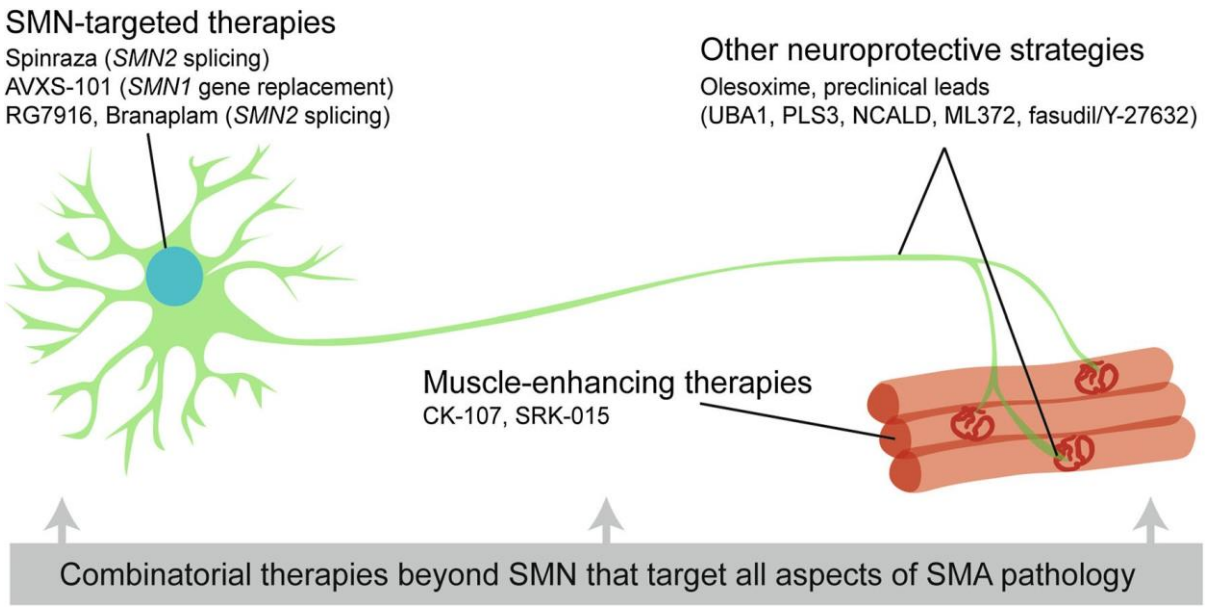

Figure 1. 4. Overview of potential therapeutic strategies in SMA. Most therapies currently under development target SMN levels, however, additional approaches are being explored and include drugs designed to enhance muscle function, provide neuroprotection and/or target systemic pathology. Combinations of these approaches will be necessary to provide robust rescue of all SMA-associated phenotypes. NCALD- neurocalcin delta, PLS3 plastin-3, SMA-spinal muscular atrophy, SMN-survival motor neuron, UBA1-ubiquitin-like modifier activating enzyme 1 (Shorrock, Gillingwater and Groen, 2018).

In summary, it has been shown here that SMA is not exclusively a motor neuron disease, and other pathologies, affecting skeletal, cardiovascular, immune and endocrine system, have been identified in SMA patients. Although very successful in improving motor functions in young and especially pre-symptomatic SMA patients, the antisense oligonucleotide approach nusinersen showed limited benefit in older population of SMA patients, and was not able to rescue systemic pathology. The gene therapy zolgensma, though administrated systemically, was also more successful in improving motor functions in younger population of SMA patients. Both of these examples show that therapies aiming to increase the levels of functional SMN may not be sufficient to completely abolish all the downstream effects of SMN loss in SMA patients. Other therapeutic approaches that target different SMA disease pathways, including proteasomal degradation, actin cytoskeleton dynamics and pathways involved in muscle growth, are currently under development. In combination with SMN-targeted approaches

they may prove useful in abolishing both neuromuscular and systemic pathology, thus bringing greater therapeutic benefit to all SMA patients.

The aim of this thesis was to identify and characterise new SMA disease pathways that could potentially be targeted therapeutically, and to determine the shared molecular fingerprint between SMA and amyotrophic lateral sclerosis (ALS).

Specific objectives were as follows:

a) To determine the molecular overlap between proteins and genes that were differentially expressed in SMA cells and tissues across at least two omics studies of SMA, so that appropriate therapeutic strategies, that can target molecules on the gene and/or protein levels, can be selected. To establish the pattern of differential expression of six protein targets in SMA tissues and cells, including UBA1, lamin A/C, GAPDH, ANXA2, NCAM and GAP43, and identify pharmaceutical compounds that have the potential to change their expression and test them in patient fibroblasts.
b) To investigate the molecular mechanism of lamin A/C dysregulation in SMA tissues and cells and determine the functional consequences of lamin A/C dysregulation in SMA patient fibroblasts. This knowledge can then be used in the development of therapies that can restore lamin A/C expression to normal levels. Considering that lamin A/C dysfunction has important implications for the heart health, it was important too to determine whether other changes to the proteome can be identified in the heart from SMA mice.
c) To identify conserved protein changes in ALS tissues and cells by comparison of published proteomic studies of ALS, and to compare these to the list of conserved protein changes in SMA tissues and cells. The aim here was to identify shared molecular overlap between SMA and ALS that can expand the knowledge of common disease pathways, so that the same therapy can be designed for treatment of SMA and ALS patients.

CHAPTER 2: Materials & Methods

2.1. Experimental models

2.1.1. Cell lines

Fibroblast cells from SMA patients (n = 3) and age/gender matched healthy controls (n = 3) were obtained from the Coriell Institute for Medical Research (NIGMS Human Genetic Cell Repository). Fibroblast cells from healthy older individuals (n = 5) were obtained from the Newcastle Biobank. Specifications for each cell line are provided in Table 2.1.

Mouse embryonic fibroblast cells (MEFs) from lamin A/C knockout (*LMNA* KO) (Sullivan *et al.*, 1999) and wild type mouse were obtained from Prof Colin L Stewart (Institute of Medical Biology, Singapore).

HEK293 cells were obtained from European Collection of Authenticated Cell Cultures. HEK293 cell culture and knockdown (KD) of ubiquitin-like modifier-activating enzyme 1 (UBA1) were performed by Dr Hannah K. Shorrock and Prof. Thomas H. Gillingwater (University of Edinburgh) as previously described (Shorrock *et al.*, 2018).

Table 2. 1. Fibroblast cell lines derived from SMA patients and healthy controls

ID	Phenotype	SMN2 copy number	Gender/Age	Biopsy source/ Tissue type	Supplier
GM00302	Healthy control	NA	Male/10 months	Unspecified/skin	Coriell Cell Repository
GM00498	Healthy control	NA	Male/3 years	Unspecified/skin	Coriell Cell Repository
GM05659	Healthy control	NA	Male/1 year	Chest/skin	Coriell Cell Repository
F152	Healthy control	NA	Female/27 years	Unspecified	Newcastle Biobank
F154	Healthy control	NA	Female/34 years	Unspecified	Newcastle Biobank
F008	Healthy control	NA	Male/39 years	Unspecified	Newcastle Biobank
F011	Healthy control	NA	Female/45 years	Unspecified	Newcastle Biobank
F067	Healthy control	NA	Female/66 years	Unspecified	Newcastle Biobank
GM00232	SMA I	2 SMN2 copies	Male/7 months	Unspecified	Coriell Cell Repository
GM09677	SMA I	3 SMN2 copies	Male/2 years	Eye/lens	Coriell Cell Repository
GM03813	SMA II	3 SMN2 copies	Male/3 years	Arm/skin	Coriell Cell Repository

Disease phenotype, SMN2 copy number, age of the donor, and biopsy source and tissue type are listed for each cell line.

2.1.2. Mouse models of SMA and ALS

The Taiwanese mouse model of severe SMA (original strain purchased from Jackson Laboratories, No.005058), heterozygous for the SMN2 transgene on Smn null background ($Smn^{-/-}$;$SMN2^{tg/+}$) (Hsieh-Li *et al.*, 2000) and age-matched phenotypically normal controls ($Smn^{+/-}$; $SMN2^{tg/o}$) were maintained in specific-pathogen-free (SPF) facilities at the University of Edinburgh. Breeding, genotyping using standard polymerase chain reaction (PCR) protocols, and tissue collection were performed by Dr Hannah K. Shorrock and Prof. Thomas H. Gillingwater (University of Edinburgh) as previously described (Riessland *et al.*, 2010). Tissue was harvested at a symptomatic time point, postnatal day 8 (P8).

The $SOD1^{G93A}$ mouse model of ALS (Gurney *et al.*, 1994), and age/gender-matched wild type (WT) littermates were obtained from the University of Oxford. Breeding, genotyping using standard PCR protocols, and tissue collection were performed by Dr Melissa Bowerman (Keele University) as previously described (Bowerman *et al.*, 2015). Tissue was harvested at late symptomatic (20 weeks) and early symptomatic (12 weeks) time points.

2.2. Aseptic cell culture

Sterile conditions were maintained at all time during cell culture.

2.2.1. Thawing of cells

After removal from the liquid nitrogen (N_2; -196°C), fibroblast cells and MEFs were first placed in the freezer (-80°C) for half an hour and then allowed to thaw either at room temperature (RT) or in a water bath (37°C). The thawed cell suspension was transferred to a universal tube (25mL) containing 10 mL of complete medium [High glucose Dulbecco's Modified Eagle Medium (DMEM; 31966021; Gibco), 10% fetal bovine serum (FBS; 10270098; Gibco) for fibroblasts or 15% FBS for MEFs, 1% non-essential amino acids (MEM-NEAA; 11140035; Gibco) and 1 % penicillin-streptomycin (PEN-STREP; 17-603E; Lonza)], in a drop-wise manner, and centrifuged on 365xg for 6 minutes (4K15; Sigma). Following centrifugation, the supernatant was carefully removed, and cell pellet was resuspended in complete medium.

2.2.2. Cell viability and cell count

Cell viability was assessed by using the trypan blue exclusion test. This test is based on the principle that live cells poses intact membranes that exclude certain dyes such as trypan blue (Strober, 2001). Dead cells would, therefore, stain blue while life cells remain transparent. For

this, 20-50 µL of cell suspension was mixed with an equal volume of 0.4% trypan blue (T6146; Sigma), incubated for 3 minutes and pipetted on to a haemocytometer. Cells in four corner squares of the haemocytometer were counted to assess the percentage of viable cells in the suspension, and cell concentration (number of viable cells per mL of medium) using following calculations:

$$\text{Cell viability (\%)} = (\text{number of live cells}/ \text{total number of cells}) \times 100$$

$$\text{Cell concentration (cells/mL)} = [(N/4) \times d] \times 10000$$

,where N/4 represents average number of viable cells across four corner squares of the haemocytometer, and d represents trypan blue dilution factor.

2.2.3. Monolayer cell culture and cell harvesting

According to calculations of the cell concentration, human fibroblasts and MEFs were seeded in tissue culture flasks (Sarstedt) containing complete medium at a density of $5x10^3$ cells/cm^2 and maintained in humidified incubator (Leec) at 37°C and 5% carbon dioxide (CO_2). Cells were grown up to 70% confluency, after which the media was removed from the flask, and the cells were incubated with trypsin/0.25 % ethylenediaminetetraacetic acid (EDTA) (25200056; Gibco) for 5 minutes at 37°C. Gentle tapping was applied to help detachment of cells from the culture flask. Trypsin activity was neutralised by addition of an equal volume of the complete medium, after which the cells were centrifuged at 365xg for 6 minutes. Supernatant was discarded, and the cells were either resuspended in a fresh volume of complete medium and reseeded, as described above, or resuspended in cold phosphate buffered saline [PBS; 0.02 M Sodium phosphate dibasic dodecahydrate ($Na_2HPO_4x12H_2O$; 71649; Sigma) and 0.15 M Sodium Chloride (NaCl; BP359; Fisher Scientific); pH 7.2 adjusted with phosphoric acid (H_3PO_4;

P-6560; Sigma)] and centrifuged at 365xg for 6 minutes. The PBS was then discarded, and the tubes were left upside-down to allow the cell pellet to dry completely. Tubes were wrapped in parafilm to prevent cell pellets from getting wet and stored on -80°C until further processing.

For immunocytochemistry analysis, cells were seeded in complete medium on glass coverslips (22mmx22mm) at a density of $2.5x10^4$ per coverslip and maintained in humidified incubator at 37°C and 5% CO_2. After reaching 70% confluency, the medium was removed, and cells were washed twice in cold PBS. The PBS was removed, and the cells were fixed in acetone (67-64-1; Fisher Scientific): methanol (67-56-1; Fisher Scientific) solution at a 50:50 ratio for 10 minutes. After removing the solution, coverslips were left to air dry, wrapped in parafilm and stored on -80°C until further processing.

2.2.4. Cryopreservation

Cells were trypsinized as explained above, and the supernatant was discarded following centrifugation at 365xg for 6 minutes. Cells were resuspended in a mixture of FBS and dimethyl sulfoxide (DMSO; BP231-100; Fisher Scientific) at 90:10 ratio, and carefully pipetted into a cryovial tube (1 mL per tube). Cryovials were stored at -80°C overnight before moving them to long-term storage in N_2.

2.3. Biochemical analyses of protein expression and localization

2.3.1. Quantitative western blotting

Quantitative western blotting is an established technique for investigating protein abundance (Bass *et al.*, 2017). Here, western blotting was used to investigate protein expression levels in

a range of tissues and cells from animal models and in human cells. These included spinal cord, brain, liver, muscle and heart from postnatal day 8 (P8) SMA mice (n = 5) and age-matched healthy controls (n = 5), spinal cord from 20-week (n = 5) and 12-week (n = 3) old ALS mice, and their respective age-matched healthy controls (n = 4), fibroblast cells from SMA patients (n = 3) and age/gender matched healthy controls (n = 3), UBA1 KD HEK cells (n = 3) and control HEK cells (n = 3), and *LMNA* KO MEFs (n = 3) and wild type MEFs (n = 3).

2.3.1.1. Protein extraction

Alongside chemical homogenization, mechanical disruption methods such as homogenization using pellet pestle and sonication were used to ensure complete protein extraction from the tissues (Bass *et al.*, 2017). Tissues were homogenized in 2x modified RIPA buffer [2% nonidet P-40 (NP-40; 155942; ICN Biomedicals), 0.5% sodium deoxycholate (D6750; Sigma), 2mM ethylenediamine tetra-acetic acid (EDTA; 104245S, BDH), 300 mM NaCl (BP358; Fisher Scientific) and 100 mM Tris-HCl, pH 7.4 (Trizma base; T1503; Sigma)] with pellet pestle (30 strokes), after which the samples were left on ice (4°C) for 10 minutes and sonicated at 5 microns for 10 seconds (Sonicrep 150; MSE). The same process was repeated two more times to ensure sufficient homogenization of the tissue. Cell pellets were resuspended in 2x modified RIPA buffer, left on ice (4°C) for 10-15 minutes, and sonicated at 5 microns for 10 seconds. Detergents NP-40 and sodium deoxycholate were used to improve extraction efficiency and protein solubilization (Dapic *et al.*, 2017). EDTA was used for inhibition of metalloproteinases and serine/threonine (Ser/Thr) phosphatase interactions (Bass *et al.*, 2017). Protein extracts were then centrifuged at 13000 RPM (Micro Centaur MSB010.CX2.5; MSE; rotor radius- 4 cm) for 5 minutes at 4°C to pellet any insoluble material.

2.3.1.2. Protein quantification

Protein concentration was determined using either Pierce™ 660nm Protein Assay Reagent (22660, Thermo Scientific) or Pierce^{TM} BCA protein assay kit (23227; Thermo Scientific).

2.3.1.2.1. Bicinchoninic acid (BCA) protein assay

Bicinchoninic acid (BCA) assay (Smith *et al.*, 1985) was performed according to instructions outlined in the guideline (23227; Thermo Scientific). Colorimetric BCA assay is based on the ability of the bicinchoninic acid to form a purple complex with cuprous ions (Cu^{1+}), which are generated under alkaline conditions by reaction of proteins with cupric ions (Cu^{2+}) (Smith *et al.*, 1985). The intensity of the colour is therefore proportional to the concentration of the protein in the sample.

Bovine serum albumin standards were prepared at an assay working range (0.125-2 mg/ml). Working reagent was prepared by mixing 50 parts of BCA reagent A with 1 part of BCA reagent B. 10 µL of each sample and standard was carefully pipetted into a well of 96-well plate, followed by addition of 200 µL of working reagent (sample to working reagent ratio = 1:20). All reactions were performed in triplicate to ensure accuracy. The plate was mixed on a plate shaker for 30 seconds, incubated at 37°C for 30 minutes, cooled to RT, and the absorbance was measured at 562nm using microplate reader (FLUOstar Omega; BMG Labtech). Samples that produced readings greater than the highest standard were further diluted and the absorbance was measured again (the dilution factor was taken into account during calculations). A standard curve was prepared in Excel by plotting average blank-corrected absorbance for each BSA standard vs. its concentration in mg/mL (example is shown in Figure 2.1). A quadratic calibration model was used to determine protein concentration (x) for each sample according to formula:

$$x = (-b+SQRT(b^2-4*a*(c-y)))/(2*a)$$

(y represents average blank-corrected absorbance of the sample, and a, b and c represent three coefficients of the quadratic equation ($y = ax^2+bx+c$)).

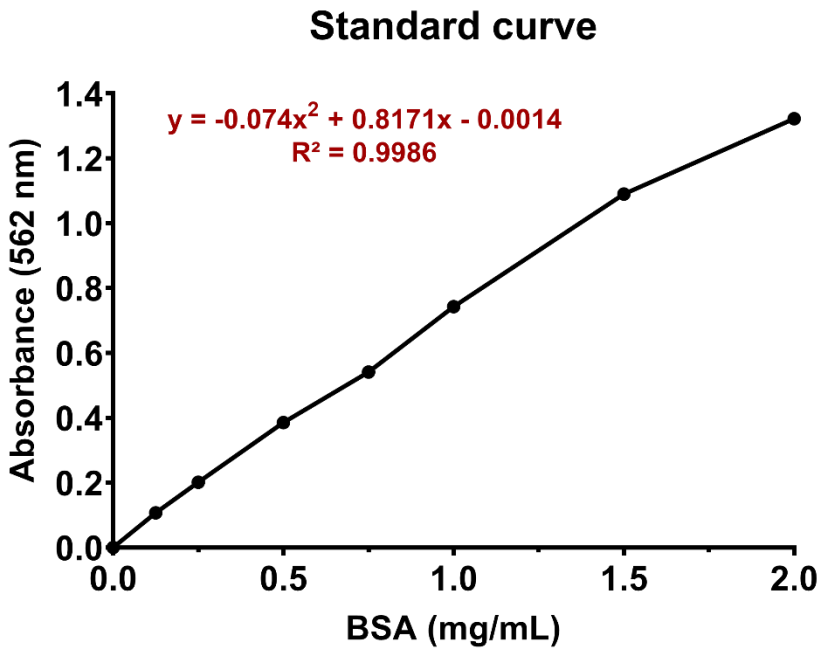

Figure 2. 1. Bovine serum albumine (BSA) standard curve. Average blank-corrected absorbance (562 nm) for each BSA standard was plotted against its concentration in mg/mL. Quadratic fit model ($y = ax^2+bx+c$) was used to determine concentration of the samples.

2.3.1.2.2. Pierce™ 660nm Protein Assay Reagent

660nm Protein Assay is colorimetric assay that relies on binding of the dye-metal complex (polyhydroxybenzenesulfoneph-thalein-type dye and a transition metal) to mainly basic amino acid residues in proteins (Antharavally *et al.*, 2009). The binding of the complex to protein causes a shift in the absorption maximum from 450 to 660 nm, which causes a change in colour from reddish-brown to green. The colour is stable and increase proportionally with protein concentrations (Antharavally *et al.*, 2009).

Bovine serum albumine (BSA; A7906; Sigma) standards were prepared in 7 serial dilutions for the analysis in assay working range (0.05–2 mg/ml of protein). 10 µL of each diluted sample

and standard, containing 0.8% of Triton X-100 (9002-93-1; Sigma), was carefully pipetted into a well of 96-well plate, following addition of 150 µL of 660nm protein assay reagent. All reactions were performed in triplicate to ensure accuracy. The plate was incubated at RT for 5 minutes, and the absorbance was measured at 660nm using microplate reader. Protein concentration in each sample was determined as described in section 2.3.1.2.1.

2.3.1.3. Sodium dodecylsulfate -polyacrylamide gel electrophoresis (SDS-PAGE)

The results from the protein assay were used to ensure equal loading for quantitative western blotting. Protein extracts were mixed with 2X SDS sample buffer [4% sodium dodecylsulfate (SDS; AM9823; Invitrogen), 10% 2-mercaptoethanol (M3148; Sigma), 20% glycerol (G9012; Sigma), 0.125 M Tris-HCl (Trizma base; T1503; Sigma; pH 6.8) and bromophenol blue (B6896; Sigma)], in a ratio of 1:1, and heated for 3 minutes at 95°C on a block heater, after which the samples were subjected to SDS-PAGE (Laemmli, 1970). 2-mercaptoethanol is used in the buffer to break disulfide bonds between cysteine residues, and SDS to facilitate solubilization of hydrophobic proteins (Bass *et al.*, 2017). Another important role of SDS is to overcome positive charge of the proteins in the sample (Bass *et al.*, 2017). Negatively charged proteins are separated by their mass, on a polyacrylamide gel by application of electrical current (Bass *et al.*, 2017). Samples and PageRuler™ Protein Ladder (26619; Thermo Scientific) were carefully loaded on Bolt™ 4-12% Bis-Tris Plus gel (NW04125BOX; Invitrogen) that was submerged in 1x SDS running buffers, MOPS (B0001; Invitrogen) or MES (B000202; Invitrogen), for separation of medium-large sized proteins or small-medium sized proteins respectively. Proteins in the sample were subject to electrophoresis at 140 V using a powerpack (PowerPac BASIC™; Biorad).

2.3.1.4. Protein transfer and immunoblotting

A slice of the gel, that did not contain protein of interest, was excised and stained with Coomassie blue dye [0.2% Coomassie Brilliant Blue R (B-0149; Sigma), 10% glacial acetic acid (64-19-7; Fisher Scientific), 20% industrial methylated spirits (IMS; Genta Medical) and 70% dH_20] for one hour or overnight, as an internal loading control for total protein. Coomassie staining is total protein loading control that showed higher linearity of protein detection compared to common housekeeping proteins such as glyceraldehyde 3-phosphate dehydrogenase (GAPDH) (Welinder and Ekblad, 2010). Coomassie dye forms complexes with proteins by binding primarily to arginine and lysine residues (Sapan, Lundblad and Price, 1999). After incubation in Coomassie blue, the gel was left in de-stain solution (10% glacial acetic acid, 20% IMS and 70% dH_20) to remove the background staining. The remaining part of a gel was assembled into a sandwich (as shown in Figure 2.2.) and submerged into transfer buffer [192 mM glycine (G7126; Sigma) and 25 mM Trizma base (T1503; Sigma)] to allow for transfer of proteins onto a nitrocellulose membrane (10600041; Amersham). Protein transfer was done overnight at 100 mA using a powerpack (PowerPac BASIC^{TM}; Biorad). The system was kept cool by cold water constantly running through a pipe that was submerged into the transfer tank.

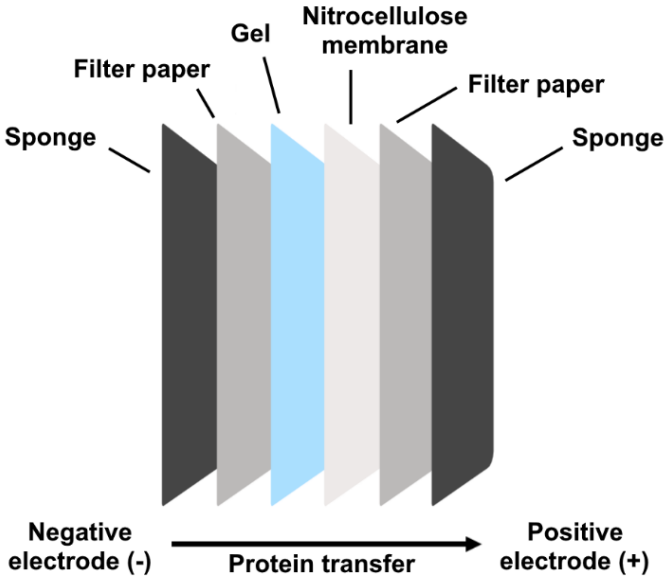

Figure 2. 2. Assembly of a sandwich for western blotting. Proteins from the gel were transferred onto a nitrocellulose membrane by assembling sandwich: sponge, filter paper, gel, nitrocellulose membrane, filter paper and sponge. The gel has to be on the negative side of the electrode to allow protein transfer onto the nitrocellulose membrane. Image created with BioRender.com.

Following protein transfer, the membrane was incubated with 4% powdered milk (Marvel) in PBS for one hour to block non-specific protein binding. The membranes were incubated with an appropriate primary antibody (Table 2.2.) in western blot (WB) buffer [1% FBS, 1% horse serum (HS; 16050130; Gibco), 0.1% BSA and 0.05% Triton X-100/ in PBS] at RT for one or two hours, followed by incubation with HRP-labelled goat anti-rabbit Ig (P0448; DAKO) or HRP-labelled goat anti-mouse Ig (P0260; DAKO) in WB buffer at 0.25 ng/mL, for one hour at RT. Between each step membranes were washed three times with PBS for five minutes. Membranes were incubated with SuperSignal™ West Femto (34904; Thermo Scientific) or SuperSignal™ West Pico (34580; Thermo Scientific) chemiluminescent substrate for 5 minutes at RT and visualised using a Gel Image Documentation system (Biorad).

Table 2. 2. Primary antibodies used in western blotting

Antibody	Supplier and catalog number	Dilution	Predicted mol. weight (kDa)	Comment
Mouse monoclonal anti-SMN	MANSMA12 2E6 (Young *et al.*, 2000)	1:100	38	
Mouse monoclonal anti-lamin AC	MANLAC1 4A7 (Manilal *et al.*, 2004)	1:100	71-66	For analyses of cell extracts
Rabbit monoclonal anti-lamin AC	ab169532; Abcam	1:1000-1:2000	74	For analyses of mouse tissues
Mouse monoclonal anti-GAPDH	NBP2-27103; Novus	1:1000-1:2000	36	
Rabbit monoclonal anti-UBA1	NBP2-67816; Novus	1:500-1:1000	130	
Mouse monoclonal anti-ANXA2	MAB3928; RD System	1:1000	40	
Rabbit monoclonal anti-NCAM	701379; Invitrogen	1:500	94, 140, 180	
Rabbit polyclonal anti-GAP43	ab16053; Abcam	1:2000	43-53	
Mouse monoclonal anti-active β-catenin	05-665; Merc Millipore	1:500	92	
Mouse monoclonal anti-β-catenin	610154; BD Trans. Lab.	1:1000-1:2000	92	
Mouse monoclonal anti-emerin	MANEM1 5D10; (Manilal *et al.*, 1996)	1:100	34	For analyses of cell extracts
Rabbit polyclonal anti-emerin	Made in the house	1:200	34	For analyses of mouse tissues
Rabbit polyclonal anti-ALDOA	NBP1-87488; Novus	1:500	40	
Rabbit polyclonal anti-SOD1	ab13498; Abcam	1:1000	18	
Rabbit polyclonal anti-CALR	NB600-103SS; Novus	1:500	55	
Mouse monoclonal anti-GRP94	sc-393402; Santa Cruz	1:50	94	Also known as HSP90B1
Rabbit monoclonal anti-Neurofilament-L	C28E10; Cell Signaling	1:1000	70	
Rabbit polyclonal anti-FAS ligand	ab15285; Abcam	1:200	31	
Mouse monoclonal anti-3-nitrotyrosine	sc-32757; Santa Cruz	1:50-1:200	NA	

Catalog number and supplier are listed for each primary antibody, together with the dilution, molecular weight of the protein target and sample type the antibodies were used on. NA-not applicable

2.3.1.5. Densitometry measurements of antibody reactive bands

Densitometry measurements of antibody reactive bands were obtained using Fiji software (v1.51) (Schindelin *et al.*, 2012). Before the analyses, images were converted to gray-scale images (Image → Type → 8-bit), and where necessary, contrast and brightness were adjusted uniformly across the gel and blot to decrease the background and enhance signal detection (Image → Adjust → Brightness/Contrast).

A rectangular box of a fixed size was drawn around the band in the first lane and marked as selection one, using a CTR+1 command. The box was then moved to the next lane and marked as selection 2 using a CTR+2 command. The same was repeated for all consecutive lanes until all bands were labelled, and the CTR+3 command was then used to draw a profile plot of each lane. Profile plot represents the relative density of the contents of the rectangle selection, where the peak corresponds to the dark band. The straight-line selection tool was used to draw a line at the base of the peak to divide the background from the peak. The surface of the peak was measured using a wand selection tool. For analysis of Coomassie stained gel, a rectangular selection tool was drawn across all lanes, to include several bands in each sample, and analysed as described above. Densitometry measurements of antibody reactive bands were normalized to densitometry measurements of the Coomassie stained gel, after which all samples were normalised to the average of control. The workflow is presented in Figure 2.3.

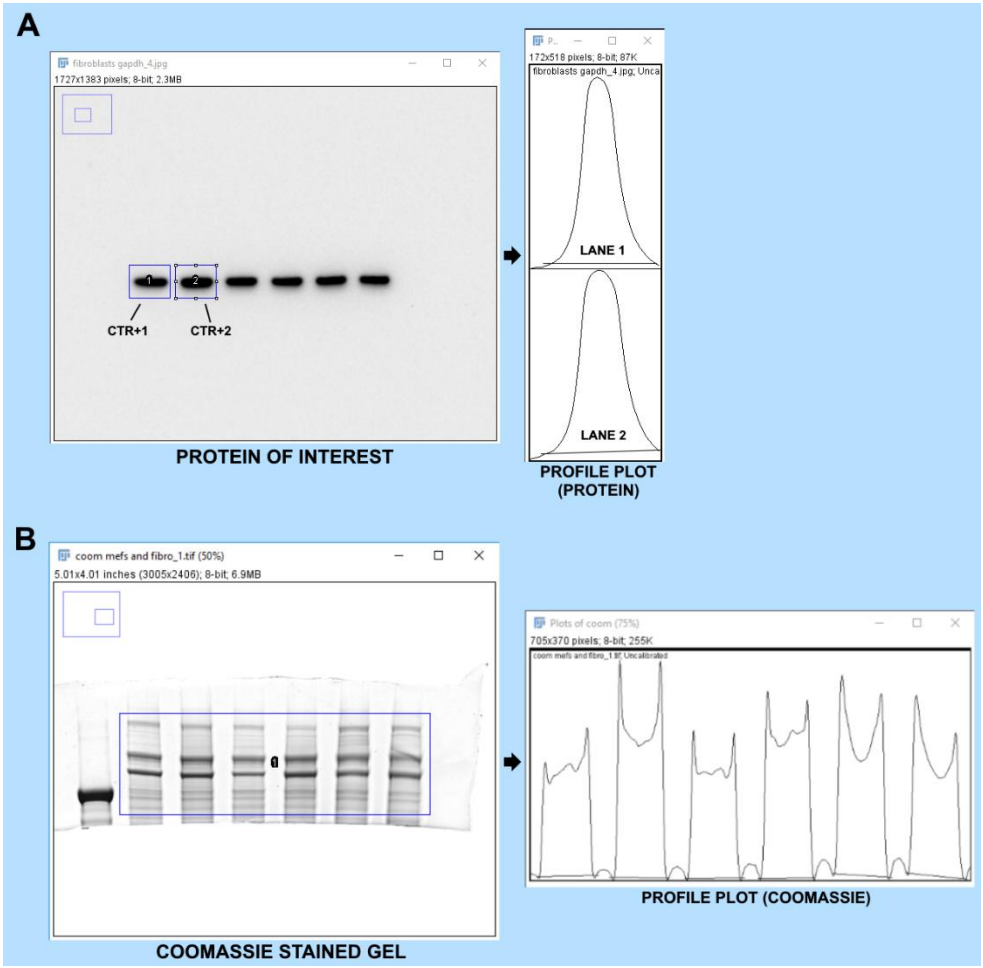

Figure 2. 3. Densitometry measurements of protein expression. Densitometry measurements of **(A)** protein of interest and **(B)** Coomassie stained gel. Rectangular box of a fixed size was drawn around protein band in each lane and across all lanes in Coomassie gel. Profile plots were generated, where peaks correspond to dark bands in each selection. The surface under the peak is proportional to the quantity of the protein in the sample.

2.3.2. Immunocytochemistry (ICC)

Fibroblasts, MEFs and HEK cells were washed with PBS (3x for 5 min) and incubated with primary antibody (Table 2.3) in immunofluorescence (IMF) buffer (1% FBS, 1% HS and 0.1% BSA/ in PBS) for one or two hours. After washing with PBS (3x for 5 min), cells were incubated with goat anti-rabbit IgG Alexa Fluor 488 or 546 (A11034 or A11010; Life Technologies), or goat anti-mouse IgG Alexa Fluor 488 or 546 (A11029 or A11030; Life Technologies) in IMF buffer for one hour at 5 µg/mL. Cells were then washed with PBS (3x for 5 min), stained with 4',6-diamidino-2-phenylindole (DAPI; D9542; Sigma; 0.4 µg/mL) for 10 minutes, washed with

PBS again (3x for 5 min) and mounted using Hydromount mounting media (National diagnostics).

Table 2. 3. Primary antibodies for immunocytochemistry analyses

Antibody	Supplier and catalog N°	Dilution	Comments
Rabbit monoclonal anti-UBA1	NBP2-67816; Novus	1:100	
Mouse monoclonal anti-lamin A	sc-71481; Santa Cruz	1:50	For all other ICC analysis
Mouse monoclonal anti-lamin A/C	MANLAC1 4A7; (Manilal *et al.*, 2004)	1:4	For analysis of lamin A/C staining in quercetin treated cells
Rabbit polyclonal anti-SMN	Made in the house	1:50	For analysis of SMN staining in MEFs
Mouse monoclonal anti-SMN	MANSMA1 11F3; (Young *et al.*, 2000)	1:4	For analysis of SMN staining in quercetin treated cells
Mouse monoclonal anti-FLAG	F3165; Sigma	1:200	
Mouse monoclonal anti active β-catenin (ABC)	05-665; Millipore	1:200	

Catalog number and supplier are listed for each primary antibody used in immunocytochemistry analysis, together with the dilution and sample type the antibodies were used on.

2.3.2.1. Imaging and quantitative analyses

Images were obtained using Leica SP5 confocal microscope (Minsky, 1988), with 63× oil immersion objective and LAS AF software (Leica Microsystems CMS GmbH). Argon, HeNe 543 and Diode 405 laser power were set to 10%, and they were used for detection of IgG Alexa Fluor 488 fluorophore, IgG Alexa Fluor 546 fluorophore and DAPI staining respectively. Imaging was performed in sequential scanning mode to avoid crosstalk between fluorophores.

2.3.2.1.1. Nuclear morphology defects

Control (GM00302, GM00498 and GM05659) and patient (GM00232, GM03813, GM09677) fibroblasts were examined for nuclear morphology defects based on the results from the previous study (van Tienen *et al.*, 2019). These included donut and honeycomb-like structures,

blebs, micronuclei and nuclear shape abnormalities (Figure 2.4). Only cells that were completely in the field of view were analysed. At least 100 cells were analysed for nuclear morphology defects in each primary cell, meaning that at least 300 cells were analysed in each group, control and SMA.

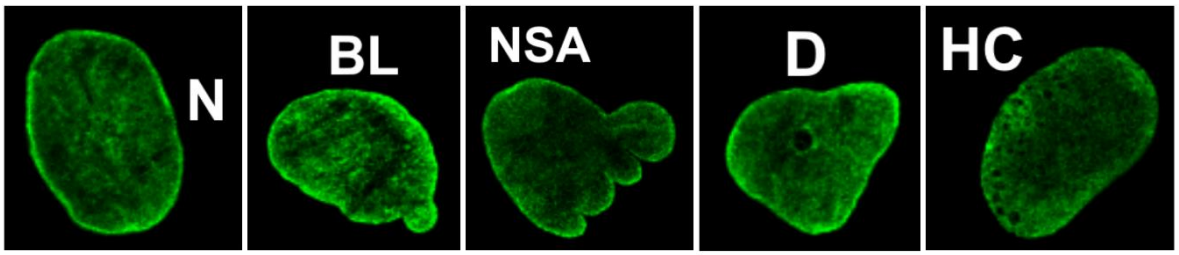

Figure 2. 4. Examples of nuclear morphology defects in SMA patient fibroblasts. N- normal fibroblast; BL-bleb; NSA-nuclear shape abnormality; D-donut-like structure; HC-honeycomb-like structure

2.3.3. Immunohistochemistry

Lumbar spinal cord sections (25 µm) from P8 SMA mice and healthy littermates, and 20 week-old ALS mice and WT littermates were permeabilised with 0.3% Triton X-100/ in PBS for ten minutes, washed with PBS (3x for 5 min) and blocked for one hour in blocking buffer (4% BSA, 0.1% Triton X-100/ in PBS) or 10% goat serum (GS)/ in PBS. Sections were incubated with rabbit monoclonal anti-calreticulin (ab92516; Abcam; 1:250) (Figure 5.9), or rabbit polyclonal anti-Fas ligand (ab15285; Abcam; 1:100) and mouse monoclonal anti-calreticulin (NBP2-50053; Novus; 1:100) (Figure 5.10A) in blocking buffer (with or without 1% GS) overnight at 4°C, and washed with PBS (3x for 5 min). After incubation with goat anti-rabbit IgG Alexa Fluor 488 or 546 (A11034 or A11010; Invitrogen) or goat anti-mouse IgG Alexa Flour 488 (A11029; Invitrogen) for one hour at 5 µg/mL, sections were washed with PBS (3x for 5 min), stained with DAPI (D9542; Sigma; 0.4 µg/mL) for 10 minutes, washed with PBS again (3x for 5 min) and mounted using Hydromount mounting media (National diagnostics). Images were obtained using Leica SP5 confocal microscope as described above.

2.3.3.1. Densitometry measurements of calreticulin staining using Fiji software

Densitometry measurements of calreticulin staining in motor neurons of the anterior horn were performed using Fiji software (v1.51) (Schindelin *et al.*, 2012). Calreticulin staining was assessed in two control and two SMA mice (P8), and in two control and two ALS mice (20 weeks). A minimum of four sections from each mouse were used in the analysis. Two fields of view (left and right anterior horn) were selected from each section (where the quality of the section allowed this) and measurements of three distinct regions that contained alpha motor neurons were taken from each field of view. A minimum of 45 measurements were made from each experimental group.

First, images were calibrated using a calibrated step tablet. A rectangular selection that filled most of the step without overlapping another one was created to measure mean grey value of the first step. The same rectangular selection was then used to measure the mean grey value of all the consecutive steps in the tablet. Measured values were plotted against standard measurements of optical density (OD) to create a calibration curve using a "Rodbard" function. OD of the negative control (IgG control) was then measured as described below. The colour (RGB) picture was converted into an 8-bit picture (Image→ Type→ 8-bit) and inverted (Edit→ Invert) for further analysis. A rectangular selection tool of fixed size was then used to measure OD of three regions of interest in each field of view. This protocol was used for measurements of all pictures, with an addition of one step. Prior to measurements of the OD, the mean OD of the negative control was subtracted from the picture to correct the background (Process→ Math→ Subtract).

2.3.4 Dot blotting

The results from the protein assay (Section 2.3.1.2) were used to ensure equal protein loading for dot blot analyses. Dot blotting is an immuno-associated technique were protein extracts are loaded directly on the nitrocellulose membrane, and the membrane is developed in the same way that a regular western blotting would be (Salazar-Anton, Tellez and Lindh, 2012). GM05659 control and GM00232 patient fibroblast extracts were used to test antibodies raised against three SMN epitopes, including mouse anti-MANSMA12 2E6, mouse anti-MANSMA2 8F7 and mouse anti-MANSMA3 8E1 (Young *et al.*, 2000), and to test mouse anti-MANLAC1 4A7 antibody raised against lamin A/C protein (Manilal *et al.*, 2004). GM00302 control and GM00232 patient fibroblast extracts were used to test mouse anti-lamin A antibody (sc-71481; Santa Cruz). Cell extracts were prepared in serial dilutions in concentration range between 1.5 mg/mL- 0.0468 mg/mL, and 2 µL of each prepared sample was carefully pipetted on to a nitrocellulose membrane in triplicates. After being left to dry for 5 minutes at RT, membranes were incubated with 4% powdered milk (Marvel) in PBS for one hour to block non-specific protein binding. Following incubation with an appropriate primary antibody (Table 2.4) in WB buffer for one hour at RT, the membranes were incubated with HRP-labelled goat anti-mouse Ig (P0260; DAKO) in WB buffer at 0.25 ng/mL, for one hour at RT. Between each step membranes were washed three times with PBS for five minutes. Membranes were incubated with SuperSignal™ West Femto (34904; Thermo Scientific) or SuperSignal™ West Pico (34580; Thermo Scientific) chemiluminescent substrate for 5 minutes at RT and visualised using a Gel Image Documentation system (Biorad).

Table 2. 4. Primary antibodies used in dot blotting

Antibody	Supplier and catalog N°	Dilution	Epitope
Mouse monoclonal anti-SMN	MANSMA2 8F7 (Young *et al.*, 2000)	1:100	aa - ASL
Mouse monoclonal anti-SMN	MANSMA3 8E1 (Young *et al.*, 2000)	1:100	Exon 5 aa- PSGP- - -P
Mouse monoclonal anti-SMN	MANSMA12 2E6 MANSMA3 8E1 (Young *et al.*, 2000)	1:100	DDT-LI—Y--A
Mouse monoclonal anti-lamin A	sc-71481; Santa Cruz	1:250	Unknown
Mouse monoclonal anti-lamin A/C	MANLAC1 4A7; (Manilal *et al.*, 2004)	1:100	aa477-485

Catalog number and supplier are listed for each primary antibody, together with the dilution and target epitope.

2.3.4.1. Densitometry measurements of antibody reactive dots using Fiji software

Densitometry measurements of antibody reactive dots were obtained using Fiji software (v1.51) (Schindelin *et al.*, 2012). Before the analyses, images were converted to gray-scale images (Image → Type → 8-bit), inverted (Edit → Invert), and where necessary, contrast and brightness or the background were adjusted uniformly across the membrane to enhance signal detection (Image → Adjust → Brightness/ Contrast or Process → Subtract Background). An oval selection tool of a fixed size was drawn around the first dot and integrated density of the selection was measured using CTR+M function. Oval selection was then moved to the next dot to measure integrated density, and the same was repeated for all consecutive dots on the membrane. The workflow is presented in Figure 2.5. R-squared (R^2) value was calculated for serial dilutions of each sample to determine accuracy of the dot blot approach. Sensitivity of the dot blot was determined by calculating the average protein levels in SMA cell line relative to control in all consecutive dilutions and comparing them to western blot analysis.

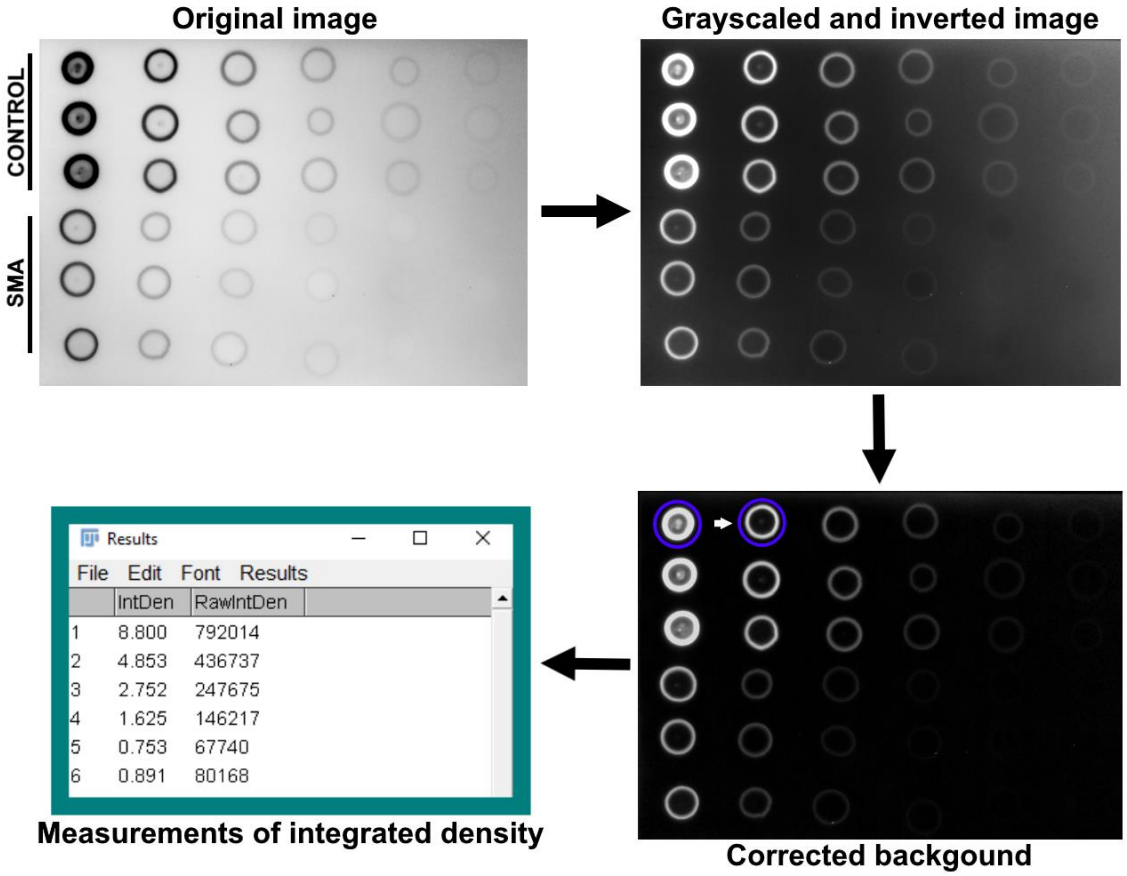

Figure 2. 5. Workflow of dot blot analysis. Image was converted to gray-scale image and inverted, and the background was adjusted uniformly across the membrane to enhance signal detection. Oval selection tool of a fixed size (blue circle) was used to measure integrated density of each dot on the membrane. Example measurements are presented for the first row of the blot.

2.3.5. Indirect enzyme-linked immunosorbent assay (ELISA)

ELISA is an immunoassay that allows quantitative and qualitative analyses of different molecules including proteins (Sakamoto *et al.*, 2018). In indirect ELISA, proteins are immobilised on the cell surface of the well and detected using a two-step antibody labelling. Protein extracts from control (GM00498) and patient (GM00232) fibroblasts were prepared at a concentration of 0.2 mg/mL to ensure equal protein loading. Seven serial dilutions of each cell extract were prepared, starting with 1:5 dilution, and a 100 µL of each dilution was carefully pipetted in ELISA 96-well plate in triplicates to allow protein immobilisation to the well surface. Following incubation with protein extracts for one hour at RT, proteins were

incubated with 4% powdered milk (Marvel) in PBS for one hour to block non-specific protein binding. After the incubation with mouse monoclonal anti-lamin A (sc-71481; Santa Cruz; 1: 250) in WB buffer for one hour, proteins were incubated with HRP-labelled goat anti-mouse Ig (P0260; DAKO) in WB buffer at 0.25 ng/mL for one hour at RT and developed with 3,3',5,5'-tetramethylbenzidine (TMB) substrate. Between each step wells were washed three times with PBS/0.1 % Triton X-100 for five minutes. In reaction with horseradish peroxidase, TMB substrate produces blue product with a maximum absorbance at 370 nm and 650 nm (Bos *et al.*, 1981). The reaction is then stopped by addition of sulfuric acid, that causes a shift in colour to yellow with a maximum absorbance at 450 nm. Blue reaction product did not develop after the addition of TMB, and so the experiment was stopped at this point.

2.4. Immunoprecipitation

Immunoprecipitation was performed as described previously (Fuller *et al.*, 2017). Anti-mouse Pan Ig-coated magnetic beads (50 µL) (11041; Invitrogen) were washed with 4% BSA/PBS (3x) to block the non-specific binding. In all steps, DynaMag^{TM} spin magnet (12320D; Invitrogen) was used to separate the beads from the solution. Beads were then incubated with 50 µL of the appropriate antibody or PBS (negative control) for 1 hour at RT with gentle rolling. Antibodies were as follows: mouse anti-lamin A/C [MANLAC1 4A7; (Manilal *et al.*, 2004); neat], mouse anti-SMN [MANSMA1 11F3; (Young *et al.*, 2000); neat] and mouse-anti 3-nitrotyrosine (sc-32757; Santa Cruz; 1:5). The beads were then washed twice with 4% BSA/PBS and once with PBS, and incubated with RIPA extracts of human fibroblast cells (75 µL), mouse heart tissue (15µl) or mouse spinal cord tissue (20 µL) for 1 hour at RT on a roller. Following incubation, the supernatant was carefully removed and stored in fresh tubes as it represents the unbound part of the pulldown. The beads were washed once with RIPA buffer and 4x with

PBS, and the captured material was eluted from the beads by heating at 90˚C for 3 minutes in 1xSDS sample buffer (30 µL for heart and spinal cord pulldown, and 75 µL for fibroblast pulldown).

Samples were then subjected to western blotting as described in section 2.3.1 to investigate potential interacting partners. Primary antibodies were as follows: mouse anti-SMN [MANSMA12 2E6 (Young *et al.*, 2000)], mouse anti-lamin A/C [MANLAC1 4A7; (Manilal *et al.*, 2004)], rabbit anti-lamin AC (ab169532; Abcam), rabbit anti-UBA1 (NBP2-67816; Novus), mouse anti-β-catenin (610154; BD Transduction Laboratories), rabbit anti-ALDOA (NBP1-87488; Novus) and mouse-anti 3-nitrotyrosine (sc-32757; Santa Cruz).

2.5. Quantitative (real time) reverse transcription polymerase chain reaction (RT-qPCR)

2.5.1. Extraction of total RNA

Total RNA was extracted using RNeasy Plus Mini kit (74134; Qiagen) according to instructions outlined in the kit guidelines. Fibroblasts cells were lysed and homogenised in 350 µL of RTL buffer containing 1% 2-mercaptoethanol (M3148; Sigma) by repeated pipetting. 600 µL of RTL buffer/2-mercaptoethanol was added to the heart tissue, and the samples were lysed and homogenised using a GentleMACS Dissociator (Miltenyi Biotec) for 45 seconds. Guanidine Isothiocyanate in the RTL buffer and 2-mercaptoethanol were used to denature and inhibit RNAases to ensure isolation of intact RNA (Wagner, 2013). Homogenized lysates were transferred to a gDNA Eliminator spin column placed in a 2 ml collection tube and centrifuged for 30 seconds at 13000 RPM (Micro Centaur MSB010.CX2.5; MSE; rotor radius- 4 cm) to remove double-stranded DNA. The column was discarded, and 1 volume (350 or 600 µL) of 70% ethanol was added to the flow-through to precipitate the RNA from the solution (Wagner,

2013). Samples were mixed by gentle pipetting, transferred to a RNeasy spin column and centrifuged for 15 seconds at 13000 RPM. In this step, total RNA binds to the membrane while down-stream contaminants, such as the ethanol, get discarded in the flow-through. RNeasy spin column with total RNA was then washed by centrifugation (13000 RPM) in RW1 buffer (700 µL) for 15 seconds, and twice in RPE buffer (500 µL), for 15 seconds and 2 minutes respectively. The RNeasy spin column was then transferred into the new collection tube and centrifuged on 13000 RPM for 1 minute to eliminate any possible carryover of buffer RPE. RNeasy spin column was placed into the new collection tube and total RNA was eluted from the column by centrifugation (13000 RPM) in 30 µL of RNase-free water for 1 minute. Total RNA was quantified with a NanoDrop ND- 1000 spectrophotometer (Thermo Fisher). Absorption ratio (OD_{260}/OD_{280} nm) was used to verify the integrity of the RNA, where ratio of 1.8-2.0 represented pure RNA.

2.5.2. Synthesis of complementary DNA (cDNA)

Total RNA was reverse transcribed using SuperScript™ VILO™ cDNA Synthesis Kit (11754050; Invitrogen) according to instructions outlined in the guideline. Total RNA from fibroblast cells (2 µg) and heart tissue (1.5 µg) was prepared in 20 µL reactions, and subjected to cDNA synthesis using a Prime Thermal Cycler (Bibby Scientific) with parameters: 25°C for 10 min (primer annealing), 42°C for 60 min (reverse transcription) and 85°C for 5 min (enzyme inactivation). Enzyme mix contains reverse transcriptase, recombinant ribonuclease inhibitor to prevent RNA/DNA degradation, and a proprietary helper protein. VILO reaction mix contains random primers, $MgCl_2$, and dNTPs.

cDNA reactions:

x µL total RNA

4 µL 5x VILO reaction mix

2 µL 10x enzyme mix

Make up to the final volume of 20 µL with RNase-free water

2.5.3. Quantitative PCR (qPCR)

Quantitative PCR (qPCR) for the *LMNA* gene was performed using a SYBR Green detection system (Ririe, Rasmussen and Wittwer, 1997), according to instructions outlined in the guideline (SYBR™ Select Master Mix; 4472903; Applied Biosystems). SYBR master mix contains: SYBR® GreenER Dye, AmpliTaq DNA polymerase, heat-labile Uracil-DNA glycosylase (UDG), ROX dye passive reference, dNTP blend containing dUTP/dTTP and optimized buffer components. In this system, fluorescent SYBR green dye forms complexes with double-stranded DNA (dsDNA), and as its fluorescence increases it can be measured at the end of each amplification cycle of qPCR (Navarro *et al.*, 2015). UDG prevents carryover and amplification of non-specific PCR products (contaminants) by removing any uracil incorporated into single- or double-stranded amplicons. The ROX dye passive reference provides an internal reference to which the reporter-dye signal can be normalized. PCR reactions were prepared to contain 3.75 ng of cDNA (fibroblast cells) or 2.8 ng of cDNA (heart tissue) in 20 µL reactions.

qPCR reactions:

x µL DNA

10 µL SYBR master mix (2X)

300 nM Forward and 300 nM Reverse primers

Make up to the final volume of 20 µL with RNase-free water

All PCR reactions were performed in triplicates. Parallel wells with no cDNA were run for each gene to control for contamination. RNA Polymerase II Subunit J (*POLR2J*) and TATA-Box binding protein (*TBP*) were used as reference genes as they have previously demonstrated stable expression across tissues (Radonić *et al.*, 2004), and their expression was not dysregulated in published transcriptomics studies of SMA. qPCR was performed using a QuantStudio 3 Real Time PCR system (Applied Biosystems) with the following parameters: 50°C for 2 min (UDG activation), 95°C for 10 min (DNA polymerase activation), and 40 cycles of 95°C for 15 sec (denaturation) and 60°C for 1 min (anneal/extend faze). Amplification plots were generated by plotting cycles on the X axes against ΔRn on y-axes, where ΔRn is defined as normalized reporter value (Rn) of an experimental reaction minus the Rn value of the baseline signal generated by the instrument. The baseline and threshold values were automatically defined by the software. Baseline value represents background fluorescence that is not taken into account during calculations. Threshold value is placed in the region of the exponential faze of the amplification plot and is used to define cycle threshold (Ct) value for each sample (Figure 2.6A). Relative gene expression was quantified using Pfaffl method (Pfaffl, 2001). First the geometric mean of reference genes (POLRJ and TBP) was subtracted from the Ct value of lamin A giving the ΔCt value, after which raw gene expression was calculated using the equation: 2^-(ΔCt). Data was presented as average raw expression of the

group. Dissociation curves were obtained for each sample to control for amplification of non-specific products and formation of primer- dimers (Navarro *et al.*, 2015) (Figure 2.6B).

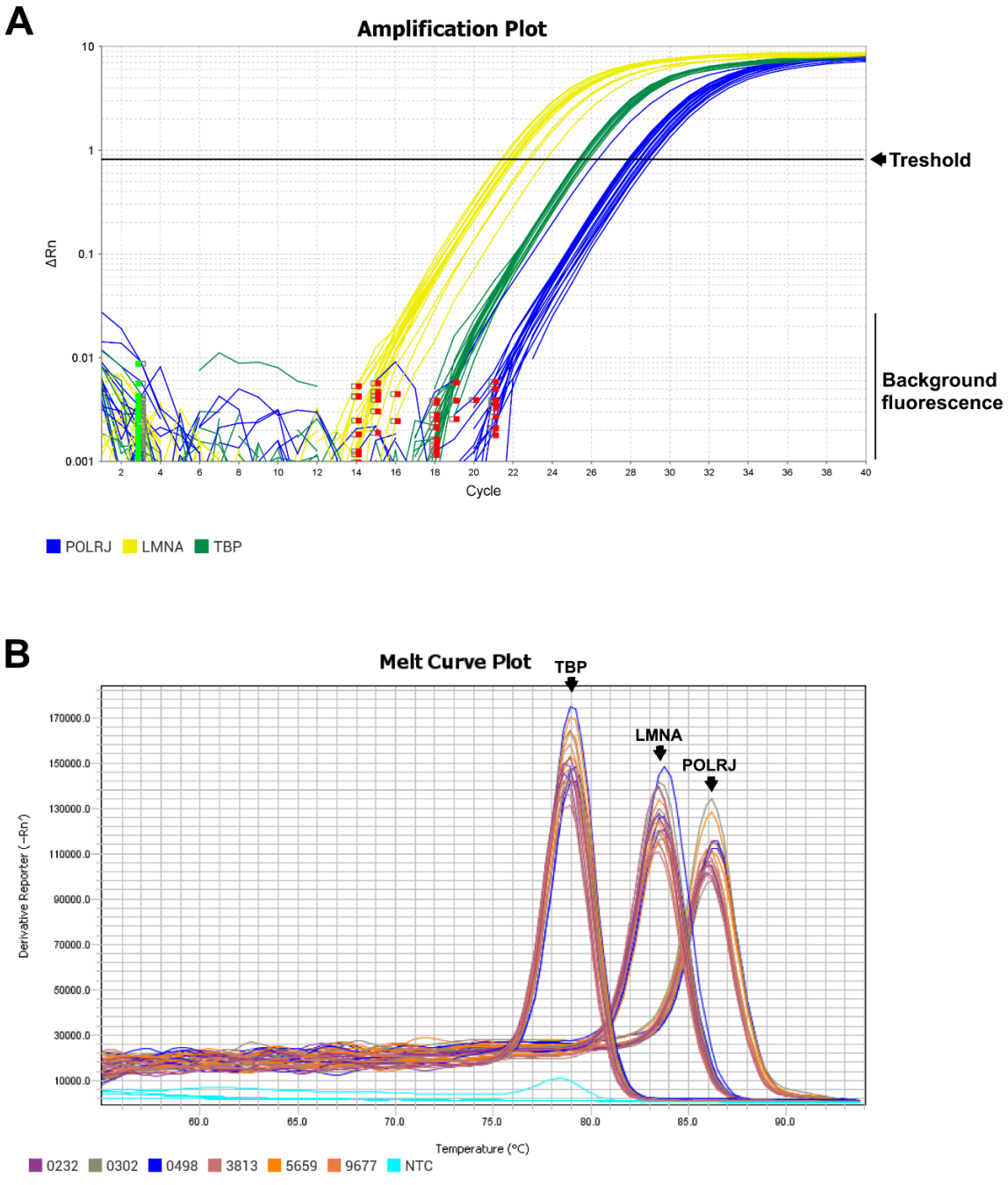

Figure 2. 6. Example of quantitative RT-PCR. Representative images showing **(A)** amplification plots and **(B)** dissociation curves for *LMNA*, *POLRJ* and TBP genes in control and SMA fibroblasts. Three peaks, corresponding to *LMNA*, *POLRJ* and *TBP*, were identified in dissociation curves, indicating absence of non-specific products and primer- dimers formations. *LMNA*- lamin A/C; *POLR2J*- RNA Polymerase II Subunit J; *TBP*- TATA-Box binding protein; NTC-no template control

2.5.3.1. Primer design and primer efficiency

Primer sequences for lamin A, *POLR2J* and *TBP* were designed using National Center for Biotechnology Information (NCBI) primer-BLAST tool (Ye *et al.*, 2012). Primers were chosen based on the ability to produce PCR product of approximately the same size (between 70-150 bp), to have similar melting temperatures (around 60°C). For the *LMNA* gene, primer pairs were also designed to recognise only lamin A isoform (exon 11 and 12). Primer sequences are listed in the Table 2.5. Efficiency of the primer pairs was determined by making serial dilutions of the cDNA and performing qPCR as described above. Log values of the cDNA were then plotted on the X axis against the C_t (cycle threshold) values on y axes to generate equation (Figure 2.7). Primer efficiency was calculated using a slope according to the equation: $E = (10^{[-1/slope]}-1) \times 100$ (Pfaffl, 2001). The theoretical maximum of 100% indicates that the amount of PCR product doubles with each cycle. Primers with the efficiency between 90%-110% are considered optimal (Wagner, 2013), and were used here for qPCR.

Table 2. 5. Primer sequences for qPCR

Target gene	Species	Sequence	Size of the PCR product
LMNA	human	F: CTCCTACCTCCTGGGCAACT R: AGGTCCCAGATTACATGATGCT	74 bp
LMNA	mouse	F: AGAGATGGGAATGACGGGGA R: CAGGCTCAGAAGCTGGGAAA	71 bp
TATA-Box Binding Protein (*TBP*)	human	F: GCATCACTGTTTCTTGGCGT R: AGAGCATCTCCAGCACACTC	78 bp
TATA-Box Binding Protein (*TBP*)	mouse	F: TCAGTTACAGGTGGCAGCAT R: GCAGGGTGATTTCAGTGCAG	83 bp
RNA Polymerase II Subunit J (*POLR2J*)	human	F: CTGGACCAAAGATCCGGGG R: GGTTTGCACACTTCTCTCCG	70 bp
RNA Polymerase II Subunit J (*POLR2J*)	mouse	F: GCTACAAAGTCCCTCACCCC R: TCCTGGGGACTGTAGTCTGG	62 bp

Forward and reverse primers for human and mouse lamin A, POLRJ and TBP genes are listed in the table, together with the size of the PCR product.

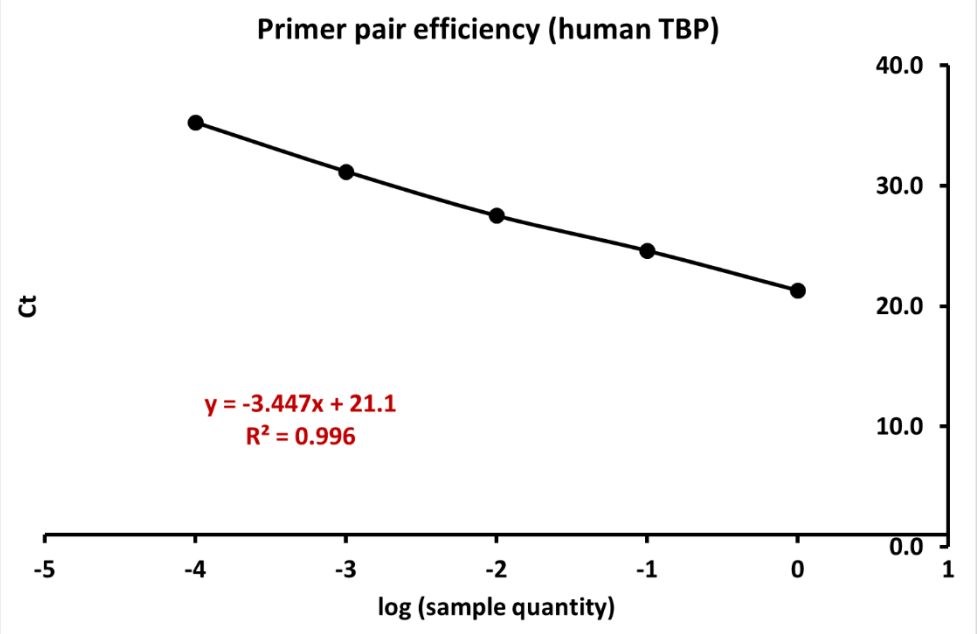

Figure 2. 7. Assessing the efficiency of a primer pair. Log values of the sample quantity were plotted on the X axis against the C_t values on the y axes to generate equation. Slop (-3.447) was plotted in the equation: E = ($10^{[-1/slope]}$ -1) x 100 to calculate primer efficiency (95%).

2.6. Functional studies

2.6.1. Cell proliferation

Control (GM05659 P14, GM00498 P17, GM00302 P20) and SMA (GM00232, GM03813, GM09677 P13) fibroblasts were thawed and grown in complete medium as described previously in section 2.2. (The number after the cell ID (i.e. P14) indicates cell passage number. Passage number was not available/known for cell lines GM03813 and GM00232). After reaching 70% confluency, the cells were trypsinized and re-seeded in T25 culture flasks containing complete medium at a density of 30 000 cells/flask. Cells were maintained in humidified incubator (Leec) at 37°C and 5% CO_2 for three days, after which the media was removed from the flask, and the cells were trypsinized and counted as described in section 2.2. Each cell line was grown in three T25 flasks (technical replicates), and each technical replicate was counted four times, meaning that 12 measurements were done for each cell line. Doubling time (DT) for each cell was calculated using equation:

$DT = \ln(2) * t / (\ln(C_2) - \ln(C_1))$

,where t represents culture duration in hours, C_2 is the number of cells at the end of the culture and C_1 is the number of seeded cells.

The same protocol was used for the proliferation experiment in young (GM05659 P15, GM00498 P17, GM00302 P22) vs old (F011 P9, F067 P8, F154 P10) healthy fibroblasts.

2.6.2. Trans-well migration assay

Control (GM00498 P17) and SMA (GM03813) fibroblasts were thawed and grown in complete medium up to 70% confluency as described previously in section 2.2. Cells were trypsinized, carefully resuspended in media without the FBS and seeded on hanging cell culture inserts

(MCMP24H48; Millipore; 5 µm pore size) at a density of 20 000 cells/insert, that were placed into 24-well plates containing complete media (schematic diagram is shown in Figure 2.8). This was done to establish a nutrient gradient and induce migration of the cells through the membrane (Harada *et al.*, 2014). Cells were maintained in humidified incubator (Leec) at 37°C and 5% CO_2 for 6, 24, 48 and 72 hours to assess optimal incubation time.

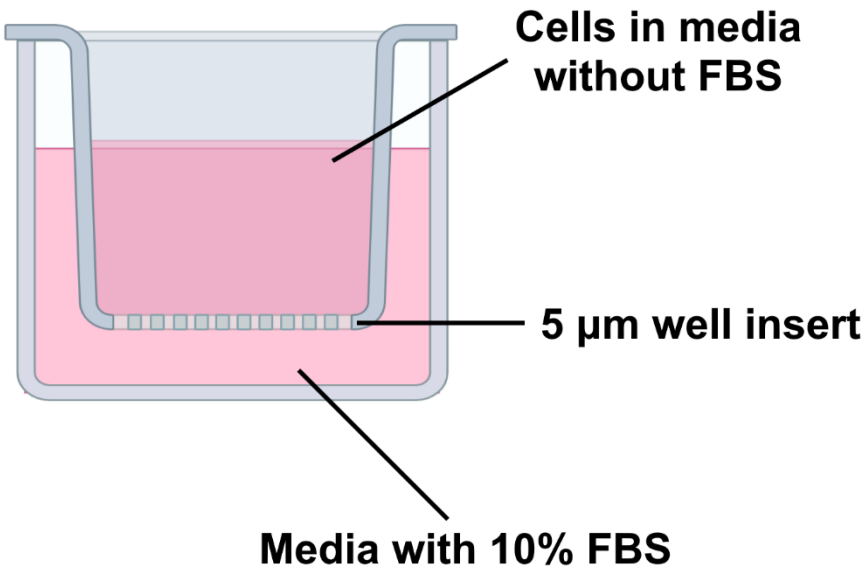

Figure 2. 8. Schematic diagram showing transwell migration assay. Cells were seeded on the apical side of the well insert to allow migration through a 5 µm well insert towards the media with FBS. Image created with BioRender.com.

2.6.2.1. Immunocytochemistry

Following incubation, the cells were washed with PBS (3x for 5 min), fixed in methanol (67-56-1; Fisher Scientific) for 5 minutes and permeabilized in 0.5% Triton X-100/PBS for 5 minutes. After incubation with mouse anti-lamin A (sc-71481; Santa Cruz; 1:100) in IMF buffer at RT for 1 hour, the cells were incubated with goat anti-mouse IgG Alexa Fluor 546 (A11030; Invitrogen; 5 µg/mL) in IMF buffer for one hour at RT, followed by incubation for 10 minutes with DAPI (D-9542; Sigma-Aldrich; 0.04 µg/mL). Between each step cells were washed with

PBS (3x for 5 minutes). The membrane was carefully cut from the insert and mounted with Hydromount, with apical side of the membrane facing up.

2.6.2.2. Imaging and cell count using Fiji software

Images were obtained using Leica SP5 confocal microscope with 63X oil immersion objective, using a Z-stack function. Z-stack function allows 3D reconstruction of the specimen (Kopecky *et al.*, 2012), and here it was used to determine the number of cells on each side of the membrane (apical or dorsal). Apical and dorsal focal planes were defined in the begin and end boxes of the Z-stack panel in LAS AF software. The number of steps was defined to 15-40, and represents the number of pictures that were taken in each Z-stack. Cells were counted using Fiji software (v1.51) (Schindelin *et al.*, 2012). The membrane was stained in blue with DAPI which served as a good guideline for the position of cells on the membrane. All pictures from one side of the membrane were uploaded into Fiji software and converted into a stack (Image → Stacks → Images to stack). The stack was then converted into a single image with a Z-project function (Image → Stacks → Z Project), with projection type set to max intensity (Figure 2.9). Cells were counted using a multi-point tool. Cells on the left and bottom edge of the picture were counted if at least half of the cell was in the field of view. Cell on the top and right edge of the picture were excluded from the analysis. Results were expressed as percentage of migrated cells (MC) using formula:

$$MC = D*100/T$$

,where D represents number of cells on the dorsal side of the membrane and T represents total number of cells.

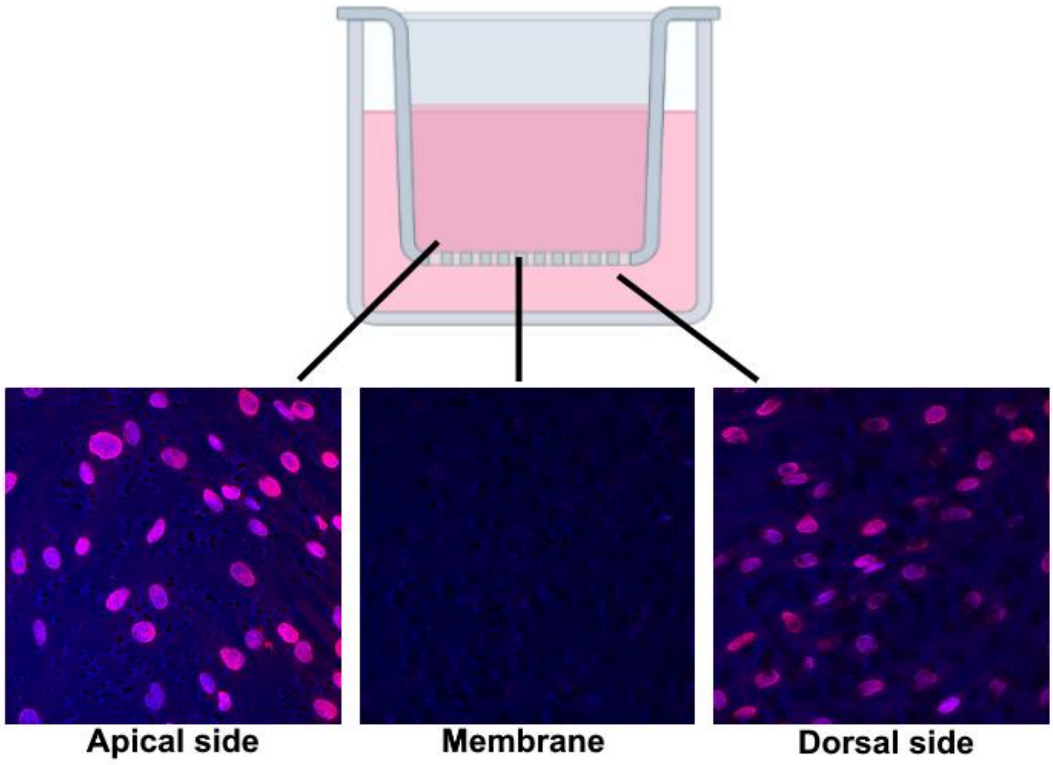

Figure 2. 9. Assessing cell migration through a 5 µm well insert. Cells on the apical and dorsal side of the membrane, and centre of the membrane are indicated on three consecutive figures (generated with stack function in Fiji). Image created with BioRender.com.

The same protocol was used to assess cell migration in control (GM05659 P13, GM00498 P16, GM00302 P20) vs SMA (GM00232, GM03813, GM09677 P14) fibroblasts, and young (GM05659 P13, GM00498 P115, GM00302 P20) vs old (F011 P7, F067 P6, F154 P8) healthy fibroblasts. Each cell line was grown in three technical replicates for 70 hours as described above, and three fields of view (Z-stacks) were taken from each technical replicate, meaning that nine fields of view were analysed in each cell.

2.7. Transfection of MEFS with wild type lamin A using electroporation

Transfection by electroporation relies on the use of high-voltage electric shocks to introduce DNA into the cell, and can be used both for transient and stable transfection of mammalian cells (Potter and Heller, 2003). *LMNA* KO MEFs were grown in cell culture up to 70%

confluency, trypsinized, neutralised and centrifuged (as described in section 2.2). Following removal of supernatant, the cells were resuspended in F12 Ham medium to a concentration of $2x10^6$ cells/mL, and 200 µL of cell suspension was gently mixed with 24 µg of pSVK3/lamin A WT plasmid. The pSVK3/lamin A WT plasmid was designed by Dr Ian Holt (Holt *et al.*, 2003). The modified pSVK3 vector adds N-terminal FLAG tag to the lamin A/C protein. Cell/plasmid mix was added to electroporation cuvette with 2 mm gap (Biorad) and the cells were electroporated using Gene Pulser (Biorad) at 1.5 kV (resistance = 200 W; capacitance = 25 mF; time constant » 0.8). Cell viability and cell concentration were assessed as described previously in section 2.2.2. Following electroporation, around 60% of cells were viable, and these were seeded in tissue culture flasks ($5x10^3$ cells/cm^2) and on glass coverslips ($2.5x10^4$ cells) containing complete medium (with 20% FBS). Cells were maintained in humidified incubator (Leec) at 37°C and 5% CO_2 for 48 hours to allow cell adhesion and expression of transfected plasmid.

2.7.1. Western blotting and immunocytochemistry

Cells were harvested for western blotting as described in section 2.2.3. Protein extraction and quantitative western blotting were done as described previously in section 2.3.1., using mouse monoclonal anti-lamin A/C [MANLAC1 4A7 (Manilal *et al.*, 2004); 1:100], mouse monoclonal anti-SMN [MANSMA12 2E6 (Young *et al.*, 2000); 1:100] and rabbit monoclonal anti-UBA1 (NBP2-67816; Novus; 1:1000) antibodies.

Cells seeded on glass coverslips were fixed in acetone: methanol solution as described in section 2.2.3. Immunocytochemistry analysis was done as described in section 2.3.2, using a mouse monoclonal anti-FLAG antibody (F3165; Sigma, 1:200). Fields of view were chosen to

capture at least 100 cells per coverslip. Three coverslips were analysed in each group, i.e. pSVK3/lamin A transfected and non-transfected cells, meaning that at least 300 cells were analysed in each group. Cells on the left and upper edge of the picture were included in the analysis if at least half of the cell was in the field of view. Results were expressed as average percentage of transfected cells (TC) using formula:

TC= FP *100/T

,where FP represents number of FLAG positive cells and T represents total number of cells.

2.8. Drug studies on control and patient fibroblasts

2.8.1. Cell culture and drug treatment

Control and patient fibroblasts were grown in cell culture as described previously in section 2.2. Briefly, the cells were seeded in tissue culture flasks containing complete medium at a density of $5x10^3$ cells/cm^2 and maintained in humidified incubator (Leec) at 37°C and 5% CO_2 until enough quantity of cells was generated for drug treatment. GM05659 control and GM00232 patient cell lines were used to investigate the effects of PDGF-BB and quercetin treatment, while GM00498 control and GM09677 patient cell lines were used to investigate the effect of trichostatin A (TSA) treatment. Cells were trypsinized and re-seeded in complete media in 6-well plates, at a concentration listed in table 2.6, for western blot analyses. For quercetin treatment, cells were also seeded on coverslips (25000 cells/coverslip) for immunocytochemistry analyses. To assess cell viability after TSA treatments, cells were seeded in 24-well plates at a concentration listed in table 2.6. Cells were maintained in humidified incubator (Leec) at 37°C and 5% CO_2 until they reached appropriate confluency so that they can be treated with an appropriate concentration of the drug (details are listed in table 2.6). To do this, drugs were first dissolved in either DMSO (quercetin and TSA) or 4mM

HCl (PDGF-BB) according to instructions outlined in the guidelines, and diluted to the concentration that is 1000x higher than the one needed in experiment. Prepared drug concentrations were then mixed with complete media at 1:1000 dilution and sterile filtered to prevent microbial contamination. Cell culture media was carefully aspirated from the cells, and media containing appropriate concentration of the drug was carefully pipetted into the wells or on coverslips. Parallel wells, containing DMSO or 4 mM HCl (vehicle control), were prepared at 1:1000 dilution with complete media. This dilution was chosen to ensure that all drug and vehicle wells contained the same final concentration of the vehicle (i.e. 0.1%). Cells grown in complete media only served as untreated controls. Three technical replicates for each group, i.e. drug treatment, vehicle and untreated cells, were set up in 6-well plates and on coverslips. Two technical replicates were used in 24-well plates. The cells were maintained in humidified incubator (Leec) at 37°C and 5% CO_2 (as listed in table 2.6).

Table 2. 6. Details of the drug treatment

Drug	Supplier and catalog N°	Seeding density (time in culture)	Drug treatment (concentration/ duration)
Western blotting (6-well plates)			
PDGF-BB	R&D Systems; 220-BB	CTR: 80000 cells/well (48 hours) SMA: 100000 cells/well (48 hours)	0 and 100 ng/mL / 24 hours
Quercetin	Sigma- Aldrich; 337951	CTR: 80000 cells/well (24 hours) SMA: 100000 cells/well (24 hours)	0, 6.25, 12.5, 25, 50 and 100 µM/ 24 hours
Trichostatin A	Santa Cruz; SC-3511	50000 cells/well (72 hours) 80000 cells/well (48 hours) 50000 cells/well (72 hours) 50000 cells/well (72 hours)	0, 50 and 100 nM/ 4 hours 0, 25, 50 and 100 nM/ 8 hours 0, 25, 50 and 100 nM/ 16 hours 0, 25, 50 and 100 nM/ 24 hours
Cell viability (24-well plates)			
Trichostatin A	Santa Cruz; SC-3511	10000 cells/well (48 hours) 20000 cells/well (72 hours) 15000 cells/well (72 hours) 15000 cells/well (72 hours)	0, 50 and 100 nM / 4 hours 0, 25, 50 and 100 nM/ 8 hours 0, 25, 50 and 100 nM/ 16 hours 0, 25, 50 and 100 nM/ 24 hours
Immunocytochemistry (coverslips)			
Quercetin	Sigma Aldrich; 337951	25000 cells/well (24 hours)	0, 6.25 and 100 µM/ 24 hours

Supplier and product code for each drug are listed in the table. Seeding density and time in the cell culture before the drug treatment are listed for each application, together with the concentration and duration of the drug treatment. The 0 concentration represent vehicle (DMSO or 4 mM HCl).

2.8.2. Cell viability

After the TSA and quercetin treatment, cell viability was assessed using trypan blue exclusion test as described in section 2.2.2. For TSA treatment, cells were seeded in duplicates in 24-well plates and two cell viability assays were performed for each well, meaning that, in each treatment group, cell viability was assessed four times. For quercetin treatment, cells plated in triplicates in 6-well plates were also used for cell viability assay, meaning that, in each treatment group, cell viability was assessed three times.

2.8.3. Protein extraction and western blotting

Cell treated with PDGF-BB and quercetin were harvested as described previously in section 2.2.3. and proteins were extracted as described in section 2.3.1.1. Cells treated with TSA were washed twice in cold PBS, and lysed directly from the plate using 100 µL of 2X modified RIPA buffer. During this procedure the plate was kept on ice (4°C). RIPA buffer was carefully pipetted across the surface of the well multiple times to ensure complete protein extraction, followed by sonication at 5 microns for 10 seconds (Sonicrep 150; MSE). Protein extracts were then centrifuged at 13000 RPM (Micro Centaur MSB010.CX2.5; MSE; rotor radius- 4 cm) for 5 minutes at 4°C to pellet any insoluble material. Cell extracts were subjected to protein assay using Pierce™ 660nm Protein Assay Reagent to determine sample protein concentration (as described in section 2.3.1.2.2). The samples were then subjected to quantitative western blotting as described in section 2.3.1, using mouse monoclonal anti-lamin A/C [MANLAC1 4A7 (Manilal *et al.*, 2004); 1:100], mouse monoclonal anti-SMN [MANSMA12 2E6 (Young *et al.*, 2000); 1:100], rabbit monoclonal anti-UBA1 (NBP2-67816; Novus; 1:500), mouse monoclonal anti-active β-catenin (05-665; Merc Millipore; 1:1000) and mouse monoclonal anti-β-catenin (610154; BD Trans. Lab.; 1:2000) antibodies.

2.8.4. Immunocytochemistry analysis of quercetin treated cells

Following quercetin treatment, cells on glass coverslips were washed in cold PBS and fixed in acetone/methanol solution as described in section 2.2.3. Immunocytochemistry analyses were done as described in section 2.3.2, using mouse monoclonal anti-lamin A/C [MANLAC1 4A7 (Manilal *et al.*, 2004); 1:4], mouse monoclonal anti-SMN [MANSMA1 11F3 (Young *et al.*, 2000); 1:4], rabbit monoclonal anti-UBA1 (NBP2-67816; Novus; 1:100) and mouse monoclonal anti-active β-catenin (05-665; Merc Millipore; 1:200) antibodies. Images were obtained using

Leica SP5 confocal microscope, with 63× oil immersion objective, as described previously in section 2.3.2.1.

2.8.4.1. GEM number

Fields of view were chosen to capture at least 100 cells per coverslip. Three coverslips were analysed in each group, i.e. 0 µM (vehicle), 6.25 µM and 100 µM quercetin, meaning that at least 300 cells were analysed in each group. Only cells that were completely visible in the field of view were included in the analysis. SMN can be found both in the cytoplasm and nucleus, and nuclear SMN is located in structures called Gemini of the coiled bodies (GEMs) (Coovert *et al.*, 1997) (Example is shown in Figure 2.10). Here, GEMs were counted in quercetin treated cells to determine the effect of a drug treatment on SMN levels. This was done because reduction in the number of GEMs was previously shown to corelate with disease severity in SMA (Coovert *et al.*, 1997), meaning that number of GEMs decreases with reduction of SMN levels.

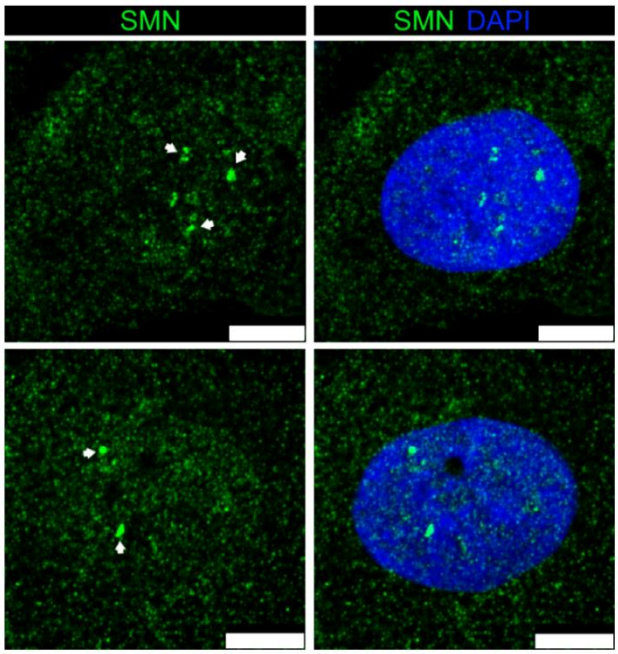

Figure 2. 10. Representative immunocytochemistry images showing GEMs in healthy fibroblasts. GEMs are indicated by arrows. Scale bar = 7.5 µm.

2.8.4.2. Densitometry measurements of nuclear staining using Fiji software

Fields of view were chosen to capture at least a 100 cells per coverslip. Three coverslips were analysed in each group, i.e. 0 µM (vehicle), 6.25 µM and 100 µM quercetin, meaning that at least 300 cells were analysed in each group. Densitometry measurements of nuclear lamin A/C, ABC and UBA1 staining were obtained using Fiji software (v1.51) (Schindelin *et al.*, 2012). First, images were calibrated using a calibrated step tablet (as described in section 2.3.3.1). OD of the nuclear region was first measured on the negative control (IgG control) as described below. The split channels function (Image → Colour → Split Channels) was first used to separate blue and green channels which automatically converted them into gray-scale images for further analyses. Pixels on the green channel (LMNA, ABC and UBA1) were inverted (Edit → Invert), while blue channel (DAPI) was used to define regions of interest. This was done by using one of the auto-threshold options, i.e. Huang or Huang2 (Image→ Adjust →Auto Threshold), where regions of interest are defined based on the intensity of staining. Measurement setting (Analyse→ Set Measurements) were defined as follows: integrated density, limit to threshold and redirect to green channel. This was done to ensure that integrated density is measured on the green channel and in the defined region of interest only. OD of the nuclear region was then measured using the analyse particles function (Analyse→ Analyse particles) with defined parameters: size (inch^2): 0.05-infinity, circularity: 0.00-1.00 and exclude on edges (to exclude cells that are not completely visible in the field of view). This protocol was then used for measurements of all pictures, with an addition of one step. Prior to measurements of the OD, the mean OD of the negative control was subtracted from the green channel to correct the background, by using subtract function (Process→ Math→ Subtract). OD measurements from each field of view were normalised to the number of cells

in the field of view, and the average OD from each field of view was used in statistical analysis.

The workflow is presented in Figure 2.11.

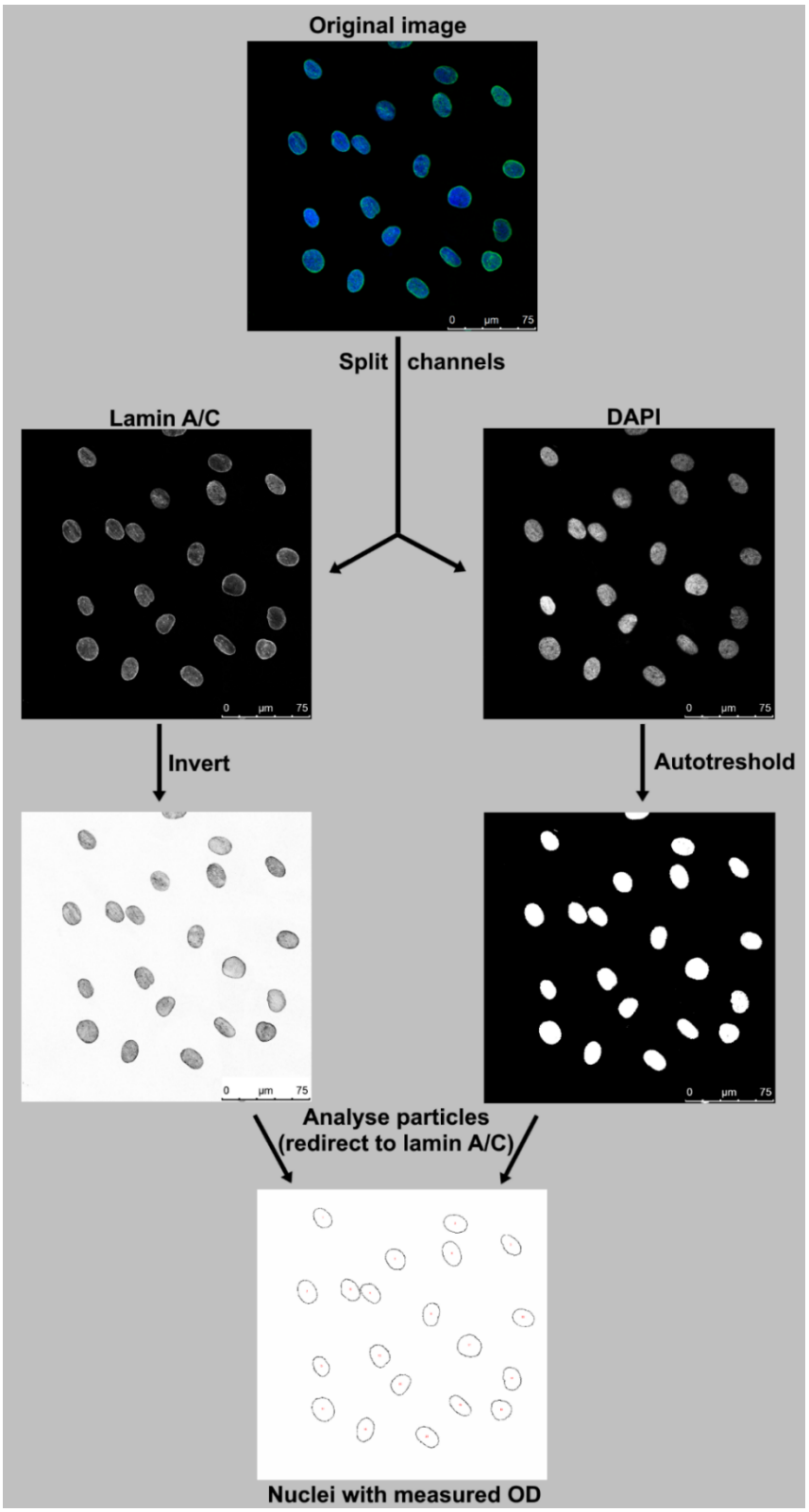

Figure 2. 11. Workflow of densitometry measurements of nuclear protein staining. OD measurements of nuclear lamin A/C staining are presented, together with all corresponding steps.

2.9. Multi-study comparison of published 'omics' studies and bioinformatics analyses

2.9.1. Identification and comparison of published transcriptomics studies of SMA

PubMed searches were performed by Dr Heidi Fuller (Keele University). The search was conducted to include studies published up to April 2016, and published studies were considered eligible for inclusion if they had applied an unbiased transcriptomics approach to identify disease-specific gene expression patterns in SMA. Further selection of studies for comparison was done by me. Studies that utilised a targeted approach (i.e. seeking specific genes) for initial gene identification were excluded from comparison. Initially 15 studies were eligible for review, but four studies were further excluded from the list due to inaccessible or incomplete data (i.e. lack of access to complete article, only some results published or accessible), leaving 11 studies in total.

All studies provided the list of genes in a standard format (i.e. official gene symbol), and so the use of DAVID gene ID conversion tool was not necessary here. Transcriptomics datasets were first extracted into a Microsoft Excel spreadsheet, and compared using Microsoft Excel's 'pivot table' function (Grech, 2018) to identify genes that appeared in multiple studies. Pivot table function is a powerful tool that allows summary of a complex data (Grech, 2018). To do this, all transcriptomics studies were first listed in column A, together with the list of differentially expressed genes listed in column B. In the pivot table function (Insert → Pivot Table) the fields were dragged into the appropriate area, meaning that column A ('Study') was dragged into the column area, and column B ('Gene') was dragged into the row area, with the output measure (value) set to 'count of genes'. The value of 1 suggested that the gene was identified as dysregulated in that specific study.

2.9.1.1. Bioinformatics analysis using DAVID and STRING 10

Database for Annotation, Visualization and Integrated Discovery (DAVID)

The Gene ontology (GO) analysis tool of the Database for Annotation, Visualization and Integrated Discovery (DAVID; version 6.8) platform (Huang, Sherman and Lempicki, 2009b, 2009a) was used to investigate the likely function of genes that showed consistent direction of differential expression across at least three transcriptomic studies of SMA. In the GO analysis, genes/proteins are systematically mapped to biological annotations (gene ontology terms), including biological process (BP), molecular function (MF) and cellular component (CC) terms (Huang, Sherman and Lempicki, 2009b). This allows identification of biological processes that may have important role in the experimental model studied. The Fisher exact test is used to calculate the p-value, by measuring the gene/protein-enrichment in annotation terms (Huang, Sherman and Lempicki, 2009b). First, the number of genes/proteins that are associated with a specific GO term is determined from the reference dataset. The reference dataset is referred in DAVID as the 'background'. The entire genome of the species that the data was derived from is usually set as a default background (Huang, Sherman and Lempicki, 2009b). In this comparison, the background was set to *Homo sapiens* since data from both human and mouse samples was included in the comparison (Section 3, Table 3.1). The number of genes/proteins that are associated with the same GO term is then determined in the input dataset. If more genes/proteins are identified in the input dataset compared to the reference dataset, the specified term is significantly enriched in the input dataset (i.e. the association is not due to a chance) (Workflow is presented in Figure 2.12). Gene ontology (GO) analysis was conducted to include terms that had at least three annotated genes and a p-value ≤0.05. Following the analysis, redundant terms (those that were describing the same function and had identical matches, i.e. gene expression and regulation of gene expression) were combined

into one term to generate the final list of enriched GO terms. Data was presented as chord diagram using the circlize package in R software (Gu *et al.*, 2014).

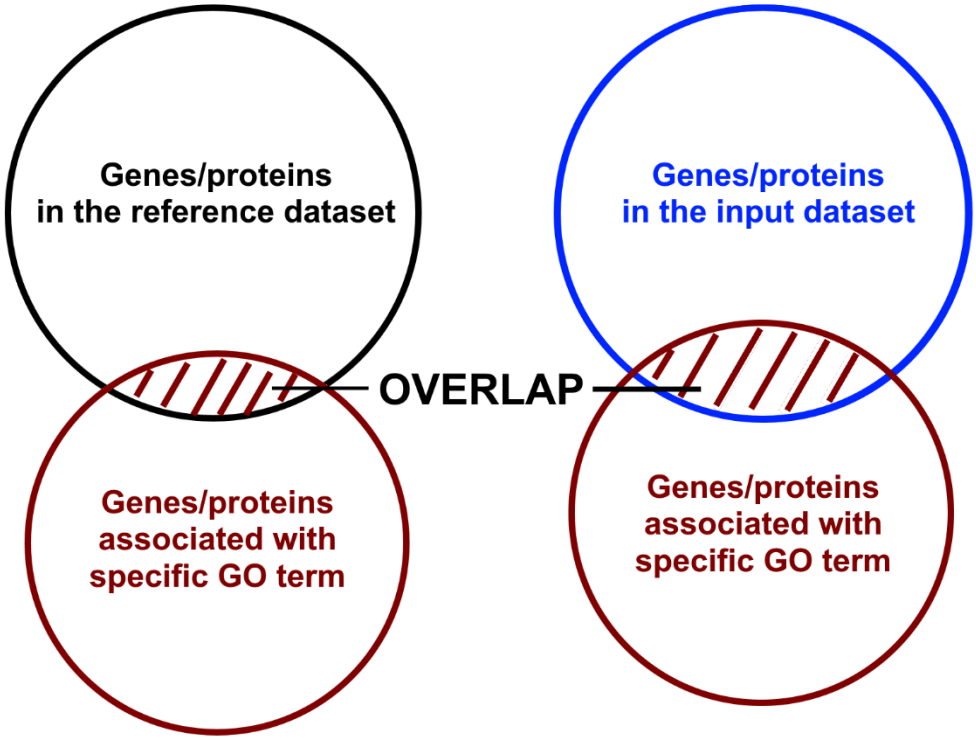

Figure 2. 12. Workflow of the enrichment analysis. If the overlap between genes/proteins in the input dataset and genes/proteins that are associated with a specific GO term is bigger compared to the reference dataset, the term is considered to be significantly enriched.

Search Tool for the Retrieval of Interacting Genes/Proteins (STRING) 10

Search Tool for the Retrieval of Interacting Genes/Proteins (STRING) 10 (Szklarczyk *et al.*, 2015) was used to identify statistically significant interactions between proteins, encoded by genes that showed consistent direction of differential expression across at least three transcriptomic studies of SMA. The STRING platform extracts data from multiple sources including KEGG Pathway Database, Reactome Pathway Database, The Biomolecular Interaction Network Database and many others[7], thus integrating information about protein

[7] https://string-db.org/cgi/help.pl?sessionId=wxWRgx0N5sDs

interactions from more than 2000 organisms (Szklarczyk *et al.*, 2015). Protein interaction represents functional relationship between two proteins that is likely contributing to a common biological purpose (Szklarczyk *et al.*, 2015).

A list of proteins was uploaded into a tab: multiple proteins, with background set to *Homo sapiens* since data from both human and mouse samples was included in the comparison. Protein association network consist of nodes (input proteins), and edges which represent the predicted functional associations (Szklarczyk *et al.*, 2015). Data was filtered to include protein associations identified with high confidence (0.700) interaction score to exclude false positive results. Confidence score is derived from seven types of evidence, each of which is scored separately (Szklarczyk *et al.*, 2017). All evidence scores are then combined to give a final interaction score. Different types of evidence are presented with a different colour in association network. A red line represents fusion evidence, where proteins are given an interaction score if their orthologs have fused into a single, protein-coding gene in at least one organism. A green line represents neighbourhood evidence, where genes are given an association score if they are consistently observed in each other's genome neighbourhood. A blue line represents co-occurrence evidence and assesses the phylogenetic distribution of orthologs of all proteins in a given organism. Proteins are given an interaction score if their orthologs show a high similarity in the distribution, i.e. if they tend to be 'present' or 'absent' in the same subsets of organisms. A purple line represents experimental evidence, where proteins are given an interaction score if they were shown to interact experimentally. A light blue line represents database evidence, where proteins are given interaction score if information about their interaction was gathered from curated databases. A yellow line represents text-mining evidence, where proteins are given an interaction score if they are often mentioned together in PubMed abstracts and in other text collections. A black line

represents co-expression evidence, where proteins are given high association score if their expression patterns are consistently similar under a variety of conditions (Szklarczyk *et al.*, 2017).

2.9.2. Comparison of the SMA proteome and transcriptome

Differentially expressed genes, identified in the comparison of published transcriptomic studies of SMA (Chapter 3, Table 3.2), were compared with the differentially expressed proteins identified in a multi-study comparison of SMA proteomic studies (Fuller, Gillingwater and Wishart, 2016) using a Microsoft Excel's 'pivot table' function (Grech, 2018) as described above.

2.9.3. Identification of upstream regulators using Ingenuity pathway analysis (IPA)

Upstream regulators of eight protein targets, SMN, lamin A/C, UBA1, GAPDH, ANXA2, GAP43, NCAM and COL6A3, were identified using a trial version of Ingenuity Pathway Analysis (IPA) (QIAGEN Inc., https://www.qiagenbioinformatics.com/products/ingenuity-pathway-analysis). The upstream regulator function of the IPA enables identification of upstream regulators that have a known mechanism of action on target proteins/genes (Krämer *et al.*, 2014). Upstream regulators include different molecules such as the transcription factors, miRNAs, drugs, growth factors etc. Two main values are generated in upstream regulators analysis, the p-value of an overlap and the Z-score. The p-value is calculated by Fisher exact test (as described in section 2.9.1.1) by looking at the overlap between the genes/proteins in the input dataset and the genes from the literature that are known to be regulated by upstream regulators. Z-score, on the other hand, gives a prediction of whether the upstream regulator is activated or inhibited based on the direction of expression change in the input dataset. This is done by

comparing the IPA database, which tells us what to expect when upstream regulator interacts with its downstream target, to the direction of differential gene/protein expression that was observed in the input dataset. Z-score of ≥2 represents the prediction of activation, while Z-score ≤ -2 represents the prediction of inhibition.

An Excel file, containing eight proteins of interest (expressed as official gene symbols) and their average fold changes across all proteomic studies, was uploaded into the IPA software (New → Core analysis → Upload), with column A defined as an ID column, and column B as an observation column. Core analysis were performed on the Expr fold change values to enable Z-score calculations. The Ingenuity Knowledge Base was defined as a reference dataset. Only experimentally determined, direct and indirect, upstream regulators were considered in the analysis. The analysis identified 307 upstream regulators that have a known mechanism of action on one or more protein targets, with a p-value ≤ 0.05. After removal of upstream regulators that were identified with just one downstream target, 78 upstream regulators were left that showed a known mechanism of action on at least two proteins. Of these, 20 upstream regulators were chemical or biological drugs that where considered for *in vitro* drug screening studies. After exclusion of toxic drugs (the ones that are used in cancer treatment), the list was reduced to eleven candidates. Drugs identified with two target proteins were further excluded from the list which left six potential drugs.

2.9.4. Identification and comparison of published proteomic studies of ALS

PubMed searches were performed initially by Joanne Stock (Keele University Masters student), and later updated by myself (DS) using combinations of the terms: “amyotrophic lateral sclerosis”, “Lou Gehrig’s disease” or “motor neuron disease” AND “proteomics” or “mass spectrometry”. The search was conducted to include studies published up to 1st July

2018, and published studies were considered eligible for inclusion if they had applied an unbiased proteomics approach to identify disease-specific protein patterns in ALS. Studies that utilised a targeted approach (i.e. seeking specific proteins) for initial protein identification were excluded. Initially 40 studies were eligible for review, but seven studies were further excluded from the list due to inaccessible or incomplete data (i.e. lack of access to complete article, only some results published or accessible), leaving 33 studies in total. Of these, 12 studies examined proteome changes in biofluids from ALS patients and 21 studies examined proteome changes in cells and tissues from ALS models.

The studies eligible for review applied a variety of strategies in data analysis and processing, and so it was necessary to establish a method of data selection for the comparison. First, only proteins changed in expression in ALS compared to healthy controls were considered for analysis. Proteins that were differentially expressed between ALS and diseased controls (e.g. Alzheimer disease), protein changes identified between different groups of ALS patients, and/or protein changes identified between different regions of the same tissue were disregarded. Results from studies that used multiple groups in proteomic comparison were filtered so that only proteins that showed differential expression between ALS and healthy controls were included in the comparison. Proteomic datasets were first extracted into a Microsoft Excel spreadsheet. To facilitate an achievable and accurate method for comparison between the studies the protein identifiers from each study were first converted to official gene symbols by using DAVID platform (Huang, Sherman and Lempicki, 2009b, 2009a). If protein identifiers were not provided, or if DAVID could not recognise the accession number, identifiers were assigned manually by searching for protein names using NCBI with the appropriate species filter to identify the corresponding accession number. Rarely, proteins

had been removed from the NCBI database and so were not included in the final analysis. Most studies presented changes in the protein expression as a fold change (FC) difference between ALS and controls, after having applied a cut-off value to identify proteins that were differentially expressed in ALS. In cases where the cut-off value for fold change was not applied, only proteins that showed at least 20% change in the expression were included in the comparison. (This value was chosen because it has been commonly used in other published proteomic studies to identify differentially expressed proteins e.g. (Mutsaers *et al.*, 2013; Wishart *et al.*, 2014; Chen *et al.*, 2016)). The final lists of gene names were then compared using Microsoft Excel's 'pivot table' function (Grech, 2018) to identify proteins that appeared in multiple studies, as described in section 2.9.1.

2.9.4.1. Bioinformatics analysis

Bioinformatics analyses were conducted on a list of proteins that showed consistent direction of differential expression across at least two proteomic studies of ALS, as described in section 2.9.1.1. Gene ontology analysis, using DAVID platform (Huang, Sherman and Lempicki, 2009b, 2009a), was conducted to include terms that had at least three annotated proteins and a p-value ≤0.05, with background set to *Homo sapiens*. Redundant terms (i.e. those that were describing the same function and had identical matches, e.g. response to oxidative stress and removal of superoxide radicals) were combined into one term. Data was presented as chord diagram using circlize package in R tool (Gu *et al.*, 2014). STRING 10 (Szklarczyk *et al.*, 2015) was used to identify statistically significant interactions between proteins that showed consistent change in expression in ALS. Association network analysis was performed with high confidence (0.700) interaction score to exclude false positive results.

2.9.5. Comparison of SMA and ALS proteome changes

Differentially expressed proteins identified in the comparison of ALS proteomic studies (Table 5.4. and 5.5.) were compared with the list of differentially expressed proteins identified in the comparison of published proteomic studies of SMA proteomic (Fuller, Gillingwater and Wishart, 2016) to investigate common molecular patterns between the two diseases. Proteins with dysregulated expression in both SMA and ALS datasets were subjected to bioinformatics analysis using DAVID (Huang, Sherman and Lempicki, 2009b, 2009a) and STRING 10 (Szklarczyk *et al.*, 2015) as described in section 2.9.4.1.

2.10. GAPDH and ALDOA activity assays

Aldolase fructose-bisphosphate A (ALDOA) and glyceraldehyde-3-phosphate dehydrogenase (GAPDH) activity were measured in spinal cord extracts from 8-days old Taiwanese mice (n = 3) and age-matched healthy controls (n = 3), 20-week old $SOD1^{G93A}$ mice (n = 3) and age-matched healthy controls (n = 5 for ALDOA, and n = 3 for GAPDH), and 12-week old $SOD1^{G93A}$ mice (n = 4 for ALDOA, and n = 3 for GAPDH) and age-matched healthy controls (n = 3), according to instructions outlined in the guidelines. ALDOA (ab196994; Abcam) and GAPDH (ab204732; Abcam) are colorimetric activity assays that rely on the reaction between the developer and the product of the ALDOA or GAPDH activity. This reaction produces a coloured product that absorbs maximally at 450 nm, where the intensity of the colour is proportional to the enzyme activity levels.

2.10.1. Protein extraction and quantification

Spinal cord tissue was homogenized in ice-cold aldolase assay buffer with pallet pestle (30 strokes), after which the samples were left on ice (4°C) for 10 minutes and sonicated at 5

microns for 10 seconds (Sonicrep 150; MSE). The same process was repeated two more times to ensure sufficient homogenization of the tissue. Protein extracts were then centrifuged at 13000 RPM (Micro Centaur MSB010.CX2.5; MSE; rotor radius- 4 cm) for 5 minutes at 4°C to pellet any insoluble material, and supernatants were transferred to a fresh tube. Because of the compatibility between buffers of the two kits (in consultation with a technical team from Abcam), samples extracted in aldolase assay buffer were also used for measurements of GAPDH activity. Pierce™ 660nm Protein Assay was used to determine protein concentration of the samples (as described in section 2.3.1.2.2). The results from a protein assay were then used to ensure equal protein loading across all samples (1 mg/mL) that would allow accurate quantification of ALDOA and GAPDH activity.

2.10.2. Measurements of ALDOA and GAPDH activity

Nicotinamide adenine dinucleotide (NADH) standards, positive control and samples were prepared for the analysis in 96-well plates according to instructions outlined in the guidelines. All reactions were prepared in duplicates in the final volume of 50 µL. NADH standards were prepared from a 1.25 mM stock solution as described in Table 2.7, and 50 µL of the solution was carefully transferred into the well. Spinal cord extracts (1 mg/mL) were diluted to the final volume of 50 µL as shown in Table 2.8. Reaction and background wells were prepared for each sample in duplicates. Positive control wells were prepared at the same dilution as corresponding samples.

Table 2. 7. NADH standards

NADH concentration (nmol/well)	0	2.5	5	7.5	10	12.5
Volume of standard (µL)	**0**	**5**	**10**	**15**	**20**	**25**
Volume of assay buffer (µL)	**125**	**120**	**115**	**110**	**105**	**100**

Recipe for each standard is given in the table.

Table 2. 8. Sample dilutions

Sample	Application and dilution
ALS (20 weeks)	**ALDOA activity- 1:20**
	GAPDH activity- 1:20
ALS (12 weeks)	**ALDOA activity- 1:80**
	GAPDH activity- 1:20
SMA (8 days)	**ALDOA activity- 1:80**
	GAPDH activity- 1:20

Dilution factors used for each sample type and assay are listed.

Reaction mix (50 µL) was then added to each standard, positive control and sample reaction well, and background mix to background sample wells (Table 2.9). Absorbance was measured at 450 nm using microplate reader (FLUOstar Omega; BMG Labtech), in a kinetic mode (every two minutes), for 1 hour at 37°C.

Table 2. 9. Reaction and background mix

Component	Reaction mix (µL)	Background mix (µL)
Assay buffer	**46 (GAPDH)** **44 (ALDOA)**	**48 (GAPDH)** **46 (ALDOA)**
Substrate	**2**	**0**
Developer	**2**	**2**
Enzyme mix*	**2**	**2**

Recipes for reaction and background mix are given. *Enzyme mix was added to the reaction and background mix only in ALDOA activity assay**.**

2.10.3. ALDOA and GAPDH activity calculations

First, the corrected absorbance was calculated for each NADH standard and sample, meaning that average absorbance of the blank (0 nmol/well) was subtracted from the average absorbance of samples and standards. Difference in absorbance (ΔOD) between the two time points was calculated for each sample according to formula:

$\Delta OD = (A_2 - A_{BG2}) - (A_1 - A_{BG1})$

(A_1 represents corrected sample absorbance at time point 1, A_2 corrected absorbance at time point 2, and A_{BG1} and A_{BG2} represent corrected background sample absorbance for each time point).

Standard curve was created in Excel by plotting the corrected absorbance for each NADH standard vs. its concentration in nmol/well. Quadratic calibration model from the standard curve was then used to obtain the amount of the NADH (nmol) for the ΔOD value (B) according to formula:

$B = (-b+SQRT(b^2-4*a*(c-\Delta OD)))/(2*a)$

, where a, b and c represent three coefficients of the quadratic equation ($y = ax^2+bx+c$).

Aldolase activity was calculated according to formula:

Aldolase activity = [B/(T2-T1) x V)]*D

(T1 and T2 represent time of the first (A_1) and second (A_2) absorbance reading in minutes, V is the sample volume added to reaction well (µL), and D is the sample dilution factor).

2.11. Quantitative iTRAQ proteomics analysis

Quantitative iTRAQ mass spectrometry analysis was performed as previously described (Fuller *et al.*, 2014). Isobaric tags for relative and absolute quantification (iTRAQ) allows for the analysis of several samples in one experiment (Fuller and Morris, 2012). This eliminates the need to do multiple experiments, thereby reducing in-between experiment variations and overall analytical time. Isobaric tags covalently bind to all primary amines in the sample, meaning that all peptides are labelled (Fuller and Morris, 2012). Each isobaric label contains a unique reporter group, peptide reactive group, and a neutral balance group, and has an overall mass of a 145 Da (Fuller and Morris, 2012). Following peptide fragmentation, the unique reporter groups break off and produce distinct ions, i.e. m/z 114, 115, 116, 117 for four-plex iTRAQ, where the signal intensity form reporter ions corresponds to relative protein abundance in the sample (Fuller and Morris, 2012).

2.11.1. Protein extraction

Frozen hearts from postnatal day 8 (P8) Taiwanese mice ($Smn^{-/-}$;$SMN2^{tg/+}$) (Hsieh-Li *et al.*, 2000) (n = 5) and healthy littermate mice (n = 5) were homogenised in 4 volumes (w/v) of extraction buffer [6 M Urea (U0631; Sigma), 2 M thiourea (T8656; Sigma), 2% 3-[(3-Cholamidopropyl)dimethylammonio]-1-propanesulfonate hydrate (CHAPS; C9426; Sigma) and 0.5% SDS (AM9823; Invitrogen)], as described in section 2.3.1.1. Urea is often used in

extraction buffers to facilitate protein denaturation and unfolding, while addition of detergents, such as SDS and CHAPS, improves solubilization of hydrophobic proteins (Dapic *et al.*, 2017). Protein extracts were centrifuged at 13000 RPM (Micro Centaur MSB010.CX2.5; MSE; rotor radius- 4 cm) for 5 minutes at 4°C to pellet any insoluble material. Components of the extraction buffer can interfere with enzymatic digestion and mass spectrometry analysis, and have to be removed from the sample before downstream analysis (Dapic *et al.*, 2017). To do this, supernatants were precipitated in 4 volumes of ice-cold acetone overnight at −20°C, and acetone precipitates were pelleted at 13000 RPM for 5 minutes at 4°C. The supernatant, containing interfering substances, was discarded, and pellets were resuspended in 200 µL of 500 mM triethylammonium bicarbonate (TEAB, T7408; Sigma) in ultrapure water to dissolve the proteins. Dissolution of proteins after acetone precipitation can be challenging (Feist and Hummon, 2015), and so several strategies have been employed here to facilitate dissolution. These included addition of the SDS to TEAB solution, to a maximum of 0.05% (4352135, Applied biosystems), and mechanical homogenisation by repeated pipetting, vortexing, sonication and the use of pellet pestles.

2.11.2. Protein quantification

50 µL of protein extract from each sample (n = 5) were pulled into one tube to make two groups, i.e. control (CTR) and SMA. The remaining samples were stored on -80°C for downstream analysis. Protein concentration was determined using Bradford reagent (B6916; Sigma) according to instructions outlined in the guideline. Bradford assay (Coomassie brilliant blue assay) is rapid and simple colorimetric assay for quantification of protein concentration (Bradford, 1976). Principles of Bradford rely on the binding of Coomassie brilliant G-250 dye to the arginine and lysine residues of the protein (Sapan, Lundblad and Price, 1999). The

reaction is performed under acidic conditions, where the formation of dye-protein complexes results in a change of colour from brown to blue that absorbs at 595 nm (Sapan, Lundblad and Price, 1999).

Bovine serum albumine standards were prepared in 8 serial dilutions for the analysis in assay working range (0.1–1.4 mg/ml of protein). 50 µL of each diluted sample and standard was added to the tube, following addition of 1 mL of Bradford reagent (sample to reagent ratio = 1:20). Content of the tube was mixed by gentle pipetting, after which a 150 µL of the mixture was loaded in 96-well plate in triplicates. Each sample, i.e. CTR and SMA, was prepared as described in three separate tubes, meaning that each sample was analysed in nine technical replicates to ensure better accuracy (3 tubes x 3 replicates). The plate was incubated at RT for 5 minutes, and absorbance was measured at 595 nm using microplate reader (FLUOstar Omega; BMG Labtech). Protein concentration in each sample was determined as described in section 2.3.1.2.1. The results were used to calculate the appropriate volume of the extract that had to be added to the tube to get 90 µg of total protein for iTRAQ labelling.

2.11.3. Sample reduction, alkylation, digestion and labelling

Samples were prepared for quantitative iTRAQ mass spectrometry analysis according to instructions outlined in the iTRAQ labelling kit (4352135, Applied biosystems). For this, 20 µL of dissolution buffer and 2 µL of reducing reagent (tris-(2-carboxyethyl) phosphine, TCEP) was added to each of the four samples containing 90 µg of total protein. SDS was not added in this step since the extracts already contained 0.05% SDS, and higher concentration could interfere with mass spectrometry analysis. The tubes were vortexed for a couple of seconds and incubated on 60°C for one hour to reduce proteins. SDS increases protein solubility, while TCEP breaks disulphide bonds between cysteine residues, both of which reduce proteome

complexity for downstream analysis (Padula *et al.*, 2017). Reduction of disulphide bonds produces thiol groups that have to be blocked to prevent reforming of disulphide bonds (Padula *et al.*, 2017). 1 µL of cysteine blocking reagent was added to samples, after which the samples were mixed and incubated at RT for 10 minutes to allow cysteine alkylation. Sequencing grade modified trypsin (Promega, V511A) was then added to samples in a ratio 1 µg trypsin/ 10 µg of protein, and the proteins were digested at 37°C overnight. iTRAQ^{TM} tagging reagents were reconstituted with 70 µL of ethanol at RT and each tag was added to appropriate sample group as follows: 114-control (P8), 115-SMA (P8). Tubes were vortexed and incubated at RT for one hour to allow the labelling, after which contents of all tubes were combined into one tube. The sample was dried with centrifugal vacuum concentrator at 41°C, and the remaining pellet was stored at -80°C until further analysis.

2.11.4. Data analysis

Mass spectrometry analysis were performed by Dr Sally L. Shirran and Dr Silvia A. Synowsky (University of St Andrews) as described (Šoltić *et al.*, 2019). Raw mass spectrometry data files were analysed by ProteinPilot software, version 5.0.1.0 (Applied Biosystems) with the ParagonTM database search and Pro GroupTM Algorithm using the UniProtKB/Swiss-Prot FASTA database. The general Paragon search analysis parameters were: type 'iTRAQ4plex (Peptide Labeled)', cysteine alkylation 'MMTS', digestion 'trypsin' as the cleavage enzyme, instrument 'TripleTOF, and species 'Mouse' for sample parameters; processing parameters were specified as 'quantitative', 'bias correction', 'background correction'; 'thorough ID' and 'biological modifications'. Proteins that showed a Protein Threshold > 5 were used for the Pro Group Algorithm to calculate the relative quantification of the protein expression, generating an error factor and p-value. A false discovery rate (FDR) analysis was performed using the

Proteomics System Performance Evaluation Pipeline (PSPEP). This approach identified 3105 proteins in total of which 2479 were identified with a 5% local false-discovery rate. For reliable quantification, proteins identified from just a single peptide were removed, after which, differentially expressed proteins were identified by removal of proteins with an expression change of less than 25%, and finally, exclusion of proteins with a p-value of >0.05 assigned to their fold changes.

2.11.5. Bioinformatics analysis

Bioinformatics were performed as described in section 2.9.1.1. GO analysis using DAVID platform (Huang, Sherman and Lempicki, 2009b, 2009a) was performed separately for upregulated and downregulated proteins, and included terms with at least two annotated proteins and p-value ≤ 0.05. Differentially expressed proteins were also analysed using the STRING 10 (Szklarczyk *et al.*, 2015) to identify statistically significant interactions between them. Association network analysis was performed with high confidence (0.700) interaction score for upregulated and with highest confidence (0.900) interaction score for downregulated proteins to exclude false positive results. In both cases the background was set to *Mus musculus*.

2.12. Statistical analyses

All statistical analyses were performed in GraphPad Prism version 8.0.1 for Windows, GraphPad Software, San Diego, California USA, www.graphpad.com. The Shapiro-Wilk test was first used to assess the distribution of the data. The unpaired two-tailed *t*-test was used for parametric data, and a Mann-Whitney *U* test for a non-parametric data, when comparing two datasets. One-way ANOVA with Dunnett's multiple comparison test was used for

parametric data, and Kruskal-Wallis test for a non-parametric data, when comparing three or more datasets. Results from dot blot analyses (Figure 3.11. and 3.12) were subjected to linear regression analysis and R^2 value was extrapolated from the graph to assess linear regression fit. Multiple t-tests with Holm-Sidak multiple comparison test was used to determine whether the difference in lamin A/C expression between control and SMA sample is statistically significant across serial dilutions (Figure 3.12). All data are presented as mean ± standard deviation (SD). Statistical significance was considered to be $p \leq 0.05$ for all analyses.

CHAPTER 3: Results

Selection of multi-target drugs that can change the expression of core differentially expressed proteins in SMA

3.1. Introduction

Two SMN-targeted therapeutic strategies, Nusinersen (Spinraza^{TM}) and Zolgensma^{TM}, are available to SMA patients, but neither of them show complete efficiency in alleviating disease symptoms in all patient populations (Finkel *et al.*, 2017; Mendell *et al.*, 2017; Mercuri *et al.*, 2018; Sumner and Crawford, 2018). Coupled with uncertainties around long-term effectiveness and extremely high price of both strategies, there is keen interest to find alternative therapeutic strategies that could, in combination with SMN-targeted therapy, offer maximum therapeutic benefit to all SMA patients (Bowerman, 2019).

Identification of novel therapeutic targets is very challenging due to high complexity of biological systems, and even greater complexity of pathological mechanisms in SMA. For example, over a 100 potential interacting partners of SMN have been identified, and considering that each one of these proteins also has its own "interactome", it is highly likely that SMN loss would affect a wide range of proteins and pathways in different cells and tissues (Fuller, Gillingwater and Wishart, 2016). Selection of proteins to be investigated in SMA disease pathways can therefore be difficult.

3.1.1. Untangling the complexity of SMA pathogenesis

An attempt to uncover the mechanism of SMA pathology has put "omics" technologies in the centre of SMA research. Unbiased, quantitative comparisons of the whole proteome (Wishart *et al.*, 2010; Aghamaleky Sarvestany *et al.*, 2014; Fuller *et al.*, 2016), transcriptome (Oprea *et al.*, 2008; Zhang *et al.*, 2013) or spliceosome (Zhang *et al.*, 2008, 2013) can identify conserved disease-related molecular changes downstream of SMN in variety of different SMA models. For example, comparison of the transcriptome profile of asymptomatic females carrying homozygous deletion of SMN1 and their SMA-affected siblings, led to discovery of two

protective modifiers in SMA, plastin 3 (Oprea *et al.*, 2008) and neurocalcin delta (Riessland *et al.*, 2017). Both proteins were subsequently studied in *in vitro* and *in vivo* models of SMA were they showed neuroprotective potential that could potentially be used in a therapy design for SMA patients (summarised in chapter 1, section 1.5.2.1). Two separate proteomics studies, using Schwann cells (Aghamaleky Sarvestany *et al.*, 2014) and hippocampus synaptosomes (Wishart *et al.*, 2014) from severe mouse models of SMA, identified dysregulation of ubiquitin-proteasome pathway which was found to be important regulator of SMA disease pathways (described in chapter 1, section 1.5.2.3). In addition, proteome comparison of the SMA patient fibroblasts with genetically matched iPSC-derived motor neurons revealed differential response of the two cell types to SMN depletion (Fuller *et al.*, 2016). When compared to their respective controls, SMA iPSC-derived motor neurons showed a higher number of dysregulated proteins then genetically matched fibroblasts, which suggests that different tissues/cells have different requirements for SMN levels. In addition, only seven of these proteins were common to both cell types, which confirms previous findings that different tissues/cells respond differently to dysregulation of SMN levels (Fuller *et al.*, 2016). All of these examples demonstrate the valuable contribution of omics technologies in investigation of complex SMA disease pathways.

3.1.1.1 Limitations of proteomics approach

Although proteomics technologies usually generate a wealth of new knowledge, two main limitations have to be considered when examining the data. First, proteomic studies utilise a variety of different experimental models and sample types to investigate disease mechanism (Fuller, Gillingwater and Wishart, 2016). This could unavoidably result in identification of model/tissues-specific pathogenic patterns that cannot be isolated or distinguished from core

molecular mechanisms in SMA pathogenesis (Fuller, Gillingwater and Wishart, 2016). Translation of these findings into other experimental models or clinical research can therefore be very challenging, and demands careful examination and selection of targets from a long list of protein changes (Wishart *et al.*, 2014). The amount of information generated using this approach represents the second challenge. Proteomics technologies usually generate extensive lists of differentially expressed proteins, of which, very few protein candidates get further experimental attention (Fuller, Gillingwater and Wishart, 2016). This process usually involves selection of proteins with the biggest fold change difference, or selection of proteins that are of specific interest to the research group, where potentially important changes might be overlooked (Fuller, Gillingwater and Wishart, 2016). Public availability of these proteomic datasets, however, represents the opportunity to systematically examine this information, to generate new knowledge of SMA disease pathways.

3.1.2. Comparison of published proteomic studies of SMA identified conserved protein response in SMA cells and tissues

One recent study used a comparative approach to interrogate a range of datasets from published proteomic studies of SMA, and successfully identified core molecular changes in SMA tissues and cells (Fuller, Gillingwater and Wishart, 2016). Nine proteomic studies, investigating proteome alterations in *in vitro* and *in vivo* models of SMA and in SMA patient samples, were included in the comparison. These included cells from SMA patients and SMA mice at different stages of differentiation, SMN depleted NSC34 cells, different tissues from SMA mice and plasma from SMA patients (Fuller, Gillingwater and Wishart, 2016). The analysis identified 66 proteins that showed differential expression across at least two proteomic studies of SMA, of which 29 showed consistent direction of differential expression, meaning that their expression levels were either increased or decreased in SMA samples compared to

control in all proteomic studies (Fuller, Gillingwater and Wishart, 2016). Of these, seven proteins showed consistent direction of differential expression across three proteomic studies of SMA, including ubiquitin-like modifier-activating enzyme 1 (UBA1), whose implication in SMA disease pathways has already been described in chapter 1, section 1.5.2.3. Identification of proteins that have already been implicated in SMA disease pathways is highly relevant, and indicates the validity of this approach to identify core pathological mechanisms in SMA. This also suggested the potential role for the remaining six proteins, lamin A/C (LMNA), glyceraldehyde 3-phosphate dehydrogenase (GAPDH), annexin A2 (ANXA2), neural cell adhesion molecule 1 (NCAM), neuromodulin (GAP43) and collagen type VI alpha 3 chain (COL6A3), in SMA disease pathways.

3.1.3. Multi-target therapies

The seven proteins identified in the multi-study comparison of published proteomic studies (Fuller, Gillingwater and Wishart, 2016) represent potential therapeutic targets in SMA, and in theory could be targeted either individually or simultaneously. Given the complexity of the SMN interactome and the potential number of SMA disease pathways (Fuller, Gillingwater and Wishart, 2016), manipulation of individual proteins is unlikely to completely alleviate disease symptoms in SMA patients. However, by targeting multiple proteins at the same time it might be possible to restore several disease pathways, and when combined with SMN-targeted therapies, this strategy could bring greater therapeutic benefit to SMA patients. There are three different approaches in the design of multi-target therapies (Hopkins, 2008). The first strategy involves a combination of different drugs, and it has been successfully used, for example, for the treatment of HIV infections (Freeman *et al.*, 2004). However, a major safety issue in the use of several drugs are drug-drug interactions (DDIs) that can cause severe

adverse reactions (Hopkins, 2008). DDIs can, for example, change pharmacokinetic properties of the drug, by altering its distribution, absorption or metabolism, and pharmacodynamic profile, where one drug can have additive or antagonistic effect on the other drug (Moore, Pollack and Butkerait, 2015). This issue can be resolved by designing multicomponent drugs, meaning that several active ingredients are formulated in one delivery system such as the capsule or inhaler (Hopkins, 2008). Pharmacokinetics and bioavailability of different substances can, however, pose a significant challenge in therapy design, and so multicomponent medicines may not always be a viable solution (Hopkins, 2008). A third strategy involves the design of a single compound that can simultaneously affect several targets (Hopkins, 2008). This strategy has advantage over the other two approaches, in terms of the safety (no drug-drug interactions) and easier management of the pharmacokinetics and bioavailability of the drug. In addition, single compounds face less barriers during approval process (Hopkins, 2008).

The aim of this chapter was to investigate the differential expression of core molecules in SMA tissues and cells, and to determine the best strategy for the selection of multi-target drugs.

The specific objectives were as follows:

a) To conduct a multi-study comparison of published transcriptomics studies of SMA to determine whether conserved changes to the proteome can be tracked back to the aberrant transcriptional regulation.
b) To investigate the differential expression of six protein targets identified in a multi-study comparison of published proteomic studies, including UBA1, lamin A/C, GAPDH, ANXA2, NCAM and GAP43, in tissues from a severe mouse model of SMA and in SMA patient fibroblast cells.
c) To identify different pharmaceutical compounds that have been associated with several protein targets listed above, and to test their ability to change the expression of target proteins in SMA patient fibroblasts.

3.2. Results

3.2.1. Multi-study identification of molecular overlap between proteomic and transcriptomic studies of SMA

Fuller, Gillingwater and Wishart have recently showed that comparison of published proteomic studies of SMA can identify core protein changes in SMA tissues/cells that might be implicated in disease pathways (Fuller, Gillingwater and Wishart, 2016). Here, a similar approach was undertaken to identify core changes to the transcriptome in SMA tissues and cells. The result of the analysis were then compared to the result of a multi-study comparison of published proteomic studies of SMA (Fuller, Gillingwater and Wishart, 2016) to identify whether protein changes in SMA are driven by aberrant transcriptional regulation. This is important question for future work, as it would help to determine whether targeting of molecules at the protein and/or gene level would be necessary to maximise the effect of therapeutic approach in SMA.

3.2.1.1. Multi-study comparison of published transcriptomic studies of SMA identifies 28 genes with consistent direction of differential expression across three studies

First, the analysis of SMA transcriptomics datasets had to be conducted to determine core molecular changes in SMA on the gene level (as described in chapter 2, section 2.9.1). Comparison of eleven published transcriptomic studies of SMA (Table 3.1) identified 608 genes that were differentially expressed across two or more studies in a range of neuromuscular tissues/cells from SMA patients and animal models of SMA (data not shown). Only 28 of the genes showed conserved change in one direction across three or more separate studies of SMA, of which 17 showed decreased expression and 11 showed increased expression (Table 3.2). Among these where genes already linked to SMA pathogenesis,

including chondrolectin (*CHODL*) (Sleigh *et al.*, 2014), doublecortin (*DCX*) (Wishart *et al.*, 2010), cyclin dependent kinase inhibitor 1A (*CDKN1A*) (Staropoli *et al.*, 2015) and complement c1q b chain (*C1QB*) (Zhang *et al.*, 2013), adding support that this is a valid approach to identify disease-related molecular changes in SMA. The remaining genes represent a molecular response to decreased levels of SMN that may have been previously overlooked.

Table 3. 1. Overview of SMA transcriptomics studies

Model/sample type	Differentially expressed genes	Reference
Mouse (severe) at P1 (pre-symptomatic) and P5 (late symptomatic)/Spinal cord	162	(Murray *et al.*, 2010)
SMN knockdown/ mouse motor neurons	3412	(Saal *et al.*, 2014)
Mouse (severe) at P3 (early symptomatic)/ Lumbar spinal cord	166	(Huo *et al.*, 2014)
Mouse (Intermediate)/ Spinal cord and kidney	279	(Zhang *et al.*, 2008)
Mouse (severe) at P1 (pre-symptomatic)/ Motor neurons and glial cells	459	(Zhang *et al.*, 2013)
SMN knockdown/ rat motor neurons	748	(Wertz *et al.*, 2016)
Mouse (severe) at P1 (pre-symptomatic), P7 (early symptomatic) and P14 (late symptomatic)/ Spinal cord	178	(Bäumer *et al.*, 2009)
Mouse (severe)/ ESC-derived motor neurons	269	(Maeda *et al.*, 2014)
Mouse (intermediate)/ Motor neurons (SMAv, SMAr)	565	(Murray *et al.*, 2015)
Muscles from type I and III SMA patients	88	(Millino *et al.*, 2009)
Myoblasts from type II SMA patients	62	(Anderson *et al.*, 2004)

SMA studies included in the transcriptomics comparison are listed in table, together with SMA model and sample type used in each study. Number of differentially expressed genes identified in each study is listed in column two. SMAv - vulnerable (abdominal) motor neurons; SMAr- less vulnerable (cranial) motor neurons.

Table 3. 2. Genes differentially expressed across three or more transcriptomic studies of SMA

Gene name (Official Gene Symbol)	SMA model	References
Decreased expression		
Survival of Motor Neuron 1, Telomeric (*SMN1*)	Mouse ESC-derived motor neurons	(Maeda *et al.*, 2014)
	Mouse spinal cords	(Murray *et al.*, 2010)
	Rat motor neurons	(Wertz *et al.*, 2016)
	Mouse kidney	(Zhang *et al.*, 2008)
	Mouse motor neurons and glial cells	(Zhang *et al.*, 2013)
	Mouse spinal cord	(Bäumer *et al.*, 2009)
Chondrolectin (*CHODL*)	Rat motor neurons	(Wertz *et al.*, 2016)
	Mouse spinal cord	(Zhang *et al.*, 2008)
	Mouse motor neurons	(Zhang *et al.*, 2013)
	Mouse spinal cord	(Bäumer *et al.*, 2009)
Collagen Type XII Alpha 1 Chain (*COL12A1*)	Mouse spinal cords	(Murray *et al.*, 2010)
	Mouse motor neurons	(Saal *et al.*, 2014)
	Rat motor neurons	(Wertz *et al.*, 2016)
	Mouse motor neurons	(Zhang *et al.*, 2013)
Protein Regulator of Cytokinesis 1 (*PRC1*)	Mouse spinal cords	(Murray *et al.*, 2010)
	Mouse motor neurons	(Saal *et al.*, 2014)
	Mouse spinal cord and kidney	(Zhang *et al.*, 2008)
	Mouse spinal cord	(Bäumer *et al.*, 2009)
PCNA Clamp Associated Factor (*PCLAF*)	Mouse spinal cords	(Murray *et al.*, 2010)
	Mouse motor neurons	(Saal *et al.*, 2014)
	Mouse spinal cord	(Huo *et al.*, 2014)
Anti-Silencing Function 1B Histone Chaperone (*ASF1B*)	Mouse spinal cords	(Murray *et al.*, 2010)
	Mouse motor neurons	(Saal *et al.*, 2014)
	Mouse kidney	(Zhang *et al.*, 2008)
Cyclin A2 (*CCNA2*)	Mouse spinal cords	(Murray *et al.*, 2010)
	Mouse motor neurons	(Saal *et al.*, 2014)
	Mouse spinal cord and kidney	(Zhang *et al.*, 2008)
Cell Division Cycle Associated 7 (*CDCA7*)	Mouse spinal cords	(Murray *et al.*, 2010)
	Mouse motor neurons	(Saal *et al.*, 2014)
	Mouse glial cells	(Zhang *et al.*, 2013)

Doublecortin (*DCX*)	Mouse ESC-derived motor neurons	(Maeda *et al.*, 2014)
	Mouse motor neurons	(Murray *et al.*, 2015)
	Mouse motor neurons	(Saal *et al.*, 2014)
Eukaryotic Translation Initiation Factor 1 (*EIF1*)	Mouse SMN-knockdown motor neurons	(Saal *et al.*, 2014)
	Rat motor neurons	(Wertz *et al.*, 2016)
	Mouse spinal cord	(Huo *et al.*, 2014)
EPH Receptor A5 (*EPHA5*)	Mouse ESC-derived motor neurons	(Maeda *et al.*, 2014)
	Mouse motor neurons	(Saal *et al.*, 2014)
	Rat motor neurons	(Wertz *et al.*, 2016)
Lumican (*LUM*)	Mouse spinal cords	(Murray *et al.*, 2010)
	Mouse spinal cord	(Zhang *et al.*, 2008)
	Mouse spinal cord	(Bäumer *et al.*, 2009)
NUF2, NDC80 Kinetochore Complex Component (*NUF2*)	Mouse motor neurons	(Saal *et al.*, 2014)
	Mouse kidney	(Zhang *et al.*, 2008)
	Mouse spinal cord	(Huo *et al.*, 2014)
PDZ Binding Kinase (*PBK*)	Mouse spinal cords	(Murray *et al.*, 2010)
	Mouse motor neurons	(Saal *et al.*, 2014)
	Mouse spinal cord	(Bäumer *et al.*, 2009)
Retrotransposon Gag Domain Containing 4 (*RGAG4*)	Mouse ESC-derived motor neurons	(Maeda *et al.*, 2014)
	Rat motor neurons	(Wertz *et al.*, 2016)
	Mouse glial cells	(Zhang *et al.*, 2013)
Solute Carrier Family 8 Member A1 (*SLC8A1*)	Mouse motor neurons	(Saal *et al.*, 2014)
	Rat motor neurons	(Wertz *et al.*, 2016)
	Mouse kidney	(Zhang *et al.*, 2008)
X-Box Binding Protein 1 (*XBP1*)	Mouse motor neurons	(Saal *et al.*, 2014)
	Rat motor neurons	(Wertz *et al.*, 2016)
	Mouse glial cells	(Zhang *et al.*, 2013)
Increased expression		
Cyclin Dependent Kinase Inhibitor 1A (*CDKN1A*)	Mouse motor neurons	(Murray *et al.*, 2015)
	Mouse kidney	(Zhang *et al.*, 2008)
	Mouse motor neurons and glial cells	(Zhang *et al.*, 2013)
	Mouse spinal cord	(Bäumer *et al.*, 2009)
B-cell CLL/Lymphoma 11A (*BCL11A*)	Mouse motor neurons	(Saal *et al.*, 2014)
	Rat motor neurons	(Wertz *et al.*, 2016)
	Mouse motor neurons	(Zhang *et al.*, 2013)
Complement C1q B Chain (*C1QB*)	Mouse motor neurons	(Saal *et al.*, 2014)
	Mouse motor neurons	(Zhang *et al.*, 2013)
	Mouse spinal cord	(Bäumer *et al.*, 2009)

C-C Motif Chemokine Ligand 3 (*CCL3*)	Mouse motor neurons	(Saal *et al.*, 2014)
	Mouse glial cells	(Zhang *et al.*, 2013)
	Mouse spinal cord	(Bäumer *et al.*, 2009)
Ectodysplasin A2 Receptor (*EDA2R*)	Mouse spinal cords	(Murray *et al.*, 2010)
	Mouse kidney	(Zhang *et al.*, 2008)
	Mouse spinal cord	(Bäumer *et al.*, 2009)
FK506 Binding Protein 5 (*FKBP5*)	Mouse spinal cord and kidney	(Zhang *et al.*, 2008)
	Mouse motor glial cells	(Zhang *et al.*, 2013)
	Mouse spinal cord	(Bäumer *et al.*, 2009)
Metallothionein 2A (*MT2A*)	Mouse spinal cords	(Murray *et al.*, 2010)
	Mouse glial cells	(Zhang *et al.*, 2013)
	Mouse spinal cord	(Bäumer *et al.*, 2009)
Paternally Expressed 3 (*PEG3*)	Mouse motor neurons	(Murray *et al.*, 2015)
	Rat motor neurons	(Wertz *et al.*, 2016)
	Mouse kidney	(Zhang *et al.*, 2008)
Sphingosine-1-Phosphate Phosphatase 2 (*SGPP2*)	Mouse motor neurons	(Saal *et al.*, 2014)
	Mouse motor neurons	(Zhang *et al.*, 2013)
	Mouse spinal cord	(Zhang *et al.*, 2008)
Small Nuclear Ribonucleoprotein Polypeptide A' (*SNRPA1*)	Mouse spinal cords	(Murray *et al.*, 2010)
	Mouse motor neurons	(Zhang *et al.*, 2013)
	Mouse spinal cord	(Bäumer *et al.*, 2009)
Zinc Finger Protein 750 (*ZNF750*)	Mouse motor neurons	(Murray *et al.*, 2015)
	Mouse motor neurons	(Zhang *et al.*, 2013)
	Mouse spinal cord	(Bäumer *et al.*, 2009)

Genes with a consistent change in expression across three or more transcriptomics studies of SMA are shown. Gene name is given, followed by the official gene symbol in brackets. Genes are listed according to direction of differential expression (genes with decreased expression are listed first, followed by genes with increased expression). SMA model and sample type used in each study are listed (studies are listed in the reference column).

GO analysis, using DAVID platform (Huang, Sherman and Lempicki, 2009b, 2009a), was conducted on the 28 genes that showed consistent direction of differential expression across three transcriptomics studies of SMA, as described in Methods chapter 2.9.1.1. The analysis revealed enrichment in terms connected to biological process, among which were nervous system development, gene expression, RNA metabolism and intracellular signalling (Figure 3.1A). STRING 10 software (Szklarczyk *et al.*, 2015) was next used to identify statistically significant associations between proteins that are encoded by the 28 genes (as described in chapter 2.9.1.1). The analysis identified association between seven of the 28 proteins (Figure 3.1B), that are connected to biological process terms like regulation of gene expression and RNA metabolism.

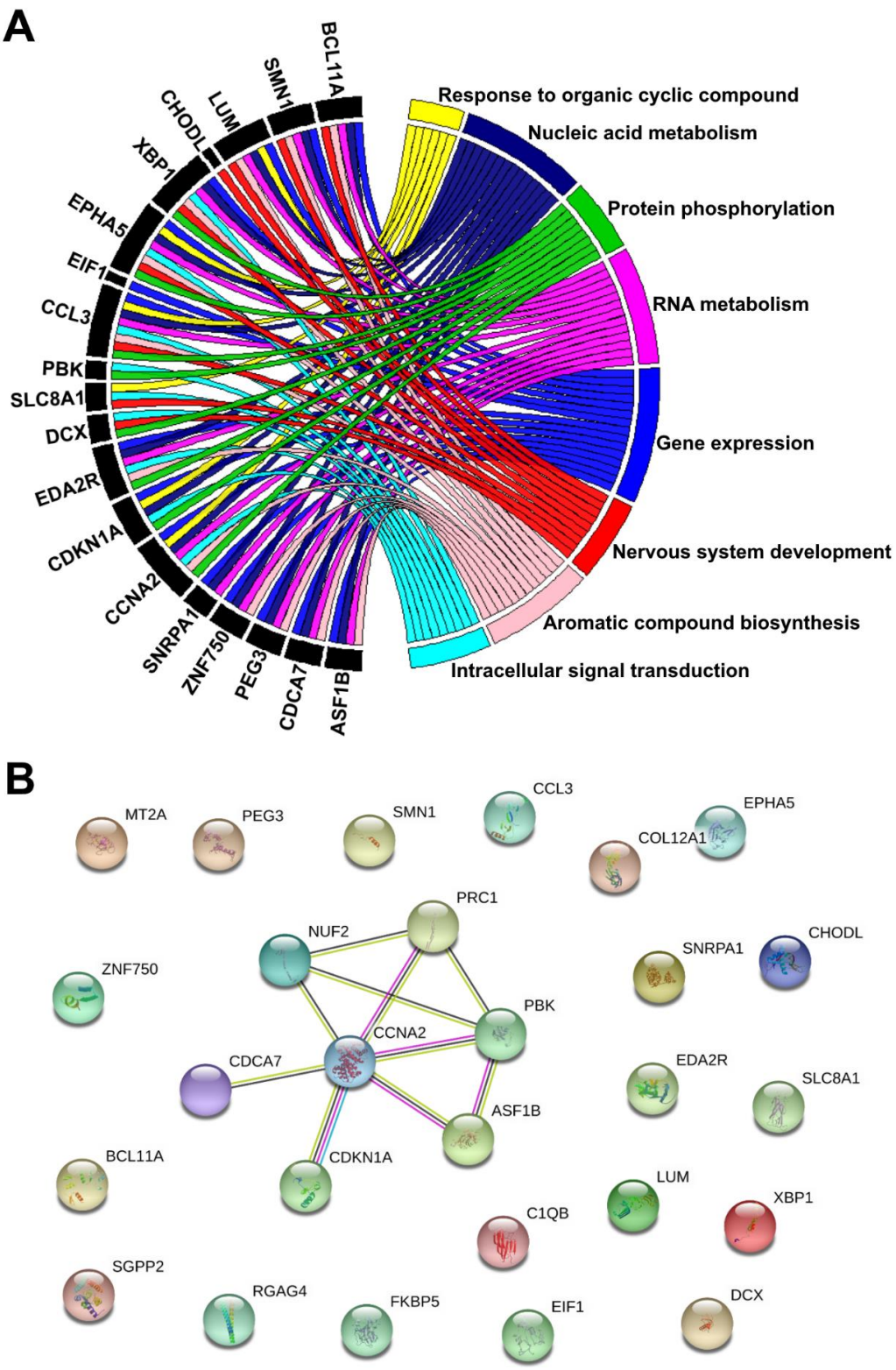

Figure 3. 1. Bioinformatics analyses of the 28 genes that were differentially expressed in the same direction across three or more transcriptomic studies of SMA. (A) Top eight enriched terms from GO biological process domain are shown in the chord diagram, together with the genes annotated to each term. **(B)** STRING 10 analysis of proteins that are encoded by 28 genes were performed with high confidence (0.700) interaction score. The analysis identified significant asocciations between seven of these proteins. The type of association between proteins is indicated by the colour (pink: experimentally determined interactors; light blue: interactors from curated database; yellow: text-mining; black: co-expression).

Although the initial number of genes, identified as being differentially expressed across two or more transcriptomic studies of SMA, was high, very few genes followed the same direction of differential expression across at least three transcriptomic studies of SMA. The 28 genes that showed consistent direction of differential expression were associated with functions like gene expression, RNA metabolism and nervous system development.

3.2.1.2 Multi-study comparison of published proteomics and transcriptomics studies of SMA identified little overlap between differentially expressed genes and proteins

The 608 genes that showed differentially expression across at least two transcriptomic studies of SMA were then compared to the list of proteins that showed differentially expression across at least two proteomic studies of SMA (Fuller, Gillingwater and Wishart, 2016). The analysis identified seven molecules that were differentially expressed at both the gene and protein level across at least two omics studies of SMA (Table 3.3). Of these, annexin A2 (ANXA2) was consistently increased at the protein level and consistently decreased at the gene level across all omics studies, while the remaining six proteins, including neural cell adhesion molecule 1 (NCAM1), glutamic-oxaloacetic transaminase 2 (GOT2), collagen type I alpha 1 chain (COL1A1), collagen type VI alpha 1 chain (COL6A1), caldesmon 1 (CALD1) and aldolase, fructose-bisphosphate A (ALDOA) showed different directions of differential expression across studies.

Table 3. 3. Seven molecules that showed dysregulated expression at protein and gene level in SMA omics studies

Protein/gene name (Official gene symbol)	Omics study (Direction of expression change)	SMA model/sample	References
Annexin A2 (ANXA2)	Proteomics (Up)	Type I patient motor neurons	(Fuller *et al.*, 2016)
	Proteomics (Up)	Mouse Schwann cells	(Aghamaleky Sarvestany *et al.*, 2014)
	Proteomics (Up)	Mouse muscle	(Mutsaers *et al.*, 2013)
	Transcriptomics (Down)	Mouse spinal cord	(Murray et al., 2010)
	Transcriptomics (Down)	Mouse spinal cord	(Zhang et al., 2008)
Aldolase, Fructose-Bisphosphate A (ALDOA)	Proteomics (Up)	Mouse Schwann cells	(Aghamaleky Sarvestany *et al.*, 2014)
	Proteomics (Up)	Mouse hippocampus synaptosomes	(Wishart *et al.*, 2014)
	Proteomics (Down)	Mouse hippocampus	(Wishart *et al.*, 2010)
	Transcriptomics (Down)	Mouse motor neurons	(Murray *et al.*, 2015)
	Transcriptomics (Down)	Rat motor neurons	(Wertz *et al.*, 2016)
Neural Cell Adhesion Molecule 1 (NCAM1)	Proteomics (Down)	Type I patient motor neurons	(Fuller *et al.*, 2016)
	Proteomics (Down)	Mouse hippocampus	(Wishart *et al.*, 2010)
	Proteomics (Down)	Type I, II and III patient plasma	(Kobayashi *et al.*, 2013)
	Transcriptomics (Up)	Rat motor neurons	(Wertz *et al.*, 2016)
	Transcriptomics (Down)	Mouse motor neurons	(Saal *et al.*, 2014)

Caldesmon 1 (CALD1)	Proteomics (Up)	Type I patient motor neurons	(Fuller et al., 2016)
	Proteomics (Up)	Mouse Schwann cells	(Aghamaleky Sarvestany et al., 2014)
	Proteomics (Down)	Type I patient skin fibroblast	(Fuller et al., 2016)
	Transcriptomics (Up)	Mouse motor neurons	(Murray et al., 2015)
	Transcriptomics (Down)	Mouse motor neurons	(Saal et al., 2014)
Glutamic-Oxaloacetic Transaminase 2 (GOT2)	Proteomics (Up)	Mouse muscle	(Mutsaers *et al.*, 2013)
	Proteomics (Down)	Type I patient motor neurons	(Fuller *et al.*, 2016)
	Transcriptomics (Down)	Rat motor neurons	(Wertz *et al.*, 2016)
	Transcriptomics (Up)	Mouse motor neurons	(Saal *et al.*, 2014)
Collagen Type I Alpha 1 Chain (COL1A1)	Proteomics (Up)	Type I patient motor neurons	(Fuller *et al.*, 2016)
	Proteomics (Up)	Mouse Schwann cells	(Aghamaleky Sarvestany *et al.*, 2014)
	Transcriptomics (Up)	Mouse motor neurons	(Murray *et al.*, 2015)
	Transcriptomics (Down)	Mouse spinal cord	(Murray et al., 2010)
	Transcriptomics (Up)	Mouse motor neurons and glial cells	(Zhang *et al.*, 2013)
Collagen Type VI Alpha 1 Chain (COL6A1)	Proteomics (Up)	Type I patient skin fibroblast	(Fuller *et al.*, 2016)
	Proteomics (Up)	Type I, II and III patient plasma	(Kobayashi *et al.*, 2013)
	Transcriptomics (Down)	Mouse spinal cord	(Murray et al., 2010)
	Transcriptomics (Up)	Mouse glial cells	(Zhang *et al.*, 2013)

Seven molecules that were differentially expressed at both the gene and protein level. Protein/gene name is given, followed by official gene symbol in brackets. Type of proteomic study, direction of differential protein/gene expression, and model and sample type are listed for each study (studies are listed in column four).

The aim here was to determine whether changes in the protein expression, identified previously in multi-study comparison of published proteomic studies of SMA (Fuller, Gillingwater and Wishart, 2016), are driven by transcriptional defects, as this could aid selection of appropriate therapies for SMA. The very few molecules that showed differential expression at both the gene and protein levels do not seem to follow the same pattern of differential expression, suggesting that changes in protein expression in SMA tissues are most likely posttranscriptional. Further research efforts where therefore focused on dysregulated proteins in SMA since they represent functional units of cellular pathways.

3.2.2. Liver tissue extracts from SMA mice showed widespread dysregulation of protein expression, while SMA mouse muscles showed very few consistent changes in protein expression compared to controls

Proteins that showed consistent direction of differential expression across three proteomic studies of SMA (Fuller, Gillingwater and Wishart, 2016) were given priority, as they may have important role in SMA disease pathways across a range of tissues. The expression of six protein targets, UBA1, lamin A/C, GAPDH, ANXA2, NCAM and GAP43, was studied in the heart, spinal cord, brain, liver and muscle tissue from late-symptomatic (P8) Taiwanese SMA mice ($Smn^{-/-}$;$SMN2^{tg/+}$), and in fibroblast cells from two type I SMA patients and one type II SMA patient (details are provided in Table 2.1) using quantitative western blotting. COL6A3 levels could not be measured reliably in patient and control fibroblasts using western blotting, due to the high background and the presence of multiple bands in the sample (data not shown), and so COL6A3 levels were not investigated biochemically in other tissues from a mouse model of SMA. The workflow for the quantitative western blotting is presented in Figure 3.2 (in all analyses a Coomassie stained gel was used as an internal, total protein loading control).

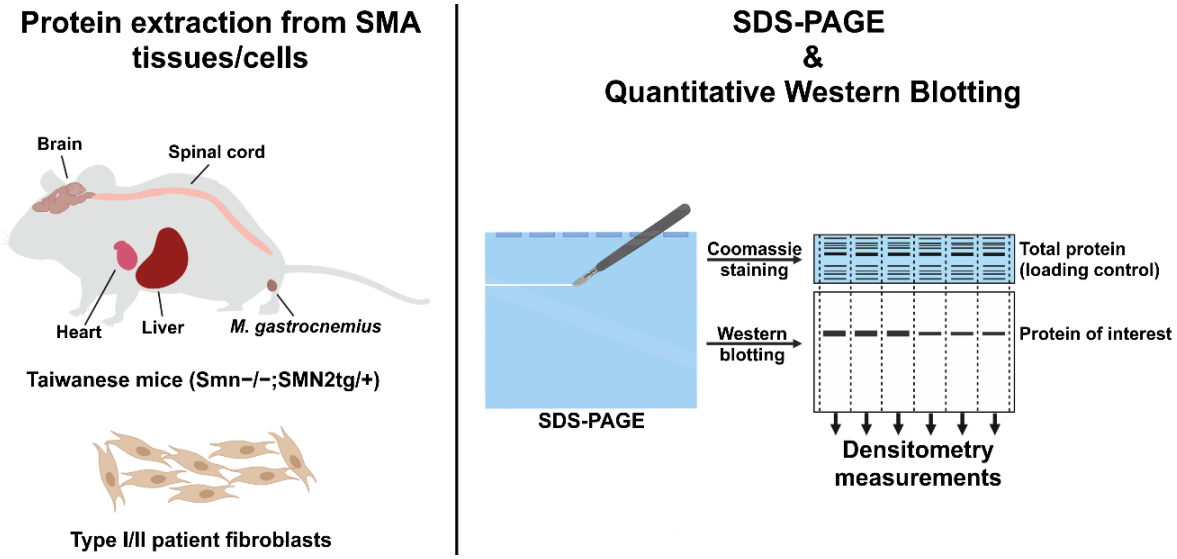

Figure 3. 2. Schematic diagram showing workflow of quantitative western blot analysis. Total protein extracts from human fibroblast cells and mouse tissues were subjected to SDS-PAGE. A part of the gel was stained with Coomassie blue as an internal, total protein loading control. Proteins from the remaining part of the gel were transferred to nitrocellulose membrane and developed with the appropriate antibody. Quantification of protein levels was performed by normalising densitometry measurements of antibody reactive bands to densitometry measurements of Coomassie stained gel. Image created with BioRender.com

The levels of SMN were first determined in tissues from 8 days old control and severe Taiwanese mice, and in control and SMA patient fibroblast cells, and they served as positive control and reference (Figure 3.3). As expected, all SMA tissues and cells showed significant reduction of SMN levels when compared to healthy controls. Liver and muscle tissue from SMA mice showed the greatest reduction of SMN levels (94%, $p < 0.001$), followed by the heart (92%, $p < 0.001$), brain (91%, $p < 0.001$) and spinal cord (88%, $p < 0.001$) tissue from SMA mice, and patient fibroblast cells (71%, $p = 0.0013$).

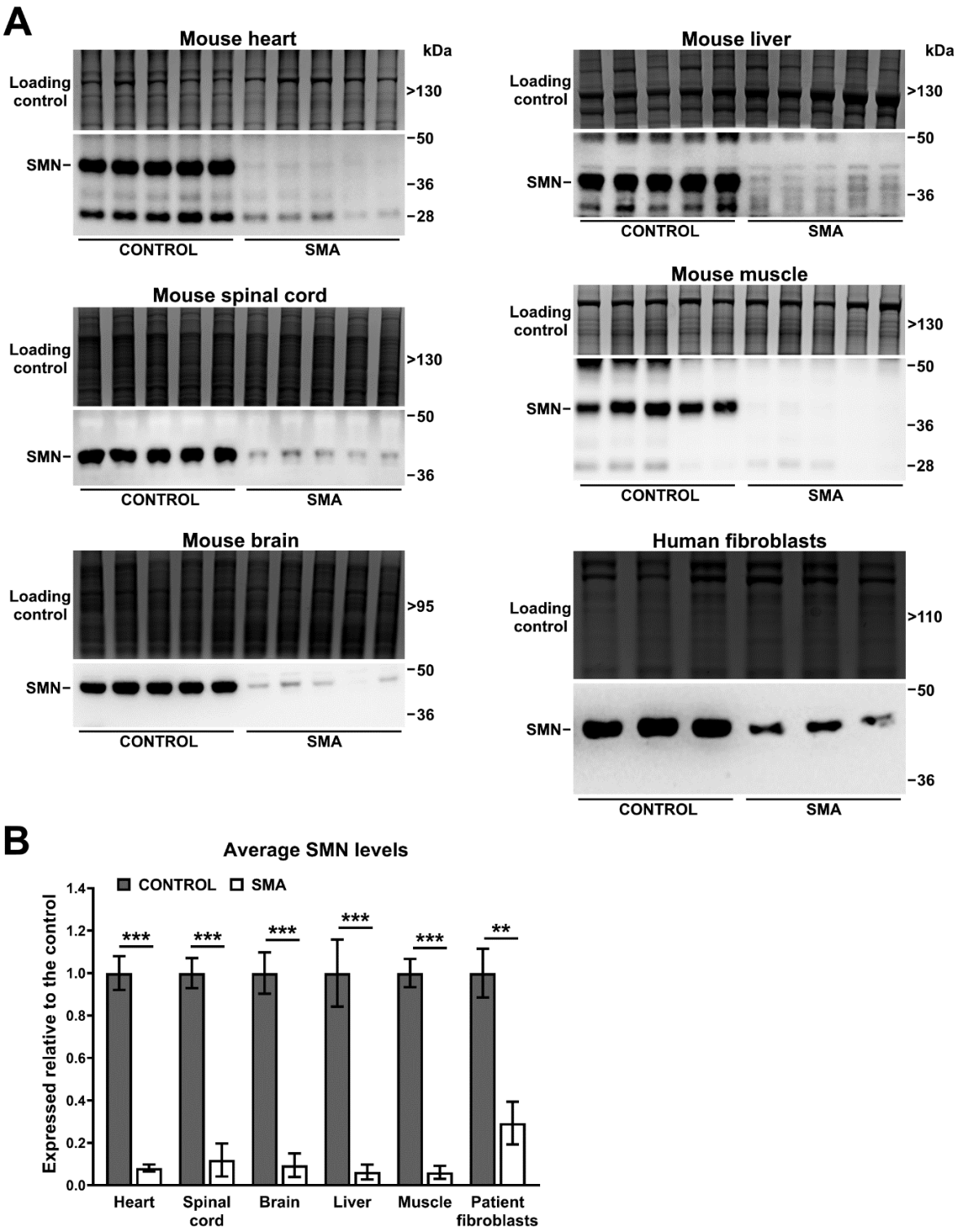

Figure 3. 3. SMN protein levels in tissues from late-symptomatic SMA mice (P8) and in patient fibroblast cells. **A)** Representative western blots showing SMN levels in the heart, spinal cord, brain, liver and muscle tissue extracts from SMA mice (n=5) and age-matched healthy controls (n=5), and in SMA patient fibroblast cells (n=3) and age-matched healthy controls (n=3). Coomassie stained gel was used as internal, total protein loading control. Fibroblast cells are listed in this order from left to the right: GM00498, GM05659, GM00302, GM03813, GM09677, GM00232. **(B)** Densitometry measurements of SMN reactive bands were first normalised to densitometry measurements of Coomassie stained gel, after which all samples were normalised to the average of control. The graph is presented as average protein levels (expressed relative to control), with error bars showing standard deviation from the mean. ** p<0.01; ***p<0.001

UBA1 levels were significantly reduced in the heart (76%, p = 0.0002) and liver extracts (66%, p = 0.0002) from SMA mice (Figure 3.4). A 59% reduction of UBA1 levels in muscles from SMA mice was not statistically significant, likely due to the large variability in protein expression between the samples in both control and SMA groups. Spinal cord and brain tissue from SMA mice, and fibroblast cells from SMA patients did not show a significant change in UBA1 levels compared to controls (Figure 3.4). The unchanged levels of UBA1 in SMA mouse spinal cord and brain tissue extracts are in contrast with proteomic studies, where UBA1 showed decreased expression across neuronal tissues, including Schwann cells and hippocampus synaptosomes from SMA mice, and iPSC-derived motor neurons from SMA patients (Fuller, Gillingwater and Wishart, 2016).

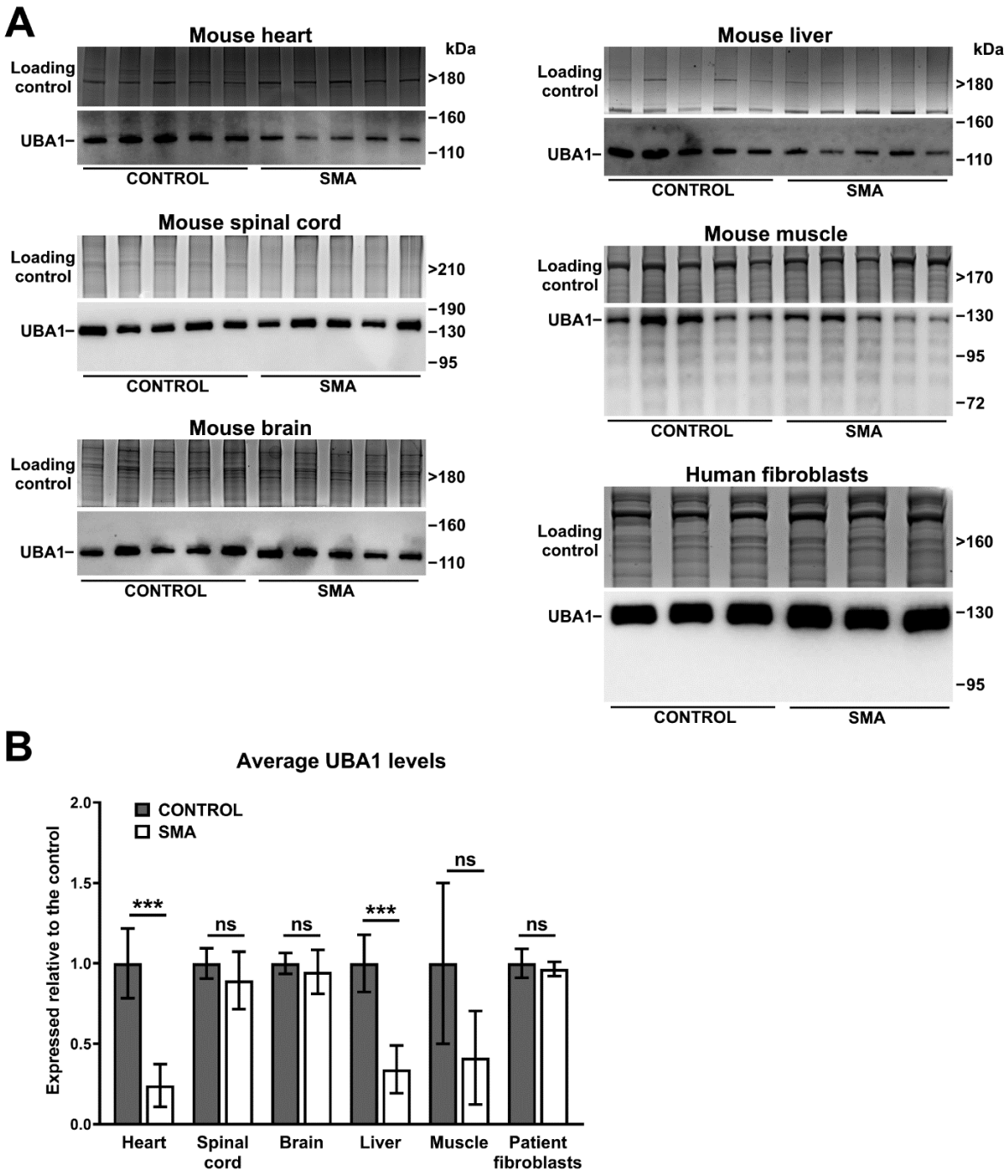

Figure 3. 4. UBA1 protein levels in tissues from late-symptomatic SMA mice (P8) and in patient fibroblast cells. (A) Representative western blots showing UBA1 levels in the heart, spinal cord, brain, liver and muscle tissue extracts from SMA mice (n=5) and age-matched healthy controls (n=5), and in SMA patient fibroblast cells (n=3) and age-matched healthy controls (n=3). Coomassie stained gel was used as internal, total protein loading control. Fibroblast cells are listed in this order from left to the right: GM00498, GM05659, GM00302, GM03813, GM09677, GM00232. **(B)** Densitometry measurements of UBA1 reactive bands were first normalised to densitometry measurements of Coomassie stained gel, after which all samples were normalised to the average of control. The graph is presented as average protein levels (expressed relative to control), with error bars showing standard deviation from the mean. ns- not significant; ***p<0.001

Widespread dysregulation of both lamin A and lamin C levels was observed in tissues from a mouse model of SMA and SMA patient fibroblasts (Figure 3.5A). A statistically significant reduction of lamin A levels was seen in SMA patient fibroblasts compared to those from healthy controls (84%, p = 0.0438), while a statistically significant upregulation of lamin A levels was found in the brain (25%, p = 0.0434), liver (52%, p = 0.0026) and heart (69%, P = 0.0007) tissue from SMA mice (Figure 3.5B). Spinal cord extracts from SMA mice did not show a significant change in lamin A expression compared to controls, but they did show a significant increase in the levels of lamin C (43%, p = 0.0078), as did the liver (42%, p = 0.0075), brain (43%, p= 0.0116) and heart (91%, P = 0.0079) (Figure 3.5B). Increased levels of lamin C in spinal cord from SMA mice are in line with proteomic studies of SMA, where increased lamin A/C expression was identified in Schwann cells from a mouse model of SMA (Aghamaleky Sarvestany *et al.*, 2014) and in SMA patient motor neurons (Fuller *et al.*, 2016). Patient fibroblast cells and skeletal muscles from SMA mice showed no significant change in lamin C expression compared to the healthy controls (Figure 3.5B). In contrast, a 45% reduction of lamin A levels in skeletal muscle extracts from SMA mice was not statistically significant, likely due to the large variability in protein expression between the samples (Figure 3.5B). This, however, is in contrast with the proteomic study of SMA where increased lamin A/C expression was identified in muscles from P5 SMA mice (Mutsaers *et al.*, 2013).

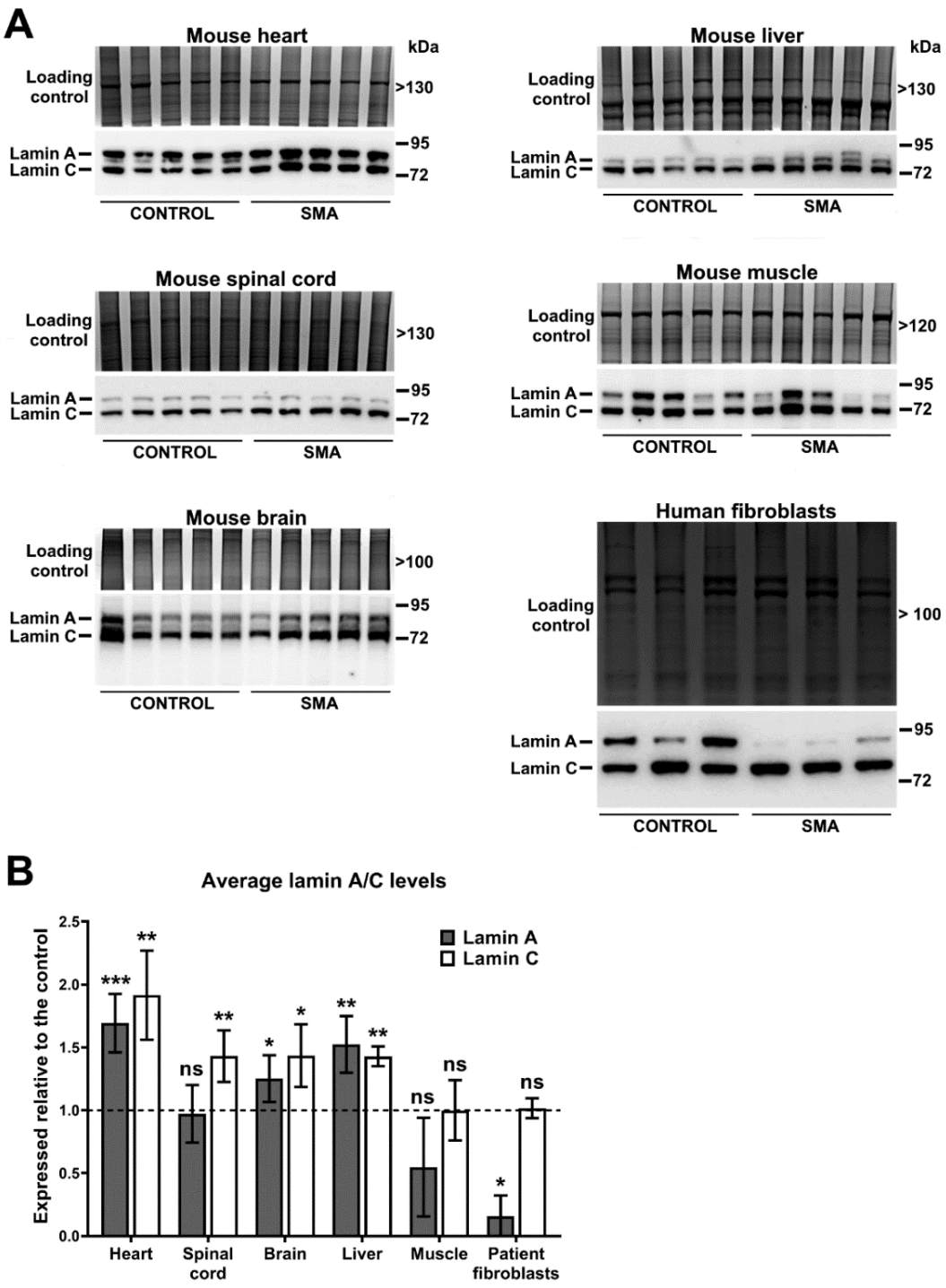

Figure 3. 5. Lamin A/C protein levels in tissues from late-symptomatic SMA mice (P8) and in patient fibroblast cells. (A) Representative western blots showing lamin A/C levels in the heart, spinal cord, brain, liver and muscle tissue extracts from SMA mice (n=5) and age-matched healthy controls (n=5), and in SMA patient fibroblast cells (n=3) and age-matched healthy controls (n=3). Coomassie stained gel was used as internal, total protein loading control. Fibroblast cells are listed in this order from left to the right: GM00498, GM05659, GM00302, GM03813, GM09677, GM00232. **(B)** Densitometry measurements of lamin A and lamin C reactive bands were first normalised to densitometry measurements of Coomassie stained gel, after which all samples were normalised to the average of control. In the liver extract, the lower band was presumed to be lamin C, and the upper two bands were presumed to be lamin A isoforms and were consequently measured together to give a single value. The graph is presented as average protein levels (expressed relative to control), with error bars showing standard deviation from the mean. The dashed line represents protein levels across healthy control tissues. ns- not significant; *p<0.05; **p<0.01; ***p<0.001

The expression of GAPDH was significantly reduced in the liver (49%, p = 0.0087) and heart (41%, p = 0.0034) tissue from SMA mice compared to age-matched healthy controls (Figure 3.6). Spinal cord, brain and muscle tissue from SMA mice, and SMA patient fibroblast cells, on the other hand, showed no significant change in GAPDH expression when compared to controls (Figure 3.6). The direction of expression change in heart and liver tissue followed the same trend as observed in proteomic studies of SMA. Once again, however, biochemical studies on mouse spinal cord and brain tissue showed different results compared to proteomic studies, where decreased GAPDH levels were identified in Schwann cells (Aghamaleky Sarvestany *et al.*, 2014) and hippocampus (Wishart *et al.*, 2010) from SMA mice.

A significant upregulation of ANXA2 levels was identified in the spinal cord from SMA mice (57%, p = 0.0119) and in fibroblast cells from SMA patients (30%, p = 0.0212) (Figure 3.7). Muscle and liver from SMA mice, on the other hand, showed a significant reduction of ANXA2 levels, 77% (p = 0.0057) and 59% (p = 0.0025) respectively. The expression of ANXA2 in the brain and heart from SMA mice was not significantly changed when compared to healthy controls (Figure 3.7). A biochemical study of spinal cord tissue showed the same trend as proteomic studies of SMA where upregulation of ANXA2 levels was identified in mouse Schwann cells (Aghamaleky Sarvestany *et al.*, 2014) and patient iPS-derived motor neurons (Fuller *et al.*, 2016). Downregulation of ANXA2 levels in muscles from SMA mice in this study is, however, in contrast with a proteomic study that showed increased ANXA2 expression in muscles from P5 SMA mice (Mutsaers *et al.*, 2013).

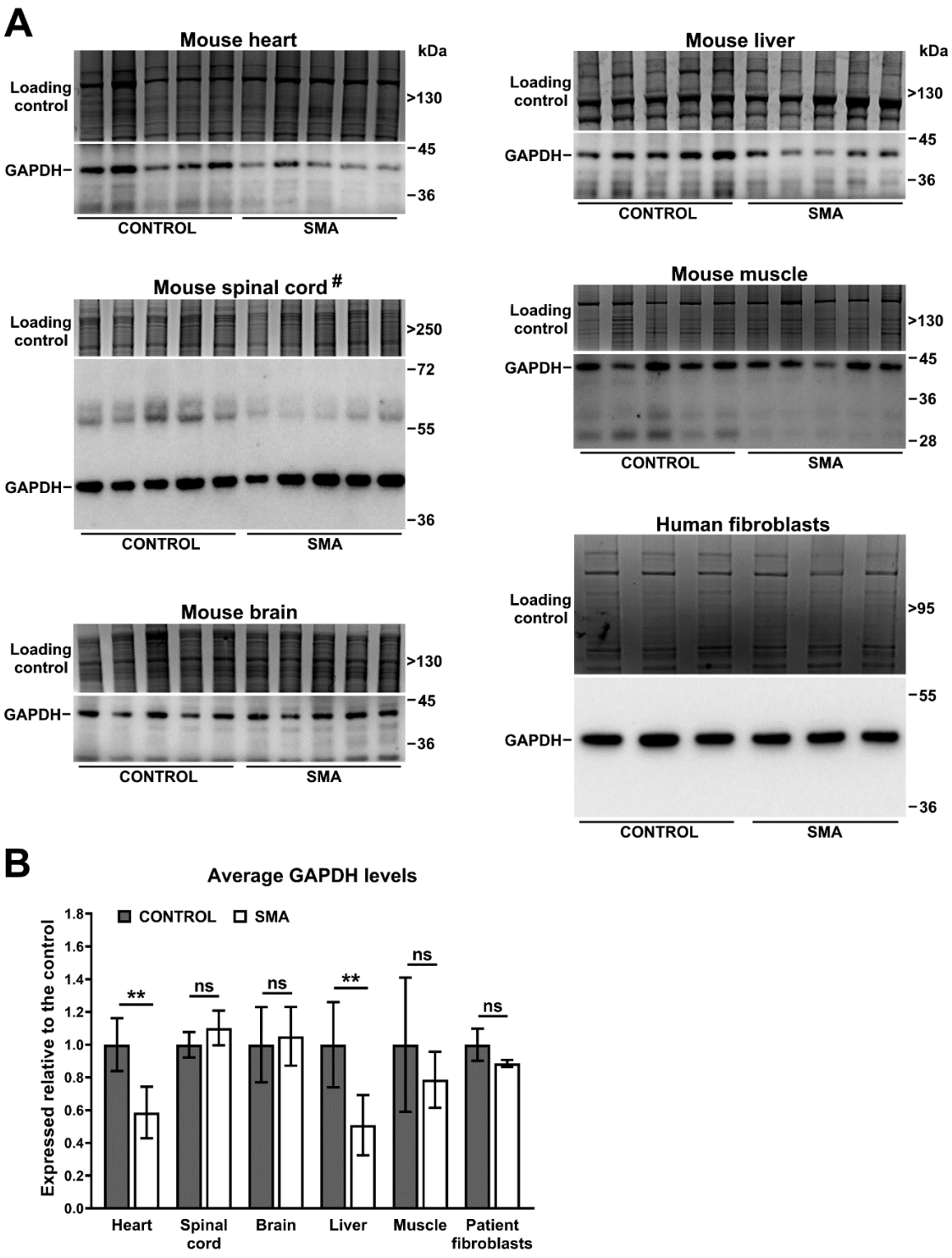

Figure 3. 6. GAPDH protein levels in tissues from late-symptomatic SMA mice (P8) and in patient fibroblast cells. A) Representative western blots showing GAPDH levels in the heart, spinal cord, brain, liver and muscle tissue extracts from SMA mice (n=5) and age-matched healthy controls (n=5), and in SMA patient fibroblast cells (n=3) and age-matched healthy controls (n=3). Coomassie stained gel was used as internal, total protein loading control. Fibroblast cells are listed in this order from left to the right: GM00498, GM05659, GM00302, GM03813, GM09677, GM00232. (#Spinal cord blot was also used in Figure 5.8). **(B)** Densitometry measurements of GAPDH reactive bands were first normalised to densitometry measurements of Coomassie stained gel, after which all samples were normalised to the average of control. The graph is presented as average protein levels (expressed relative to control), with error bars showing standard deviation from the mean. ns- not significant; **p<0.01

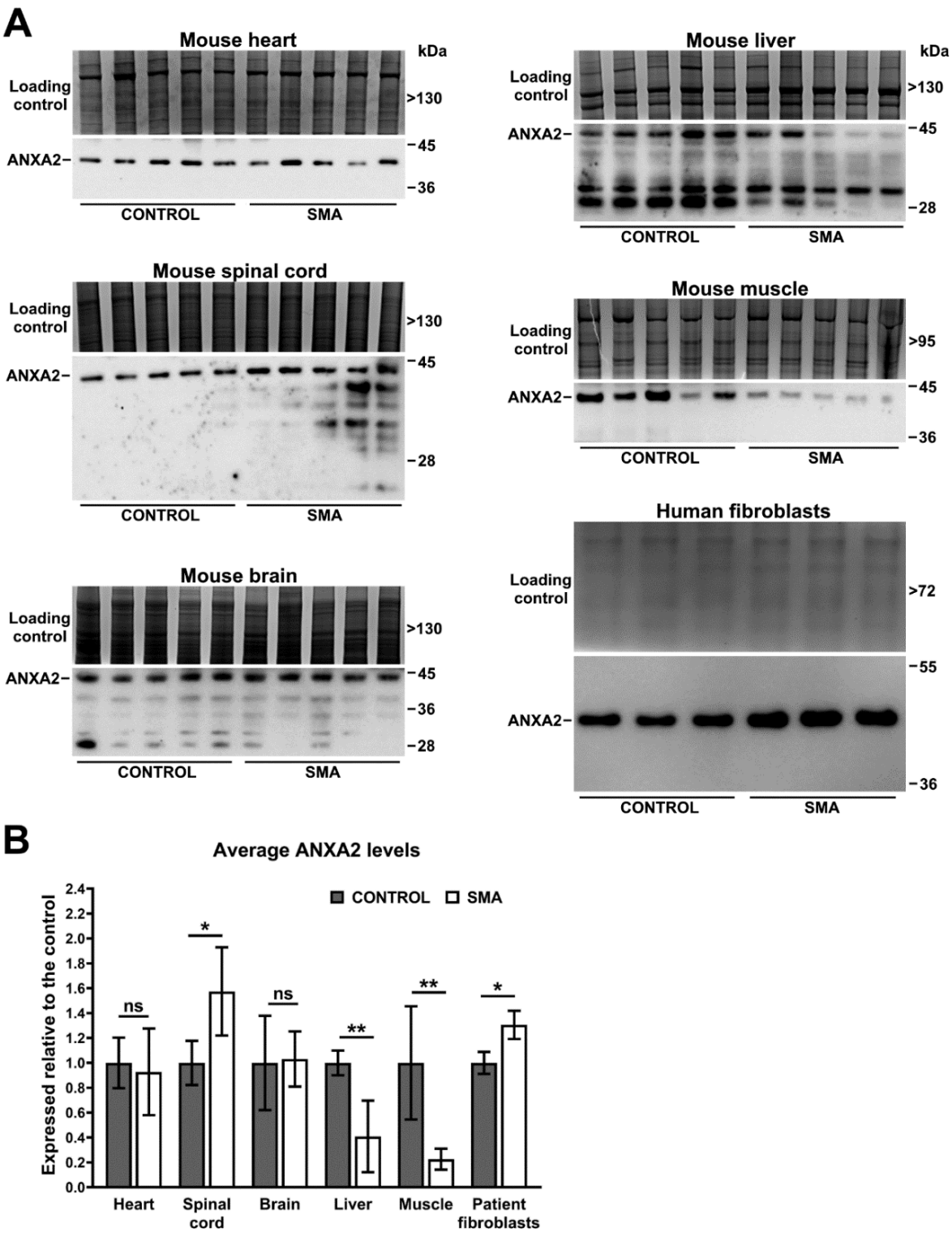

Figure 3. 7. ANXA2 protein levels in tissues from late-symptomatic SMA mice (P8) and in patient fibroblast cells. (A) Representative western blots showing ANXA2 levels in the heart, spinal cord, brain, liver and muscle tissue extracts from SMA mice (n=5) and age-matched healthy controls (n=5), and in SMA patient fibroblast cells (n=3) and age-matched healthy controls (n=3). Coomassie stained gel was used as internal, total protein loading control. Fibroblast cells are listed in this order from left to the right: GM00498, GM05659, GM00302, GM03813, GM09677, GM00232. **(B)** Densitometry measurements of ANXA2 reactive bands were first normalised to densitometry measurements of Coomassie stained gel, after which all samples were normalised to the average of control. The graph is presented as average protein levels (expressed relative to control), with error bars showing standard deviation from the mean. ns- not significant; *p<0.05; **p<0.01

GAP43[8] and NCAM[9] are almost exclusively found in neuronal tissues and so their expression levels were determined biochemically only in spinal cord and brain from a mouse model of SMA (Figure 3.8). GAP43 and NCAM expression were not significantly changed in either spinal cord or brain tissue from SMA mice compared to controls. These results are in contrast with proteomic studies of SMA, where decreased expression of both GAP43 and NCAM was identified in mouse hippocampus and patient iPSC-derived motor neurons, and decreased expression of GAPD43 was also identified in hippocampus synaptosomes from SMA mice (Fuller, Gillingwater and Wishart, 2016).

[8] https://www.proteinatlas.org/ENSG00000172020-GAP43/tissue
[9] https://www.proteinatlas.org/ENSG00000149294-NCAM1/tissue

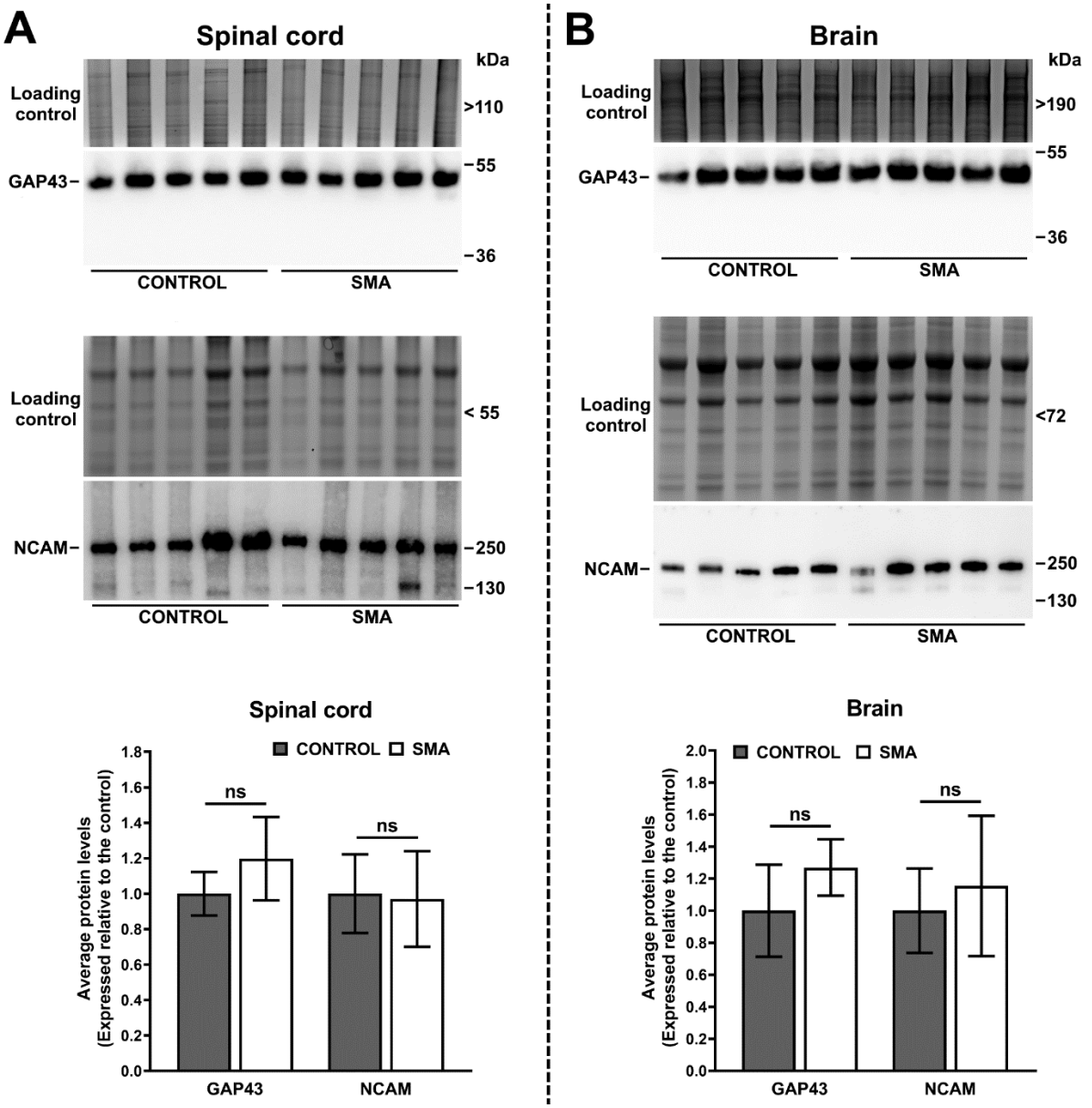

Figure 3. 8. GAP43 and NCAM protein levels in spinal cord and brain from late-symptomatic SMA mice (P8). Representative western blots showing GAP43 and NCAM levels in **(A)** spinal cord and **(B)** brain tissue extracts from SMA mice (n=5) and age-matched healthy controls (n=5). Coomassie stained gel was used as internal, total protein loading control. Densitometry measurements of GAP43 and NCAM reactive bands were first normalised to densitometry measurements of Coomassie stained gel, after which all samples were normalised to the average of control. Graphs are presented as average protein levels (expressed relative to control), with error bars showing standard deviation from the mean. ns- not significant

In summary, quantitative western blot analyses of SMA mouse tissues and SMA patient fibroblasts identified widespread dysregulation of SMN, UBA1, lamin A/C, GAPDH and ANXA2 expression levels, where the direction of expression change varied depending on the tissue examined (Table 3.4). As expected, SMN levels were decreased in all cells/tissues examined, while a reduction of UBA1 levels was identified in the heart and liver tissue from SMA mice. Lamin A and/or C expression was increased in all tissues from a mouse model of SMA, except in skeletal muscles, while patient fibroblasts showed decreased expression of lamin A isoform only. SMA mouse heart and liver tissue showed reduction of GAPDH levels, while ANXA2 expression was significantly reduced in the liver and muscle tissue from SMA mice. SMA mouse spinal cord and patient fibroblast cells, on the other hand, showed upregulation of ANXA2 levels. No obvious link between the pattern of UBA1, lamin A/C, GAPDH or ANXA2 expression change and the level of SMN reduction was observed in SMA tissues.

Table 3. 4. Overview of protein levels in tissues from a mouse model of SMA and in SMA patient fibroblasts

Protein	Mouse					Patient fibroblasts	Proteomic studies
	Heart	Spinal cord	Brain	Liver	Muscle		
SMN	-92%	-88%	-91%	-94%	-94%	-71%	NA
UBA1	-76%	-11%	-5%	-66%	-59%	-3%	↓
LAMIN A	+69%	-3%	+25%	+52%	-45%	-84%	↑
LAMIN C	+92%	+43%	+43%	+43%	-1%	+2%	↑
GAPDH	-41%	+10%	+5%	-49%	-21%	-11%	↓
ANXA2	-7%	+57%	+3%	-59%	-77%	+31%	↑
GAP43	/	+20%	+30%	/	/	/	↓
NCAM	/	-3%	+15%	/	/	/	↓

SMN, UBA1, LAMIN A/C, GAPDH, ANXA2, GAP43 and NCAM levels in the heart, spinal cord, brain, liver and muscle tissue from SMA mice, and in SMA patient fibroblast cells, as identified by western blotting. The results are expressed as average percent reduction (-) or increase (+) of protein expression in SMA samples relative to the control. The last column indicates direction of differential expression that was identified in proteomic studies of SMA. The direction of differential expression is indicated by an arrow, ↓ (downregulated) and ↑ (upregulated). /- protein expression was not studied biochemically in this sample; NA- not applicable

3.2.3. *In vitro* drug screening studies in control and SMA patient fibroblast cells

The widespread dysregulation of UBA1, lamin A/C, GAPDH and ANXA2 levels across a range of SMA tissues and cells indicated that these proteins might have a role in SMA disease pathways. Alongside SMN, restoration of UBA1, lamin A/C, GAPDH or ANXA2 expression to the levels observed in control healthy tissues might represent an attractive therapeutic approach in SMA, and so it was of interest to next identify drugs that have the potential to manipulate the expression of these proteins. Of specific interest were drugs that have the potential to target several of these proteins simultaneously as they might achieve greater therapeutic benefit compared to drugs that target individual proteins. Indeed, this was already demonstrated in a mouse model of SMA where a combination of two therapeutic strategies, aimed at increasing the levels of SMN protein and decreasing the levels of modifying factor neurocalcin

delta (NCALD), showed better results in improving neuromuscular pathology compared to SMN-targeted therapy alone (Torres-Benito *et al.*, 2019).

3.2.3.1. Selection of an appropriate experimental technique for protein expression measurements

In vitro drug screening studies were performed in fibroblast cells from SMA patients and healthy controls, where the main outcome was the ability of the drug to restore the expression of proteins of interest to the levels observed in control cells. First, however, an appropriate experimental technique, that would enable quick, accurate and sensitive protein expression measurements, had to be determined to ensure the maximum efficiency of drug screening studies. Several approaches are available for protein expression measurements including, for example, western blotting, dot blot and ELISA (Salazar-Anton, Tellez and Lindh, 2012). Western blotting was used throughout this study to measure differences in protein expression between control and SMA samples, and so it was used here as a reference to establish accuracy and sensitivity of the other two methods.

SMA and control cell extracts were first normalised to total protein, to ensure that an equal amount of starting material was loaded in each experiment. Cell extracts were prepared in triplicates in serial dilutions to establish the accuracy and sensitivity of protein expression measurements (the workflow is presented in Figure 3.9). Accuracy was determined by measuring protein levels across serial dilutions in one sample and calculating the R-squared (R^2) value. R^2 describes the linear relationship between two variables, where the value of 1 represents perfect linear relationship, and 0 describes no linear relationship between variables (Schneider, Hommel and Blettner, 2010). Sensitivity was measured by quantifying protein levels in SMA cells relative to control in all consecutive dilutions, and comparing them

to western blot analysis. This was done to determine the concentration range within which the difference in protein expression between control and SMA samples can be accurately measured.

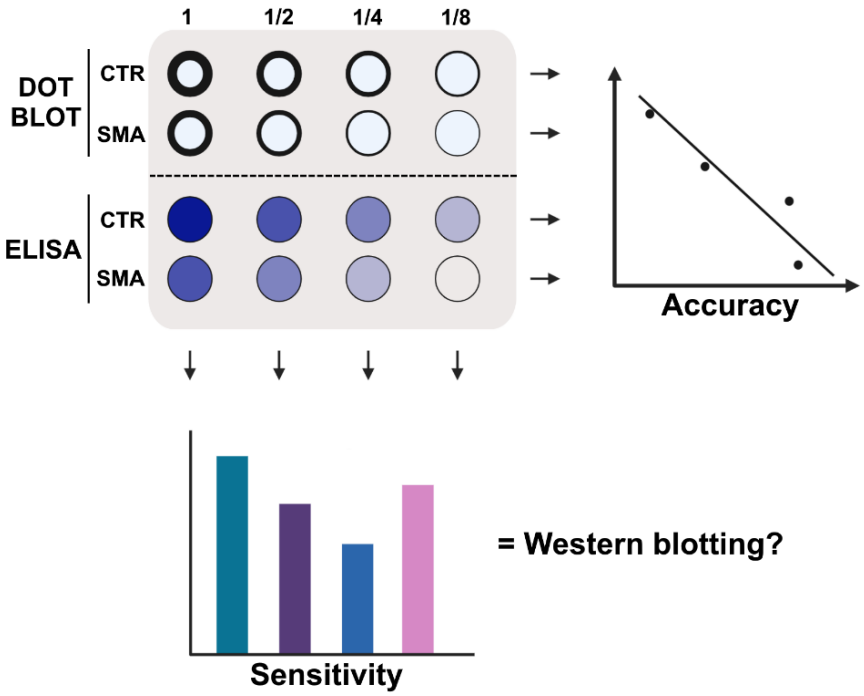

Figure 3. 9. Workflow of dot blot and ELISA. Linear correlation between protein levels and serial dilutions determines the accuracy of the method. Sensitivity is determined by comparing the relative SMN levels in SMA tissues (across different dilutions) to the results of western blot analysis.

3.2.3.1.1. Dot blot analysis showed good accuracy and sensitivity for measurements of SMN expression in patient fibroblasts, but failed to detect a change in lamin A levels

Dot blotting is an immuno-associated technique were protein extracts are loaded directly on the nitrocellulose membrane, and the membrane is developed in the same way that a regular western blotting would be (Salazar-Anton, Tellez and Lindh, 2012). Protein levels are visualised as dots and densitometry measurements are performed using Image J software (as described in chapter 2, section 2.3.4). The dot blot approach was first tested on SMN as one of the primary targets in therapy design. Three SMN antibodies, MANSMA12 2E6, MANSMA2 8F7 and MANSMA3 8E1, raised against different SMN epitopes (Young *et al.*, 2000), were used for

dot blot analyses on control (GM05659) and patient (GM00232) fibroblasts (Figure 3.10). This was done to determine whether this method is reliable and reproducible when different antibodies are used. Nitrocellulose membranes developed with MANSMA12 and MANSMA2 antibodies showed a clear SMN signal (Figure 3.10A and 3.10B). MANSMA3, on the other hand, produced a weak SMN signal and strong background (Figure 3.10C), indicating that the antibody is perhaps not suitable for dot blot analysis. This would make quantification unreliable, and so SMN levels were not measured on dot blot developed with MANSMA3 antibody.

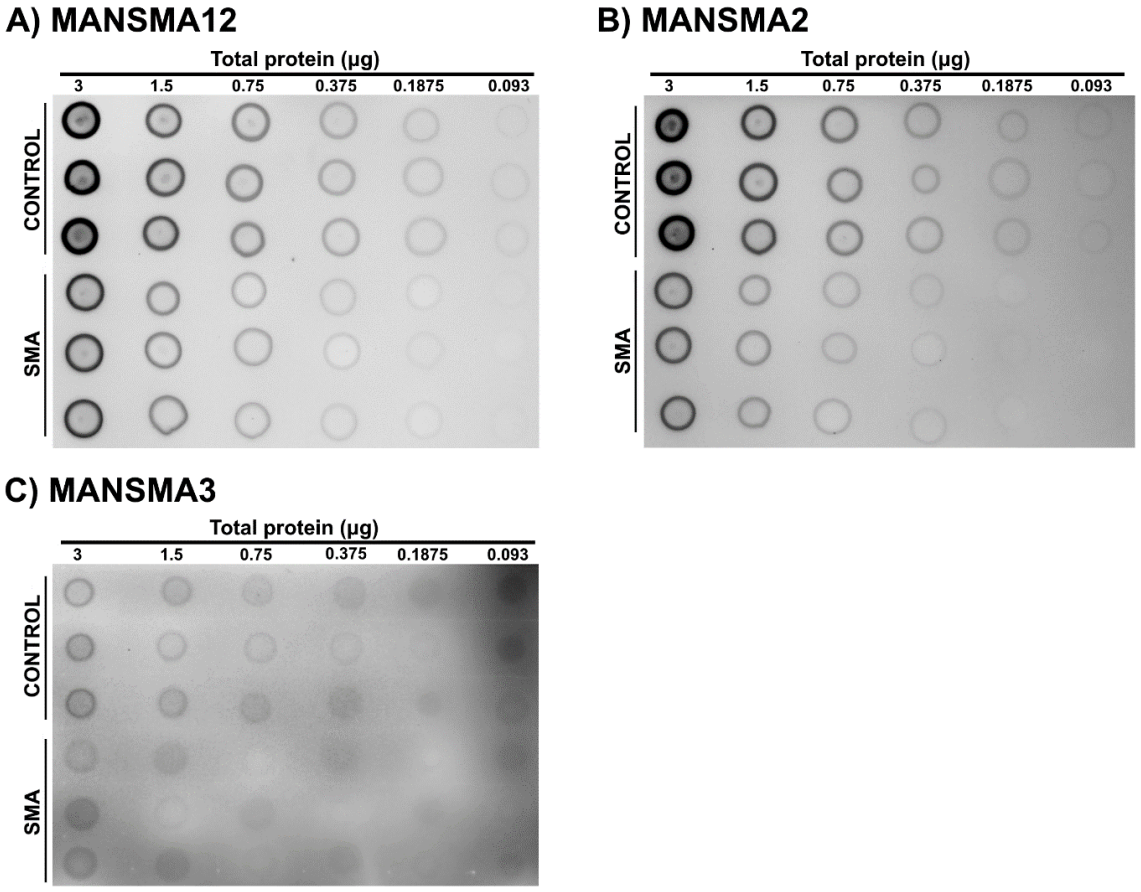

Figure 3. 10. SMN protein levels in control (GM5659) and patient (GM00232) fibroblast cells, following dot blot analyses. Membranes were developed with three SMN antibodies **(A)** MANSMA12 2E6, **(B)** MANSMA2 8F7 and **(C)** MANSMA3 8E1. Control and SMA cell extracts were analysed in triplicates in six serial dilutions (expressed as µg of total protein).

Membranes developed with MANSMA12 and MANSMA2 were then analysed as described in Figure 3.9, taking into account seven exposure times, including three below and three above the automatic exposure. (The length of automatic exposure is determined by the number of saturated pixels within the imaging software, and represents the optimal exposure time). Different exposure times were analysed to account for variability introduced during image acquisition. Analyses identified R^2 values between 0.99 and 0.94 for all exposure times in both control (Figure 3.11A) and SMA (Figure 3.11B) samples, and for both antibodies, indicating a good linear relationship between the data. In control samples, however, a decrease in R^2 value was identified in longer exposure times with both antibodies (Figure 3.11A), indicating that overexpression of pixels can decrease the accuracy of measurements. This trend was not observed in SMA samples (Figure 3.11B), likely because SMN signal is weaker compared to control, and pixels are less likely to be overexpressed with longer exposure time.

Quantification of SMN levels in SMA cells compared to controls, with both antibodies, showed variable results for different dilutions (Figure 3.11C). When compared to results from western blot analysis, where average SMN levels across three SMA cells were at approximately 30% compared to controls (Figure 3.3), MANSMA12 antibody produced similar results in a range between 0.75-0.1875 µg of total protein, where SMN levels were at 41.3%, 39.6% and 37.8%, across all exposure times (Figure 3.11C). MANSMA2 on the other hand showed comparable results to western blotting in a range between 1.5-0.375 µg of total protein, with SMN levels being at 33%, 34% and 38.4% in SMA cells across all exposure times (Figure 3.11C). Quantification was unreliable for the highest (3 µg) and the lowest (0.093 µg) concentration (with both antibodies, and across all exposure times), where SMN levels in SMA cells were at about 50% to those observed in control cells, or higher (Figure 3.11C). These results suggest that the sensitivity range for dot blot analysis is between 1.5 and 0.1875 µg of total protein.

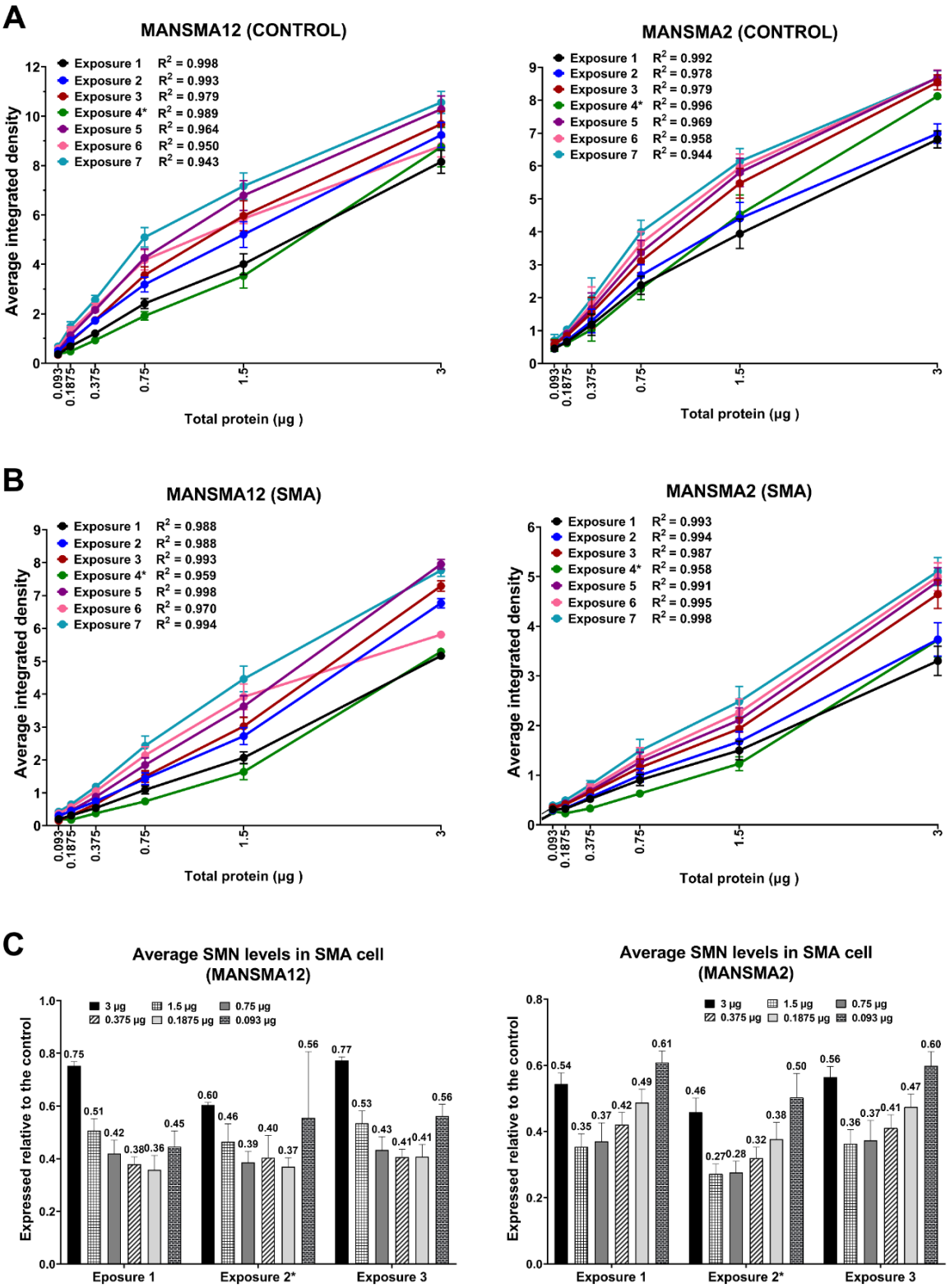

Figure 3. 11. Dot blot analyses of SMN protein levels in control (GM5659) and patient (GM00232) fibroblast extracts. Correlation between serial dilutions (expressed as µg of total protein) and average SMN levels in **(A)** control and **(B)** SMA fibroblast extracts using MANSMA12 and MANSMA2 antibodies. R-squared (R^2) was calculated for each exposure time (n = 7) to determine the strength of linear correlation. **(C)** Average levels of SMN in patient fibroblasts (expressed relative to the control), in three different exposure times. Numbers above the bars indicate relative SMN levels in SMA cells across different dilutions. *Exposure 4 in panels A) and B), and exposure 2 in panel C) indicate automatic exposure.

The same approach was then used to determine the accuracy and sensitivity of lamin A/C expression measurements in control (GM05659) and patient (GM00232) fibroblasts. Lamin A/C protein levels were dysregulated across a range of SMA tissues and cells (Figure 3.5), indicating that it may be involved in SMA disease pathways. Because of this it became one of the primary targets of *in vitro* drug screening studies, and so it was important to know whether a dot blot approach can be used for measurements of lamin A/C levels. For this, a membrane was developed with anti-lamin A/C antibody (MANLAC1 4A7) (Figure 3.12A) that had been used previously for western blot analysis (Figure 3.5). Weaker linear correlation between lamin A/C expression and serial dilutions was observed in both control and SMA samples, 0.95 and 0.889 respectively (Figure 3.12B). This is likely caused by weak lamin A/C signal in lower concentration range that made quantification unreliable (Figure 3.12A), and so other exposure times were not examined here. In contrast to western blot analysis (Figure 3.5), lamin A/C levels were not significantly changed in SMA samples compared to control in dot blot analysis (Figure 3.12C). This could be explained by the fact that only lamin A isoform showed differential expression in SMA patient fibroblasts using western blotting (Figure 3.5), and so in dot blot analysis changes in lamin A expression could have been masked by unchanged levels of lamin C. To test this hypothesis, an antibody that recognises only lamin A isoform was used for dot blot analysis in control (GM00302) and patient (GM00232) fibroblasts (Figure 3.12D). Once again, quantification of lamin A levels in the lower concentration range was unreliable in control fibroblasts, which skewed linear correlation ($R^2 = 0.96$) between lamin A expression and serial dilutions (Figure 3.12E). In addition, lamin A expression showed no significant change in SMA patient fibroblasts compared to controls (Figure 3.12F). Although the same amount of total protein was initially loaded based on the results from protein assay, differences in loading between control and SMA samples could still be plausible. Since it is not

possible to check the loading in dot blot analyses, it makes it the biggest limitation of this approach.

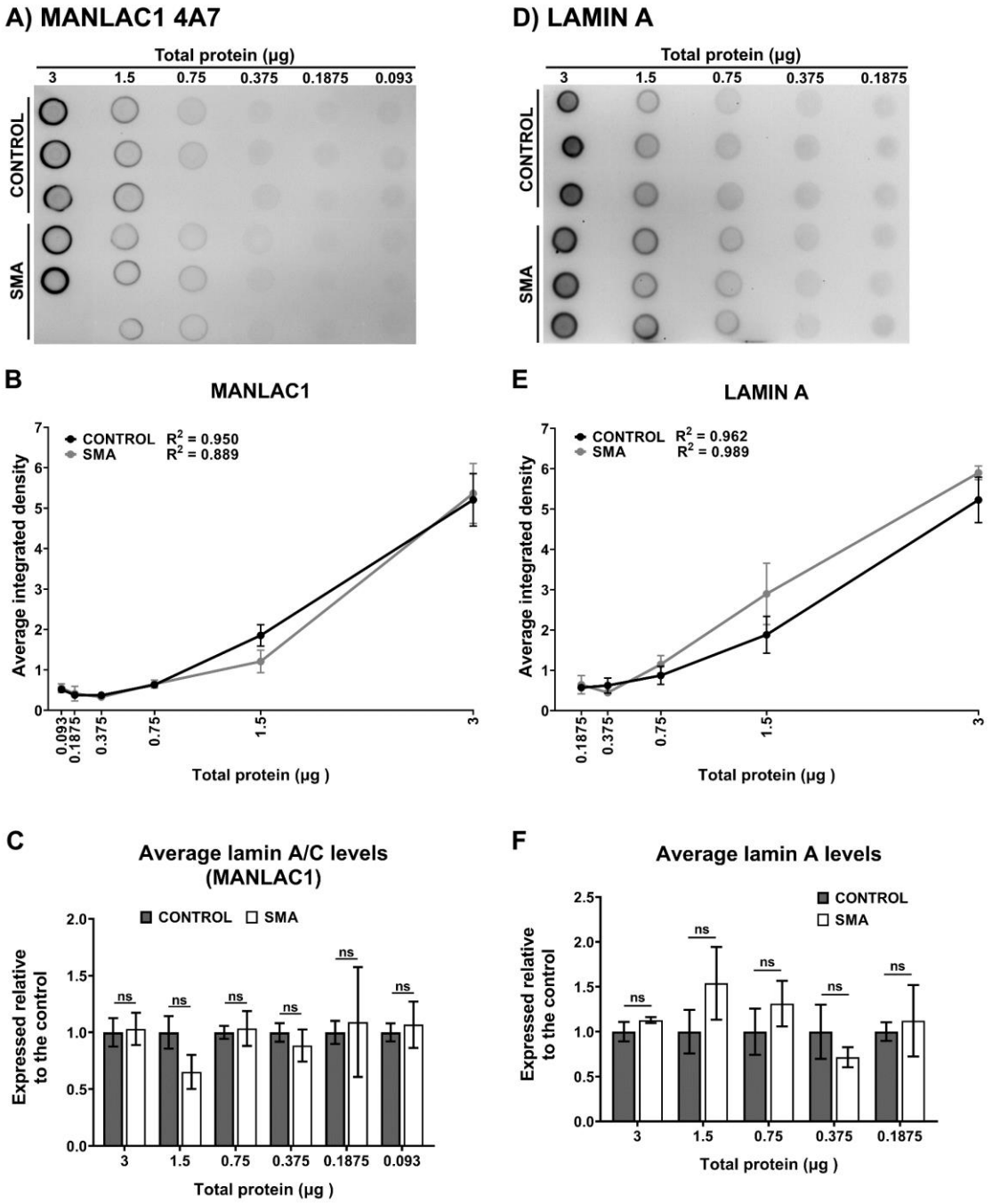

Figure 3. 12. Dot blot analysis of lamin A/C protein levels in SMA patient and control fibroblast extracts. (A) Lamin A/C (MANLAC1 4A7) and **(D)** lamin A levels in control and patient fibroblast extracts across serial dilutions (expressed as µg of total protein). Control and SMA cell extracts were analysed in triplicates. **(B, E)** Correlation between serial dilutions and average lamin A/C and lamin A levels in control and SMA cells. R-squared (R^2) represents strength of linear correlation. **(C, F)** Average levels of lamin A/C and lamin A in control and patient fibroblasts (expressed relative to the control) across serial dilutions. Ns- not significant

3.2.3.1.2. Lamin A was not identified in control and patient fibroblasts using enzyme-linked immunosorbent assay (ELISA)

Since dot blot analysis did not show good sensitivity for measurement of lamin A/C levels, a lamin A specific antibody was next used to test the accuracy and sensitivity of ELISA approach as described above (Figure 3.9). Control and SMA cell extracts were analysed in triplicates, in seven serial dilutions. The analysis, however, did not produce any visible signal, and so the absorbance of wells was not measured on the plate reader.

To summarize, the dot blot approach showed good accuracy and sensitivity for quantification of SMN levels in SMA patient fibroblasts, however, it was not sensitive enough to detect changes in expression of lamin A specific isoform. Examination of lamin A levels, using indirect ELISA, produced no results, which is likely the consequence of technical problems with the antibody. This then means that other antibodies, that can detect lamin A and lamin C specific isoforms, would have to be tested for dot blot and ELISA analyses. Western blotting, on the other hand, is an established method in this laboratory and was shown to be a reliable method for measurements of protein expression across different sample types (Eaton *et al.*, 2013). Western blotting was therefore chosen for verification of protein expression in drug screening studies.

3.2.3.2. Network pharmacology identified 20 new drugs that have the potential to change the expression of at least two protein targets

Selection of candidate therapeutics that have the potential to target multiple proteins of interest can be challenging and demands application of systemic approach such as the network pharmacology. Network pharmacology uses different resources, such as omics datasets and publicly available databases, and computational techniques to study interactions between drugs and complex biological systems (Azuaje, 2013). These analyses are used to generate prediction models that can facilitate understanding of drug action and its impact on biological system. This knowledge is clinically translational, and it can be used, for example, for identification of new therapeutic compounds or optimisation of existing treatments (Azuaje, 2013). Casas et *al.*, for example, used network pharmacology to identify additional therapeutic targets in ischemic stroke, and this was confirmed experimentally (Casas *et al.*, 2019). Combined inhibition of NADPH oxidase (NOX), primary therapeutic target in ischemic stroke, and nitric oxide synthase (NOS), newly identified therapeutic target, enhanced the efficiency of the treatment, which was evident by reduced cell death, reduced infarct size and preserved neuromotor function in a mouse model of ischemic stroke (Casas *et al.*, 2019). In another study, network pharmacology was applied to the develop new algorithm that can be used to predict adverse effects for both clinically approved drugs and new compounds (Gottlieb *et al.*, 2011). By examining inflammatory bowel disease (IBD) gene expression datasets, Dudley et *al.* identified topiramate, an anticonvulsant drug used in epilepsy, as a potential compound that could be repurposed for the treatment of IBD (Dudley *et al.*, 2011). Therapeutic benefit of topiramate was demonstrated *in vivo,* in rodent model of IBD, where topiramate treated mice exhibited improved pathology, including reduced swelling and ulceration, and decreased gross inflammation compared to untreated controls (Dudley *et al.*,

2011). All of these examples show that network pharmacology has real clinical applications, and can be used to guide development of safer and more efficient therapeutic approaches.

Here, network pharmacology approach was used to identify new drugs that could potentially be repurposed for SMA. Drug repurposing is an attractive approach in therapy design because drugs tested in clinical trials have established pharmacokinetic and pharmacodynamic profiles (Durães, Pinto and Sousa, 2018), which significantly reduces the costs and the time of a drug design compared to development of new compounds (Durães, Pinto and Sousa, 2018). This is extremely important in SMA therapy design due to high cost and differential effects of available drugs (Hoolachan, Sutton and Bowerman, 2019). Upstream regulators of eight protein targets, SMN, lamin A/C, UBA1, GAPDH, ANXA2, GAP43, NCAM and COL6A3, identified in a multi-study comparison of published proteomic studies and investigated biochemically here, were analysed using a trial version of Ingenuity Pathway Analysis (IPA) software. The analysis identified 78 upstream regulators that have a known mechanism of action on at least two proteins (data not shown), meaning they were shown to alter the expression/ activity of molecules at the gene and/or protein level. Of these, 20 upstream regulators were chemical or biological drugs (Table 3.5) that were taken into consideration for *in vitro* drug studies in fibroblast cells. The priority was given to compounds that are safe and tolerable in clinical use, and commercially available for a reasonable price, as this would facilitate translation of the treatment into clinic. After removal of drugs that show high toxicity, i.e. those that are used in the treatment of different cancers like cisplatin [10], the list was reduced to nine candidates, including trichostatin A, dexamethasone, sirolimus, valproic acid, calcitriol, agn194204,

[10] https://www.cancerresearchuk.org/about-cancer/cancer-in-general/treatment/cancer-drugs/drugs/cisplatin

curcumin, desmopressin and lovastatin. To further reduce the number of potential candidate drugs, drugs that were identified with only two downstream targets, including curcumin, desmopressin and lovastatin were excluded from the list. Of the six remaining drugs, dexamethasone induced neurodegeneration in the brain of rat pups (Feng *et al.*, 2009) which makes it unsuitable for SMA infants and young children, and sirolimus treatment decreased the lifespan of SMA and ALS mice compared to untreated animals (Custer and Androphy, 2014). Histone deacetylase inhibitor valproic acid (VPA) was already tested in clinical trials on type I, II and III SMA patients, but showed limited benefit in improving muscle strength and motor function in SMA patients (Swoboda *et al.*, 2010; Darbar *et al.*, 2011; Kissel *et al.*, 2011, 2014). This left three potential candidates: trichostatin A, calcitriol and agn194204, of which trichostatin A was associated with five protein targets, COL6A3, GAP43, LMNA, NCAM1, SMN, and was therefore chosen as first candidate for *in vitro* drug studies.

Table 3. 5. Upstream regulators of eight protein targets

Upstream regulator	Molecule type	p-value of the overlap	Activation Z-score	Protein targets
Cisplatin	chemical drug	3.02E-06	1.503	ANXA2, GAP43, LMNA, NCAM1, SMN1/SMN2
Decitabine	chemical drug	3.36E-06	0.447	ANXA2, COL6A3, GAP43, NCAM1, UBA1
Trichostatin A	chemical drug	5.64E-06	-1.397	COL6A3, GAP43, LMNA, NCAM1, SMN1/SMN2
Dexamethasone	chemical drug	4.35E-03	1.111	GAP43, GAPDH, NCAM1, SMN1/SMN2
Sirolimus	chemical drug	2.40E-05	-0.218	GAP43, LMNA, NCAM1, UBA1
Valproic acid	chemical drug	5.45E-04		GAP43, NCAM1, SMN1/SMN2
Calcitriol	chemical drug	9.00E-04		ANXA2, GAPDH, NCAM1
Agn194204	chemical drug	2.31E-05		ANXA2, GAPDH, LMNA
5-fluorouracil	chemical drug	9.16E-05		ANXA2, GAP43, GAPDH
Methotrexate	chemical drug	0.00333		GAP43, GAPDH
Tamoxifen	chemical drug	0.00458		GAP43, GAPDH
Tazemetostat	chemical drug	0.00496		GAP43, NCAM1
Curcumin	chemical drug	0.00704		NCAM1, SMN1/SMN2
Doxorubicin	chemical drug	0.0101		ANXA2, NCAM1
Methylprednisolone	chemical drug	0.0152		ANXA2, SMN1/SMN2
Camptothecin	chemical drug	0.0195		ANXA2, GAPDH
Vincristine	chemical drug	0.000121		GAP43, NCAM1
Oxaliplatin	chemical drug	0.000199		ANXA2, GAP43
Desmopressin	biologic drug	0.000495		GAPDH, LMNA
Lovastatin	chemical drug	0.00118		GAP43, LMNA

Upstream regulators of eight protein targets are listed in the table (only upstream regulators that are known to act on at least two proteins are shown). Only chemical and biological drugs are presented, together with the p-value of the overlap and activation Z-score. Overlap p-value is used to identify likely upstream regulators based on significant overlap between dataset genes/proteins and known targets regulated by upstream regulator. Activation Z-score gives a prediction of whether the upstream regulator is activated (positive value) or inhibited (negative value) based on the direction of expression change in the input dataset. Z-score of ≥2 represents the prediction of activation, while Z-score ≤ -2 represents the prediction of inhibition.

3.2.3.2.1. Trichostatin A does not significantly change SMN and lamin A/C levels

Trichostatin A (TSA) is an antifungal antibiotic and selective histone deacetylase inhibitor that showed promising anti-cancer activity in different cancer subtypes (Lernoux *et al.*, 2018), and the beneficial effect of TSA was already demonstrated in SMA (Avila *et al.*, 2007; Liu *et al.*, 2014). For example, TSA treatment increased the levels of SMN mRNA in SMA patient fibroblasts, and increased SMN mRNA and protein levels in the brain, spinal cord and liver tissue from a severe mouse model of SMA ($Smn^{-/-}SMN2^{+/+}SMN\Delta7^{+/+}$)**.** In addition, TSA treatment attenuated weight loss, improved neuromuscular pathology and increased survival in severe SMA mice (Avila *et al.*, 2007). An SMN-independent beneficial effect of TSA was also demonstrated in intermediate mouse model of SMA ($Smn^{2B/-}$) (Liu *et al.*, 2014). Embryonic fibroblasts and myoblasts, and brain, spinal cord, muscle, heart and liver tissue from $Smn^{2B/-}$ mice showed no significant change in SMN protein levels following TSA treatment, however, improved neuromuscular pathology and survival were identified in $Smn^{2B/-}$ mice (Liu *et al.*, 2014). This would then suggest that TSA also has an SMN-independent mechanism of action, possibly through regulation of lamin A/C levels (Table 3.5). Indeed, increase in lamin A/C expression was previously observed in TSA-treated fibroblasts from Hutchinson-Gilford progeria syndrome (HGPS) patients and healthy controls (Columbaro *et al.*, 2005) and in mouse embryonic fibroblasts (MEFs) (Galiová *et al.*, 2008).

Here, SMN and lamin A/C protein expression was first studied in control (GM00498) and SMA (GM09677) fibroblasts treated with 50 nM and 100 nM TSA for four hours (Figure 3.13C and 3.13D) to determine whether TSA has the ability to regulate their expression *in vitro*. Justification for that comes from *in vitro* study on SMA patient fibroblasts, where a maximum increase in SMN mRNA levels was observed four to five hours following exposure to 50 nM

TSA (Avila *et al.*, 2007), and so it was of interest to see whether this translates to protein level. In addition to SMN and lamin A/C, UBA1 levels were also examined in TSA treated cells (Figure 3.13C and 3.13D). The role for UBA1 in SMA disease pathways was well characterised across different models of SMA (Wishart *et al.*, 2014; Powis *et al.*, 2016; Shorrock *et al.*, 2018), which makes it one of the primary targets of non-SMN therapeutic approaches. Cell viability was around 90% in all treatment groups, in both control and SMA fibroblast cells (Figure 3.13A and 3.13B), meaning the treatment was well tolerated. Quantitative analyses, using western blotting, did not identify a statistically significant difference in SMN, lamin A, lamin C or UBA1 expression following trichostatin treatment in control fibroblasts (Figure 3.13E). In SMA fibroblasts, SMN and lamin A/C levels were not significantly changed in TSA treated group, while the levels of UBA1 were significantly decreased in vehicle, 50 nM and 100 nM TSA treated group for 30% ($p = 0.0382$), 37% ($p = 0.0166$) and 38% ($p = 0.0168$) respectively (Figure 3.13F). Significant reduction of UBA1 levels in the vehicle group suggested that vehicle (DMSO) might be responsible for changes in UBA1 expression in all treatment groups. However, technical problems, such as the variable efficiency of protein transfer onto the nitrocellulose membrane and unreliable quantification of UBA1 levels caused by low signal intensity, are also possible and should be considered when interpreting the results.

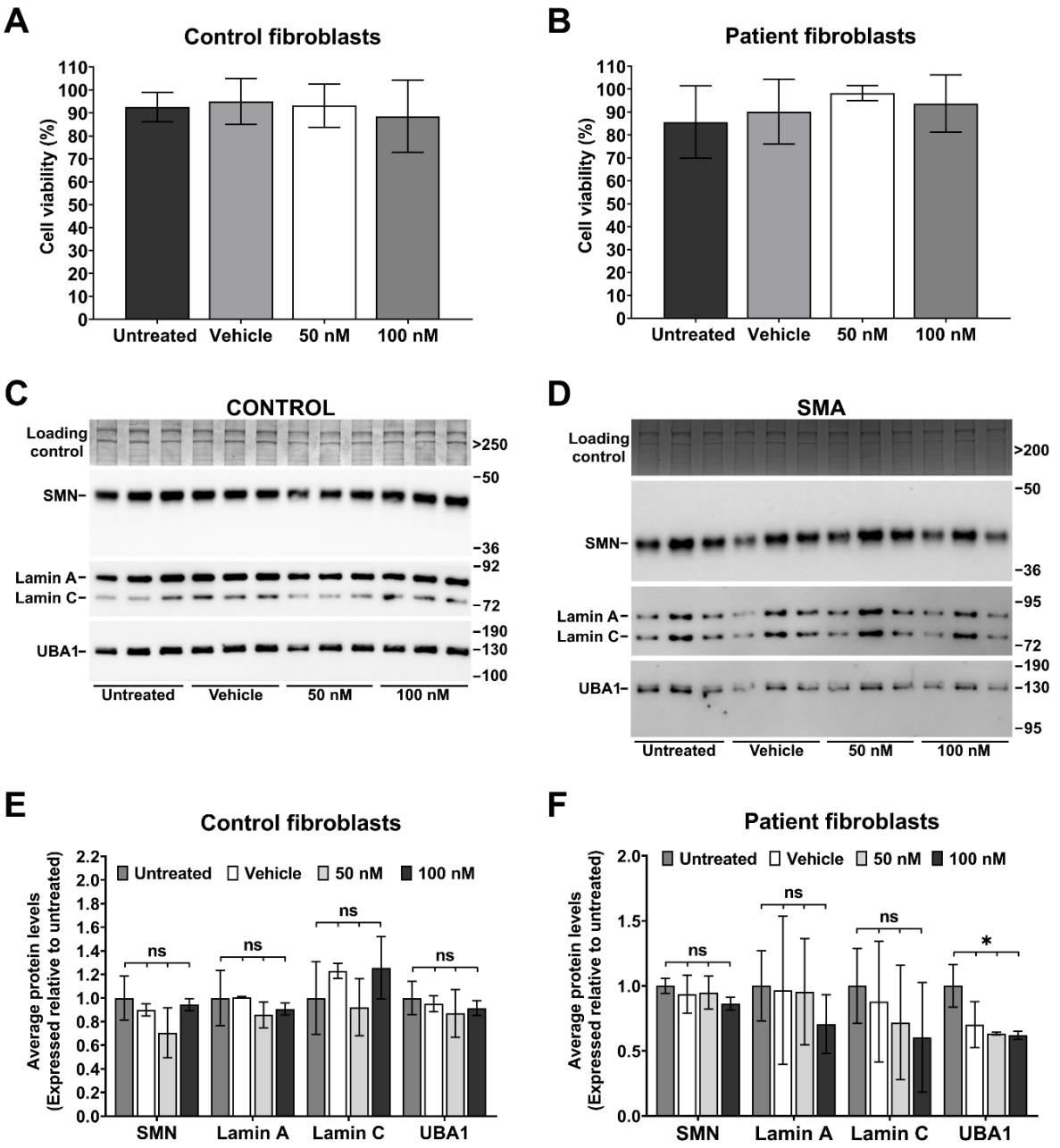

Figure 3. 13. SMN, lamin A/C and UBA1 protein levels in control and patient fibroblasts treated with trichostatin A (TSA). Cell viability in **(A)** control and **(B)** patient fibroblasts treated with 50 nM and 100 nM TSA for four hours. Two technical replicates were used in each group: untreated (media only), vehicle (DMSO) and TSA (50 nM and 100 nM). Graphs are presented as average cell viability, with error bars showing standard deviation from the mean. Representative western blots showing SMN, lamin A/C and UBA1 levels in **(C)** control and **(D)** patient fibroblasts treated with 50 nM and 100 nM TSA. Three technical replicates were used in each group: untreated (media only), vehicle (DMSO) and TSA (50 nM and 100 nM). Coomassie stained gel was used as internal, total protein loading control. Quantification of SMN, lamin A/C and UBA1 levels in **(E)** control and **(F)** patient fibroblasts. Densitometry measurements of SMN, lamin A, lamin C and UBA1 reactive bands were first normalised to densitometry measurements of Coomassie stained gel, after which all samples were normalised to the average of untreated. Graphs are presented as average protein levels (expressed relative to untreated), with error bars showing standard deviation from the mean. TSA- trichostatin A; ns- not significant; *$p \leq 0.05$.

It is possible that a four-hour treatment is not sufficient to induce changes in SMN or lamin A/C protein levels. For example, HGSP patient fibroblasts (Columbaro *et al.*, 2005) and MEFs (Galiová *et al.*, 2008) showed increased levels of lamin A/C after a 24-hour exposure to TSA. It was therefore important to investigate whether longer treatment could change the expression of proteins of interest. SMA fibroblasts were next exposed to 25 nM, 50 nM and 100 nM of TSA for 8-, 16- and 24 hours to examine the expression of SMN, lamin A/C and UBA1 (Figure 3.14B, 3.14C and 3.14D). Cell viability was between 95% and 100% in all groups and across all three time points (Figure 3.14A). SMN, lamin A and lamin C did not show a significant change in expression after 8, 16 and 24-hour exposure to TSA in any concentration examined (Figure 3.14E, 3.14F and 3.14G). UBA1 expression was not significantly changed after 16- and 24-hour exposure to TSA, however, a significant reduction of UBA1 levels (22%, $p = 0.0328$) (Figure 3.14E) was identified in cells treated with 50 nM TSA for 8 hours. It would be hard to speculate whether this is a true finding or a result of technical problems, such as the variable efficiency of protein transfer or unreliable quantification of UBA1 levels. This experiment would thus need to be repeated again before making any conclusions.

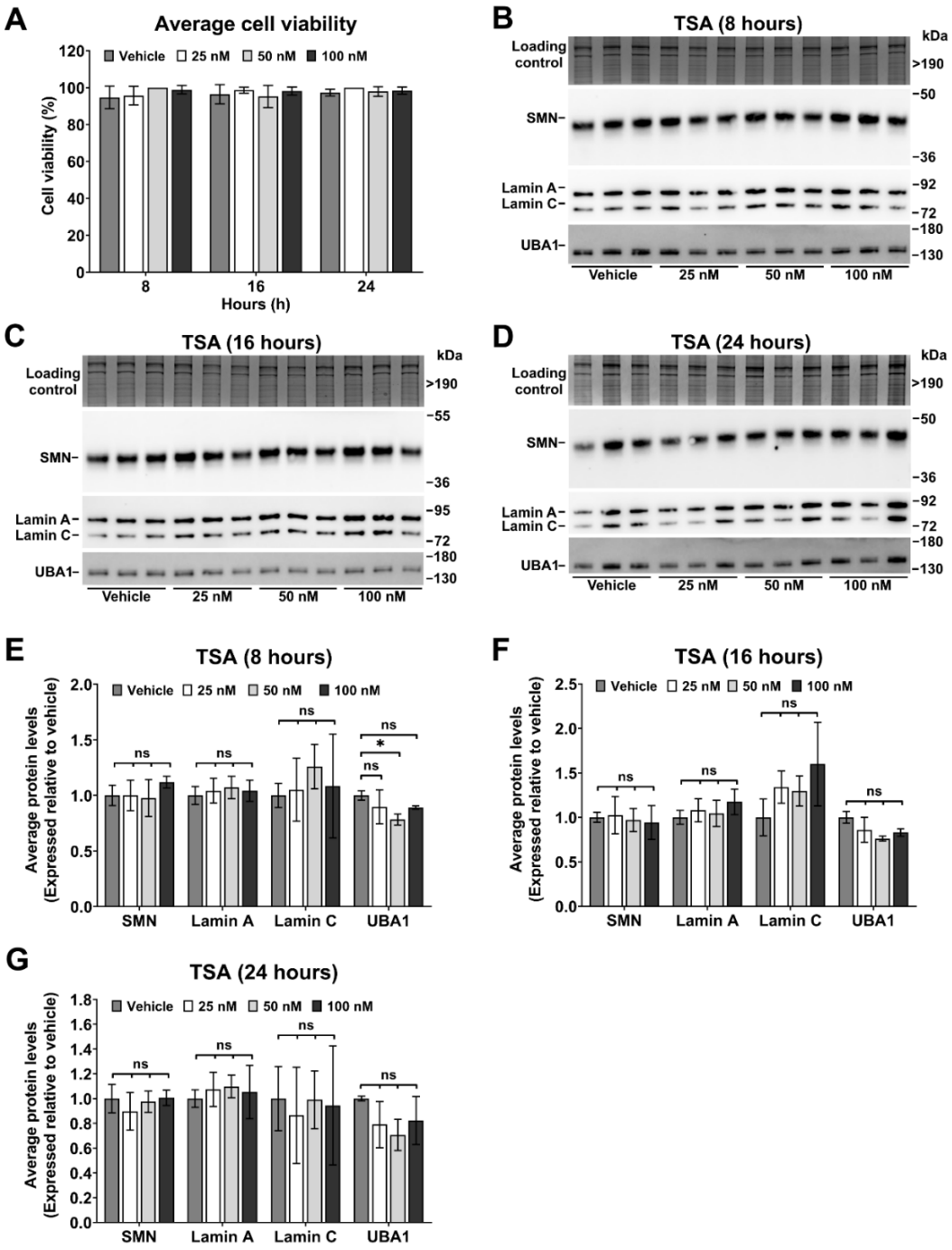

Figure 3. 14. SMN, lamin A/C and UBA1 protein levels in patient fibroblasts treated with trichostatin A (TSA). **(A)** Cell viability in patient fibroblasts treated with 25 nM, 50 nM and 100 nM TSA for 8, 16 and 24 hours. Two technical replicates were used in each group: vehicle (DMSO) and TSA (25 nM, 50 nM and 100 nM). Graphs are presented as average cell viability, with error bars showing standard deviation from the mean. Representative western blots showing SMN, lamin A/C and UBA1 levels in patient fibroblasts following exposure to TSA for **(B)** 8, **(C)** 16 and **(D)** 24 hours. Three technical replicates were used in each group: vehicle (DMSO) and TSA (25 nM, 50 nM and 100 nM). Coomassie stained gel was used as internal, total protein loading control. Quantification of SMN, lamin A/C and UBA1 levels in cells exposed to TSA for **(E)** 8, **(F)** 16 and **(G)** 24 hours. Densitometry measurements of SMN, lamin A, lamin C and UBA1 reactive bands were first normalised to densitometry measurements of Coomassie stained gel, after which all samples were normalised to the average of vehicle. Graphs are presented as average protein levels (expressed relative to vehicle), with error bars showing standard deviation from the mean. TSA- trichostatin A. ns- not significant; *p ≤ 0.05

In summary, SMN and lamin A/C levels were not significantly changed in TSA treated cells in any of the concentrations or exposure times used, while a significant reduction of UBA1 levels was identified in patient fibroblasts treated with TSA for 4 and 8 hours. However, additional experiments are needed to investigate whether TSA can change the expression of UBA1.

3.2.3.3. Identification of possible multi-target drugs using PubMed search engine

Since trichostatin A did not show promising results in regulating the expression of target proteins, a more direct approach was undertaken to identify other potential drug candidates. A PubMed search was conducted to identify drugs with the potential to target multiple proteins of interest, including SMN, lamin A/C and UBA1. This approach was chosen because research has shown that targeting SMA modifiers like NCALD, in combination with a SMN-targeted approach, brings greater therapeutic benefit to SMA mice (Torres-Benito *et al.*, 2019). Identifying a single drug that can achieve this offers an attractive alternative to combinatorial approach, in terms of the safety (no drug-drug interactions) and easier management of the pharmacokinetics and bioavailability of the drug (Hopkins, 2008). Two drugs, PDGF-BB and quercetin, were identified and tested in control and patient fibroblasts to determine whether they can change the expression of target proteins.

3.2.3.3.1. Quantification of SMN and lamin A/C protein levels was unreliable in PDGF-BB treated fibroblasts

Platelet-derived growth factor BB (PDGF-BB) plays an important role in cell proliferation, differentiation and migration, and is being used in the clinics to improve wound-healing (Andrae, Gallini and Betsholtz, 2008). PDGF treatment increased lamin A/C phosphorylation in NIH/3T3 fibroblasts (Fields *et al.*, 1990), which was identified as an important regulator of

lamin A/C turnover (Cho *et al.*, 2019). For example, increased phosphorylation promotes lamin A/C turnover, whereas decreased phosphorylation promotes lamin A/C stability (Cho *et al.*, 2019). In addition, treatment of neuronal progenitor cells (NPCs) with PDGF-BB resulted in upregulation of microRNA-9 (miR-9) levels (Yang *et al.*, 2013), a negative regulator of lamin A expression in neuronal tissues (Jung *et al.*, 2012), and miR-9 expression was dysregulated across a range of SMA tissues/cells, including spinal cord and muscles from severe SMA mice (Catapano *et al.*, 2016), and SMA patient fibroblasts (Wang *et al.*, 2014). A two-fold upregulation of SMN protein levels was previously observed in SMA patient fibroblasts following 72-hour exposure to 100 ng/mL PDGF-BB, using both immunocytochemistry and western blotting (Makhortova *et al.*, 2011). The same study identified no significant change in SMN expression after 24- and 48-hour exposure to the same concentration of PDGF-BB, however, they used immunocytochemistry approach for quantitative analysis (Makhortova *et al.*, 2011), which might not be sensitive enough to detect small changes in SMN expression. Western blotting was therefore used here as a more sensitive quantitative approach to determine whether 100 ng/mL PDGF-BB treatment for 24 hours can change SMN expression in control (GM05659) and SMA (GM00232) fibroblasts (Figure 3.15A and 3.15B). The analyses identified no significant change in SMN levels in control or patient fibroblasts treated with PDGF-BB (Figure 3.15C and 3.15D). However, quantification of SMN levels was unreliable because of the large variability in SMN expression within the group (Figure 3.15A and 3.15B). Quantification of lamin A and lamin C levels was unreliable in both control and SMA fibroblasts because of the large variability in lamin A/C expression in all treatment groups (Figure 3.15C and 3.15D). The only significant difference in lamin A expression was identified in vehicle treated group from control fibroblasts (Figure 3.15C), which could be a result of different technical problems during protein extraction and/or protein detection. Although, a vehicle (4

mM HCl) specific effect on lamin A expression cannot be excluded at this point without further experiments, especially not without the cell viability assay that is missing here.

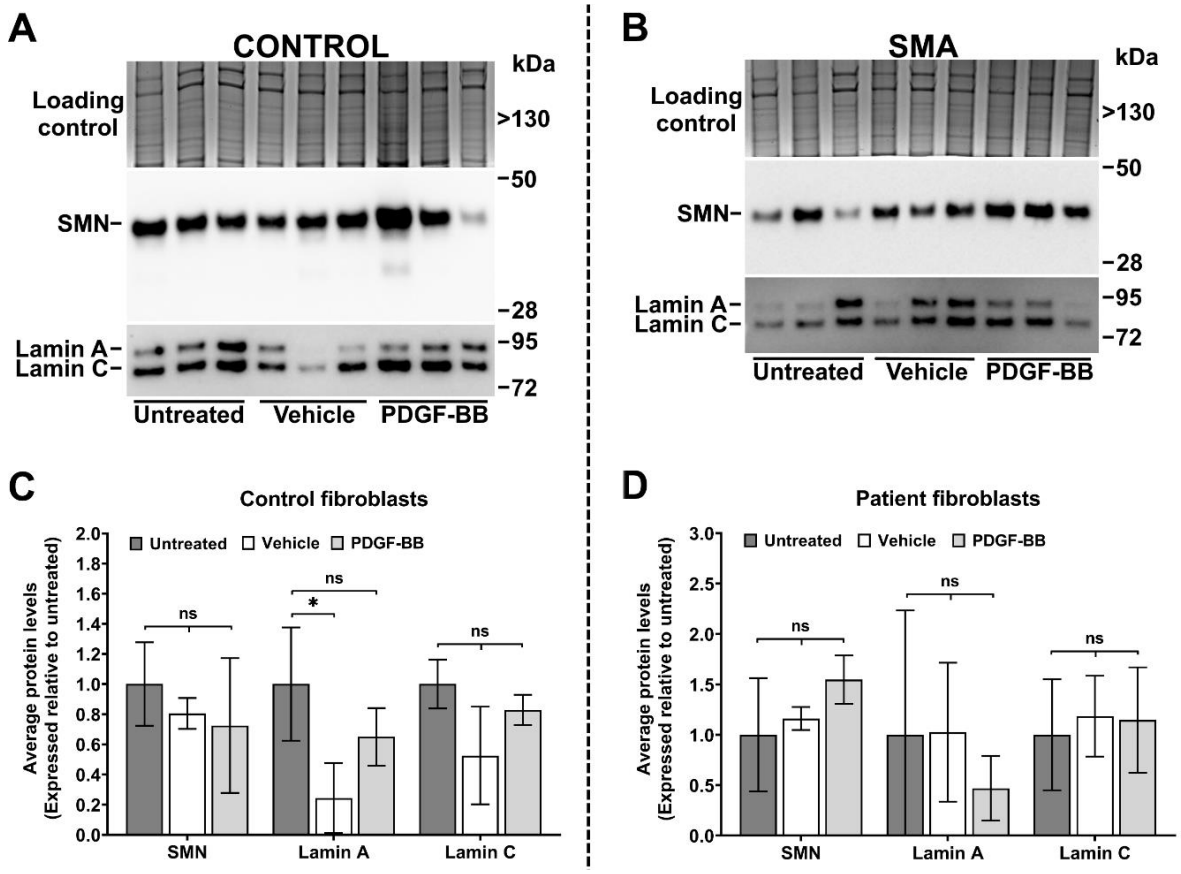

Figure 3. 15. SMN and lamin A/C protein levels in control and patient fibroblasts treated with PDGF-BB. Representative western blots showing SMN and lamin A/C levels in **(A)** control and **(B)** patient fibroblasts treated with 100 ng/mL PDGF-BB. Three technical replicates were used in each group: untreated (media only), vehicle (4 mM HCl) and PDGF-BB (100 ng/mL). Coomassie stained gel was used as internal, total protein loading control. Quantification of SMN, lamin A and lamin C levels in **(C)** control and **(D)** patient fibroblasts. Densitometry measurements of SMN and lamin A/C reactive bands were first normalised to densitometry measurements of Coomassie stained gel, after which all samples were normalised to the average of control. Graphs are presented as average protein levels (expressed relative to untreated), with error bars showing standard deviation from the mean. ns- not significant, * $p \leq 0.05$

In summary, treatment of fibroblast cells with PDGF-BB did not offer new insights into mechanisms of drug action in SMA. Control and patient fibroblasts treated with PDGF-BB showed large variability in SMN and lamin A/C expression within all groups.

3.2.3.3.2. A dose-dependent reduction of SMN, lamin A/C and active β-catenin levels, and increase of UBA1 levels in quercetin treated patient fibroblasts

Quercetin is natural flavonoid with anti-inflammatory, anti-oxidant and anti-cancer properties that is widely available as a food supplement (Wanga *et al.*, 2011). Quercetin already demonstrated therapeutic benefit *in vivo*, in zebrafish, *Drosophila* and mouse models of SMA (Wishart *et al.*, 2014). For example, quercetin treatment rescued axonal defects in SMA zebrafish, ameliorated NMJ pathology in *Drosophila* and mouse models of SMA, and restored muscle fiber dimeter and improved muscle strength in a mouse model of SMA (Wishart *et al.*, 2014). The study provided several pieces of evidence that quercetin has protective effect on neuromuscular pathology in animal models of SMA (Wishart *et al.*, 2014), however, the molecular mechanism of quercetin action in SMA tissues remains unknown. In a separate study, increased SMN2 mRNA levels were identified in SMA patient fibroblast cells treated with quercetin, with no significant change observed at the protein level, however, they used actin as a loading control for western blot analysis (Uzunalli *et al.*, 2015). Considering that changes in actin expression have already been identified in spinal cord from SMA mice (Eaton *et al.*, 2013), normalization of SMN expression to actin could be unreliable. In addition, a 24-hour exposure to quercetin reduced levels of lamin A and lamin C levels in NCOL-1 cells (Herzog *et al.*, 2004).

Here, the ability of quercetin to change the expression of SMN and lamin A/C was studied in control (GM05659) and patient fibroblast cells (GM00232), where cells were treated with 100 µM of quercetin for 24 hours (Figure 3.16A and 3.16B). These parameters were chosen because patient fibroblast cells treated with 100 µM of quercetin for 24 hours showed increased levels of SMN2 mRNA, however, SMN protein levels were not investigated for this

dose (Uzunalli *et al.*, 2015). The same study investigated SMN protein levels in patient fibroblasts treated with 20 µM of quercetin and found no significant change in SMN expression compared to untreated group. However, they used actin as a loading control which could have made quantification unreliable, and so it was important to determine whether quercetin has the ability to change SMN protein levels by using total protein as a loading control. Interestingly, a reduction of SMN levels was identified in control and patient fibroblasts following quercetin treatment, and a lower molecular weight band was observed in drug treated cells (Figure 3.16A and 3.16B). Measurements of the upper band showed significant reduction of SMN levels in both control and patient fibroblasts, for 27% ($p = 0.0347$) and 52% ($p = 0.0167$) respectively (Figure 3.16C and 3.16D). Both SMN bands were then measured together to account for the possibility that quercetin induces SMN degradation. When both bands were taken into account, average SMN levels in quercetin treated control cells were similar to those observed in vehicle and untreated group (Figure 3.16C). In SMA cells, a 30% reduction of SMN levels was observed in quercetin treated group when bands were measured together, however, the change was not statistically significant likely because of the variability in SMN expression between technical replicates of the treatment group (Figure 3.16D). Lamin A and lamin C expression were not significantly changed in either control or SMA fibroblasts following quercetin treatment (Figure 3.16C and 3.16D). Inhibition of β-catenin signalling was proposed as possible mechanism of quercetin action in SMA, however, this was not verified biochemically (Wishart *et al.*, 2014). To test this hypothesis, total β-catenin levels were investigated in patient fibroblasts treated with quercetin (Figure 3.16B), however, no significant change in β-catenin expression was identified in cells following drug treatment (Figure 3.16D).

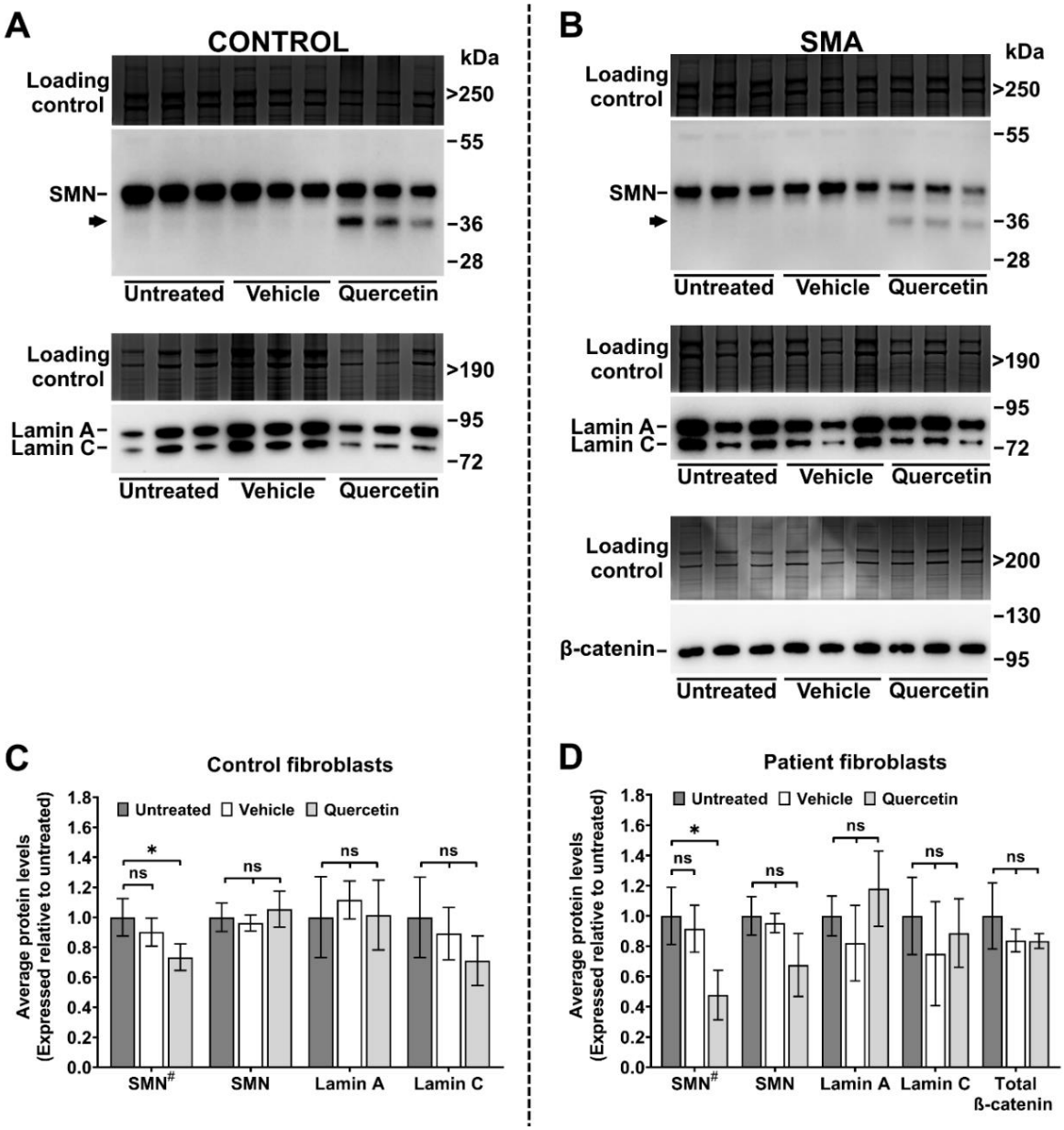

Figure 3. 16. SMN, lamin A/C and total β-catenin protein levels in fibroblasts treated with quercetin. Representative western blots showing **(A)** SMN and lamin A/C levels in control fibroblasts, and **(B)** SMN, lamin A/C and total β-catenin levels in patient fibroblasts treated with 100 µM of quercetin. Three technical replicates were used in each group: untreated (media only), vehicle (DMSO) and quercetin (100 µM). Coomassie stained gel was used as internal, total protein loading control. Arrows indicate possible SMN degradation product. Quantification of **(C)** SMN and lamin A/C levels in control fibroblasts, and **(D)** SMN, lamin A/C and β-catenin levels in patient fibroblasts. Densitometry measurements of SMN, lamin A, lamin C and β-catenin reactive bands were first normalised to densitometry measurements of Coomassie stained gel, after which all samples were normalised to the average of untreated. Graphs are presented as average protein levels (expressed relative to untreated), with error bars showing standard deviation from the mean. SMN$^{\#}$-only upper SMN band was subjected to densitometry measurements. ns- not significant

Although Uzunalli et *al.* showed good cell viability in patient fibroblast cell treated with 100 µM of quercetin for 24 hours (Uzunalli *et al.*, 2015), a 72-hour exposure to 100 µM quercetin, for example, reduced cell proliferation in NCOL-1 cell line (Herzog *et al.*, 2004). In addition, incubation with 150 µM quercetin activated apoptosis in NCOL-1 cells, which was evident by increased caspase-3 activity and DNA fragmentation (Herzog *et al.*, 2004). An additional SMN band in the quercetin treated group suggested increased SMN degradation which could be indicative of apoptotic process, however it is impossible to conclude anything without the cell viability test. To test this, patient fibroblasts (GM00232) were treated with incremental concentrations of quercetin, including 6.25 µM, 12.5 µM, 25 µM, 50 µM and 100 µM, to determine whether the same effect on SMN expression can be observed across different doses of quercetin (Figure 3.17B). Cell viability was assessed for all doses of quercetin using a trypan blue exclusion test. All treated groups showed good cell viability, with values between 96% and 100% (Figure 3.17A).

A dose dependent reduction of SMN levels was identified in quercetin treated cells starting with 8% in 12.5 µM treatment, 12% in 25 µM treatment, 50% in 50 µM treatment and 66% in 100 µM treatment (Figure 3.17C). Statistical significance of these results could not be determined due to the low group size (i.e. n=2). The lower molecular band in SMN blot, observed previously in Figure 3.16 in quercetin treated cells, was not as distinct here (Figure 3.17B). In contrast to results from a 100 µM quercetin treatment, where no change in lamin A/C levels was observed in fibroblasts cells (Figure 3.16), a dose dependent reduction of lamin A and lamin C levels was identified in quercetin treated cells (Figure 3.17C). A 64% reduction of lamin A levels was observed in cell treated with 12.5 µM quercetin, 85% in cells treated with 25 µM quercetin, 93% in cells treated with 50 µM quercetin and 92% in cells treated with

100 µM quercetin. Lamin C levels where reduced by 39% in cells treated with 12.5 µM quercetin, 80% in cells treated with 25 µM quercetin, and 94% and 93% in cell treated with 50 µM and 100 µM quercetin respectively (Figure 3.17C). A dose dependent decrease in nuclear (active) β-catenin expression was identified previously in SW480 and HEK293 cells incubated with quercetin (Park *et al.*, 2005). This means that changes in active β-catenin levels could have been masked in quercetin treated cells when total β-catenin levels where examined (Figure 3.16). Indeed, investigation of active β-catenin (ABC) levels in quercetin treated cells revealed a dose dependent reduction of ABC levels, where treatment with 25 µM quercetin showed 40% reduction, treatment with 50 µM quercetin showed 75% reduction and treatment with 100 µM quercetin showed 81% reduction in ABC levels compared to vehicle treated group (Figure 3.17C). A dose-dependent reduction of active β-catenin, SMN and lamin A/C levels suggested activation of proteasome pathway in SMA patient fibroblasts. Proteasome activation was identified previously in HFL-1 cells treated with 2 µg/mL quercetin (Chondrogianni *et al.*, 2010), which is comparable to the lowest concentration of quercetin used in this study, i.e. 6.25 µM. UBA1 levels were therefore investigated in quercetin treated cells to determine whether activation of ubiquitin-proteasome system could be responsible for reduction of SMN, lamin A/C and active β-catenin levels (Figure 3.17A). Indeed, increased levels of UBA1 were observed in quercetin treated cells, with 29%, 31%, and 33% increase identified in 25 µM, 50 µM and 100 µM concentrations respectively (Figure 3.17C).

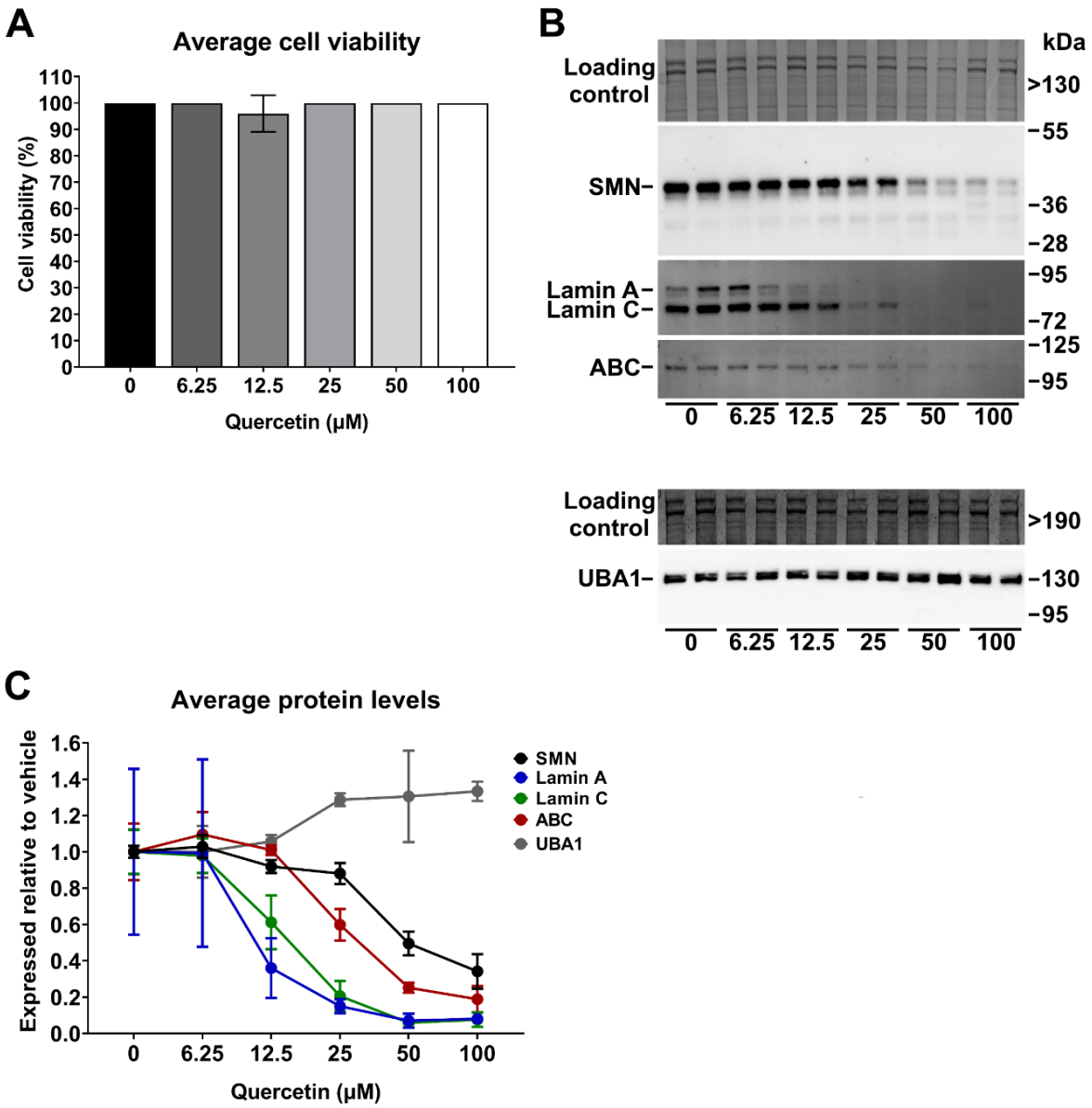

Figure 3. 17. SMN, lamin A/C, UBA1 and active β-catenin (ABC) protein levels in patient fibroblasts treated with quercetin. (A) Cell viability in patient fibroblasts treated with 0 µM (DMSO), 6.25 µM, 12.5 µM, 25 µM, 50 µM and 100 µM quercetin. Three technical replicates were used in each group. Graph is presented as average cell viability, with error bars showing standard deviation from the mean. **(B)** Representative western blots showing SMN, lamin A/C, ABC and UBA1 levels in patient fibroblasts treated with 0 µM (DMSO), 6.25 µM, 12.5 µM, 25 µM, 50 µM and 100 µM quercetin. Two technical replicates were used in each group. Coomassie stained gel was used as internal, total protein loading control. **(C)** Quantification of SMN, lamin A/C, ABC and UBA1 levels in patient fibroblasts. Densitometry measurements of SMN, lamin A, lamin C, ABC and UBA1 reactive bands were first normalised to densitometry measurements of Coomassie stained gel, after which all samples were normalised to the average of control. Graph is presented as average protein levels (expressed relative to vehicle), with error bars showing standard deviation from the mean. ABC- active β-catenin. *p ≤ 0.05; ***p ≤ 0.001

In summary, quercetin treatment did not affect cell viability, however, a dose-dependent downregulation of SMN, lamin A/C and active β-catenin level, and a small upregulation of UBA1 levels was observed in quercetin treated cells.

To explore the potential mechanism of quercetin action in SMA fibroblast cells, SMN, lamin A/C, ABC and UBA1 expression were next investigate in SMA fibroblast cells (GM00232) treated with 6.25 µM and 100 µM quercetin using immunocytochemistry approach (Figure 3.18, 3.19 and 3.20). These concentrations were chosen because 6.25 µM quercetin did not affect SMN, lamin A/C, UBA1 and ABC protein levels in previous experiment, while 100 µM quercetin induced the biggest change in expression of all four proteins (Figure 3.17). No obvious difference in SMN and lamin A/C expression or localization was observed between quercetin and vehicle treated group (Figure 3.18A and 3.19A). ABC and UBA1 levels, on the other hand, did seem increased in cells treated with 100 µM quercetin (Figure 3.20A and 3.20B). To quantify these results, lamin A/C, ABC and UBA1 levels were measured in the nucleus of quercetin and vehicle treated cells as described in methods section 2.8.4.2. Nuclear SMN is located in structures called Gemini of the coiled bodies (GEMs) (Coovert *et al.*, 1997), and reduction in the number of GEMs was previously shown to corelate with disease severity in SMA (Coovert *et al.*, 1997). In addition, increased number of GEMs was identified in phenylbutyrate treated patient fibroblasts (Andreassi *et al.*, 2004). This suggested that GEM number can be used to assess the effect of a drug treatment on SMN, and so GEMs were counted in quercetin treated fibroblasts. When compared to vehicle where 0.9% of cells showed GEMs, GEMs were identified in 2.9% cells treated with 6.25 µM quercetin and in 1.3% cells treated 100 µM quercetin (Figure 3.18B). Lamin A/C levels were not significantly changed in cells treated with 100 µM quercetin, however, although visually not obvious, a statistically

significant reduction of lamin A/C levels (30%, p=0.0419) was identified in cells treated with 6.25 µM quercetin (Figure 3.19B). A statistically significant increase in ABC levels was identified in cells treated with 6.25 µM quercetin (38%, p=0.0349) and 100 µM quercetin (78%, p<0.001) (Figure 3.20C). Nuclear UBA1 levels were significantly upregulated in cells treated with 100 µM quercetin (111%, p<0.001), while no change in UBA1 expression was observed in 6.25 µM quercetin (Figure 3.20D).

A

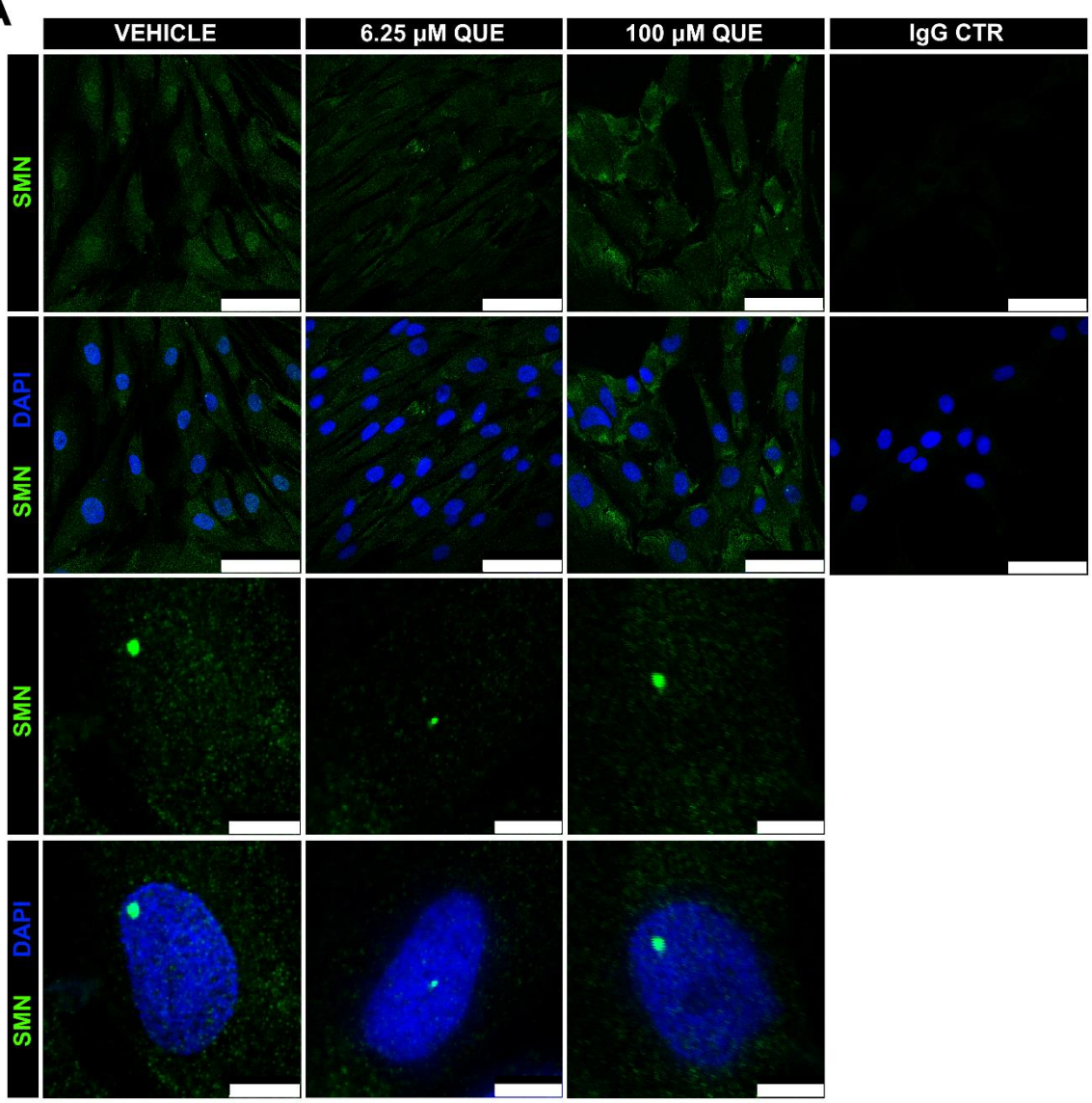

B

Treatment	Total number of cells	Cell with		Percentage (%) of cells containing GEMs
		1 GEM	3 GEMs	
Vehicle	334	3	0	0.9
6.25 µM quercetin	340	9	1	2.9
100 µM quercetin	300	4	0	1.3

Figure 3. 18. SMN in SMA patient fibroblasts. Representative immunocytochemistry images showing **(A)** SMN (green) staining in SMA patient fibroblasts (GM00232) treated with quercetin, with DAPI shown in blue. Three technical replicates were used in each group: vehicle (DMSO), quercetin (6.25 µM and 100 µM). Lower magnification images (scale bar = 75 µm), higher magnification images (scale bar = 7.5 µm). **(B)** Quantification of GEM number in SMA patient fibroblasts following quercetin treatment. Total number of cells counted, and the number and percentage of cells that contained GEMs are presented in vehicle and quercetin treated groups.

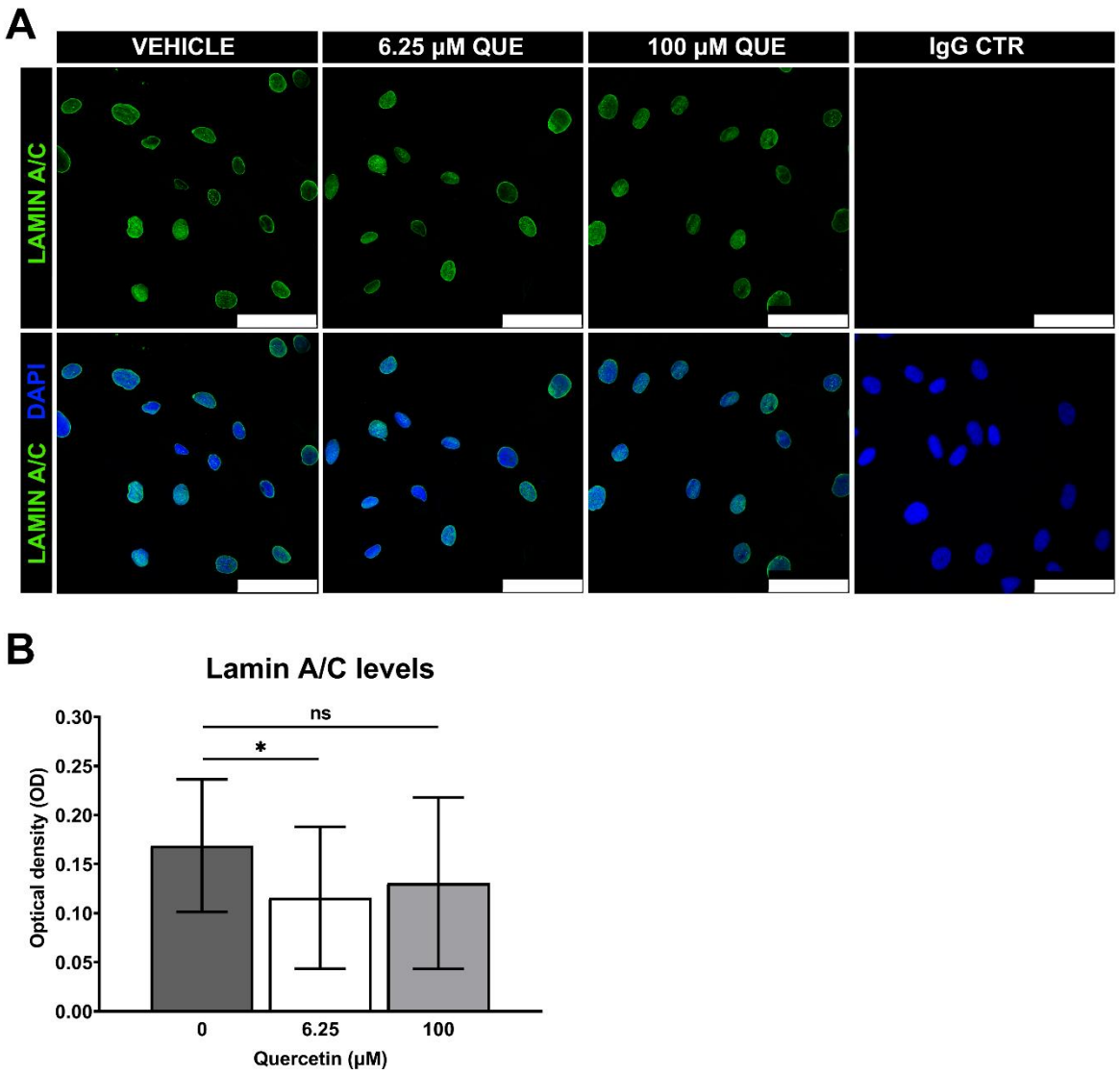

Figure 3. 19. Lamin A/C staining in SMA patient fibroblasts. (A) Representative immunocytochemistry images showing lamin A/C (green) staining in SMA patient fibroblasts (GM00232) treated with quercetin, with DAPI shown in blue. Three technical replicates were used in each group: vehicle (DMSO), quercetin (6.25 µM and 100 µM). Scale bar = 75 µm. **(B)** The graph is presented as average optical density, with error bars showing standard deviation from the mean. ns-not significant; *p<0.05

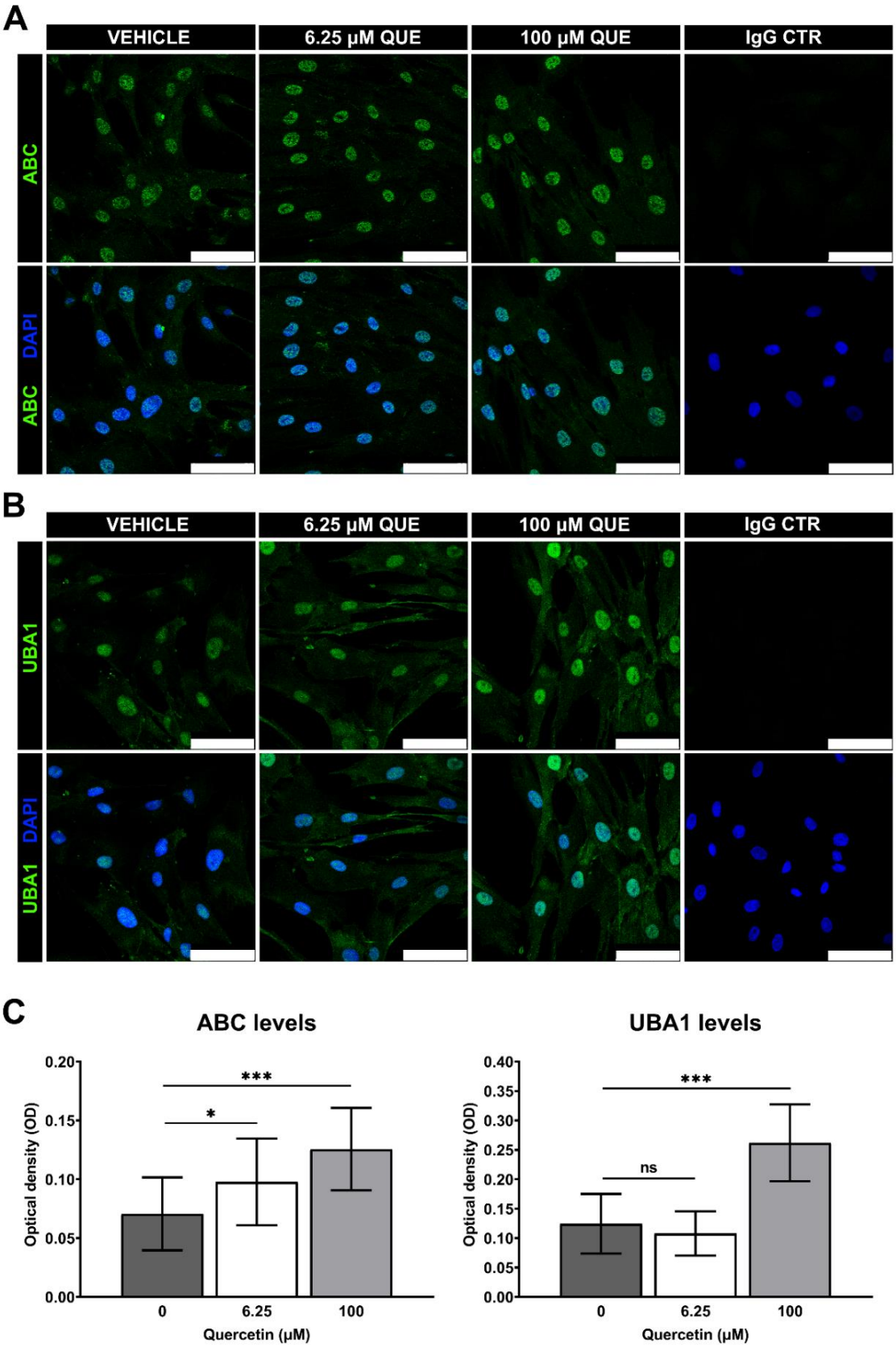

Figure 3. 20. ABC and UBA1 staining in SMA patient fibroblasts. Representative immunocytochemistry images showing **(A)** ABC (green) and **(B)** UBA1 (green) staining in SMA patient fibroblasts (GM00232) treated with quercetin, with DAPI shown in blue. Three technical replicates were used in each group: vehicle (DMSO), quercetin (6.25 µM and 100 µM). Scale bar = 75 µm. **(C)** Graphs are presented as average optical density, with error bars showing standard deviation from the mean. ns-not significant; *p<0.05, ***p<0.001

Of the four proteins examined, only UBA1 showed upregulation in cells treated with 100 µM quercetin, both by western blotting and immunocytochemistry. Others, including SMN, lamin A/C and ABC showed contradictory results using two different techniques.

In summary:

a) Multi-study comparison of published transcriptomic studies of SMA identified widespread dysregulation of gene expression in different animal and cell models of SMA. However, very few commonalities were observed between the list of differentially expressed genes and proteins, identified in multi-study comparisons of published omics studies, suggesting that changes to the SMA proteome are not driven by aberrant transcriptional regulation.

b) Western blot analyses identified widespread dysregulation of SMN, UBA1, lamin A/C, GAPDH and ANXA2 protein levels in spinal cord, brain, liver, heart and muscle tissue from a severe mouse model of SMA, and in fibroblasts from SMA patients. Of the tissues/cells examined, liver showed the greatest number of differentially expressed proteins, where SMN, UBA1, ANXA2 and GAPDH levels were significantly reduced, and lamin A/C levels were significantly upregulated. Skeletal muscles, on the other hand, showed very few significant changes in protein expression, likely because of the big variability in protein expression within the group. NCAM and GAP43 expression was not significantly changed in spinal cord and brain tissue from a severe mouse model of SMA.

c) Identification of pharmaceutical compounds that have the potential to restore the expression of several proteins to the levels observed in control fibroblasts proved to be very challenging. A change in expression of SMN, lamin A/C and UBA1 was not

observed in control and SMA patient fibroblasts treated with trichostatin A and PDGF-BB. In addition, large variability in SMN, lamin A/C and UBA1 expression within the group was identified in both drug treatments which made quantification unreliable. Quercetin, on the other hand, decreased the expression of SMN, lamin A/C and active β-catenin in a dose dependent manner, and a small upregulation of UBA1 levels was also identified in quercetin treated cells. However, SMN reduction is not a desirable effect in SMA therapy design, and so therapeutic benefit of quercetin remains to be investigated in more detail.

3.3. Discussion

3.3.1. Multi-study comparison of published transcriptomic studies of SMA identified 28 genes with a consistent direction of differential expression across at least three studies

Eleven published transcriptomics studies were compared to identify core gene expression changes in SMA, that may have been overlooked when datasets were considered in isolation (Section 3.2.1.1). Studies ustilised a range of neuromuscular tissues/cells, including SMA mouse spinal cord at diffrent stages of disease development (Zhang *et al.*, 2008; Bäumer *et al.*, 2009; Murray *et al.*, 2010; Huo *et al.*, 2014), mouse motor neurons (Zhang *et al.*, 2013; Maeda *et al.*, 2014; Saal *et al.*, 2014; Murray *et al.*, 2015), rat motor neurons (Wertz *et al.*, 2016), SMA patient myoblasts (Anderson *et al.*, 2004) and muscles, and SMA mouse kidney (Zhang *et al.*, 2008). Only 28 genes showed a consistent direction of diferential expression across three or more studies of SMA. Considering that transcriptomic studies utilised mostly neuromuscular tissues, and that 608 genes were initially identified as being differentially expressed in at least two transcriptomic studies of SMA, the number of core gene changes in SMA is surprisingly low. This could be attributed to genetic differences between SMA models, and/or the the different response of tissues/cells to SMN reduction at diffrerent stages of the disease development (Groen *et al.*, 2018). The 28 genes that showed consistent direction of diferential expression across at least three transcriptomic studies of SMA were connected to functions like regulation of gene expression and RNA metabolism. This may not be surprising considering that SMN controls different aspects of RNA metabolism, including transcription, pre-mRNA splicing, mRNA trafficking and translation (described in more detail in chapter 1, section 1.2.2).

Nevertheless, the 28 genes may represent a core response in SMA tissues/cells, and some of these have already been linked to SMA disease pathogenesis, including chondrolectin (CHODL). Decreased expression of CHODL mRNA was identified in four transcriptomic studies of SMA (Zhang *et al.*, 2008, 2013; Bäumer *et al.*, 2009; Wertz *et al.*, 2016), and this result was confirmed biochemically in SMN-knockdown motor neurons (Wertz *et al.*, 2016). In addition, CHODL knockdown arrested axonal growth in zebrafish, while overexpression of *CHODL* prevented motor neurons from growing axons out of the spinal cord (Zhong *et al.*, 2012), thus indicating that correct expression is important for normal motor neuron development.

3.3.2. Seven molecules were dysreglated at the gene and protein level in at least two omics studies of SMA

Proteins identified in a multi-study comparison of published proteomic studies (Fuller, Gillingwater and Wishart, 2016), were compared to the list of differentially expressed genes identified in this study (Section 3.2.1.1), to determine whether changes in protein expression can be tracked back to the aberrant transcription. This was done to gain insights into whether it might be necessary to target molecules at the protein and/or gene level to maximise the effect of the therapeutic approach. The analysis identified seven molecules that were differentially expressed at both the gene and protein levels. This may not be surprising since different experimental models and samples have been used across different omics studies, and at different stages of disease development, and could reflect the tissue/model specific differences in protein/gene expression. However, a recent study in an *in vitro* model of ALS did show little overlap between differentially expressed genes and proteins in the same experimental model (Kim *et al.*, 2017). The lack of overlap between proteomic and transcriptomic studies of SMA could therefore be a real finding, suggesting that changes in protein expression in SMA are caused by aberrant post-transcriptional regulation. Indeed,

perturbed post-transcriptional gene regulation in SMA has been associated with several defective RNA processing pathways, including those that regulate RNA splicing (Gabanella *et al.*, 2007), RNA stability and translation (Saal *et al.*, 2014).

3.3.3. An overview of protein expression in SMA mouse tissues and patient fibroblasts

Having shown that changes in SMA proteome are not regulated by aberrant transcriptional regulation, the research was next focused on differentially expressed proteins. Of the seven proteins investigated here, including SMN, UBA1, lamin A/C, GAPDH, ANXA2, GAP43 and NCAM, five showed dysregulated expression across different tissues from a mouse model of SMA, and in patient fibroblast cells. Liver and heart from SMA mice showed the greatest number of dysregulated proteins, while SMA mouse skeletal muscles and brain showed dysregulated expression of one more protein alongside SMN, ANXA2 and lamin A/C respectively. This could possibly be explained by the fact that only specific brain regions showed vulnerability to reduced levels of SMN (Wishart *et al.*, 2010). For example, morphological changes in hippocampus were observed from pre-symptomatic stage of the disease in severe mouse model of SMA mice, while primary somatosensory cortex remained unaffected throughout disease progression (Wishart *et al.*, 2010). The contribution of unaffected or less vulnerable regions of the brain to the overall protein expression trends in whole brain extracts, could possibly mask changes that are restricted to vulnerable regions like the hippocampus. The same logic could then be applied to the spinal cord tissue, where protein expression in unaffected cell populations or spinal cord regions could mask changes that are specific to vulnerable alpha motor neurons. For example, Boyd et *al.* identified a five-fold difference in expression of phosphoglycerate kinase 1 (PGK1) between vulnerable and resistant motor neuron populations in a mouse model of SMA (Boyd *et al.*, 2017). Investigation

of protein expression in vulnerable regions of the brain and spinal cord would therefore be necessary to establish the precise pattern of protein expression in SMA tissues.

Muscle tissue, on the other hand, showed large variability in protein expression within the group, with non-significant changes in protein expression. For example, 60% reduction in UBA1 levels in skeletal muscles from SMA mice was not statistically significant in this study, while a separate study showed significant reduction of UBA1 levels in skeletal muscles from two severe mouse models of SMA at symptomatic stage of the disease (Wishart *et al.*, 2014), thus indicating that reliable quantification of UBA1 levels in skeletal muscles from SMA mice was hampered here for technical reasons. Differences in protein extraction efficiency of specific proteins are possible and could explain variability between the samples. In addition, Murgia et *al.* analysed protein profiles of four fiber-types in mouse soleus and *extensor digitorum longus* muscles, using a proteomics approach, and identified widespread differences in protein expression between different muscle fibers (Murgia *et al.*, 2015). These results were verified biochemically in mouse skeletal muscle sections, by analysing isocitrate dehydrogenase (IDH) expression across four fiber-types (Murgia *et al.*, 2015; Schiaffino, Reggiani and Murgia, 2019). Since only a small piece of M. *gastrocnemius* from each animal was analysed in this study, it is possible that different samples contained different fiber ratios. This suggests that different samples would have different absolute protein levels, and could explain why large sample variability is observed despite the equal loading.

When taken together, western blot analyses confirmed that several proteins, identified in the multi-study comparison of published SMA proteomic studies (Fuller, Gillingwater and Wishart, 2016), show dysregulation in SMA tissues/cells. However, this study also showed that quantification of protein expression can be challenging, and different technical aspects such

as the differential response of vulnerable regions of the tissue or the origin of the sample, have to be taken into account in future analyses.

3.3.3.1 Survival of motor neuron protein (SMN) was reduced in all tissues from a severe mouse model of SMA and in SMA patient fibroblasts

As expected, SMN expression was decreased in all tissues examined, with muscle and liver showing the greatest reduction of SMN levels, followed by the heart, brain and spinal cord from SMA mice, and patient fibroblast cells. SMN expression was analysed previously in tissues from a mouse model of SMA in a study by Groen et *al.* (Groen *et al.*, 2018), where the lowest SMN levels were identified in the muscle and heart tissue from SMA mice, followed by the liver, brain and spinal cord (Groen *et al.*, 2018). The results of SMN analyses across SMA mouse tissues were largely comparable between the two studies, where the difference in SMN expression in comparable tissues did not exceed 5% across both studies.

3.3.3.2. Ubiquitin-like modifier activating enzyme 1 (UBA1) expression was reduced in the heart and liver tissue from a mouse model of SMA

Ubiquitin-like modifier activating enzyme 1 (UBA1) is a well characterised modifier of SMA disease pathways (Wishart *et al.*, 2014; Powis *et al.*, 2016), and its expression levels were investigated previously across tissues from severe mouse model of SMA (Powis *et al.*, 2016). The greatest reduction of UBA1 levels was identified in the heart, followed by the liver, muscle, kidney, lung and spinal cord from SMA mice, while brain showed small increase in UBA1 levels (Powis *et al.*, 2016). UBA1 followed a similar expression trend in SMA mouse tissues in this study, where a statistically significant reduction of UBA1 levels was identified in the heart and liver, while non-significant reduction was identified in the muscle, spinal cord and brain tissue

from SMA mice (Figure 3.4). In addition, UBA1 expression was not significantly changed in SMA patient fibroblast cells.

Although tissues followed the same expression trend, with the exception of brain, differences in UBA1 expression of approximately 5-40% were established between the studies, depending on the tissue examined. Powis et *al.* showed that UBA1 levels decrease with disease progression in tissues from a mouse model of SMA (Powis *et al.*, 2016), and greater reduction of UBA1 levels in tissues from P8 SMA mice (used in this study) compared to P7 mice (Powis *et al.*, 2016) could therefore reflect the disease progression. The choice of the detection system is another factor to consider, since fluorescent western blotting shows higher linear range and sensitivity compared to the enhanced chemiluminescence (ECL) western blotting (Eaton *et al.*, 2014). In this study ECL western blotting was used to quantify UBA1 levels, while Powis et *al.* used fluorescent western blotting (Powis *et al.*, 2016).

Reduction of UBA1 levels was already shown to be conserved pathology in SMA, in mouse and zebrafish models of SMA and in SMA patient motor neurons, leading to widespread dysregulation of ubiquitin-proteasome pathway in SMA (Wishart *et al.*, 2014; Powis *et al.*, 2016). Systemic restoration of UBA1 levels, for example, corrected defects in ubiquitin pathway, improved neuromuscular pathology and increased survival in severe SMA mice (Powis *et al.*, 2016). In addition, heart and liver, two tissues that showed the most dramatic decrease in UBA1 levels in this study (Figure 3.4), had improved pathology following restoration of UBA1 levels in SMA mice (Powis *et al.*, 2016). The number of megakaryocytes and nucleated erythrocytes was reduced in SMA mouse liver, indicating partial rescue of liver pathology following AAV9-UBA1 treatment, while SMA mouse hearts showed increased size

and weight (Powis *et al.*, 2016). Perturbations in ubiquitin-proteasome system have already been associated with different heart pathologies (Li, Johnson and Su, 2018), and so dysregulation of ubiquitin-proteasome system could have important function in cardiac pathology in SMA.

3.3.3.3. Lamin A/C expression was increased in the brain, spinal cord, liver and heart tissue from a mouse model of SMA

Lamin A/C was increased across three proteomic studies of SMA, including mouse Schwann cells (Aghamaleky Sarvestany *et al.*, 2014), mouse muscles (Mutsaers *et al.*, 2013) and type I patient motor neurons (Fuller *et al.*, 2016). In line with this, upregulation of lamin A/C levels was identified here across a range of tissues from a mouse model of SMA. Lamin A expression was upregulated in the heart, brain and liver tissue from SMA mice, while lamin C showed increased levels in the heart, spinal cord, liver and brain tissue from a mouse model of SMA. In addition, increased levels of lamin A/C were identified in the heart from SMA mice using immunohistochemistry approach (Šoltić *et al.*, 2019).

Interestingly, an additional band, presumed to be pre-lamin A, was observed in the liver tissue from SMA mice but was not observed in the liver from healthy littermate controls (Figure 3.5). Accumulation of pre-lamin A, as a result of zinc metallopeptidase STE24 (ZMPSTE24) knockdown, was previously shown to increase the levels of reactive oxygen species (ROS) and activate senescence pathways in skin fibroblasts (Sieprath *et al.*, 2015), and in different liver diseases increased hepatocyte senescence significantly impaired liver functions and regeneration (Huda *et al.*, 2019). Accumulation of pre-lamin A might thus lead to hepatocyte senescence in the liver of SMA mice and compromise normal functioning of the liver.

Patient fibroblasts were the only sample that showed statistically significant reduction of lamin A levels compared to controls. Control fibroblasts showed variability in lamin A expression, where GM05659 cells showed lower lamin A levels compared to two other control cells, GM00498 and GM00302 respectively. This expression pattern could be a result of biological variability between cells, since a previous study already showed variable levels of lamin A/C mRNA in primary human ovarian surface epithelial cells (Capo-chichi *et al.*, 2011). In addition, expression of lamin A/C was shown to correlate with the cell density in 2D cell culture (Zonderland *et al.*, 2019), and so differences in lamin A/C expression in this study could have been introduced by the seeding density (cell confluency).

3.3.3.4. Glyceraldehyde 3-phosphate dehydrogenase (GAPDH) expression was reduced in the liver and heart tissue from a mouse model of SMA

Reduced GAPDH levels were identified using a proteomics approach in type I, II and III patient plasma (Kobayashi *et al.*, 2013), and in Schwann cells (Aghamaleky Sarvestany *et al.*, 2014) and hippocampus (Wishart *et al.*, 2010) from SMA mice, however, to date GAPDH has not been investigated biochemically in SMA tissues and cells. Here, GAPDH levels were decreased in the liver and heart tissue from SMA mice, while spinal cord, brain and muscles from SMA mice, and SMA patient fibroblasts showed no significant change in GAPDH expression compared to controls.

High energy demanding tissues, such as muscles and neuronal tissues rely on glycolysis to meet their energy demands (Jang *et al.*, 2016), and so defective glycolytic machinery is likely to disturb their proper functioning. Indeed, defects in energy production, including glycolysis, have already been identified in mouse and zebrafish models of SMA. For example, glycolytic

enzyme phosphoglycerate kinase 1 (PGK1) showed reduced expression in spinal cord and heart tissue from a mouse model of SMA, and PGK1 knockdown in zebrafish embryos induced SMA-like axonal outgrowth defects (Boyd *et al.*, 2017). Dysregulation of GAPDH levels in SMA mouse heart, for example, could have detrimental consequences on the heart health during remodelling and dedifferentiation (Szibor *et al.*, 2014). Remodelling and dedifferentiation of adult cardiomyocytes are adaptive processes intended to protect the cardiomyocytes in times of mechanical and/or molecular stress. In this process, high-energy demanding contractile apparatus is degraded to reduce the oxygen-dependent generation of ATP, and the heart relies on glycolysis to maintain energy demands (Szibor *et al.*, 2014). Altered expression and/or activity of glycolytic machinery would therefore impair glycolysis, promoting instability and cell death of cardiomyocytes.

In addition, GAPDH is housekeeping protein often used as a loading control for western blot analyses. Identification of reduced levels of GAPDH in SMA tissues therefore implies that some results from SMA studies, that used GAPDH as a loading control, may need to be re-examined (Fuller, Gillingwater and Wishart, 2016). In addition, perturbations in other common housekeepers, such as actin and tubulin, have also been identified in SMA tissues (Eaton *et al.*, 2013), emphasising the need to use total protein as a reliable loading control for quantitative analyses in SMA tissues.

3.3.3.5. Annexin A2 (ANXA2) expression was increased in the spinal cord from SMA mice and in SMA patient fibroblasts, but decreased in SMA mouse muscles

Several pieces of evidence implicate annexin A2 (ANXA2) in SMA disease pathways. First, an interaction between ANXA2 and SMN was identified in C2C12 muscle and PC12 neuronal cells

expressing SMN fusion protein using a mass spectrometry approach, and this interaction was verified biochemically in C2C12 and PC12 cell cultures (Shafey *et al.*, 2010). Increased ANXA2 levels were identified previously in proteomic studies of SMA, in mouse Schwann cells (Aghamaleky Sarvestany *et al.*, 2014) and in patient iPSC-derived motor neurons (Fuller *et al.*, 2016), and in line with this, upregulation of ANXA2 levels was identified here in the spinal cord from SMA mice and in SMA patient fibroblasts. The role for ANXA2 in neuronal cell differentiation and development was established previously in PC12 neuronal cells, where increased levels of ANXA2 corelated with cell differentiation, while knockdown of ANXA2 protein and mRNA levels inhibited neuronal differentiation (Jacovina *et al.*, 2001). In addition, colocalization between ANXA2 mRNA and SMN protein was identified previously in axons of NSC-34 cells, and this colocalization was dramatically reduced in SMN-depleted cells despite the general increase in ANXA2 mRNA levels (Rage *et al.*, 2013). The increased expression of ANXA2 in SMA mouse spinal cord could, therefore, be a compensatory mechanism to reduced SMN levels.

A significant reduction of ANXA2 levels in the liver from SMA mice was identified here at the protein level, and at the mRNA level in the study by Szunyogova et *al.* (Szunyogova *et al.*, 2016). Brain and heart tissue from SMA mice showed no significant change in ANXA2 expression compared to controls. In contrast to the proteomic study of SMA that identified increased ANXA2 levels in muscles from P5 SMA mice (Mutsaers *et al.*, 2013), ANXA2 levels were decreased in muscles from P8 SMA mice in this study. Different animal models, at different stages of the development, and different muscle used in each study could offer some explanation for the discrepancy between the studies. Nevertheless, both increased and decreased ANXA2 levels were shown to have effect on muscle pathology. For example, ANXA2

deficient mice showed progressive muscle weakness with aging, and ANXA2 deficient muscles showed poor myofiber repair (Defour *et al.*, 2017). However, ANXA2 also has a role in the inflammatory response (Swisher, Khatri and Feldman, 2007), and knockout of ANXA2 inhibited chronic muscle inflammation and adipogenic replacement of muscle cells, and improved muscle function in dysferlin deficient mice (Defour *et al.*, 2017). ANXA2 homeostasis seems to be important for muscle health, and so both increased and decreased ANXA2 levels could have a role in muscle pathology in SMA.

3.3.3.6. Neural cell adhesion molecule 1 (NCAM) and neuromodulin (GAP43) levels were not changed in spinal cord and brain extracts from a mouse model of SMA

NCAM is a cell surface protein important for cell adhesion, and it has been implicated in different functions including neurite outgrowth, myelination, organization of synapses and myogenesis (Gnanapavan and Giovannoni, 2013). Structural and functional defects in NMJs were observed in NCAM-deficient mice, including smaller NMJs and problems with signal transduction (Rafuse, Polo-Parada and Landmesser, 2000). Decreased expression of NCAM was identified across three proteomic studies of SMA, including patient motor neurons (Fuller *et al.*, 2016), patient plasma (Kobayashi *et al.*, 2013) and mouse hippocampus (Wishart *et al.*, 2010). Here, the expression of NCAM was not significantly changed in spinal cord and brain tissues from a mouse model of SMA mice, which may not be surprising since proteomic studies of SMA examined vulnerable regions of the spinal cord and brain (section 3.3.3).

GAP43 is neuronal protein involved in a range of functions, including axonal growth, neuronal regeneration and plasticity (Hao Le *et al.*, 2017). Proteomic studies of SMA identified decreased expression of GAP43 in patient motor neurons (Fuller *et al.*, 2016), mouse hippocampus (Wishart *et al.*, 2010) and mouse hippocampus synaptosomes (Wishart *et al.*,

2014). Decreased GAP43 mRNA and protein levels were previously reported in cultured motor neurons from a mouse model of SMA (Fallini *et al.*, 2016), and decreased GAP43 mRNA levels were identified in motor neurons from a zebrafish model of SMA (Hao Le *et al.*, 2017). In addition, reduced GAP43 mRNA and protein levels were observed in neuron growth cones from SMA mice, indicating that SMN is important for correct localization and translation of GAP43 mRNA (Fallini *et al.*, 2016). The same study showed no significant change in GAP43 levels in whole spinal cord and brain extracts from SMA mice (Fallini *et al.*, 2016). In line with this, no change in GAP43 expression was identified in SMA mouse spinal cord and brain tissues in this study, suggesting that changes restricted to vulnerable regions are masked in whole tissue extracts (section 3.3.3).

Analyses of vulnerable regions like hippocampus and lumbar spinal cord would help to determine the expression pattern of NCAM and GAP43 in SMA. Since both proteins are implicated in axonal outgrowth and maintenance of neuronal function, perturbed expression or localization of NCAM and GAP43 are likely to have important role in motor neuron vulnerability in SMA. Alongside SMN, NCAM and GAP43 therefore represent attractive targets for neuronal-specific therapy design in SMA.

3.3.4. Western blotting is a sensitive and accurate method for measurement of protein expression in fibroblast cells

Dot blotting and ELISA techniques were compared to the western blotting to identify the appropriate technique for measurement of protein expression in drug screening studies, where both the accuracy and sensitivity of measurements were assessed on SMN and lamin A/C levels.

The dot blot approach showed good accuracy and sensitivity for quantification of SMN levels in SMA patient fibroblasts, using two different antibodies, MANSMA12 and MANSMA2, while MANSMA3 antibody produced weak SMN signal (Section 3.2.3.1.1). Detection of changes in lamin A expression in patient fibroblast extracts, using an antibody raised against lamin A/C (MANLAC1 4A7), might have been masked by unchanged levels of lamin C. It is possible too that different amounts of total protein from control and patient fibroblasts were loaded on the nitrocellulose membrane, and could explain why changes in lamin A expression, using lamin A specific antibody, were not detected in patient fibroblasts. The inability to use loading control is thus the biggest limitation of dot blotting.

Indirect ELISA, on the other hand, failed to detect lamin A in control and patient fibroblasts (Section 3.2.3.1.2). Although a positive control was not used in ELISA, western blotting previously showed that lamin A is present in fibroblasts extracts (Figure 3.5), indicating the low sensitivity of the method used (i.e. indirect ELISA). This problem could be resolved by using sandwich ELISA that can increase the sensitivity range of the detection (Aydin, 2015). Indeed, sandwich ELISA has been successfully used for detection of SMN levels in a range of SMA cells/tissues, including peripheral blood mononuclear cells (PBMC) (Kobayashi et al., 2011) and fibroblast cells (Nguyen et al., 2008) from SMA patients, and brain, spinal cord and muscles from a severe mouse model of SMA (Kobayashi et al., 2011). In addition, sandwich ELISA showed good sensitivity for detecting small changes in SMN expression (20-30%) following exposure to valproate or phenylbutyrate, indicating it can be reliably used in drug screening studies (Nguyen et al., 2008).

To summarize, the dot blot approach showed good accuracy and sensitivity for quantification of SMN levels in SMA patient fibroblasts, however, it was not sensitive enough to detect changes in expression of lamin A specific isoform. Examination of lamin A levels, using indirect ELISA, produced no results. This then means that other antibodies, that can detect lamin A and lamin C specific isoforms, would have to be tested for dot blot and ELISA analyses. When doing so, it would be of interest do compare indirect and sandwich ELISA, taking into account the sensitivity and the cost of each approach. In addition, both techniques would have to be optimized for a range of other protein targets, including for example, UBA1, which would consume more time and resources.

Western blotting, on the other hand, is an established technique for measurement of protein expression in this lab. It can detect isoform specific changes in expression using one antibody, where variability in protein expression between samples can be corrected using loading control (Figure 3.2). In addition, western blotting can assess the expression levels of two proteins on the same blot, if they are not of similar molecular weight, and can be used to detect changes in posttranslational profile of proteins (Wilson, Garton and Fuller, 2016). In contrast to ELISA, however, western blotting is not a high-throughput method (Nguyen *et al.*, 2008), i.e. only small number of samples can be screened at a time, which can lead to logistic problems as demonstrated in Figure 3.17. When all is taken into account, western blotting seems to offer the best sensitivity, however, it would not be a good platform for high-throughput drug screening.

3.3.5. Selection of appropriate therapeutic targets for in vitro drug studies in control and patient fibroblasts

Since very few molecules showed differential expression at both the gene and protein level (Table 3.3), chemical compounds were selected based on their potential to manipulate the expression of seven protein targets that were investigated biochemically in this study (Section 3.2.2). Identification of compounds that have the ability to change the expression of several of these proteins at the same time would likely induce better therapeutic response in SMA patients, since multiple pathogenic pathways would be targeted at the same time (Torres-Benito *et al.*, 2019). Network pharmacology approach was first applied to do this, and identified 20 drugs which were then filtered to three potential candidates. Of these, trichostatin A was selected for in vitro studies because it showed association to 5 proteins of interest, among which were SMN and lamin A/C.

Trichostatin A (TSA) did not significantly change the expression of SMN, lamin A/C and UBA1

SMN protein expression was not changed in patient fibroblast cells in this study, even after a 24-hour exposure to TSA (Figure 3.14). This is perhaps not surprising since the maximum increase in SMN mRNA levels was previously identified in SMA patient fibroblast cells 4 hours after the treatment, after which the levels dropped drastically and went below the basal levels (Avila *et al.*, 2007). This would suggest that SMN mRNA levels are rapidly degraded and/or that mRNA is not efficiently translated. The latter explanation is supported by the finding that SMN reduction causes widespread defects in translation machinery in SMA tissues (Bernabò *et al.*, 2017). A similar trend was observed in the severe mouse model of SMA ($Smn^{-/-}$ $SMN2^{+/+}SMN\Delta7^{+/+}$), where a single dose of TSA produced small increase in SMN mRNA levels, without an obvious change in protein levels (Avila *et al.*, 2007). In contrast, however, repeated TSA injections induced an upregulation of both SMN mRNA and protein levels in SMA mouse

tissues (Avila *et al.*, 2007), indicating that constant upregulation of SMN gene expression is necessary to induce efficient translation.

Another study showed SMN-independent improvement of neuromuscular pathology and survival in SMA mice (Liu *et al.*, 2014), suggesting that TSA acts on other pathogenic pathways in SMA. One of these could be lamin A/C, since TSA treatment was shown to upregulate expression of lamin A/C *in vitro*, in fibroblast cells from HGPS patients (Columbaro et *al.*, 2005) and in MEFs (Galiová et *al.*, 2008). In contrast, lamin A/C expression was not significantly changed in this study (Figure 3.13 and 3.14). Changes in lamin A/C expression in HGPS fibroblasts could be explained by the drug concentration (Columbaro et *al.*, 2005), where 15x higher concentration was used compared to concentration used in this study (i.e. 100 nM). However, it is not clear why the same drug treatment (100 nM for 24 hours), used here and in MEFs (Galiová et *al.*, 2008), produced different results.

A small reduction of UBA1 levels was identified in all concentrations and time points in patient fibroblasts, one of which, 50 nM exposure for 8 hours, showed a significant difference compared to vehicle. However, considering that other drug concentrations and exposure times did not show statistically significant difference, the result may be a false positive. In addition, quantification of UBA1 levels is likely unreliable because of the low signal intensity.

PDGF-BB treatment did not change SMN and lamin A/C expression in control or SMA patient fibroblasts

The results from PDGF-BB treatment indicate technical problems, such as the variable efficiency of the protein extraction and/or protein transfer onto the nitrocellulose membrane. Differences in lamin A/C expression could have also been introduced by the seeding density

(cell confluency) (Zonderland *et al.*, 2019). Although seeding density has been controlled in drug experiments, uneven distribution of cells in the well could have caused differences in confluency within the well, which could affect lamin A/C expression.

Since both SMN and lamin A/C showed large sample variability within the group in control and patient fibroblasts, it is not possible to conclude at this stage whether lamin A/C and SMN expression change after 24-hour treatment with 100 ng/mL PDGF-BB. The biggest limitation of this experiment is the lack of a positive control, i.e. drug treatment that was previously shown to increase SMN expression in fibroblast cells (100 ng/mL PDGF-BB for 72 hours). The dose and time response would have to be established for PDGF-BB treatment to determine its effect on SMN and lamin A/C levels.

Quercetin induces a dose-dependent decrease in SMN, lamin A/C and active beta-catenin levels, and an increase in UBA1 levels in patient fibroblast cells

Consistent with previous reports of beta-catenin signalling inhibition (Park *et al.*, 2005) and lamin A/C reduction (Herzog *et al.*, 2004), quercetin treatment decreased active β-catenin and lamin A/C levels in a dose dependent manner in patient fibroblast cells (Figure 3.17). Surprisingly, however, a dose-dependent reduction of SMN was also identified in patient fibroblasts using western blotting (Figure 3.17), suggesting a possible negative effect of quercetin treatment. Indeed, induction of apoptosis following quercetin treatment was identified previously in two separate studies (Herzog *et al.*, 2004; Gelebart *et al.*, 2008). For example, a dose dependent decrease in cell proliferation was observed after a 72-hour exposure to quercetin in NCOL-1 cell line, with EC_{50}-values for half-maximal growth-inhibition of 53.4 µM (Herzog *et al.*, 2004). A significant reduction of cell viability was also identified in three cancer cell lines treated with 10 µM and 50 µM quercetin for 48 hours (Gelebart *et al.*,

2008). However, cell viability of patient fibroblasts was not affected here after exposure to 6.25-100 μM quercetin for 24 hours (Figure 3.17). It is possible, however, that cancer cells and fibroblasts would react differently to quercetin treatment, since another study showed a beneficial effect of quercetin on proliferation of HFL-1 cells (human foetal lung fibroblasts) (Chondrogianni *et al.*, 2010). Inhibition of proteasome activity was reported in cancer cells treated with quercetin, and is thought to be the major cause of quercetin-induced cancer cell death (Klappan *et al.*, 2012). In contrast, however, proteasome activation was identified in HFL-1 cells treated with 2 μg/mL quercetin (Chondrogianni *et al.*, 2010), which is comparable to the lowest concentration of quercetin used in this study, i.e. 6.25 μM. In addition, increased activity of proteasomal system was observed in Neuro 2a cell line expressing mutated huntingtin after the exposure to 20 μM of quercetin (Chakraborty *et al.*, 2015). Here, a small increase in UBA1 levels was identified in quercetin treated cells, starting with the 25 μM concentration (Figure 3.17). Since UBA1 is the first essential protein in proteasomal degradation, increased levels of UBA1 following quercetin treatment indicate that activation of ubiquitin-proteasome system might be responsible, at least in part, for the reduction of SMN, lamin A/C and active β-catenin levels in SMA. This hypothesis is further supported by immunocytochemistry analysis showing increased UBA1 levels in the nucleus of patient fibroblasts treated with 100 μM quercetin (Figure 3.20). This analysis also suggested that quercetin treatment selectively induces expression and/or translocation of the nuclear UBA1 isoform, UBA1a. Further experiments are clearly needed to elucidate the precise mechanism of quercetin action on UBA1 expression. This could be done, for example, by studying the expression of UBA1, after the drug treatment, using isoform specific antibodies. Nevertheless, induction of UBA1 expression and proteasomal degradation is proposed here as one of the potential molecular mechanisms of quercetin action in SMA tissues.

However, some differences have been identified between the two experiments (Figures 3.16 and 3.17), and so these results should be taken with caution. For example, a lower SMN molecular band, identified in control and patient fibroblasts treated with one dose of quercetin (100 μM) (Figure 3.16), was not as distinct in the dose response experiment (Figure 3.17). Similarly, reduction of lamin A/C levels that was detected in a dose response (Figure 3.17) was not apparent in the first experiment (Figure 3.16). This raises a question of whether quercetin had a different effect in two drug treatments, and why is that so. In addition, immunocytochemistry analysis of SMN, lamin A/C and ABC (Figures 3.18, 3.19 and 3.20) expression did not agree with the results from western blotting (figure 3.17). ABC showed the most dramatic differences, where increased ABC levels were identified in quercetin treated cells using immunocytochemistry approach (Figure 3.20), compared to reduction of ABC levels identified by western blotting (Figure 3.17), thus indicating possible technical problems with protein detection. Indeed, technical problems using the same ABC antibody where already demonstrated in a previous study, where a strong cross-reaction of ABC antibody with an unknown nuclear antigen was detected in β-catenin knockout F9 cells (Maher *et al.*, 2009). Similarly, the lamin A/C (MANLAC1 4A7) antibody, that was used here in immunocytochemistry experiment, also showed positive staining in *LMNA* KO MEFs, thus suggesting that the antibody cross-reacts with a nuclear antigen (Appendix 1). Quantification of lamin A/C and ABC levels in quercetin treated cells, using immunocytochemistry, is therefore unreliable. Another limitation of this study is the small group size that limited statistical analysis in quercetin treated cells (Figure 3.17).

The results do, however, raise the question of quercetin action in SMA tissues: Can quercetin treatment induce the same changes in the expression of SMN, lamin A/C, ABC and UBA1 *in*

vivo? Quercetin treatment rescued axonal defects in SMA zebrafish, ameliorated NMJ pathology in *Drosophila* and mouse models of SMA, restored muscle fiber dimeter and improved muscle strength in a mouse model of SMA, however, survival of SMA mice was not improved with quercetin treatment (Wishart *et al.*, 2014). On the other hand, activation of the proteasomal system, by systemic restoration of UBA1 levels in a mouse model of SMA, rescued neuromuscular and peripheral organ pathology, and improved survival of SMA mice without affecting SMN expression (Powis *et al.*, 2016). This would then suggest that initial benefit of quercetin treatment, possibly through induction of proteasomal degradation, would be counteracted by excessive degradation of proteins like SMN and lamin A/C that are important for cell stability. It could help to explain why quercetin treatment restored neuromuscular pathology in SMA mice but had no benefit on their survival (Wishart *et al.*, 2014). It is possible too that quercetin would have a different effect on protein expression *in vivo*, since metabolic degradation of quercetin would likely produce metabolites that have different biological activity compared to quercetin alone (Almeida *et al.*, 2018). Further studies are clearly warranted to assess the molecular mechanism of quercetin action in SMA, *in vitro* and *in vivo*, if quercetin or its derivatives are to be used in SMA therapy design.

3.4. Conclusion

The aim of this study was to determine whether proteins identified in a multi-study comparison of published proteomic studies of SMA, including UBA1, lamin A/C, GAPDH, ANXA2, NCAM and GAP43, are differentially expressed in SMA tissues and cells. This knowledge would then be used to facilitate selection of pharmaceutical compounds that have the potential to regulate the expression of several of these proteins. However, selection of pharmaceutical compounds proved to be very challenging. Although drugs with the potential

to change the expression of target proteins were identified, using both network pharmacology approach and PubMed search, when tested in fibroblasts showed no effect on expression of target proteins or produced unwanted effects, like reduction of SMN expression in the case of quercetin treatment. In addition, technical problems, i.e. variability in protein expression within the treatment groups made quantification of protein expression unreliable. Further work is clearly warranted to determine whether multi-target drugs might be viable strategy in SMA therapy design.

CHAPTER 4: Results

Lamin A/C is mechanistically linked to UBA1, a known regulator of SMA disease pathways, and contributes to cardiac pathology in SMA

4.1. Introduction

4.1.1. Diversity of proximal spinal muscular atrophy (SMA)

Spinal muscular atrophies (SMAs) are a heterogeneous group of neuromuscular disorders, clinically characterised by motor neuron loss in the spinal cord and lower brainstem, muscle weakness and atrophy. They are roughly divided into proximal SMAs and distal SMAs (DSMAs), based on the limb region primarily affected by muscle weakness, where proximal SMA is traditionally referred to as SMA (Farrar and Kiernan, 2015). In 95% of the cases, autosomal recessive loss of *SMN1* gene is the cause of the proximal SMA, while the minority of cases link to mutations in other genes (Wirth *et al.*, 1999) (summarised in Table 4.1.). They are all characterized mostly, not exclusively, by proximal limb weakness, but show heterogeneity in mode of inheritance, age of the onset, severity of the motor function impairments and differential involvement of other organ systems (Table 4.1). For clarity, proximal SMA is referred from here on as SMA.

Table 4. 1. Genetics and clinical features of proximal spinal muscular atrophy

Type of SMA	Gene	Inheritance	Clinical manifestation	Common clinical features	References
SMN-related SMA	*SMN*	Autosomal recessive	Onset: SMA type I: before 6 months SMA type II: between 6-18 months SMA type III: after 18 months SMA type IV: adulthood Proximal weakness of lower and upper limbs associated with muscle atrophy Diaphragm and facial muscles relatively spared Death by the age of 2 years (SMA type I) or adolescence/early adulthood (SMA type II) caused by respiratory failure	Problems with swallowing and breathing (SMA type I and II) Scoliosis (SMA type I-III)	(Dubowitz, 1995)
SMA with respiratory distress and stridor	*SCO2*	Autosomal recessive	Onset: infantile Generalised muscle weakness and hypotonia associated with muscle atrophy (similar to SMA type I) Respiratory insufficiency and stridor Lactic acidosis Death usually in infancy/early childhood caused by heart failure	Hypertrophic cardiomyopathy Spasticity Ptosis and strabismus	(Salviati *et al.*, 2002) (Tarnopolsky *et al.*, 2004) (Pronicki *et al.*, 2010)
Lower limb SMA with respiratory distress	*PLEKHG5*	Autosomal recessive	Onset: early childhood Proximal weakness of lower limbs associated with muscle atrophy (early evolvement of hand and foot muscles) Progressive weakening of all muscle leading to respiratory insufficiency	Dorso-lumbar scoliosis and hyperlordosis Foot deformities (bilateral equinus varus)	(Maystadt *et al.*, 2006) (Maystadt *et al.*, 2007)

SMA-PCH	*EXOSC8* *EXOSC3* *EXOSC9* *TSEN54* *RARS2* *VRK1* *SLC25A46*	Autosomal recessive	Onset: congenital-infantile Loss of spinal cord anterior horn motor neurons Cerebellum and brainstem atrophy (pontocerebellar hypoplasia) Diffuse muscle weakness Death: infancy-adulthood (often caused by respiratory failure/complications)	Microcephaly Impared vision and hearing Hypomyelination	(Boczonadi *et al.*, 2014) (Wan *et al.*, 2012) (Burns et *al.*, 2018) (Simonati *et al.*, 2011) (Namavar *et al.*, 2011) (Renbaum *et al.*, 2009) (Van Dijk *et al.*, 2017)
Prenatal SMA with congenital bone fractures	*TRIP4* *ASCC1*	Autosomal recessive	Onset: prenatal Decreased or absent fetal movement Generalised hypotonia and muscle atrophy Long bone fractures (femur and humerus) Distal and proximal joint contractures Dysphagia Respiratory distress Death in infancy due to respiratory failure	Premature birth Microretrognathia Hypertelorism High-arched palate Pulmonary hypoplasia Patent ductus arteriosus	(Knierim *et al.*, 2016)
SMA-MDS	*TK2*	Autosomal recessive	Onset: infancy Severe proximal limb weakness and associated with muscle atrophy Areflexia Scoliosis		(Mancuso *et al.*, 2002)
SMA associated with GMG	*HEXA*	Autosomal recessive	Onset: childhood-adolescent Proximal weakness of lower and upper limbs associated with muscle atrophy	Weakness and atrophy of paravertebral muscles and interossei Dysarthria Tendon reflexes good in upper limbs but unobtainable in the lower limb	(Navon *et al.*, 1995) (Navon *et al.*, 1997)
SMALED1	*DYNC1H1*	Autosomal dominant	Onset: mostly early childhood (congenital- adulthood) Proximal lower limb weakness associated with muscle atrophy	Foot deformities (equinovarus or valgus feet and pes cavus or planus)	(Harms *et al.*, 2012) (Tsurusaki *et al.*, 2012) (Scoto *et al.*, 2015)

			Disease progression is slow or static Upper limbs mostly spared No sensory involvement	Joint contractures (hips, knees and ankles) Mild to moderate cognitive impairments and behavioural comorbidities (ADHD, autism, dyslexia)	(Niu *et al.*, 2015) (Beecroft *et al.*, 2017) (Das *et al.*, 2018) (Chan *et al.*, 2018)
SMALED2	*BICD2*	Autosomal dominant	Onset: mostly early childhood (congenital- adulthood) Proximal and distal lower limb weakness associated with muscle atrophy Disease progression is slow or static Mild or no upper limb weakness	Ankle and knee contractures Foot deformities (equinovarus feet and pes cavus or planus) Skeletal deformities (lumbal hyperlordosis, scoliosis and scapular winging) Congenital dislocation of the hips	(Peeters *et al.*, 2013) (Neveling *et al.*, 2013) (Oates *et al.*, 2013) (Rossor *et al.*, 2015) (Bansagi *et al.*, 2015) (Fiorillo *et al.*, 2016) (Rudnik-Schöneborn *et al.*, 2016)
SMA-PME	*ASAH1*	Autosomal recessive	Onset: childhood-adolescence (rarely adulthood) Proximal muscle weakness of lower and upper limbs associated with muscle atrophy Generalized epilepsy with absences and myoclonic seizures Death usually in juvenile age/ early adulthood (often caused by respiratory complications) Adult cases show slower disease progression without myoclonic epilepsy[#]	Loss of consciousness Tongue fasciculations Difficulties swallowing (dysphagia) Scoliosis	(Zhou *et al.*, 2012) (Rubboli *et al.*, 2015) (Giráldez *et al.*, 2015) (Oguz Akarsu *et al.*, 2016) (Yildiz *et al.*, 2018) (Filosto *et al.*, 2016)[#] (Ame van der Beek *et al.*, 2019)[#]
Early onset SMA with respiratory failure	*RBM7*	Autosomal recessive	Onset: infancy Proximal and distal upper and lower limb weakness associated with muscle atrophy Respiratory dificulties Death in early childhood caused by respiratory failure		(Giunta *et al.*, 2016)

Adult SMA	*VAPB*	Autosomal dominant	Onset: adulthood Proximal muscle weakness of lower and upper limbs associated with muscle atrophy Fasciculations and cramps	Autonomic dysfunction (choking, chronic intestinal constipation, sexual dysfunction) Abdominal muscle weakness Lordosis	(Nishimura *et al.*, 2004) (Marques *et al.*, 2006)
SMA with cardiac involvement	*LMNA*	Autosomal dominant	Onset: mostly adulthood (childhood-adulthood) Proximal muscle weakness of lower limbs associated with muscle atrophy Cardiac abnormalities (dilated cardiomyopathy, conduction disease, heart rhythm problems) Death associated with heart problems		(Rudnik-Schöneborn *et al.*, 2007) (Iwahara *et al.*, 2015)
Adult SMA with respiratory failure	*MAPT*	Autosomal dominant	Onset: adulthood Proximal upper limb weakness (proximal lower limb weakness usually presents with disease progression) Dyspnea and respiratory difficulties Death caused by respiratory failure	Lumbar backache	(Di Fonzo *et al.*, 2014)
ADSMA	*SETX*	Autosomal dominant	Onset: adolescent-adulthood Proximal and distal muscle weakness of lower and upper limbs associated with muscle atrophy Slow disease progression		(Rudnik-Schöneborn *et al.*, 2012)
SBMA	*AR*	X-linked	Onset: adulthood (the age of onset inversely correlates with the size of the CAG-repeat expansion within the AR gene) Proximal and distal limb and bulbar muscle weakness associated with muscle atrophy Dysarthria and dysphagia Slow disease progression	Tremors and cramps Androgen insensitivity (gynaecomastia and sexual dysfunction)	(La Spada *et al.*, 1991) (Atsuta *et al.*, 2006) (Rhodes *et al.*, 2009) (Grunseich *et al.*, 2014)

SMAX2	*UBE1*	X-linked	Onset: congenital-infantile Proximal muscle weakness and generalized hypotonia associated with muscle atrophy (similar to SMA type I) Decreased foetal movement Contractures (elbows, fingers, hips, knees, wrists and ankles) Areflexia Death usually in infancy	Fractures of femur and humerus Cryptorchidism Tongue fasciculations	(Greenberg *et al.*, 1988) (Dlamini *et al.*, 2013) (Jedrzejowska, Jakubowska-Pietkiewicz and Kostera-Pruszczyk, 2015)

Genetics and clinical features of proximal spinal muscular atrophies are listed in the table, followed by corresponding references. Adjusted according to (Farrar and Kiernan, 2015). SMA- spinal muscular atrophy; SMA type I (also known as Werdnig-Hoffmann disease); SMA type III (also known as Kugelberg-Welander disease); SMA-PCH- spinal muscular atrophy with pontocerebellar hypoplasia; SMA-MDS- spinal muscular atrophy with mitochondrial DNA (mtDNA) depletion syndrome; GMG- GM_2 gangliosidosis; SMA-LED1- spinal muscular atrophy, lower extremity predominant; SMA-LED2- spinal muscular atrophy, lower extremity predominant 2; SMA-PME- spinal muscular atrophy with progressive myoclonic epilepsy; ADSMA- autosomal dominant proximal SMA; SBMA- spinal and bulbar muscular atrophy (also known as Kennedy disease); SMAX2- X-linked spinal muscular atrophy; [#]Adult onset SMA caused by mutations in ASAHA1 without myoclonic epilepsy

4.1.2. Some SMA-causing genes are implicated in SMN-dependent disease pathways

Some SMA-causing genes are implicated in SMN-dependent disease pathways, including for example, senataxin (*SETX*) and ubiquitin-like modifier activating enzyme 1 (*UBA1*). The autosomal dominant proximal spinal muscular atrophy (ADSMA)- causing gene *SETX* (Rudnik-Schöneborn *et al.*, 2012) acts as a transcription regulator and regulator of genome stability (Groh *et al.*, 2017). SETX is involved in the repair of DNA double-strand breaks (DSBs) and R-loops (DNA-RNA hybrids) (Groh *et al.*, 2017). SETX dysregulation was also observed in SMN-dependent SMA (Kannan *et al.*, 2018). For example, decreased SETX protein levels were identified in SMN-deficient HeLa cells, SMA patient fibroblasts and cultured spinal cord neurons from SMA mice, which coincided with the increased accumulation of R-loops and DSBs (Kannan *et al.*, 2018). Decreased SETX levels were also observed *in vivo*, in spinal cords from type I SMA patients and in mouse model of SMA, and overexpression of SMN in patient fibroblasts and cultured mouse spinal cord neurons restored SETX levels and decreased R-loop accumulation. In addition, overexpression of SETX alone was sufficient to decrease R-loop accumulation in SMA patient fibroblasts and cultured mouse spinal cord neurons, indicating that low levels of SETX are directly responsible for genomic instability in SMA cells/tissues (Kannan *et al.*, 2018).

Mutations in the *UBA1* gene, which encodes the ubiquitin-like modifier activating enzyme 1 (UBA1) protein, cause a form of X-linked infantile SMA (SMAX2) (Ramser *et al.*, 2008), and a role for UBA1 in SMN-dependent pathways has also been well characterised across several models of SMA. At the protein level, UBA1 was reduced in zebrafish and mouse models of SMA, and in iPSC-derived motor neurons from patients with type I SMA (Wishart *et al.*, 2014; Fuller *et al.*, 2016; Powis *et al.*, 2016). Pharmacological or genetic suppression of UBA1 was

sufficient to induce an SMA-like phenotype in zebrafish, thus demonstrating that UBA1 directly contributes to SMA disease pathways (Wishart *et al.*, 2014). Restoration of UBA1 levels increased motor performance in zebrafish and mouse models of SMA, as well as increased survival and improved systemic pathology in SMA mice (Powis *et al.*, 2016).

Investigation of two downstream targets of UBA1 pathways, β-catenin and glycine-tRNA ligase (GARS), provided further insights into fundamental molecular mechanism that drive pathology in different tissues (Wishart *et al.*, 2014; Shorrock *et al.*, 2018). β-catenin signaling pathways play important role in motor neuron differentiation and stability, and increased β-catenin levels were restricted to neuromuscular system in a mouse model of SMA (Wishart *et al.*, 2014). In line with this, pharmacological inhibition of β-catenin levels decreased motor neuron loss and restored muscle fiber diameters in SMA mice, and ameliorated NMJ pathology in zebrafish, *Drosophila* and mouse models of SMA, but did not prevent systemic pathology in SMA mice (Wishart *et al.*, 2014). Similarly, increased expression of GARS in spinal cords from SMA mice was restricted to sensory neurons (Shorrock *et al.*, 2018). Mutations in *GARS* are known to cause Charcot-Marie-Tooth disease Type 2D (CMT2D), typically characterised by sensory impairment, but also a type of SMA, called distal spinal muscular atrophy type V (Antonellis *et al.*, 2003). Dysregulation of UBA1/GARS pathways disrupted sensory neuron fate and altered sensory-motor connectivity in SMA mice, both of which were corrected following restoration of UBA1 levels (Shorrock *et al.*, 2018).

Mutations in *LMNA*, the lamin A/C encoding gene, cause an adult form of SMA (Rudnik-Schöneborn *et al.*, 2007; Iwahara *et al.*, 2015). Rudnik-Schöneborn et *al.*, for example, described two cases of proximal SMA caused by mutations in *LMNA* gene (Rudnik-Schöneborn

et al., 2007). Both SMA patients developed proximal muscle weakness in adulthood, experienced cardiac problems with disease progression and were provided with a pacemaker. Examination of family history revealed high frequency of cardiac abnormalities and sudden unexplained cardiac deaths (Rudnik-Schöneborn *et al.*, 2007). The third patient, initially diagnosed with type III SMA, experienced muscle weakness in their lower limbs since early childhood and had cardiac involvement that required a pacemaker to be fitted at the age of 45 (Iwahara *et al.*, 2015). As in the previous two cases of SMA, examination of family history revealed increased incidence of cardiac problems and sudden deaths (Iwahara *et al.*, 2015). The evidence to implicate lamin A/C in SMN-dependent disease pathways first came from a multi-study proteomic comparison (Fuller, Gillingwater and Wishart, 2016), where increased expression of lamin A/C was identified across three separate proteomic studies of SMA, including in iPSC-derived motor neurons from type I SMA patients (Fuller *et al.*, 2016), Schwann cells (Aghamaleky Sarvestany *et al.*, 2014) and muscles (Mutsaers *et al.*, 2013) from a mouse model of SMA. In addition, identification of widespread dysregulation of lamin A/C levels in fibroblast cells from SMA patients and in different tissues from a mouse model of SMA (chapter 3, Figure 3.5), provided further support that lamin A/C might be an important regulator of SMA disease pathways. Of specific interest was the heart, where a two-fold increase in lamin A/C expression was identified at the protein level, suggesting that lamin A/C might play an important role in heart pathology. Indeed, mutations in the *LMNA* gene have already been implicated in a wide range of neuromuscular conditions that present with some form of cardiac pathology, including Emery-Dreifuss muscular dystrophy (Bonne *et al.*, 1999), limb-girdle muscular dystrophy 1B (Ki *et al.*, 2002), dilated cardiomyopathy (Fatkin *et al.*, 1999) and an adult form of SMA (Rudnik-Schöneborn *et al.*, 2007; Iwahara *et al.*, 2015).

Evidence of the heart's involvement in SMN-dependent SMA are not lacking either. For example, a systematic review of the literature in 2017 found 58 studies that reported on a total of 264 SMA patients with cardiac abnormalities (Wijngaarde *et al.*, 2017). A common finding among the 77 patients with the most severe type of SMA (type I) was structural pathology, observed mainly in the septum and/or cardiac outflow tract. All of the 63 type II SMA patients identified in the literature search had ECG abnormalities, while the 124 patients with type III SMA had cardiac rhythm disorders and/or structural abnormalities. In addition to the numerous reports of cardiac defects among SMA patients, the systematic review identified 14 studies that have documented cardiac pathology in mouse models of SMA (Wijngaarde *et al.*, 2017). Common macroscopic findings include decreased heart size and decreased thickness of the left ventricular wall and interventricular septum, while a frequent microscopic observation was cardiac fibrosis, which was detected at a pre-symptomatic stage of the disease in both severe and intermediate mouse models of SMA (Shababi *et al.*, 2010; Cobb *et al.*, 2013; Wijngaarde *et al.*, 2017). A more recent study of a severe mouse model of SMA at pre- and early symptomatic time points confirmed many of these previous findings, but also noted significant molecular defects, such as the reduced microvasculature, increased oxidative stress and apoptosis in the heart from early symptomatic SMA mice (Maxwell *et al.*, 2018). Despite this knowledge, molecular defects that drive pathology in SMA heart are not well investigated.

The aim of this chapter was to investigate the molecular mechanism of lamin A/C dysregulation in SMA tissues, and gain insight into its role in SMA disease pathways.

The specific objectives were as follows:

a) To investigate the molecular mechanism(s) of lamin A/C dysregulation in SMA tissues/cells
b) To determine the functional consequences of lamin A/C dysregulation in SMA patient fibroblasts
c) Mutations in the *LMNA* gene cause heart defects, and lamin A/C was dysregulated in the heart from Taiwanese SMA mice. To investigate whether other heart defects can be seen in SMN-dependent SMA, an unbiased view of the proteome was taken in the heart from a mouse model of SMA.

4.2. Results

4.2.1. Investigation of the molecular mechanism of lamin A/C dysregulation in SMA

In chapter 3, widespread dysregulation of lamin A/C protein levels was identified in the heart, brain, spinal cord and liver from a mouse model of SMA, and in SMA patient fibroblasts, with differing directions of expression change depending on the tissue/cell type examined (Chapter 3, Figure 3.5). Here, lamin A/C was further investigated at the mRNA and protein levels to determine the molecular mechanism of its dysregulation in SMA. Lamin A transcript levels were first investigated in SMA tissues/ cells to determine whether perturbed gene expression can explain the direction of differential protein expression, after which, lamin A/C was investigated in connection to SMN and UBA1 disease pathways to try to elucidate the mechanism of its dysregulation in SMA. Understanding the molecular mechanism of lamin A/C dysregulation in SMA may have important implications in SMA therapy design. It may aid selection of appropriate therapeutic strategies that could target lamin A/C dysregulation in SMA*. i.e.* targeting lamin A/C at the gene and/or protein level.

4.2.1.1. Lamin A transcript levels were not changed in SMA patient fibroblasts or in the heart from a mouse model of severe SMA

It was of interest to first determine whether dysregulation of lamin A/C levels can be tracked back to the aberrant transcriptional regulation. Lamin A transcript levels were therefore investigated in SMA patient fibroblasts and SMA mouse heart (where lamin A protein levels were lowest, and highest, compared to controls, respectively) (Chapter 3, Figure 3.5). Since only the lamin A isoform showed dysregulation at the protein level in SMA patient fibroblasts, primers for qPCR were designed to specifically recognise lamin A isoform (as described in 2.5.3.1). RT-qPCR analyses showed no significant change in lamin A transcript levels in the

heart from SMA mice and patient fibroblasts (Figure 4.1), indicating that dysregulation of lamin A/C expression occurred post-transcriptionally.

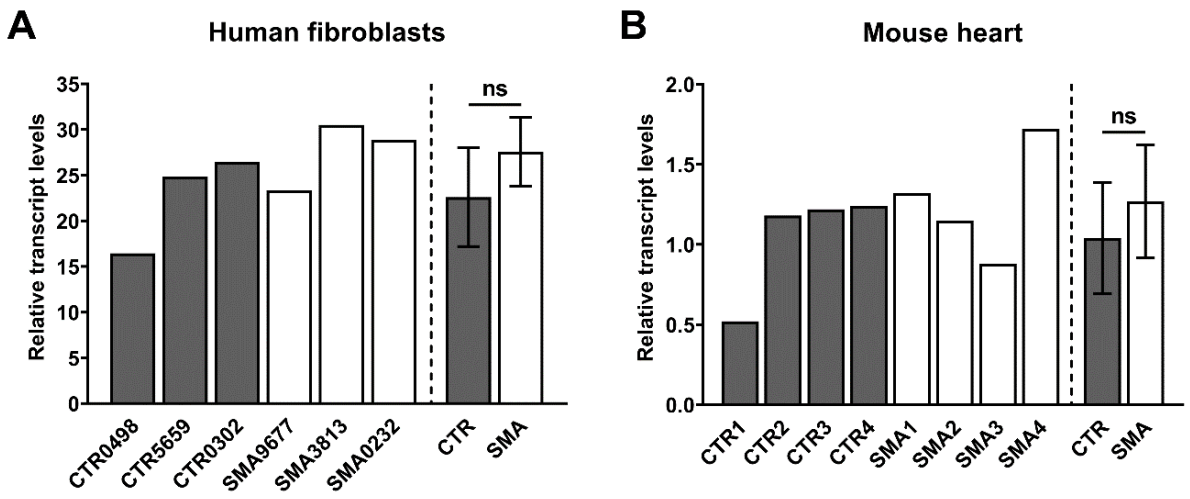

Figure 4. 1. Lamin A transcript levels are not dysregulated in SMA patient fibroblasts and heart tissue from a mouse model of SMA. Lamin A transcript levels in the **(A)** heart from SMA mice (n = 4) and healthy controls (n = 4) and in **(B)** fibroblasts from SMA patients (n = 3) and healthy controls (n = 3). Expression levels of lamin A were normalized to the geometric mean of POLR2J and TBP. Individual values for each sample and average of the group are presented, with error bars showing standard deviation from the mean. CTR- control; ns—not significant

4.2.1.2. Interaction between lamin A/C and SMN was undetectable in healthy fibroblast cells and in heart tissue extracts from control and SMA mice

Lamin A/C was previously identified as a potential SMN interactor using a mass spectrometry approach in PC12 neuronal and C2C12 muscle cell lines expressing fusion SMN proteins (Shafey *et al.*, 2010), however, this has not been verified biochemically. An SMN-lamin A/C interaction might be important for lamin A/C stability in healthy cells, and could possible explain lamin A/C dysregulation in the environment of low levels of SMN. To test this hypothesis, a physical interaction between lamin A/C and SMN was investigated in three healthy fibroblast cell lines using an immunoprecipitation technique (as described in methods section 2.4). Lamin A/C was successfully pulled down using a lamin A/C antibody attached to

magnetic beads, however, SMN was not detected in the eluate from three control fibroblasts (Figure 4.2A). The same was observed in the SMN pulldown, where both SMN and lamin A/C were easily detected in fibroblast cells by western blot analyses, however, lamin A/C was undetectable in the eluates from SMN pulldown in all three control fibroblast lines (Figure 4.2B). Two additional bands in the SMN blot, in eluates from both lamin A/C and SMN pulldown, represent the small and large subunits of the immunoglobulin (Figure 4.2A. and 4.2B). This result may not be surprising since an interaction between lamin A/C and SMN was identified previously in neuronal and muscle cells (Shafey *et al.*, 2010), and may be restricted to specific tissues/cells.

The possible interaction between SMN and lamin A/C was next investigated in the heart from control and SMA mice (Figure 4.2C). Heart was of particular interest because it showed the greatest upregulation of lamin A/C levels in SMA mice (chapter 3, Figure 3.5), and it already has an established role in the maintenance of heart health (Rudnik-Schöneborn *et al.*, 2007; Iwahara *et al.*, 2015), meaning that perturbed SMN-lamin A/C interaction might be responsible for heart defects in SMA. Lamin A/C was successfully pulled down in both control and SMA heart extracts, and a weak SMN band was also observed in the eluate from both samples, suggesting that a small amount of SMN could be interacting with lamin A/C in the heart tissue. However, the weak SMN band was also observed in the eluate from the negative control (Figure 4.2C), indicating that observed interaction between lamin A/C and SMN in heart extracts could be false positive. (The negative control refers to fibroblast extracts incubated with magnetic beads without the antibody). In addition, extra bands were observed across all samples (indicated by + sign), but the reason for this is unclear.

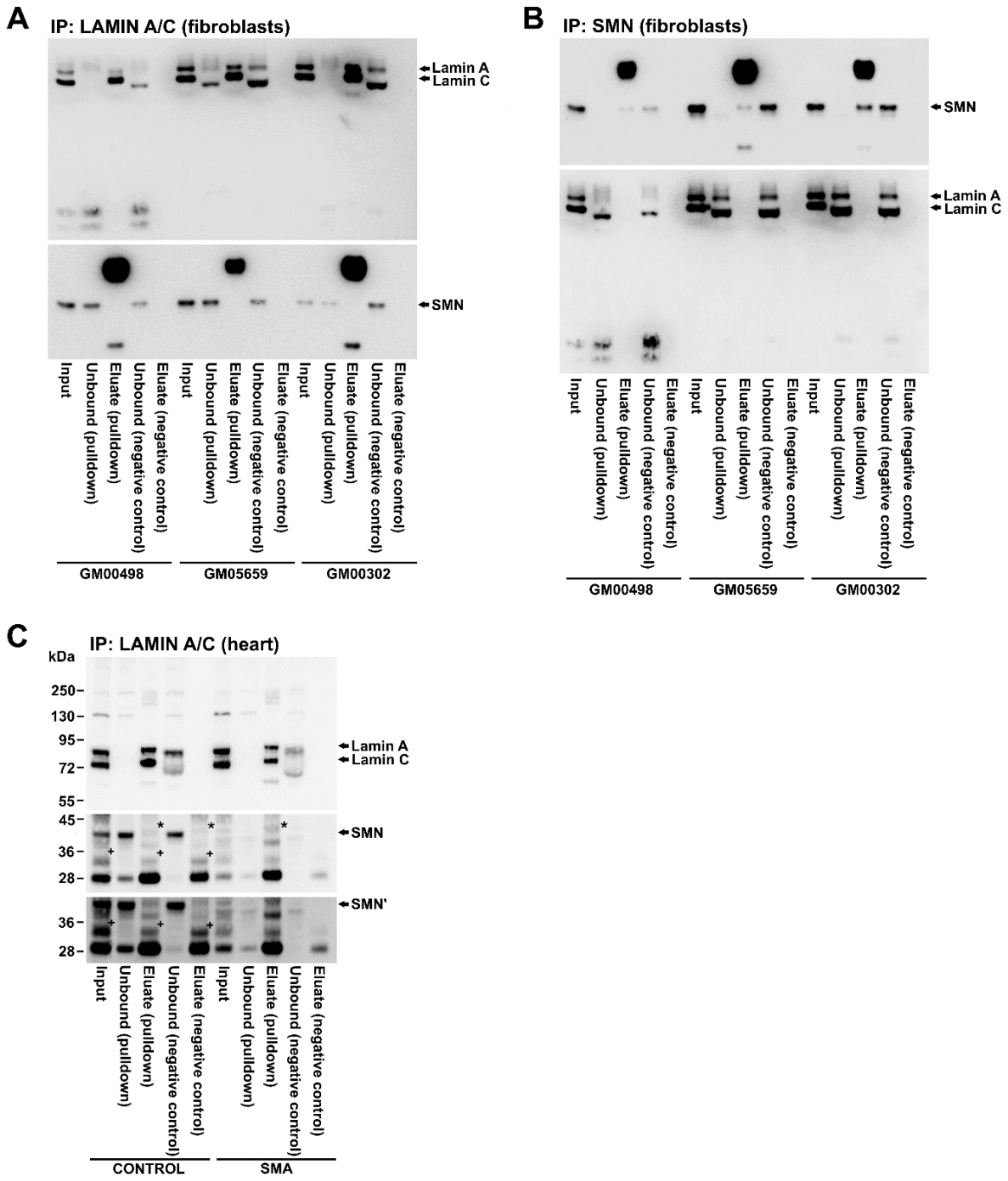

Figure 4. 2. Interaction between Lamin A/C and SMN was not identified in human fibroblasts and mouse heart tissues. Western blots showing lamin A/C and SMN expression in three healthy fibroblasts after immunoprecipitation with **(A)** anti-lamin A/C and **(B)** anti-SMN antibodies. **(C)** Western blots showing lamin A/C and SMN expression in heart tissue extracts from control and SMA mice after immunoprecipitation with anti-lamin A/C antibody. (Lamin A/C blot was also used in Figure 4.7C). Negative control lanes refer to fibroblast/ heart extracts incubated with magnetic beads without the antibody. SMN'-longer exposure time; *SMN band was observed in the eluate from lamin A/C pulldown and negative control; $^{+}$Additional bands were detected in SMN blot, in the input and eluate from both lamin A/C pulldown and negative control.

In summary, the unchanged lamin A transcript levels in SMA patient fibroblasts and heart from SMA mice suggest that dysregulation of lamin A/C protein levels can be attributed to the aberrant posttranscriptional regulation. In addition, a direct physical interaction between lamin A/C and SMN was not established in human fibroblasts or mouse heart tissues, suggesting that dysregulation of lamin A/C levels is driven by other mechanism in SMA tissues.

4.2.1.3 Lamin A/C and UBA1 are mechanistically linked

Interestingly, heart, followed by the liver showed the greatest increase of lamin A levels and the greatest reduction of UBA1 levels in SMA mice compared to controls (Chapter, 3, Figures 3.4 and 3.3), suggesting a possible link between lamin A/C and UBA1 pathways in SMA. Mutations in the genes that encode for lamin A/C and UBA1 are associated with an SMA phenotype (Ramser *et al.*, 2008) (Rudnik-Schöneborn *et al.*, 2007; Ramser *et al.*, 2008; Iwahara *et al.*, 2015), and UBA1 has already been implicated in SMN-dependent SMA disease pathways (Wishart *et al.*, 2014; Shorrock *et al.*, 2018). For example, perturbations in ubiquitin-proteasome pathway (UBA1 being one of the essential components of this pathway) were directly responsible for increased levels of β-catenin (Wishart *et al.*, 2014) and GARS (Shorrock *et al.*, 2018) that drive motor and sensory neuron pathology in SMA. Lamin A/C was therefore investigated in relation to UBA1 pathways to determine whether deceased UBA1 expression might be responsible for lamin A/C expression defects in SMA tissues.

4.2.1.3.1. Lamin A/C and UBA1 follow an inverse pattern of expression in healthy tissues/cells

A western blot study of lamin A/C, UBA1 and SMN relative protein expression levels was first conducted using equal amounts of total protein from heart, muscle, liver, brain and spinal

cord tissue extracts from healthy control mice and from healthy human fibroblasts (Figure 4.3). The analyses revealed a strong inverse pattern of lamin A/C and UBA1 expression where fibroblast cells, heart and muscle tissue had high relative levels of lamin A/C and low relative levels of UBA1. Liver, brain and spinal cord, on the other hand showed the opposite pattern, with low relative levels of lamin A/C and high relative levels of UBA1. SMN followed the same expression trend as UBA1 across the tissues examined.

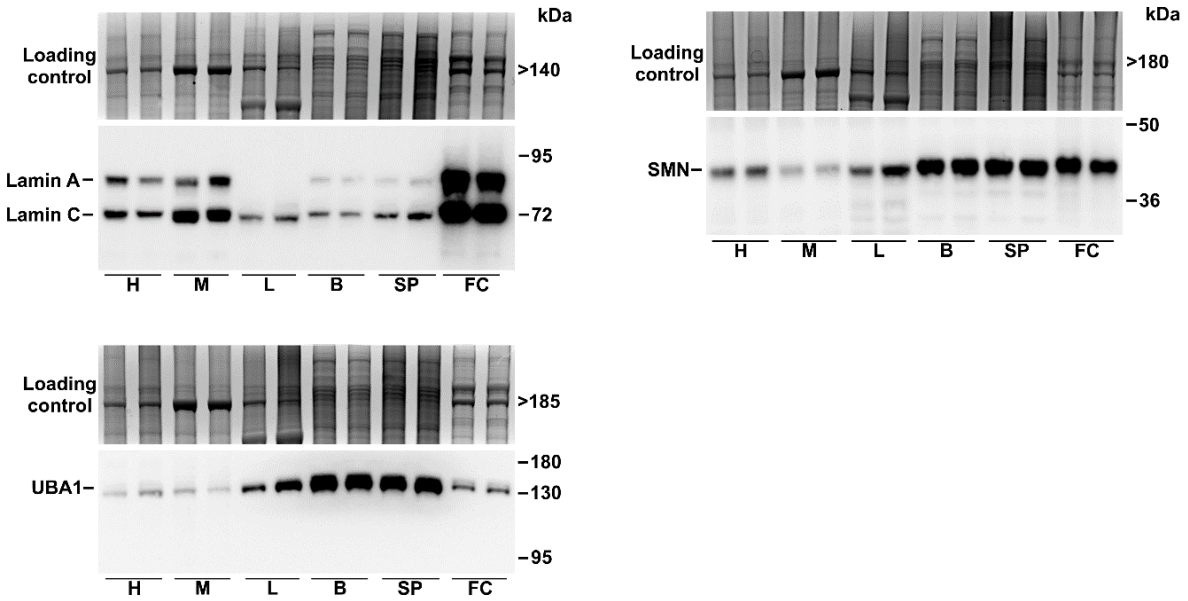

Figure 4. 3. UBA1 and lamin A/C showed the opposite expression trend across healthy mouse tissues and human cells. Western blots showing lamin A/C, UBA1 and SMN protein levels in the heart, muscle, liver, brain and spinal cord tissue from healthy mice (n=2) and in fibroblasts from healthy individuals (n=2). Fibroblasts are listed in this order: GM00498, GM00302. H-heart; M-muscle; L-liver; B-brain; SP-spinal cord; FC-fibroblast cells

4.2.1.3.2. Lamin A/C and UBA1 are able to regulate each other's expression

The inverse pattern of UBA1 and lamin A/C expression across tissues suggested a mechanistic link between the two proteins, which could rely on the ubiquitin-proteasome pathway. To determine whether UBA1 regulates lamin A/C turnover, lamin A/C expression was investigated in UBA1 knockdown human embryonic kidney (HEK) cells (provided by Dr Hannah K. Shorrock and Prof. Thomas H. Gillingwater). A 95% reduction of UBA1 levels in HEK cells was confirmed by western blotting and immunostaining (Figure 4.4A and 4.4B). A 43% upregulation of lamin A expression ($p = 0.0398$) was identified in UBA1 KD HEK cells using western blotting, independent of changes to lamin C and SMN expression (Figure 4.4A). Lamin A localization, on the other hand, was unaffected in UBA1 KD HEK cells compared to controls (Figure 4.4C).

The unchanged levels of lamin C in UBA1 knockdown HEK cells suggest that UBA1-mediated protein degradation cannot completely explain the inverse pattern of lamin A/C and UBA1 expression in healthy tissues. It was of interest therefore to determine whether lamin A/C regulates UBA1 stability. To investigate this, UBA1 expression and localization were investigated in mouse embryonic fibroblast cells lacking the *LMNA* gene (*LMNA* KO MEFs) (Sullivan *et al.*, 1999). As expected, lamin A/C was undetectable In *LMNA* KO MEFs by western blotting and immunocytochemistry (Figure 4.5A and 4.5B). Western blot analyses identified a 55% downregulation of UBA1 levels ($p = 0.0053$) and a 21% downregulation of SMN (21%, $p = 0.0016$) compared to healthy controls (Figure 4.5A). The cytoplasm was more spread in *LMNA* KO MEFs compared to wild type MEFs, however, SMN and UBA1 localization seemed unchanged when compared to wild type MEFs (Figure 4.5C and 4.5D).

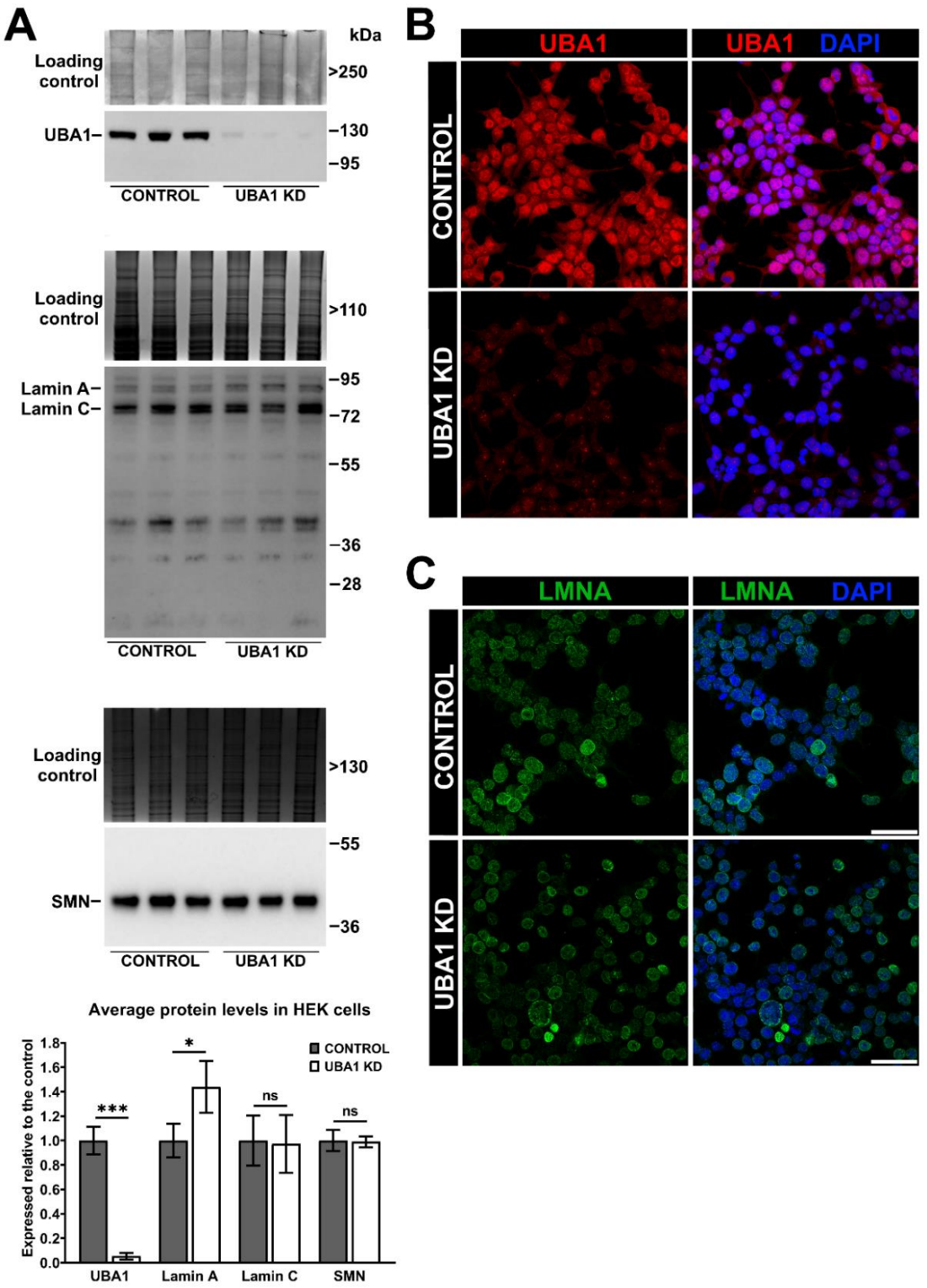

Figure 4. 4. Lamin A expression was increased in UBA1 KD HEK cells. (A) Western blots showing lamin A/C, UBA1 and SMN protein levels in UBA1 KD and control HEK cells (n=3), where n=3 represents technical replicates. Coomassie stained gel was used as internal, total protein loading control. Densitometry measurements of UBA1, lamin A, lamin C and SMN reactive bands were first normalised to densitometry measurements of Coomassie stained gel, after which all samples were normalised to the average of control. The graph is presented as average protein levels (expressed relative to the control), with error bars showing standard deviation from the mean. Representative immunocytochemistry images showing **(B)** UBA1 (red) and **(C)** lamin A (green) staining in UBA1 KD and control HEK cells, with DAPI shown in blue. Scale bar = 50 µm. ns-not significant; *p<0.05; ***p<0.001

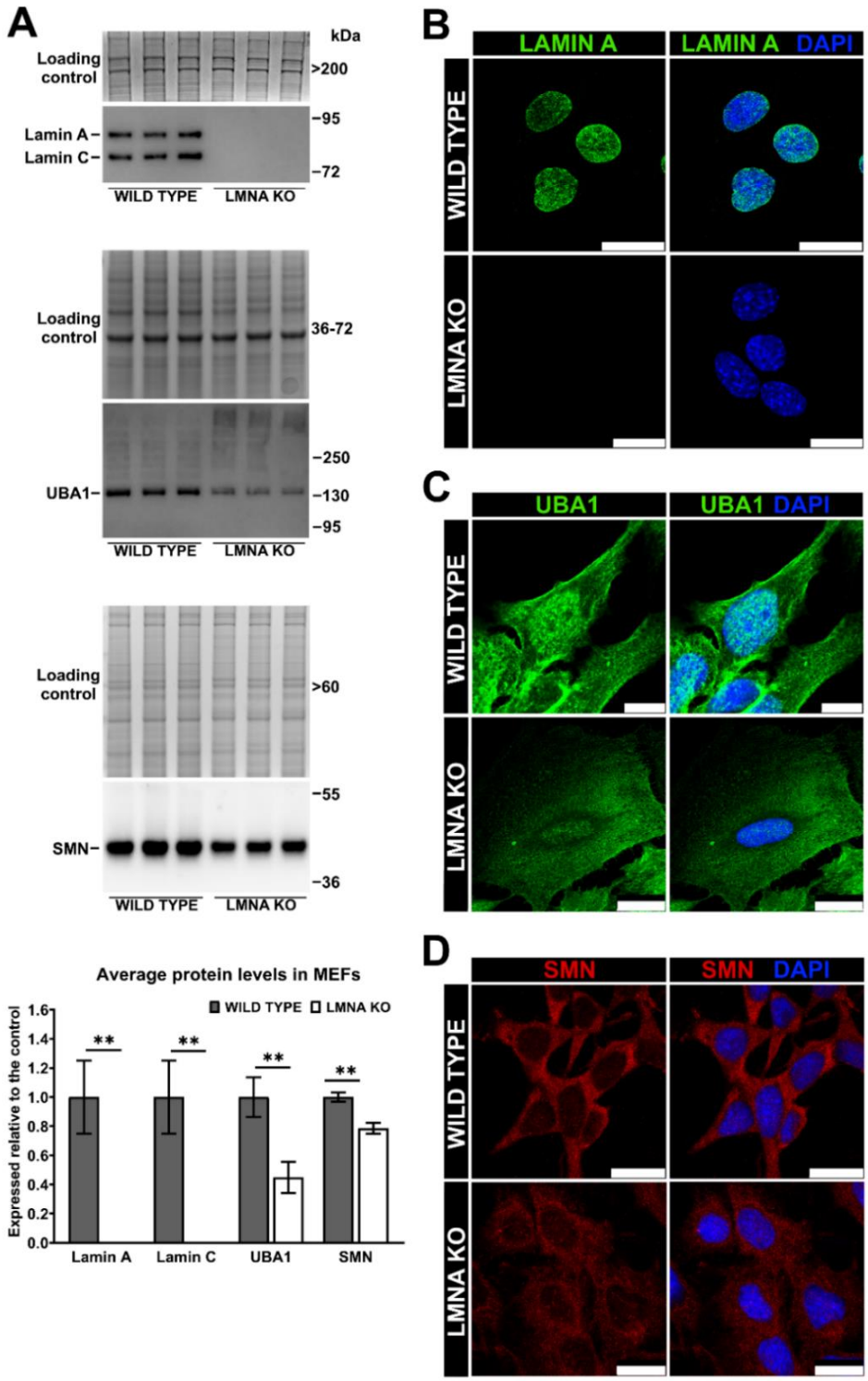

Figure 4. 5. SMN and UBA1 expression were decreased in LMNA KO MEFs. (A) Western blots showing lamin A/C, UBA1 and SMN protein levels in *LMNA* KO and wild type MEFs (n=3), where n=3 represents technical replicates. Coomassie stained gel was used as internal, total protein loading control. Densitometry measurements of UBA1, lamin A, lamin C and SMN reactive bands were first normalised to densitometry measurements of Coomassie stained gel, after which all samples were normalised to the average of control. The graph is presented as average protein levels (expressed relative to the control), with error bars showing standard deviation from the mean. Representative immunocytochemistry images showing **(B)** lamin A (green), **(C)** UBA1 (green) and **(D)** SMN (red) staining in *LMNA* KO and wild type MEFs, with DAPI shown in blue. Scale bar = 25 µm, except in wild type MEFs stained with UBA1 where scale bar = 10 µm. **p<0.01

Having demonstrated that UBA1 and SMN are decreased in MEFs from a LMNA deficient mouse, it was next of interest to determine whether restoration of lamin A/C levels can reverse defects in SMN and UBA1 expression. For this, *LMNA* KO MEFs were transfected with a recombinant *LMNA* plasmid expressing FLAG tag (pSVK3), as described in section 2.7. Western blot analysis showed no significant difference in lamin A/C expression in *LMNA* KO MEFs following transfection (Figure 4.6A), suggesting that transfection did not work. In addition, binding of the antibody to the epitope is conformation-dependent (Nguyen et *al*., 2008), and addition of a tag to the protein can affect its conformation. To account for the possibility that lamin A/C was not detected in transfected cells due to the inability of lamin A/C antibody (MANLAC1 4A7) to bind the epitope, MEFs transfected with lamin A-FLAG were stained with anti-FLAG antibody (Figure 4.6B). Immunocytochemistry analysis showed very few FLAG positive cells (5%±1.7), thus confirming the low transfection efficiency in *LMNA* KO MEFs. As expected, western blot analyses showed unchanged levels of both UBA1 and SMN in cells transfected with recombinant lamin A-FLAG (Figure 4.6A).

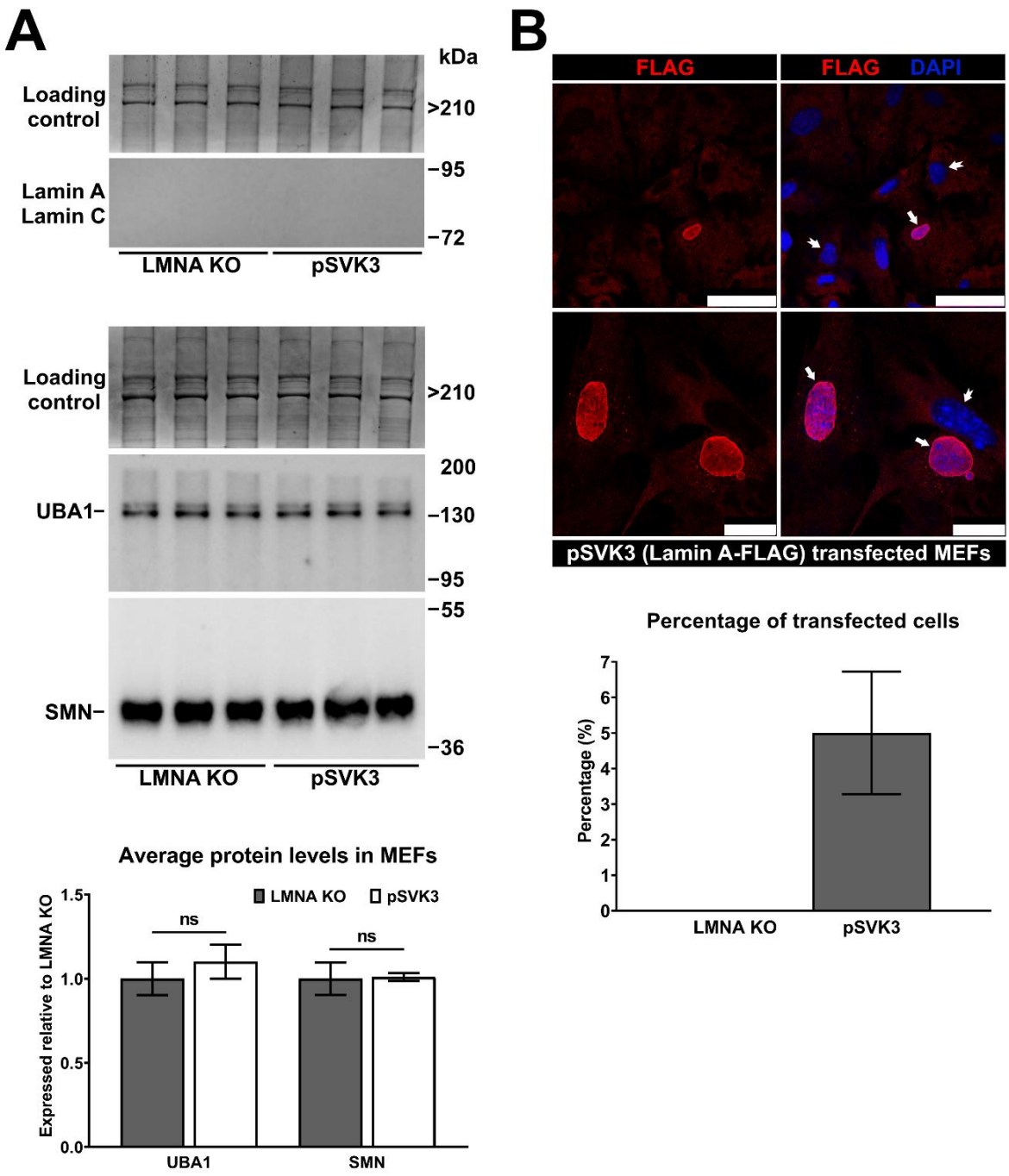

Figure 4. 6. Low transfection efficiency in *LMNA* KO MEFs. (A) Western blots showing lamin A/C, SMN and UBA1 levels in *LMNA* KO MEFs and in *LMNA* KO MEFs transfected with recombinant lamin A-FLAG plasmid (pSVK3) (n=3), where n=3 represents technical replicates. Coomassie stained gel was used as internal, total protein loading control. Densitometry measurements of UBA1 and SMN reactive bands were first normalised to densitometry measurements of Coomassie stained gel, after which all samples were normalised to the average of *LMNA* KO. The graph is presented as average protein levels (expressed relative to the *LMNA* KO), with error bars showing standard deviation from the mean. **(B)** Representative immunocytochemistry images showing FLAG (red) staining in *LMNA* KO MEFs transfected with lamin A-FLAG plasmid (pSVK3), with DAPI shown in blue. Cells that were successfully transfected are indicated by an arrow, with non-transfected cells indicated by chevron arrow. Scale bar = 75 µm in the first row and scale bar = 25 µm in the second row. The graph is showing percentage of transfected cells, with error bars showing standard deviation from the mean. ns- not significant

The inverse pattern of lamin A/C and UBA1 expression across healthy tissues implicated that lamin A/C and UBA1 might be mechanistically linked, and indeed experiments on UBA1 knockdown HEK cells and *LMNA* KO MEFs showed that lamin A/C and UBA1 are able to regulate each other's expression.

4.2.1.3.3. Lamin A/C colocalizes with UBA1 in fibroblast cells, and interacts with beta-catenin in mouse heart tissue

UBA1 already has an established role in SMA (Wishart *et al.*, 2014; Powis *et al.*, 2016; Shorrock *et al.*, 2018), and lamin A/C is emerging as a potential modulator of disease pathways in SMA, especially in the context of heart pathology. Establishing the link between UBA1 and lamin A/C may offer the opportunity to therapeutically target two SMA disease pathways at the same time which may offer better therapeutic benefit to SMA patients. To further explore the relationship between them, lamin A and UBA1 staining was examined in three control and three SMA patient fibroblast cell lines (Figure 4.7A). On average, 57% of control fibroblasts and 47% of patient fibroblasts showed co-localisation between UBA1 and lamin A at the nuclear periphery (Figure 4.7B), suggesting they might be physically interacting. To investigate this possibility, control and SMA mouse heart extracts were subjected to immunoprecipitation using a lamin A/C monoclonal antibody attached to magnetic beads. Although both lamin A/C and UBA1 were easily detected in SMA and control heart extracts by western blot analyses, UBA1 was undetectable in the eluates following lamin A/C pull-down (Figure 4.7C).

Both lamin A/C and UBA1 are implicated in the regulation of β-catenin (Wishart *et al.*, 2014; Bermeo *et al.*, 2015; Le Dour, Macquart, *et al.*, 2017). UBA1, for example, controls the stability of β-catenin through the canonical ubiquitin-proteasome pathway, and deficiency in UBA1

protein levels leads to β-catenin accumulation and neuromuscular pathology in SMA (Wishart *et al.*, 2014). Lamin A/C was shown to control the dynamics of the Wnt/β-catenin signalling pathway, where lamin A/C overexpression increased nuclear levels of β-catenin and activated the Wnt signalling pathway to promote osteoblast differentiation (Bermeo *et al.*, 2015). The same study also provided evidence of an interaction between lamin A/C and β-catenin by immunoprecipitation of nuclear proteins from mesenchymal stem cells (MSCs) forcibly overexpressing lamin A/C (Bermeo *et al.*, 2015). There is a possibility, therefore, that lamin A/C and UBA1 converge on the β-catenin signalling pathway. β-catenin levels were next examined in control and SMA heart tissue extracts to determine whether interaction between lamin A/C and β-catenin occurs under normal physiological conditions (Figure 4.7C). Indeed, a small proportion of the total β-catenin co-immunoprecipitated with lamin A/C from both SMA and control heart extracts (Figure 4.7C).

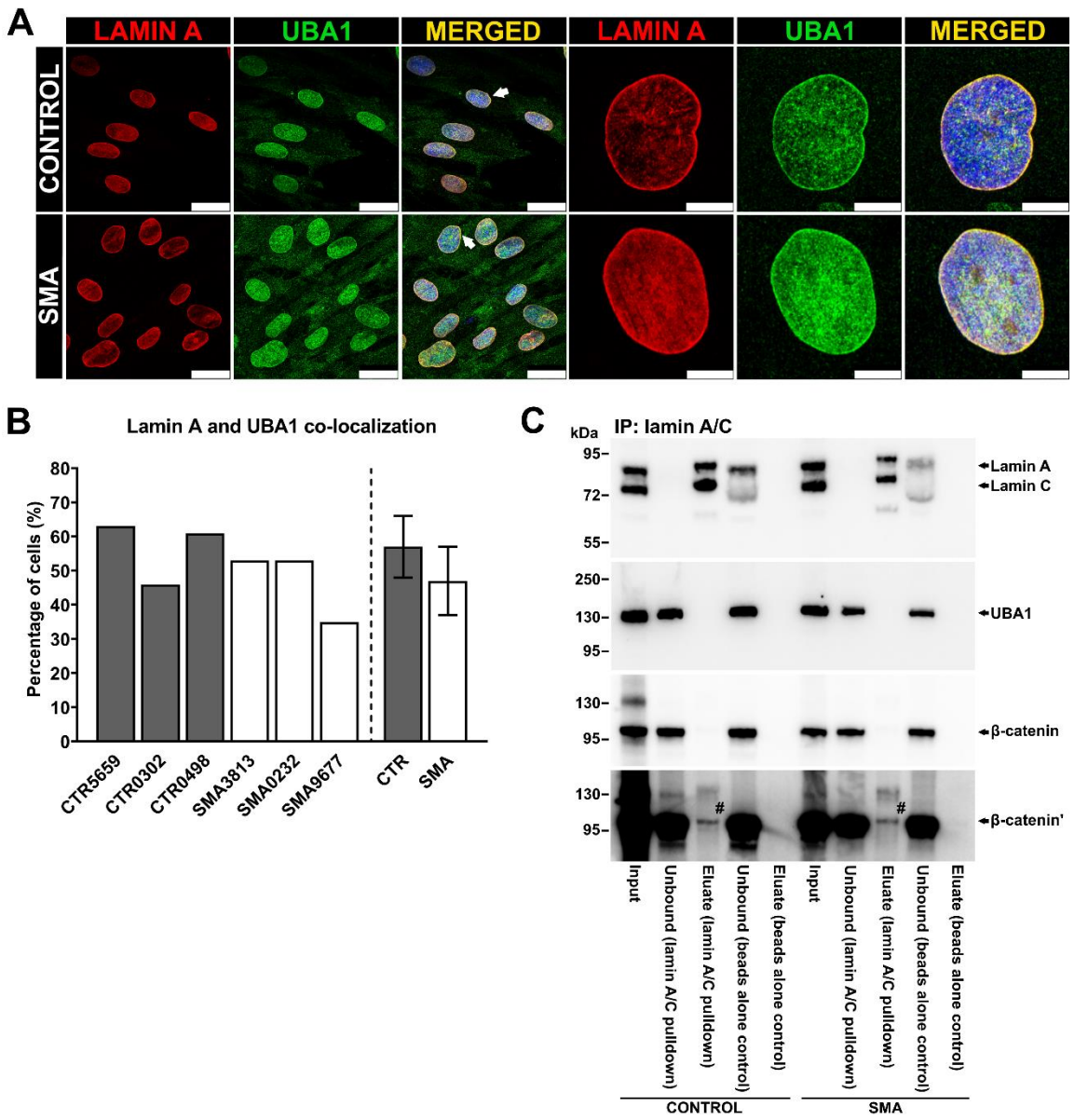

Figure 4. 7. Lamin A/C interacts with β-catenin in the heart of control and SMA mice. (A) Representative immunocytochemistry images showing lamin A and UBA1 staining in control and SMA patient fibroblast cells. Arrows in the lower magnification images indicate cells with the most obvious UBA1 staining at the nuclear periphery. Scale bar = 25 µm. Scale bar = 10 µm (control) and 7.5 µm (SMA) in higher magnification images. **(B)** The graph is presented as percentage of fibroblasts cells that showed lamin A and UBA1 co-localization. Individual values for each cell and average of the group are presented, with error bars showing standard deviation from the mean. **(C)** Western blots showing lamin A/C, UBA1 and β-catenin expression in the heart tissue from control and SMA mice after immunoprecipitation with anti-lamin A/C antibody (Lamin A/C blot was also used in Figure 4.2C). Beads alone control lanes refer to heart extracts incubated with magnetic beads without the antibody, and represent negative control. #β-catenin band was detected in the eluate from lamin A/C pulldown in both control and SMA samples, but was not observed in the eluate from the beads alone control.

When taken together, these experiments demonstrate a mechanistic link between lamin A/C and UBA1. Lamin A/C and UBA1 regulate each other's expression, they are both observed at the nuclear rim in human fibroblasts, and immunoprecipitation experiments highlighted β-catenin signalling as a potential pathway upon which they both converge.

4.2.2. Functional consequences of lamin A/C dysregulation in SMA patient fibroblasts

It was of interest to next determine the functional consequences of lamin A/C dysregulation in SMA tissues/cells as this would help to determine the role of lamin A/C in SMA disease pathways.

4.2.2.1. Lamin localization is not changed in SMA patient fibroblasts

Lamin A localization was first investigated in control (GM00302, GM05659, GM00498) and patient (GM00232, GM03813, GM09677) fibroblasts (Figure 4.8). This was done because dysregulation of lamin A/C localization was previously shown to induce molecular defects in HEK293 cells and mouse cardiomyocyte cell line (Carmosino *et al.*, 2016; Gerbino *et al.*, 2017). For example, in HEK cells expressing R321X lamin A/C mutant, lamin A/C was mis-localised to the endoplasmic reticulum (ER) which induced ER stress response and altered calcium (Ca^{2+}) dynamics. In addition, mouse cardiomyocytes carrying a different lamin A/C mutation (D243Gfs∗4) showed mis-localization of lamin A/C to the ER, altered Ca^{2+} dynamics and defective electrical coupling (Gerbino *et al.*, 2017). It was important, therefore, to investigate whether altered lamin A/C localization might be implicated in SMA disease pathways. Immunocytochemistry analysis were conducted on control and SMA patient fibroblasts to investigate the subcellular distribution of lamin A levels, however, no difference in lamin A localization was observed in SMA patient fibroblasts when compared to controls (Figure 4.8).

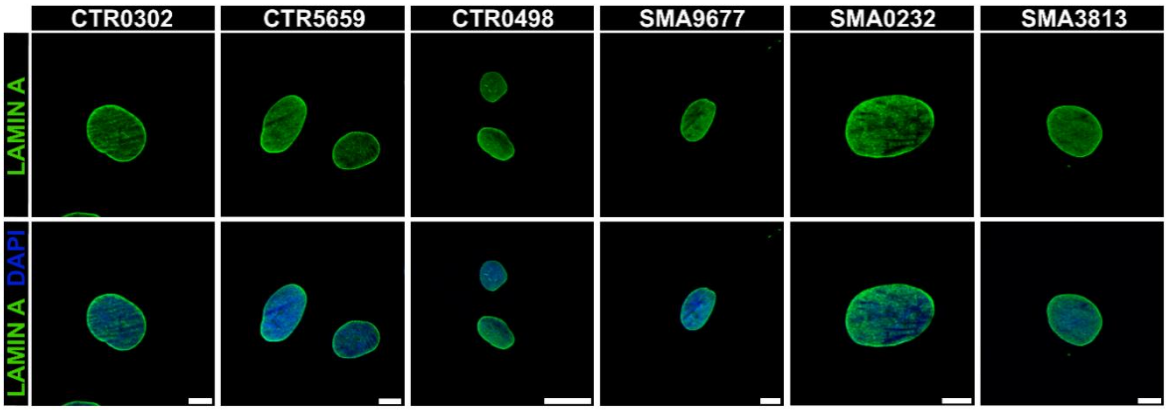

Figure 4. 8. Lamin A localization is not changed in SMA patient fibroblasts. Representative immunocytochemistry images showing lamin A staining in fibroblasts from SMA patients (n = 3) and healthy controls (n = 3). Scale bar = 10 µm, except in CTR0498 (scale bar = 25 µm) and SMA0232 (scale bar = 7.5 µm).

4.2.2.2. SMA patient fibroblasts showed increased number of nuclear defects

Nuclear abnormalities were occasionally observed in SMA patient fibroblasts during the analysis of lamin A localization. Interestingly, one recent study characterised nuclear morphology defects in fibroblast cells carrying different lamin A/C mutations (van Tienen *et al.*, 2019). The cells were derived from patients with a range of conditions including Emery-Dreifuss muscular dystrophy, dilated cardiomyopathy, HGPS and lipodystrophy. The study demonstrated 77% sensitivity, where 10 out 13 cells carrying likely pathogenic mutation where identified as laminopathies, based on the increased number of cells showing nuclear morphology defects (van Tienen *et al.*, 2019). More importantly, this study showed that nuclear morphology defects are conserved across a range of conditions associated with defects in nuclear lamins. Similar defects in SMA patient fibroblasts would suggest that changes in lamin A expression are likely to have functional consequences for the cell. Here, fibroblast cells stained with lamin A were examined retrospectively to determine the extent of nuclear defects in SMA patient fibroblasts compared to control. Based on the results from the previous study (van Tienen *et al.*, 2019), cells were examined for morphology defects such as the donut and honeycomb-like structures, blebs, micronuclei and nuclear shape

abnormalities (examples are shown in Figure 4.9). On average, 4.3% of healthy control cells showed nuclear abnormalities (Table 4.2) which is comparable to the previous study where nuclear abnormalities were identified in 4.8% of control cells (van Tienen *et al.*, 2019). Interestingly, GM00232 cell line showed very few abnormal nuclei (2.9%), while 20.3% and 14.9% of nuclei showed morphological defects in GM03813 and GM09677 cells lines respectively (Table 4.2). The most common type of nuclear malformation was bleb, followed by the donut-like structure. Nuclear morphology defects suggest that lamin A dysregulation could have pathological consequences in SMA patient fibroblasts. The analysis would, however, have to be repeated on a larger number of patient fibroblasts, to determine whether nuclear morphology defects are a conserved phenotype in SMA.

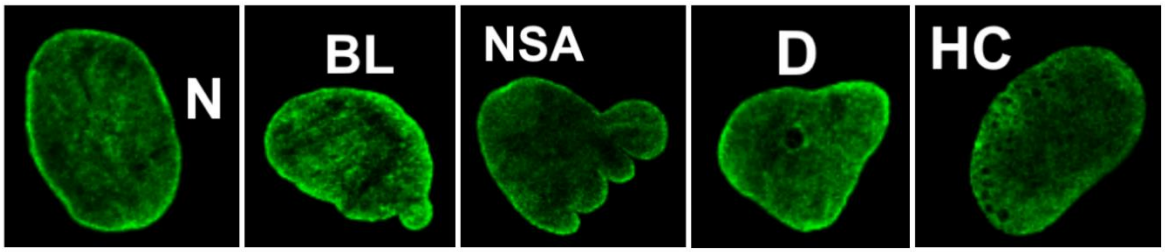

Figure 4. 9. SMA patient fibroblasts show nuclear morphology defects. Examples of nuclear morphology defects in SMA patient fibroblasts. N- normal fibroblast; BL-bleb; D-donut-like structure; HC-honeycomb-like structure; NSA-nuclear shape abnormalit

Table 4. 2. Nuclear morphology defects in control and SMA patient fibroblasts

Cell line	% abnormal nuclei	# abnormal nuclei	# normal nuclei	# total nuclei	BL	MI	D	HC	NSA	D+BL
CTR5659	5.9	6	95	101	1	1	4	0	0	0
CTR0498	4.3	5	111	116	2	0	2	0	1	0
CTR0302	2.7	3	109	112	2	0	1	0	0	0
SMA9677	14.9	15	86	101	13	0	0	2	0	0
SMA0232	2.9	3	99	102	1	0	2	0	0	0
SMA3813	20.3	26	102	128	22	0	0	0	3	1

Nuclear morphology defects in three control and three SMA fibroblasts. Number of abnormal and normal nuclei, as well as total number of nuclei is listed in the table. Type of malformation found in each cell is listed in the table: BL-blebs; MI-micronuclei; D-donut-like structures; HC-honeycomb-like structures; NSA-nuclear shape abnormalities

4.2.2.3. Proliferation and migration are not altered in SMA patient fibroblasts

Previous work has shown that increased and decreased lamin A/C expression affected cell proliferation and migration, with differing results observed depending on the *in vitro* model used (Kong *et al.*, 2012; Harada *et al.*, 2014). In the prostate cancer cell lines, LNCaP, DU145, and PC3, for example, downregulation of lamin A/C levels decreased cell migration, while lamin A/C overexpression increased migration of all three cell lines in a 2D and 3D environment (Kong *et al.*, 2012). In addition, proliferation was decreased in LNCaP, DU145, and PC3 cell lines following lamin A/C knockdown, and increased in all three cell lines overexpressing lamin A/C (Kong *et al.*, 2012). Harada et *al.*, on the other hand, found that lamin A/C knockdown increases migration of lung carcinoma-derived A549 cells, glioblastoma-derived U251 cells and MSCs in 2D and 3D environment, and A549 cell proliferation was not affected following lamin A/C knockdown (Harada *et al.*, 2014). This would then mean that proliferation and migration of different cells in SMA tissues could have been affected by lamin

A/C dysregulation, which could result in aberrant development of tissues that is often observed in SMA (discussed in chapter 1, section 1.3). To investigate this hypothesis, SMA patient fibroblasts were used for functional studies, as this *in vitro* model of SMA was readily available in the laboratory.

Cell proliferation was first determined by measuring cell doubling time in three control (GM00302, GM05659, GM00498) and three patient (GM00232, GM03813, GM09677) fibroblasts (as described in section 2, section 2.6.1). On average, SMA fibroblasts showed a longer doubling time (67.3± 18.9 hours) compared to control cells (48.3±7.57 hours), meaning their proliferation rate was decreased compared to control cells, however, this difference was not statistically significant (Figure 4.10A). Interestingly, of the three fibroblasts cells examined, GM09677, showed the highest proliferation rate, which was comparable to all three healthy fibroblasts. GM09677 was also the only cell derived from the eye lens, while others, that have a known biopsy source, originate from the skin (Table 2.1).

Cell migration was next assessed by a 3D migration assay (as described in chapter 2, section 2.6.2). The speed of cell migration in confined space, such as the extracellular matrix (ECM), depends on the physical properties of the nucleus, i.e. size, shape, and rigidity. Deformation of the nucleus to the 1/10 of its original size, for example, was shown to be the lower limit for cell migration in a range of cells, including tumour cell lines, T-cells and neutrophils (Wolf *et al.*, 2013). Deformation of the nucleus for factor 2-5, on the other hand, was shown sustainable for cell migration, but at the same time affected the rate of migration (Wolf *et al.*, 2013). Since the average diameter of fibroblast cells is 20-30 µm (Figure 4.8), the 5 µm pore well inserts were chosen for the experiment. This pore size provides sufficient challenge to

cell migration, where the effect of lamin A/C expression (i.e. cell rigidity) could be assessed on fibroblast cell migration. First, one control (GM00498) and one patient (GM003813) fibroblast cell line were plated on the apical side of the 5 μm well insert, and cell migration was assessed after 6, 24, 48 and 72 hours to determine the optimal time for the large-scale experiment (Figure 4.10B). In control and patient fibroblasts equally, no migration was observed after 6 hours, with very few cells observed on the dorsal side of the membrane after 24 hours. However, the number of migrating cells increased after 48 and 72 hours in cell culture. This data was then used to set up a migration assay, with three control (GM00302, GM05659, GM00498) and three patient (GM00232, GM03813, GM09677) fibroblasts, where the cells were allowed to migrate for 70 hours (Figure 4.10C). No significant difference in migration rate between control and patient fibroblasts was observed following 70 hours in cell culture.

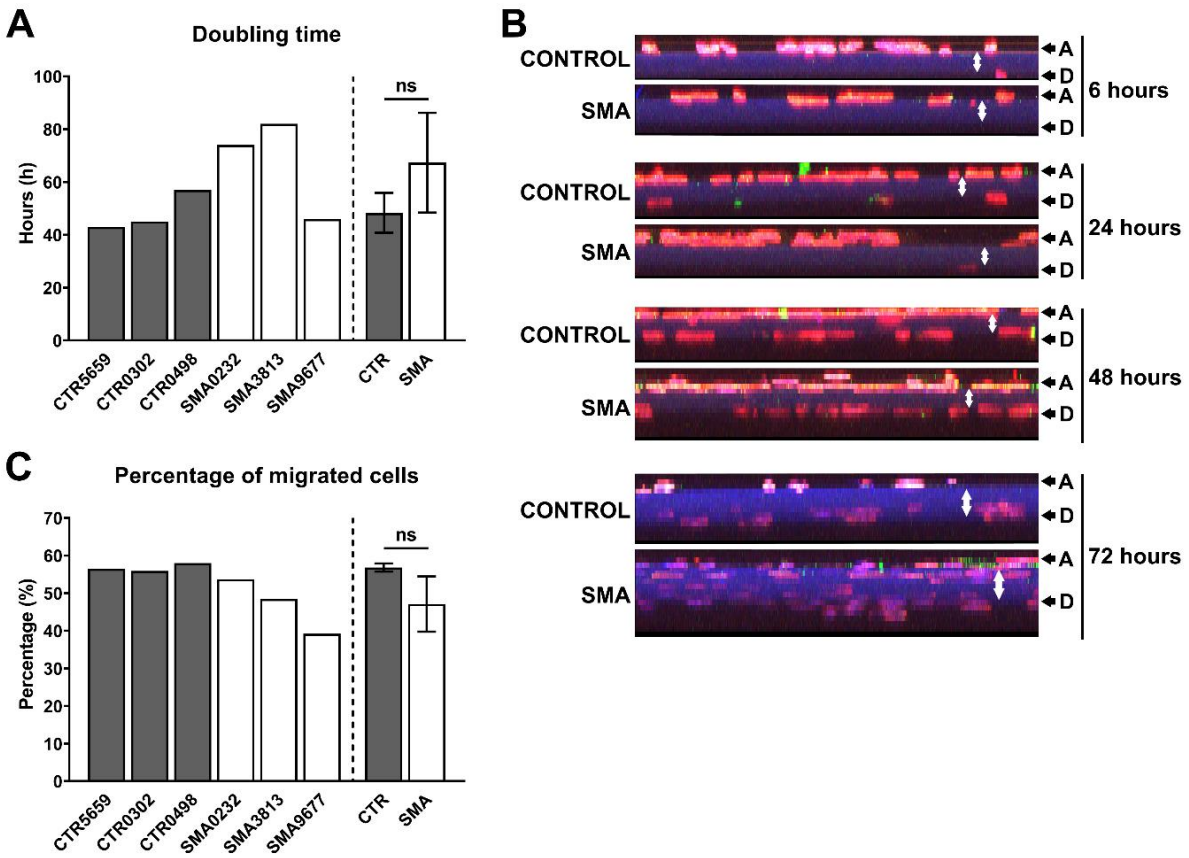

Figure 4. 10. Cell proliferation and migration are not affected in SMA patient fibroblasts. (A) Cell proliferation expressed as doubling time in fibroblast cells from SMA patients (n = 3) and healthy controls (n = 3). Individual values for each cell and average of the group are presented, with error bars showing standard deviation from the mean. **(B)** Orthogonal view of the 3D projection showing migration of control (GM00498) and patient (GM003813) fibroblasts through a 5 µm pore size membrane after 6, 24, 48 and 72 hours in cell culture. The membrane is stained blue with DAPI, and fibroblast cells are shown in red (lamin A). Up-down arrows indicate membrane thickness, where A stands for apical, and D for dorsal side of the membrane. **(C)** The percentage of cells that migrated through a 5 µm pore size membrane was assessed in control (n = 3) and patient (n = 3) fibroblasts after 70 hours in cell culture. Individual values for each cell and average of the group are presented, with error bars showing standard deviation from the mean. CTR- control; ns—not significant

In summary, functional studies did not show significant changes in cell proliferation or migration in SMA patient fibroblasts. In addition, lamin A localization was not changed in SMA patient fibroblasts. The increased number of patient fibroblast cells that showed nuclear morphology defects does, however, indicate that dysregulation of lamin A/C levels is likely to induce pathological changes in cells which are to be explored in the future.

4.2.3. Lamin A/C levels decrease with aging

Mutations in the lamin A/C gene, *LMNA,* have been implicated in Hutchinson-Gilford progeria syndrome (HGPS), a premature aging syndrome, and a role for lamin A/C in normal physiological aging has been demonstrated in human fibroblast cells (Scaffidi and Misteli, 2006), and in mouse cardiomyocytes (Afilalo *et al.*, 2007) and osteoblasts (Duque and Rivas, 2006). Reduction of lamin A/C levels, for example, was identified in fibroblasts from older healthy individuals (81-96 years) compared to the younger healthy individuals (7-11 years) (Scaffidi and Misteli, 2006). In addition, nuclear defects, similar to the ones observed in HGPS patient fibroblasts, where observed in older cells, including an increased number of foci containing phosphorylated H2A.X Variant Histone (H2AX), thus directly implicating lamin A/C in aging process (Scaffidi and Misteli, 2006). Development of new therapies and better clinical care has created an aging population of SMA patients, with new phenotypes that differ from the natural history of the disease (Tizzano and Finkel, 2017; Schorling, Pechmann and Kirschner, 2020). In the case of nusinersen, for example, where neuronal tissue is the only target of the treatment, peripheral pathologies are still a concern (Tizzano and Finkel, 2017), and a major question is whether natural aging could affect/exacerbate these pathologies in SMA patients. In the case of fibroblast cells, for example, further reduction of lamin A/C levels could bring lamin A/C levels below the crucial point where different cell functions, like proliferation and migration, could be affected.

Lamin A/C expression was first examined by western blotting in a range of fibroblast cells from healthy individuals (10 month, 1, 3, 27, 34, 39, 45 and 66 years) to verify previous results, and to expand the knowledge of age-dependent lamin A/C changes by using a wider age-range of fibroblast cells (Figure 4.11A). When compared to the average lamin A/C levels across three

young cells, an average reduction of 65% in lamin A levels and 70% in lamin C levels ($p = 0.0213$) was observed across five older cells. Interestingly, cells from a 27-year old female and a 39-years old male showed a 25% reduction of lamin A/C levels, while the levels of both lamin A and C were almost undetectable in fibroblasts from other three female subjects, i.e. 34, 45 and 66 years. Though it is not possible to conclude from a single sample, this result suggests a possibility that changes in lamin A/C expression with aging could also be gender-dependent, however, a large scale study would have to be conducted to investigate this in detail. Another important observation is that lamin A levels were lower in fibroblasts from a 1-year old (GM05659) compared to two other young subjects (10-month old corresponding to GM00302, and a 3-year old corresponding to GM00498), and two adult subjects (27 and 39 years).

Having confirmed that both lamin A and lamin C levels decrease with aging, it was next of interest to investigate whether this reduction would affect cell proliferation and migration. Proliferation and migration rate were, therefore, investigated in three older cell lines that showed the greatest reduction of lamin A/C levels (34, 45 and 66 years), and three younger cell lines (10 m, 1 and 3 years) as described in chapter 2, section 2.6. The analyses showed no significant change in proliferation or migration rate between young and old fibroblast cells (Figure 4.11B and 4.11C).

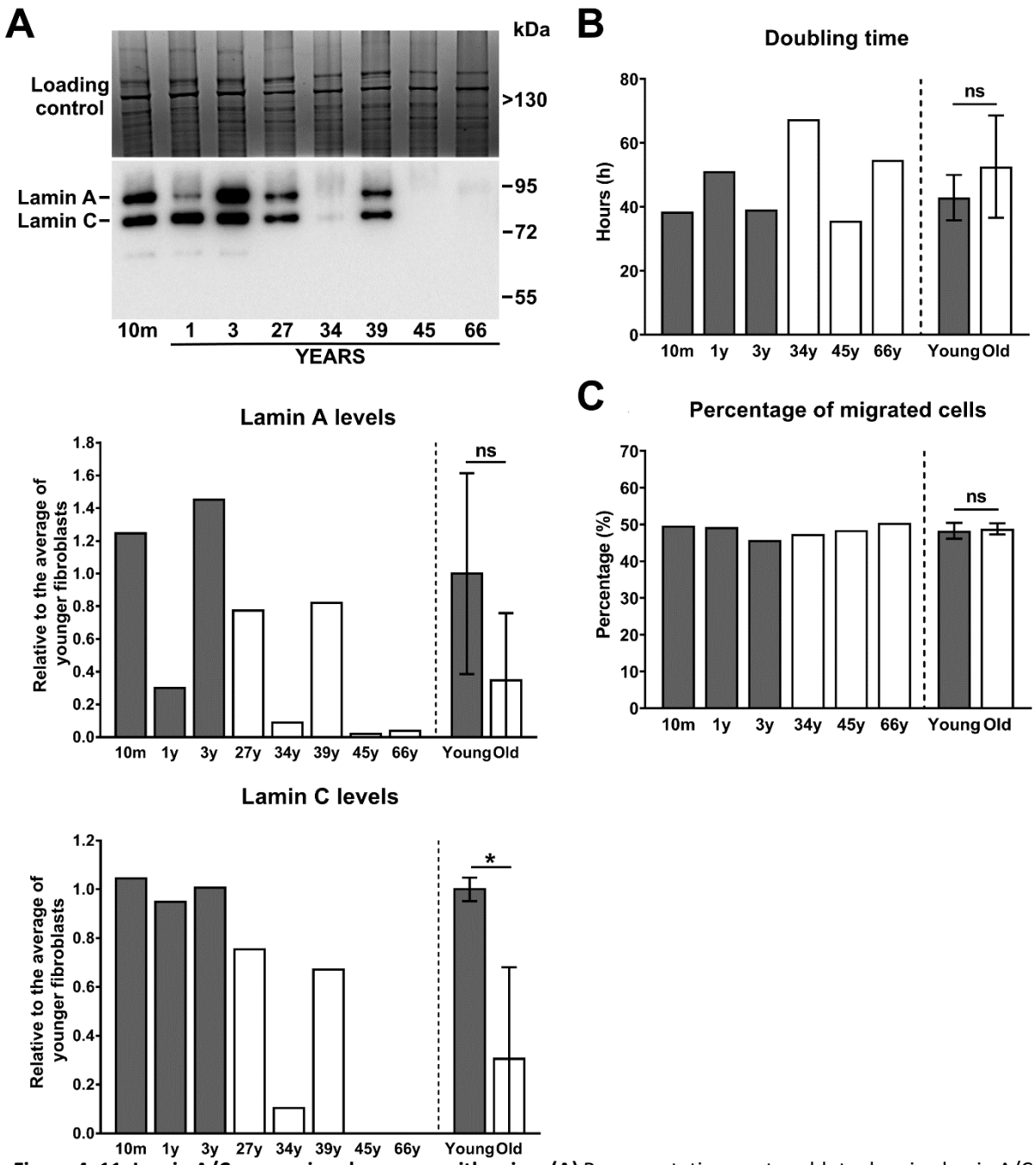

Figure 4. 11. Lamin A/C expression decreases with aging. (A) Representative western blots showing lamin A/C levels in healthy fibroblasts of different ages. Coomassie stained gel was used as internal, total protein loading control. Fibroblast cells are listed in chronological order from the youngest to the oldest one (left to right): GM00302, GM05659, GM00498, F152, F154, F008, F011, F067. Densitometry measurements of lamin A and lamin C reactive bands were first normalised to densitometry measurements of Coomassie stained gel, after which all samples were normalised to the average of young group (first three cells). **(B)** Cell proliferation and **(C)** migration were assessed in healthy fibroblast cells from younger (n = 3) and older (n = 3) individuals. Fibroblast cells are listed in chronological order from the youngest to the oldest one (left to right): GM00302, GM05659, GM00498, F154, F011, F067. Cell proliferation is expressed as doubling time, and cell migration as percentage of cells that migrated through a 5 µm pore size membrane after 70 hours in cell culture. Individual values for each cell line and average of the group are presented, with error bars showing standard deviation from the mean. m- month; y- year; ns—not significant; *p<0.05

In summary, western blot analyses identified decreased lamin A/C levels in healthy fibroblasts from older individual, confirming previous results of age-dependent changes in lamin A/C expression. Functional studies did not, however, identify significant changes in cell proliferation or migration in older healthy fibroblasts cells.

4.2.4. Heart pathology in SMA

Structural and functional cardiac defects were reported in numerous studies in SMA patients and mouse models of SMA (Wijngaarde *et al.*, 2017), however, only one study to date undertook a systematic approach to examine molecular defects in the heart from Taiwanese mouse model of severe SMA (Sheng *et al.*, 2018). Transcriptomic study identified numerous changes in the heart from early symptomatic Taiwanese mice, of which 205 genes were downregulated and 269 genes were upregulated (Sheng *et al.*, 2018). Several of these changes were tracked back to a pre-symptomatic time-point, suggesting that cardiac defects might be attributable, at least in part, to cell autonomous mechanisms (Sheng *et al.*, 2018). And whilst it has generated novel insights about changes to the transcriptome, proteomic insights into the SMA heart are lacking.

4.2.4.1. Quantitative proteomics analysis identified widespread molecular defects in the heart tissue from severe SMA mice

Here, a quantitative comparison of the SMA and age-matched control heart proteome was undertaken using iTRAQ^{TM} mass spectrometry approach (as described in methods section 2.11), to determine whether depletion of SMN protein levels leads to alterations to the heart proteome. This approach identified 3105 proteins in total (data not shown), of which 2479 were identified with a 5% local false-discovery rate. After filtering the data (as described in

section 2.11.4), 383 proteins were identified as differentially expressed in SMA mouse heart compared to controls. Of these, 177 proteins were increased and 206 were decreased in expression in SMA mouse heart compared to controls (Appendix 2). Among these was lamin A/C that showed a statistically significant 4-fold increase in the heart from Taiwanese SMA mice when compared to controls.

Gene ontology (GO) analysis using the DAVID platform (Huang, Sherman and Lempicki, 2009b, 2009a) highlighted enriched biological processes and cellular components relating to the up- and down-regulated proteins, respectively (Appendix 3). A relatively high proportion of up-regulated proteins were found to be blood-specific (n=16), and although this compliments a previous report of blood pooling in the hearts of the Taiwanese SMA mouse model (Maxwell *et al.*, 2018), these proteins were excluded from further analysis to retain focus on changes specific to the heart tissue. After also removing keratin-associated proteins (n=4), the remaining proteins were then subject to analysis using STRING 10 (Szklarczyk *et al.*, 2015) to identify statistically significant associations between them. Comparison of the resulting networks with the GO analysis output (Appendix 3) identified protein clusters associated with highly enriched molecular and/or biological processes (Figure 4.12). For the up-regulated proteins, enriched processes included organization and/or regulation of the cytoskeleton, cell junction, and extracellular matrix (Figure 4.12A), while clusters of down-regulated proteins were associated with translation and metabolic processes (Figure 4.12B).

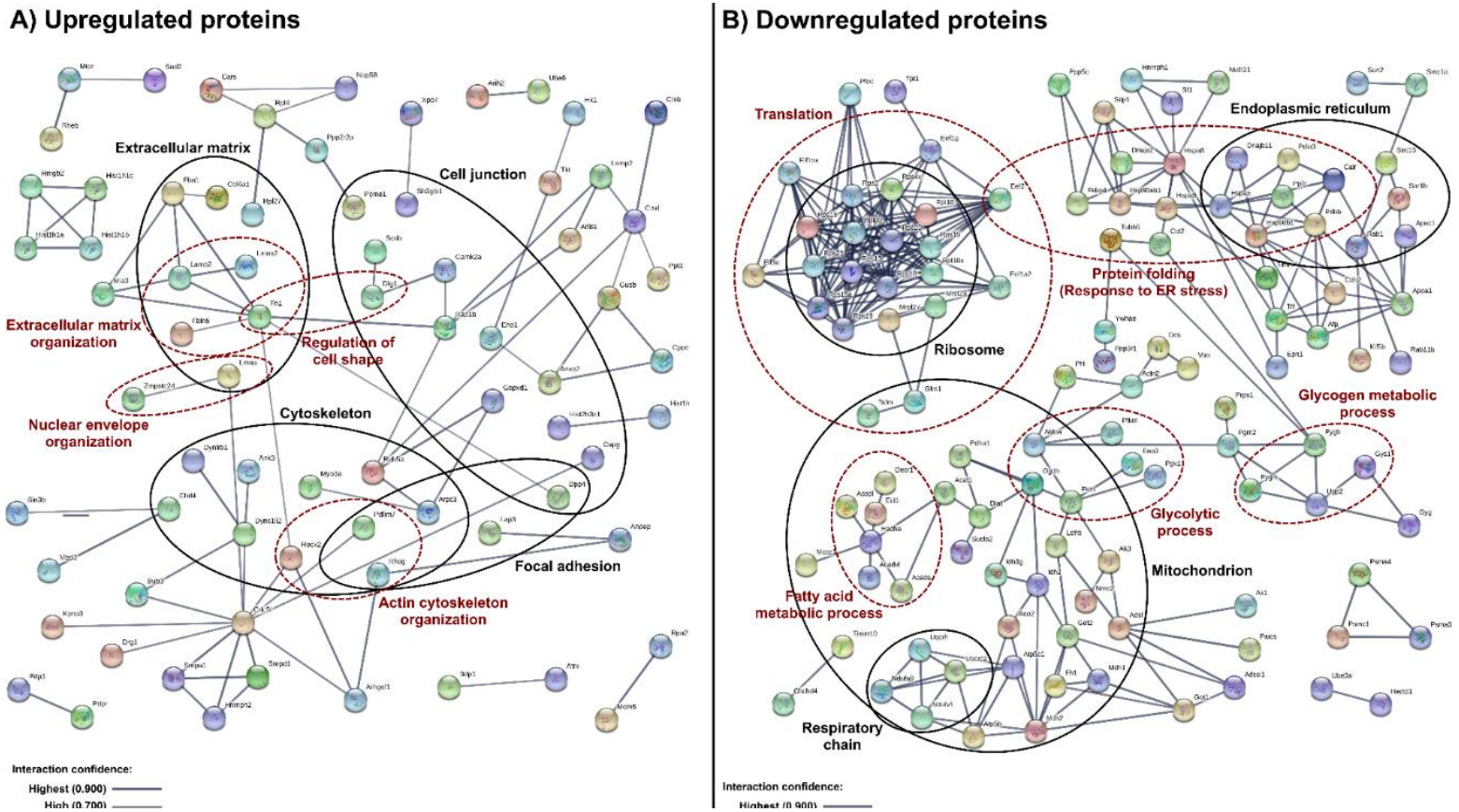

Figure 4. 12. Bioinformatics analysis of the proteins dysregulated in heart tissue from SMA mice. A) Upregulated proteins and **(B)** downregulated proteins were subjected to STRING 10 analysis. Protein associations were identified with high confidence (0.700) interaction score for **(A)** upregulated and with the highest confidence (0.900) interaction score for **(B)** downregulated proteins. The thickness and colour of the lines indicate confidence of the interaction (see legend inset in figure). Protein networks were compared to the GO analysis output (Appendix 3). The analysis identified protein clusters that associate with enriched GO terms in the cellular component (black) and biological process (red) domain. Proteins annotated to each term are shown in corresponding circles.

In summary, it was shown here that:

a) The molecular mechanism of lamin A/C dysregulation in SMA tissues/cells does not rely on aberrant transcriptional regulation, nor is it likely to be dependent on the physical interaction between SMN and lamin A/C, and remains to be further investigated. However, a mechanistic link between lamin A/C and UBA1, a known regulator of disease pathways, was identified in UBA1 knockdown HEK cells and *LMNA* KO MEFs where lamin A/C and UBA1 were shown to regulate each other's expression. In addition, it was shown here that lamin A/C interacts with β-catenin under normal physiological conditions in the heart from control and SMA mice. Considering that UBA1 is a known β-catenin interacting partner, it is possible that lamin A/C and UBA1 converge on β-catenin signalling pathway, which could have important implications for SMA therapy design.

b) Decreased levels of lamin A in SMA patient fibroblasts did not significantly affect cell proliferation and migration. An increased number of dysmorphic nuclei, identified in SMA patient fibroblasts, indicates that decreased levels of lamin A could cause defects in nuclear stability.

c) The highest upregulation of lamin A/C levels in the heart tissue from SMA mice suggested that lamin A/C might be implicated in the heart pathology in SMA. This is supported by numerous finding of severe heart defect caused by mutations in *LMNA* gene. In addition, widespread dysregulation of proteome was identified in SMA mouse heart. Dysregulated proteins were associated with metabolic processes and cytoskeletal and extracellular matrix organisation, indicating de-differentiation process in cardiomyocytes.

4.3. Discussion

4.3.1. Dysregulation of lamin A/C protein levels in SMA tissues and cells is not caused by aberrant transcription

Lamins A and C, A-type lamins, are filament proteins of the nuclear lamina that provide structural support to the nucleus (Naetar, Ferraioli and Foisner, 2017). They are encoded by the *LMNA* gene, whose alternative splicing gives rise to two isoforms, pre-lamin A and lamin C, where mature lamin A is produced by post-translational modifications of pre-lamin A (Lin and Worman, 1993). In addition to maintaining nuclear integrity, lamin A and C are involved in several other functions including mechanosignaling, chromatin organization and regulation of gene expression (Naetar, Ferraioli and Foisner, 2017).

Interestingly, mutations in lamin A/C gene are associated with an adult form of SMA (Rudnik-Schöneborn *et al.*, 2007; Iwahara *et al.*, 2015), and increased expression of lamin A/C was previously identified in three proteomic studies of SMA, including mouse Schwann cells (Aghamaleky Sarvestany *et al.*, 2014), mouse muscles (Mutsaers *et al.*, 2013) and type I patient motor neurons (Fuller *et al.*, 2016). The widespread dysregulation of lamin A and C levels, identified in SMA tissues and cells by western blotting (chapter 3, Figure 3.5), provided further evidence that lamin A/C might be implicated in SMA disease pathways. For example, a statistically significant upregulation of both lamin A and C levels was identified in the heart, liver and brain from a mouse model of SMA, while spinal cord tissue from SMA mice showed significant upregulation of lamin C levels only. In line with this, immunohistochemistry analysis showed increased levels of lamin A/C in the heart from 8 days old SMA mice (Šoltić *et al.*, 2019). In addition, dysregulation of lamin A/C levels seems to occur post-transcriptionally

since both SMA patient fibroblasts and SMA mouse heart tissue showed unchanged lamin A transcript levels (Figure 4.1).

4.3.2. Lamin A/C does not interact with SMN in human fibroblast and mouse heart tissue

Immunoprecipitation experiments using both SMN and lamin A/C antibodies showed no evidence that SMN and lamin A/C physically interact in healthy fibroblast cells. This may not be surprising since lamin A/C was previously identified as SMN interactor in PC12 neuronal and C2C12 muscle cell lines (Shafey *et al.*, 2010), meaning that SMN-lamin A/C interaction might be cell type specific. Indeed, the same study identified a range of SMN interactors that were specific to either PC12 or C2C12 cells, and some of these interactions were found only in specific stages of cell differentiation, thus emphasizing the dynamic nature of the protein interactions (Shafey *et al.*, 2010). A pulldown of lamin A/C from the heart tissue of control and SMA mice, on the other hand, showed inconclusive results. Although a small amount of SMN was identified in the eluate from the pulldown, bands were also detected in the negative control lanes which indicates the non-specific binding of proteins to the beads (Louche, Salcedo and Bigot, 2017). It is important to note though that an interaction between lamin A/C and SMN cannot be ruled out on this basis since physiological interactions may occur between a minor proportion of the total protein present and/or may be vulnerable to disruption by protein extraction methods (Kubben *et al.*, 2010). This could be tested in future using different buffers (with /without detergents, low /high salt, sonication vs no sonication etc). The biggest limitation of both pulldowns is the absence of the positive control, i.e. verified lamin A/C and SMN interactors that could identify potential problems with the extraction method.

4.3.3. Lamin A/C and UBA1 are mechanistically linked

A role for lamin A/C in SMA is strengthened by experiments showing a mechanistic link between lamin A/C and UBA1, a key contributor to SMN-dependent disease pathways (Wishart *et al.*, 2014; Powis *et al.*, 2016; Shorrock *et al.*, 2018). For example, a strong inverse pattern of lamin A/C and UBA1 expression was identified in healthy mouse tissues and fibroblasts from healthy individuals (Figure 4.3). Heart, muscles, and fibroblasts showed high relative levels of lamin A/C and low relative levels of UBA1, whereas, spinal cord, brain and liver showed low relative levels of lamin A/C and high relative levels of UBA1. This pattern of lamin A/C expression is not surprising, since a previous study already showed that lamin A/C expression correlates with tissue stiffness (Swift *et al.*, 2013). Stiffer tissues like heart and muscles induce high levels of mechanical stress, and so high levels of lamin A/C are necessary for the maintenance of nuclear stability (Swift *et al.*, 2013). The inverse pattern of UBA1 expression, on the other hand, was a new finding, and suggested that UBA1 might be implicated in the regulation of lamin A/C homeostasis through a canonical ubiquitin-proteasome pathway. Upregulation of lamin A levels in UBA1 knockdown HEK cells supported this idea (Figure 4.4). However, the unchanged levels of lamin C, following UBA1 knockdown, indicate that lamin A/C homeostasis is also regulated by other mechanisms like phosphorylation (Cho *et al.*, 2019). In addition, downregulation of UBA1 and SMN expression was identified in *LMNA* KO MEFs (Figure 4.5), suggesting that lamin A/C might also play a role in SMN and UBA1 homeostasis. Indeed, several studies showed that lamin A/C directly binds to DNA to regulate gene expression (summarised in (Naetar, Ferraioli and Foisner, 2017)), and decreased expression of both SMN and UBA1, following lamin A/C knockout, gives additional evidence for the role of lamin A/C in transcription regulation.

To further investigate the role for lamin A/C in the regulation of UBA1 and SMN expression, *LMNA* KO MEFs were transfected with wild type lamin A (Figure 4.6). This was done to assess whether restoration of lamin A/C levels can correct UBA1 and SMN expression defects in *LMNA* KO MEFs, however, this was not possible due to the low transfection efficiency (5% of cells). This indicated possible technical problems, since a 38% transfection efficiency was identified previously in *LMNA* KO MEFs, using the same method and the same lamin A plasmid (Holt *et al.*, 2003). One possibility is that long-term storage compromised plasmid integrity, i.e. 15 years at -20°C. In addition, some cells, especially primary cells, electroporate poorly and are easily killed by high voltage (Potter and Heller, 2003). Indeed, approximately 40% of cells were lost during electroporation which could explain low transfection efficiency in *LMNA* KO MEFs. Before further experiments are undertaken, both plasmid integrity and optimal electroporation conditions would have to be determined to reduce cell death and increase the efficiency of the transfection rate.

4.3.3.1 Lamin A/C and UBA1 converge on β-catenin signalling

Further evidence for the mechanistic link between lamin A/C and UBA1 was provided in control and patient fibroblasts, where UBA1 co-localized with lamin A at the nuclear lamina (Figure 4.7A). A physical interaction between lamin A/C and UBA1 was not identified in the heart from control and SMA mice, however, a small amount of total β-catenin was successfully pulled down using a lamin A/C antibody (Figure 4.7C). Lamin A/C and UBA1 might thus converge on the β-catenin signalling pathway, since both proteins were implicated in its regulation (Wishart *et al.*, 2014; Bermeo *et al.*, 2015; Le Dour, Macquart, *et al.*, 2017). UBA1, for example, controls the stability of β-catenin through the canonical ubiquitin-proteasome pathway, and deficiency in UBA1 protein levels leads to β-catenin accumulation and

neuromuscular pathology in SMA (Wishart *et al.*, 2014). Pharmacological inhibition of β-catenin signalling, using quercetin, ameliorated neuromuscular pathology in *Drosophila*, zebrafish and mouse models of SMA (Wishart *et al.*, 2014). Results from this study suggest that the mechanism of quercetin action might be due, at least in part, to the upregulation of UBA1 levels (chapter 3, Figure 3.17). At the same time quercetin induced a dose-dependent reduction of lamin A/C, beta catenin and SMN levels in patient fibroblasts, indicating a mechanistic link between lamin A/C, UBA1, β-catenin and SMN pathways that could together contribute to SMA pathogenesis. In addition, defective Wnt/β-catenin signalling was also found to contribute to the pathology of dilated cardiomyopathy caused by mutation in *LMNA* gene (Le Dour, Macquart, *et al.*, 2017). Decreased expression of several components of Wnt/β-catenin pathway, including β-catenin, was identified in the heart from a mouse model of *LMNA* cardiomyopathy (Le Dour, Macquart, *et al.*, 2017). Interestingly, pharmacological activation of WNT/β-catenin signalling improved cardiac pathology in a mouse model of *LMNA* cardiomyopathy, directly implicating it in disease pathways in cardiomyopathy associated with *LMNA* mutation (Le Dour, Macquart, *et al.*, 2017). In a separate study, lamin A/C was shown to regulate the differentiation fate of mesenchymal stem cells (MSCs) by controlling dynamics of the Wnt/β-catenin signalling pathway (Bermeo *et al.*, 2015). Lamin A/C overexpression, for example, increased nuclear levels of β-catenin and activated the Wnt signalling pathway to promote osteoblast differentiation (Bermeo *et al.*, 2015). The same study also provided evidence of an interaction between lamin A/C and β-catenin by immunoprecipitation of nuclear proteins from MSCs forcibly overexpressing lamin A/C (Bermeo *et al.*, 2015). Here, this knowledge was further expanded, by demonstrating that lamin A/C and β-catenin interact in heart extracts under normal physiological conditions. In a recent study, β-catenin was implicated in regulation of mechanosignaling by connecting adherens junctions to actin

cytoskeleton (Towbin *et al.*, 2019). This is enabled by direct interaction of β-catenin with transmembrane protein N-cadherin on one end**,** and through interactions with α-catenin and vinculin on the other side that bind to actin cytoskeleton (Towbin *et al.*, 2019).

It seems likely that UBA1 and lamin A/C converge on β-catenin signalling pathway, since they both have important functions in the regulation of its stability. It is possible, for example, that increased levels of lamin A/C are responsible, at least in part, for increased levels of β-catenin in neuromuscular tissues from SMA mice that was directly implicated in motor neuron degeneration (Wishart *et al.*, 2014). There is evidence too, that lamin A/C might be directly implicated in regulation of UBA1 levels, perhaps through regulation of its transcriptional activity. The exact link between lamin A/C and UBA1 pathways, however, remains to be determined, as it might have important implications in SMA therapy design. Carefully designed therapies that could restore the expression of all these targets may need to be designed to increase the therapeutic benefit in SMA patients.

4.3.4. Functional consequences of lamin A/C dysregulation in SMA cells and tissues

4.3.4.1. Cell proliferation and migration were not significantly changed in SMA fibroblast cells

Reduced cell proliferation and migration rates were identified in SMA patient fibroblasts compared to control cells, however, this change was not statistically significant (Figure 4.10). This could be explained by the fact that only lamin A levels were reduced in patient cells compared to controls, while the levels of lamin C stayed unchanged. This change in lamin A levels may not be sufficient to recapitulate changes in proliferation and migration that were previously identified in cells with lamin A/C knockdown (Kong *et al.*, 2012; Harada *et al.*, 2014).

However, different technical considerations have to be taken into account when interpreting the results, especially since SMA cells showed variable proliferation rates. Of the three SMA fibroblast cell lines examined, GM09677 showed the highest proliferation rate (comparable to all three healthy fibroblasts). GM09677 was also the only cell derived from the eye lens, while others, that have a known biopsy source, originate from the skin (Table 2.1). Indeed, biopsy location might offer an explanation for differences in proliferation ad migration rate between SMA cells. For example, it was shown previously that skin fibroblasts from the abdominal scar tissue have higher proliferation rate compared to skin fibroblasts from the back of the ear and the eyelid (Fernandes *et al.*, 2016), and in a separate study, fetal lung and skin fibroblasts derived from the same individual showed different migration rates (Kondo and Yonezawa, 1992). In line with this, widespread differences in gene expression profiles were identified between fibroblast cells derived from different anatomical locations (Chang *et al.*, 2002). Genes implicated in cell proliferation and migration were among those identified, thus supporting the idea that biopsy location has important implications for cell dynamics (Chang *et al.*, 2002). Another important consideration is passage number. For example, migration rate of fetal skin fibroblasts decreased with higher passage number, while fetal lung fibroblasts showed consistent migration throughout passages (Kondo and Yonezawa, 1992). In addition, reduction in proliferation rate was observed in skin fibroblasts with higher passage number (Ng *et al.*, 2009). Unfortunately, not all information (i.e. passage number and biopsy source) were available for fibroblast cells (Table 2.1) and so complete control of experimental conditions was not possible.

In conclusion, proliferation and migration were not significantly changed in SMA patient fibroblasts, although interpretation of results was hampered here for technical reasons. It

would be of interest in the future to assess how lamin A/C dysregulation affects SMA patient cell proliferation and migration, as this may have important implications for cell/tissue health and integrity. When doing so, both biopsy source and passage number should be taken into account to facilitate interpretation of results.

4.3.4.2. Nuclear morphology defects are present in SMA patient fibroblasts

SMA patient fibroblasts showed increased number of dysmorphic nuclei compared to healthy age-matched healthy controls (Table 4.2). The same nuclear morphology defects were previously observed in fibroblast cells from Emery-Dreifuss, dilated cardiomyopathy, HGPS and lipodystrophy patients caused by lamin A/C mutations (van Tienen *et al.*, 2019), and downregulation of lamin A/C levels in ovarian surface epithelial cells was sufficient to induce nuclear morphology defects (Capo-chichi *et al.*, 2011). Aberrant nuclei could thus be more susceptible to apoptosis compared to control cells, either because of the altered response to mechanical stress or altered gene expression (Mallampalli *et al.*, 2005).

4.3.4.3. Proliferation and migration rate were not significantly changed in fibroblast cells from older healthy individuals

There are several lines of evidence that implicate lamin A/C in aging. For example, accumulation of truncated pre-lamin A protein progerin (Δ50 lamin A) is a pathological feature of premature aging syndrome, Hutchinson-Gilford progeria syndrome (HGPS) (Verstraeten *et al.*, 2008), and a small amount of progerin was detected previously in healthy fibroblast cells of different ages (Scaffidi and Misteli, 2006). In addition, increased number of TP53-binding protein 1 (53BP1) foci and increased levels of histone γ-H2AX, markers of DNA damage, were identified in HGPS patient fibroblasts, indicating altered DNA damage response that promotes

genomic instability and cell apoptosis in HGPS cells (Liu *et al.*, 2005). Similarly, the percentage of nuclei with phospho- H2AX foci was significantly higher in fibroblasts from older individuals compared to younger individuals (Scaffidi and Misteli, 2006), suggesting that the same mechanism is responsible for aging in healthy and HGSP fibroblasts. Reduction of lamin A/C levels is another feature of aging cells, and was previously reported by immunocytochemistry in dermal fibroblasts from older healthy individuals (81-96 years) compared to younger heathy individuals (7-11 years) (Scaffidi and Misteli, 2006). Here, a drastic reduction of lamin A/C levels was identified by western blotting in fibroblasts from healthy individuals starting from the age of 27 (Figure 4.11A), which expands the knowledge of age-dependent changes in lamin A/C levels in healthy fibroblasts. Increased number of γ-H2AX foci was observed in LMNA depleted 293 cells treated with interstrand cross-link agents, indicating compromised DNA damage response (Singh *et al.*, 2013), and in human skin fibroblasts, lamin A/C knockdown induced production of ROS (Sieprath *et al.*, 2015). In a separate study a link between DNA damage, ROS production and cell apoptosis was established (Kang *et al.*, 2012). For example, overexpression of histone H2AX and/or its accumulation as a result of DNA damage, was shown to be sufficient to increase production of ROS in human osteosarcoma (U2OS) and human mammary epithelia (HBL100) cell lines (Kang *et al.*, 2012). When taken together, these findings indicate that reduction of lamin A/C levels might be directly responsible for compromised DNA damage response in aging cells that results in genomic instability and cell death.

A key question here is: can age-related changes in lamin A/C levels affect the pathology in aging population of SMA patients? For example, decreased cell proliferation was identified previously in lamin A/C depleted human fibroblasts (Sieprath *et al.*, 2015). It is possible

therefore that further reduction of lamin A/C levels in SMA fibroblast cells, as a consequence of aging, would exacerbate defects in cell dynamics. Since fibroblasts from adult SMA patients were not available for these experiments, cell proliferation and migration were assessed in older healthy fibroblasts that showed the greatest reduction of lamin A/C levels (Figure 4.11). No significant difference in proliferation or migration rate was identified between older and younger cells, which is in line with previous studies showing similar doubling times between fibroblasts of different ages (Ng *et al.*, 2009; Moulin *et al.*, 2011). However, it is possible too, that different passage numbers and/or biopsy locations masked changes between two fibroblast populations. Indeed, one previous study showed that older fibroblasts (77 years) migrate slower compared to the younger fibroblasts (36-years), and in both cases cell migration decreased with increasing passage number (Kondo and Yonezawa, 1992). The most obvious consequence of reduced fibroblast migration is impaired skin wound healing (Li *et al.*, 2004) which could significantly decrease the quality of life of SMA patients. Though the question remains: how would an age-dependent reduction of lamin A/C levels affect other SMA tissues/cells that showed increased levels of lamin A/C? In the heart tissue, for example, increased levels of lamin A/C are likely implicated in the heart pathology. Can reduction of lamin A/C levels improve heart pathology, or will reduction of lamin A/C levels induce mechanical stress in cardiomyocytes and lead to cell apoptosis? Liver tissue from SMA mice, on the other hand, showed increased levels of pre-lamin A, which could result in cell senescence as shown previously in skin fibroblasts (Sieprath *et al.*, 2015). It was already shown that liver function declines with aging in healthy individuals (Cieslak *et al.*, 2016), and this can be linked, at least in part, to the decreased DNA repair activity, identified in hepatocytes from old SMA mice (Intano *et al.*, 2003). This would then mean that aging process could exacerbate liver dysfunction in SMA, where decreased levels of lamin A/C are likely to impair DNA damage

response and induce cell apoptosis. All of these questions warrant further experimental attention to determine the best strategy in development of therapies for aging population of SMA patients.

4.3.5. Lamin A/C is likely implicated in the regulation of SMA heart pathology

Mutations in *LMNA* gene cause a spectrum of disorders known as laminopathies, the majority of which prominently feature cardiac pathology, including autosomal dominant Emery-Dreifuss muscular dystrophy (EDMD) (Bonne *et al.*, 1999), limb-girdle muscular dystrophy 1B (LGMD1B) (Ki *et al.*, 2002), dilated cardiomyopathy (DCM) (Fatkin *et al.*, 1999) and an adult from of SMA (Rudnik-Schöneborn *et al.*, 2007; Iwahara *et al.*, 2015). Remarkably, some mutations in the *LMNA* gene can result in different pathologies (Kang, Yoon and Park, 2018). For example, a missense mutation (c.1130G > T) in exon 6 of *LMNA* gene, found in a case of adult onset SMA (Rudnik-Schöneborn *et al.*, 2007), has also been attributed to LGMD1B (Ki *et al.*, 2002); both of which share heart conduction problems and dilated cardiomyopathy. This indisputable link between lamin A/C mutations and cardiac pathology in a wide range of conditions, including a rare form of SMA, leaves very little doubt that correct functioning of lamin A/C is a key requirement for the maintenance of cardiac health. The finding here that lamin A/C is robustly increased in heart tissue from a mouse model of SMA therefore strongly suggests that lamin A/C is responsible, at least in part, for previously reported cardiac defects in SMA.

Lamin A/C expression levels correlate with tissue stiffness, where rigid tissues have the highest levels and softer tissues the least (Swift *et al.*, 2013), and this expression trend has functional implications for cell stability and cell dynamics (Harada *et al.*, 2014). In stiff tissues like heart

and bone, where cells sustain higher levels of mechanical stress, higher lamin A/C levels protect the integrity of the genome by stiffening the nucleus (Swift *et al.*, 2013). However, if overexpressed, lamin A/C was shown to alter cell dynamics (Kong *et al.*, 2012; Harada *et al.*, 2014). Kong et *al.*, for example, showed increased migration rate of three prostate cancer cell lines, following overexpression of lamin A/C levels (Kong *et al.*, 2012), while Harada et *al.*, found that lamin A/C overexpression decreases migration of lung carcinoma-derived A549 cells (Harada *et al.*, 2014). This therefore suggests that changes in lamin A/C expression may be most pathologically relevant in SMA in highly mechanically active tissues such as the heart, where increased expression of lamin A/C is likely to impair its proper functioning. Indeed, increased rigidity of human and rat cardiomyocytes increased the extent to which cells/tissues resist deformation (i.e. passive tension) *in vitro* (Borbély *et al.*, 2005; Røe *et al.*, 2017), and *in vivo* rat experiments showed that higher passive tension slows the dynamics of myocardium contractions and induces functional heart defects (Røe *et al.*, 2017). Increased cardiomyocyte rigidity was also identified in a cell model carrying D192G mutation in *LMNA* gene, where mutant lamin A and lamin C accumulate as distinct foci in the nucleus (Lanzicher *et al.*, 2015). This mutation causes severe dilated cardiomyopathy in humans (Lanzicher *et al.*, 2015), which strongly mirrors the phenotype previously observed in severe and mild mouse models of SMA, including thinning of ventricle walls and interventricular septum (Shababi *et al.*, 2010; Maxwell *et al.*, 2018), and dilation of ventricles (Heier *et al.*, 2010; Bogdanik *et al.*, 2015; Maxwell *et al.*, 2018). The pathological end-point of dilated cardiomyopathy is systolic heart failure where the heart cannot pump blood properly. This would be evidenced by decreased ejection fraction and blood pooling in ventricles; both of which were identified in SMA mice (Heier *et al.*, 2010; Shababi *et al.*, 2012; Bogdanik *et al.*, 2015; Maxwell *et al.*, 2018) and SMA patients (Yasuma, Kuru and Konagaya, 2004; Roos *et al.*, 2009; Iwahara *et al.*, 2015). In the context of

SMN-dependent SMA, it seems highly likely, therefore, that increased levels of lamin A/C would lead to stiffening of the cardiomyocytes, impeding their ability to contract properly and inducing the cardiac defects previously reported in SMA. In addition, cardiac fibrosis has been described in patients harbouring a LMNA mutation (van Tintelen *et al.*, 2007; Le Dour, Wu, *et al.*, 2017), and was frequently reported in SMA patients and mouse models of SMA (Wijngaarde *et al.*, 2017), even at a pre-symptomatic stage of the disease in both severe and intermediate mouse models of SMA (Shababi *et al.*, 2010; Cobb *et al.*, 2013). Cardiac fibrosis is a key contributor to myocardial rigidity (Røe *et al.*, 2017), and supports the idea that increased rigidity of cardiac muscle could be responsible for pathological defects in SMA hearts.

The fact that fibrosis is observed at a pre-symptomatic stage of the disease gives confidence that lamin A/C dysregulation might also be an early phenotype in SMA heart. This is supported by studies showing direct relationship between tissues stiffness and lamin A/C expression (Buxboim *et al.*, 2014). Phosphorylation, for example, was identified as an important regulator of lamin A/C turnover, where hypo-phosphorylation promotes lamin A/C stability and decreases its degradation (Cho *et al.*, 2019), and this process seems to depend on the rigidity of ECM (Buxboim *et al.*, 2014). For example, *in-vitro* investigation of MSCs showed that stiffer matrix promotes lamin A/C dephosphorylation in favour of the genome stability (Buxboim *et al.*, 2014). Indeed, western blot analysis did indicate a small difference in electrophoretic mobility of lamin A and C between control and SMA heart tissue samples, indicating possible differences in the post-translational status of lamin A/C (Appendix 4). The lower position of lamin A/C bands in SMA heart samples compared to control samples suggest that lamin A/C hypo-phosphorylation could indeed be responsible for increased lamin A/C levels in SMA heart

tissue, and possible other tissues from a mouse model of SMA. This may also help to explain why changes in lamin A/C protein levels in the heart form SMA mice and patient fibroblasts could not be tracked back to the aberrant transcription. Additional experiments are clearly warranted to determine whether changes in phosphorylation state of lamin A/C exist between control and SMA samples in all tissues examined, as this would help to explain the mechanism of lamin A/C dysregulation in SMA tissues. Antibodies that are raised against phosphorylated lamin A/C, and are available commercially, could thus help to answer this question. This may have important implications in SMA therapy design to determine the best approach to target lamin A/C dysregulation.

4.3.5.1. Widespread molecular defects in the heart from a severe mouse model of SMA

The arguments above (section 4.3.5) support the hypothesis that lamin A/C dysregulation is likely to be responsible, at least in part, for previously reported cardiac defects in SMA, but other proteins identified in proteomics screen also offer insight into the molecular defects underlying cardiac abnormalities in SMA. For example, two such proteins, SUN domain-containing protein 2 (SUN2) (Taranum *et al.*, 2012) and cell division cycle 5-like protein (Cdc5l) (Zahr and Jaalouk, 2018), are known lamin A/C interactors and may provide further insights into lamin A/C-associated pathways in SMA. Like *LMNA*, mutations in *SUN2*, the gene encoding the SUN2 protein, have been associated with Emery-Dreifuss muscular dystrophy, a neuromuscular disorder often associated with cardiac defects (Meinke *et al.*, 2014). Cdc5l, on the other hand, is a known splicing complex component that appears to require lamin A/C in order to regulate its assembly and targeting to the spliceosomal complex (Zahr and Jaalouk, 2018). Alterations to this interaction may therefore affect splicing, further exacerbating the downstream molecular consequences of reduced SMN expression. It is interesting to note that

a large proportion of the downregulated proteins in the SMA mouse heart were associated with translation, and re-enforces previous work showing that the SMN protein plays fundamental roles in protein translation (Sanchez *et al.*, 2013; Bernabò *et al.*, 2017). It is also highly relevant that a large proportion of the downregulated proteins in the SMA heart to be associated with metabolic processes, while the upregulated proteins were strongly associated with cytoskeletal and extracellular matrix organisation (Figure 4.12). Imbalances in contractile performance or energy supply are known to promote remodelling and dedifferentiation of adult cardiomyocytes; the consequences of which include cytoskeletal rearrangement, restructuring of contractile apparatus, and reduced oxidative metabolism (Szibor *et al.*, 2014). Ironically, it seems that these adaptive processes - presumably intended to protect the cardiomyocytes in times of mechanical and/or molecular stress – can lead to adverse consequences for the heart (Szibor *et al.*, 2014). Disruption of the actin cytoskeleton, for example, can impair contractile properties of cardiomyocytes and was implicated in initiation of cardiomyocyte apoptosis (Communal *et al.*, 2002). Here, a model is proposed of how lamin A/C dysregulation, together with other molecular changes, may contribute to cardiac pathology in SMA (Figure 4.13).

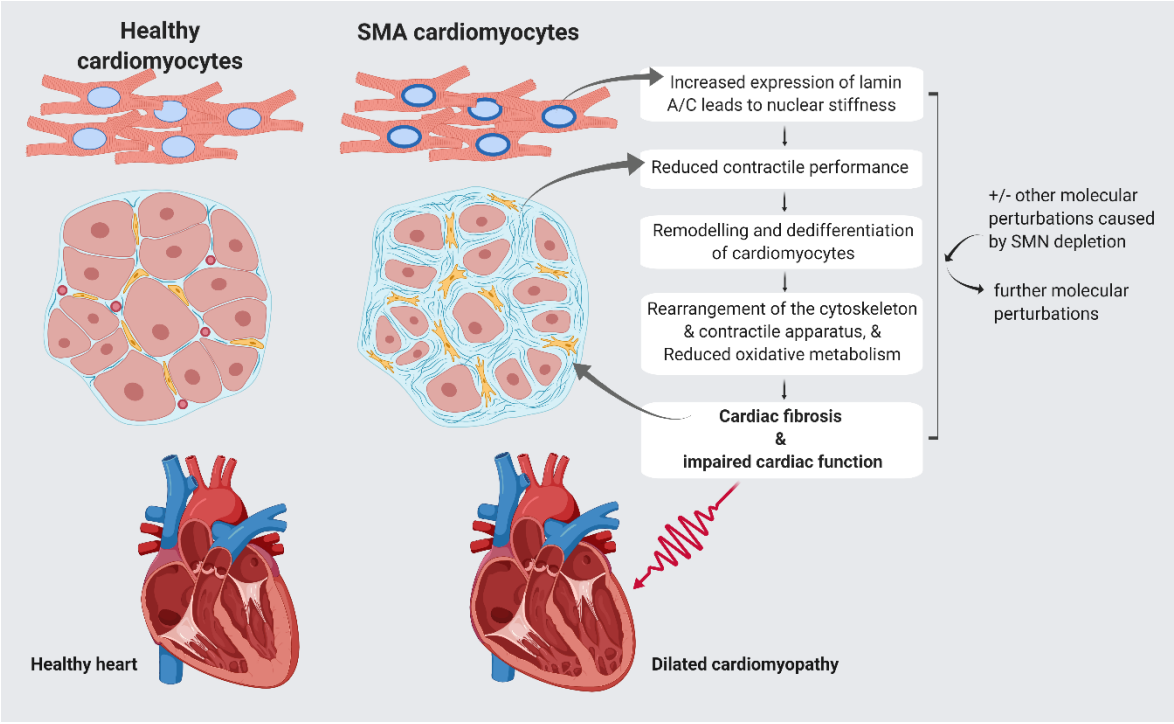

Figure 4. 13. Model of how lamin A/C dysregulation, in combination with other molecular changes, may contribute to cardiac pathology in SMA. A model is proposed in which lamin A/C up-regulation, in combination with other molecular changes that occur in SMA, may lead to cardiac fibrosis and impaired cardiac function. Thinner ventricle walls and dilated ventricles in SMA heart are clinical features of dilated cardiomyopathy.

4.4. Conclusion

The widespread dysregulation of lamin A/C levels, coupled with the nuclear morphology defects that were identified in SMA patient fibroblasts indicate that lamin A/C might have an important role in SMA disease pathways. This is supported by experiments showing mechanistic link between lamin A/C and UBA1, a known regulator of SMA disease pathways. It would be of interest in the future to explore lamin A/C expression in cells and tissues throughout the natural history of disease progression in SMA to determine whether lamin A/C is an early pathology in SMA, and to investigate the functional consequences of lamin A/C dysregulation in SMA cells and tissues. This might be especially relevant for tissues like the heart, where early dysregulation of lamin A/C expression could contribute to the heart pathology in SMA. Moreover, identification of upstream regulators of lamin A/C may help to unravel the tissue-specific regulatory mechanisms that act on lamin A/C in response to SMN depletion. Regulation of lamin A/C levels through phosphorylation is one possibility that should be explored in SMA, as it may have important implications for SMA therapy design. For example, increasing lamin A/C phosphorylation and turnover (Buxboim *et al.*, 2014) could be sufficient to restore normal levels of lamin A/C in SMA tissues. This could be achieved, for example, by using dephosphorylation inhibitors, such as the okadaic acid that was previously shown to phosphorylate nuclear proteins like p80 coilin (Lyon *et al.*, 1997). However, caution should be taken, since downregulation of lamin A/C might also have negative effect on SMA cells. i.e. induce cell death (Harada *et al.*, 2014). Indeed, in cells that are already stressed by SMN depletion, decreasing the levels of lamin A/C might have unwanted effect on cell stability. For example, reduction of lamin A/C levels could lead to reduction of UBA1 levels (as observed in Figure 4.5), which could in turn hamper protein turnover. Establishing the precise link between lamin A/C and UBA1 pathways in SMA disease pathogenesis should therefore be

the aim of future studies, to ensure the best efficiency of SMA therapy design. It would be important too, to monitor SMA patient health longitudinally to determine whether new phenotypes emerge with increasing age. Therapies primarily designed to target neuronal tissues, such as Nusinersen, are especially relevant in this context since they are unlikely to rescue peripheral pathologies. This knowledge, together with a broader understanding of the interplay between lamin A/C and other regulators of SMA disease pathways, would help to isolate the most appropriate targets for therapy design that could, in combination with SMN-targeted therapy, offer maximum therapeutic benefit to all SMA patients.

CHAPTER 5: Results

Multi-Study proteomic and bioinformatic identification of molecular overlap between Amyotrophic lateral sclerosis (ALS) and Spinal muscular atrophy (SMA)

5.1. Introduction

Deletions and mutations within the *SMN1* gene account for more than 95% of SMA cases, resulting in insufficient levels of the ubiquitously-expressed survival of motor neuron (SMN) protein (Bowerman *et al.*, 2018). On the pathological level, SMA is characterised by the loss of motor neurons in the anterior horn of the spinal cord ("lower motor neurons") and muscle atrophy. Interestingly, the loss of lower motor neurons is also a primary pathology in amyotrophic lateral sclerosis (ALS), an adult form of motor neuron disease (Bowerman *et al.*, 2018). In contrast to SMA, however, only 10% of ALS cases have known etiology, while 90% of ALS patients present with sporadic ALS (Bowerman *et al.*, 2018).

Despite variation in the genetic basis of fALS and sALS, there is little difference recognized in their clinical presentation (aside from younger age at presentation in fALS) or any phenotypic pattern related to different genes (Naganska and Matyja, 2011; Ravits *et al.*, 2013). This would suggest that the disease mechanisms of ALS likely converge on common molecular pathways, that ultimately result in similar phenotypes. This then raises the question of whether there are general regulatory pathways that drive disease pathology in both ALS and SMA, that may prove useful for guiding research into therapeutic development.

5.1.1. Amyotrophic lateral sclerosis (ALS)

Amyotrophic lateral sclerosis (ALS), also known as Charcot's disease or Lou Gehrig's disease, is the most common adult form of motor neuron disease, characterised by progressive muscle wasting due to loss of motor neurons in the anterior horn of the spinal cord ("lower motor neurons") and spasticity due to loss of cortical neurons ("upper motor neurons") (Naganska and Matyja, 2011). In ALS, 90% of cases occur sporadically (sALS), while only 10% of cases are attributable to a familial form of ALS (fALS) that typically follow an autosomal dominant

inheritance pattern (Mathis *et al.*, 2019). Mutations in more than 30 genes have been linked to cases of familial ALS, the most common of which include superoxide dismutase 1 (*SOD1*) gene, TAR DNA Binding protein-43 (*TDP-43*) gene, fused-in-sarcoma (*FUS*) gene, and a hexonucleotide repeat within the *C9orf72* gene (Mathis *et al.*, 2019). The frequency of mutations depends on the geographical region where, for example, mutations in the *C9orf72* gene have the highest frequency in European fALS patients (33.7%), followed by *SOD1* (14.8%), *TDP-43* (4.2%) and *FUS* (2.8%) (Mathis *et al.*, 2019). In comparison, Asian fALS patients most commonly present with mutations in SOD1 (30%), whereas, *C9orf72* accounts for only 2.3% of all fALS cases (Mathis *et al.*, 2019).

5.1.1.1 ALS disease pathways

Glutamate excitotoxicity

Research into ALS disease pathways identified several molecular mechanisms that contribute to motor neuron degeneration in both sALS and fALS (summarised in Figure 5.1). Glutamate excitotoxicity is one of the first described mechanisms, and has been identified in fALS and sALS patients, and in animal models of ALS (Ilieva, Polymenidou and Cleveland, 2009). The neurotransmitter glutamate is synthesized in presynaptic neuron terminals and is realised into the synaptic cleft during signal transduction for activation of postsynaptic receptors. Glutamate recycling is mediated by several transporter proteins, including the glial protein, excitatory amino acid transporter 2 (EAAT2) (Zarei *et al.*, 2015). In ALS, the loss of EAAT2 protein results in the build-up of glutamate in synaptic cleft that has a toxic effect on motor neurons. Reduced EAAT2 expression was demonstrated in spinal cord and motor cortex from sALS patients (Glenn Lin *et al.*, 1998), and in ventral horn spinal cord sections from pre-symptomatic $SOD1^{G93A}$ mice (Howland *et al.*, 2002). The reduction of EAAT2 protein levels is

thought to be driven by aberrant mRNA processing (Glenn Lin *et al.*, 1998) and/or transcription deficiency (Yang *et al.*, 2009). For example, increased levels of aberrant EAAT2 transcripts were identified in spinal cord and motor cortex from sALS patients, and *in vitro* expression studies in COS7 cell line suggested that unstable truncated proteins, translated from this transcripts, get rapidly degraded (Glenn Lin *et al.*, 1998). Decreased efficiency of EAAT2 transcription, identified in lumbar spinal cord from $SOD1^{G93A}$ mice, offers additional explanation for decreased EAAT2 protein levels in ALS tissues (Yang *et al.*, 2009). Glutamate accumulation leads to overactivation of glutamate receptors, N-methyl-d-aspartic acid (NMDA) and alpha-amino-3-hydroxy-5-methylisoxazole-4-propionate (AMPA), and consequent Ca^{2+} influx that overwhelms mitochondrial and ER storage capacities (Ilieva, Polymenidou and Cleveland, 2009). Dysregulation of Ca^{2+} homeostasis can directly activate apoptotic pathways, but Ca^{2+} is also known to contribute to apoptosis indirectly (Foran and Trotti, 2009). For example, Ca^{2+} can activate catabolic enzymes, i.e. nucleases and proteases, resulting in irreversible damage that promotes cell death, and induces production of ROS (Foran and Trotti, 2009).

Protein aggregation and ER stress

Misfolded protein aggregation and induction of endoplasmic reticulum (ER) stress is another mechanism known to contribute to ALS pathology. Insoluble protein aggregates have been identified in a range of neuronal tissues in ALS, including spinal cord from sALS and fALS patients (Neumann *et al.*, 2006; Atkin *et al.*, 2008; Forsberg *et al.*, 2010), hippocampus and neocortex from sALS patients (Neumann *et al.*, 2006) and spinal cord from symptomatic $SOD1^{L126Z}$ and $SOD1^{G93A}$ mice (Deng *et al.*, 2006; Furukawa *et al.*, 2006). Accumulation of misfolded proteins triggers the unfolded protein response (UPR), an adaptive process that

promotes protein homeostasis by improving the folding capacity of the cell and clearing of the misfolded proteins (Rozas *et al.*, 2017). Indeed, increased expression of folding machinery was demonstrated in the spinal cord from sALS patients (Ilieva *et al.*, 2007; Atkin *et al.*, 2008; Hetz *et al.*, 2009) and fALS patients (Hetz *et al.*, 2009; Farg *et al.*, 2012), and in spinal cord from mutant SOD1 (Atkin *et al.*, 2006; Kikuchi *et al.*, 2006) and TDP-43 mice (Walker *et al.*, 2013). In addition, upregulation of protein folding machinery was observed in early symptomatic (Kikuchi *et al.*, 2006) and pre-symptomatic stages of the disease (Atkin *et al.*, 2008) in $SOD1^{G93A}$ mice, thus indicating that ER stress is early pathology in ALS. Chronic ER stress triggers the UPR-mediated cell death pathway (Rozas *et al.*, 2017), and in ALS, chronic ER stress is maintained by impaired expression and/or function of the UPR machinery (Nishitoh *et al.*, 2008). For example, impaired function of the ER-associated degradation (ERAD) pathway could explain the toxic accumulation of mutant SOD1 in ALS (Nishitoh *et al.*, 2008). An interaction between SOD1 mutants and derlin-1, a crucial component of the ERAD pathway, was demonstrated in the spinal cord and brain from $SOD1^{G93A}$ mice, and in SOD1 mutant HEK293 and NSC34 cell cultures, with no specific interaction detected between WT SOD1 and derlin-1. Binding of mutant SOD1 to derlin-1 was sufficient to inhibit ERAD pathway in HEK293 cell line and was proposed as a mechanism that drives accumulation of mutant SOD1 in ALS (Nishitoh *et al.*, 2008). In addition, overexpression of derlin-1 reduced mutant SOD1 aggregate formation, supressed ER stress and improved the viability of Neuro2a cell line (Mori *et al.*, 2010).

Structural and functional mitochondria abnormalities

Structural and functional abnormalities in mitochondria were also shown to play an important role in ALS pathogenesis. For example, structural abnormalities in mitochondria, such as

fragmentation, swelling and abnormal cristae have been identified in muscles and spinal cord from sALS patients (Chung and Suh, 2002; Sasaki and Iwata, 2007), and in spinal cord from $SOD1^{G93A}$ mice (Kong and Xu, 1998). On a functional level, ALS mitochondria showed abnormal oxidative respiration and ATP production, increased production of ROS and altered Ca^{2+} homeostasis (Zarei *et al.*, 2015). For example, decreased activity of mitochondrial respiratory chain complexes was detected in the spinal cord from sALS and fALS patients (Wiedemann *et al.*, 2002), in muscles from sALS patients (Wiedemann *et al.*, 1998; Vielhaber *et al.*, 2000), and in the spinal cord from $SOD1^{G93A}$ mouse model of ALS (Jung, Higgins and Xu, 2002; Mattiazzi *et al.*, 2002). In addition, ATP synthesis was significantly diminished in the spinal cord from $SOD1^{G93A}$ mice, and taken together with impaired function of respiratory chain complexes, suggests perturbations in energy production that are likely to contribute to motor neuron degeneration in ALS (Mattiazzi *et al.*, 2002).

Abnormalities in respiratory chain complexes could offer an explanation for increased oxidative stress in ALS, since defects in complex I are known to increase the production of ROS (Tan, Pasinelli and Trotti, 2014). Indeed, increased oxidative stress was detected in spinal cord and muscles from sALS and fALS patients (Pedersen *et al.*, 1998; Vielhaber *et al.*, 2000; Wiedemann *et al.*, 2002), and in spinal cord from $SOD1^{G93A}$ mouse model of ALS (Andrus *et al.*, 1998). If left unresolved, oxidative stress can cause severe damage to biological molecules that triggers cell death, and was thus proposed as important pathological mechanism in ALS neuron death (Tan, Pasinelli and Trotti, 2014).

Higher intracellular Ca^{2+} levels, caused by overactivation of glutamate receptors (described above), were shown critical in ALS pathogenesis, however, intrinsic defect in mitochondria

Ca^{2+} handling have also been implicated in motor neuron vulnerability (Tan, Pasinelli and Trotti, 2014). For example, Ca^{2+} buffering capacity was significantly decreased in spinal cord and brain mitochondria from $SOD1^{G93A}$ mice before the symptom onset (Damiano *et al.*, 2006), and it was attributed, at least in part, to decreased activity of mitochondrial calcium uniporter, a channel that mediates Ca^{2+} uptake into mitochondria (Fuchs *et al.*, 2013). Altered buffering capacity of mitochondria is thought to contributes to accumulation of calcium in cytosol, therefore enhancing glutamate excitotoxic effect, and promoting production of ROS (Manfredi and Xu, 2005)

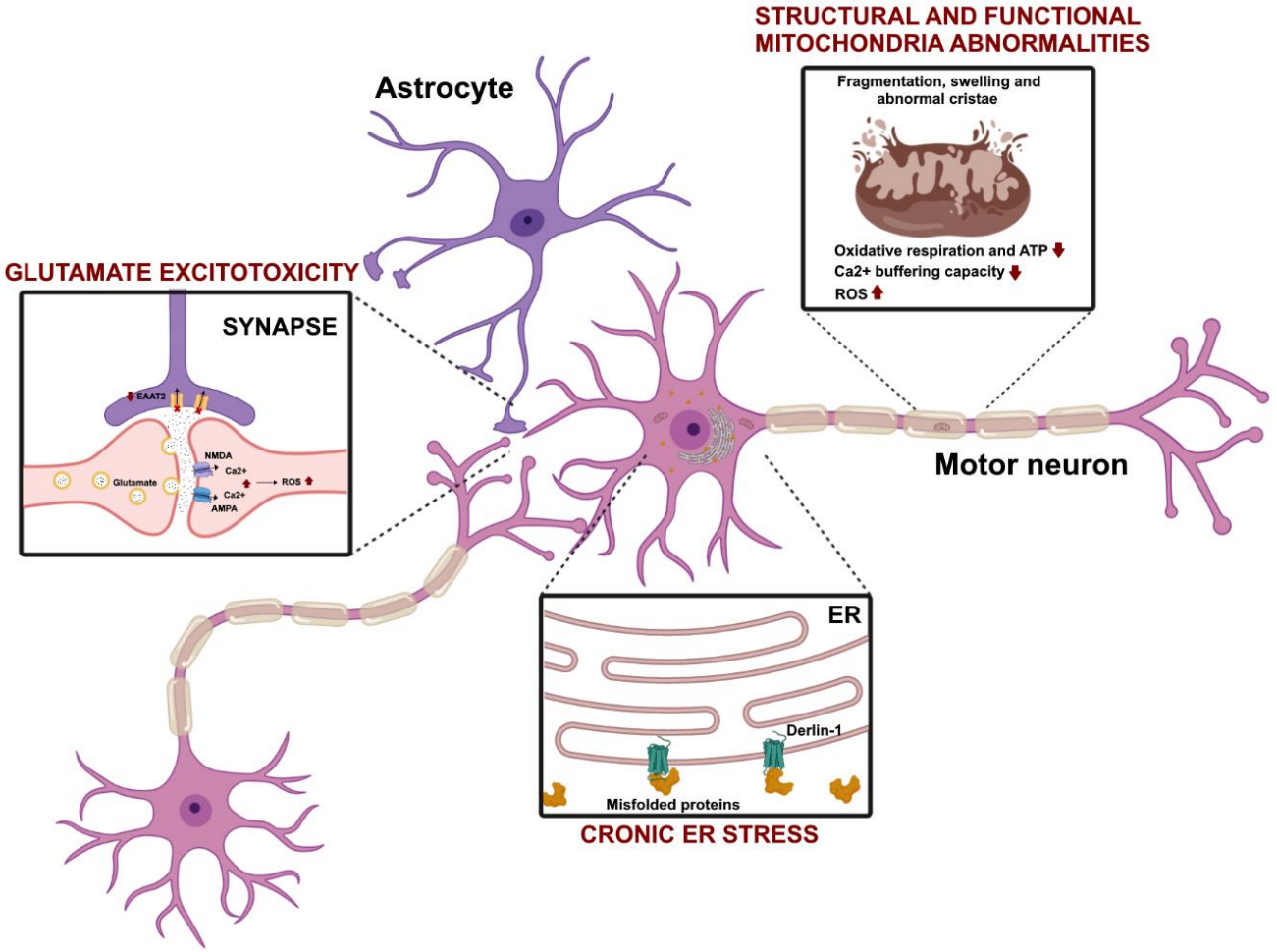

Figure 5. 1. Disease pathways in ALS. Excitotoxicity, ER stress and mitochondrial dysfunction are well characterised disease mechanisms in ALS. ROS-reactive oxygen species; EAAT2-excitatory amino acid transporter 2; NMDA- N-methyl-d-aspartic acid; AMPA- alpha-amino-3-hydroxy-5-methylisoxazole-4-propionate**.** Image created with BioRender.com.

5.1.2. Therapeutic strategies in ALS and SMA

There is no cure for either disease, though some progress has been made in recent years towards the development of therapies that may extend survival or alleviate symptoms (reviewed most recently for SMA (Waldrop and Kolb, 2019), and for ALS (Nowicka *et al.*, 2019)).

First, treatment available to ALS patients was Riluzol (commercially known as Rilutek), approved for clinical use in 1995, which may prolong survival by 2–3 months (Nowicka *et al.*, 2019). The precise mechanism of riluzol action is not well established, although it has been shown to decrease glutamate toxicity by targeting several of its pathways; riluzol inhibits glutamate release from neuronal terminals, it inactivates voltage-dependent sodium channels, and has antagonist action on glutamate receptor NMDA (Zarei *et al.*, 2015). Edaravone, also known as Radicava, was recently approved by the FDA to slow disease progression in ALS patients in the USA (Nowicka *et al.*, 2019). Indeed, inhibition of motor neuron function deterioration was demonstrated in 137 ALS patients following treatment with edaravone, however, only patients at an early stage of the disease (i.e. within 2 years of onset), and with forced vital capacity of 80% or more where included in the study (Abe *et al.*, 2017). The therapeutic benefit of edaravone has not been demonstrated in the wider population of ALS patients (Nowicka *et al.*, 2019), and was therefore rejected for clinical use by the European Medicines Agency[11]. The mechanism of action is not well defined, but it seems that edaravone exhibits antioxidant activity that helps to eliminate reactive oxygen species and reduces oxidative injury in neurons and neighbouring glia cells (Nowicka *et al.*, 2019).

[11] https://www.ema.europa.eu/en/medicines/human/withdrawn-applications/radicava

Research into SMA therapy resulted in development of two approaches, the antisense oligonucleotide drug Nusinersen (Spinraza^{TM}), and adeno-associated virus-based gene replacement therapy Zolgensma^{TM}, both of which have been approved for clinical use in the last three years (reviewed in chapter 1, section 1.5.1). Though undoubtedly an enormous step forward, none of the strategies that have been developed so far show complete efficiency (Finkel *et al.*, 2017; Mendell *et al.*, 2017; Mercuri *et al.*, 2018; Sumner and Crawford, 2018). Coupled with uncertainties around long-term effectiveness and extremely high price of both strategies, there is keen interest to find alternative therapeutic strategies that could, in combination with SMN-targeted therapy, offer maximum therapeutic benefit to all SMA patients (Bowerman, 2019).

5.1.3. Pathogenic commonalities between ALS and SMA

Targeting the same pathogenic mechanism in SMA and ALS, for example, represents an attractive approach in therapy design, as it would allow more rapid and cost-effective identification of new treatments for both diseases. It is not surprising, therefore, that the potential molecular similarities between ALS and SMA are receiving significant attention (Gama-Carvalho *et al.*, 2017; Bowerman *et al.*, 2018; Hensel and Claus, 2018).

5.1.3.1. Altered RNA metabolism

Physical interactions between SMA and ALS- associated proteins offer the first line of evidence that the two disease converge on common mechanisms. For example, FUS and SMN interacted in NSC34 cells and mouse brain tissue extracts (Groen *et al.*, 2013), while an interaction between SOD1 and SMN was detected in spinal cords from wild type and SOD1^{G93A} mice (Groen *et al.*, 2013). In mouse primary neurons expressing ALS-associated FUS mutant

protein, SMN was redistributed to cytoplasmic FUS aggregates causing a reduction in axonal SMN levels (Groen *et al.*, 2013). Considering the role for SMN in regulation of axonal mRNA trafficking and translation (described in detail in chapter 1, section 1.2.2.2), reduction of axonal SMN levels could be responsible, at least in part, for axonal defect in FUS model of ALS (Groen *et al.*, 2013). In addition, reduction of SMN levels was observed in spinal cords from $SOD1^{G93A}$ mice, and further depletion of SMN protein levels aggravated disease progression in ALS mice (Turner *et al.*, 2009). Overexpression of SMN rescued axonal defects in primary neuron cultures expressing transgenic FUS (Groen *et al.*, 2013), and rescued motor neuron loss and improved motor function in $SOD1^{G93A}$ mouse model of ALS (Turner *et al.*, 2014), suggesting that SMN has the potential to modify ALS disease pathways.

Interestingly, loss of GEMs, nuclear complexes that have essential role in biogenesis of snRNP (revised in chapter 1, section 1.2.2.1), was identified in ALS patient fibroblasts that carry mutations in FUS and TDP43 (Yamazaki *et al.*, 2012) and in spinal cord motor neurons from a transgenic $SOD1^{G86R}$ mouse model of ALS (Kariya *et al.*, 2012; Turner *et al.*, 2014). In SMA, loss of GEMs was first reported in SMA patient fibroblast cells, where the degree of loss correlated with disease severity (Coovert *et al.*, 1997). The loss of GEMs seems to be a conserved pathology in ALS and SMA, and suggests perturbations in RNA metabolism, specifically the pre-mRNA splicing, as a common pathological mechanism in both diseases. Indeed, splicing defects have been identified in different tissues from intermediate and severe mouse models of SMA, including spinal cord, brain and kidney (Zhang *et al.*, 2008; Bäumer *et al.*, 2009), and in motor neurons from severe SMA mice (Huo *et al.*, 2014). In ALS, widespread splicing defects have been identified in the brain from TDP43 and FUS transgenic mice (Lagier-Tourenne *et al.*, 2012).

5.1.3.2. Intrinsic muscle defects

Muscle atrophy is usually associated with the functional loss of motor neurons in both SMA and ALS, however, intrinsic muscle defects including for example, dysregulation of myogenic program and defective satellite cell function, have been recognised in the pathogenesis of both diseases (Bowerman *et al.*, 2018). By specifically depleting SMN in murine skeletal muscles, Cifuentes-Diaz et *al.* demonstrated severe muscular dystrophy phenotype, providing one of the earliest evidence that intrinsic muscle defects contribute to disease pathogenesis in SMA (Cifuentes-Diaz *et al.*, 2001). In addition, muscle-specific restoration of SMN levels was sufficient to increase muscle fiber size, and improve survival and motor functions in SMA mice (Martinez *et al.*, 2012). The same effect was confirmed in SOD1 transgenic mice, where muscle-specific expression of SOD1 mutants (G93A and G37R) induced progressive muscle atrophy and abnormalities in NMJs, including smaller motor endplates and loss of innervation (Dobrowolny *et al.*, 2008; Wong and Martin, 2010).

Early pre-symptomatic reduction in the expression of myogenic regulatory factors, including paired box protein Pax7 (Pax7), myoblast determination protein (MyoD) and myogenin, has been detected in muscles from severe ($Smn^{-/-}$;SMN2) and intermediate ($Smn^{2B/-}$) mouse models of SMA (Boyer *et al.*, 2014). Decreased expression of all three factors was confirmed at symptomatic stage of the disease in severe mouse models of SMA ($Smn^{-/-}$;SMN2, $Smn^{-/-}$;SMN2;Δ7), while $Smn^{2B/-}$ mice demonstrated increased expression levels of all three factors with the onset of disease symptoms (Boyer *et al.*, 2014). In the $SOD1^{G93A}$ mouse model of ALS, the expression of myogenic factors including Pax7, MyoD, myogenic factor 5 (Myf5), and myogenin, was altered at the mRNA and protein levels at pre and early- symptomatic stages of the disease (Manzano *et al.*, 2011). Disruption of the myogenic program indicates possible defects in the muscle development in both disease, but this has only been confirmed in SMA

by histological analysis of muscle sections in $Smn^{2B/-}$ and $Smn^{-/-}$;SMN2 mouse models (Boyer *et al.*, 2014). The analysis identified reduction in myofiber size and increased number of myofibers with centrally located nuclei (Boyer *et al.*, 2014), the later one being an indication of maturation defects (Bowerman *et al.*, 2018). Indeed, myoblasts from $Smn^{2B/-}$ mice showed defective fusion *in vitro* by generating less myotubes compared to controls (Boyer *et al.*, 2014), and the same defect was observed in SMN deficient C2C12 myoblast cell line (Shafey, Côté and Kothary, 2005).

In addition, satellite cells from skeletal muscles of pre-symptomatic $SOD1^{G93A}$ mice demonstrated lower proliferation rate *in vitro* when compared to controls (Manzano *et al.*, 2013). Satellite cells from skeletal muscles from early symptomatic SMA mice did not show altered proliferation, however, defects in the differentiation potential of SMA satellite cells have been demonstrated *in vitro* (Hayhurst *et al.*, 2012). The cells undergo earlier differentiation compared to control cells, but fail to efficiently finish differentiation, as evidenced by decreased myotube formation in cell cultures (Hayhurst *et al.*, 2012).

5.1.3.3. Neuroinflammation

Astrocytes and microglia have an important role in maintaining motor neuron health and function, and naturally they received significant attention in SMA and ALS pathogenesis as non-cell autonomous mechanisms of motor neuron injury. For example, murine $SOD1^{G93A}$ glial cells significantly reduced viability of $SOD1^{G93A}$ and wild type motor neurons in co-culture, providing evidence that healthy and disease motor neurons an both affected by defective microglia (Di Giorgio *et al.*, 2007). Murine microglia and human astrocytes expressing mutant SOD1 proteins, G93A and G37R respectively, demonstrated the same toxic effect on human ESC-derived motor neurons (Di Giorgio *et al.*, 2008; Marchetto *et al.*, 2008). This effect was

also demonstrated *in vivo* in mouse models of ALS, where selective deletion of mutant SOD1 in astrocytes delayed disease onset (Wang, Gutmann and Roos, 2011), prolonged survival and reduced microgliosis in ALS mice (Wang, Gutmann and Roos, 2011; Yamanaka *et al.*, 2011).

Changes typical of reactive astrocytes have been described in type I SMA patient iPSC-derived astrocytes and spinal cord sections from SMA patients (McGivern *et al.*, 2013; Rindt *et al.*, 2015), and in ventral horn spinal cord sections from severe SMA mice (McGivern *et al.*, 2013; Tarabal *et al.*, 2014; Rindt *et al.*, 2015). These include upregulation of glial fibrillary acidic protein (GFAP) and nestin (McGivern *et al.*, 2013; Tarabal *et al.*, 2014; Rindt *et al.*, 2015), and changes in cell morphology, including enlarged cell bodies and short thick processes (McGivern *et al.*, 2013). Increased expression of proinflammatory cytokines, including interleukin 1β (IL-1β) and interleukin 8 (IL-8), has been reported in spinal cords from SMA patients and SMA mice, both of which are markets of glial activation (Rindt *et al.*, 2015). Restoration of SMN levels specifically in astrocytes improved motor function and survival of SMA mice, improved NMJ pathology and supressed production of pro-inflammatory cytokines in lumbar spinal cord (Rindt *et al.*, 2015). Increased levels of proinflammatory factors such as interferon gamma 1 (IFNγ) and prostaglandin D were also detected in glia cells from $SOD1^{G93A}$ mouse model of ALS (Di Giorgio *et al.*, 2008; Aebischer *et al.*, 2011). The collection of evidence indicates an active role of glial cells in ALS and SMA pathology, where activation of proinflammatory response in astrocytes and microglia aggravates motor neuron injury and contributes to motor neuron death in both diseases.

5.1.3.4. Actin cytoskeleton alterations

Actin cytoskeleton was first implicated in SMA by the finding that SMN and profilins, important regulators of actin cytoskeleton dynamics, interact in Hela cell extracts (Giesemann *et al.*, 1999). Profilin-2, a neuronal specific profilin isoform, demonstrated stronger binding to SMN compared to profilin-1 (Giesemann *et al.*, 1999), and this interaction was validated in NSC34 cell line (Nölle *et al.*, 2011). In addition, mutations in profilin-1 have been implicated in cases of fALS (Wu *et al.*, 2012). Profilins bind globular (G)-actin and regulate its polymerization to filamentous (F)-actin by dual action; profilin binds G-actin that dissociates from the filament and facilitates ADP- to ATP-G-actin recycling; profilin assists in filament elongation by adding ATP-G-actin to the capped end of the filament, a process known as transient capping (Hensel and Claus, 2018).

Knockdown of both profilin isoforms inhibited neurite outgrowth in PC12 cells and induced accumulation of SMN in cytoplasmic aggregates (Sharma *et al.*, 2005). Increased levels of profilin-2a isoform were identified in SMN depleted PC12 cells (Bowerman, Shafey and Kothary, 2007). In addition, in vitro polymerisation experiments showed that SMN in combination with profilin-2a increases actin polymerization compared to profilin-2a alone (Sharma *et al.*, 2005), indicating a functional link between the two proteins in the regulation of actin dynamics. Although the precise mechanism of SMN action on actin polymerization has yet to be determined, it was proposed that SMN accelerates the release of profilin from filament-bound actin after capping, a process that is necessary for further filament elongation (Hensel and Claus, 2018). Another theory proposes a role for SMN in preventing profilin inhibition; with SMN loss, profilin binding domain could become more accessible for phosphorylation, which is known to have inhibitory effect on profilin binding to actin. Indeed, profilin hyperphosphorylation has been identified in SMN deficient PC12 cells and in spinal

cord from symptomatic SMA mice, and activation of ROCK pathway was proposed as a mechanism that induces profilin phosphorylation (Nölle *et al.*, 2011). This was confirmed in a separate study in PC12 cells where SMN depletion increased formation of profilin-2-ROCK complexes (Bowerman, Shafey and Kothary, 2007).

A range of mutations in profilin-1 have been identified in fALS cases, most of which showed typical ALS pathology characterised by cytoplasmic protein aggregations (Hensel and Claus, 2018). Protein aggregates have also been identified in HEK293 and Neuro2a cell cultures carrying ALS-associated profilin-1 mutants, some of which contained TDP-43 protein (Wu *et al.*, 2012; Smith *et al.*, 2015). Transgenic mice carrying profilin mutations recapitulated pathologies observed in ALS patients, including the loss of motor neurons and progressive muscle wasting, accumulation of insoluble protein aggregates in motor neurons and increased ubiquitin levels (Yang *et al.*, 2016; Fil *et al.*, 2017). Protein aggregation and impaired proteasomal degradation indicate toxic gain of function of mutant profilin-1, however, in a study by Yung et *al.*, motor neuron degeneration preceded protein aggregation in a transgenic mouse model carrying profilin-1 mutation (Yang *et al.*, 2016). This result indicates that other mechanisms, like impaired ability of profilin to regulate actin dynamics may be crucial in early stages of the disease, although the contribution of protein aggregates to motor neuron pathology cannot be ruled out (Hensel and Claus, 2018). Indeed, mutations identified in the actin-binding domain of profilin-1 directly affected the affinity of profilin to bind actin (Hensel and Claus, 2018). The precise mechanisms of action of profilin mutants on the dynamics of actin cytoskeleton remains to be investigated, so does the role for profilin in the pathogenesis of sALS and non-profilin-associated fALS.

5.1.3.5. Altered architecture of the spleen and thymus

Compromised spleen development was identified in severe (Taiwanese and $SMN^{-/-}$; SMN2) and intermediate (Smn^{2B-}) mouse models of SMA, as evidenced by the failure of the spleen to grow and develop mature morphology (Deguise *et al.*, 2017; Khairallah *et al.*, 2017; Thomson *et al.*, 2017). During normal postnatal development, homogenous spleen tissue differentiates into distinct red and white pulp, and the spleen develops defined capsule and trabeculae (Thomson *et al.*, 2017). In contrast, spleens from SMA mice maintained homogenous morphology throughout development, with no segregation between red and white pulp (Deguise *et al.*, 2017; Khairallah *et al.*, 2017; Thomson *et al.*, 2017), and failed to develop defined capsule and trabeculae (Thomson *et al.*, 2017). Pathological changes in the spleen were also confirmed in approximately 50% of type I SMA patients (Thomson *et al.*, 2017). Similarly, spleen from symptomatic $SOD1^{G93A}$ mice had reduced size and weight and altered morphology as demonstrated by immunohistochemistry analysis (Banerjee *et al.*, 2008).

Morphological abnormalities in thymus have been observed in symptomatic stage of the disease in severe ($SMN^{-/-}$; SMN2) and intermediate (Smn^{2B-}) mouse models of SMA, including decreased size, thinner cortex, reduced cell content, and increased number of apoptotic bodies and tangible body macrophages (Deguise *et al.*, 2017). Decreased size, reduced cell content and loss of typical structures (e.g. cortex and medulla) have also been identified in $SOD1^{G93A}$ mouse model of ALS at symptomatic stage of the disease (Seksenyan *et al.*, 2010).
In both diseases, the expression and distribution of immune cells was altered. For example, B-lymphocytes in the spleen from both SMA and ALS mice showed reduced numbers and altered localization when compared to healthy controls (Banerjee *et al.*, 2008; Deguise *et al.*, 2017; Thomson *et al.*, 2017), and a general reduction in the number of circulating lymphocytes was

identified in the blood from severe SMA mice (Thomson *et al.*, 2017). Diffuse distribution and expression pattern of T cells was also evident in the spleen from SMA and ALS mice (Banerjee *et al.*, 2008; Deguise *et al.*, 2017). For example, increased levels of killer ($CD8^+$) and helper ($CD4^+$) T cells were detected in the spleen from SMA mice (Deguise *et al.*, 2017; Khairallah *et al.*, 2017), while ALS mice demonstrated increased levels of natural killer T (NKT) cell, $CD4^+$ naïve T cells, but decreased levels of $CD4^+$ memory T cells. (Finkelstein *et al.*, 2011).

Despite the wealth of knowledge showing shared pathological features between SMA and ALS, the precise molecular overlap between SMA and ALS is still unknown. The aim of this chapter was to identify the molecular overlap between SMA and ALS, and gain insights into shared disease pathways between the two diseases that would help in the development of therapies for both SMA and ALS patients.

The specific objectives were as follows:

a) To identify core protein changes in ALS tissues/cells by comparison of published proteomic studies of ALS, and investigate their likely function by using bioinformatics.
b) To identify core molecular overlap between SMA and ALS, by comparing the results from an ALS multi-study comparison to the previously published dataset of conserved molecular alterations in SMA, and gain insights into the likely function of these proteins by using bioinformatics tools.
c) To investigate the expression of five protein targets, identified as differentially expressed in both SMA and ALS, in spinal cord from comparable mouse models of ALS and SMA.

5.2. Results

5.2.1. Overview of ALS proteomic studies

A total of 33 proteomic studies of ALS were eligible for comparison (as described in the methods section 2.9.4) (Table 5.1), and as expected, the number of differentially expressed proteins identified in studies correlated with the sensitivity of the method used, with label-free technologies having identified by far the greatest number of protein changes compared to 2D-gel approaches. Samples from animal models and ALS patients were equally represented across studies (Table 5.1), and were derived from a range of sources, including ALS patient cerebrospinal fluid (CSF) (Ranganathan *et al.*, 2005, 2007; Pasinetti *et al.*, 2006; Brettschneider *et al.*, 2008; Ryberg *et al.*, 2010; Von Neuhoff *et al.*, 2012; Mendonça *et al.*, 2012; Varghese *et al.*, 2013; Collins *et al.*, 2015; Chen *et al.*, 2016; Thompson *et al.*, 2018), ALS patient serum (De Benedetti *et al.*, 2017), ALS patient muscles (Conti *et al.*, 2014; Elf *et al.*, 2014), ALS patient blood mononuclear cells (PBMC) (Nardo *et al.*, 2011), ALS patient spinal cord (Engelen-Lee *et al.*, 2017), ALS patient prefrontal cortex (Umoh *et al.*, 2018), a range of cell models (Allen *et al.*, 2003; Fukada *et al.*, 2004; Stalekar *et al.*, 2015; Schwenk *et al.*, 2016), and tissues/cells from various mouse and rat models of ALS including astrocytes (Basso *et al.*, 2013), skeletal muscles (Staunton, Jockusch and Ohlendieck, 2011), ventral roots (Zhou *et al.*, 2010), embryonic motor neurons (Duplan *et al.*, 2010), spinal cord (Strey *et al.*, 2004; Massignan *et al.*, 2007; Basso *et al.*, 2009; Bastone *et al.*, 2009; Bergemalm *et al.*, 2009; Li *et al.*, 2010; Sharma *et al.*, 2016), and hippocampus (Shin *et al.*, 2005).

Table 5. 1. ALS proteomic studies used in the comparison

Reference	Sample Type/ ALS model	Differentially exp. proteins	Analysis platform	Protein Database
(Chen *et al.*, 2016)	Patient CSF	35/35	iTRAQ; API QSTAR XL (Applied Biosystems)	UniProt/ Swiss-Prot
(Collins *et al.*, 2015)	Patient CSF	123/110	Label-Free; linear ion trap (ThermoFisher Scientific)	UniProt/Swiss-Prot
(Varghese *et al.*, 2013)	Patient CSF	48/47	iTRAQ; LTQ-Orbitrap Velos (Thermo Electron)	Human Protein Database (NCBI)
(Mendonça *et al.*, 2012)	Patient CSF	17*/17	2D electrophoresis; Voyager-DE Pro MALDI-TOF (Applied Biosystems)	NCBI and UniProt/ Swiss-Prot
(Von Neuhoff *et al.*, 2012)	Patient CSF	153/11	Peak recognition (statistical analysis; linear Microflex MALDI-TOF (Bruker)	Entrez Protein Database
(Ryberg *et al.*, 2010)	Patient CSF	33/7	SELDI-TOF-MS	Empirical Proteomics Ontology Knowledge Base
(Brettschneider *et al.*, 2008)	Patient CSF	6/5	2D-DIGE; Voyager DE-STR (Applied Biosystems)	NCBI database
(Ranganathan *et al.*, 2005)	Patient CSF	52^{+}/3	SELDI-TOF-MS/MS; Ciphergen ProteinChip Reader (Ciphergen Biosystems)	UniProt/Swiss-Prot
(Ranganathan *et al.*, 2007)	Patient CSF	10/2 (PM-ALS) $^{+}$ 9/2 (L-ALS) $^{+}$	SELDI-TOF-MS; Ciphergen ProteinChip Reader (Ciphergen Biosystems)	UniProt/Swiss-Prot
(Pasinetti *et al.*, 2006)	Patient CSF	3/2	SELDI-TOF-MS	Unknown

(Thompson *et al.*, 2018)	Patient CSF	3/3	UHPLC LC-MS/MS; Q Exactive HF tandem mass spectrometer (Thermo Fisher Scientific)	UniProt
(De Benedetti *et al.*, 2017)	Patient serum	7/7	2D-GE; SYNAPT-MS G1 (Waters Corporation)	UniProt
(Schwenk *et al.*, 2016)	Rat neurons/ TDP-43 Knockdown	63/63	Label-free; Orbitrap Q Exactive (Thermo Fisher Scientific)	UniProt/Swiss-Prot
(Sharma *et al.*, 2016)	Patient CSF injected into rat spinal cord/MF	49/48	iTRAQ; LTQ-Orbitrap Velos (Thermo Electron)	RefSeq
(Stalekar *et al.*, 2015)	SH-SY5Y cells/ TDP-43 Loss	273/270	Label-free; LTQ Orbitrap XL (Thermo Fisher Scientific)	UniProt/Swiss-Prot
(Conti *et al.*, 2014)	Patient muscle	5/5	2D-GE; API QStar PULSAR (AB-Sciex)	UniProt/Swiss-Prot
(Elf *et al.*, 2014)	Patient muscle	11/11	Stable-isotope dimethyl labels; 7 T hybrid LTQ FT Ultra mass spectrometer (ThermoFisher Scientific)	UniProt/Swiss-Prot
(Basso *et al.*, 2013)	Mouse astrocytes/ SOD1 G93A	31/31	2D-GE; Reflex III MALDI-TOF (Bruker Daltonics)	UniProt/Swiss-Prot
(Nardo *et al.*, 2011)	Patient blood mononuclear cells	44/44	2D DIGE; 4800 MALDI TOF/TOF (Applied Biosystems)	UniProt/Swiss-Prot
(Bastone *et al.*, 2009)	Mouse spinal cord/ Wobbler Mouse	13/13	2D DIGE; Model 6430 Ion Trap (Agilent Technologies)	NCBI
(Zhou *et al.*, 2010)	Mouse ventral roots/ SOD1 G93A	$14^{\#}$/14	Label Free; LTQ (Thermo Finnigan)	UniProt/Swiss-Prot

(Duplan *et al.*, 2010)	Mouse embryonic motor neurons/ SOD1 G85R	6/4	2D-GE; UltraFlex MALDI TOF/TOF (Bruker-Franzen Analytik)	UniProt/Swiss-Prot
(Bergemalm *et al.*, 2009)	Mouse spinal cord/ SOD1 G127X	53/47	2D-DIGE; Voyager DE-STR MALDI-TOF (Applied Biosystems)	UniProt/Swiss-Prot
(Staunton, Jockusch and Ohlendieck, 2011)	Mouse muscle/ Wobbler Mouse	31/26	2D-GE; Reflex III MALDI-TOF (Bruker Daltonics)	UniProt/Swiss-Prot
(Basso *et al.*, 2009)	Mouse spinal cord (IF)/ SOD1 G93A	32/32	2DE; Reflex III MALDI-TOF (Bruker Daltonics)	UniProt/Swiss-Prot
(Massignan *et al.*, 2007)	Mouse spinal cord (pre-symptomatic)/ SOD1 G93A	15/15	2D-GE; ReflexIII MALDI mass spectrometer (Bruker Daltonics)	UniProt/Swiss-Prot
(Strey *et al.*, 2004)	Mouse spinal cord / SOD1 G93A	7/7	2D-GE; VG 2E Tofspec laser desorption time of flight mass spectrometer (Waters)	NCBI
(Fukada *et al.*, 2004)	NSC34 cells (MF)/ SOD1 G93A	40/38	2D-GE; Qstar XL Q-TO (Applied Biosystems)	NCBI and UniProt/ Swiss-Prot
(Li *et al.*, 2010)	Rat spinal cord (MF)/ SOD1 G93A	40/40	2D-GE; MudPIT RCADiA platform	Saccharomyces Genome Database/ Ensembl
(Allen *et al.*, 2003)	NSC34 cells/ SOD1 G93A/G37R	7/7	2D-GE; Voyager-DE STR (Perspective Biosystems)	UniProt/Swiss-Prot
(Shin *et al.*, 2005)	Mouse hippocampus/ Tg152 line overexpressing hSOD1	41/41	2D-GE; Ultraflex MALDI TOF/TOF (Bruker Daltonics)	NCBI and UniProt/ Swiss-Prot

(Engelen-Lee *et al.*, 2017)	Patient anterior and posterior horn	32/18 (AH) 3/3 (PH)	2D-GE; LTQ linear ion trap mass spectrometer (ThermoFisher Scientific)	UniProt
(Umoh *et al.*, 2018)	Patient prefrontal cortex	103/101	Label-free; Fusion mass spectrometer (ThermoFisher Scientific)	UniProt

ALS studies included in the proteomic comparison are listed in table, together with ALS model, sample type, analysis platform and database used in each study. Number of differentially expressed proteins identified in each study/ number of those proteins that were included in the comparison are listed in column three. * Proteins were considered significantly changed if they were identified in ALS samples, but not in CTR samples. † Significantly changed proteins in ALS were identified by applying second-pass peak selection with a signal to noise ratio of 1.5 and $p < 0.01$. # By dynamically adjusting the p-value cut-off, p-value of 0.05 was chosen for the identification of significantly changed proteins in ALS. PM-ALS- samples from ALS patients taken post-mortem; L-ALS- samples from living patients; CSF- cerebrospinal fluid; IF- insoluble fraction; MF- mitochondrial fraction; AH-anterior horn; PH-posterior horn.

5.2.2. Identification of protein changes in biofluids from ALS patients

Protein expression changes in biofluids may not necessarily correlate with protein changes at the cellular level and may in fact be contradictory. It is possible that secretion or leakage of proteins into the CSF or serum may, for example, be accompanied by a concomitant decrease of expression levels in tissues (Anderson and Anderson, 2002). Thus, studies that utilised cells/tissues were compared separately to those that examined biofluids.

Comparison across the 12 proteomic studies that examined biofluids from ALS patients (Ranganathan *et al.*, 2005, 2007; Pasinetti *et al.*, 2006; Brettschneider *et al.*, 2008; Ryberg *et al.*, 2010; Von Neuhoff *et al.*, 2012; Mendonça *et al.*, 2012; Varghese *et al.*, 2013; Collins *et al.*, 2015; Chen *et al.*, 2016; De Benedetti *et al.*, 2017; Thompson *et al.*, 2018) identified 11 proteins that were consistently changed in the same direction across at least two studies (Table 5.2). Of these, one protein – cystatin C - was decreased in expression across four separate studies (Ranganathan *et al.*, 2005, 2007; Pasinetti *et al.*, 2006; Ryberg *et al.*, 2010) and one protein – chitinase 3-like protein 1 - was increased in expression across three separate studies (Von Neuhoff *et al.*, 2012; Varghese *et al.*, 2013; De Benedetti *et al.*, 2017). The remaining eight proteins showed opposing directions of differential expression (Table 5.3).

Table 5. 2. Proteins differentially expressed in the same direction in biofluids from ALS patients

Protein name (official gene symbol)	References	Sample Type
Decreased expression		
Cystatin C (CST3)	(Ranganathan et al., 2005)	Patient CSF
	(Ranganathan et al., 2007)	Patient CSF
	(Pasinetti et al., 2006)	Patient CSF
	(Ryberg et al., 2010)	Patient CSF
Alpha-1-Acid Glycoprotein 1 (ORM1)	(Varghese et al., 2013)	Patient CSF
	(Chen et al., 2016)	Patient CSF
Apolipoprotein A-IV (APOA4)	(Von Neuhoff et al., 2012)	Patient CSF
	(De Benedetti et al., 2017)	Patient serum
Haptoglobin (HP)	(Varghese et al., 2013)	Patient CSF
	(Chen et al., 2016)	Patient CSF
Neurosecretory Protein VGF (VGF)	(Pasinetti et al., 2006)	Patient CSF
	(Von Neuhoff et al., 2012)	Patient CSF
Ribonuclease Pancreatic (RNASE1)	(Ryberg et al., 2010)	Patient CSF
	(Chen et al., 2016)	Patient CSF
Transferrin (TF)	(Brettschneider et al., 2008)	Patient CSF
	(Varghese et al., 2013)	Patient CSF
Increased expression		
Chitinase 3-Like Protein 1 (CHI3L1)	(Von Neuhoff et al., 2012)	Patient CSF
	(Varghese et al., 2013)	Patient CSF
	(De Benedetti et al., 2017)	Patient serum
Chitinase 3-Like Protein 2 (CHI3L2)	(Varghese et al., 2013)	Patient CSF
	(Collins et al., 2015)	Patient CSF
Chitotriosidase-1 (CHIT1)	(Varghese et al., 2013)	Patient CSF
	(De Benedetti et al., 2017)	Patient serum
Hemoglobin Subunit Alpha 1 (HBA1)	(Ryberg et al., 2010)	Patient CSF
	(Chen et al., 2016)	Patient CSF

Proteins with a consistent change in expression in biofluids from ALS patients across two or more proteomic studies are shown. Proteins are listed according to direction of differential expression (proteins with increased expression are listed first, followed by proteins with decreased expression). Protein name is given, followed by official gene symbol in brackets. Studies and ALS patient sample type are listed in columns two and three. CSF-cerebrospinal fluid

Table 5. 3. Proteins that showed contradictory direction of differential expression in biofluids from ALS patients across at least two proteomic studies

Protein name (official gene symbol)	Increased expression	Decreased expression
Transthyretin (TTR)	(Ryberg et al., 2010)*	(Ranganathan et al., 2005) (Ranganathan et al., 2007) (De Benedetti et al., 2017)
Hemoglobin Subunit Beta (HBB)	(Ryberg et al., 2010) (Chen et al., 2016)	(Varghese et al., 2013)
Protein AMBP (AMBP)	(De Benedetti et al., 2017)	(Von Neuhoff et al., 2012) (Chen et al., 2016)
Apolipoprotein A-II (APOA2)	(Chen et al., 2016)	(De Benedetti et al., 2017)
Apolipoprotein B-100 (APOB)	(Varghese et al., 2013)	(Collins et al., 2015)
Prothrombin (F2)	(Varghese et al., 2013)	(Von Neuhoff et al., 2012)
Testican-2 (SPOCK2)	(Chen et al., 2016)	(Collins et al., 2015)
Zinc-Alpha-2-Glycoprotein (AZGP1)	(Brettschneider et al., 2008)	(Chen et al., 2016)

Proteins that showed contradictory change in expression in biofluids from ALS patients in two or more proteomic studies. Protein name is given, followed by official gene symbol in brackets. Studies that identified increased or decreased protein expression are listed in column two and three. *CysGly-transthyretin-modified form of transthyretin generated by oxidative damage.

Gene ontology analysis was performed using the DAVID software as described in methods section 2.9.4.1 (Huang, Sherman and Lempicki, 2009b, 2009a) to investigate the likely function of the 11 proteins that showed a consistent change in expression. “Establishment of localization” was the most enriched biological process term, with seven of the eleven proteins mapping to it (Figure 5.2A), and complementary to this, 9 of the 11 proteins were associated with the term “vesicles”; eight of which were connected to the term “extracellular vesicles” (Figure 5.2B). STRING 10 (Szklarczyk *et al.*, 2015) analysis identified association network between four proteins: HBA1, HP, TF and ORM1 (Figure 5.2C), all of which appear to be plasma-derived proteins.

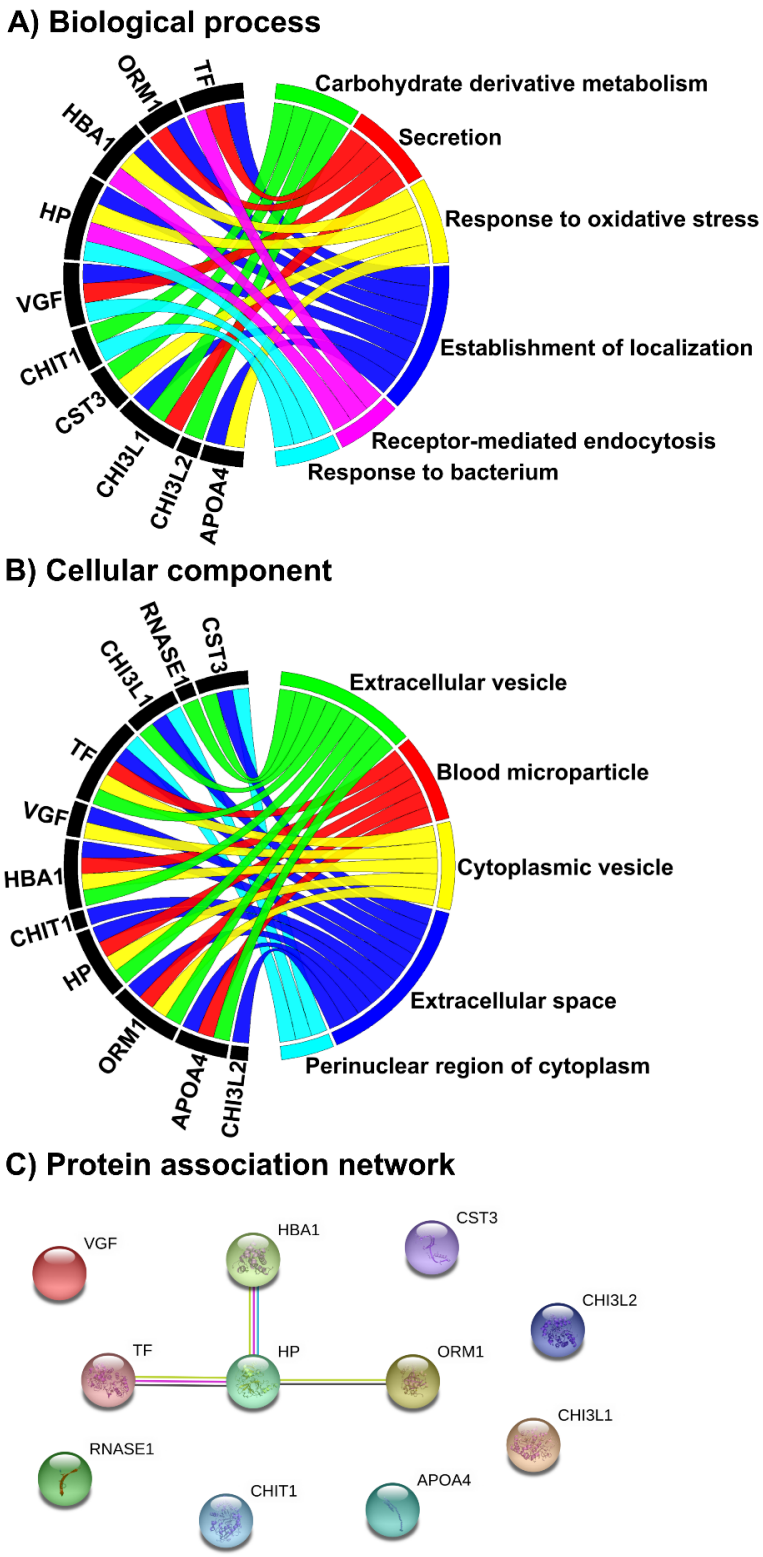

Figure 5. 2. Bioinformatics analysis of eleven proteins that showed consistent change in expression across biofluids from ALS patients. Gene ontology analysis revealed enriched terms connected to **(A)** biological process, **(B)** cellular component. Enriched terms are shown in the chord diagram, together with the proteins annotated to each term. **(C)** STRING 10 analysis identified association network between four proteins: HBA1- haemoglobin subunit alpha 1, HP- haptoglobin, ORM1- alpha-1-acid glycoprotein 1 and TF- transferrin. The type of association is indicated by the colour (pink: experimentally determined interactors; light blue: interactors form curated database; black: co-expression; yellow: text-mining).

5.2.3 Multi-study proteomic identification of conserved molecular response in cells/tissues from ALS patients and animal models of ALS

Comparison of the 21 studies that investigated proteome changes in tissues and cells from ALS patients and animal models identified 80 proteins that were differentially expressed across two or more studies. Of these, 42 proteins showed a consistent direction of differential expression (Table 5.4), eleven of which were upregulated across three or more studies: aldolase A, superoxide dismutase 1 and 2, 14-3-3 protein gamma, calreticulin, glyceraldehyde-3-phosphate dehydrogenase, heat shock protein 1, heat shock protein family A member 8, peroxiredoxin 2 and 6 and glial fibrillary acidic protein. The remaining 38 proteins showed a contradictory direction of expression in different studies (Table 5.5).

Table 5. 4. Proteins that showed consistent direction of differential expression in ALS cells and tissues across two or more proteomic studies

Protein (Official Gene Symbol)	References	Sample Type/ ALS Model
Increased expression		
Aldolase A (ALDOA)	(Fukada *et al.*, 2004)	NSC34 cells (MF)/ SOD1 G93A
	(Staunton, Jockusch and Ohlendieck, 2011)	Mouse muscle/ Wobbler Mouse
	(Bastone *et al.*, 2009)	Mouse spinal cord/ Wobbler Mouse
	(Nardo *et al.*, 2011)	Patient blood mononuclear cells
	(Basso *et al.*, 2013)	Mouse astrocytes/ SOD1 G93A
Superoxide Dismutase 2 (SOD2)	(Bergemalm *et al.*, 2009)	Mouse spinal cord/ SOD1 G127X
	(Li *et al.*, 2010)	Rat spinal cord (MF)/ SOD1 G93A
	(Nardo *et al.*, 2011)	Patient blood mononuclear cells
	(Stalekar *et al.*, 2015)	SH-SY5Y cells/ TDP-43 Loss
Superoxide Dismutase 1 (SOD1)	(Strey *et al.*, 2004)	Mouse spinal cord / SOD1 G93A
	(Basso *et al.*, 2009)	Mouse spinal cord (IF)/ SOD1 G93A
	(Staunton, Jockusch and Ohlendieck, 2011)	Mouse muscle/ Wobbler Mouse

Peroxiredoxin 2 (PRDX2)	(Duplan *et al.*, 2010)	Mouse embryonic motor neurons/ SOD1 G85R
	(Nardo *et al.*, 2011)	Patient blood mononuclear cells
	(Stalekar *et al.*, 2015)	SH-SY5Y cells/ TDP-43 Loss
14-3-3 Protein Gamma (YWHAG)	(Basso *et al.*, 2009)	Mouse spinal cord (IF)/ SOD1 G93A
	(Bergemalm *et al.*, 2009)	Mouse spinal cord/ SOD1 G127X
	(Stalekar *et al.*, 2015)	SH-SY5Y cells/ TDP-43 Loss
Heat Shock Protein 1 (HSPB1)	(Strey *et al.*, 2004)	Mouse spinal cord / SOD1 G93A
	(Basso *et al.*, 2009)	Mouse spinal cord (IF)/ SOD1 G93A
	(Stalekar *et al.*, 2015)	SH-SY5Y cells/ TDP-43 Loss
Calreticulin (CALR)	(Zhou *et al.*, 2010)	Mouse ventral roots/ SOD1 G93A
	(Nardo *et al.*, 2011)	Patient blood mononuclear cells
	(Stalekar *et al.*, 2015)	SH-SY5Y cells/ TDP-43 Loss
Heat Shock Protein Family A, Member 8 (HSPA8)	(Basso *et al.*, 2009)	Mouse spinal cord (IF)/ SOD1 G93A
	(Nardo *et al.*, 2011)	Patient blood mononuclear cells
	(Stalekar *et al.*, 2015)	SH-SY5Y cells/ TDP-43 Loss
Peroxiredoxin 6 (PRDX6)	(Strey *et al.*, 2004)	Mouse spinal cord / SOD1 G93A
	(Nardo *et al.*, 2011)	Patient blood mononuclear cells
	(Bastone *et al.*, 2009)	Mouse spinal cord/ Wobbler Mouse
Glial Fibrillary Acidic Protein (GFAP)	(Basso *et al.*, 2009)	Mouse spinal cord (IF)/ SOD1 G93A
	(Basso *et al.*, 2013)	Mouse astrocytes/ SOD1 G93A
	(Umoh *et al.*, 2018)	Patient prefrontal cortex
Glyceraldehyde-3-Phosphate Dehydrogenase (GAPDH)	(Basso *et al.*, 2009)	Mouse spinal cord (IF)/ SOD1 G93A
	(Staunton, Jockusch and Ohlendieck, 2011)	Mouse muscle/ Wobbler Mouse
	(Bastone *et al.*, 2009)	Mouse spinal cord/ Wobbler Mouse
Valosin Containing Protein (VCP)	(Basso *et al.*, 2009)	Mouse spinal cord (IF)/ SOD1 G93A
	(Elf *et al.*, 2014)	Patient muscle
Septin 9 (SEPT9)	(Zhou *et al.*, 2010)	Mouse ventral roots/ SOD1 G93A
	(Stalekar *et al.*, 2015)	SH-SY5Y cells/ TDP-43 Loss
Malate Dehydrogenase 1 (MDH1)	(Basso *et al.*, 2009)	Mouse spinal cord (IF)/ SOD1 G93A
	(Bergemalm *et al.*, 2009)	Mouse spinal cord/ SOD1 G127X
Actin, Alpha Cardiac Muscle 1 (ACTC1)	(Staunton, Jockusch and Ohlendieck, 2011)	Mouse muscle/ Wobbler Mouse
	(Stalekar *et al.*, 2015)	SH-SY5Y cells/ TDP-43 Loss
NADH Dehydrogenase [Ubiquinone] Iron-Sulfur Protein 8, Mitochondrial (NDUFS8)	(Fukada *et al.*, 2004)	NSC34 cells (MF)/ SOD1 G93A
	(Engelen-Lee *et al.*, 2017)	Patient anterior and posterior horn

Calumenin (CALU)	(Zhou *et al.*, 2010) (Stalekar *et al.*, 2015)	Mouse ventral roots/ SOD1 G93A SH-SY5Y cells/ TDP-43 Loss
Creatine Kinase, Mitochondrial 1 (CKMT1B)	(Basso *et al.*, 2009) (Bastone *et al.*, 2009)	Mouse spinal cord (IF)/ SOD1 G93A Mouse spinal cord/ Wobbler Mouse
Glutamate Dehydrogenase (GLUD1)	(Basso *et al.*, 2009) (Bastone *et al.*, 2009)	Mouse spinal cord (IF)/ SOD1 G93A Mouse spinal cord/ Wobbler Mouse
Apolipoprotein E (APOE)	(Strey *et al.*, 2004) (Zhou *et al.*, 2010)	Mouse spinal cord / SOD1 G93A Mouse ventral roots/ SOD1 G93A
Enoyl Coenzyme A Hydratase, Short Chain 1 (ECHS1)	(Massignan *et al.*, 2007) (Basso *et al.*, 2013)	Mouse spinal cord (pre-symptomatic)/ SOD1 G93A Mouse astrocytes/ SOD1 G93A
Single Stranded DNA Binding Protein 1 (SSBP1)	(Li *et al.*, 2010) (Stalekar *et al.*, 2015)	Rat spinal cord (MF)/ SOD1 G93A SH-SY5Y cells/ TDP-43 Loss
Glycerol Phosphate Dehydrogenase 2 (GPD2)	(Basso *et al.*, 2009) (Bastone *et al.*, 2009)	Mouse spinal cord (IF)/ SOD1 G93A Mouse spinal cord/ Wobbler Mouse
Aldolase C (ALDOC)	(Basso *et al.*, 2009) (Basso *et al.*, 2013)	Mouse spinal cord (IF)/ SOD1 G93A Mouse astrocytes/ SOD1 G93A
Glutamine Ammonia Ligase (GLUL)	(Basso *et al.*, 2009) (Bastone *et al.*, 2009)	Mouse spinal cord (IF)/ SOD1 G93A Mouse spinal cord/ Wobbler Mouse
Endoplasmic Reticulum Protein 29 (ERP29)	(Bergemalm *et al.*, 2009) (Nardo *et al.*, 2011)	Mouse spinal cord/ SOD1 G127X Patient blood mononuclear cells
Isocitrate Dehydrogenase 2 (IDH2)	(Basso *et al.*, 2009) (Li *et al.*, 2010)	Mouse spinal cord (IF)/ SOD1 G93A Rat spinal cord (MF)/ SOD1 G93A
Lactate Dehydrogenase B (LDHB)	(Basso *et al.*, 2009) (Nardo *et al.*, 2011)	Mouse spinal cord (IF)/ SOD1 G93A Patient blood mononuclear cells
Decreased expression		
Neurosecretory protein VGF (VGF)	(Stalekar *et al.*, 2015) (Umoh *et al.*, 2018)	SH-SY5Y cells/ TDP-43 Loss Patient prefrontal cortex
Myosin Light Chain, Phosphorylatable, Fast Skeletal Muscle (MYLPF)	(Zhou *et al.*, 2010) (Conti *et al.*, 2014)	Mouse ventral roots/ SOD1 G93A Patient muscle
Nudix Motif 2 (NUDT2)	(Bergemalm *et al.*, 2009) (Sharma *et al.*, 2016)	Mouse spinal cord/ SOD1 G127X Patient CSF injected into rat spinal cord/MF
Adenylate Kinase 2 (AK2)	(Fukada *et al.*, 2004) (Li *et al.*, 2010)	NSC34 cells (MF)/ SOD1 G93A Rat spinal cord (MF)/ SOD1 G93A

Far Upstream Element-Binding Protein 1 (FUBP1)	(Nardo *et al.*, 2011) (Stalekar *et al.*, 2015)	Patient blood mononuclear cells SH-SY5Y cells/ TDP-43 Loss
Filamin A (FLNA)	(Nardo *et al.*, 2011) (Basso *et al.*, 2013)	Patient blood mononuclear cells Mouse astrocytes/ SOD1 G93A
Golgin B1 (GOLGB1)	(Nardo *et al.*, 2011) (Stalekar *et al.*, 2015)	Patient blood mononuclear cells SH-SY5Y cells/ TDP-43 Loss
Heat Shock Protein Family D, Member 1 (HSPD1)	(Li *et al.*, 2010) (Stalekar *et al.*, 2015)	Rat spinal cord (MF)/ SOD1 G93A SH-SY5Y cells/ TDP-43 Loss
Acyl- Coenzyme A Dehydrogenase, Medium Chain (ACADM)	(Fukada *et al.*, 2004) (Elf *et al.*, 2014)	NSC34 cells (MF)/ SOD1 G93A Patient muscle
Nadh Dehydrogenase 1 Beta Subcomplex Subunit 10 (NDUFB10)	(Fukada *et al.*, 2004) (Stalekar *et al.*, 2015)	NSC34 cells (MF)/ SOD1 G93A SH-SY5Y cells/ TDP-43 Loss
Solute Carrier Family 25, Member 4 (SLC25A4)	(Li *et al.*, 2010) (Stalekar *et al.*, 2015)	Rat spinal cord (MF)/ SOD1 G93A SH-SY5Y cells/ TDP-43 Loss
Ubiquinol-Cytochrome C Reductase Core Protein I (UQCRC1)	(Basso *et al.*, 2013) (Stalekar *et al.*, 2015)	Mouse astrocytes/ SOD1 G93A SH-SY5Y cells/ TDP-43 Loss
Chaperonin Containing Tcp1 Subunit 6a (CCT6A)	(Fukada *et al.*, 2004) (Stalekar *et al.*, 2015)	NSC34 cells (MF)/ SOD1 G93A SH-SY5Y cells/ TDP-43 Loss
2',3'-Cyclic Nucleotide 3' Phosphodiesterase (CNP)	(Bergemalm *et al.*, 2009) (Stalekar *et al.*, 2015)	Mouse spinal cord/ SOD1 G127X SH-SY5Y cells/ TDP-43 Loss

Proteins that showed consistent direction of differential expression in cells and tissues in at least two proteomic studies of ALS. Proteins are listed according to direction of differential expression (proteins with increased expression are listed first, followed by proteins with decreased expression). Protein name is given, followed by official gene symbol in brackets. ALS model and sample type used in each study are listed (studies are listed in the reference column). IF- insoluble fraction; MF- mitochondrial fraction

Table 5. 5. Proteins that showed contradictory direction of differential expression in cells and tissues across two or more proteomic studies of ALS

Protein (Official Gene Symbol)	Increased expression	Decreased expression
Prolyl 4-Hydroxylase Subunit Beta (P4HB)	(Massignan *et al.*, 2007) (Basso *et al.*, 2009) (Zhou et al., 2010) (Nardo et al., 2011)	(Basso *et al.*, 2013)
Phosphoglycerate Mutase 1 (PGAM1)	(Bastone *et al.*, 2009) (Bergemalm *et al.*, 2009) (Nardo *et al.*, 2011)	(Shin *et al.*, 2005) (Massignan *et al.*, 2007) (Stalekar *et al.*, 2015)
Peptidylprolyl Isomerase A (PPIA)	(Massignan *et al.*, 2007) (Basso *et al.*, 2009) (Nardo *et al.*, 2011)	(Basso *et al.*, 2013)
Dihydropyrimidinase-Like 2 (DPYSL2)	(Basso *et al.*, 2009) (Bastone *et al.*, 2009)	(Shin *et al.*, 2005) (Bergemalm *et al.*, 2009) (Basso *et al.*, 2013)
Pyruvate Kinase, Muscle (PKM)	(Basso *et al.*, 2009) (Bastone *et al.*, 2009)	(Shin *et al.*, 2005) (Basso *et al.*, 2013)
NADH Dehydrogenase Fe-S Protein 1 (NDUFS1)	(Basso *et al.*, 2009)	(Shin *et al.*, 2005) (Li *et al.*, 2010)
Enolase 1 (ENO1)	(Massignan *et al.*, 2007) (Basso *et al.*, 2009)	(Nardo *et al.*, 2011) (Basso *et al.*, 2013)
ATP Synthase, H+ Transporting, Mitochondrial F1 Complex, Alpha Subunit 1 (ATP5A1)	(Basso *et al.*, 2009)	(Fukada *et al.*, 2004) (Shin *et al.*, 2005) (Basso *et al.*, 2013)
Tubulin Alpha 1b (TUBA1B)	(Shin *et al.*, 2005)	(Fukada *et al.*, 2004)

	(Stalekar *et al.*, 2015)	
Voltage-Dependent Anion Channel 1 (VDAC1)	(Basso *et al.*, 2013)	(Fukada *et al.*, 2004) (Bergemalm *et al.*, 2009)
Transketolase (TKT)	(Bastone *et al.*, 2009) (Stalekar *et al.*, 2015)	(Basso *et al.*, 2013)
Pyruvate Dehydrogenase E1 Alpha 1 (PDHA1)	(Massignan *et al.*, 2007) (Basso *et al.*, 2009)	(Fukada *et al.*, 2004)
4-Aminobutyrate Aminotransferase (ABAT)	(Bastone *et al.*, 2009) (Li *et al.*, 2010)	(Bergemalm *et al.*, 2009)
Atp Synthase, H+ Transporting, Mitochondrial F1 Complex, Beta Polypeptide (ATP5B)	(Shin *et al.*, 2005) (Nardo *et al.*, 2011)	(Nardo *et al.*, 2011) (Stalekar *et al.*, 2015)
Aconitase 2 (ACO2)	(Fukada *et al.*, 2004) (Basso *et al.*, 2009) (Bastone *et al.*, 2009)	(Fukada *et al.*, 2004)
Vimentin (VIM)	(Basso *et al.*, 2009) (Basso *et al.*, 2013) (Stalekar *et al.*, 2015)	(Basso *et al.*, 2013)
Heat Shock Protein Family A, Member 5 (HSPA5)	(Engelen-Lee *et al.*, 2017)	(Fukada *et al.*, 2004) (Nardo *et al.*, 2011) (Basso *et al.*, 2013)
Actin Beta (ACTB)	(Nardo *et al.*, 2011) (Basso *et al.*, 2013)	(Umoh *et al.*, 2018)
Phosphoglycerate kinase 1 (PGK1)	(Shin *et al.*, 2005) (Bastone *et al.*, 2009) (Nardo *et al.*, 2011)	(Bastone *et al.*, 2009) (Nardo *et al.*, 2011)

Tubulin Beta-2B Chain (TUBB2B)	(Shin *et al.*, 2005) (Stalekar *et al.*, 2015)	(Umoh *et al.*, 2018)
Glutathione S-Transferase Mu 1 (GSTM1)	(Umoh *et al.*, 2018)	(Allen *et al.*, 2003)
Dipeptidyl Peptidase 3 (DPP3)	(Engelen-Lee *et al.*, 2017)	(Umoh *et al.*, 2018)
Prohibitin (PHB)	(Basso *et al.*, 2013)	(Li *et al.*, 2010)
Tubulin, Beta 4b (TUBB4B)	(Basso *et al.*, 2013)	(Stalekar *et al.*, 2015)
Electron Transferring Flavoprotein, Alpha (ETFA)	(Massignan *et al.*, 2007)	(Bergemalm *et al.*, 2009)
Actin, Gamma, Cytoplasmic 1 (ACTG1)	(Bergemalm *et al.*, 2009)	(Fukada *et al.*, 2004)
Annexin A5 (ANXA5)	(Basso *et al.*, 2009)	(Bergemalm *et al.*, 2009)
Creatine Kinase, Muscle (CKM)	(Staunton, Jockusch and Ohlendieck, 2011)	(Zhou *et al.*, 2010) (Staunton, Jockusch and Ohlendieck, 2011)
Crystallin, Alpha B (CRYAB)	(Basso *et al.*, 2009)	(Basso *et al.*, 2013)
Growth Factor Receptor-Bound Protein 2 (GRB2)	(Stalekar *et al.*, 2015)	(Bergemalm *et al.*, 2009)
Hexosaminidase Subunit Alpha (HEXA)	(Zhou *et al.*, 2010)	(Sharma *et al.*, 2016)
Heat Shock Protein 90 Alpha Family Class A Member 1 (HSP90AA1)	(Basso *et al.*, 2009)	(Stalekar *et al.*, 2015)
Isocitrate Dehydrogenase 3 (NAD+) Beta (IDH3B)	(Li *et al.*, 2010)	(Fukada *et al.*, 2004)
Heat Shock Protein 90, Beta (Grp94), Member 1 (HSP90B1)	(Basso *et al.*, 2009)	(Basso *et al.*, 2013)
Mitogen-Activated Protein Kinase 1 (MAPK1)	(Basso *et al.*, 2009)	(Basso *et al.*, 2013)
Lon Peptidase 1 (LONP1)	(Stalekar *et al.*, 2015)	(Fukada *et al.*, 2004)
Dynamin 1 (DNM1)	(Bergemalm *et al.*, 2009) (Umoh *et al.*, 2018)	(Shin *et al.*, 2005)

2,4-Dienoyl Coa Reductase 1 (DECR1)	(Li *et al.*, 2010)	(Stalekar *et al.*, 2015)

Proteins that showed contradictory direction of differential expression in cells and tissues in at least two proteomic studies of ALS. Protein name is given, followed by official gene symbol in brackets. Studies that identified increased or decreased protein expression are listed in column two and three.

GO analysis of the 42 proteins using the DAVID platform (Huang, Sherman and Lempicki, 2009b, 2009a) highlighted enriched biological process terms, including programmed cell death, protein transport and localization, response to oxidative stress and metabolism (Figure 5.3A). Cellular component GO analysis returned a range of terms, but similar to the bioinformatics finding from the CSF studies, the greatest number (i.e. 64%) of annotated proteins were associated with the term “extracellular vesicles” (Figure 5.3B). Proteins were then subjected to analysis using STRING 10 (Szklarczyk et al., 2015) to identify statistically significant associations between them (Figure 5.4). Comparison of the resulting networks with the GO analysis output (Figure 5.3) identified strong association between mitochondrial and endoplasmic reticulum proteins that are involved in the control of energy homeostasis, oxidative stress response and protein homeostasis (Figure 5.4). Within the networks, glyceraldehyde-3-phosphate dehydrogenase (GAPDH) was found to have the greatest number of known associations, linking with proteins involved in each of the three main domains.

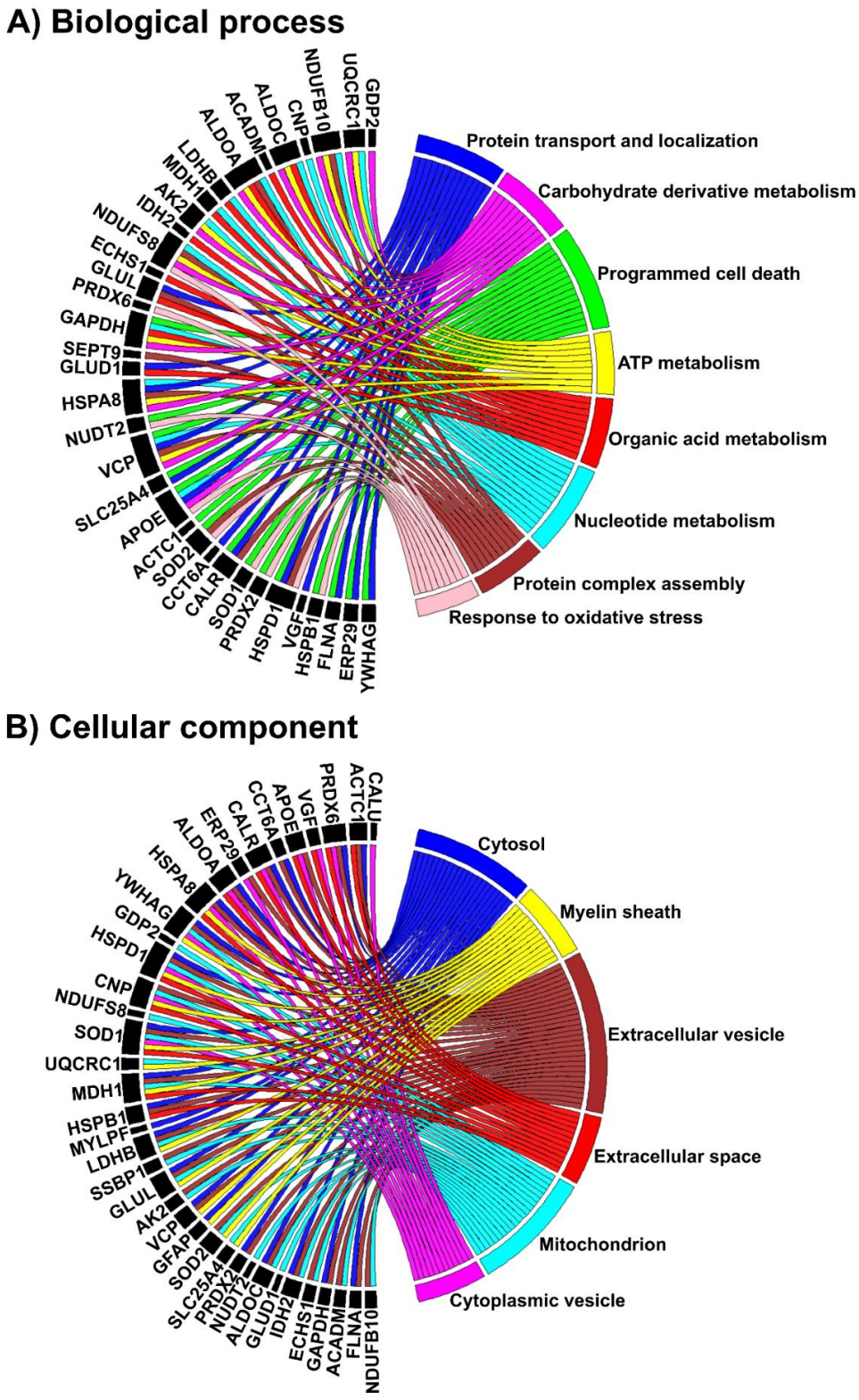

Figure 5. 3. Gene ontology analysis of the proteins consistently changed in the same direction in ALS tissues and cells. Gene ontology analysis revealed enriched terms connected to **(A)** biological processes and **(B)** cellular component. Top eight enriched terms from biological process domain, and top six enriched terms from cellular component domain are shown in the chord diagram, together with the proteins annotated to each term.

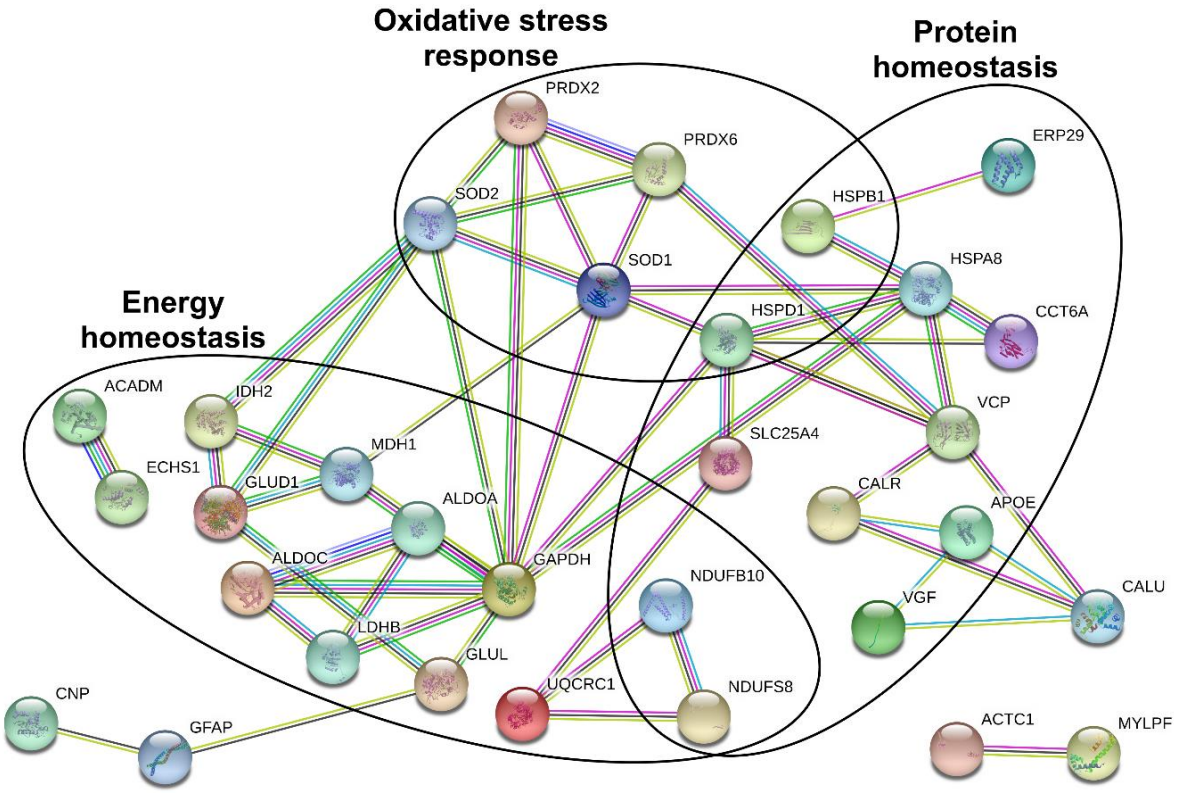

Figure 5.4. STRING 10 analysis of the proteins consistently changed in the same direction in ALS tissues and cells. Protein associations were identified with high confidence (0.700) interaction score, and only proteins that demonstrated significant associations are shown in the figure. The type of association between proteins is indicated by the colour (pink: experimentally determined interactors; light blue: interactors form curated database; grey: protein homology; black: co-expression; yellow: text-mining; dark blue: gene co-occurrence; green: gene neighbourhood). Three functional groups of proteins associated with regulation of oxidative stress, energy homeostasis and protein homeostasis were identified in the network from Figure 5.3.

5.2.4. Multi-study proteomic identification of conserved molecular changes in both SMA and ALS

To identify conserved protein changes common to SMA and ALS, differentially expressed proteins identified in the ALS multi-study comparison (Table 5.2 – 5.5) were compared with the differentially expressed proteins identified in a previous multi-study comparison of SMA proteomic datasets (Fuller, Gillingwater and Wishart, 2016). Fifteen proteins, summarised in Figure 5.5, were found to be differentially expressed in both diseases.

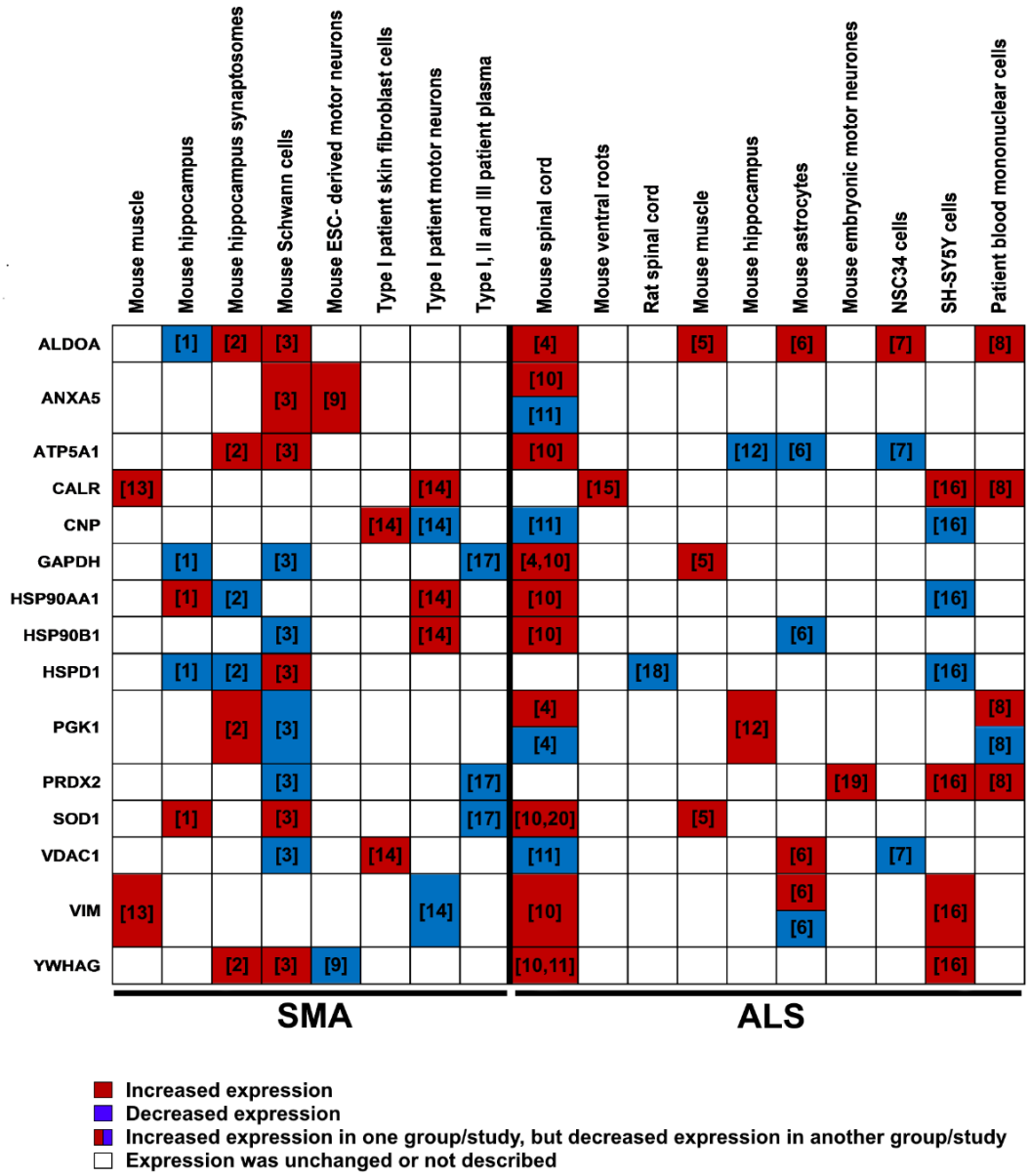

[1] Wishart et al. (2010), Hum. Mol. Genet., 19, 4216–4228
[2] Wishart et al. (2014), J. Clin. Invest., 124, 1821–1834
[3] Aghamaleky Sarvestany et al. (2014), J. Proteome Res., 13, 4546–4557
[4] Bastone et al. (2009), J Proteome Res., 8, 5229–5240
[5] Staunton et al. (2011), Biochem Biophys Res Commun, 406, 595–600
[6] Basso et al. (2013), J. Biol. Chem., 288, 15699 –15711
[7] Fukada et al. (2004), Mol Cell Proteomics., 3, 1211–1223
[8] Nardo et al. (2011), PLoS One, 6, e25545
[9] Wu et al. (2011), BMC Neurosci., 12, 25
[10] Basso et al. (2009), PLoS One, 4, e8130
[11] Bergemalm et al. (2009), Mol. Cell. Proteomics, 8, 1306–1317
[12] Shin et al. (2005), Neurochem. Int., 46, 641–653
[13] Mutsaers et al. (2013), Genome Med, 5, 95
[14] Fuller et al. (2016), Front. Cell. Neurosci., 9, 506
[15] Zhou et al. (2010), J Proteome Res., 9, 5133–5141
[16] Stalekar et al. (2015), Neuroscience, 293, 157–170
[17] Kobayashi et al. (2013), PLoS One, 8, e60113
[18] Li et al. (2010), Proc Natl Acad Sci U S A., 107, 21146–21151
[19] Duplan et al. (2010), J. Neurosci., 30, 785–796
[20] Strey et al. (2004), Am. J. Pathol., 165, 1701–1718

Figure 5.5. Proteins differentially expressed in both SMA and ALS proteomic studies. Heat map of proteins that were differentially expressed in both SMA and ALS proteomic studies. Protein names are presented as official gene symbols. The reference for each study is given in the corresponding squares of the heat map and in the Figure legend. Experimental model and sample type used in each study are indicated above the table. ALDOA- aldolase, fructose-bisphosphate A; ANXA5- annexin A5; ATP5A1- ATP synthase subunit alpha mitochondrial; CALR- calreticulin; CNP- 2,3-cyclic nucleotide 3-phosphodiesterase; GAPDH- glyceraldehyde-3-phosphate dehydrogenase; HSP90AA1- heat shock protein HSP 90 alpha; HSP90B1- heat shock protein 90 beta family member 1; HSPD1- heat shock protein family D, member 1; PGK1- phosphoglycerate kinase 1; PRDX2- peroxiredoxin 2; SOD1- superoxide dismutase 1; VDAC1- voltage dependent anion channel 1; VIM- vimentin; YWHAG- 14-3-3 protein gamma.

String 10 analysis revealed a strong association network between 14 of the 15 proteins (Figure 5.6). Programmed cell death was one of the most enriched biological process GO terms (Figure 5.7A) and is likely describing the downstream consequences of disease pathogenesis. Other highly enriched terms included regulation of immune system, regulation of protein metabolism, cytoskeleton organization, and mitochondrial transport and organization. Strikingly, all fifteen proteins identified in the comparison were associated with the cellular component term “extracellular vesicles” (Figure 5.7B).

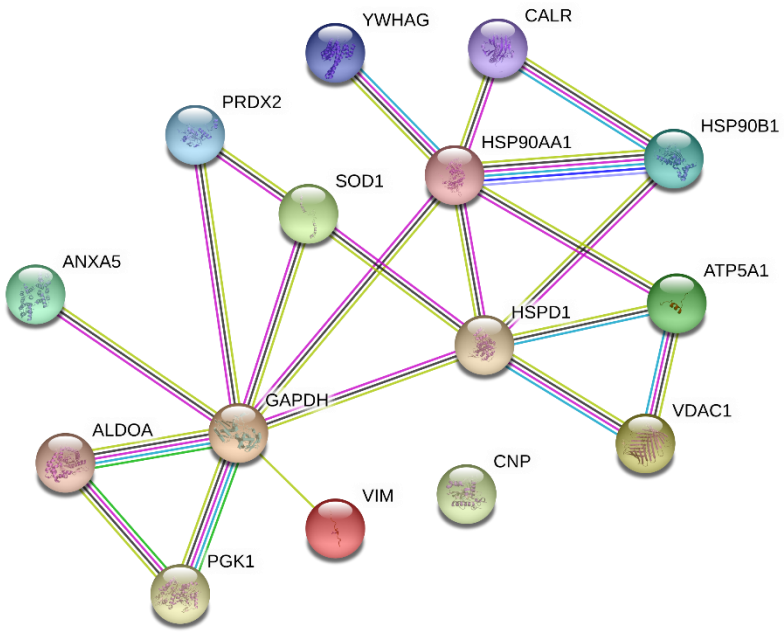

Figure 5. 6. String 10 association network of proteins that were differentially expressed in SMA and ALS. The analysis revealed strong association network between 14 of the 15 proteins. The type of the association between proteins is indicated by the colour (pink: experimentally determined interactors; light blue: interactors form curated databases; grey: protein homology; black: co-expression; yellow: text-mining; dark blue: gene co-occurrence; green: gene neighbourhood).

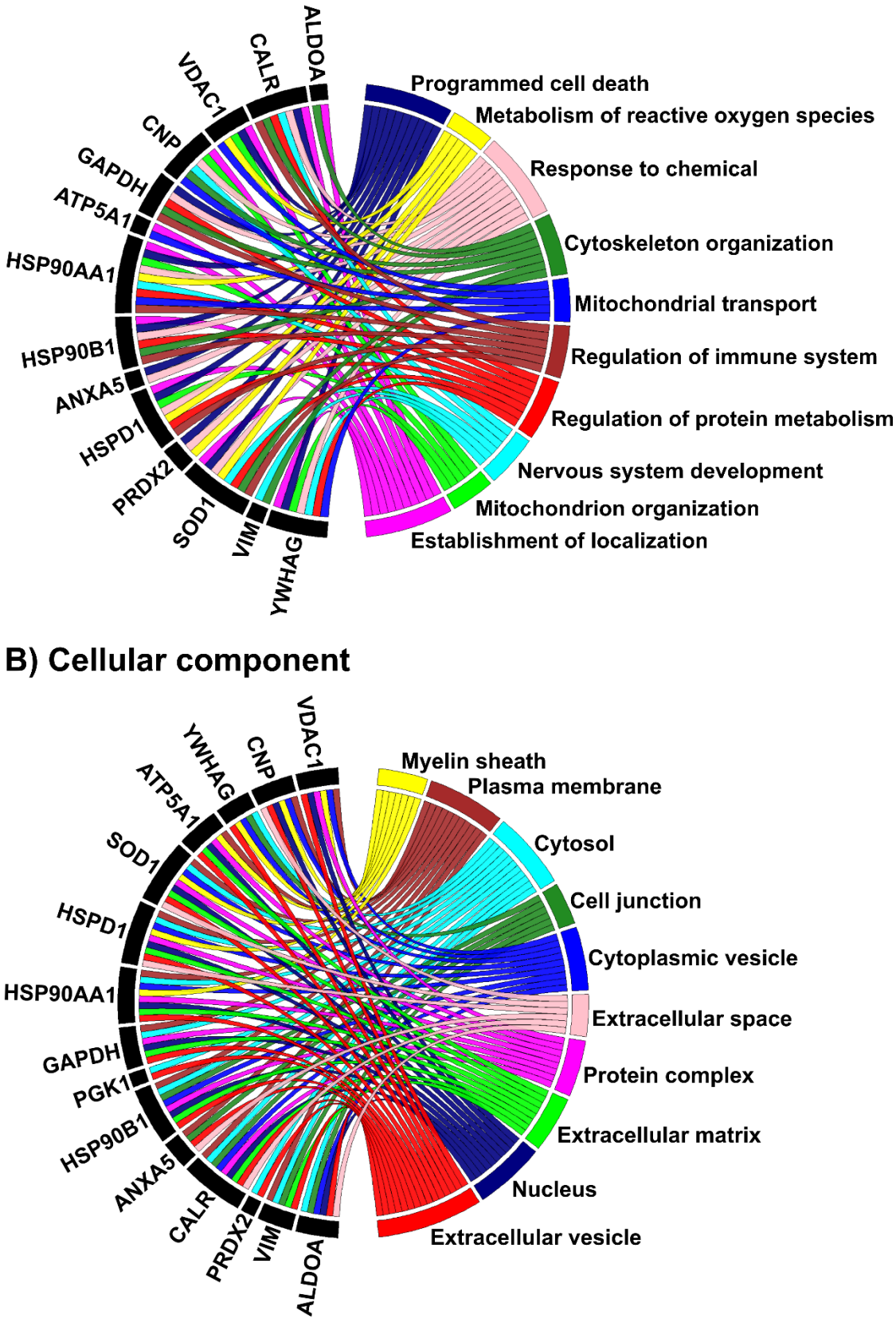

Figure 5. 7. Gene ontology analysis of the fifteen proteins differentially expressed in both SMA and ALS proteomic studies. Gene ontology analysis revealed enriched terms connected to **(A)** biological process and **(B)** cellular component. Top ten enriched terms from each domain are shown in the chord diagram, together with the proteins annotated to each term.

In summary, multi-study comparison of published proteomic studies of ALS and SMA identified fifteen proteins that were found to be differentially expressed in both diseases. Enriched terms associated with regulation of protein metabolism, regulation of immune system and mitochondrial transport were identified in the bioinformatics analysis, and all 15 proteins were linked to the GO cellular component term “extracellular vesicles”.

5.2.5. Verification of differential protein expression in spinal cords from SMA and ALS mice

Having established the core molecular overlap between SMA and ALS, it was next important to verify these changes biochemically in SMA and ALS tissues to establish how translatable these findings are to different biological systems. Spinal cord extracts from a mouse model of ALS ($SOD1^{G93A}$) and a mouse model of SMA (severe ‘Taiwanese’ model; $Smn^{-/-}$;$SMN2^{tg/+}$) at late symptomatic time-points (20 weeks and 8 days respectively), and from age-matched healthy controls were subjected to western blot analyses to determine the expression levels of five protein targets, including SOD1, CALR, ALDOA, GAPDH and HSP90B1 (Figure 5.8A and 5.8B). Only one of these proteins, calreticulin (CALR), was dysregulated in ALS and SMA spinal cords, and increased calreticulin expression in spinal cord extracts from ALS mice (73%, $p = 0.0028$) was in line with proteomic studies of ALS (Figure 5.5). Decreased calreticulin expression, identified in spinal cord extracts from SMA mice (22%, $p = 0.0079$), was in contrast with proteomic studies of SMA that showed increased calreticulin expression in iPSC-derived motor neurons from type I SMA patients and in SMA mouse muscles (Figure 5.5). As expected, SOD1 was significantly increased in ALS spinal cords ($p < 0.0001$), with no significant change observed in the spinal cord from SMA mice. ALDOA and GAPDH did not show a statistically significant change in expression in ALS and SMA spinal cords compared to healthy controls. It was not possible to reliably quantify the expression of HSP90B1 in spinal cords from ALS and

SMA mice due to low signal intensity, and/ or the presence of non-specific bands in samples (Figure 5.8A), both of which indicate technical problems with the antibody.

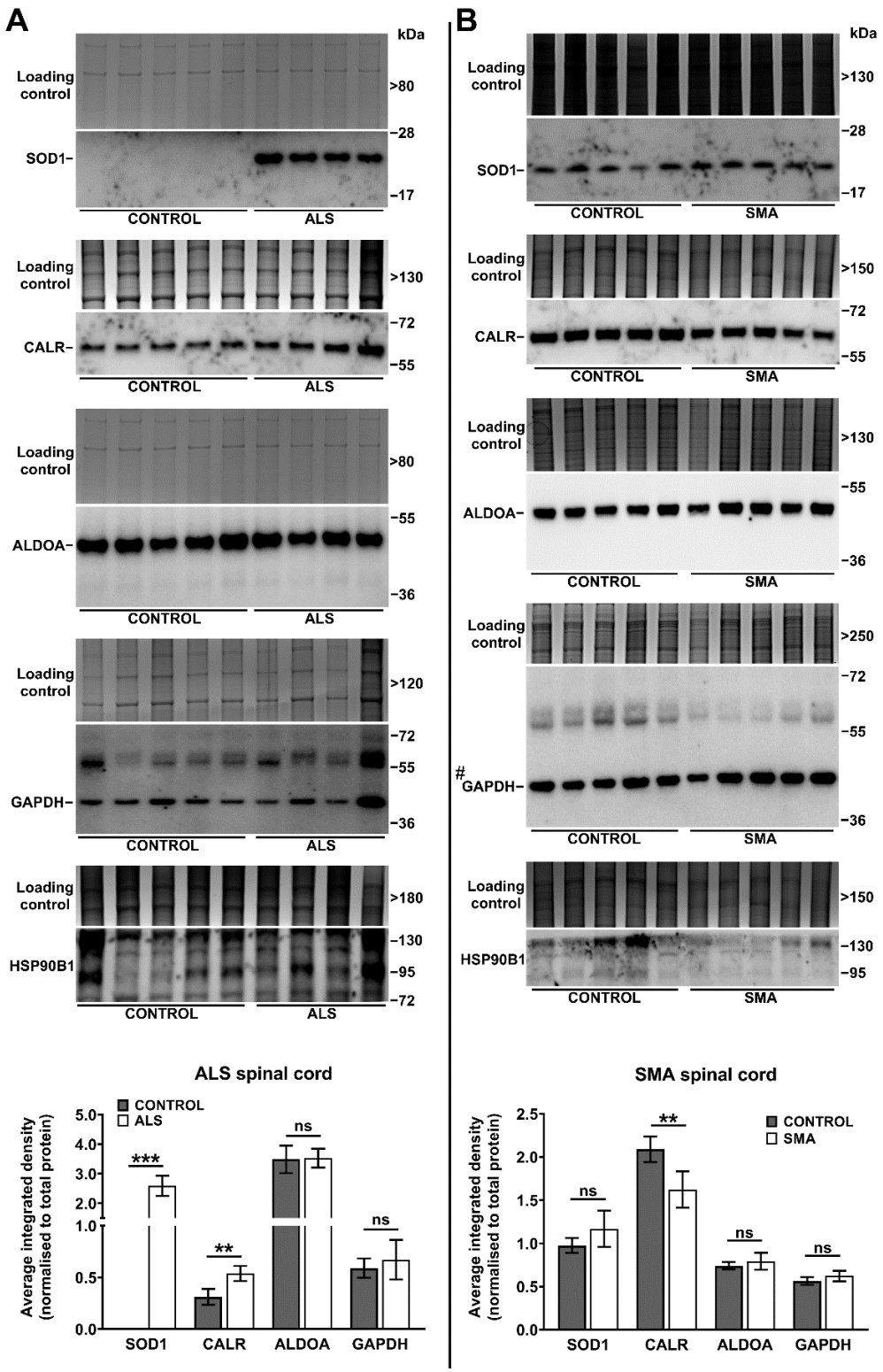

Figure 5.8. Verification of protein targets in spinal cord extracts from late-symptomatic ALS mice (20 week) and late-symptomatic SMA mice (P8). Representative western blots showing SOD1, CALR, ALDOA, GAPDH and HSP90B1 protein levels in **(A)** spinal cords from ALS mice (n=4) and age-matched healthy controls (n=5) and in **(B)** spinal cords from SMA mice (n=5) and age-matched healthy controls (n=5). ([#]GAPDH graph was also used in Figure 3.6). Graphs are presented as average integrated density (normalised to Coomassie stained gel), with error bars showing standard deviation from the mean. ALDOA- aldolase, fructose-bisphosphate A; CALR- calreticulin; GAPDH- glyceraldehyde-3-phosphate dehydrogenase; HSP90B1- heat shock protein 90 beta family member 1; SOD1- superoxide dismutase 1; ns-not significant; ** p<0.01; ***p<0.001

5.2.6. Calreticulin expression is dysregulated in spinal cord tissue from ALS and SMA mice

Calreticulin was the only protein that showed dysregulated expression in both ALS and SMA spinal cord extracts (Figure 5.8). However, the direction of expression change in SMA mouse spinal cord was in contrast with proteomic studies, where iPSC-derived motor neurons from type I SMA patients (Fuller et al., 2016) and SMA mouse muscle (Mutsaers et al., 2013) showed increased CALR levels. Differences in calreticulin expression in different cell populations could, according to a theory proposed by Bernard-Marissal et *al.* (Bernard-Marissal et *al.*, 2012), have contributed to the overall calreticulin expression levels in spinal cord, masking changes that were previously reported to be specific to vulnerable lower motor neurons. They show that reduction of calreticulin levels is restricted to lumbar motor neurons form $SOD1^{G93A}$ mice, since no obvious change in calreticulin expression was detected in thoracic motor neurons (Bernard-Marissal et *al.*, 2012). In addition, differences in calreticulin expression have been identified between different motor neuron populations within the lumbar spinal cord, where vulnerable motor neurons showed decreased calreticulin levels, and resistant motor neurons showed unchanged calreticulin levels when compared to control (Bernard-Marissal et al., 2012). To determine the contribution of vulnerable motor neuron population to the overall calreticulin expression trends in ALS and SMA spinal cords, lumbar spinal cord sections from late-symptomatic ALS (20 weeks) and SMA mice (P8), and age-matched healthy controls were stained with an antibody against calreticulin (Figure 5.9). The analysis of the ventral horn of lumbar spinal cord sections from control and SMA mice closely aligned with the quantitative western blotting, showing reduction of calreticulin levels by an average of 25% in SMA compared to controls ($p<0.001$) (Figure 5.9B). A significant difference in calreticulin expression was not detected by immunohistochemistry analysis of ALS and control lumbar spinal cord sections (Figure 5.9A).

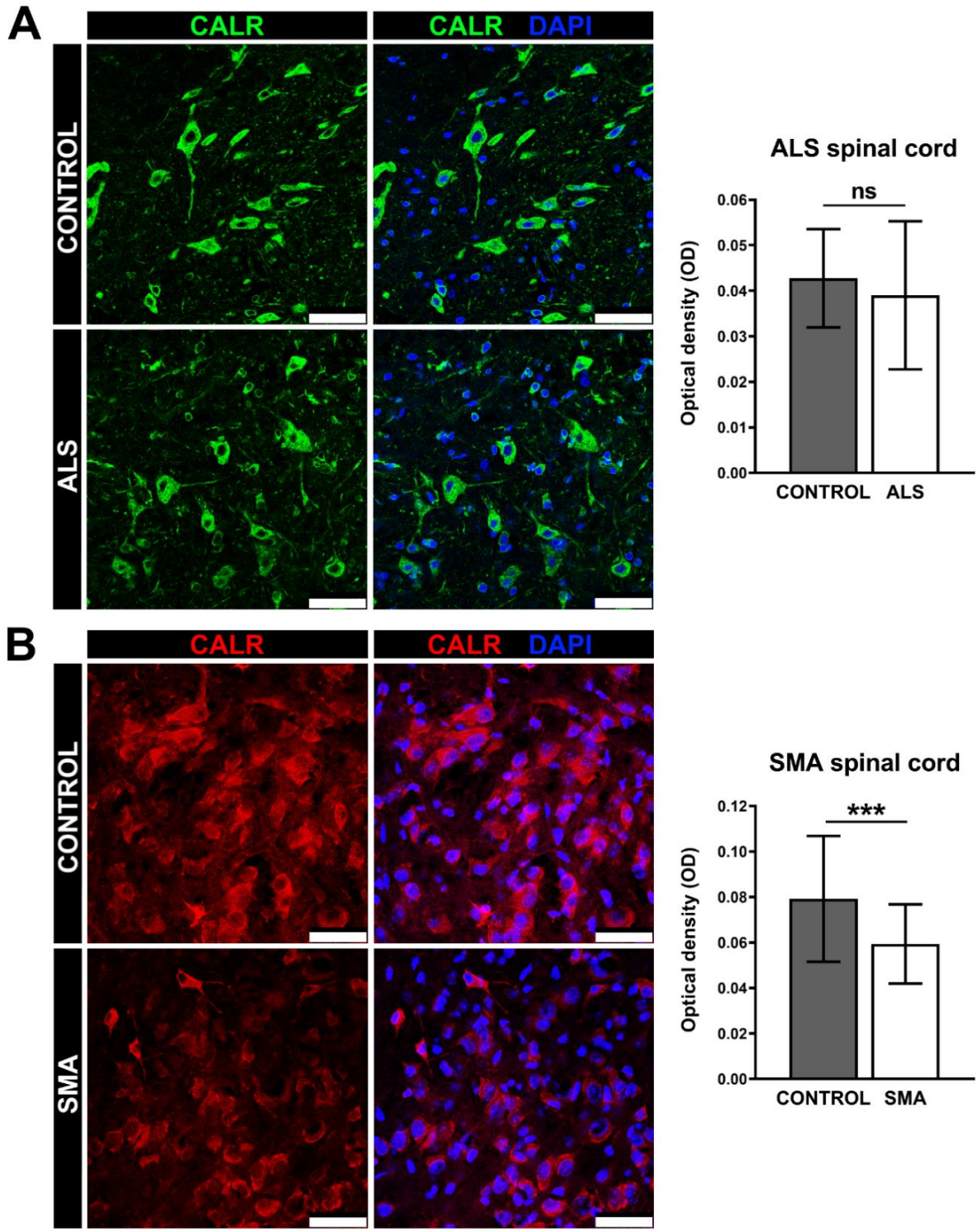

Figure 5.9. Reduced levels of calreticulin in lumbar spinal cords from late-symptomatic SMA mice. Representative immunohistochemistry images showing calreticulin expression in the ventral horn of lumbar spinal cord sections in **(A)** 20-week old control and ALS mice, and in **(B)** control and SMA mice (P8). Scale bar = 50 µm. Densitometry measurements of calreticulin levels in alpha motor neurons are presented as mean optical density, with error bars showing standard deviation from the mean. CALR- calreticulin; ns-not significant; *** $p<0.001$

In vitro studies of cultured mouse motor neurons demonstrated that activation of Fas/NO pathway specifically induces cell death in $SOD1^{G93A}$ and $SOD1^{G85R}$ vulnerable motor neurons, without affecting the survival of healthy cells (Raoul et al., 2006; Bernard-Marissal et al., 2012). Several proteins of this pathway including Fas ligand (FasL), whose binding to the Fas receptor initiates the pathway, demonstrated increased expression in lumbar spinal cord sections from $SOD1^{G93A}$ and $SOD1^{G85R}$ mice at the pre-symptomatic stage of the disease (Raoul et al., 2006), and ALS mice deficient for FasL function ($SOD1^{G93A}$; $FasL^{-/-}$) demonstrated increased survival and decreased motor neuron loss in lumbar spinal cord (Petri et al., 2006). In SMA, activation of Fas death pathway was identified in iPSC-derived motor neurons from type I SMA patients (Sareen et *al.,* 2012), while no significant change in FasL expression was demonstrated in whole spinal cord extracts from SMA mice (P8) (Tsai et al., 2006). By studying $SOD1^{G93A}$ motor neurons *in vitro*, Bernard-Marissal et *al.* demonstrated that activation of Fas/NO pathway triggers reduction of calreticulin levels, which in turn promotes ER stress and further activation of Fas/NO pathway leading to the vicious cycle of changes that result in motor neuron death (Bernard-Marissal et *al.*, 2012). To investigate whether the same mechanism might be responsible for calreticulin downregulation in vulnerable motor neurons in SMA, lumbar spinal cord sections from SMA mouse and healthy control were stained for FasL and calreticulin (Figure 5.10A). Calreticulin showed clear staining in ventral horn motor neurons from SMA and control mice, however, no specific FasL staining was detected in either SMA or control sections. To determine whether FasL detection was hampered for technical reasons, including the tissue processing method and/or immunohistochemistry protocol used in the study, the FasL antibody was next tested in quantitative western blotting on whole spinal cord extracts from SMA and control mice (Figure 5.10B). Surprisingly, the analysis showed strong cross-reaction of anti-FasL antibody with protein standards (indicated by arrow

in Figure 5.10B). To facilitate detection of specific bands, the blot had to be re-imaged with protein ladder outside of the field of view. Following this, three bands, in the range of 55-130 kDa, were detected in spinal cord extracts from SMA mice and healthy controls (indicated by chevron arrows in Figure 5.10B), however none of these correspond to monomeric FasL (~30 kDa). Western blot analysis of spinal cord extracts from ALS and control mice demonstrated the same cross-reaction of anti-FasL antibody with protein standards (Figure 5.10C). The greatest limitation of this study is the lack of positive control, i.e. purified FasL or extract of cells exposed to nitric oxide (NO) as in Bernard-Marissal et *al.* (Bernard-Marissal et *al.*, 2012). Positive control can confirm possible technical problems with the antibody, and since one was not used in this study, it is not possible to determine with certainty whether the Fas pathway is activated or not in spinal cord tissue from SMA and ALS mice.

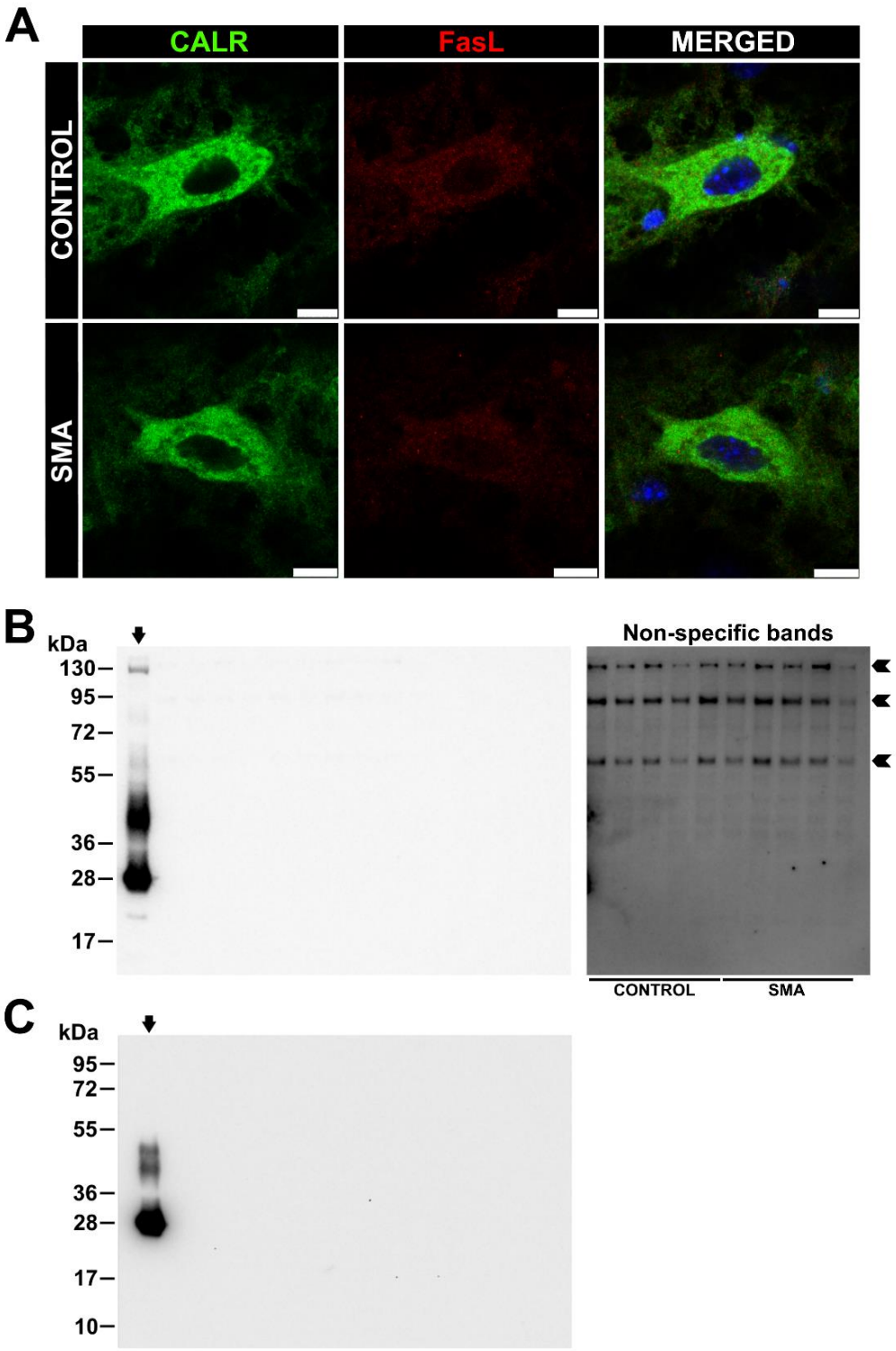

Figure 5.10. FasL antibody cross-reacts with proteins of the ladder in spinal cord extracts from late-symptomatic ALS (20 week) and SMA mice (P8). (A) Representative immunohistochemistry images showing calreticulin and FasL expression in the ventral horn of lumbar spinal cord sections from SMA mouse and age-matched healthy control. Scale bar = 10 µm. Representative western blots showing FasL protein levels in **(B)** spinal cords from SMA mice (n=5) and age-matched healthy controls (n=5), and in **(C)** spinal cords from ALS mice (n=4) and age-matched healthy controls (n=5). Arrows indicate cross-reaction of FasL antibody with protein standards. Chevron arrows indicate non-specific bands, detected when protein ladder was moved outside of the field of view. CALR- calreticulin; FasL- Fas ligand

In summary, calreticulin showed the opposite direction of differential expression in whole spinal cord extracts from ALS and SMA mice, and decreased expression of calreticulin, identified in spinal cords from SMA mice, was in contrast with proteomic studies of SMA. The link between calreticulin dysregulation and Fas death pathway was not observed in ventral horn motor neurons from SMA mice.

5.2.7. ALDOA and GAPDH activity in spinal cord extracts from ALS and SMA mice

Glycolysis is the main source of ATP in high energy demanding tissues like muscles and neuronal tissues (Jang *et al.*, 2016), and defects in energy homeostasis, caused by abnormal glycolysis, were shown to contribute to selective death of vulnerable motor neurons and muscle atrophy in mouse models of SMA (Boyd *et al.*, 2017) and ALS (Palamiuc *et al.*, 2015). Two glycolytic enzymes identified in this study, aldolase fructose-bisphosphate A (ALDOA) and glyceraldehyde-3-phosphate dehydrogenase (GAPDH) (Kanungo *et al.*, 2018), showed no significant change in expression in spinal cord extracts from late-symptomatic ALS mice (20 weeks) and late-symptomatic SMA mice (P8) (Figure 5.8). In a separate study, GAPDH protein levels were unchanged in muscles from symptomatic $SOD1^{G93A}$ mice (130 days) and late-symptomatic $SOD1^{H46R/H48Q}$ mice (230 days), however, a significant reduction of GAPDH activity was identified in muscles from both mouse models of ALS (Pierce et *al.*, 2008). There is a possibility therefore that ALDOA and GAPDH activity might be dysregulated in spinal cord extracts from late-symptomatic ALS and SMA mice despite showing unchanged protein levels. In addition, oxidative stress was identified as a shared link between ALS and SMA (Figure 5.7A), and exposure to oxidative stress was previously shown to decrease the activity of both GAPDH (Pierce et *al.*, 2008) and ALDOA (Koeck et *al.*, 2004) *in vitro*. To test this hypothesis, ALDOA and GAPDH activity levels were investigated in whole spinal cord extracts from late-

symptomatic ALS mice (20 weeks) and late-symptomatic SMA mice (P8), and in age-matched healthy controls as described in chapter 2, section 2.10 (Figure 5.11A and 5.11B). Neither ALDOA or GAPDH showed a change in activity levels in spinal cord extracts from late-symptomatic SMA mice, however, a statistically significant reduction of ALDOA (64%, $p < 0.0001$) and GAPDH (42%, $p = 0.0452$) activity was identified in spinal cord extracts from late-symptomatic ALS mice when compared to controls (Figure 5.11C and 5.11D). It was of interest to next determine whether changes in ALDOA and GAPDH activity can be detected at an earlier stage of the disease, as this would suggest that metabolic changes drive motor neuron pathology in ALS. ALDOA and GAPDH activity levels were not significantly changed in spinal cord extracts from early-symptomatic ALS mice (12 week) compared to age-matched healthy controls (Figure 5.12A). As expected, western blot analysis showed no significant change in ALDOA and GAPDH protein levels in spinal cord extracts from 12-week old ALS mice (Figure 5.12B) (western blot analysis of ALDOA expression in 12-week old ALS mice were conducted by Dr Heidi Fuller (Keele) and are presented here for the purpose of comparison).

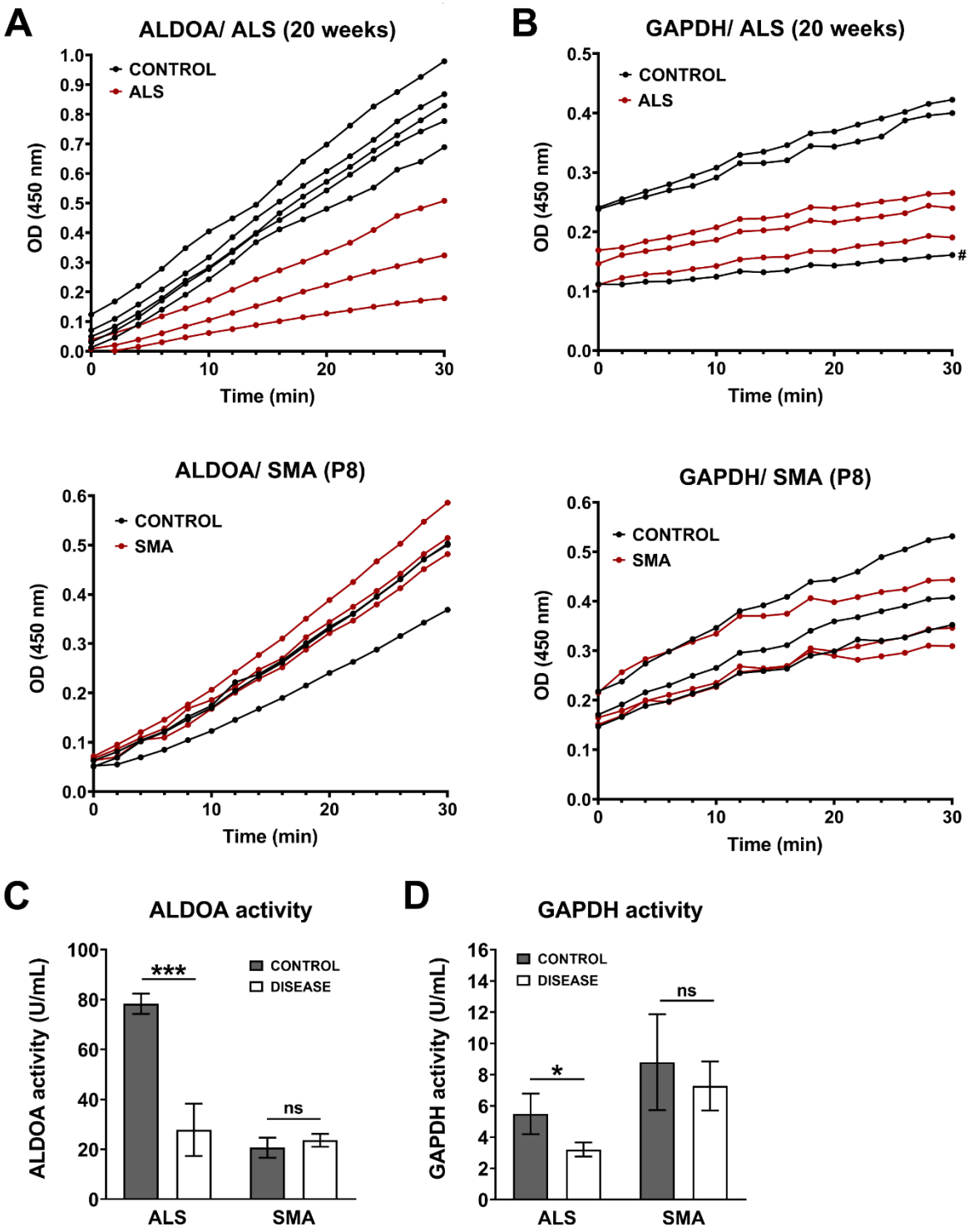

Figure 5.11. ALDOA and GAPDH activity levels are deceased in spinal cord extracts from late-symptomatic ALS mice (20 week). (A) ALDOA activity, measured as optical density (OD) over time, in spinal cord extracts from 20-week old ALS mice (n = 3) and age-matched healthy controls (n = 5), and in spinal cord extracts from 8-days old SMA mice (n = 3) and age-matched healthy controls (n = 3). **(B)** GAPDH activity, measured as optical density (OD) over time, in spinal cord extracts from 20-week old ALS mice and 8-days old SMA mice (n = 3) and their respective age-matched healthy controls (n = 3). #Lower GAPDH activity of this sample is caused by higher dilution factor, which was taken into account during quantitative analysis. Graphs are presented as average **(C)** ALDOA and **(D)** GAPDH activity levels, with error bars showing standard deviation from the mean. ALDOA- aldolase, fructose-bisphosphate A; GAPDH- glyceraldehyde-3-phosphate dehydrogenase; ns- not significant; *p<0.05; *** p<0.001

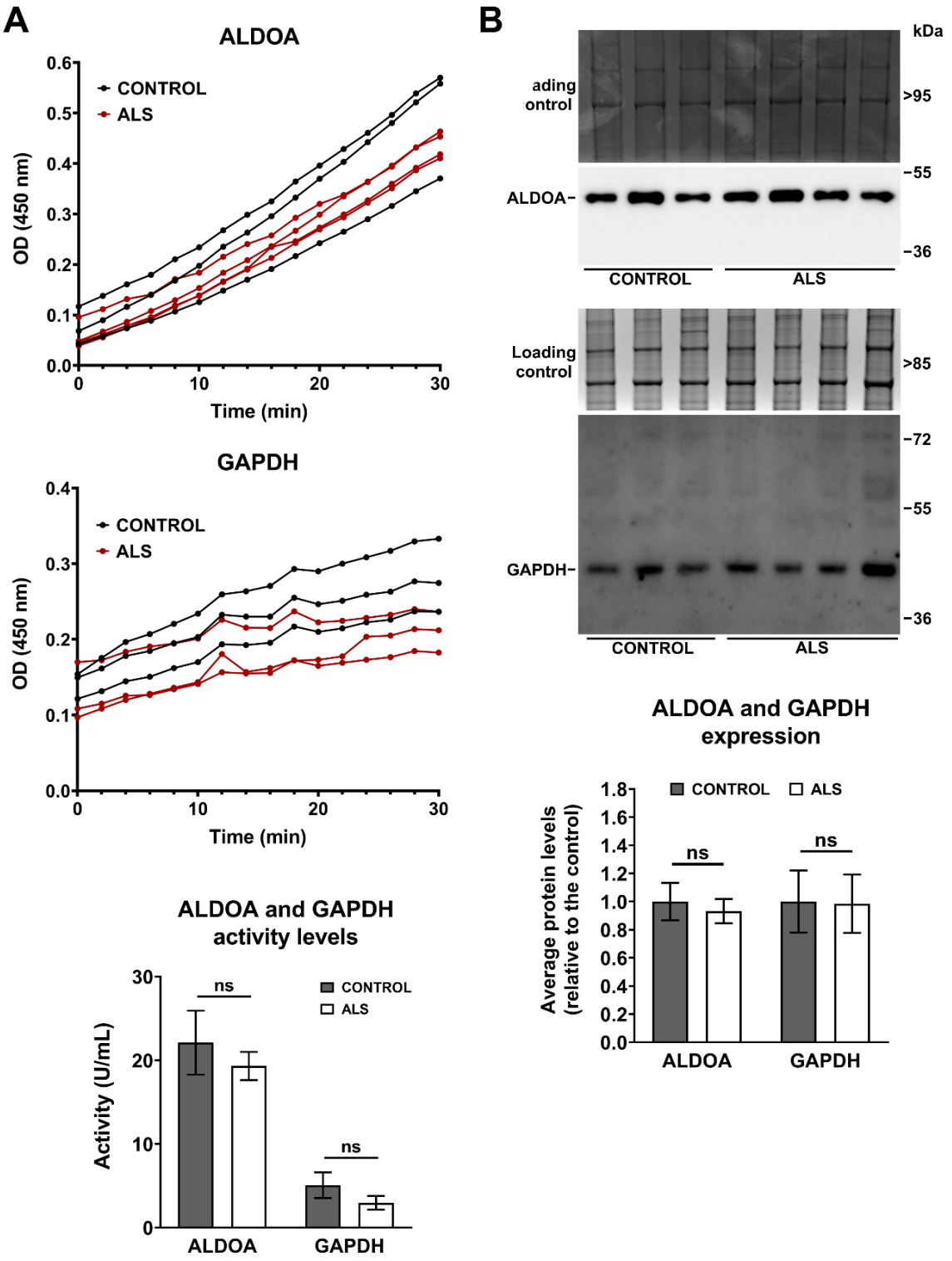

Figure 5. 12. ALDOA and GAPDH expression and activity are not changed in spinal cord extracts from early-symptomatic ALS mice (12 week). (A) ALDOA and GAPDH activity, measured as optical density (OD) over time, in spinal cord extracts from 12-week old ALS mice (n = 4 for ALDOA, and n = 3 for GAPDH) and age-matched healthy controls (n = 3). Graph is presented as average ALDOA and GAPDH activity levels, with error bars showing standard deviation from the mean. **(B)** Representative western blots showing ALDOA and GAPDH protein levels in spinal cords from 12-week old ALS mice (n = 4) and age-matched healthy controls (n = 3). The graph is presented as average protein levels (expressed relative to the control), with error bars showing standard deviation from the mean. ALDOA- aldolase, fructose-bisphosphate A; GAPDH- glyceraldehyde-3-phosphate dehydrogenase; ns- not significant

In summary, a statistically significant reduction of ALDOA and GAPDH activity was identified in spinal cord extracts from late-symptomatic ALS mice. In addition, defects in ALDOA and GAPDH activity seem to be an ALS specific pathology, since SMA mouse spinal cords showed no significant change in ALDOA and GAPDH activity levels compared to controls.

Protein tyrosine nitration increases *in vitro* as a result of oxidative stress (Koeck et al., 2004), and it was shown to be responsible for decreased GAPDH and ALDOA activity *in vitro* (Koeck et al., 2004; Palamalai and Miyagi, 2010). Oxidative stress is an important pathological feature in ALS (Tan, Pasinelli and Trotti, 2014), and increased nitrotyrosine levels were identified previously in spinal cords from pre- and early symptomatic ALS mice (Bruijn et al., 1997; Ferrante et al., 1997; Casoni et al., 2005). To date, however, protein tyrosine nitration has not been investigated as a direct mechanism of dysregulated ALDOA and GAPDH activity in ALS. To test this hypothesis, equal amounts of total protein from spinal cord extracts of 20-week old ALS and control mice were immunoprecipitated with mouse antibody raised against 3-nitrotyrosine and subjected to western blot analysis to detect nitrotyrosine and ALDOA (Figure 5.13A). ALDOA was easily detected in the input and unbound part of the pulldown but was absent from the eluate in both control and ALS samples. When the blot was developed with anti-nitrotyrosine antibody, two bands, most likely corresponding to large and small subunits of the mouse IgG, were identified in the eluate from control and ALS samples, however, no specific nitrotyrosine bands were observed in either of the sample. This would suggest technical problems with the antibody (e.g. it is not suitable for immunoprecipitation) since nitrotyrosine did not pull itself down, and so GAPDH protein levels were not investigated in this experiment. It is possible too that proteins are not nitrated in spinal cords from 20-week old ALS mice, and/or that protein nitration is below the levels of detection in whole spinal cord

extracts. This is supported by the finding that nitrotyrosine bands were not detected in the input from either control or ALS spinal cord extracts in the pulldown experiment (Figure 5.13A). To test this hypothesis, 20 µg of total protein was used for western blot analysis of ALS and control spinal cord extract to increase the sensitivity of signal detection, however, the same result was demonstrated in this experiment showing no specific nitrotyrosine bands in control and ALS samples (Figure 5.13B). The only band detected had a molecular weight of around 55 kDa and likely represents the large subunit of mouse IgG. It is still not possible to reliably interpret these results, since a positive control, that could validate the sensitivity of the antibody, was not used in this experiment.

Aldolase A is glycolytic enzyme that catalyses the reversible conversion of fructose-1,6-bisphosphate to glyceraldehyde 3-phosphate and dihydroxyacetone phosphate (Kanungo et al., 2018). There is also evidence to support the role for ALDOA in regulating neurofilament light (NF-L) mRNA stability (Canete-Soler et al., 2005). For example, ALDOA and NF-L mRNA demonstrated interaction in Neuro-2a cell line and in mouse brain extracts, and constitutive ectopic expression of ALDOA induced NF-L mRNA degradation in Neuro-2a cell line (Canete-Soler et al., 2005). As a subunit of neurofilament proteins, NF-L regulates cell shape, and is involved in control of different neuronal functions including signal conduction, synaptic vesicle trafficking and neurite growth (Didonna and Opal, 2019). NF-L subunit is required for initiation of neurofilament assembly, and defects in NF-L expression or function are therefore likely to impair different neuronal functions (Didonna and Opal, 2019). Nuclease activity was proposed as a mechanism by which ALDOA controls the stability of NF-L mRNA (Canete-Soler et al., 2005), and since ALDOA already demonstrated perturbed glycolytic activity in spinal cord extracts from 20-week old ALS mice (Figure 5.10C), it was of interest to next determine

whether ALDOA nuclease activity is also affected in ALS. Decreased NF-L mRNA levels were previously identified in cervical motor neurons from sporadic ALS patients (Wong, He and Strong, 2000), and so the aim here was to determine whether NF-L dysregulation translates functionally on the protein level. NF-L expression was analysed in spinal cord extracts from late-symptomatic ALS mice and age-matched healthy controls using quantitative western blotting (Figure 5.13C). The analysis identified decreased NF-L protein levels in spinal cord extracts from 20-week old ALS mice, however the change was not statistically significant, likely caused by big sample variability in control group.

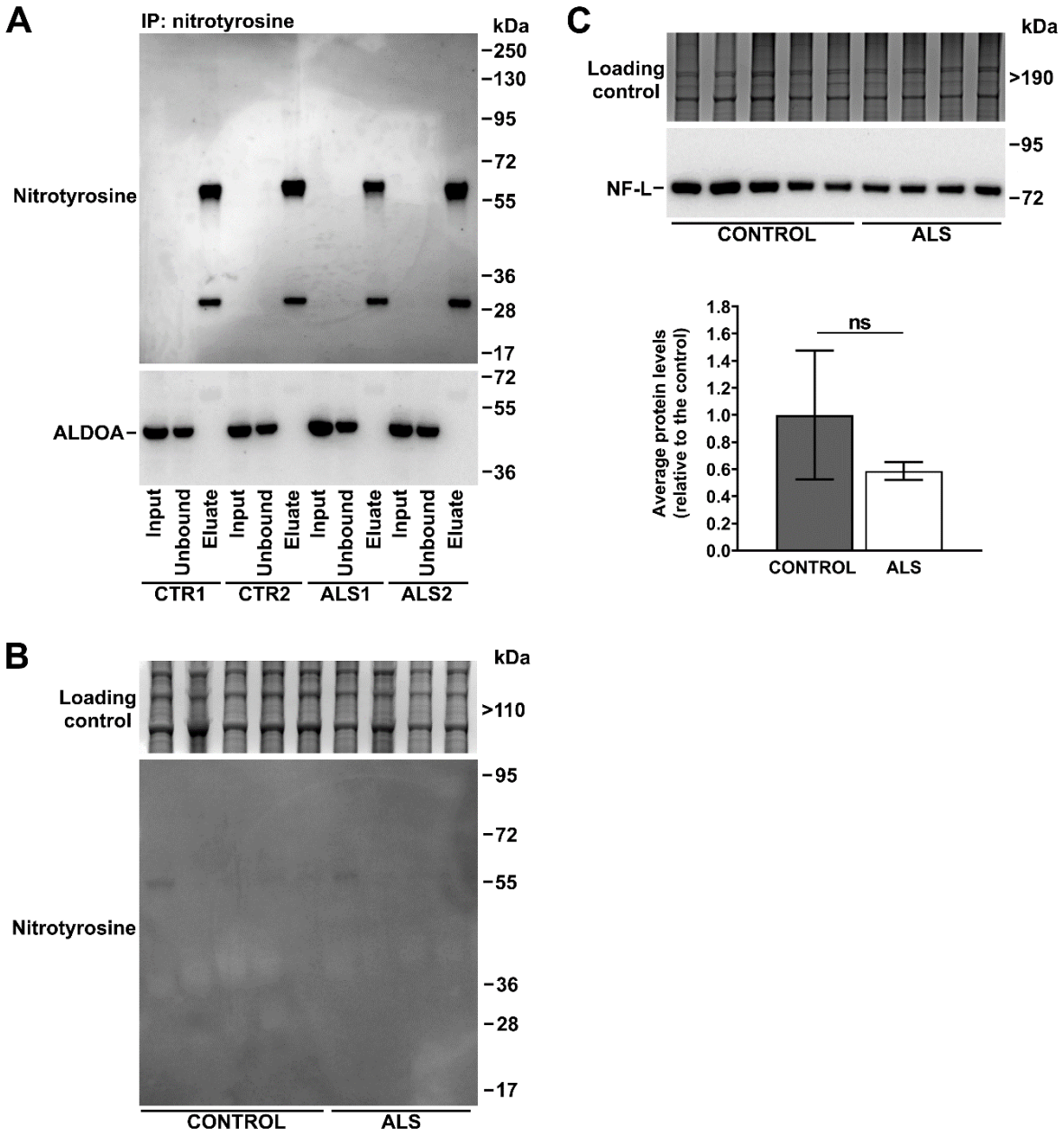

Figure 5.13. Protein nitration was not detected in spinal cord extracts from late-symptomatic ALS mice (20 week). (A) Western blots showing nitrotyrosine and ALDOA protein levels in spinal cord extracts from control (n = 2) and ALS (n = 2) mice after immunoprecipitation with anti-nitrotyrosine antibody. Specific nitrotyrosine bands were not detected in control or ALS spinal cords. Bands in the eluate represent large and small subunits of mouse IgG. Western blots showing **(B)** nitrotyrosine and **(C)** NF-L levels in spinal cord extracts from ALS mice (n = 4) and age-matched healthy controls (n = 5). The graph is presented as average protein levels (expressed relative to the control), with error bars showing standard deviation from the mean. CTR- control; ALDOA- aldolase, fructose-bisphosphate A; NF-L- light-neurofilament; ns- not significant

Protein tyrosine nitration was not identified in spinal cord extracts from 20-week old ALS mice. It is not possible, however, to determine at this point whether this is a true finding or a result of technical problems with the antibody. Finding of decreased NF-L protein levels in spinal

cord extracts from ALS mice suggested that ALDOA nuclease activity might also be altered in ALS. The result was, however, statistically insignificant, and to be confirmed, this hypothesis requires further experimental attention.

In summary:

a) The multi-study comparison identified 42 proteins that showed consistent direction of differential expression across at least two proteomic studies of ALS. These proteins were associated with mitochondrial and endoplasmic reticulum functions such as the control of energy homeostasis, oxidative stress response and protein homeostasis.

b) Fifteen proteins identified in the comparison of ALS and SMA proteomic datasets represent core molecular overlap between SMA and ALS, and are associated with functions like regulation of protein metabolism, regulation of immune system and mitochondrial transport. All fifteen proteins were also associated with extracellular vesicles, indicating alterations in exosome transport as a shared link between SMA and ALS.

c) Biochemical analyses of the five proteins, SOD1, CALR, ALDOA, GAPDH and HSP90B1, showed very few similarities between SMA and ALS. Calreticulin was the only protein that showed dysregulated expression in the spinal cord from symptomatic SMA and ALS mice, where increased expression was identified in the spinal cord from ALS mice and decreased expression was identified in the spinal cord from SMA mice. Although no significant change was detected in ALDOA and GAPDH protein levels, the activity of both proteins was decreased in the spinal cord extracts from late-symptomatic ALS mice.

5.3. Discussion

5.3.1. Differentially expressed proteins in biofluids from ALS patients

Eleven proteins were consistently changed in the same direction in ALS patient biofluids across at least two proteomic studies (Table 5.2), some of which like putative auxiliary biomarker, cystatin C (Zhu *et al.*, 2018), have already gained significant attention in the context of ALS. The neurosecretory protein VGF emerged in recent years as a potential biomarker of disease progression, having demonstrated decreased levels in post-mortem spinal cord samples from sporadic ALS patients (Shimazawa *et al.*, 2010), in plasma and fibroblast cells from sporadic and familial ALS patients in an advanced stage of the disease (Brancia *et al.*, 2016), and in CSF from ALS patients, the levels of VGF decreased with disease progression (Zhao *et al.*, 2008). In addition, decreased levels of VGF were identified at a pre-symptomatic stage of the disease in CSF, serum and in lumbar and cervical spinal cord sections from transgenic $SOD1^{G93A}$ mice (Zhao *et al.*, 2008; Brancia *et al.*, 2016), suggesting VGF as a potential modifier of disease pathogenesis in ALS. For example, overexpression of *VGF* prevented ER-stress induced cell death in SH-SY5Y cell cultures (Shimazawa *et al.*, 2010), and *in-vitro* restoration of VGF levels in motor neurons derived from $SOD1^{G93A}$ mice demonstrated neuroprotective action, highlighting VGF as a potential therapeutic target in ALS (Zhao *et al.*, 2008).

A relatively high number of blood-derived proteins was detected in the comparison, including for example, Hemoglobin subunit alpha 1 (HBA1) and Hemoglobin subunit beta (HBB), both of which are indicators of blood contamination in CSF, most likely caused by poor quality control during sample processing (Barschke *et al.*, 2017). Another source of blood-derived proteins is CSF itself, as it is mainly the product of plasma filtration. Abundant proteins originating from blood can hamper detection of CNS-specific proteins and are usually removed from the

sample prior to proteomics analysis (Hu, Loo and Wong, 2006), however, the efficiency of the protein depletion varies depending on the method used (Polaskova *et al.*, 2010). This and other technical variabilities between different proteomics approaches can significantly alter sensitivity of the protein detection (Barschke *et al.*, 2017). It is perhaps not surprising that comparison identified very few similarities, emphasising the need to standardize proteomics protocols that would enable reliable and reproducible comparison between the studies.

5.3.2. Differentially expressed proteins in ALS patient samples and animal models of ALS associate with mitochondria and endoplasmic reticulum (ER)

Comparison of published proteomic studies that utilised tissues and cells from patients and animal models of ALS identified 42 proteins with a consistent direction of differential expression across at least two studies, some of which appear to have been overlooked when these datasets were considered in isolation. One such protein, aldolase A, for example, was increased in expression in five separate studies (Fukada *et al.*, 2004; Bastone *et al.*, 2009; Nardo *et al.*, 2011; Staunton, Jockusch and Ohlendieck, 2011; Basso *et al.*, 2013). Given its importance in glycolysis (Magistretti and Allaman, 2015), overexpression of this protein is highly likely to reflect perturbed metabolic activity. Indeed, mitochondrial dysfunction (Tan, Pasinelli and Trotti, 2014) and ER stress (Rozas *et al.*, 2017) are known early pathological features and a major contributing factor of motor neuron death in ALS. Not surprisingly, most of the dysregulated proteins identified in tissues and cells from ALS patients and models were associated with energy homeostasis, oxidative stress response and control of protein stability, confirming the importance of ER and mitochondria in ALS disease pathways.

Another important finding is that most proteins with a consistent direction of differential expression across ALS proteomic studies were associated with extracellular vesicles.

Significant attention has been given to extracellular vesicles in the context of neurodegenerative disorders, including ALS, as a potential source of biomarkers and as a possible mechanism of misfolded protein spreading in CNS (Quek and Hill, 2017). Mutant SOD1 and TDP-43 proteins are among molecules whose prion-like properties, facilitated by exosome transport, are thought to contribute to spreading of protein misfolding in ALS (Quek and Hill, 2017).

5.3.3. Impaired protein metabolism and mitochondrial dysfunction are shared pathologies in ALS and SMA

Interestingly, all fifteen proteins identified in the comparison between ALS and SMA proteomics studies were also associated with extracellular vesicles. Increased levels of exosomes were recently reported in culture media from SMN-depleted cells, SMA patient fibroblasts, and in serum from SMA patients and mouse model of SMA (Nash *et al.*, 2017), indicating alterations in exosome transport as a shared link between SMA and ALS.

Other enriched terms, identified in the bioinformatics analysis of the 15 proteins that were differentially expressed in ALS and SMA, included cell death, protein metabolism and mitochondria-associated functions. Considering the role for protein aggregation and ER stress in ALS pathology (Section 5.1.1), it is not surprising that four out of fifteen proteins identified, including CALR, HSPD1, HSP90B1 and HSP90AA1, are chaperones that promote correct folding of proteins. In spinal cord tissue from $SOD1^{G93A}$ mice upregulation of proteins in the UPR pathway was identified at a pre-symptomatic stage of the disease (Atkin *et al.*, 2008) directly implicating it in ALS pathogenesis. Using transcriptomics approach, Ng et *al.* also demonstrated activation of the UPR pathway in induced pluripotent derived-motor neurons from type I SMA patients, the results of which were verified by qPCR analyses in motor

neurons from type I and type II SMA patients (Ng *et al.*, 2015). An inverse correlation between the levels of SMN protein and the degree of ER stress was identified in human motor neuron cultures *in vitro*, and pharmacological inhibition of the UPR pathway increased the survival of motor neurons from type I SMA patients (Ng *et al.*, 2015).

In recent years, ER-Golgi protein trafficking has also been identified as a shared link between SMA and ALS. Impaired ER-Golgi transport mechanisms can trigger ER stress and Golgi alterations, ultimately leading to induction of the cell death-related pathways (Preston *et al.*, 2009; Atkin *et al.*, 2014). Indeed, dysregulated ER-Golgi trafficking was observed as an early event in embryonic cortical and motor neurons in a mouse model of ALS (Soo *et al.*, 2015), and in NSC34 cells expressing mutant SOD1, dysregulation of ER-Golgi trafficking preceded protein aggregation, ER stress, Golgi fragmentation and axon degeneration (Atkin *et al.*, 2014). Overexpression of Ras-related protein Rab 1A (Rab1), a master regulator of ER-Golgi transport, restored ER-Golgi trafficking and prevented induction of ER stress, formation of intracellular aggregations and apoptosis in *in vitro* model of ALS (Soo *et al.*, 2015). Several studies also indicate a role for defective ER-Golgi transport in SMA. SMN interacts with coatomer subunit alpha (α-COP), a member of coat protein complex I (COPI) vesicles that mediate ER-Golgi transport (Peter *et al.*, 2011; Ting *et al.*, 2012; Custer *et al.*, 2013; Li *et al.*, 2015), and knockdown of *α-COP* caused SMN accumulation in Golgi apparatus of neuron-like NSC34 cells (Ting *et al.*, 2012) and produced developmental defects in motor neuron-like NSC34 cells and primary cortical murine neurons (Li *et al.*, 2015). Overexpression of human *α-COP* reversed motor neuron defects in SMN-depleted NSC34 cells (Custer *et al.*, 2013; Li *et al.*, 2015) and in motor neurons from a zebrafish model of SMA (Li *et al.*, 2015). In a most recent study,

transgenic expression of *α-COP* increased survival and improved muscle pathology in a severe mouse model of SMA (Custer *et al.*, 2019).

Dysregulation of protein metabolism has been demonstrated on multiple levels in SMA and ALS, however, investigation of specific protein targets, in comparable models of ALS and SMA, is needed to elucidate precise molecular mechanisms of protein metabolism dysregulation. Identification of similarities and differences in specific disease pathways in ALS and SMA would aid the selection of protein targets for therapy design that could bring benefit to both patient populations. With this in mind, the expression of several protein targets, identified in this study, was investigated in SMA and ALS spinal cords, starting with the calreticulin.

5.3.4. Calreticulin is dysregulated in spinal cord from symptomatic ALS and SMA mice

Calreticulin is a multifunctional protein involved in a range of processes, including the regulation of Ca^{2+} homeostasis in the ER, chaperone activity in secretory pathways, folding of nascent proteins, regulation of immune system, and modulation of cell adhesion (Gelebart, Opas and Michalak, 2005). Calreticulin was previously identified from proteomic studies as having increased levels in iPSC-derived motor neurons from type I SMA patients (Fuller *et al.*, 2016) and in SMA mouse muscle (Mutsaers *et al.*, 2013), and this was verified biochemically in muscles from SMA mice and SMA patients (Mutsaers *et al.*, 2013). In contrast, a statistically significant decrease of calreticulin levels was observed in spinal cord extracts and in motor neurons of lumbar spinal cord sections from late symptomatic SMA mice. In proteomic studies of ALS, calreticulin was found to be increased in the ventral roots from the spinal cord of ALS $SOD1^{G93A}$ mice (Zhou *et al.*, 2010), blood mononuclear cells from ALS patients (Nardo *et al.*, 2011), and in TDP-43 knockdown SH-SY5Y cells (Stalekar *et al.*, 2015), and in agreement with

this, increased levels of calreticulin were also found in spinal cord extracts from late-symptomatic ALS SOD1^{G93A} mice. This is, however, in contrast with a biochemical study of lower motor neurons isolated from ALS SOD1^{G93A} mice that reported decreased expression of calreticulin (Bernard-Marissal *et al.*, 2012). Differences in calreticulin expression in different cell populations could have contributed to the overall calreticulin expression levels in spinal cord, masking changes that were previously reported to be specific to vulnerable lower motor neurons (Bernard-Marissal et *al.*, 2012). In addition, it has been shown that calreticulin levels increase under stress conditions prior to being secreted to the cell surface; a process that is associated with the functional role of calreticulin in apoptosis (Tarr *et al.*, 2010). It is thus possible that opposing directions of perturbed calreticulin expression reflect ongoing cycles of apoptosis in vulnerable motor neurons. The time-course of disease is another potential variable to consider, since Bernard-Marissal *et al.* (Bernard-Marissal *et al.*, 2012) studied ALS mice up to 110 days of age, compared to the later time-point of 140 days in the present study.

5.3.4.1. Activation of Fas death pathway was not observed in spinal cord from SMA and ALS mice

Activation of Fas/NO pathway was previously demonstrated *in vitro* in motor neurons carrying mutant SOD1^{G93A} and SOD1^{G85R} (Raoul *et al.*, 2006; Bernard-Marissal *et al.*, 2012), and in iPSC-derived motor neurons from type I SMA patients (Sareen *et al.*, 2012), and in SOD1^{G93A} motor neurons, activation of Fas pathway was responsible for reduction of calreticulin levels (Bernard-Marissal *et al.*, 2012). It appears that only one study to date investigated FasL expression *in vivo* in SMA mouse model, and identified no significant change in FasL expression in whole spinal cords from SMA mice (P8) compared to healthy controls (Tsai *et al.*, 2006). However, as shown before, changes in protein expression may be restricted to vulnerable

motor neurons (Bernard-Marissal *et al.*, 2012) and may not be easily detectable in whole spinal cord extracts. To investigate whether the same mechanism might be responsible for calreticulin downregulation in vulnerable motor neurons in SMA, the expression of FasL was investigated in lumbar spinal cord sections from SMA mouse and healthy control. Immunohistochemistry analysis of ventral horn motor neurons did not identify specific FasL staining in either SMA or control spinal cord sections. The cross-reaction between anti-FasL antibody and protein ladder, following western blot analysis of SMA and control spinal cord extracts, indicated technical problems with the antibody. After removing the protein ladder outside of the field of view, three bands were identified, none of which corresponded to monomeric FasL. Some of these bands may correspond to FasL dimer and trimer, as they were previously identified in COS cell line, after chemical crosslinking of FasL and under non-reducing conditions (Tanaka *et al.*, 1995). None of these conditions are applicable to experimental design in this study, and so it is likely that these are non-specific bands caused by antibody cross-reaction. However, without a positive control it is not possible to determine with certainty whether Fas pathway is activated in spinal cord from SMA or ALS mice.

5.3.5. Unchanged SOD1 expression in the spinal cord of symptomatic SMA mice

Transgenic SOD1 mice, carrying high copy number of mutant SOD1 gene, have been developed to investigate SOD1 disease pathways (Turner and Talbot, 2008), and can explain the increased expression of SOD1 identified in spinal cord extracts from late-symptomatic ALS mice. There are several lines of evidence that support the role for SMN in ALS disease pathways, including the reduction of SMN levels in spinal cords from $SOD1^{G93A}$ mice (Turner *et al.*, 2009), and the beneficial effect of SMN overexpression on neuromuscular pathology in $SOD1^{G86R}$ model of ALS (Kariya *et al.*, 2012). However, very few studies support the link

between SOD1 and SMA disease pathways. For example, one study investigated SOD1 mRNA levels in SMA patient iPSC-derived motor neurons and astrocytes, but found no significant change in SMA cells compared to controls (Patitucci and Ebert, 2016), and in a mouse model of SMA, overexpression of *SOD1* showed no benefit on survival of SMA mice (Turner *et al.*, 2009). In this study, no significant change in SOD1 protein expression was identified in spinal cords from SMA mice compared to healthy controls, although it is possible that changes in SOD1 expression in vulnerable cell populations would be masked in whole spinal cord extracts (Bernard-Marissal *et al.*, 2012). Indeed, in proteomic studies of SMA upregulation of SOD1 levels was identified in Schwann cells (Aghamaleky Sarvestany *et al.*, 2014) and hippocampus (Wishart *et al.*, 2010) from severe mouse models of SMA. Increased production of reactive oxygen species, identified in motor neuron cultures from SMA mice and human ESC-derived motor neurons (Wang, Zhang and Li, 2013; Miller *et al.*, 2016) supports this theory, as it is likely to increase the expression of proteins involved in oxidative stress response, including the SOD1. It would be of interest, therefore, to investigate the expression of SOD1 and other markers of oxidative stress in pathologically affected lumbar spinal cord sections, to determine the extent of oxidative stress in SMA motor neurons *in vivo*. This is important since oxidative stress indicates impaired mitochondrial health and function that can be detrimental for the survival of motor neurons (Miller *et al.*, 2016), and could be contributing to SMA pathology.

5.3.6. Unchanged levels of ALDOA and GAPDH in spinal cord extracts from symptomatic ALS and SMA mice

In this study, western blot analyses showed unchanged protein levels of ALDOA and GAPDH in whole spinal cord extracts from ALS and SMA mice. This is perhaps not surprising since none of the SMA proteomic studies, that identified decreased GAPDH expression, investigated

protein profile in spinal cord tissue (Fuller, Gillingwater and Wishart, 2016), and to date, GAPDH has not been investigated biochemically in spinal cord tissue from SMA mice. In addition, there are no published studies that investigated ALDOA protein levels in ALS or SMA tissues.

Upregulation of ALDOA and GAPDH levels was identified in a proteomic study that investigated protein changes in spinal cord from a Wobbler mouse model (Bastone *et al.*, 2009). Wobbler mice represent general model of neurodegeneration where motor neuron loss is restricted to cervical region of the spinal cord (Bastone *et al.*, 2009). The purpose of this study was to identify proteins involved in mechanisms of motor neuron degeneration in general, that would facilitate investigation of disease pathways in ALS models with heterogeneous genetic background (Bastone *et al.*, 2009). However, increased ALDOA and GAPDH levels, identified in cervical but not lumbar spinal cord from Wobbler mice, possibly reflect the primary pathology in this mouse model (Bastone *et al.*, 2009), and may not necessarily recapitulate changes that are specific to ALS or SMA disease pathways. For example, increased levels of GAPDH, identified in proteomic study in skeletal muscles from a Wobbler mouse model, and verified biochemically by quantitative western blotting (Staunton, Jockusch and Ohlendieck, 2011), contradict the results from $SOD1^{G93A}$ mouse model of ALS, where GAPDH levels were decreased in muscles from ALS mice compared to healthy controls (Desseille *et al.*, 2017).

Here, GAPDH levels were also decreased in the heart and liver tissue from a severe mouse model of SMA using western blotting, and in addition to the spinal cord, unchanged levels of GAPDH were demonstrated in the brain and muscle tissues from SMA mice, and in SMA

patient fibroblast cells (Figure 3.6). Proteomic studies of SMA identified downregulation of GAPDH levels in hippocampus (Wishart *et al.*, 2010) and Schwann cells (Aghamaleky Sarvestany *et al.*, 2014) from SMA mice, and in SMA patient plasma (Kobayashi *et al.*, 2013), and so it is possible that differential expression of GAPDH in vulnerable regions of the tissue examined (i.e. spinal cord and brain) would get masked in whole tissue extracts.

5.3.7. Impaired ALDOA and GAPDH activity are pathological features of symptomatic ALS mice

Decreased GAPDH activity was previously demonstrated in skeletal muscles from symptomatic ALS mice (Pierce *et al.*, 2008), and in line with this, reduction of ALDOA and GAPDH activity levels was identified in spinal cord extracts from late-symptomatic ALS mice in this study. In contrast, spinal cord extracts from late-symptomatic SMA mice showed no significant change in ALDOA and GAPDH activity when compared to age-matched controls. Oxidative stress can inform about the possible activity defects, since it was shown to hamper the activity of both GAPDH and ALDOA (Koeck *et al.*, 2004; Palamalai and Miyagi, 2010). Investigation of oxidative stress in *in vitro* and *in vivo* models of SMA, however, showed contradicting results (Wang, Zhang and Li, 2013; Miller *et al.*, 2016; Patitucci and Ebert, 2016), where motor neuron cultures from SMA mice and human ESC-derived motor neurons showed increased production of reactive oxygen species (Wang, Zhang and Li, 2013; Miller *et al.*, 2016). SMA patient iPSC-derived motor neurons and astrocytes, on the other hand, showed decreased levels of reactive oxygen species, and lumbar spinal cord sections from severe SMA mice showed unchanged levels of oxidative stress marker 8-hydroxydeoxyguanosine (Patitucci and Ebert, 2016). It would be difficult to speculate, therefore, whether unchanged GAPDH and ALDOA activity are a real finding in SMA spinal cords, or whether examination of vulnerable regions of the spinal cord could produce different results. In addition, increased ALDOA

activity levels in CSF from ALS patients (Diószeghy, Mechler and Csenkér, 1981) and in serum from type III SMA patients (Mastaglia and Walton, 1971), indicate that different mechanisms might be responsible for defects in enzyme activity in different ALS and SMA tissues.

5.3.7.1. Protein nitration was not detected in spinal cord extracts from symptomatic ALS mice

Increased nitrotyrosine levels were shown to impair activity of both ALDOA and GAPDH *in vitro* (Koeck et *al.*, 2004; Palamalai and Miyagi, 2010), but to date, nitration of ALDOA and GAPDH has not been investigated specifically in ALS models as a mechanism of dysregulated enzyme activity. Here, anti-nitrotyrosine antibody was used to pulldown nitrated proteins from spinal cords of control and ALS mice, however, subsequent western blot analysis did not identify specific nitrotyrosine bands in either control or ALS mice samples. In addition, western blot analysis of whole spinal cord extracts (20µL) from symptomatic ALS mice confirmed the results from the pulldown, indicating that protein nitration is not present in ALS mouse spinal cords. However, without a positive control (i.e. nitrated purified aldolase A (Koeck *et al.*, 2004)) this result cannot be interpreted, since technical problems with the antibody are also possible. Increased nitrotyrosine levels were previously identified in lumbar and thoracic spinal cord from sALS and fALS patients (Beal *et al.*, 1997), in the anterior horn neurons (Sasaki *et al.*, 2001) and in whole spinal cords and cerebral cortex from transgenic SOD1 mice (Bruijn *et al.*, 1997; Ferrante *et al.*, 1997; Casoni *et al.*, 2005). In addition, Casoni et *al.* identified several protein targets that showed nitration in spinal cord from pre-symptomatic ALS mice, GAPDH being one of them (Sasaki *et al.*, 2001). Several studies strongly implicate nitrative stress in ALS pathogenesis, and so further research is needed to determine the role for protein nitration in GAPDH and ALDOA activity. Elucidating the mechanism of ALDOA and GAPDH

activity perturbations *in vivo* would help to develop targeted therapies, aiming to restore metabolic defects and slow disease progression in ALS.

5.3.8. Neurofilament-L levels are not changed in spinal cord from ALS mice

As a subunit of neurofilament proteins, NF-L regulates different neuronal functions including signal conduction, synaptic vesicle trafficking and neurite growth (Didonna and Opal, 2019). Neurofilament light (NF-L) is well characterised diagnostic and prognostic marker in ALS, (Poesen and Van Damme, 2019), and neurofilament abnormalities have also been directly implicated in ALS disease pathogenesis (Williamson *et al.*, 1998; Wong, He and Strong, 2000). Decreased NF-L mRNA levels were previously identified in cervical motor neurons from sporadic ALS patients (Wong, He and Strong, 2000), and ALDOA was shown to control the stability of NF-L mRNA through its nuclease activity (Canete-Soler et al., 2005). It was of interest, therefore, to determine whether NF-L is dysregulated on the protein level in this study, as this would indicate changes in ALDOA nuclease activity. Western blot analysis did identify reduction of NF-L protein levels in spinal cord extracts from late-symptomatic ALS mice. This difference, however, was not statistically significant, likely because of the large variability in protein expression within the group. It would be of interest in the future to determine NF-L expression at both the mRNA and protein level in ALS mouse spinal cords, since perturbations in NF-L expression are likely to affect neuronal function on multiple levels. If the results showed statistically significant difference, further experiments would need to be conducted to demonstrate that ALDOA is driving these defects, including the comparison of ALDOA activity from ALS and control samples *in vitro*.

5.4. Conclusion and future work

5.4.1. ALS-specific disease pathways and therapies

The main purpose of this work was to determine whether analysis of big data, in combination with bioinformatics analysis can help unravel complex disease mechanisms and facilitate selection of drug targets. Multi-study comparison identified 42 proteins that showed consistent direction of differential expression in ALS tissues and cells across at least two proteomic studies, and bioinformatics analysis implicated them in functions including protein metabolism, oxidative stress response and energy production. Within these functions, different pathways have already been implicated in ALS disease pathogenesis, including for example, UPR pathway (Nishitoh *et al.*, 2008) and glycolysis (Palamiuc *et al.*, 2015), confirming the validity of this approach.

Identification of several proteins that have not been previously implicated in ALS, offers the opportunity to expand knowledge of existing disease pathways or to provide explanation for novel mechanisms that drive pathology in ALS. The glycolytic enzymes GAPDH (Basso *et al.*, 2009; Bastone *et al.*, 2009; Staunton, Jockusch and Ohlendieck, 2011) and ALDOA (Fukada *et al.*, 2004; Bastone *et al.*, 2009; Nardo *et al.*, 2011; Staunton, Jockusch and Ohlendieck, 2011; Basso *et al.*, 2013) are a good example, as their expression levels were increased across at least three proteomic studies of ALS, however, in depth studies of ALDOA and GAPDH expression and function in ALS are missing. Glycolysis is the main source of ATP in high energy demanding tissues like muscles and neuronal tissues (Jang *et al.*, 2016). Alterations in the expression or function of glycolytic enzymes, such as ALDOA and GAPDH, are likely to induce defects in energy production that is crucial for the maintenance of neuromuscular health (Kanungo *et al.*, 2018). Unchanged ALDOA and GAPDH protein levels, identified biochemically

in spinal cord from ALS mice, were not in accordance with proteomic studies of ALS, however, differences between experimental models used in each study could explain these discrepancies (revised in section 5.3.6). Importantly the activity of both proteins was altered at a symptomatic stage of the disease in ALS mouse spinal cords, potentially implicating them in disease mechanisms in ALS.

Determining the mechanism of perturbed ALDOA and GAPDH activity is crucial for the development of appropriate therapies. Protein nitration is one possible mechanism (Koeck et *al.*, 2004; Palamalai and Miyagi, 2010), and although it was not demonstrated in this study, protein nitration has been implicated in ALS pathogenesis (Beal *et al.*, 1997; Ferrante *et al.*, 1997; Sasaki *et al.*, 2001; Casoni *et al.*, 2005). Further studies to examine protein nitration in spinal cord tissue, and its implication in GAPDH and ALDOA activity defects, are needed. When doing so it would be important to expand the research by including other pathologically relevant tissues like muscles, since increased nitrotyrosine levels (Wong and Martin, 2010) and decreased GAPDH activity (Pierce *et al.*, 2008) have previously been demonstrated in skeletal muscles from ALS mice.

Antioxidant compounds or inhibitors of inducible nitric oxide synthase (iNOS) represent potential therapeutic strategies for reducing protein nitration (Sasaki *et al.*, 2001). iNOS is one of the enzymes that produces high quantities of NO, and has been implicated in protein nitration in ALS (Sasaki *et al.*, 2001). Aminoguanidine, selective iNOS inhibitor, has shown success in reducing the levels of nitrotyrosine in A549 cell cultures stimulated with inflammatory cytokines (Aulak *et al.*, 2001), and in a rat model of radiculopathy (Lee *et al.*, 2013), and attenuated muscle weakness in radiculopathy rats (Lee *et al.*, 2013). Edaravone,

antioxidant compound, has shown therapeutic benefit in ALS patients, where reduced nitrotyrosine levels were detected in CSF of treated patients (Sawada, 2017). However, as demonstrated previously in clinical trials with edaravone (Nowicka *et al.*, 2019), targeting oxidative stress and protein nitration is likely to have beneficial effect at earlier stages of the disease, and can only slow disease progression in ALS patients.

A combinatorial approach, with therapies that would, for example, aim to restore intrinsic muscle defects or decrease protein aggregation, could bring greater benefit to ALS patients. Indeed, several compounds have been effective in decreasing protein aggregates in animal and *in vitro* models of ALS (Nowicka *et al.*, 2019). These include migration inhibitory factor and [4,5-bis{(N-carboxy methyl imidazolium)methyl}acridine] dibromide, that successfully decreased SOD1 and TDP-43 aggregates (Nowicka *et al.*, 2019), and could potentially be used in combination with antioxidant compounds to alleviate disease symptoms in a wider population of ALS patients.

5.4.2. SMA and ALS commonalities

The molecular overlap between ALS and SMA consists of fifteen proteins, most of which were implicated in the regulation of protein metabolism and mitochondria-associated functions. Specific pathways, like activation of the unfolded protein repose (UPR) (Atkin *et al.*, 2008; Ng *et al.*, 2015) and defects in glycolysis (Palamiuc *et al.*, 2015; Boyd *et al.*, 2017), have already been implicated in the pathogenesis of both diseases. The fifteen proteins identified here represent the opportunity to study the same pathogenic mechanism in comparable models of ALS and SMA. However, as demonstrated in this study, different factors (technical and biological) can make this very challenging.

Of the five proteins investigated in this study using western blotting, only calreticulin showed changed expression in spinal cords from ALS and SMA mice. Detection of HSP90B1 was unreliable, likely because of the poor antibody specificity. SOD1 showed increased expression only in the spinal cord from ALS mice, while expression of both GAPDH and ALDOA was unchanged in ALS and SMA tissues. There are several possible explanations for discrepancies between ALS and SMA studies:

a) First, protein levels in different cell populations or unaffected regions of the spinal cord could have masked protein changes that are restricted to vulnerable motor neurons (Bernard-Marissal *et al.*, 2012), thus hampering detection of differential expression in whole spinal cord extracts.

b) The experimental model/sample type used in proteomic studies in comparison to biochemical study could also help to explain some differences. For example, none of the SMA proteomic studies used spinal cord tissue (Fuller, Gillingwater and Wishart, 2016), suggesting that changes in protein expression might be tissue specific. On the other hand, proteomic studies of ALS studied protein profiles in spinal cord from Wobbler mouse model (Bastone *et al.*, 2009), making it challenging to correlate this results to the whole spinal cord extracts from $SOD1^{G93A}$ mice used in this study.

c) Some protein changes might be induced or exacerbated with aging (Krisko and Radman, 2019), and so eight days old SMA mice and 20-week old ALS mice, although pathologically comparable, might not necessarily have the same molecular response at given time-points.

When taken together, biochemical studies of spinal cord tissue identified very few similarities between ALS and SMA, and one of these was calreticulin. Calreticulin showed increased expression in the spinal cord from ALS mice, but decreased expression in the spinal cord from SMA mice. Designing therapeutic strategies that would simultaneously target calreticulin expression in ALS and SMA would therefore be very challenging, and individual strategies would have to be applied in each disease.

Genetic approaches for restoring calreticulin levels in spinal cord from ALS and SMA mice could be used to assess the effect on NMJ pathology, muscle strength and survival in transgenic mouse models. This could be achieved by a knockdown of calreticulin levels in ALS, and by calreticulin overexpression in SMA. There is a possibility, however, that decreasing the levels of calreticulin in spinal cord from ALS mice would not be beneficial, since overexpression of calreticulin in murine $SOD1^{G93A}$ motor neurons showed a positive effect on cell survival (Bernard-Marissal *et al.*, 2012). In addition, examination of calreticulin expression in other tissues from SMA and ALS mice would help to determine whether systemic or neuronal-specific restoration of calreticulin levels is necessary. This is important since both increased and decreased levels of calreticulin were shown to impair proper functioning of the heart (Gelebart, Opas and Michalak, 2005).

The second approach to therapy design involves identification of upstream regulators of calreticulin expression, and several of these have been identified using IPA software (Stock, unpublished Master's dissertation, 2017). Some of these are already in clinical use, including Formoterol, beta-2 receptor agonist used in asthma and chronic obstructive pulmonary

disease[12], and Azathioprine, anti-inflammatory drug used in rheumatoid arthritis and Crohn's disease[13] (Stock, unpublished Master's dissertation, 2017). Because they already have established pharmacokinetic and pharmacodynamic profiles, these compounds are especially interesting for drug repurposing (Durães, Pinto and Sousa, 2018). Formoterol, for example, could be an interesting choice for SMA, since it was shown to increase calreticulin expression in human bronchial smooth muscle cells (Miglino *et al.*, 2012). In addition, treatment with Formoterol significantly improved cognitive functions and restored synaptic density in hippocampus of Ts65Dn mouse model of Down syndrome (Phillips *et al.*, 2016), showing its beneficial effect on neuronal tissue.

Although the same biological functions are impaired in ALS and SMA, biochemical studies of spinal cord from SMA and ALS mice produced very little evidence that these changes converge on the same molecular mechanism. Comparison of proteomic studies has shown useful for identifying core molecular changes in individual diseases, however, a clear molecular link between SMA and ALS disease pathways remains to be established. Standardising methods for proteomics dataset deposition and presentation would perhaps give better results in the future analysis (Martens and Vizcaíno, 2017). Not all proteomic studies publicly present complete lists of differentially expressed proteins, while even smaller number of studies present raw (unfiltered) data. This can undoubtedly lead to the loss of important information that can compromise the integrity of data reanalysis. Comparison of raw datasets would thus allow for stringent data processing, increasing the sensitivity and reliability of detected information, and allow for better correlation between proteomics and biochemical studies.

[12] https://bnf.nice.org.uk/drug/formoterol-fumarate.html
[13] https://bnf.nice.org.uk/drug/azathioprine.html

Chapter 6: General discussion and conclusion

It is becoming evident that SMN-targeted therapies are not sufficient to completely ameliorate pathology in SMA patients (Finkel *et al.*, 2017; Mendell *et al.*, 2017; Mercuri *et al.*, 2018; Sumner and Crawford, 2018), and other non-SMN targeted approaches, like neuroprotection and muscle enhancers (Shorrock, Gillingwater and Groen, 2018), are already under development to try to tackle this problem. However, most non-SMN strategies are still focused on preserving motor neuron and/or muscle health (chapter 1, section 1.5.2), and so peripheral pathologies remain largely overlooked in SMA therapy design. Understanding the molecular mechanisms that drive disease pathology in individual tissues is crucial for the development of therapies that can target both neuromuscular and systemic pathology. Here, core protein changes in SMA, identified by comparison of published proteomic studies of SMA (Fuller, Gillingwater and Wishart, 2016), were investigated biochemically across tissues from severe Taiwanese mouse model of SMA and in SMA patient fibroblasts, and four of these proteins, lamin A/C, UBA1, GAPDH and ANXA2, showed widespread dysregulation in SMA tissues and cells. These proteins might have important role in SMA disease pathways across a range of tissues, and are therefore worthy of further experimental attention.

Increased levels of lamin A/C, for example, might offer an explanation for previously reported cardiac defects in SMA patients and mouse models of SMA, including thinning of the ventricle walls and interventricular septum (Shababi *et al.*, 2010; Maxwell *et al.*, 2018), dilation of ventricles (Heier *et al.*, 2010; Bogdanik *et al.*, 2015; Maxwell *et al.*, 2018), and decreased ejection fraction and blood pooling in ventricles (Yasuma, Kuru and Konagaya, 2004; Roos *et al.*, 2009; Heier *et al.*, 2010; Shababi *et al.*, 2012; Bogdanik *et al.*, 2015; Iwahara *et al.*, 2015; Maxwell *et al.*, 2018). Further work is clearly warranted to investigate lamin A/C expression throughout natural history of disease progression in SMA heart, and to determine the

molecular mechanism of lamin A/C dysregulation in SMA tissues/cells. Knowledge of the molecular mechanism of lamin A/C dysregulation would aid selection of appropriate therapeutic approaches that can restore lamin A/C expression to the levels observed in control tissues/cells. These could then be tested *in vivo* to determine whether systemic restoration of lamin A/C levels can rescue peripheral pathology in SMA, with the specific interest in the heart.

It is worth noting too that most of these proteins, including lamin A/C, GAPDH and ANXA2, showed both increased and decreased expression in SMA, depending on the tissue/cell type examined. These findings highlighted the differential response of different SMA tissues/cells to low levels of SMN, however, they also opened a range of new questions that need to be addressed. For example, does differential protein expression have pathological significance in all cells and tissues examined, and if so, how can these proteins be therapeutically targeted? Systemic targeting could result in unwanted protein expression changes, meaning that tissue-specific approach in therapy design would have to be applied to restore protein levels to the ones observed in healthy tissues. Selection of drugs that have the potential to target several of these proteins at the same time would therefore be even more challenging. Indeed, drugs that have the potential to change the expression of target proteins were already identified in this thesis using two different approaches, network pharmacology approach and PubMed search. However, when tested in fibroblast cells, the drugs showed no effect on expression of target proteins or produced unwanted effects. In addition, technical problems, including large variability in protein expression within the treatment group, have also been encountered during drug studies which made interpretation of results extremely difficult. The mixed pattern of protein expression across different tissues represents yet another challenge for the design of therapies that can effectively target several disease pathways at the same time.

A multi-study comparison approach was also used here to identify conserved protein changes in ALS cells and tissues, with the aim to compare these to the list of conserved protein changes from a multi-study comparison of published proteomic studies of SMA (Fuller, Gillingwater and Wishart, 2016). This was done to identify pathogenic commonalities between SMA and ALS that could potentially be used in a therapy design for both diseases. Fifteen molecules were identified as differentially expressed in proteomic studies of SMA and ALS, however, when investigated biochemically proteins showed little overlap. Calreticulin was the only protein that showed differential expression in the spinal cord from both SMA and ALS mice, with the opposite direction of expression change identified in each model. This means that individual strategies would likely have to be applied in each disease to normalise calreticulin levels, which would prevent development of drug repurposing strategies in SMA and ALS. However, the lack of overlap between SMA and ALS could also be a result of different biological and technical variations, and so further research in needed to establish a clear molecular link between SMA and ALS disease pathways.

The multi-study comparison did, however, successfully identify conserved protein changes in ALS tissues and cells, some of which were investigated biochemically in the spinal cord from $SOD1^{G93A}$ mouse model of ALS. For example, two essential enzymes of glycolysis, GAPDH and ALDOA, showed decreased activity in the spinal cord from symptomatic ALS mice. Glycolysis is the main source of ATP in high energy demanding tissues like muscles and neuronal tissues (Jang *et al.*, 2016), and so altered function of ALDOA and GAPDH is likely to have pathological implications for neuromuscular tissues in ALS. Therapeutic targeting of glycolytic pathways could be used as a strategy to preserve motor neuron and muscle health in ALS, although,

further studies are also warranted to determine the exact mechanism of ALDOA and GAPDH dysregulation in ALS tissues.

In conclusion, the work presented here demonstrated that published proteomic studies contain valuable information that are often deposited in supplementary files and disregarded in the future work. These proteomic datasets were exploited here to investigate conserved protein changes across a range of SMA and ALS tissues and cells. Information, extracted using this approach, can be used to expand the understanding of known disease mechanisms or inform about the new potential disease pathways, which could then be used to develop new therapies for all patients. Development of therapies that can tackle systemic pathology in SMA remains one of the main goals of research and clinical community, and data presented here might be useful in achieving this goal.

References

Abe, K. *et al.* (2017) 'Safety and efficacy of edaravone in well defined patients with amyotrophic lateral sclerosis: a randomised, double-blind, placebo-controlled trial.', *The Lancet Neurology*. Elsevier, 16(7), pp. 505–512. doi: 10.1016/S1474-4422(17)30115-1.

Ackermann, B. *et al.* (2013) 'Plastin 3 ameliorates spinal muscular atrophy via delayed axon pruning and improves neuromuscular junction functionality', *Human Molecular Genetics*, 22(7), pp. 1328–1347. doi: 10.1093/hmg/dds540.

Aebischer, J. *et al.* (2011) 'IFNγ triggers a LIGHT-dependent selective death of motoneurons contributing to the non-cell-autonomous effects of mutant SOD1', *Cell Death and Differentiation*. Nature Publishing Group, 18(5), pp. 754–768. doi: 10.1038/cdd.2010.143.

Afilalo, J. *et al.* (2007) 'Age-related changes in lamin A/C expression in cardiomyocytes', *Am J Physiol Heart Circ Physiol*, 293(3), pp. H1451–H1456. doi: 10.1152/ajpheart.01194.2006.

Aghamaleky Sarvestany, A. *et al.* (2014) 'Label-Free Quantitative Proteomic Profiling Identifies Disruption of Ubiquitin Homeostasis As a Key Driver of Schwann Cell Defects in Spinal Muscular Atrophy', *Journal of Proteome Research*, 13, pp. 4546–4557.

Akten, B. *et al.* (2011) 'Interaction of survival of motor neuron (SMN) and HuD proteins with mRNA cpg15 rescues motor neuron axonal deficits.', *Proceedings of the National Academy of Sciences of the United States of America*, 108(25), pp. 10337–42. doi: 10.1073/pnas.1104928108.

Al-Zaidy, S. A. and Mendell, J. R. (2019) 'From Clinical Trials to Clinical Practice: Practical Considerations for Gene Replacement Therapy in SMA Type 1', *Pediatric Neurology*, 100, pp. 3–11. doi: 10.1016/j.pediatrneurol.2019.06.007.

Allen, S. *et al.* (2003) 'Analysis of the cytosolic proteome in a cell culture model of familial amyotrophic lateral sclerosis reveals alterations to the proteasome, antioxidant defenses, and

nitric oxide synthetic pathways.', *Journal of Biological Chemistry*, 278(8), pp. 6371–6383. doi: 10.1074/jbc.M209915200.

Almeida, A. F. *et al.* (2018) 'Bioavailability of Quercetin in Humans with a Focus on Interindividual Variation', *Comprehensive Reviews in Food Science and Food Safety*, 17(3), pp. 714–731. doi: 10.1111/1541-4337.12342.

Ame van der Beek, N. *et al.* (2019) 'A new case of SMA phenotype without epilepsy due to biallelic variants in ASAH1', *European Journal of Human Genetics*. Nature Publishing Group, pp. 337–339. doi: 10.1038/s41431-018-0250-z.

Anderson, K. N. *et al.* (2004) 'Expression profiling in spinal muscular atrophy reveals an RNA binding protein deficit', *Neuromuscular Disorders*, 14, pp. 711–722. doi: 10.1016/j.nmd.2004.08.009.

Anderson, N. L. and Anderson, N. G. (2002) 'The human plasma proteome: history, character, and diagnostic prospects', *Mol Cell Proteomics*, 1(11), pp. 845–867. doi: 10.1074/mcp.R200007-MCP200.

Andrae, J., Gallini, R. and Betsholtz, C. (2008) 'Role of platelet-derived growth factors in physiology and medicine', *Genes and Development*. Cold Spring Harbor Laboratory Press, pp. 1276–1312. doi: 10.1101/gad.1653708.

Andreassi, C. *et al.* (2004) 'Phenylbutyrate increases SMN expression in vitro: relevance for treatment of spinal muscular atrophy', *European Journal of Human Genetics*, 12, pp. 59–65. doi: 10.1038/sj.ejhg.5201102.

Andrus, P. K. *et al.* (1998) 'Protein Oxidative Damage in a Transgenic Mouse Model of Familial Amyotrophic Lateral Sclerosis', *Journal of Neurochemistry*, 71(5), pp. 2041–2048. doi: 10.1046/j.1471-4159.1998.71052041.x.

Antharavally, B. S. *et al.* (2009) 'Quantitation of proteins using a dye-metal-based colorimetric

protein assay', *Analytical Biochemistry*, 385, pp. 342–345. doi: 10.1016/j.ab.2008.11.024.

Antonellis, A. *et al.* (2003) 'Glycyl tRNA synthetase mutations in Charcot-Marie-Tooth disease type 2D and distal spinal muscular atrophy type V', *American journal of human genetics*. Elsevier, 72(5), pp. 1293–1299. doi: 10.1086/375039.

Atkin, J. D. *et al.* (2006) 'Induction of the unfolded protein response in familial amyotrophic lateral sclerosis and association of protein-disulfide isomerase with superoxide dismutase 1', *Journal of Biological Chemistry*, 281(40), pp. 30152–30165. doi: 10.1074/jbc.M603393200.

Atkin, J. D. *et al.* (2008) 'Endoplasmic reticulum stress and induction of the unfolded protein response in human sporadic amyotrophic lateral sclerosis', *Neurobiology of Disease*, 30(3), pp. 400–407. doi: 10.1016/j.nbd.2008.02.009.

Atkin, J. D. *et al.* (2014) 'Mutant SOD1 inhibits ER-Golgi transport in amyotrophic lateral sclerosis', *Journal of Neurochemistry*, 129(1), pp. 190–204. doi: 10.1111/jnc.12493.

Atsuta, N. *et al.* (2006) 'Natural history of spinal and bulbar muscular atrophy (SBMA): a study of 223 Japanese patients', *Brain*, 129, pp. 1446–1455. doi: 10.1093/brain/awl096.

Aulak, K. S. *et al.* (2001) 'Proteomic method identifies proteins nitrated in vivo during inflammatory challenge', *PNAS*, 98(21), pp. 12056–12061. doi: 10.1073/pnas.221269198.

Avila, A. M. *et al.* (2007) 'Trichostatin A increases SMN expression and survival in a mouse model of spinal muscular atrophy', *Journal of Clinical Investigation*, 117(3), pp. 659–671. doi: 10.1172/JCI29562.derived.

Aydin, S. (2015) 'A short history, principles, and types of ELISA, and our laboratory experience with peptide/protein analyses using ELISA', *Peptides*. Elsevier Inc., 72, pp. 4–15. doi: 10.1016/j.peptides.2015.04.012.

Azuaje, F. (2013) 'Drug interaction networks: An introduction to translational and clinical applications', *Cardiovascular Research*, 97(4), pp. 631–641. doi: 10.1093/cvr/cvs289.

Baccon, J. *et al.* (2002) 'Identification and Characterization of Gemin7, a Novel Component of the Survival of Motor Neuron Complex', *THE JOURNAL OF BIOLOGICAL CHEMISTRY*, 277(35), pp. 31957–31962. doi: 10.1074/jbc.M203478200.

Bach, J. R. (2007) 'Medical Considerations of Long-Term Survival of Werdnig–Hoffmann Disease', *American Journal of Physical Medicine & Rehabilitation*, 86(5), pp. 349–355. doi: 10.1097/PHM.0b013e31804b1d66.

Banerjee, R. *et al.* (2008) 'Adaptive immune neuroprotection in G93A-SOD1 amyotrophic lateral sclerosis mice', *PLoS ONE*, 3(7), p. e2740. doi: 10.1371/journal.pone.0002740.

Bansagi, B. *et al.* (2015) 'LETTER TO THE EDITOR The p.Ser107Leu in BICD2 is a mutation "hot spot" causing distal spinal muscular atrophy', *Brain*, 138, p. e391. doi: 10.1093/brain/awv159.

Baranello, G. *et al.* (2019) 'Evolution of bone mineral density, bone metabolism and fragility fractures in Spinal Muscular Atrophy (SMA) types 2 and 3', *Neuromuscular Disorders*. Elsevier B.V., 29(7), pp. 525–532. doi: 10.1016/j.nmd.2019.06.001.

Barschke, P. *et al.* (2017) 'Proteomic studies in the discovery of cerebrospinal fluid biomarkers for amyotrophic lateral sclerosis', *Expert Review of Proteomics*, 14(9), pp. 769–777. doi: 10.1080/14789450.2017.1365602.

Bass, J. J. *et al.* (2017) 'An overview of technical considerations for Western blotting applications to physiological research', *Scandinavian Journal of Medicine and Science in Sports*, 27(1), pp. 4–25. doi: 10.1111/sms.12702.

Basso, M. *et al.* (2009) 'Characterization of detergent-insoluble proteins in ALS indicates a causal link between nitrative stress and aggregation in pathogenesis', *PLoS ONE*, 4(12), p. e8130. doi: 10.1371/journal.pone.0008130.

Basso, M. *et al.* (2013) 'Mutant Copper-Zinc superoxide dismutase (SOD1) induces protein secretion pathway alterations and exosome release in astrocytes: Implications for disease

spreading and motor neuron pathology in amyotrophic lateral sclerosis', *JOURNAL OF BIOLOGICAL CHEMISTRY*. in Press, 288(22), pp. 15699 –15711. doi: 10.1074/jbc.M112.425066.

Bastone, A. *et al.* (2009) 'Proteomic profiling of cervical and lumbar spinal cord reveals potential protective mechanisms in the wobbler mouse, a model of motor neuron degeneration', *J Proteome Res.*, 8(11), pp. 5229–5240. doi: 10.1021/pr900569d.

Battaglia, G. *et al.* (1997) 'Expression of the SMN gene, the spinal muscular atrophy determining gene, in the mammalian central nervous system', *Human Molecular Genetics*, 6(11), pp. 1961–1971. doi: 10.1093/hmg/6.11.1961.

Battle, D. J. *et al.* (2007) 'SMN-independent Subunits of the SMN Complex: IDENTIFICATION OF A SMALL NUCLEAR RIBONUCLEOPROTEIN ASSEMBLY INTERMEDIATE', *TE JOURNAL OF BIOLOGICAL CHEMISTRY*, 282(38), pp. 27953–27959. doi: 10.1074/jbc.M702317200.

Bäumer, D. *et al.* (2009) 'Alternative splicing events are a late feature of pathology in a mouse model of spinal muscular atrophy', *PLoS Genetics*, 5(12), p. e1000773. doi: 10.1371/journal.pgen.1000773.

Beal, M. F. *et al.* (1997) 'Increased 3-nitrotyrosine in both sporadic and familial amyotrophic lateral sclerosis', *Annals of Neurology*. John Wiley & Sons, Ltd, 42(4), pp. 644–654. doi: 10.1002/ana.410420416.

Beecroft, S. J. *et al.* (2017) 'Expanding the phenotypic spectrum associated with mutations of DYNC1H1', *Neuromuscular Disorders*. Elsevier B.V., 27(7), pp. 607–615. doi: 10.1016/j.nmd.2017.04.011.

De Benedetti, S. *et al.* (2017) 'Serum Proteome in a Sporadic Amyotrophic Lateral Sclerosis Geographical Cluster', *Proteomics - Clinical Applications*, 11(11–12). doi: 10.1002/prca.201700043.

Bergemalm, D. *et al.* (2009) 'Changes in the spinal cord proteome of an amyotrophic lateral

sclerosis murine model determined by differential in-gel electrophoresis', *Molecular & Cellular Proteomics*, 8(6), pp. 1306–1317. doi: 10.1074/mcp.M900046-MCP200.

Bermeo, S. *et al.* (2015) 'Lamin A/C Acts as an Essential Factor in Mesenchymal Stem Cell Differentiation Through the Regulation of the Dynamics of the Wnt/β-Catenin Pathway', *Journal of Cellular Biochemistry*, 116(10), pp. 2344–2353. doi: 10.1002/jcb.25185.

Bernabò, P. *et al.* (2017) 'In Vivo Translatome Profiling in Spinal Muscular Atrophy Reveals a Role for SMN Protein in Ribosome Biology', *Cell Reports*, 21, pp. 953–965. doi: 10.1016/j.celrep.2017.10.010.

Bernard-Marissal, N. *et al.* (2012) 'Reduced calreticulin levels link endoplasmic reticulum stress and Fas-triggered cell death in motoneurons vulnerable to ALS', *The Journal of Neuroscience*, 32(14), pp. 4901– 4912. doi: 10.1523/JNEUROSCI.5431-11.2012.

Bertini, E. *et al.* (2017) 'Safety and efficacy of olesoxime in patients with type 2 or non-ambulatory type 3 spinal muscular atrophy: a randomised, double-blind, placebo-controlled phase 2 trial', *The Lancet Neurology*, 16(7), pp. 513–522. doi: 10.1016/S1474-4422(17)30085-6.

Bertrandy, S. *et al.* (1999) 'The RNA-binding properties of SMN: deletion analysis of the zebrafish orthologue defines domains conserved in evolution.', *Human molecular genetics*, 8(5), pp. 775–782. doi: ddc102 [pii].

Boczonadi, V. *et al.* (2014) 'EXOSC8 mutations alter mRNA metabolism and cause hypomyelination with spinal muscular atrophy and cerebellar hypoplasia', *NATURE COMMUNICATIONS*, 5, p. 4287. doi: 10.1038/ncomms5287.

Bogdanik, L. P. *et al.* (2015) 'Systemic, postsymptomatic antisense oligonucleotide rescues motor unit maturation delay in a new mouse model for type II/III spinal muscular atrophy', *PNAS*, 112(43), pp. E5863–E5872. doi: 10.1073/pnas.1509758112.

Bonne, G. *et al.* (1999) 'Mutations in the gene encoding lamin A/C cause autosomal dominant Emery-Dreifuss muscular dystrophy', *Nature Genetics*, 21(3), pp. 285–288. doi: 10.1038/6799.

Boon, K.-L. *et al.* (2009) 'Zebrafish survival motor neuron mutants exhibit presynaptic neuromuscular junction defects', *Human Molecular Genetics*, 18(19), pp. 3615–3625. doi: 10.1093/hmg/ddp310.

Borbély, A. *et al.* (2005) 'Cardiomyocyte Stiffness in Diastolic Heart Failure', *Circulation*, 111(6), pp. 774–781. doi: 10.1161/01.CIR.0000155257.33485.6D.

Bordet, T. *et al.* (2010) 'Olesoxime (TRO19622): A novel mitochondrial-targeted neuroprotective compound', *Pharmaceuticals*, 3(2), pp. 345–368. doi: 10.3390/ph3020345.

Bos, E. S. *et al.* (1981) '3,3',5,5' -Tetramethylbenzidine As An Ames Test Negative Chromogen For Horse-Radish Peroxidase In Enzyme-Immunoassay', *Journal of Immunoassay*, 2(3–4), pp. 187–204. doi: 10.1080/15321818108056977.

Bose, J. K. *et al.* (2008) 'TDP-43 Overexpression Enhances Exon 7 Inclusion during the Survival of Motor Neuron Pre-mRNA Splicing', *THE JOURNAL OF BIOLOGICAL CHEMISTRY*. JBC Papers in Press, 283(43), pp. 28852–28859. doi: 10.1074/jbc.M805376200.

Bowerman, M. *et al.* (2009) 'SMN, profilin IIa and plastin 3: A link between the deregulation of actin dynamics and SMA pathogenesis', *Molecular and Cellular Neuroscience*. Elsevier Inc., 42(1), pp. 66–74. doi: 10.1016/j.mcn.2009.05.009.

Bowerman, M. *et al.* (2010) 'Rho-kinase inactivation prolongs survival of an intermediate SMA mouse model', *Human Molecular Genetics*, 19(8), pp. 1468–1478. doi: 10.1093/hmg/ddq021.

Bowerman, M. *et al.* (2012) 'Glucose metabolism and pancreatic defects in spinal muscular atrophy', *Annals of Neurology*, 72(2), pp. 256–268. doi: 10.1002/ana.23582.

Bowerman, M. *et al.* (2015) 'Tweak regulates astrogliosis, microgliosis and skeletal muscle atrophy in a mouse model of amyotrophic lateral sclerosis', *Human Molecular Genetics*,

24(12), pp. 3440–3456. doi: 10.1093/hmg/ddv094.

Bowerman, M. *et al.* (2018) 'Pathogenic commonalities between spinal muscular atrophy and amyotrophic lateral sclerosis: Converging roads to therapeutic development', *European Journal of Medical Genetics*, 61(11), pp. 685–698. doi: 10.1016/j.ejmg.2017.12.001.

Bowerman, M. (2019) 'Funding for spinal muscular atrophy research must continue', *Future Neurol*, 14(2). doi: 10.2217/fnl-2019-0001.

Bowerman, M., Shafey, D. and Kothary, R. (2007) 'Smn depletion alters profilin II expression and leads to upregulation of the RhoA/ROCK pathway and defects in neuronal integrity', *Journal of Molecular Neuroscience*, 32(2), pp. 120–131. doi: 10.1007/s12031-007-0024-5.

Boyd, P. J. *et al.* (2017) 'Bioenergetic status modulates motor neuron vulnerability and pathogenesis in a zebrafish model of spinal muscular atrophy', *PLoS Genet*, 13(4), p. e1006744. doi: 10.1371/journal.pgen.1006744.

Boyer, J. G. *et al.* (2014) 'Myogenic program dysregulation is contributory to disease pathogenesis in spinal muscular atrophy', *Human Molecular Genetics*, 23(16), pp. 4249–4259. doi: 10.1093/hmg/ddu142.

Bradford, M. M. (1976) 'A rapid and sensitive method for the quantitation of microgram quantities of protein utilizing the principle of protein-dye binding', *Analytical Biochemistry*, 72(1–2), pp. 248–254. doi: 10.1016/0003-2697(76)90527-3.

Brahe, C. *et al.* (2005) 'Phenylbutyrate increases SMN gene expression in spinal muscular atrophy patients.', *European Journal of Human Genetics*, 13(2), pp. 256–259. doi: 10.1038/sj.ejhg.5201320.

Brancia, C. *et al.* (2016) 'VGF Protein and Its C-Terminal Derived Peptides in Amyotrophic Lateral Sclerosis: Human and Animal Model Studies', *PLoS ONE*, 11(10), p. e0164689. doi: 10.1371/journal.pone.0164689.

Brettschneider, J. *et al.* (2008) 'Proteome analysis of cerebrospinal fluid in amyotrophic lateral sclerosis (ALS)', *Neurochem Res*, 33, pp. 2358–2363. doi: 10.1007/s11064-008-9742-5.

Brichta, L. *et al.* (2003) 'Valproic acid increases the SMN2 protein level: a well-known drug as a potential therapy for spinal muscular atrophy', *Human Molecular Genetics*, 12(19), pp. 2481–2489. doi: 10.1093/hmg/ddg256.

Briese, M. *et al.* (2006) 'SMN, the Product of the Spinal Muscular Atrophy-Determining Gene, Is Expressed Widely but Selectively in the Developing Human Forebrain', *The Journal of comparative neurology*, 497(2), pp. 808–816. Available at: http://onlinelibrary.wiley.com/doi/10.1002/cne.21010/pdf.

Briese, M. *et al.* (2009) 'Deletion of smn-1, the Caenorhabditis elegans ortholog of the spinal muscular atrophy gene, results in locomotor dysfunction and reduced lifespan', *Human Molecular Genetics*, 18(1), pp. 97–104. doi: 10.1093/hmg/ddn320.

Bruijn, L. I. *et al.* (1997) 'Elevated free nitrotyrosine levels, but not protein-bound nitrotyrosine or hydroxyl radicals, throughout amyotrophic lateral sclerosis (ALS)-like disease implicate tyrosine nitration as an aberrant in vivo property of one familial ALS-linked superoxide di', *Proceedings of the National Academy of Sciences of the United States of America*, 94(14), pp. 7606–7611. doi: 10.1073/pnas.94.14.7606.

Bürglen, L. *et al.* (1996) 'Structure and organization of the human survival motor neurone (SMN) gene', *Genomics*, 32(3), pp. 479–482. doi: 10.1006/geno.1996.0147.

Buxboim, A. *et al.* (2014) 'Matrix elasticity regulates lamin-A,C phosphorylation and turnover with feedback to actomyosin', *Curr Biol*, 24(16), pp. 1909–1917. doi: 10.1016/j.cub.2014.07.001.

Canete-Soler, R. *et al.* (2005) 'Aldolases A and C Are Ribonucleolytic Components of a Neuronal Complex That Regulates the Stability of the Light-Neurofilament mRNA', *Journal of*

Neuroscience, 25(17), pp. 4353–4364. doi: 10.1523/jneurosci.0885-05.2005.

Capo-chichi, C. D. *et al.* (2011) *Nuclear envelope structural defects cause chromosomal numerical instability and aneuploidy in ovarian cancer*, *BMC Medicine*. doi: 10.1186/1741-7015-9-28.

Carissimi, C. *et al.* (2006) 'Gemin8 Is a Novel Component of the Survival Motor Neuron Complex and Functions in Small Nuclear Ribonucleoprotein Assembly', *THE JOURNAL OF BIOLOGICAL CHEMISTRY*, 281(12), pp. 8126–8134. doi: 10.1074/jbc.M512243200.

Carmosino, M. *et al.* (2016) 'The expression of Lamin A mutant R321X leads to endoplasmic reticulum stress with aberrant Ca 2+ handling', *Journal of Cellular and Molecular Medicine*, 20(11), pp. 2194–2207. doi: 10.1111/jcmm.12926.

Cartegni, L. and Krainer, A. R. (2002) 'Disruption of an SF2/ASF-dependent exonic splicing enhancer in SMN2 causes spinal muscular atrophy in the absence of SMN', *Nature Genetics*, 30(4), pp. 377–384. doi: 10.1038/ng854.

Casas, A. I. *et al.* (2019) 'From single drug targets to synergistic network pharmacology in ischemic stroke', *PNAS*, 116(14), pp. 7129–7136. doi: 10.1073/pnas.1820799116.

Casoni, F. *et al.* (2005) 'Protein nitration in a mouse model of familial amyotrophic lateral sclerosis: Possible multifunctional role in the pathogenesis', *Journal of Biological Chemistry*, 280(16), pp. 16295–16304. doi: 10.1074/jbc.M413111200.

Catapano, F. *et al.* (2016) 'Altered Levels of MicroRNA-9, -206, and -132 in Spinal Muscular Atrophy and Their Response to Antisense Oligonucleotide Therapy', *Molecular Therapy—Nucleic Acids*. Official journal of the American Society of Gene & Cell Therapy, 5(7), p. e331. doi: 10.1038/mtna.2016.47.

Chakraborty, J. *et al.* (2015) 'Quercetin improves the activity of the ubiquitin-proteasomal system in 150Q mutated huntingtin-expressing cells but exerts detrimental effects on

neuronal survivability', *Journal of Neuroscience Research*, 93(10), pp. 1581–1591. doi: 10.1002/jnr.23618.

Chan, S. H. S. *et al.* (2018) 'A recurrent de novo DYNC1H1 tail domain mutation causes spinal muscular atrophy with lower extremity predominance, learning difficulties and mild brain abnormality', *Neuromuscular Disorders*. Elsevier B.V., 28(9), pp. 750–756. doi: 10.1016/j.nmd.2018.07.002.

Chan, Y. B. *et al.* (2003) 'Neuromuscular defects in a Drosophila survival motor neuron gene mutant', *Human Molecular Genetics*, 12(12), pp. 1367–1376. doi: 10.1093/hmg/ddg157.

Chang, H. C.-H. *et al.* (2008) 'Modeling Spinal Muscular Atrophy in Drosophila', *PLoS ONE*, 3(9), p. e3209. doi: 10.1371/journal.pone.0003209.

Chang, H. Y. *et al.* (2002) 'Diversity, topographic differentiation, and positional memory in human fibroblasts', *PNAS*, 99(20), pp. 12877–12882. Available at: www.ncbi.nlm.nih.gov (Accessed: 30 December 2019).

Charnas, L. *et al.* (2017) 'Safety and efficacy findings in the first-in-human trial (FIH) of the oral splice modulator branaplam in type 1 spinal muscular atrophy (SMA): interim results', *Neuromuscular Disorders*, 27(2), pp. S207–S208. doi: 10.1016/j.nmd.2017.06.408.

Chen, Y. *et al.* (2016) 'Proteomic analysis of cerebrospinal fluid in amyotrophic lateral sclerosis', *EXPERIMENTAL AND THERAPEUTIC MEDICINE*, 11, pp. 2095–2106. doi: 10.3892/etm.2016.3210.

Chiriboga, C. A. *et al.* (2016) 'Results from a phase 1 study of nusinersen (ISIS-SMNRx) in children with spinal muscular atrophy.', *Neurology*, 86(10), pp. 890–897. doi: 10.1212/WNL.0000000000002445.

Cho, S. *et al.* (2019) 'Mechanosensing by the Lamina Protects against Nuclear Rupture, DNA Damage, and Cell-Cycle Arrest', *Developmental Cell*. Elsevier Inc., 49(6), pp. 920–935. doi:

10.1016/j.devcel.2019.04.020.

Cho, Sunghee *et al.* (2014) 'HnRNP M facilitates exon 7 inclusion of SMN2 pre-mRNA in spinal muscular atrophy by targeting an enhancer on exon 7', *Biochimica et Biophysica Acta*. Elsevier B.V., 1839(4), pp. 306–315. doi: 10.1016/j.bbagrm.2014.02.006.

Chondrogianni, N. *et al.* (2010) 'Anti-ageing and rejuvenating effects of quercetin', *Experimental Gerontology*. Elsevier Inc., 45(10), pp. 763–771. doi: 10.1016/j.exger.2010.07.001.

Chung, M. J. and Suh, Y. L. (2002) 'Ultrastructural changes of mitochondria in the skeletal muscle of patients with amyotrophic lateral sclerosis', *Ultrastructural Pathology*, 26(1), pp. 3–7. doi: 10.1080/01913120252934260.

Cieslak, K. P. *et al.* (2016) 'Liver function declines with increased age', *HPB*, 18, pp. 691–696. doi: 10.1016/j.hpb.2016.05.011.

Cifuentes-Diaz, C. *et al.* (2001) 'Deletion of Murine SMN Exon 7 Directed to Skeletal Muscle Leads to Severe Muscular Dystrophy', *The Journal of Cell Biology*, 152(5), pp. 1107–1114. Available at: http://www.jcb.org/cgi/content/full/152/5/1107 (Accessed: 20 March 2017).

Cifuentes-Diaz, C. *et al.* (2002) 'Neurofilament accumulation at the motor endplate and lack of axonal sprouting in a spinal muscular atrophy mouse model', *Human Molecular Genetics*, 11(12), pp. 1439–1447. Available at: https://oup.silverchair-cdn.com/oup/backfile/Content_public/Journal/hmg/11/12/10.1093_hmg_11.12.1439/2/ddf140.pdf?Expires=1490184014&Signature=IDb9JwzLj2QXJsNNPyXL7TqjNyfABgqVVEOC5kG--m8ALgXUkmzbQ-rbS8R7PXMdocGl-mL7B~3JBvBRV3sawqT1MEZ65RBpvdUMH2yokIGAxtUF (Accessed: 18 March 2017).

Cobb, M. S. *et al.* (2013) 'Development and characterization of an SMN2-based intermediate mouse model of Spinal Muscular Atrophy', *Human Molecular Genetics*, 22(9), pp. 1843–1855.

doi: 10.1093/hmg/ddt037.

Collins, M. A. *et al.* (2015) 'Label-Free LC−MS/MS Proteomic Analysis of Cerebrospinal Fluid Identifies Protein/Pathway Alterations and Candidate Biomarkers for Amyotrophic Lateral Sclerosis', *Journal of Proteome Research*, 14, p. 4486−4501. doi: 10.1021/acs.jproteome.5b00804.

Columbaro, M. *et al.* (2005) 'Rescue of heterochromatin organization in Hutchinson-Gilford progeria by drug treatment', *Cellular and Molecular Life Sciences*, 62(22), pp. 2669–2678. doi: 10.1007/s00018-005-5318-6.

Communal, C. *et al.* (2002) 'Functional consequences of caspase activation in cardiac myocytes', *PNAS*, 99(9), pp. 6252–6256. doi: 10.1073_pnas.0920229.

Conti, A. *et al.* (2014) 'Increased expression of Myosin binding protein H in the skeletal muscle of amyotrophic lateral sclerosis patients', *Biochimica et Biophysica Acta*, 1842(1), pp. 99–106. doi: 10.1016/j.bbadis.2013.10.013.

Coovert, D. D. *et al.* (1997) 'The survival motor neuron protein in spinal muscular atrophy', *Human Molecular Genetics*, 6(8), pp. 1205–1214. doi: 10.1093/hmg/6.8.1205.

Corti, S. *et al.* (2012) 'Genetic Correction of Human Induced Pluripotent Stem Cells from Patients with Spinal Muscular Atrophy', *Science Translational Medicine*, 4(165), p. 165ra162. doi: 10.1126/scitranslmed.3004108.

Crawford, T. O. *et al.* (1999) 'Abnormal Fatty Acid Metabolism in Childhood Spinal Muscular Atrophy', *Annals of Neurology*, 45(3), pp. 337–343.

Custer, S. K. *et al.* (2013) 'Dilysine motifs in exon 2b of SMN protein mediate binding to the COPI vesicle protein a-COP and neurite outgrowth in a cell culture model of spinal muscular atrophy', *Human Molecular Genetics*, 22(20), pp. 4043–4052. doi: 10.1093/hmg/ddt254.

Custer, S. K. *et al.* (2019) 'Interaction between alpha-COP and SMN ameliorates disease

phenotype in a mouse model of spinal muscular atrophy', *Biochemical and Biophysical Research Communications*. Elsevier Ltd, 514(2), pp. 530–537. doi: 10.1016/j.bbrc.2019.04.176.

Custer, S. K. and Androphy, E. J. (2014) 'Autophagy dysregulation in cell culture and animals models of Spinal Muscular Atrophy', *Mol cell neurosci.*, 61, pp. 133–140. doi: 10.1016/j.mcn.2014.06.006.

d'Ydewalle, C. *et al.* (2017) 'The Antisense Transcript SMN-AS1 Regulates SMN Expression and Is a Novel Therapeutic Target for Spinal Muscular Atrophy', *Neuron*. Elsevier Inc., 93, pp. 66–79. doi: 10.1016/j.neuron.2016.11.033.

D'Ydewalle, C. and Sumner, C. J. (2015) 'Spinal Muscular Atrophy Therapeutics: Where do we Stand?', *Neurotherapeutics*, 12(2), pp. 303–316. doi: 10.1007/s13311-015-0337-y.

Damiano, M. *et al.* (2006) 'Neural mitochondrial Ca2+ capacity impairment precedes the onset of motor symptoms in G93A Cu/Zn-superoxide dismutase mutant mice', *Journal of Neurochemistry*, 96(5), pp. 1349–1361. doi: 10.1111/j.1471-4159.2006.03619.x.

Dapic, I. *et al.* (2017) 'Fast and Simple Protocols for Mass Spectrometry-Based Proteomics of Small Fresh Frozen Uterine Tissue Sections', *Analytical Chemistry*, 89(20), pp. 10769–10775. doi: 10.1021/acs.analchem.7b01937.

Darbar, I. A. *et al.* (2011) 'Evaluation of muscle strength and motor abilities in children with type II and III spinal muscle atrophy treated with valproic acid', *BMC Neurology*, 11, p. 36. doi: 10.1186/1471-2377-11-36.

Das, J. *et al.* (2018) 'A missense mutation in DYNC1H1 gene causing spinal muscular atrophy – Lower extremity, dominant', *Neurologia i Neurochirurgia Polska*. Polish Neurological Society, 52(2), pp. 293–297. doi: 10.1016/j.pjnns.2017.12.004.

Defour, A. *et al.* (2017) 'Annexin A2 links poor myofiber repair with inflammation and

adipogenic replacement of the injured muscle', *Human Molecular Genetics*, 26(11), pp. 1979–1991. doi: 10.1093/hmg/ddx065.

Deguise, M.-O. *et al.* (2017) 'Immune dysregulation may contribute to disease pathogenesis in spinal muscular atrophy mice', *Human Molecular Genetics*, 26(4), pp. 801–819. doi: 10.1093/hmg/ddw434.

Deguise, M. *et al.* (2019) 'Abnormal fatty acid metabolism is a core component of spinal muscular atrophy', *Annals of Clinical and Translational Neurology*, 6(8), pp. 1519–1532. doi: 10.1002/acn3.50855.

Deng, H.-X. *et al.* (2006) 'Conversion to the amyotrophic lateral sclerosis phenotype is associated with intermolecular linked insoluble aggregates of SOD1 in mitochondria', *PNAS*, 103(18), pp. 7142–7147. Available at: https://www.ncbi.nlm.nih.gov/pmc/articles/PMC1447523/pdf/zpq7142.pdf (Accessed: 15 May 2018).

Desseille, C. *et al.* (2017) 'Specific Physical Exercise Improves Energetic Metabolism in the Skeletal Muscle of Amyotrophic-Lateral-Sclerosis Mice', *Front. Mol. Neurosci.*, 10(332). doi: 10.3389/fnmol.2017.00332.

Didonato, C. J. *et al.* (2001) 'Regulation of murine survival motor neuron (Smn) protein levels by modifying Smn exon 7 splicing', *Human Molecular Genetics*, 10(23), pp. 2727–2736. Available at: https://oup.silverchair-cdn.com/oup/backfile/Content_public/Journal/hmg/10/23/10.1093_hmg_10.23.2727/1/102727.pdf?Expires=1490437510&Signature=eOyKWPpR2aqkKGJfjqTLj0ICNbEYaMJGR8a7xYNZNjC9Aw9jMV2jwBMN1tIqptxu9Kq71dZZB8a4xhFGcMkNo5vHj~yzDz3-l4br4I~TRWUhK1gC (Accessed: 21 March 2017).

Didonna, A. and Opal, P. (2019) 'The role of neurofilament aggregation in neurodegeneration:

lessons from rare inherited neurological disorders', *Molecular Neurodegeneration* , 14(19). doi: 10.1186/s13024-019-0318-4.

Van Dijk, T. *et al.* (2017) 'Pontocerebellar hypoplasia with spinal muscular atrophy (PCH1): identification of SLC25A46 mutations in the original Dutch PCH1 family', *Brain*, 140(1–4), p. e46. doi: 10.1093/brain/awx147.

Dimitriadi, M. *et al.* (2010) 'Conserved Genes Act as Modifiers of Invertebrate SMN Loss of Function Defects', *PLoS Genetics*, 6(10), p. e1001172. doi: 10.1371/journal.pgen.1001172.

Diószeghy, P., Mechler, F. and Csenkér, E. (1981) 'Investigations on enzyme activity in the serum and CSF of patients with neuromuscular diseases.', *Archiv fur Psychiatrie und Nervenkrankheiten*, 230(4), pp. 307–14. Available at: http://www.ncbi.nlm.nih.gov/pubmed/7316727 (Accessed: 12 April 2018).

Dlamini, N. *et al.* (2013) 'Clinical and neuropathological features of X-linked spinal muscular atrophy (SMAX2) associated with a novel mutation in the UBA1 gene', *Neuromuscular Disorders*. Elsevier B.V., 23(5), pp. 391–398. doi: 10.1016/j.nmd.2013.02.001.

Dobrowolny, G. *et al.* (2008) 'Skeletal Muscle Is a Primary Target of SOD1 G93A -Mediated Toxicity', *Cell Metabolism*, 8, pp. 425–436. doi: 10.1016/j.cmet.2008.09.002.

Le Dour, C., Macquart, C., *et al.* (2017) 'Decreased WNT/b-catenin signalling contributes to the pathogenesis of dilated cardiomyopathy caused by mutations in the lamin a/C gene', *Human Molecular Genetics*, 26(2), pp. 333–343. doi: 10.1093/hmg/ddw389.

Le Dour, C., Wu, W., *et al.* (2017) 'Extracellular matrix remodeling and transforming growth factor-β signaling abnormalities induced by lamin A/C variants that cause lipodystrophy', *Journal of Lipid Research*, 58(1), pp. 151–163. doi: 10.1194/jlr.M071381.

Dubowitz, V. (1995) 'Chaos in the classification of SMA: A possible resolution', *Neuromuscular Disorders*, 5(1), pp. 3–5. doi: 10.1016/0960-8966(94)00075-K.

Dubowitz, V. (1999) 'Very severe spinal muscular atrophy (SMA type 0): an expanding clinical phenotype.', *European journal of paediatric neurology : EJPN : official journal of the European Paediatric Neurology Society*, 3(2), pp. 49–51. doi: 10.1053/ejpn.1999.0181.

Dudley, J. T. *et al.* (2011) 'Computational repositioning of the anticonvulsant topiramate for inflammatory bowel disease', *Sci Transl Med.*, 3(96), p. 96ra76. doi: 10.1126/scitranslmed.3002648.Computational.

Duplan, L. *et al.* (2010) 'Collapsin response mediator protein 4a (CRMP4a) is upregulated in motoneurons of mutant SOD1 mice and can trigger motoneuron axonal degeneration and cell death', *The Journal of Neuroscience*, 30(2), pp. 785–796. doi: 10.1523/JNEUROSCI.5411-09.2010.

Duque, G. and Rivas, D. (2006) 'Age-related changes in lamin A/C expression in the osteoarticular system: Laminopathies as a potential new aging mechanism', *Mechanism of Ageing and Development*, 127, pp. 378–383. doi: 10.1016/j.mad.2005.12.007.

Duque, S. I. *et al.* (2015) 'A large animal model of Spinal Muscular Atrophy and correction of phenotype', *Ann Neurol*, 77(3), pp. 399–414. doi: 10.1002/ana.24332.

Durães, F., Pinto, M. and Sousa, E. (2018) 'Old Drugs as New Treatments for Neurodegenerative Diseases', *Pharmaceuticals*, 11(44). doi: 10.3390/ph11020044.

Eaton, S. L. *et al.* (2013) 'Total Protein Analysis as a Reliable Loading Control for Quantitative Fluorescent Western Blotting', *PLOS ONE*, 8(8), p. e72457. doi: 10.1371/journal.pone.0072457.

Eaton, S. L. *et al.* (2014) 'A guide to modern quantitative fluorescent western blotting with troubleshooting strategies', *Journal of visualized experiments*, (93), p. e52099. doi: 10.3791/52099.

Ebert, A. D. and Svendsen, C. N. (2010) 'Stem cell model of spinal muscular atrophy', *Arch*

Neurol, 67(6), pp. 665–669. doi: 10.1001/archneurol.2010.89.

Edens, B. M. *et al.* (2015) 'Molecular mechanisms and animal models of spinal muscular atrophy', *Biochimica et Biophysica Acta*, 1852(4), pp. 685–692. doi: 10.1016/j.bbadis.2014.07.024.

Elf, K. *et al.* (2014) 'Alterations in muscle proteome of patients diagnosed with amyotrophic lateral sclerosis', *Journal of Proteomics*, 108, pp. 55–64. doi: 10.1016/j.jprot.2014.05.004.

Engelen-Lee, J. *et al.* (2017) 'Proteomic profiling of the spinal cord in ALS: decreased ATP5D levels suggest synaptic dysfunction in ALS pathogenesis', *Amyotrophic Lateral Sclerosis and Frontotemporal Degeneration*, 18(3–4), pp. 210–220. doi: 10.1080/21678421.2016.1245757.

Fallini, C. *et al.* (2011) 'The Survival of Motor Neuron (SMN) Protein Interacts with the mRNA-Binding Protein HuD and Regulates Localization of Poly(A) mRNA in Primary Motor Neuron Axons', *J. Neurosci.*, 31(10), pp. 3914–3925. doi: 10.1523/JNEUROSCI.3631-10.2011.The.

Fallini, C. *et al.* (2016) 'Deficiency of the Survival of Motor Neuron Protein Impairs mRNA Localization and Local Translation in the Growth Cone of Motor Neurons', *The Journal of Neuroscience*, 36(13), pp. 3811–3820. doi: 10.1523/JNEUROSCI.2396-15.2016.

Fallini, C., Bassell, G. J. and Rossoll, W. (2012) 'Spinal muscular atrophy: The role of SMN in axonal mRNA regulation', *Brain Research*. Elsevier B.V., 1462, pp. 81–92. doi: 10.1016/j.brainres.2012.01.044.

Farg, M. A. *et al.* (2012) 'Mutant FUS induces endoplasmic reticulum stress in amyotrophic lateral sclerosis and interacts with protein disulfide-isomerase', *Neurobiology of Aging*, 33, pp. 2855–2868. Available at: https://ac.els-cdn.com/S0197458012001546/1-s2.0-S0197458012001546-main.pdf?_tid=442a37da-d95f-452d-a770-b17de14f211b&acdnat=1523350711_264c32e237bf6e03c85f8758888500f1.

Farrar, M. a and Kiernan, M. C. (2015) 'The Genetics of Spinal Muscular Atrophy: Progress and

Challenges.', *Neurotherapeutics*, 12(2), pp. 290–302. doi: 10.1007/s13311-014-0314-x.

Fatkin, D. *et al.* (1999) 'Missense Mutations in the Rod Domain of the Lamin A/C Gene as Causes of Dilated Cardiomyopathy and Conduction-System Disease', *New England Journal of Medicine*, 341(23), pp. 1715–1724. doi: 10.1056/NEJM199912023412302.

Feist, P. and Hummon, A. B. (2015) 'Proteomic challenges: Sample preparation techniques for Microgram-Quantity protein analysis from biological samples', *International Journal of Molecular Sciences*, 16(2), pp. 3537–3563. doi: 10.3390/ijms16023537.

Feldkötter, M. *et al.* (2002) *Quantitative Analyses of SMN1 and SMN2 Based on Real-Time LightCycler PCR: Fast and Highly Reliable Carrier Testing and Prediction of Severity of Spinal Muscular Atrophy*, *Am. J. Hum. Genet*.

Feng, Y. *et al.* (2009) 'Dexamethasone induces neurodegeneration but also up-regulates vascular endothelial growth factor A in neonatal rat brains', *Neuroscience*. IBRO, 158(2), pp. 823–832. doi: 10.1016/j.neuroscience.2008.10.024.

Fernandes, I. R. *et al.* (2016) 'Fibroblast sources: Where can we get them?', *Cytotechnology*, 68, pp. 223–228. doi: 10.1007/s10616-014-9771-7.

Ferrante, R. J. *et al.* (1997) 'Increased 3-Nitrotyrosine and oxidative damage in mice with a human copper/zinc superoxide dismutase mutation', *Annals of Neurology*, 42(3), pp. 326–334. doi: 10.1002/ana.410420309.

Fields, A. P. *et al.* (1990) 'Role of nuclear protein kinase C in the mitogenic response to platelet-derived growth factor', *Journal of Cell Science*, 96(1), pp. 107–114.

Fil, D. *et al.* (2017) 'Mutant Profilin1 transgenic mice recapitulate cardinal features of motor neuron disease', *Human Molecular Genetics*, 26(4), pp. 686–701. doi: 10.1093/hmg/ddw429.

Filosto, M. *et al.* (2016) 'ASAH1 variant causing a mild SMA phenotype with no myoclonic epilepsy: a clinical, biochemical and molecular study', *European Journal of Human Genetics*,

24, pp. 1578–1583. doi: 10.1038/ejhg.2016.28.

Finkel, R. S. *et al.* (2016) 'Treatment of infantile-onset spinal muscular atrophy with nusinersen: a phase 2, open-label, dose-escalation study', *The Lancet*. Elsevier Ltd, 388(10063), pp. 3017–3026. doi: 10.1016/S0140-6736(16)31408-8.

Finkel, R. S. *et al.* (2017) 'Nusinersen versus Sham Control in Infantile-Onset Spinal Muscular Atrophy', *New England Journal of Medicine*, 377(18), pp. 1723–1732. doi: 10.1056/NEJMoa1702752.

Finkelstein, A. *et al.* (2011) 'Abnormal changes in NKT cells, the IGF-1 axis, and liver pathology in an animal model of ALS', *PLoS ONE*, 6(8), p. e22374. doi: 10.1371/journal.pone.0022374.

Fiorillo, C. *et al.* (2016) 'Beyond spinal muscular atrophy with lower extremity dominance: cerebellar hypoplasia associated with a novel mutation in BICD2', *European Journal of Neurology*, 23(4), pp. e19–e21. doi: 10.1111/ene.12914.

Di Fonzo, A. *et al.* (2014) 'Lower motor neuron disease with respiratory failure caused by a novel MAPT mutation', *Neurology*, 82(22), pp. 1990–1998. doi: 10.1212/WNL.0000000000000476.

Foran, E. and Trotti, D. (2009) 'Glutamate transporters and the excitotoxic path to motor neuron degeneration in amyotrophic lateral sclerosis', *Antioxidants and Redox Signaling*, 11(7), pp. 1587–1602. doi: 10.1089/ars.2009.2444.

Forsberg, K. *et al.* (2010) 'Novel Antibodies Reveal Inclusions Containing Non-Native SOD1 in Sporadic ALS Patients', *PLoS ONE*, 5(7), p. e11552. doi: 10.1371/journal.pone.0011552.

Foust, K. D. *et al.* (2010) 'Rescue of the spinal muscular atrophy phenotype in a mouse model by early postnatal delivery of SMN', 28(3), pp. 271–274. doi: 10.1038/nbt.1610.Rescue.

Freeman, G. A. *et al.* (2004) 'Design of non-nucleoside inhibitors of HIV-1 reverse transcriptase with improved drug resistance properties. 2', *Journal of Medicinal Chemistry*, 47(24), pp.

5923–5936. doi: 10.1021/jm040072r.

Frugier, T. *et al.* (2000) 'Nuclear targeting defect of SMN lacking the C-terminus in a mouse model of spinal muscular atrophy', *Human Molecular Genetics*, 9(5), pp. 849–858. Available at: https://oup.silverchair-cdn.com/oup/backfile/Content_public/Journal/hmg/9/5/10.1093_hmg_9.5.849/1/090849.pdf?Expires=1490369350&Signature=exuQYjmRkNWR0qVmICAGm-~wN48bSKfZ6VseFyive~qY-cvLbEwKvIXbqaMVKzPBWQ5EC0mhwxKoLJSH9sB3P3yNSnniOmzeasDgo6AML7MISdpzaw5LG (Accessed: 20 March 2017).

Fuchs, A. *et al.* (2013) 'Selective mitochondrial Ca2+ uptake deficit in disease endstage vulnerable motoneurons of the SOD1G93A mouse model of amyotrophic lateral sclerosis', *The Journal of Physiology*, 591(10), pp. 2723–2745. doi: 10.1113/jphysiol.2012.247981.

Fujak, A. *et al.* (2010) 'Fractures in proximal spinal muscular atrophy', *Arch Orthop Trauma Surg*, 130, pp. 775–780. doi: 10.1007/s00402-010-1096-1.

Fujak, A. *et al.* (2013) 'Natural course of scoliosis in proximal spinal muscular atrophy type II and IIIa: descriptive clinical study with retrospective data collection of 126 patients.', *BMC Musculoskelet Disord*, 14, p. 283. doi: 10.1186/1471-2474-14-283.

Fukada, K. *et al.* (2004) 'Mitochondrial Proteomic Analysis of a Cell Line Model of Familial Amyotrophic Lateral Sclerosis', *Mol Cell Proteomics.*, 3(12), pp. 1211–1223. doi: 10.1074/mcp.M400094-MCP200.

Fuller, H. R. *et al.* (2014) 'The rat striatum responds to nigro-striatal degeneration via the increased expression of proteins associated with growth and regeneration of neuronal circuitry', *Proteome Science*, 12, p. 20. doi: 10.1186/1477-5956-12-20.

Fuller, H. R. *et al.* (2016) 'Spinal Muscular Atrophy Patient iPSC-Derived Motor Neurons Have

Reduced Expression of Proteins Important in Neuronal Development.', *Frontiers in cellular neuroscience*, 9, p. 506. doi: 10.3389/fncel.2015.00506.

Fuller, H. R. *et al.* (2017) 'Monoclonal antibody Py recognizes neurofilament heavy chain and is a selective marker for large diameter neurons in the brain', *Brain Structure and Function*. Springer Berlin Heidelberg, 222(2), pp. 867–879. doi: 10.1007/s00429-016-1252-7.

Fuller, H. R., Gillingwater, T. H. and Wishart, T. M. (2016) 'Commonality amid diversity: Multi-study proteomic identification of conserved disease mechanisms in spinal muscular atrophy', *Neuromuscular Disorders*. Elsevier B.V., 26(9), pp. 560–569. doi: 10.1016/j.nmd.2016.06.004.

Fuller, H. R. and Morris, G. E. (2012) 'Quantitative Proteomics Using iTRAQ Labeling and Mass Spectrometry', in Leung, D. H.-C. (ed.) *Integrative Proteomics*. February,. InTech, pp. 347–362. doi: 10.5772/31469.

Furukawa, Y. *et al.* (2006) 'Disulfide cross-linked protein represents a significant fraction of ALS-associated Cu, Zn-superoxide dismutase aggregates in spinal cords of model mice', *PNAS*, 103(18), pp. 7148–7153. doi: 10.1073/pnas.0602048103.

Gabanella, F. *et al.* (2007) 'Ribonucleoprotein assembly defects correlate with spinal muscular atrophy severity and preferentially affect a subset of spliceosomal snRNPs', *PLoS ONE*, 2(9), p. e921. doi: 10.1371/journal.pone.0000921.

Galiová, G. *et al.* (2008) 'Chromatin changes induced by lamin A/C deficiency and the histone deacetylase inhibitor trichostatin A', *European Journal of Cell Biology*, 87(5), pp. 291–303. doi: 10.1016/j.ejcb.2008.01.013.

Gama-Carvalho, M. *et al.* (2017) 'Linking Amyotrophic Lateral Sclerosis and Spinal Muscular Atrophy through RNA-transcriptome homeostasis: a genomics perspective.', *Journal of neurochemistry*, 141, pp. 12–30. doi: 10.1111/jnc.13945.

Garbes, L. *et al.* (2009) 'LBH589 induces up to 10-fold SMN protein levels by several

independent mechanisms and is effective even in cells from SMA patients non-responsive to valproate', *Human Molecular Genetics*, 18(19), pp. 3645–3658. doi: 10.1093/hmg/ddp313.

Gelebart, P. *et al.* (2008) 'Constitutive activation of the Wnt canonical pathway in mantle cell lymphoma', *Blood*, 112(13), pp. 5171–5179. doi: 10.1182/blood-2008-02-139212.

Gelebart, P., Opas, M. and Michalak, M. (2005) 'Calreticulin, a Ca2+-binding chaperone of the endoplasmic reticulum', *The International Journal of Biochemistry & Cell Biology*, 37, pp. 260–266. doi: 10.1016/j.biocel.2004.02.030.

Gerbino, A. *et al.* (2017) 'Functional Characterization of a Novel Truncating Mutation in Lamin A/C Gene in a Family with a Severe Cardiomyopathy with Conduction Defects', *Cell Physiol Biochem*, 44, pp. 1559–1577. doi: 10.1159/000485651.

Giesemann, T. *et al.* (1999) 'A role for polyproline motifs in the spinal muscular atrophy protein SMN. Profilins bind to and colocalize with SMN in nuclear gems', *Journal of Biological Chemistry*, 274(53), pp. 37908–37914. doi: 10.1074/jbc.274.53.37908.

Gilliam, T. C. *et al.* (1990) 'Genetic homogeneity between acute and chronic forms of spinal muscular atrophy', *Nature*, 345, pp. 823–825. doi: 10.1016/0021-9797(80)90501-9.

Di Giorgio, F. P. *et al.* (2007) 'Non–cell autonomous effect of glia on motor neurons in an embryonic stem cell–based ALS model', *Nat Neurosci.*, 10(5), pp. 608–614. doi: 10.1038/nn1885.

Di Giorgio, F. P. *et al.* (2008) 'Human Embryonic Stem Cell-Derived Motor Neurons Are Sensitive to the Toxic Effect of Glial Cells Carrying an ALS-Causing Mutation', *Cell Stem Cell*. Elsevier Inc., 3(6), pp. 637–648. doi: 10.1016/j.stem.2008.09.017.

Giráldez, B. G. *et al.* (2015) 'Uniparental disomy as a cause of spinal muscular atrophy and progressive myoclonic epilepsy: Phenotypic homogeneity due to the homozygous c.125C>T mutation in ASAH1', *Neuromuscular Disorders*. Elsevier Ltd, 25(3), pp. 222–224. doi:

10.1016/j.nmd.2014.11.007.

Giunta, M. *et al.* (2016) 'Altered RNA metabolism due to a homozygous RBM7 mutation in a patient with spinal motor neuropathy', *Human Molecular Genetics*. Oxford University Press, 25(14), pp. 2985–2996. doi: 10.1093/hmg/ddw149.

Glenn Lin, C.-L. *et al.* (1998) *Aberrant RNA Processing in a Neurodegenerative Disease: the Cause for Absent EAAT2, a Glutamate Transporter, in Amyotrophic Lateral Sclerosis*, *Neuron*. Bruijn and Cleveland. Available at: https://www.cell.com/action/showPdf?pii=S0896-6273%2800%2980997-6 (Accessed: 4 September 2019).

Gnanapavan, S. and Giovannoni, G. (2013) 'Neural cell adhesion molecules in brain plasticity and disease', *Multiple Sclerosis and Related Disorders*. Elsevier, 2(1), pp. 13–20. doi: 10.1016/j.msard.2012.08.002.

Godena, V. K. and Ning, K. (2017) 'Phosphatase and tensin homologue: a therapeutic target for SMA', *Signal Transduction and Targeted Therapy*, 2, p. e17038. doi: 10.1038/sigtrans.2017.38.

Gottlieb, A. *et al.* (2011) 'PREDICT: A method for inferring novel drug indications with application to personalized medicine', *Molecular Systems Biology*. Nature Publishing Group, 7, p. 496. doi: 10.1038/msb.2011.26.

Gouarné, C. *et al.* (2013) 'Olesoxime protects embryonic cortical neurons from camptothecin intoxication by a mechanism distinct from BDNF', *British Journal of Pharmacology*, 168, pp. 1975–1988. doi: 10.1111/bph.12094.

Grech, V. (2018) 'WASP (Write a Scientific Paper) using Excel – 2: Pivot tables', *Early Human Development*, 117, pp. 104–109. doi: 10.1016/j.earlhumdev.2018.01.003.

Greenberg, F. *et al.* (1988) 'X-linked Infantile Spinal Muscular Atrophy', *Am J Dis Child.*, 142(2), pp. 217–219.

Groen, E. J. N. *et al.* (2013) 'ALS-associated mutations in FUS disrupt the axonal distribution and function of SMN', *Human Molecular Genetics*, 22(18), pp. 3690–3704. doi: 10.1093/hmg/ddt222.

Groen, E. J. N. *et al.* (2018) 'Temporal and tissue-specific variability of SMN protein levels in mouse models of spinal muscular atrophy', *Human Molecular Genetics*, 27(16), pp. 2851–2862. doi: 10.1093/hmg/ddy195.

Groh, M. *et al.* (2017) 'Senataxin: Genome Guardian at the Interface of Transcription and Neurodegeneration', *Journal of Molecular Biology*. Elsevier Ltd, 429(21), pp. 3181–3195. doi: 10.1016/j.jmb.2016.10.021.

Grunseich, C. *et al.* (2014) 'Early onset and novel features in a spinal and bulbar muscular atrophy patient with a 68 CAG repeat', *Neuromuscular Disorders*, 24, pp. 978–981. doi: 10.1016/j.nmd.2014.06.441.

Gu, Z. *et al.* (2014) 'Genome analysis:circlize implements and enhances circular visualization in R', *BIOINFORMATICS APPLICATIONS NOTE*, 30(19), pp. 2811–2812. doi: 10.1093/bioinformatics/btu393.

Gurney, M. E. *et al.* (1994) 'Motor neuron degeneration in mice that express a human Cu,Zn superoxide dismutase mutation.', *Science*, 264(5166), pp. 1772–5. doi: 10.1016/j.bbrc.2011.02.099.

Hao, L. T. *et al.* (2013) 'Temporal requirement for SMN in motoneuron development', *Human Molecular Genetics*, 22(13), pp. 2612–2625. doi: 10.1093/hmg/ddt110.

Hao Le, T. *et al.* (2017) 'HuD and the Survival Motor Neuron Protein Interact in Motoneurons and Are Essential for Motoneuron Development, Function, and mRNA Regulation', *The Journal of Neuroscience*, 37(48), pp. 11559 –11571. doi: 10.1523/JNEUROSCI.1528-17.2017.

Harada, T. *et al.* (2014) 'Nuclear lamin stiffness is a barrier to 3D migration, but softness can

limit survival', *Journal of Cell Biology*, 204(5), pp. 669–682. doi: 10.1083/jcb.201308029.

Harding, B. N. *et al.* (2015) 'Spectrum of neuropathophysiology in spinal muscular atrophy type I', *Journal of neuropathology and experimental neurology*, 74(1), pp. 15–24. doi: 10.1097/NEN.0000000000000144.

Harms, M. B. *et al.* (2012) 'Mutations in the tail domain of DYNC1H1 cause dominant spinal muscular atrophy.', *Neurology*, 78(22), pp. 1714–20. doi: 10.1212/WNL.0b013e3182556c05.

Hayhurst, M. *et al.* (2012) 'A cell-autonomous defect in skeletal muscle satellite cells expressing low levels of survival of motor neuron protein', *Developmental Biology*, 368(2), pp. 323–334. doi: 10.1016/j.ydbio.2012.05.037.

Hebert, M. D. *et al.* (2001) 'Coilin forms the bridge between Cajal bodies and SMN, the spinal muscular atrophy protein', *Genes and Development*, 15(20), pp. 2720–2729. doi: 10.1101/gad.908401.

Heier, C. R. *et al.* (2010) 'Arrhythmia and cardiac defects are a feature of spinal muscular atrophy model mice', *Human Molecular Genetics*, 19(20), pp. 3906–3918. doi: 10.1093/hmg/ddq330.

Hensel, N. and Claus, P. (2018) 'The Actin Cytoskeleton in SMA and ALS: How Does It Contribute to Motoneuron Degeneration?', *Neuroscientist*, 24(1), pp. 54–72. doi: 10.1177/1073858417705059.

Hensel, N., Kubinski, S. and Claus, P. (2020) 'The Need for SMN-Independent Treatments of Spinal Muscular Atrophy (SMA) to Complement SMN-Enhancing Drugs', *Front. Neurol.*, 11, p. 45. doi: 10.3389/fneur.2020.00045.

Herzog, A. *et al.* (2004) 'Identification of biomarkers for the initiation of apoptosis in human preneoplastic colonocytes by proteome analysis', *International Journal of Cancer*, 109(2), pp. 220–229. doi: 10.1002/ijc.11692.

Hetz, C. *et al.* (2009) 'XBP-1 deficiency in the nervous system protects against amyotrophic lateral sclerosis by increasing autophagy', *Genes and Development*, 23(19), pp. 2294–2306. doi: 10.1101/gad.1830709.

Hofmann, Y. *et al.* (2000) 'Htra2-β1 stimulates an exonic splicing enhancer and can restore full-length SMN expression to survival motor neuron 2 (SMN2)', *PNAS*, 97(17), pp. 9618–9623. Available at: www.pnas.orgcgidoi10.1073pnas.160181697 (Accessed: 29 January 2020).

Hofmann, Y. and Wirth, B. (2002) 'hnRNP-G promotes exon 7 inclusion of survival motor neuron (SMN) via direct interaction with Htra2-b1', *Human Molecular Genetics*, 11(17), pp. 2037–2049. Available at: https://academic.oup.com/hmg/article-abstract/11/17/2037/589960 (Accessed: 29 January 2020).

Holm, I. E., Alstrup, A. K. O. and Luo, Y. (2016) 'Genetically modified pig models for neurodegenerative disorders', *Journal of Pathology*, 238(2), pp. 267–287. doi: 10.1002/path.4654.

Holt, I. *et al.* (2003) 'Effect of pathogenic mis-sense mutations in lamin A on its interaction with emerin in vivo', *Journal of Cell Science*, 116(14), pp. 3027–3035. doi: 10.1242/jcs.00599.

Hoolachan, J. M., Sutton, E. R. and Bowerman, M. (2019) 'Teaching an old drug new tricks: repositioning strategies for spinal muscular atrophy', *Future Neurology*, 14(3), p. FNL25. doi: 10.2217/fnl-2019-0006.

Hopkins, A. L. (2008) 'Network pharmacology: The next paradigm in drug discovery', *Nature Chemical Biology*, 4(11), pp. 682–690. doi: 10.1038/nchembio.118.

Howland, D. S. *et al.* (2002) 'Focal loss of the glutamate transporter EAAT2 in a transgenic rat model of SOD1 mutant-mediated amyotrophic lateral sclerosis (ALS)', *PNAS*, 99(3), pp. 1604–1609. doi: 10.1073_pnas.032539299.

Hsieh-Li, H. M. *et al.* (2000) 'A mouse model for spinal muscular atrophy', *Nature Genetics*.

Nature Publishing Group, 24(1), pp. 66–70. doi: 10.1038/71709.

Hu, S., Loo, J. A. and Wong, D. T. (2006) 'Human body fluid proteome analysis', *Proteomics*, 6(23), pp. 6326–6353. doi: 10.1002/pmic.200600284.

Hua, Y. *et al.* (2008) 'Antisense Masking of an hnRNP A1/A2 Intronic Splicing Silencer Corrects SMN2 Splicing in Transgenic Mice', *The American Journal of Human Genetics*, 82, pp. 834–848. doi: 10.1016/j.ajhg.2008.01.014.

Hua, Y. *et al.* (2011) 'Peripheral SMN restoration is essential for long-term rescue of a severe spinal muscular atrophy mouse model', *Nature*. Nature Publishing Group, 478(7367), pp. 123–126. doi: 10.1038/nature10485.

Huang, D. W., Sherman, B. T. and Lempicki, R. A. (2009a) 'Bioinformatics enrichment tools: paths toward the comprehensive functional analysis of large gene lists', *Nucleic Acids Research*, 37(1), pp. 1–13. doi: 10.1093/nar/gkn923.

Huang, D. W., Sherman, B. T. and Lempicki, R. A. (2009b) 'Systematic and integrative analysis of large gene lists using DAVID bioinformatics resources', *Nature Protocols*. Nature Publishing Group, 4(1), pp. 44–57. doi: 10.1038/nprot.2008.211.

Hubers, L. *et al.* (2011) 'HuD interacts with survival motor neuron protein and can rescue spinal muscular atrophy-like neuronal defects', *Human Molecular Genetics*, 20(3), pp. 553–579. doi: 10.1093/hmg/ddq500.

Huda, N. *et al.* (2019) 'Hepatic senescence, the good and the bad', *World J Gastroenterol*, 25(34), pp. 5069–5081. doi: 10.3748/wjg.v25.i34.5069.

Hunter, G. *et al.* (2014) 'SMN-dependent intrinsic defects in Schwann cells in mouse models of spinal muscular atrophy', *Human Molecular Genetics*, 23(9), pp. 2235–2250. doi: 10.1093/hmg/ddt612.

Hunter, G. *et al.* (2016) 'Restoration of SMN in Schwann cells reverses myelination defects and

improves neuromuscular function in spinal muscular atrophy', *Human Molecular Genetics*, 25(13), pp. 2853–2861. doi: 10.1093/hmg/ddw141.

Huo, Q. *et al.* (2014) 'Splicing changes in SMA mouse motoneurons and SMN-depleted neuroblastoma cells: evidence for involvement of splicing regulatory proteins.', *RNA biology*, 11(11), pp. 1430–46. doi: 10.1080/15476286.2014.996494.

Hwee, D. T. *et al.* (2015) 'The Small-Molecule Fast Skeletal Troponin Activator, CK-2127107, Improves Exercise Tolerance in a Rat Model of Heart Failure s', *THE JOURNAL OF PHARMACOLOGY AND EXPERIMENTAL THERAPEUTICS*, 353, pp. 159–168. doi: 10.1124/jpet.114.222224.

Ilieva, E. V. *et al.* (2007) 'Oxidative and endoplasmic reticulum stress interplay in sporadic amyotrophic lateral sclerosis', *Brain*, 130(12), pp. 3111–3123. doi: 10.1093/brain/awm190.

Ilieva, H., Polymenidou, M. and Cleveland, D. W. (2009) 'Non–cell autonomous toxicity in neurodegenerative disorders: ALS and beyond', *J. Cell Biol.* , 187(6), pp. 761–772. doi: 10.1083/jcb.200908164.

Intano, G. W. *et al.* (2003) *Age-related Base Excision Repair Activity in Mouse Brain and Liver Nuclear Extracts*, *Journal of Gerontology: BIOLOGICAL SCIENCES*. Available at: https://academic.oup.com/biomedgerontology/article-abstract/58/3/B205/684114 (Accessed: 4 January 2020).

Ito, Y. *et al.* (2003) 'Thalamic lesions in a long-surviving child with spinal muscular atrophy type I: MRI and EEG findings', *Brain and Development*, 26(1), pp. 53–56. doi: 10.1016/S0387-7604(03)00075-5.

Iwahara, N. *et al.* (2015) 'A novel lamin A/C gene mutation causing spinal muscular atrophy phenotype with cardiac involvement: report of one case.', *BMC neurology*, 15(1), p. 269. doi: 10.1186/s12883-015-0269-5.

Jacovina, A. T. *et al.* (2001) 'Neuritogenesis and the Nerve Growth Factor-induced Differentiation of PC-12 Cells Requires Annexin II-mediated Plasmin Generation', *Journal of Biological Chemistry*, 276(52), pp. 49350–49358. doi: 10.1074/jbc.M106289200.

Jang, S. *et al.* (2016) 'Glycolytic enzymes localize to synapses under energy stress to support synaptic function', *Neuron*, 90(2), pp. 278–291. doi: 10.1016/j.neuron.2016.03.011.

Jedrzejowska, M., Jakubowska-Pietkiewicz, E. and Kostera-Pruszczyk, A. (2015) 'X-linked spinal muscular atrophy (SMAX2) caused by de novo c.1731C>T substitution in the UBA1 gene', *Neuromuscular Disorders*, 25(8), pp. 661–666. doi: 10.1016/j.nmd.2015.05.001.

Jung, C., Higgins, C. M. J. and Xu, Z. (2002) 'A quantitative histochemical assay for activities of mitochondrial electron transport chain complexes in mouse spinal cord sections', *Journal of Neuroscience Methods*, 114(2), pp. 165–172. doi: 10.1016/S0165-0270(01)00524-6.

Jung, H.-J. *et al.* (2012) 'Regulation of prelamin A but not lamin C by miR-9, a brain-specific microRNA', *PNAS*, 109(7), pp. E423–E431. doi: 10.1073/pnas.1111780109.

Kaifer, K. A. *et al.* (2017) 'Plastin-3 extends survival and reduces severity in mouse models of spinal muscular atrophy', *JCI Insight.*, 2(5), p. e89970. doi: 10.1172/jci.insight.89970.

Kang, M. A. *et al.* (2012) 'DNA damage induces reactive oxygen species generation through the H2AX-Nox1/Rac1 pathway', *Cell Death and Disease*, 3, p. e249. doi: 10.1038/cddis.2011.134.

Kang, S.-M., Yoon, M.-H. and Park, B.-J. (2018) 'Laminopathies; Mutations on single gene and various human genetic diseases', *BMB Rep.*, 51(7), pp. 327–337. doi: 10.5483/BMBRep.2018.51.7.113.

Kannan, A. *et al.* (2018) 'Combined deficiency of Senataxin and DNA-PKcs causes DNA damage accumulation and neurodegeneration in spinal muscular atrophy', *Nucleic Acids Research*. Oxford University Press, 46(16), pp. 8326–8346. doi: 10.1093/nar/gky641.

Kanungo, S. *et al.* (2018) 'Glycogen metabolism and glycogen storage disorders', *Annals of Translational Medicine*, 6(24). doi: 10.21037/atm.2018.10.59.

Kariya, S. *et al.* (2008) 'Reduced SMN protein impairs maturation of the neuromuscular junctions in mouse models of spinal muscular atrophy', *Human Molecular Genetics*, 17(16), pp. 2552–2569. doi: 10.1093/hmg/ddn156.

Kariya, S. *et al.* (2012) 'Mutant superoxide dismutase 1 (SOD1), a cause of amyotrophic lateral sclerosis, disrupts the recruitment of SMN, the spinal muscular atrophy protein to nuclear Cajal bodies', *Human Molecular Genetics*, 21(15), pp. 3421–3434. doi: 10.1093/hmg/dds174.

Kariya, S. *et al.* (2014) 'Requirement of enhanced Survival Motoneuron protein imposed during neuromuscular junction maturation', *The Journal of Clinical Investigation*, 124(2), pp. 785–800. doi: 10.1172/JCI72017.

Kashima, T. and Manley, J. L. (2003) 'A negative element in SMN2 exon 7 inhibits splicing in spinal muscular atrophy', *Nature Genetics*, 34(4), pp. 460–463. doi: 10.1038/ng1207.

Khairallah, M.-T. *et al.* (2017) 'SMN deficiency negatively impacts red pulp macrophages and spleen development in mouse models of spinal muscular atrophy', *Human Molecular Genetics*, 26(5), pp. 932–941. doi: 10.1093/hmg/ddx008.

Khatri, I. A. *et al.* (2008) 'Low bone mineral density in spinal muscular atrophy', *Journal of clinical neuromuscular disease*, 10(1), pp. 11–17. doi: 10.1097/CND.0b013e318183e0fa.

Ki, C.-S. *et al.* (2002) *Identification of lamin A/C (LMNA) gene mutations in Korean patients with autosomal dominant Emery-Dreifuss muscular dystrophy and limb-girdle muscular dystrophy 1B*, *J Hum Genet*. Available at: http://genetics.med.harvard.edu/ (Accessed: 17 March 2019).

Kikuchi, H. *et al.* (2006) 'Spinal cord endoplasmic reticulum stress associated with a microsomal accumulation of mutant superoxide dismutase-1 in an ALS model', *PNAS*, 103(15),

pp. 6025–6030. Available at: https://www.ncbi.nlm.nih.gov/pmc/articles/PMC1458691/pdf/zpq6025.pdf (Accessed: 7 September 2019).

Kim, J.-E. *et al.* (2017) 'Altered nucleocytoplasmic proteome and transcriptome distributions in an in vitro model of amyotrophic lateral sclerosis', *PLoS ONE*, 12(4), p. e0176462. doi: 10.1371/journal.pone.0176462.

Kirschner, J. *et al.* (2014) 'Somatropin treatment of spinal muscular atrophy: A placebo-controlled, double-blind crossover pilot study', *Neuromuscular Disorders*, 24, pp. 134–142. doi: 10.1016/j.nmd.2013.10.011.

Kissel, J. T. *et al.* (2011) 'SMA CARNI-VAL TRIAL PART II: A Prospective, Single- Armed Trial of L-Carnitine and Valproic Acid in Ambulatory Children with Spinal Muscular Atrophy', *PLoS ONE*, 6(7), p. e21296. doi: 10.1371/journal.pone.0021296.

Kissel, J. T. *et al.* (2014) 'SMA valiant trial: A prospective, double-blind, placebo-controlled trial of valproic acid in ambulatory adults with spinal muscular atrophy', *Muscle & Nerve*. John Wiley & Sons, Ltd, 49(2), pp. 187–192. doi: 10.1002/mus.23904.

Klappan, A. K. *et al.* (2012) 'Proteasome inhibition by quercetin triggers macroautophagy and blocks mTOR activity', *Histochemistry and Cell Biology*, 137(1), pp. 25–36. doi: 10.1007/s00418-011-0869-0.

Knierim, E. *et al.* (2016) 'Mutations in Subunits of the Activating Signal Cointegrator 1 Complex Are Associated with Prenatal Spinal Muscular Atrophy and Congenital Bone Fractures', *The American Journal of Human Genetics*, 98, pp. 473–489. doi: 10.1016/j.ajhg.2016.01.006.

Kobayashi, D. T. *et al.* (2011) 'Utility of survival motor neuron ELISA for spinal muscular atrophy clinical and preclinical analyses', *PLoS ONE*, 6(8), p. e24269. doi: 10.1371/journal.pone.0024269.

Kobayashi, D. T. *et al.* (2013) 'SMA-MAP: A Plasma Protein Panel for Spinal Muscular Atrophy', *PLoS ONE*, 8(4), p. e60113. doi: 10.1371/journal.pone.0060113.

Koeck, T. *et al.* (2004) 'Tyrosine Nitration Impairs Mammalian Aldolase A Activity', *Molecular & Cellular Proteomics*, 3(6), pp. 548–557. doi: 10.1074/mcp.m300141-mcp200.

Kondo, H. and Yonezawa, Y. (1992) 'Changes in the migratory ability of human lung and skin fibroblasts during in vitro aging and in vivo cellular senescence', *Mechanisms of Ageing and Development*, 63(3), pp. 223–233. doi: 10.1016/0047-6374(92)90001-T.

Kong, J. and Xu, Z. (1998) 'Massive mitochondrial degeneration in motor neurons triggers the onset of amyotrophic lateral sclerosis in mice expressing a mutant SOD1', *Journal of Neuroscience*, 18(9), pp. 3241–3250.

Kong, L. *et al.* (2012) 'Lamin A / C protein is overexpressed in tissue-invading prostate cancer and promotes prostate cancer cell growth , migration and invasion through the PI3K / AKT / PTEN pathway', *Carcinogenesis*, 33(4), pp. 751–759. doi: 10.1093/carcin/bgs022.

Kopecky, B. J. *et al.* (2012) 'Three-dimensional reconstructions from optical sections of thick mouse inner ears using confocal microscopy', *J Microsc.*, 248(3), pp. 292–298. doi: 10.1111/j.1365-2818.2012.03673.x.

Krämer, A. *et al.* (2014) 'Causal analysis approaches in Ingenuity Pathway Analysis', *BIOINFORMATICS*, 30(4), pp. 523–530. doi: 10.1093/bioinformatics/btt703.

Krisko, A. and Radman, M. (2019) 'Protein damage, ageing and age-related diseases', *Open Biology*, 9(3), p. 180249. doi: 10.1098/rsob.180249.

Kubben, N. *et al.* (2010) 'Identification of differential protein interactors of lamin A and progerin', *Nucleus*, 1(6), pp. 513–525. doi: 10.4161/nucl.1.6.13512.

Kye, M. J. *et al.* (2014) 'SMN regulates axonal local translation via miR-183/mTOR pathway', *Human Molecular Genetics*, 23(23), pp. 6318–6331. doi: 10.1093/hmg/ddu350.

Laemmli, U. K. (1970) ‘Cleavage of Structural Proteins during the Assembly of the Head of Bacteriophage T4’, *Nature*, 227, pp. 680–685.

Lagier-Tourenne, C. *et al.* (2012) ‘Divergent roles of ALS-linked proteins FUS/TLS and TDP-43 intersect in processing long pre-mRNAs’, *Nature Neuroscience*. Nature Publishing Group, 15(11), pp. 1488–1497. doi: 10.1038/nn.3230.

Lanzicher, T. *et al.* (2015) ‘The Cardiomyopathy Lamin A/C D192G Mutation Disrupts Whole-Cell Biomechanics in Cardiomyocytes as Measured by Atomic Force Microscopy Loading-Unloading Curve Analysis’, *Scientific Reports* , 5(13388). doi: 10.1038/srep13388.

Le, T. T. *et al.* (2005) ‘SMNΔ7, the major product of the centromeric survival motor neuron (SMN2) gene, extends survival in mice with spinal muscular atrophy and associates with full-length SMN’, *Human Molecular Genetics*, 14(6), pp. 845–587. Available at: https://oup.silverchair-cdn.com/oup/backfile/Content_public/Journal/hmg/14/6/10.1093_hmg_ddi078/2/ddi078.pdf?Expires=1490369398&Signature=Rg-vOe9oiRQVD9kMlTAhBwHEeLTll9Q8e~9ix875goMiYyLpi37ecS5HvzFQMWq7fxeQb4CqfwEx5EkRNpAEjW44yg75l--g047t8b~pPz9MoO85QmcNx (Accessed: 20 March 2017).

Lecker, S. H., Goldberg, A. L. and Mitch, W. E. (2006) ‘Protein Degradation by the Ubiquitin-Proteasome Pathway in Normal and Disease States’, *Journal of the American Society of Nephrology*, 17(7), pp. 1807–1819. doi: 10.1681/ASN.2006010083.

Lee, S. J. *et al.* (2013) ‘Inhibition of nitric oxide mediated protein nitration: therapeutic implications in experimental radiculopathy.’, *Spine*, 38(20), pp. 1749–1753. doi: 10.1097/BRS.0b013e3182a085d9.

Lefebvre, S. *et al.* (1995) ‘Identification and characterization of a spinal muscular atrophy-determining gene’, *Cell*, 80(1), pp. 155–165. doi: 10.1016/0092-8674(95)90460-3.

Lernoux, M. *et al.* (2018) 'Anti-cancer effects of naturally derived compounds targeting histone deacetylase 6-related pathways', *Pharmacological Research*. Elsevier Ltd, 129, pp. 337–356. doi: 10.1016/j.phrs.2017.11.004.

Li, H. *et al.* (2015) 'α-COP binding to the survival motor neuron protein SMN is required for neuronal process outgrowth.', *Human molecular genetics*. Oxford University Press, 24(25), pp. 7295–7307. doi: 10.1093/hmg/ddv428.

Li, J., Johnson, J. A. and Su, H. (2018) 'Ubiquitin and Ubiquitin-like proteins in cardiac disease and protection.', *Current drug targets*. NIH Public Access, 19(9), pp. 989–1002. doi: 10.2174/1389450117666151209114608.

Li, Q. *et al.* (2010) 'ALS-linked mutant superoxide dismutase 1 (SOD1) alters mitochondrial protein composition and decreases protein import', *Proc Natl Acad Sci U S A.*, 107(49), pp. 21146–21151. doi: 10.1073/pnas.1014862107.

Li, W. *et al.* (2004) 'Mechanism of Human Dermal Fibroblast Migration Driven by Type I Collagen and Platelet-derived Growth Factor-BB', *Molecular Biology of the Cell*, 15, pp. 294–309. doi: 10.1091/mbc.E03.

Lin, F. and Worman, H. J. (1993) 'Structural Organization of the Human Gene Encoding Nuclear Lamin A and Nuclear Lamin C', *THe JOURNAL OF BIOLOGICAL CHEMISTRY*, 268(22), pp. 16321–16326. Available at: http://www.jbc.org/content/268/22/16321.full.pdf (Accessed: 28 June 2017).

Ling, K. K. Y. *et al.* (2010) 'Synaptic Defects in the Spinal and Neuromuscular Circuitry in a Mouse Model of Spinal Muscular Atrophy', *PLoS ONE*, 5(11), p. e15457. doi: 10.1371/journal.pone.0015457.

Ling, K. K. Y. *et al.* (2012) 'Severe neuromuscular denervation of clinically relevant muscles in a mouse model of spinal muscular atrophy', *Human Molecular Genetics*, 21(1), pp. 185–195.

doi: 10.1093/hmg/ddr453.

Lipnickid, S. L. *et al.* (2019) 'Systemic nature of spinal muscular atrophy revealed by studying insurance claims', *PLoS ONE*, 14(3), p. e0213680. doi: 10.1371/journal.pone.0213680.

Little, D. *et al.* (2015) 'PTEN Depletion Decreases Disease Severity and Modestly Prolongs Survival in a Mouse Model of Spinal Muscular Atrophy', *Molecular Therapy*, 23(2), pp. 270–277. doi: 10.1038/mt.2014.209.

Liu, B. *et al.* (2005) 'Genomic instability in laminopathy-based premature aging', *Nature Medicine*, 11(7), pp. 780–785. doi: 10.1038/nm1266.

Liu, H. *et al.* (2014) 'The Smn-Independent Beneficial Effects of Trichostatin A on an Intermediate Mouse Model of Spinal Muscular Atrophy', *PLoS ONE*, 9(7), p. e101225. doi: 10.1371/journal.pone.0101225.

Long, K. K. *et al.* (2019) 'Specific inhibition of myostatin activation is beneficial in mouse models of SMA therapy', *Human Molecular Genetics*, 28(7), pp. 1076–1089. doi: 10.1093/hmg/ddy382.

Lorson, C. L. *et al.* (1999) 'A single nucleotide in the SMN gene regulates splicing and is responsible for spinal muscular atrophy.', *Proceedings of the National Academy of Sciences of the United States of America*, 96(11), pp. 6307–11. doi: 10.1073/pnas.96.11.6307.

Lorson, M. A. *et al.* (2011) 'Disruption of the Survival Motor Neuron (SMN) gene in pigs using ssDNA', *Transgenic Res*, 20(6), pp. 1293–1304. doi: 10.1007/s11248-011-9496-8.

Louche, A., Salcedo, S. P. and Bigot, S. (2017) 'Protein–Protein Interactions: Pull-Down Assays', in *Bacterial Protein Secretion Systems: Methods and Protocols*, pp. 247–255. doi: 10.1007/978-1-4939-7033-9.

Lunn, M. R. and Wang, C. H. (2008) 'Spinal muscular atrophy', *Lancet*, 371, pp. 2120–2133. doi: 10.1016/S0140-6736(08)60921-6.

Lyon, C. E. *et al.* (1997) 'Inhibition of protein dephosphorylation results in the accumulation of splicing snRNPs and coiled bodies within the nucleolus', *Experimental Cell Research*, 230(1), pp. 84–93. doi: 10.1006/excr.1996.3380.

Maeda, M. *et al.* (2014) 'Transcriptome Profiling of Spinal Muscular Atrophy Motor Neurons Derived from Mouse Embryonic Stem Cells', *PLoS ONE*, 9(9), p. e106818. doi: 10.1371/journal.pone.0106818.

Magistretti, P. J. and Allaman, I. (2015) 'A cellular perspective on brain energy metabolism and functional imaging', *Neuron*, 86(4), pp. 883–901. doi: 10.1016/j.neuron.2015.03.035.

Maher, M. T. *et al.* (2009) 'Issues associated with assessing nuclear localization of N-terminally unphosphorylated β-catenin with monoclonal antibody 8E7', *Biology Direct*, 4, p. 5. doi: 10.1186/1745-6150-4-5.

Makhortova, N. R. *et al.* (2011) 'A screen for regulators of survival of motor neuron protein levels', *Nature Chemical Biology*, 7(8), pp. 544–552. doi: 10.1038/nchembio.595.

Mallampalli, M. P. *et al.* (2005) 'Inhibiting farnesylation reverses the nuclear morphology defect in a HeLa cell model for Hutchinson-Gilford progeria syndrome', *PNAS*, 102(40), p. 14417. Available at: www.pnas.orgcgidoi10.1073pnas.0503712102 (Accessed: 5 January 2020).

Mancuso, M. *et al.* (2002) 'Mitochondrial DNA depletion: Mutations in thymidine kinase gene with myopathy and SMA', *Neurology*, 59(8), pp. 1197–1202. doi: 10.1212/01.WNL.0000028689.93049.9A.

Manfredi, G. and Xu, Z. (2005) 'Mitochondrial dysfunction and its role in motor neuron degeneration in ALS', *Mitochondrion*, 5(2), pp. 77–87. doi: 10.1016/j.mito.2005.01.002.

Manilal, S. *et al.* (1996) 'The Emery-Dreifuss muscular dystrophy protein, emerin, is a nuclear membrane protein', *Human Molecular Genetics*, 5(6), pp. 801–808. doi:

10.1093/hmg/5.6.801.

Manilal, S. *et al.* (2004) 'A lamin A/C beta-strand containing the site of lipodystrophy mutations is a major surface epitope for a new panel of monoclonal antibodies.', *Biochimica et biophysica acta*, 1671(1–3), pp. 87–92. doi: 10.1016/j.bbagen.2004.01.008.

Manzano, R. *et al.* (2011) 'Altered expression of myogenic regulatory factors in the mouse model of amyotrophic lateral sclerosis', *Neurodegenerative Diseases*, 8(5), pp. 386–396. doi: 10.1159/000324159.

Manzano, R. *et al.* (2013) 'Altered in vitro proliferation of mouse SOD1-G93A skeletal muscle satellite cells', *Neurodegenerative Diseases*, 11(3), pp. 153–164. doi: 10.1159/000338061.

Marchetto, M. C. N. *et al.* (2008) 'Non-Cell-Autonomous Effect of Human SOD1G37R Astrocytes on Motor Neurons Derived from Human Embryonic Stem Cells', *Cell Stem Cell*. Elsevier Inc., 3(6), pp. 649–657. doi: 10.1016/j.stem.2008.10.001.

Marques, V. D. *et al.* (2006) 'Expanding the phenotypes of the Pro56Ser VAPB mutation: Proximal SMA with dysautonomia', *Muscle & Nerve*, 34(6), pp. 731–739. doi: 10.1002/mus.20657.

Martens, L. and Vizcaíno, J. A. (2017) 'A Golden Age for Working with Public Proteomics Data', *Trends in Biochemical Sciences*. Elsevier Ltd, 42(5), pp. 333–341. doi: 10.1016/j.tibs.2017.01.001.

Martinez, T. L. *et al.* (2012) 'Survival Motor Neuron Protein in Motor Neurons Determines Synaptic Integrity in Spinal Muscular Atrophy', *The Journal of Neuroscience*, 32(25), pp. 8703–8715. doi: 10.1523/JNEUROSCI.0204-12.2012.

Massignan, T. *et al.* (2007) 'Proteomic analysis of spinal cord of presymptomatic amyotrophic lateral sclerosis G93A SOD1 mouse', *Biochemical and Biophysical Research Communications*, 353(3), pp. 719–725. doi: 10.1016/j.bbrc.2006.12.075.

Mastaglia, F. L. and Walton, J. (1971) 'Histological and histochemical changes in skeletal muscle from cases of chronic juvenile and early adult spinal muscular atrophy (the Kugelberg-Welander syndrome)', *Journal of the Neurological Sciences*, 12(1), pp. 15–44.

Mathis, S. *et al.* (2019) 'Genetics of amyotrophic lateral sclerosis : A review', *Journal of the Neurological Sciences*, 399, pp. 217–226. doi: 10.1016/j.jns.2019.02.030.

Mattiazzi, M. *et al.* (2002) 'Mutated human SOD1 causes dysfunction of oxidative phosphorylation in mitochondria of transgenic mice', *Journal of Biological Chemistry*, 277(33), pp. 29626–29633. doi: 10.1074/jbc.M203065200.

Maxwell, G. K. *et al.* (2018) 'Developmental and degenerative cardiac defects in the Taiwanese mouse model of severe spinal muscular atrophy', *Journal of Anatomy*, 232(6), pp. 965–978. doi: 10.1111/joa.12793.

Maystadt, I. *et al.* (2006) 'A gene for an autosomal recessive lower motor neuron disease with childhood onset maps to 1p36', *Neurology*, 67(1), pp. 120–124. doi: 10.1212/01.wnl.0000223834.55225.2d.

Maystadt, I. *et al.* (2007) 'The Nuclear Factor kB-Activator Gene PLEKHG5 Is Mutated in a Form of Autosomal Recessive Lower Motor Neuron Disease with Childhood Onset', *Am. J. Hum. Genet*, 81(1), pp. 67–76. doi: 10.1086/518900.

McGivern, J. V *et al.* (2013) 'Spinal muscular atrophy astrocytes exhibit abnormal calcium regulation and reduced growth factor production', *Glia*, 61(9), pp. 1418–1428. doi: 10.1002/glia.22522.

Mcwhorter, M. L. *et al.* (2003) 'Knockdown of the survival motor neuron (Smn) protein in zebrafish causes defects in motor axon outgrowth and pathfinding', *The Journal of Cell Biology*. Rockefeller University Press, 162(5), pp. 919–931. doi: 10.1083/jcb.200303168.

McWhorter, M. L. *et al.* (2008) 'The SMN Binding Protein Gemin2 is not Involved in Motor

Axon Outgrowth', *Developmental Neurobiology*, 68(2), pp. 182–194. doi: 10.1002/dneu.20582.

Meinke, P. *et al.* (2014) 'Muscular Dystrophy-Associated SUN1 and SUN2 Variants Disrupt Nuclear-Cytoskeletal Connections and Myonuclear Organization', *PLoS Genet.* , 10(9), p. e1004605. doi: 10.1371/journal.pgen.1004605.

Melki, J. *et al.* (1990) 'Mapping of acute (type I) spinal muscular atrophy to chromosome 5q12-q14', *The Lancet*, 336(8710), pp. 271–273. doi: 10.1016/0140-6736(90)91803-I.

Mendell, J. R. *et al.* (2017) 'Single-Dose Gene-Replacement Therapy for Spinal Muscular Atrophy', *New England Journal of Medicine*, 377(18), pp. 1713–1722. doi: 10.1056/NEJMoa1706198.

Mendonça, D. M. F. *et al.* (2012) 'Neuroproteomics: an insight into ALS', *Neurological Research*, 34(10), pp. 937–943. doi: 10.1179/1743132812Y.0000000092.

Mentis, G. Z. *et al.* (2011) 'Early Functional Impairment of Sensory-Motor Connectivity in a Mouse Model of Spinal Muscular Atrophy', *Neuron*, 69, pp. 453–467. Available at: http://www.cell.com/neuron/pdf/S0896-6273(10)01080-9.pdf (Accessed: 20 March 2017).

Mercuri, E. *et al.* (2007) 'Randomized, double-blind, placebo-controlled trial of phenylbutyrate in spinal muscular atrophy', *Neurology*, 68(1), pp. 51–55. doi: 10.1212/01.wnl.0000249142.82285.d6.

Mercuri, E. *et al.* (2018) 'Nusinersen versus Sham Control in Later-Onset Spinal Muscular Atrophy', *New England Journal of Medicine*, 378(7), pp. 625–635. doi: 10.1056/NEJMoa1710504.

Mercuri, E., Bertini, E. and Iannaccone, S. T. (2012) 'Childhood spinal muscular atrophy: controversies and challenges', *Lancet Neurology*. Elsevier Ltd, 11(5), pp. 443–452. doi: 10.1016/S1474-4422(12)70061-3.

Miglino, N. *et al.* (2012) 'Calreticulin Is a Negative Regulator of Bronchial Smooth Muscle Cell Proliferation', *Journal of Allergy*, 2012, p. 783290. doi: 10.1155/2012/783290.

Miguel-Aliaga, I. *et al.* (2000) 'Disruption of SMN function by ectopic expression of the human SMN gene in Drosophila', *FEBS Letters*, 486, pp. 99–102. Available at: http://ac.els-cdn.com/S0014579300022432/1-s2.0-S0014579300022432-main.pdf?_tid=4f5c0bb6-0bc1-11e7-afb5-00000aab0f6b&acdnat=1489831234_096eadb7d4f8d8c04b2b239b38c4bbf1 (Accessed: 18 March 2017).

Miller, N. *et al.* (2016) 'Motor neuron mitochondrial dysfunction in spinal muscular atrophy', *Human Molecular Genetics*, 25(16), pp. 3395–3406. doi: 10.1093/hmg/ddw262.

Millino, C. *et al.* (2009) 'Different atrophy-hypertrophy transcription pathways in muscles affected by severe and mild spinal muscular atrophy', *BMC Medicine*, 7(14). doi: 10.1186/1741-7015-7-14.

Minsky, M. (1988) 'Memoir on Inventing the Confocal Scanning Microscope', *Scanning*, 10, pp. 128–138.

Mohseni, J. *et al.* (2016) 'Transcript, methylation and molecular docking analyses of the effects of HDAC inhibitors, SAHA and Dacinostat, on SMN2 expression in fibroblasts of SMA patients', *Journal of Human Genetics*. Nature Publishing Group, 61(9), pp. 823–830. doi: 10.1038/jhg.2016.61.

Mohseni, J., Zabidi-Hussin, Z. A. M. H. and Sasongko, T. H. (2013) 'Histone deacetylase inhibitors as potential treatment for spinal muscular atrophy', *Genetics and Molecular Biology*, 36(3), pp. 299–307. Available at: www.sbg.org.br (Accessed: 11 February 2020).

Monani, U. R. *et al.* (2000) 'The human centromeric survival motor neuron gene (SMN2) rescues embryonic lethality in Smn(-/-) mice and results in a mouse with spinal muscular atrophy.', *Human molecular genetics*, 9(3), pp. 333–339. doi: 10.1093/hmg/ddm236.

Monani, U. R. *et al.* (2003) 'A transgene carrying an A2G missense mutation in the SMN gene modulates phenotypic severity in mice with severe (type I) spinal muscular atrophy', *The Journal of Cell Biology*. Rockefeller University Press, 160(1), pp. 41–52. doi: 10.1083/jcb.200208079.

Monani, U. R. (2005) 'Spinal muscular atrophy: A deficiency in a ubiquitous protein; a motor neuron-specific disease', *Neuron*, 48(6), pp. 885–896. doi: 10.1016/j.neuron.2005.12.001.

Moore, N., Pollack, C. and Butkerait, P. (2015) 'Adverse drug reactions and drug–drug interactions with over-the-counter NSAIDs', *Therapeutics and Clinical Risk Management*, 11, pp. 1061–1075. doi: 10.2147/TCRM.S79135.

Mori, A. *et al.* (2010) 'Derlin-1 overexpression ameliorates mutant SOD1-induced endoplasmic reticulum stress by reducing mutant SOD1 accumulation', *Neurochemistry International*, 58, pp. 344–353. doi: 10.1016/j.neuint.2010.12.010.

Morris, G. E. (2008) 'The Cajal body', *Biochimica et Biophysica Acta*, 1783(11), pp. 2108–2115. doi: 10.1016/j.bbamcr.2008.07.016.

Moulin, V. *et al.* (2011) 'In Vitro Culture Methods of Skin Cells for Optimal Skin Reconstruction by Tissue Engineering', in Prof. Daniel Eberli (ed.) *Regenerative Medicine and Tissue Engineering - Cells and Biomaterials*. InTech, pp. 195–208. doi: 10.5772/20341.

Muqit, M. M. K. and Feany, M. B. (2002) 'Modelling neurodegenerative diseases in Drosophila: a fruitful approach?', *NATURE REVIEWS NEUROSCIENCE*, 3, pp. 237–243.

Murdocca, M. *et al.* (2012) 'IPLEX Administration Improves Motor Neuron Survival and Ameliorates Motor Functions in a Severe Mouse Model of Spinal Muscular Atrophy', *Molecular Medicine*, 8, pp. 1076–1085. doi: 10.2119/molmed.2012.00056.

Murgia, M. *et al.* (2015) 'Single muscle fiber proteomics reveals unexpected mitochondrial specialization', *EMBO reports*, 16(3), pp. 387–395. doi: 10.15252/embr.201439757.

Murray, L. M. *et al.* (2010) 'Pre-symptomatic development of lower motor neuron connectivity in a mouse model of severe spinal muscular atrophy', *Hum Mol Genet*, 19(3), pp. 420–433. doi: 10.1093/hmg/ddp506.

Murray, L. M. *et al.* (2015) 'Transcriptional profiling of differentially vulnerable motor neurons at pre-symptomatic stage in the Smn 2b / - mouse model of spinal muscular atrophy', *Acta Neuropathologica Communications*. Acta Neuropathologica Communications, 3(55), pp. 1–17. doi: 10.1186/s40478-015-0231-1.

Mutsaers, C. A. *et al.* (2013) 'Label-free proteomics identifies Calreticulin and GRP75/Mortalin as peripherally accessible protein biomarkers for spinal muscular atrophy', *Genome Med*, 5, p. 95. doi: 10.1186/gm498.

Naetar, N., Ferraioli, S. and Foisner, R. (2017) 'Lamins in the nuclear interior − life outside the lamina', *Journal of Cell Science*, 130, pp. 2087–2096. doi: 10.1242/jcs.203430.

Naganska, E. and Matyja, E. (2011) 'Amyotrophic lateral sclerosis - looking for pathogenesis and effective therapy.', *Folia neuropathologica*, 49(1). Available at: http://www.ncbi.nlm.nih.gov/pubmed/21455838 (Accessed: 23 May 2018).

Namavar, Y. *et al.* (2011) 'Clinical, neuroradiological and genetic findings in pontocerebellar hypoplasia', *Brain*, 134(1), pp. 143–156. doi: 10.1093/brain/awq287.

Narayanan, U. *et al.* (2004) 'Coupled in vitro import of U snRNPs and SMN, the spinal muscular atrophy protein', *Molecular Cell*, 16(2), pp. 223–234. doi: 10.1016/j.molcel.2004.09.024.

Nardo, G. *et al.* (2011) 'Amyotrophic lateral sclerosis multiprotein biomarkers in peripheral blood mononuclear cells', *PLoS ONE*, 6(10), p. e25545. doi: 10.1371/journal.pone.0025545.

Nash, L. A. *et al.* (2017) 'Survival Motor Neuron Protein is Released from Cells in Exosomes: A Potential Biomarker for Spinal Muscular Atrophy OPEN', *SCIENTIFIC REPORTS*, 7(13859). doi: 10.1038/s41598-017-14313-z.

Navarro, E. *et al.* (2015) 'Real-time PCR detection chemistry', *Clinica Chimica Acta*. Elsevier B.V., 439, pp. 231–250. doi: 10.1016/j.cca.2014.10.017.

Navon, R. *et al.* (1995) 'A new mutation in the hexa gene associated with a spinal muscular atrophy phenotype', *Neurology*, 45(3), pp. 539–543. doi: 10.1212/WNL.45.3.539.

Navon, R. *et al.* (1997) 'Juvenile-onset spinal muscular atrophy caused by compound heterozygosity for mutations in the HEXA gene', *Annals of Neurology*, 41(5), pp. 631–638. doi: 10.1002/ana.410410512.

Nery, F. C. *et al.* (2019) 'Impaired kidney structure and function in spinal muscular atrophy', *Neurol Genet*, 5, p. e353. doi: 10.1212/NXG.0000000000000353.

Von Neuhoff, N. *et al.* (2012) 'Monitoring CSF Proteome Alterations in Amyotrophic Lateral Sclerosis: Obstacles and Perspectives in Translating a Novel Marker Panel to the Clinic', *PLOS ONE*, 7(9), p. e44401. doi: 10.1371/journal.pone.0044401.

Neumann, M. *et al.* (2006) 'Ubiquitinated TDP-43 in frontotemporal lobar degeneration and amyotrophic lateral sclerosis', *Science*, 314(5796), pp. 130–133. doi: 10.1126/science.1134108.

Neveling, K. *et al.* (2013) 'Mutations in BICD2, which Encodes a Golgin and Important Motor Adaptor, Cause Congenital Autosomal-Dominant Spinal Muscular Atrophy', *The American Journal of Human Genetics*, 92, pp. 946–954. doi: 10.1016/j.ajhg.2013.04.011.

Ng, M. H. *et al.* (2009) 'Correlation of donor age and telomerase activity with in vitro cell growth and replicative potential for dermal fibroblasts and keratinocytes', *Journal of Tissue Viability*. Elsevier Ltd, 18(4), pp. 109–116. doi: 10.1016/j.jtv.2009.06.003.

Ng, S.-Y. *et al.* (2015) 'Genome-Wide RNA-Seq of Human Motor Neurons Implicates Selective ER Stress Activation in Spinal Muscular Atrophy', *Cell Stem Cell*, 17(5), pp. 569–584. doi: 10.1016/j.stem.2015.08.003.

Nguyen, M. thi *et al.* (2008) 'A two-site ELISA can quantify upregulation of SMN protein by drugs for spinal muscular atrophy', *Neurology*, 71(22), pp. 1757–1763. doi: 10.1212/01.wnl.0000313038.34337.b1.

Ning, K. *et al.* (2010) 'PTEN depletion rescues axonal growth defect and improves survival in SMN-deficient motor neurons', *Human Molecular Genetics*, 19(16), pp. 3159–3168. doi: 10.1093/hmg/ddq226.

Nishimura, A. L. *et al.* (2004) *A Mutation in the Vesicle-Trafficking Protein VAPB Causes Late-Onset Spinal Muscular Atrophy and Amyotrophic Lateral Sclerosis*, *Am. J. Hum. Genet*. doi: https://doi.org/10.1086/425287.

Nishitoh, H. *et al.* (2008) 'ALS-linked mutant SOD1 induces ER stress- and ASK1-dependent motor neuron death by targeting Derlin-1', *Genes and Development*, 22(11), pp. 1451–1464. doi: 10.1101/gad.1640108.

Niu, Q. *et al.* (2015) 'A NOVEL DYNC1H1 MUTATION CAUSING SPINAL MUSCULAR ATROPHY WITH LOWER EXTREMITY PREDOMINANCE', *Neurol Genet*, 1, p. e20. doi: 10.1212/NXG.0000000000000017.

Nölle, A. *et al.* (2011) 'The spinal muscular atrophy disease protein SMN is linked to the Rho-kinase pathway via profilin', *Human Molecular Genetics*, 20(24), pp. 4865–4878. doi: 10.1093/hmg/ddr425.

Nowicka, N. *et al.* (2019) 'Risk Factors and Emerging Therapies in Amyotrophic Lateral Sclerosis', *International Journal of Molecular Sciences*, 20(11), p. 2616. doi: 10.3390/ijms20112616.

Oates, E. C. *et al.* (2013) 'Mutations in BICD2 Cause Dominant Congenital Spinal Muscular Atrophy and Hereditary Spastic Paraplegia', *The American Journal of Human Genetics*, 92, pp. 965–973. doi: 10.1016/j.ajhg.2013.04.018.

Ogino, S. *et al.* (2002) 'Genetic risk assessment in carrier testing for spinal muscular atrophy', *American Journal of Medical Genetics*, 110(4), pp. 301–307. doi: 10.1002/ajmg.10425.

Oguz Akarsu, E. *et al.* (2016) 'Eyelid myoclonic status epilepticus: A rare phenotype in spinal muscular atrophy with progressive myoclonic epilepsy associated with ASAH1 gene mutation', *Seizure*, 42, pp. 49–51. doi: 10.1016/j.seizure.2016.09.007.

Ohuchi, K. *et al.* (2019) 'Notch signaling Mediates Astrocyte Abnormality in spinal Muscular Atrophy Model systems', *Scientific reports*, 9, p. 3701. doi: 10.1038/s41598-019-39788-w.

Oprea, G. E. *et al.* (2008) 'Plastin 3 Is a Protective Modifier of Autosomal Recessive Spinal Muscular Atrophy', *Science*, 320(5875), pp. 524–527. doi: 10.1126/science.1155085.

Ottesen, E. W. (2017) 'ISS-N1 makes the first FDA-approved drug for spinal muscular atrophy', *Translational Neuroscience*, 8(1), pp. 1–6. doi: 10.1515/tnsci-2017-0001.

Padula, M. P. *et al.* (2017) 'A Comprehensive Guide for Performing Sample Preparation and Top-Down Protein Analysis', *Proteomes*, 5(2), p. 11. doi: 10.3390/proteomes5020011.

Palacino, J. *et al.* (2015) 'SMN2 splice modulators enhance U1-pre-mRNA association and rescue SMA mice', *Nature Chemical Biology*, 11, pp. 511–517. doi: 10.1038/nCHeMBIO.1837.

Palamalai, V. and Miyagi, M. (2010) 'Mechanism of glyceraldehyde-3-phosphate dehydrogenase inactivation by tyrosine nitration', *PROTEIN SCIENCE*, 19(2), p. 255—262. doi: 10.1002/pro.311.

Palamiuc, L. *et al.* (2015) 'A metabolic switch toward lipid use in glycolytic muscle is an early pathologic event in a mouse model of amyotrophic lateral sclerosis', *EMBO Mol Med*, 7, pp. 526–546. doi: 10.15252/emmm.201404433.

Park, C. H. *et al.* (2005) 'Quercetin, a potent inhibitor against β-catenin/Tcf signaling in SW480 colon cancer cells', *Biochemical and Biophysical Research Communications*, 328(1), pp. 227–234. doi: 10.1016/j.bbrc.2004.12.151.

Pasinetti, G. M. *et al.* (2006) 'Identification of potential CSF biomarkers in ALS', *Neurology*, 66(8), pp. 1218–1222. doi: 10.1212/01.wnl.0000203129.82104.07.

Patitucci, T. N. and Ebert, A. D. (2016) 'SMN deficiency does not induce oxidative stress in SMA iPSC-derived astrocytes or motor neurons', *Human Molecular Genetics*, 25(3), pp. 514–523. doi: 10.1093/hmg/ddv489.

Pedersen, W. A. *et al.* (1998) 'Protein modification by the lipid peroxidation product 4-hydroxynonenal in the spinal cords of amyotrophic lateral sclerosis patients', *Annals of Neurology*. John Wiley & Sons, Ltd, 44(5), pp. 819–824. doi: 10.1002/ana.410440518.

Pedrotti, S. *et al.* (2010) 'The splicing regulator Sam68 binds to a novel exonic splicing silencer and functions in SMN2 alternative splicing in spinal muscular atrophy', *EMBO Journal*. Nature Publishing Group, 29(7), pp. 1235–1247. doi: 10.1038/emboj.2010.19.

Peeters, K. *et al.* (2013) 'Molecular Defects in the Motor Adaptor BICD2 Cause Proximal Spinal Muscular Atrophy with Autosomal-Dominant Inheritance', *The American Journal of Human Genetics*, 92, pp. 955–964. doi: 10.1016/j.ajhg.2013.04.013.

Peter, C. J. *et al.* (2011) 'The COPI vesicle complex binds and moves with survival motor neuron within axons', *Human Molecular Genetics*, 20(9), pp. 1701–1711. doi: 10.1093/hmg/ddr046.

Petri, S. *et al.* (2006) 'Loss of Fas ligand-function improves survival in G93A-transgenic ALS mice', *Journal of the Neurological Sciences*, 251(1–2), pp. 44–49. doi: 10.1016/j.jns.2006.08.013.

Pfaffl, M. W. (2001) 'A new mathematical model for relative quantification in real-time RT-PCR', *Nucleic acids research*, 29(9), p. e45. Available at: http://www.ncbi.nlm.nih.gov/pubmed/11328886 (Accessed: 19 November 2018).

Phillips, C. *et al.* (2016) 'Noradrenergic System in Down Syndrome and Alzheimer's Disease A Target for Therapy.', *Current Alzheimer research*, 13(1), pp. 68–83. Available at:

http://www.ncbi.nlm.nih.gov/pubmed/26391048 (Accessed: 29 September 2019).

Pierce, A. *et al.* (2008) 'GAPDH Is Conformationally and Functionally Altered in Association with Oxidative Stress in Mouse Models of Amyotrophic Lateral Sclerosis', *Journal of Molecular Biology*, 382, pp. 1195–1210. doi: 10.1016/j.jmb.2008.07.088.

Poesen, K. and Van Damme, P. (2019) 'Diagnostic and prognostic performance of neurofilaments in ALS', *Frontiers in Neurology*, 9(1167). doi: 10.3389/fneur.2018.01167.

Poirier, A. *et al.* (2018) 'Risdiplam distributes and increases SMN protein in both the central nervous system and peripheral organs', *Pharmacol Res Perspect.*, 6(6), p. e00447. doi: 10.1002/prp2.447.

Polaskova, V. *et al.* (2010) 'High-abundance protein depletion: Comparison of methods for human plasma biomarker discovery', *Electrophoresis*, 31(3), pp. 471–482. doi: 10.1002/elps.200900286.

Potter, H. and Heller, R. (2003) 'Transfection by Electroporation', *Curr Protoc Mol Biol.*, 62(1), pp. 9.3.1-9.3.6. doi: 10.1002/0471142727.mb0903s62.

Powis, R. A. *et al.* (2016) 'Systemic restoration of UBA1 ameliorates disease in spinal muscular atrophy', *JCI Insight*, 1(11), p. e87908. doi: 10.1172/jci.insight.87908.

Prather, R. S. *et al.* (2013) 'Genetically Engineered Pig Models for Human Diseases', *Annual Review of Animal Biosciences*, 1, pp. 203–219. doi: 10.1146/annurev-animal-031412-103715.

Preston, A. M. *et al.* (2009) 'Reduced endoplasmic reticulum (ER)-to-Golgi protein trafficking contributes to ER stress in lipotoxic mouse beta cells by promoting protein overload', *Diabetologia*, 52, pp. 2369–2373. doi: 10.1007/s00125-009-1506-5.

Prior, T. W. (2010) 'Spinal Muscular Atrophy: Newborn and Carrier Screening', *Obstetrics and Gynecology Clinics of North America*. Elsevier, pp. 23–36. doi: 10.1016/j.ogc.2010.03.001.

Pronicki, M. *et al.* (2010) 'A homozygous mutation in the SCO2 gene causes a spinal muscular

atrophy like presentation with stridor and respiratory insufficiency', *European Journal of Paediatric Neurology*, 14(3), pp. 253–260. doi: 10.1016/j.ejpn.2009.09.008.

Quek, C. and Hill, A. F. (2017) 'The role of extracellular vesicles in neurodegenerative diseases', *Biochemical and Biophysical Research Communications*, 483(4), pp. 1178–1186. doi: 10.1016/j.bbrc.2016.09.090.

Radonić, A. *et al.* (2004) 'Guideline to reference gene selection for quantitative real-time PCR.', *Biochemical and biophysical research communications*, 313(4), pp. 856–62. doi: 10.1016/j.bbrc.2003.11.177.

Rafuse, V. F., Polo-Parada, L. and Landmesser, L. T. (2000) 'Structural and functional alterations of neuromuscular junctions in NCAM-deficient mice', *Journal of Neuroscience*, 20(17), pp. 6529–6539. doi: 10.1523/jneurosci.20-17-06529.2000.

Rage, F. *et al.* (2013) 'Genome-wide identification of mRNAs associated with the protein SMN whose depletion decreases their axonal localization', *RNA*, 19(12), pp. 1755–1766. doi: 10.1261/rna.040204.113.

Raker, V. A. *et al.* (1999) *Spliceosomal U snRNP Core Assembly: Sm Proteins Assemble onto an Sm Site RNA Nonanucleotide in a Specific and Thermodynamically Stable Manner*, *MOLECULAR AND CELLULAR BIOLOGY*. Available at: http://mcb.asm.org/ (Accessed: 20 February 2020).

Ramser, J. *et al.* (2008) 'Rare Missense and Synonymous Variants in UBE1 Are Associated with X-Linked Infantile Spinal Muscular Atrophy', *American Journal of Human Genetics*, 82(1), pp. 188–193. doi: 10.1016/j.ajhg.2007.09.009.

Ranganathan, S. *et al.* (2005) 'Proteomic profiling of cerebrospinal fluid identifies biomarkers for amyotrophic lateral sclerosis', *J Neurochem.*, 95(5), pp. 1461–1471. doi: 10.1111/j.1471-4159.2005.03478.x.

Ranganathan, S. *et al.* (2007) 'Comparative proteomic profiling of cerebrospinal fluid between

living and post mortem ALS and control subjects', *Amyotroph Lateral Scler*, 8(6), pp. 373–379. doi: 10.1080/17482960701549681.

Raoul, C. *et al.* (2006) 'Chronic activation in presymptomatic amyotrophic lateral sclerosis (ALS) mice of a feedback loop involving Fas, Daxx, and FasL', *Proc Natl Acad Sci U S A*, 103(15), pp. 6007–6012. doi: 10.1073/pnas.0508774103.

Ravits, J. *et al.* (2013) 'Deciphering amyotrophic lateral sclerosis: What phenotype, neuropathology and genetics are telling us about pathogenesis', *Amyotrophic Lateral Sclerosis and Frontotemporal Degeneration*, 14(sup1), pp. 5–18. doi: 10.3109/21678421.2013.778548.

Renbaum, P. *et al.* (2009) 'Spinal Muscular Atrophy with Pontocerebellar Hypoplasia Is Caused by a Mutation in the VRK1 Gene', *The American Journal of Human Genetics*, 85, pp. 281–289. doi: 10.1016/j.ajhg.2009.07.006.

Rhodes, L. E. *et al.* (2009) 'Clinical features of spinal and bulbar muscular atrophy', *Brain*, 132, pp. 3242–3251. doi: 10.1093/brain/awp258.

Riessland, M. *et al.* (2006) 'The benzamide M344, a novel histone deacetylase inhibitor, significantly increases SMN2 RNA/protein levels in spinal muscular atrophy cells', *hum genet*, 120, pp. 101–110. doi: 10.1007/s00439-006-0186-1.

Riessland, M. *et al.* (2010) 'SAHA ameliorates the SMA phenotype in two mouse models for spinal muscular atrophy', *Human Molecular Genetics*, 19(8), pp. 1492–1506. doi: 10.1093/hmg/ddq023.

Riessland, M. *et al.* (2017) 'Neurocalcin Delta Suppression Protects against Spinal Muscular Atrophy in Humans and across Species by Restoring Impaired Endocytosis', *The American Journal of Human Genetics*, 100(2), pp. 297–315. doi: 10.1016/j.ajhg.2017.01.005.

Rindt, H. *et al.* (2015) 'Astrocytes influence the severity of spinal muscular atrophy', *Human Molecular Genetics*, 24(14), pp. 4094–4102. doi: 10.1093/hmg/ddv148.

Ririe, K. M., Rasmussen, R. P. and Wittwer, C. T. (1997) 'Product differentiation by analysis of DNA melting curves during the polymerase chain reaction', *Analytical Biochemistry*, 245(2), pp. 154–160. doi: 10.1006/abio.1996.9916.

Rochette, C. F., Gilbert, N. and Simard, L. R. (2001) 'SMN gene duplication and the emergence of the SMN2 gene occurred in distinct hominids: SMN2 is unique to Homo sapiens', *Human Genetics*, 108(3), pp. 255–266. doi: 10.1007/s004390100473.

Røe, A. T. *et al.* (2017) 'Increased passive stiffness promotes diastolic dysfunction despite improved Ca2+ handling during left ventricular concentric hypertrophy', *Cardiovascular Research*, 113, pp. 1161–1172. doi: 10.1093/cvr/cvx087.

Roos, M. *et al.* (2009) 'Malignant Ventricular Arrhythmia in a Case of Adult Onset of Spinal Muscular Atrophy (Kugelberg-Welander Disease)', *J Cardiovasc Electrophysiol*, 20, pp. 342–344. doi: 10.1111/j.1540-8167.2008.01327.x.

Rossoll, W. *et al.* (2003) 'Smn, the spinal muscular atrophy- determining gene product, modulates axon growth and localization of β-actin mRNA in growth cones of motoneurons', *The Journal of Cell Biology*, 163(4), pp. 801–812. doi: 10.1083/jcb.200304128.

Rossor, A. M. *et al.* (2015) 'Phenotypic and molecular insights into spinal muscular atrophy due to mutations in BICD2', *Brain*, 138, pp. 293–310. doi: 10.1093/brain/awu356.

Rozas, P. *et al.* (2017) 'The ER proteostasis network in ALS: Determining the differential motoneuron vulnerability', *Neuroscience Letters*. Elsevier Ireland Ltd, 636, pp. 9–15. doi: 10.1016/j.neulet.2016.04.066.

Rubboli, G. *et al.* (2015) 'Spinal muscular atrophy associated with progressive myoclonic epilepsy: A rare condition caused by mutations in ASAH1', *Epilepsia*, 56(5), pp. 692–698. doi: 10.1111/epi.12977.

Rudnik-Schöneborn, S. *et al.* (2007) 'Mutations of the LMNA gene can mimic autosomal

dominant proximal spinal muscular atrophy', *Neurogenetics*, 8(2), pp. 137–142. doi: 10.1007/s10048-006-0070-0.

Rudnik-Schöneborn, S. *et al.* (2010) 'Digital necroses and vascular thrombosis in severe spinal muscular atrophy', *Muscle and Nerve*, 42(1), pp. 144–147. doi: 10.1002/mus.21654.

Rudnik-Schöneborn, S. *et al.* (2012) 'SETX gene mutation in a family diagnosed autosomal dominant proximal spinal muscular atrophy', *Neuromuscular Disorders*, 22(3), pp. 258–262. doi: 10.1016/j.nmd.2011.09.006.

Rudnik-Schöneborn, S. *et al.* (2016) 'Autosomal dominant spinal muscular atrophy with lower extremity predominance: A recognizable phenotype of BICD2 mutations', *Muscle & Nerve*, 54(3), pp. 496–500. doi: 10.1002/mus.25114.

Ryberg, H. *et al.* (2010) 'Discovery and verification of amyotrophic lateral sclerosis biomarkers by proteomics', *Muscle & Nerve*, 42(1), pp. 104–111. doi: 10.1002/mus.21683.

Saal, L. *et al.* (2014) 'Subcellular transcriptome alterations in a cell culture model of spinal muscular atrophy point to widespread defects in axonal growth and presynaptic differentiation', *RNA*, 20(11), pp. 1789–1802. doi: 10.1261/rna.047373.114.

Sakamoto, S. *et al.* (2018) 'Enzyme-linked immunosorbent assay for the quantitative/qualitative analysis of plant secondary metabolites', *Journal of Natural Medicines*, 72, pp. 32–42. doi: 10.1007/s11418-017-1144-z.

Salazar-Anton, F., Tellez, A. and Lindh, J. (2012) 'Evaluation of an immunodot blot technique for the detection of antibodies against Taenia solium larval antigens', *Parasitology Research*, 110(6), pp. 2187–2191. doi: 10.1007/s00436-011-2747-z.

Salviati, L. *et al.* (2002) 'Cytochrome c Oxidase Deficiency Due to a Novel SCO2 Mutation Mimics Werdnig-Hoffmann Disease', *ARCH NEUROL*, 59, pp. 862–865.

Sanchez, G. *et al.* (2013) 'A novel function for the survival motoneuron protein as a

translational regulator', *Human Molecular Genetics*, 22(4), pp. 668–684. doi: 10.1093/hmg/dds474.

Sapan, C. V, Lundblad, R. L. and Price, N. C. (1999) 'Colorimetric protein assay techniques.', *Biotechnology and applied biochemistry*, 29 (Pt 2), pp. 99–108. doi: 10.1111/j.1470-8744.1999.tb00538.x.

Sareen, D. *et al.* (2012) 'Inhibition of apoptosis blocks human motor neuron cell death in a stem cell model of spinal muscular atrophy', *PLoS ONE*, 7(6), p. e39113. doi: 10.1371/journal.pone.0039113.

Sasaki, S. *et al.* (2001) 'Inducible Nitric Oxide Synthase (iNOS) and Nitrotyrosine Immunoreactivity in the Spinal Cords of Transgenic Mice with a G93A Mutant SOD1 Gene', *Journal of Neuropathology & Experimental Neurology*. Narnia, 60(9), pp. 839–846. doi: 10.1093/jnen/60.9.839.

Sasaki, S. and Iwata, M. (2007) 'Mitochondrial alterations in the spinal cord of patients with sporadic amyotrophic lateral sclerosis', *Journal of Neuropathology and Experimental Neurology*, 66(1), pp. 10–16. doi: 10.1097/nen.0b013e31802c396b.

Sawada, H. (2017) 'Clinical efficacy of edaravone for the treatment of amyotrophic lateral sclerosis', *Expert Opinion on Pharmacotherapy*. Taylor & Francis, 18(7), pp. 735–738. doi: 10.1080/14656566.2017.1319937.

Scaffidi, P. and Misteli, T. (2006) 'Lamin A-Dependent Nuclear Defects in Human Aging', *Science*, 312, pp. 1059–1063. Available at: http://science.sciencemag.org/content/312/5776/1059/tab-pdf (Accessed: 25 April 2017).

Schiaffino, S., Reggiani, C. and Murgia, M. (2019) 'Fiber type diversity in skeletal muscle explored by mass spectrometry-based single fiber proteomics.', *Histol Histopathol.*, p. 18170. doi: 10.14670/HH-18-170.

Schindelin, J. *et al.* (2012) 'Fiji: an open-source platform for biological-image analysis', *Nature Methods*. Nature Publishing Group, 9(7), pp. 676–682. doi: 10.1038/nmeth.2019.

Schleef, M. *et al.* (2006) 'Long-Term Stability Study and Topology Analysis of Plasmid DNA By Capillary Gel Electrophoresis', *BioProcess International*, 4(8), pp. 38–40. Available at: www.agilent.com (Accessed: 19 December 2019).

Schneider, A., Hommel, G. and Blettner, M. (2010) 'Linear regression analysis -', *Deutsches Ärzteblatt International*, 107(44), pp. 776–782. doi: 10.3238/arztebl.2010.0776.

Schorling, D. C., Pechmann, A. and Kirschner, J. (2020) 'Advances in Treatment of Spinal Muscular Atrophy – New Phenotypes, New Challenges, New Implications for Care', *Journal of Neuromuscular Diseases*, 7(1), pp. 1–13. doi: 10.3233/JND-190424.

Schrank, B. *et al.* (1997) 'Inactivation of the survival motor neuron gene, a candidate gene for human spinal muscular atrophy, leads to massive cell death in early mouse embryos', *Proc. Natl. Acad. Sci. USA*, 94, pp. 9920–9925. Available at: http://www.pnas.org/content/94/18/9920.full.pdf (Accessed: 20 March 2017).

Schreml, J. *et al.* (2012) 'Severe SMA mice show organ impairment that cannot be rescued by therapy with the HDACi JNJ-26481585', *European Journal of Human Genetics*, 21(10), pp. 643–652. doi: 10.1038/ejhg.2012.222.

Schwenk, B. M. *et al.* (2016) 'TDP-43 loss of function inhibits endosomal trafficking and alters trophic signaling in neurons', *The EMBO Journal*, 35(21), pp. 2350–2370. doi: 10.15252/embj.201694221.

Scoto, M. *et al.* (2015) 'Novel mutations expand the clinical spectrum of DYNC1H1-associated spinal muscular atrophy', *Neurology*, 84, pp. 668–679. Available at: http://sift.jcvi.org/ (Accessed: 27 November 2019).

Seksenyan, A. *et al.* (2010) 'Thymic involution, a co-morbidity factor in amyotrophic lateral

sclerosis', *Journal of Cellular and Molecular Medicine*, 14(10), pp. 2470–2482. doi: 10.1111/j.1582-4934.2009.00863.x.

Sen, A. *et al.* (2013) 'Genetic circuitry of Survival motor neuron, the gene underlying spinal muscular atrophy', *PNAS*, 110(26), pp. E2371–E2380. doi: 10.1073/pnas.1301738110.

Shababi, M. *et al.* (2010) 'Cardiac defects contribute to the pathology of spinal muscular atrophy models', *Human Molecular Genetics*, 19(20), pp. 4059–4071. doi: 10.1093/hmg/ddq329.

Shababi, M. *et al.* (2012) 'Partial restoration of cardio-vascular defects in a rescued severe model of spinal muscular atrophy', *Journal of Molecular and Cellular Cardiology*. Elsevier Ltd, 52(5), pp. 1074–1082. doi: 10.1016/j.yjmcc.2012.01.005.

Shababi, M., Lorson, C. L. and Rudnik-Schöneborn, S. S. (2014) 'Spinal muscular atrophy: A motor neuron disorder or a multi-organ disease?', *Journal of Anatomy*, 224(1), pp. 15–28. doi: 10.1111/joa.12083.

Shafey, D. *et al.* (2010) 'Identification of Novel Interacting Protein Partners of SMN Using Tandem Affinity Purification', *Journal of Proteome Research*, 9, pp. 1659–1669. doi: 10.1021/pr9006987.

Shafey, D., Côté, P. D. and Kothary, R. (2005) 'Hypomorphic Smn knockdown C2C12 myoblasts reveal intrinsic defects in myoblast fusion and myotube morphology', *Experimental Cell Research*, 311, pp. 49–61. doi: 10.1016/j.yexcr.2005.08.019.

Shanmugarajan, S. *et al.* (2009) 'Bone loss in survival motor neuron (Smn−/− SMN2) genetic mouse model of spinal muscular atrophy', *Journal of Pathology*, 219, pp. 52–60. doi: 10.1002/path.2566.

Sharma, A. *et al.* (2005) 'A role for complexes of survival of motor neurons (SMN) protein with gemins and profilin in neurite-like cytoplasmic extensions of cultured nerve cells',

Experimental Cell Research, 309(1), pp. 185–197. doi: 10.1016/j.yexcr.2005.05.014.

Sharma, A. *et al.* (2016) 'Cerebrospinal Fluid from Sporadic Amyotrophic Lateral Sclerosis Patients Induces Mitochondrial and Lysosomal Dysfunction', *Neurochemical Research*, 41(5), pp. 965–984. doi: 10.1007/s11064-015-1779-7.

Sheng, L. *et al.* (2018) 'Downregulation of Survivin contributes to cell-cycle arrest during postnatal cardiac development in a severe spinal muscular atrophy mouse model.', *Human molecular genetics*. Oxford University Press, 27(3), pp. 486–498. doi: 10.1093/hmg/ddx418.

Shimazawa, M. *et al.* (2010) 'An Inducer of VGF Protects Cells against ER Stress- Induced Cell Death and Prolongs Survival in the Mutant SOD1 Animal Models of Familial ALS', *PLoS ONE*, 5(12), p. e15307. doi: 10.1371/journal.pone.0015307.

Shin, J.-H. *et al.* (2005) 'Proteome analysis in hippocampus of mice overexpressing human Cu/Zn-superoxide dismutase 1', *Neurochemistry International*, 46(8), pp. 641–653. doi: 10.1016/j.neuint.2004.06.017.

Shorrock, H. K. *et al.* (2018) 'UBA1/GARS-dependent pathways drive sensory-motor connectivity defects in spinal muscular atrophy', *Brain*, 141(10), pp. 2878–2894. doi: 10.1093/brain/awy237.

Shorrock, H. K., Gillingwater, T. H. and Groen, E. J. N. (2018) 'Overview of Current Drugs and Molecules in Development for Spinal Muscular Atrophy Therapy', *Drugs*, 78, pp. 293–305. doi: 10.1007/s40265-018-0868-8.

Sieprath, T. *et al.* (2015) 'Sustained accumulation of prelamin A and depletion of lamin A/C both cause oxidative stress and mitochondrial dysfunction but induce different cell fates', *Nucleus*, 6(3), pp. 236--246. doi: 10.1080/19491034.2015.1050568.

Simic, G. (2008) 'Pathogenesis of proximal autosomal recessive spinal muscular atrophy', *Acta Neuropathologica*, 116(3), pp. 223–234. doi: 10.1007/s00401-008-0411-1.

Simonati, A. *et al.* (2011) 'TSEN54 mutation in a child with pontocerebellar hypoplasia type 1', *Acta Neuropathol*, 121, pp. 671–673. doi: 10.1007/s00401-011-0823-1.

Singh, M. *et al.* (2013) 'Lamin A/C Depletion Enhances DNA Damage-Induced Stalled Replication Fork Arrest', *Molecular and Cellular Biology*, 33(6), pp. 1210–1222. doi: 10.1128/MCB.01676-12.

Singh, N. K. *et al.* (2006) 'Splicing of a Critical Exon of Human Survival Motor Neuron Is Regulated by a Unique Silencer Element Located in the Last Intron', *MOLECULAR AND CELLULAR BIOLOGY*, 26(4), pp. 1333–1346. doi: 10.1128/MCB.26.4.1333-1346.2006.

Singh, R. N. *et al.* (2017) 'Diverse role of survival motor neuron protein', *Biochimica et Biophysica Acta*. Elsevier B.V., 1860(3), pp. 299–315. doi: 10.1016/j.bbagrm.2016.12.008.

Singh, R. N. and Singh, N. N. (2018) 'Mechanism of Splicing Regulation of Spinal Muscular Atrophy Genes', *Adv Neurobiol.*, 20, pp. 31–61. doi: 10.1007/978-3-319-89689-2_2.

Sison, S. L. *et al.* (2017) 'Astrocyte-produced miR-146a as a mediator of motor neuron loss in spinal muscular atrophy', *Human Molecular Genetics*, 26(17), pp. 3409–3420. doi: 10.1093/hmg/ddx230.

Sleigh, J. N. *et al.* (2011) 'A novel Caenorhabditis elegans allele, smn-1(cb131), mimicking a mild form of spinal muscular atrophy, provides a convenient drug screening platform highlighting new and pre-approved compounds', *Human Molecular Genetics*, 20(2), pp. 245–260. doi: 10.1093/hmg/ddq459.

Sleigh, J. N. *et al.* (2014) 'Chondrolectin affects cell survival and neuronal outgrowth in in vitro and in vivo models of spinal muscular atrophy', *Human Molecular Genetics*, 23(4), pp. 855–869. doi: 10.1093/hmg/ddt477.

Sleigh, J. N., Gillingwater, T. H. and Talbot, K. (2011) 'The contribution of mouse models to understanding the pathogenesis of spinal muscular atrophy.', *Disease models & mechanisms*,

4(4), pp. 457–467. doi: 10.1242/dmm.007245.

Smith, B. N. *et al.* (2015) 'Novel mutations support a role for Profilin 1 in the pathogenesis of ALS', *Neurobiology of Aging*. Elsevier Inc, 36(3), pp. 1602.e17-1602.e27. doi: 10.1016/j.neurobiolaging.2014.10.032.

Smith, P. K. *et al.* (1985) 'Measurement of protein using bicinchoninic acid', *Analytical Biochemistry*, 150(1), pp. 76–85. doi: 10.1016/0003-2697(85)90442-7.

Šoltić, D. *et al.* (2018) 'Multi-Study Proteomic and Bioinformatic Identification of Molecular Overlap between Amyotrophic Lateral Sclerosis (ALS) and Spinal Muscular Atrophy (SMA)', *Brain Sciences*, 8(12). doi: 10.3390/brainsci8120212.

Šoltić, D. *et al.* (2019) 'Lamin A/C dysregulation contributes to cardiac pathology in a mouse model of severe spinal muscular atrophy', *Human Molecular Genetics*, 28(21), pp. 3515–3527. doi: 10.1093/hmg/ddz195.

Somers, E. *et al.* (2016) 'Vascular Defects and Spinal Cord Hypoxia in Spinal Muscular Atrophy', *Annals of Neurology*, 79(2), pp. 217–230. doi: 10.1002/ana.24549.

Soo, K. Y. *et al.* (2015) 'Rab1-dependent ER-Golgi transport dysfunction is a common pathogenic mechanism in SOD1, TDP-43 and FUS-associated ALS', *Acta Neuropathologica*, 130(5), pp. 679–697. doi: 10.1007/s00401-015-1468-2.

Soubrouillard, C. *et al.* (1995) 'Expression of developmentally regulated cytoskeleton and cell surface proteins in childhood spinal muscular atrophies', *Journal of the Neurological Sciences*, 133(1–2), pp. 155–163. doi: 10.1016/0022-510X(95)00182-2.

La Spada, A. R. *et al.* (1991) 'Androgen receptor gene mutations in X-linked spinal and bulbar muscular atrophy', *Nature*, 352(6330), pp. 77–79. Available at: http://www.nature.com/doifinder/10.1038/352077a0%5Cnfile:///Articles/1991/Spada/Nature 1991 Spada.pdf%5Cnpapers3://publication/doi/10.1038/352077a0.

Stalekar, M. *et al.* (2015) 'Proteomic analyses reveal that loss of TDP-43 affects RNA processing and intracellular transport', *Neuroscience*, 293, pp. 157–170. doi: 10.1016/j.neuroscience.2015.02.046.

Staropoli, J. F. *et al.* (2015) 'Rescue of gene-expression changes in an induced mouse model of spinal muscular atrophy by an antisense oligonucleotide that promotes inclusion of SMN2 exon 7', *Genomics*. Academic Press Inc., 105(4), pp. 220–228. doi: 10.1016/j.ygeno.2015.01.007.

Staunton, L., Jockusch, H. and Ohlendieck, K. (2011) 'Proteomic analysis of muscle affected by motor neuron degeneration: the wobbler mouse model of amyotrophic lateral sclerosis', *Biochem Biophys Res Commun*, 406, pp. 595–600. doi: 10.1016/j.bbrc.2011.02.099.

Strey, C. W. *et al.* (2004) 'Dysregulation of stathmin, a microtubule-destabilizing protein, and up-regulation of Hsp25, Hsp27, and the antioxidant peroxiredoxin 6 in a mouse model of familial amyotrophic lateral sclerosis', *American Journal of Pathology*, 165(5), pp. 1701–1718. doi: 10.1016/S0002-9440(10)63426-8.

Strober, W. (2001) 'Trypan Blue Exclusion Test of Cell Viability', in *Current Protocols in Immunology*. John Wiley & Sons Inc., p. A.3B.1-A.3B.2. doi: 10.1002/0471142735.ima03bs21.

Sturm, S. *et al.* (2019) 'A phase 1 healthy male volunteer single escalating dose study of the pharmacokinetics and pharmacodynamics of risdiplam (RG7916, RO7034067), a *SMN2* splicing modifier', *British Journal of Clinical Pharmacology*. Blackwell Publishing Ltd, 85(1), pp. 181–193. doi: 10.1111/bcp.13786.

Sullivan, T. *et al.* (1999) 'Loss of A-type Lamin Expression Compromises Nuclear Envelope Integrity Leading to Muscular Dystrophy', *The Journal of Cell Biology*, 147(5), pp. 913–919. Available at: http://www.jcb.org (Accessed: 28 June 2017).

Sumner, C. J. and Crawford, T. O. (2018) 'Two breakthrough gene-targeted treatments for

spinal muscular atrophy: challenges remain', *Journal of Clinical Investigation*, 128(8), pp. 3219–3227. doi: 10.1172/JCI121658.

Sunyach, C. *et al.* (2012) 'Olesoxime delays muscle denervation, astrogliosis, microglial activation and motoneuron death in an ALS mouse model', *Neuropharmacology*. Elsevier Ltd, 62(7), pp. 2346–2353. doi: 10.1016/j.neuropharm.2012.02.013.

Swift, J. *et al.* (2013) 'Nuclear Lamin-A Scales with Tissue Stiffness and Enhances Matrix-Directed Differentiation', *Science*, 341, pp. 965–966. doi: 10.1126/science.1243643.

Swisher, J. F. A., Khatri, U. and Feldman, G. M. (2007) 'Annexin A2 is a soluble mediator of macrophage activation', *Journal of Leukocyte Biology*, 82(5), pp. 1174–1184. doi: 10.1189/jlb.0307154.

Swoboda, K. J. *et al.* (2009) 'Phase II Open Label Study of Valproic Acid in Spinal Muscular Atrophy', *PLoS ONE*, 4(5), p. e5268. doi: 10.1371/journal.pone.0005268.

Swoboda, K. J. *et al.* (2010) 'SMA CARNI-VAL Trial Part I: Double-Blind, Randomized, Placebo-Controlled Trial of L-Carnitine and Valproic Acid in Spinal Muscular Atrophy', *PLoS ONE*, 5(8), p. e12140. Available at: http://journals.plos.org/plosone/article/file?id=10.1371/journal.pone.0012140&type=printable (Accessed: 26 March 2017).

Szibor, M. *et al.* (2014) 'Remodeling and dedifferentiation of adult cardiomyocytes during disease and regeneration', *Cell. Mol. Life Sci*, 71(10), pp. 1907–1916. doi: 10.1007/s00018-013-1535-6.

Szklarczyk, D. *et al.* (2015) 'STRING v10: protein–protein interaction networks, integrated over the tree of life', *Nucleic Acids Research*, 43. doi: 10.1093/nar/gku1003.

Szklarczyk, D. *et al.* (2017) 'The STRING database in 2017: quality-controlled protein-protein association networks, made broadly accessible', *Nucleic Acids Research*, 45, pp. D362–D368.

doi: 10.1093/nar/gkw937.

Szunyogova, E. *et al.* (2016) 'Survival Motor Neuron (SMN) protein is required for normal mouse liver development', *Scientific reports*, 6, p. 34635. doi: 10.1038/srep34635.

Takahashi, K. *et al.* (2007) 'Induction of Pluripotent Stem Cells from Adult Human Fibroblasts by Defined Factors', *Cell*, 131, pp. 861–872. doi: 10.1016/j.cell.2007.11.019.

Tan, W., Pasinelli, P. and Trotti, D. (2014) 'Role of mitochondria in mutant SOD1 linked amyotrophic lateral sclerosis', *Biochim Biophys Acta*, 1842(8), pp. 1295–1301. doi: 10.1016/j.bbadis.2014.02.009.

Tanaka, M. *et al.* (1995) *Expression of the functional soluble form of human Fas ligand in activated lymphocytes*, *The EMBO Journal*. Available at: https://www.ncbi.nlm.nih.gov/pmc/articles/PMC398190/pdf/emboj00030-0083.pdf (Accessed: 8 August 2019).

Tarabal, O. *et al.* (2014) 'Mechanisms involved in spinal cord central synapse loss in a mouse model of spinal muscular atrophy', *Journal of Neuropathology and Experimental Neurology*, 73(6), pp. 519–535. doi: 10.1097/NEN.0000000000000074.

Taranum, S. *et al.* (2012) 'LINC complex alterations in DMD and EDMD/CMT fibroblasts', *European Journal of Cell Biology*, 91(8), pp. 614–628. doi: 10.1016/j.ejcb.2012.03.003.

Tarnopolsky, M. A. *et al.* (2004) 'Novel SCO2 mutation (G1521A) presenting as a spinal muscular atrophy type I phenotype', *American Journal of Medical Genetics*, 125A(3), pp. 310–314. doi: 10.1002/ajmg.a.20466.

Tarr, J. M. *et al.* (2010) 'A mechanism of release of calreticulin from cells during apoptosis', *J. Mol. Biol.*, 401(5), pp. 799–812. doi: 10.1016/j.jmb.2010.06.064.

Taylor, J. E. *et al.* (1998) 'Correlation of SMNt and SMNc gene copy number with age of onset and survival in spinal muscular atrophy', *European Journal of Human Genetics*, 6, pp. 467–474.

Available at: http://www.stockton-press.co.uk/ejhg (Accessed: 20 February 2020).

Tein, I. *et al.* (1995) 'Fatty acid oxidation abnormalities in childhood-onset spinal muscular atrophy: Primary or secondary defect(s)?', *Pediatric Neurology*, 12(1), pp. 21–30. doi: 10.1016/0887-8994(94)00100-G.

Thompson, A. G. *et al.* (2018) 'Cerebrospinal Fluid Macrophage Biomarkers in Amyotrophic Lateral Sclerosis', *Annals of Neurology*, 83(2), pp. 258–268. doi: 10.1002/ana.25143.

Thomson, A. K. *et al.* (2017) 'Survival of motor neurone protein is required for normal postnatal development of the spleen', *Journal of Anatomy*, 230, pp. 337–346. doi: 10.1111/joa.12546.

van Tienen, F. H. J. *et al.* (2019) 'Assessment of fibroblast nuclear morphology aids interpretation of LMNA variants', *European Journal of Human Genetics*, 27(3), pp. 389–399. doi: 10.1038/s41431-018-0294-0.

Ting, C.-H. *et al.* (2012) 'The spinal muscular atrophy disease protein SMN is linked to the Golgi network', *PLOS ONE*, 7(12), p. e51826. doi: 10.1371/journal.pone.0051826.

van Tintelen, J. P. *et al.* (2007) 'Severe Myocardial Fibrosis Caused by a Deletion of the 5' End of the Lamin A/C Gene', *Journal of the American College of Cardiology*, 49(25), pp. 2430–2439. doi: 10.1016/j.jacc.2007.02.063.

Tizzano, E. F. and Finkel, R. S. (2017) 'Spinal muscular atrophy: A changing phenotype beyond the clinical trials', *Neuromuscular Disorders*. Elsevier B.V., 27(10), pp. 883–889. doi: 10.1016/j.nmd.2017.05.011.

Torres-Benito, L. *et al.* (2019) 'NCALD Antisense Oligonucleotide Therapy in Addition to Nusinersen further Ameliorates Spinal Muscular Atrophy in Mice', *American Journal of Human Genetics*. Cell Press, 105(1), pp. 221–230. doi: 10.1016/j.ajhg.2019.05.008.

Towbin, J. A. *et al.* (2019) '2019 HRS expert consensus statement on evaluation, risk

stratification, and management of arrhythmogenic cardiomyopathy', *Heart Rhythm*, 16(11), pp. e301–e372. doi: 10.1016/j.hrthm.2019.05.007.

Tsai, L.-K. *et al.* (2012) 'IGF-1 delivery to CNS attenuates motor neuron cell death but does not improve motor function in type III SMA mice', *Neurobiology of Disease*, 45, pp. 272–279. doi: 10.1016/j.nbd.2011.06.021.

Tsai, L.-K. *et al.* (2014) 'Systemic administration of a recombinant AAV1 vector encoding IGF-1 improves disease manifestations in SMA mice', *Molecular Therapy*, 22(8), pp. 1450–1459. doi: 10.1038/mt.2014.84.

Tsai, M. S. *et al.* (2006) 'Abolishing Bax-Dependent Apoptosis Shows Beneficial Effects on Spinal Muscular Atrophy Model Mice', *Molecular Therapy*, 13(6), pp. 1149–1155. doi: 10.1016/j.ymthe.2006.02.008.

Tsurusaki, Y. *et al.* (2012) 'A DYNC1H1 mutation causes a dominant spinal muscular atrophy with lower extremity predominance', *Neurogenetics*, 13, pp. 327–332. doi: 10.1007/s10048-012-0337-6.

Tu, W.-Y. *et al.* (2017) 'Spinal muscular atrophy: Factors that modulate motor neurone vulnerability', *Neurobiology of Disease*, 102, pp. 11–20. doi: 10.1016/j.nbd.2017.01.011.

Turner, B. J. *et al.* (2009) 'Survival motor neuron deficiency enhances progression in an amyotrophic lateral sclerosis mouse model', *Neurobiology of Disease*, 34, pp. 511–517. doi: 10.1016/j.nbd.2009.03.005.

Turner, B. J. *et al.* (2014) 'Overexpression of survival motor neuron improves neuromuscular function and motor neuron survival in mutant SOD1 mice', *Neurobiology of Aging*, 35, pp. 906–915. doi: 10.1016/j.neurobiolaging.2013.09.030.

Turner, B. J. and Talbot, K. (2008) 'Transgenics, toxicity and therapeutics in rodent models of mutant SOD1-mediated familial ALS', *Progress in Neurobiology*, 85, pp. 94–134. doi:

10.1016/j.pneurobio.2008.01.001.

Umoh, M. E. *et al.* (2018) 'A proteomic network approach across the ALS-FTD disease spectrum resolves clinical phenotypes and genetic vulnerability in human brain', *EMBO Molecular Medicine*, 10(1), pp. 48–62. doi: 10.15252/emmm.201708202.

Uzunalli, G. *et al.* (2015) 'Effects of flavonoid quercetin on survival of motor neuron gene expression', *Cell Biology International*, 39(3), pp. 350–354. doi: 10.1002/cbin.10395.

Vai, S. *et al.* (2015) 'Bone and Spinal Muscular Atrophy', *Bone*. Elsevier Inc., 79, pp. 116–120. doi: 10.1016/j.bone.2015.05.039.

Varghese, A. M. *et al.* (2013) 'Chitotriosidase-a putative biomarker for sporadic amyotrophic lateral sclerosis', *Clinical Proteomics*, 10(19). doi: 10.1186/1559-0275-10-19.

Verstraeten, V. L. R. M. *et al.* (2008) 'Increased mechanosensitivity and nuclear stiffness in Hutchinson-Gilford progeria cells: Effects of farnesyltransferase inhibitors', *Aging Cell*, 7(3), pp. 383–393. doi: 10.1111/j.1474-9726.2008.00382.x.

Vielhaber, S. *et al.* (2000) 'Mitochondrial DNA abnormalities in skeletal muscle of patients with sporadic amyotrophic lateral sclerosis', *Brain*, 123(7), pp. 1339–1348. doi: 10.1093/brain/123.7.1339.

De Vivo, D. C. *et al.* (2019) 'Nusinersen initiated in infants during the presymptomatic stage of spinal muscular atrophy: Interim efficacy and safety results from the Phase 2 NURTURE study', *Neuromuscular Disorders*. Elsevier B.V., 29(11), pp. 842–856. doi: 10.1016/j.nmd.2019.09.007.

Wadman, R. I. *et al.* (2016) 'A Comparative Study of SMN Protein and mRNA in Blood and Fibroblasts in Patients with Spinal Muscular Atrophy and Healthy Controls', *PLoS ONE*, 11(11), p. e0167087. doi: 10.1371/journal.pone.0167087.

Wagner, E. M. (2013) 'Monitoring Gene Expression: Quantitative Real-Time RT-PCR', in Freeman, L. A. (ed.) *Lipoproteins and Cardiovascular Disease: Methods and Protocols*. Springer

Science+Business Media, pp. 19–45.

Waldrop, M. A. and Kolb, S. J. (2019) 'Current Treatment Options in Neurology-SMA Therapeutics', *Curr Treat Options Neurol*, 21(6), p. 25. doi: 10.1007/s11940-019-0568-z.

Walker, A. K. *et al.* (2013) 'ALS-Associated TDP-43 Induces Endoplasmic Reticulum Stress, Which Drives Cytoplasmic TDP-43 Accumulation and Stress Granule Formation', *PLOS ONE*, 8(11), p. e81170. doi: 10.1371/journal.pone.0081170.

Wan, J. *et al.* (2012) 'Mutations in the RNA exosome component gene EXOSC3 cause pontocerebellar hypoplasia and spinal motor neuron degeneration', *Nat Genet*, 44(6), pp. 704–708. doi: 10.1038/ng.2254.

Wang, L.-T. *et al.* (2014) 'Survival of motor neuron protein downregulates miR-9 expression in patients with spinal muscular atrophy', *Kaohsiung Journal of Medical Sciences*, 30, pp. 229–234. doi: 10.1016/j.kjms.2013.12.007.

Wang, L., Gutmann, D. H. and Roos, R. P. (2011) 'Astrocyte loss of mutant SOD1 delays ALS disease onset and progression in G85R transgenic mice', *Human Molecular Genetics*, 20(2), pp. 286–293. doi: 10.1093/hmg/ddq463.

Wang, Z.-B., Zhang, X. and Li, X.-J. (2013) 'Recapitulation of spinal motor neuron-specific disease phenotypes in a human cell model of spinal muscular atrophy', *Cell Research*, 23(3), pp. 378–393. doi: 10.1038/cr.2012.166.

Wanga, R. E. *et al.* (2011) 'Biotinylated Quercetin as an Intrinsic Photoaffinity Proteomics Probe for the Identification of Quercetin Target Proteins', *Bioorg Med Chem.*, 19(16), pp. 4710–4720. doi: 10.1016/j.bmc.2011.07.005.

Wasserman, H. M. *et al.* (2017) 'Low bone mineral density and fractures are highly prevalent in pediatric patients with spinal muscular atrophy regardless of disease severity', *Neuromuscul Disord*, 27(4), pp. 331–337. doi: 10.1016/j.nmd.2017.01.019.

Welinder, C. and Ekblad, L. (2010) 'Coomassie Staining as Loading Control in Western Blot Analysis', *J. Proteome Res*, 10, pp. 1416–1419. doi: 10.1021/pr1011476.

Wertz, M. H. *et al.* (2016) 'Cell-type-specific miR-431 dysregulation in a motor neuron model of spinal muscular atrophy', *Human Molecular Genetics*, 0(0), pp. 1–14. doi: 10.1093/hmg/ddw084.

Wiedemann, F. R. *et al.* (1998) 'Impairment of mitochondrial function in skeletal muscle of patients with amyotrophic lateral sclerosis', *Journal of Neurological Sciences*, 156, pp. 65–72.

Wiedemann, F. R. *et al.* (2002) 'Mitochondrial DNA and respiratory chain function in spinal cords of ALS patients', *Journal of Neurochemistry*, 80(4), pp. 616–625. doi: 10.1046/j.0022-3042.2001.00731.x.

Wijngaarde, C. A. *et al.* (2017) 'Cardiac pathology in spinal muscular atrophy: a systematic review', *Orphanet Journal of Rare Diseases*. Orphanet Journal of Rare Diseases, 12(1), p. 67. doi: 10.1186/s13023-017-0613-5.

Williamson, T. L. *et al.* (1998) *Absence of neurofilaments reduces the selective vulnerability of motor neurons and slows disease caused by a familial amyotrophic lateral sclerosis-linked superoxide dismutase 1 mutant*, *Proc. Natl. Acad. Sci. USA*. doi: 10.1073/pnas.95.16.9631.

Wilson, E. L., Garton, M. and Fuller, H. R. (2016) 'Anti-epileptic drugs and bone loss: Phenytoin reduces pro-collagen I and alters the electrophoretic mobility of osteonectin in cultured bone cells', *Epilepsy Research*. Elsevier B.V., 122, pp. 97–101. doi: 10.1016/j.eplepsyres.2016.03.002.

Winkler, C. *et al.* (2005) 'Reduced U snRNP assembly causes motor axon degeneration in an animal model for spinal muscular atrophy', *Genes and Development*, 19, pp. 2320–2330. doi: 10.1101/gad.342005.

Wirth, B. *et al.* (1999) 'Quantitative analysis of survival motor neuron copies: identification of

subtle SMN1 mutations in patients with spinal muscular atrophy, genotype-phenotype correlation, and implications for genetic counseling', *American journal of human genetics*, 64(5), pp. 1340–1356. doi: S0002-9297(07)62279-4 [pii]\n10.1086/302369.

Wirth, B. *et al.* (2006) 'Mildly affected patients with spinal muscular atrophy are partially protected by an increased SMN2 copy number', *Hum Genet*, 119, pp. 422–428. doi: 10.1007/s00439-006-0156-7.

Wirth, B., Brichta, L. and Hahnen, E. (2006) 'Spinal Muscular Atrophy: From Gene to Therapy', *Seminars in Pediatric Neurology*, 13(2), pp. 121–131. doi: 10.1016/j.spen.2006.06.008.

Wirth, B., Garbes, L. and Riessland, M. (2013) 'How genetic modifiers influence the phenotype of spinal muscular atrophy and suggest future therapeutic approaches', *Current Opinion in Genetics and Development*. Elsevier Ltd, 23(3), pp. 330–338. doi: 10.1016/j.gde.2013.03.003.

Wishart, T. M. *et al.* (2010) 'SMN deficiency disrupts brain development in a mouse model of severe spinal muscular atrophy.', *Human molecular genetics*, 19(21), pp. 4216–28. doi: 10.1093/hmg/ddq340.

Wishart, T. M. *et al.* (2014) 'Dysregulation of ubiquitin homeostasis and β-catenin signaling promote spinal muscular atrophy', *The Journal of Clinical Investigation*, 124(4), pp. 1821–1834. doi: 10.1172/JCI71318DS1.

Wolf, K. *et al.* (2013) 'Physical limits of cell migration: control by ECM space and nuclear deformation and tuning by proteolysis and traction force.', *The Journal of cell biology*. The Rockefeller University Press, 201(7), pp. 1069–1084. doi: 10.1083/jcb.201210152.

Woll, M. G. *et al.* (2016) 'Discovery and Optimization of Small Molecule Splicing Modifiers of Survival Motor Neuron 2 as a Treatment fr Spinal Muscular Atrophy', *J. Med. Chem.*, 59, pp. 6070–6085. doi: 10.1021/acs.jmedchem.6b00460.

Wong, M. and Martin, L. J. (2010) 'Skeletal muscle-restricted expression of human SOD1

causes motor neuron degeneration in transgenic mice', *Human Molecular Genetics*, 19(11), pp. 2284–2302. doi: 10.1093/hmg/ddq106.

Wong, N. K. Y., He, B. P. and Strong, M. J. (2000) *Characterization of Neuronal Intermediate Filament Protein Expression in Cervical Spinal Motor Neurons in Sporadic Amyotrophic Lateral Sclerosis (ALS)00*, *Journal of Neuropathology and Experimental Neurology*. doi: 10.1093/jnen/59.11.972.

Workman, E. *et al.* (2009) 'A SMN missense mutation complements SMN2 restoring snRNPs and rescuing SMA mice', *Human Molecular Genetics*, 18(12), pp. 2215–2229. doi: 10.1093/hmg/ddp157.

Wu, C. *et al.* (2012) 'Mutations in the Profilin 1 Gene Cause Familial Amyotrophic Lateral Sclerosis', *Nature*, 488(7412), pp. 499–503. doi: 10.1038/nature11280.

Yamanaka, K. *et al.* (2011) 'Astrocytes as determinants of disease progression in inherited ALS', *Nature Neuroscience*, 11(3), pp. 251–253. doi: 10.1038/nn2047.Astrocytes.

Yamatani, H. *et al.* (2010) 'Proteomics analysis of the temporal changes in axonal proteins during maturation', *Developmental Neurobiology*. John Wiley & Sons, Ltd, 70(7), pp. 523–537. doi: 10.1002/dneu.20794.

Yamazaki, T. *et al.* (2012) 'FUS-SMN protein interactions link the motor neuron diseases ALS and SMA', *Cell Rep.*, 2(4), pp. 799–806. doi: 10.1016/j.celrep.2012.08.025.

Yang, C. *et al.* (2016) 'Mutant PFN1 causes ALS phenotypes and progressive motor neuron degeneration in mice by a gain of toxicity', *PNAS*, 113(41), pp. E6209–E6218. doi: 10.1073/pnas.1605964113.

Yang, L. *et al.* (2013) 'Involvement of miR-9/MCPIP1 axis in PDGF-BB-mediated neurogenesis in neuronal progenitor cells', *Cell Death and Disease*. Nature Publishing Group, 4(12), p. e960. doi: 10.1038/cddis.2013.486.

Yang, Y. *et al.* (2009) 'Pre-synaptic regulation of astroglial excitatory neurotransmitter transporter GLT1', *Neuron*, 61(6), pp. 880–894. doi: 10.1016/j.neuron.2009.02.010.

Yasuma, F., Kuru, S. and Konagaya, M. (2004) 'Dilated Cardiomyopathy in Kugelberg-Welander Disease: Coexisting Sleep Disordered Breathing and Its Treatment with Continuous Positive Airway Pressure', *Internal Medicine*, 43(10), pp. 951–954.

Ye, J. *et al.* (2012) 'Primer-BLAST: A tool to design target-specific primers for polymerase chain reaction', *BMC Bioinformatics*, 13, p. 134. Available at: http://www.biomedcentral.com/1471-2105/13/134 (Accessed: 29 December 2019).

Yildiz, E. P. *et al.* (2018) 'Spinal muscular atrophy with progressive myoclonic epilepsy linked to mutations in ASAH1', *Clinical Neurology and Neurosurgery*. Elsevier B.V., 164, pp. 47–49. doi: 10.1016/j.clineuro.2017.11.008.

Yoshida, M. *et al.* (2015) 'Modeling the early phenotype at the neuromuscular junction of spinal muscular atrophy using patient-derived iPSCs', *Stem Cell Reports*. The Authors, 4, pp. 561–568. doi: 10.1016/j.stemcr.2015.02.010.

Young, P. J. *et al.* (2000) 'The Relationship between SMN, the spinal muscular atrophy protein, and nuclear coiled bodies in differentiated tissues and cultured cells', *Experimental Cell Research*, 256(2), pp. 365–374. doi: 10.1006/excr.2000.4858.

Young, P. J. *et al.* (2002) *SRp30c-dependent stimulation of survival motor neuron (SMN) exon 7 inclusion is facilitated by a direct interaction with hTra2β1*, *Human Molecular Genetics*.

Zahr, H. C. and Jaalouk, D. E. (2018) 'Exploring the Crosstalk Between LMNA and Splicing Machinery Gene Mutations in Dilated Cardiomyopathy', *Front. Genet*, 9(231). doi: 10.3389/fgene.2018.00231.

Zarei, S. *et al.* (2015) 'A comprehensive review of amyotrophic lateral sclerosis.', *Surgical neurology international*. Wolters Kluwer -- Medknow Publications, 6, p. 171. doi:

10.4103/2152-7806.169561.

Zelano, J. *et al.* (2006) 'Expression of nectin-1, nectin-3, N-cadherin, and NCAM in spinal motoneurons after sciatic nerve transection', *Experimental Neurology*, 201(2), pp. 461–469. doi: 10.1016/j.expneurol.2006.04.026.

Zerres, Klaus; Rudnik-Schöneborn, S. (1995) 'Natural History in Proximal Spinal Muscular Atrophy. Clinical Analysis of 445 Patients and Suggestions for a Modification of Existing Classifications', *Arch Neurol*, 52, pp. 518–523.

Zhang, H. L. *et al.* (2003) 'Active transport of the survival motor neuron protein and the role of exon-7 in cytoplasmic localization', *J. Neurosci.*, 23(16), pp. 6627–6637. doi: 23/16/6627 [pii].

Zhang, Z. *et al.* (2008) 'SMN Deficiency Causes Tissue-Specific Perturbations in the Repertoire of snRNAs and Widespread Defects in Splicing', *Cell*, 133(4), pp. 585–600. doi: 10.1016/j.cell.2008.03.031.

Zhang, Z. *et al.* (2013) 'Dysregulation of synaptogenesis genes antecedes motor neuron pathology in spinal muscular atrophy.', *PNAS*, 110(48), pp. 19348–19353. doi: 10.1073/pnas.1319280110.

Zhao, Z. *et al.* (2008) 'Vgf is a novel biomarker associated with muscle weakness in amyotrophic lateral sclerosis (ALS), with a potential role in disease pathogenesis', *Int. J. Med. Sci*, 5(2), pp. 92–99. Available at: https://www.ncbi.nlm.nih.gov/pmc/articles/PMC2323610/pdf/ijmsv05p0092.pdf (Accessed: 12 June 2018).

Zhong, Z. *et al.* (2012) 'Chondrolectin Mediates Growth Cone Interactions of Motor Axons with an Intermediate Target', *The Journal of Neuroscience*, 32(13), pp. 4426–4439. doi: 10.1523/JNEUROSCI.5179-11.2012.

Zhou, J.-Y. *et al.* (2010) 'Galectin-3 is a candidate biomarker for ALS: Discovery by a proteomics approach', *J Proteome Res.*, 9(10), pp. 5133–5141. doi: 10.1021/pr100409r.

Zhou, J. *et al.* (2012) 'Spinal Muscular Atrophy Associated with Progressive Myoclonic Epilepsy Is Caused by Mutations in ASAH1', *The American Journal of Human Genetics*, 91, pp. 5–14. doi: 10.1016/j.ajhg.2012.05.001.

Zhu, Y. *et al.* (2018) 'Aberrant Levels of Cystatin C in Amyotrophic Lateral Sclerosis: a Systematic Review and Meta Analysis', *International Journal of Biological Sciences*, 14(9), pp. 1041–1053. doi: 10.7150/ijbs.25711.

Zonderland, J. *et al.* (2019) 'Dimensionality changes actin network through lamin A and C and zyxin'. doi: 10.1101/752691.

Appendix

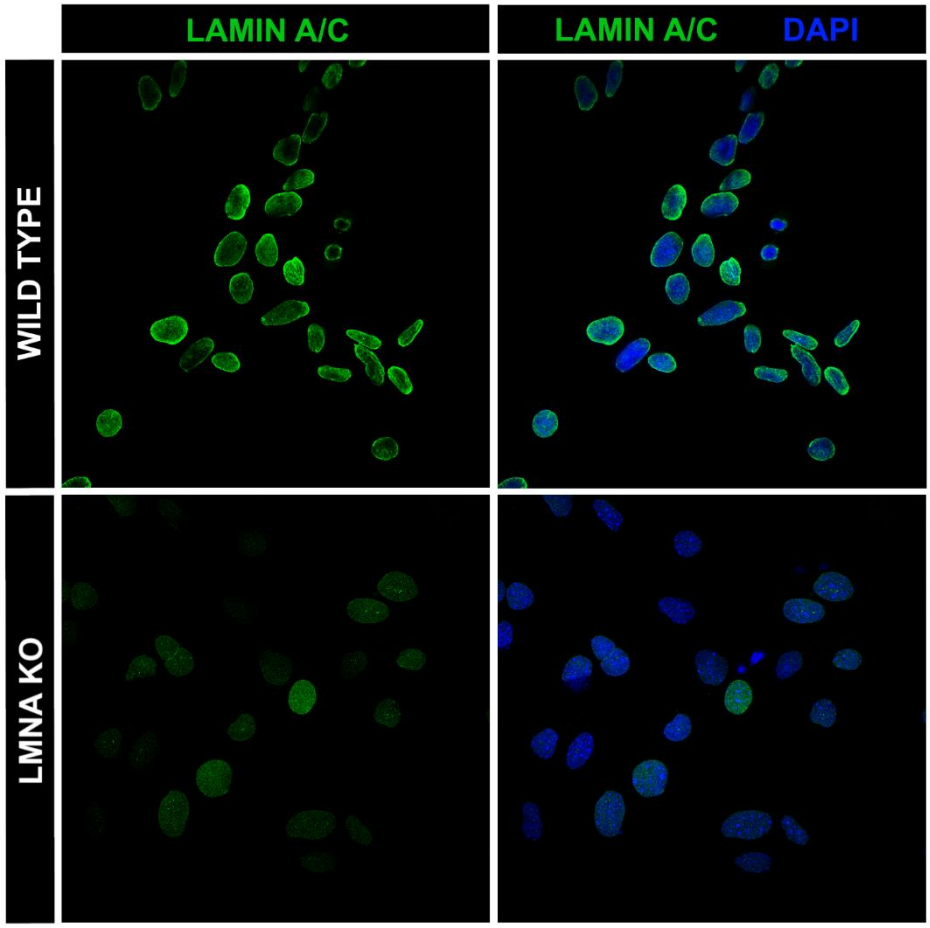

Appendix 1. MANLAC 4A7 cross-reaction in *LMNA* KO MEFs. Representative immunocytochemistry images showing lamin A/C staining in wild type and *LMNA* KO cells, with DAPI shown in blue.

Appendix 2. Proteins that were differentially expressed when SMA and control mouse heart tissue extracts were quantitatively compared using iTRAQ mass spectrometry

Accession	Name	Peptides (95%)	Fold change (SMA:CTR)	p-value (SMA:CTR)	EF (SMA:CTR)
INCREASED EXPRESSION					
sp|Q6ZQH8|NU188_MOUSE	Nucleoporin NUP188 homolog OS=Mus musculus GN=Nup188 PE=1 SV=2	3	99.083	0.036	1.000
sp|Q62219|TGFI1_MOUSE	Transforming growth factor beta-1-induced transcript 1 protein OS=Mus musculus GN=Tgfb1i1 PE=1 SV=2	2	99.083	0.032	1.000
sp|Q9Z0P4|PALM_MOUSE	Paralemmin-1 OS=Mus musculus GN=Palm PE=1 SV=1	3	99.083	0.020	1.000
sp|O54946|DNJB6_MOUSE	DnaJ homolog subfamily B member 6 OS=Mus musculus GN=Dnajb6 PE=1 SV=4	3	99.083	0.020	1.000
sp|P39655|LOX12_MOUSE	Arachidonate 12-lipoxygenase, 12S-type OS=Mus musculus GN=Alox12 PE=1 SV=4	3	99.083	0.019	1.000
sp|P11798|KCC2A_MOUSE	Calcium/calmodulin-dependent protein kinase type II subunit alpha OS=Mus musculus GN=Camk2a PE=1 SV=2	9	99.083	0.019	1.000
sp|Q8BFS6|CPPED_MOUSE	Calcineurin-like phosphoesterase domain-containing protein 1 OS=Mus musculus GN=Cpped1 PE=2 SV=1	5	99.083	0.018	1.000
sp|P62627|DLRB1_MOUSE	Dynein light chain roadblock-type 1 OS=Mus musculus GN=Dynlrb1 PE=1 SV=3	2	87.902	0.021	2.291
sp|Q9D6V8|PAIP2_MOUSE	Polyadenylate-binding protein-interacting protein 2 OS=Mus musculus GN=Paip2 PE=2 SV=1	3	87.902	0.021	2.291
sp|O08734|BAK_MOUSE	Bcl-2 homologous antagonist/killer OS=Mus musculus GN=Bak1 PE=1 SV=2	2	87.902	0.020	2.291
sp|Q7TSQ8|PDPR_MOUSE	Pyruvate dehydrogenase phosphatase regulatory subunit, mitochondrial OS=Mus musculus GN=Pdpr PE=2 SV=1	3	87.902	0.020	2.291
sp|Q91WV0|NC2B_MOUSE	Protein Dr1 OS=Mus musculus GN=Dr1 PE=2 SV=1	2	87.902	0.020	2.291
sp|P61967|AP1S1_MOUSE	AP-1 complex subunit sigma-1A OS=Mus musculus GN=Ap1s1 PE=1 SV=1	3	87.902	0.020	2.291
sp|Q9Z1K6|ARI2_MOUSE	E3 ubiquitin-protein ligase ARIH2 OS=Mus musculus GN=Arih2 PE=2 SV=1	2	87.902	0.020	2.291

sp|Q924C1|XPO5_MOUSE	Exportin-5 OS=Mus musculus GN=Xpo5 PE=2 SV=1	4	87.902	0.020	2.291
sp|Q8C7R4|UBA6_MOUSE	Ubiquitin-like modifier-activating enzyme 6 OS=Mus musculus GN=Uba6 PE=1 SV=1	3	87.902	0.019	2.291
sp|Q61210|ARHG1_MOUSE	Rho guanine nucleotide exchange factor 1 OS=Mus musculus GN=Arhgef1 PE=1 SV=2	3	87.902	0.019	2.291
sp|Q62193|RFA2_MOUSE	Replication protein A 32 kDa subunit OS=Mus musculus GN=Rpa2 PE=1 SV=1	2	87.902	0.019	2.291
sp|Q9DCG9|TR112_MOUSE	tRNA methyltransferase 112 homolog OS=Mus musculus GN=Trmt112 PE=2 SV=1	2	87.902	0.019	2.291
sp|P70333|HNRH2_MOUSE	Heterogeneous nuclear ribonucleoprotein H2 OS=Mus musculus GN=Hnrnph2 PE=1 SV=1	18	87.902	0.019	2.291
sp|P12265|BGLR_MOUSE	Beta-glucuronidase OS=Mus musculus GN=Gusb PE=2 SV=2	3	87.902	0.019	2.291
sp|Q60649|CLPB_MOUSE	Caseinolytic peptidase B protein homolog OS=Mus musculus GN=Clpb PE=1 SV=1	2	87.902	0.019	2.291
sp|P84096|RHOG_MOUSE	Rho-related GTP-binding protein RhoG OS=Mus musculus GN=Rhog PE=2 SV=1	2	87.902	0.018	2.291
sp|Q61646|HPT_MOUSE	Haptoglobin OS=Mus musculus GN=Hp PE=1 SV=1	2	87.902	0.018	2.291
sp|Q9JLN9|MTOR_MOUSE	Serine/threonine-protein kinase mTOR OS=Mus musculus GN=Mtor PE=1 SV=2	8	87.902	0.018	2.291
sp|P61458|PHS_MOUSE	Pterin-4-alpha-carbinolamine dehydratase OS=Mus musculus GN=Pcbd1 PE=1 SV=2	3	87.096	0.021	2.270
sp|Q91WG2|RABE2_MOUSE	Rab GTPase-binding effector protein 2 OS=Mus musculus GN=Rabep2 PE=2 SV=3	2	87.096	0.018	2.270
sp|Q3SXD3|HDDC2_MOUSE	HD domain-containing protein 2 OS=Mus musculus GN=Hddc2 PE=2 SV=1	3	87.096	0.017	2.270
sp|O88531|PPT1_MOUSE	Palmitoyl-protein thioesterase 1 OS=Mus musculus GN=Ppt1 PE=2 SV=2	5	86.298	0.018	2.249
sp|Q8VEH3|ARL8A_MOUSE	ADP-ribosylation factor-like protein 8A OS=Mus musculus GN=Arl8a PE=2 SV=1	5	83.946	0.018	2.270
sp|Q91VC4|PLVAP_MOUSE	Plasmalemma vesicle-associated protein OS=Mus musculus GN=Plvap PE=2 SV=1	2	82.414	0.021	2.291
sp|O35344|IMA3_MOUSE	Importin subunit alpha-3 OS=Mus musculus GN=Kpna3 PE=1 SV=1	4	79.433	0.020	2.312
sp|Q6DVA0|LEMD2_MOUSE	LEM domain-containing protein 2 OS=Mus musculus GN=Lemd2 PE=1 SV=1	2	73.790	0.018	2.421

sp|P59242|CING_MOUSE	Cingulin OS=Mus musculus GN=Cgn PE=1 SV=1	2	67.298	0.020	2.466
sp|Q80UY2|KCMF1_MOUSE	E3 ubiquitin-protein ligase KCMF1 OS=Mus musculus GN=Kcmf1 PE=2 SV=1	2	67.298	0.019	2.489
sp|Q62141|SIN3B_MOUSE	Paired amphipathic helix protein Sin3b OS=Mus musculus GN=Sin3b PE=1 SV=2	2	62.517	0.020	2.559
sp|Q3UHU5|SOGA2_MOUSE	Protein SOGA2 OS=Mus musculus GN=Soga2 PE=1 SV=1	4	61.944	0.016	4.055
sp|P97311|MCM6_MOUSE	DNA replication licensing factor MCM6 OS=Mus musculus GN=Mcm6 PE=1 SV=1	6	61.376	0.021	2.655
sp|P17095|HMGA1_MOUSE	High mobility group protein HMG-I/HMG-Y OS=Mus musculus GN=Hmga1 PE=1 SV=4	2	32.211	0.002	5.105
sp|P84228|H32_MOUSE	Histone H3.2 OS=Mus musculus GN=Hist1h3b PE=1 SV=2	29	27.797	0.000	2.270
sp|Q61102|ABCB7_MOUSE	ATP-binding cassette sub-family B member 7, mitochondrial OS=Mus musculus GN=Abcb7 PE=1 SV=3	6	25.351	0.000	2.965
sp|P46467|VPS4B_MOUSE	Vacuolar protein sorting-associated protein 4B OS=Mus musculus GN=Vps4b PE=1 SV=2	3	23.550	0.001	1.959
sp|P82349|SGCB_MOUSE	Beta-sarcoglycan OS=Mus musculus GN=Sgcb PE=1 SV=1	5	20.701	0.001	4.446
sp|Q3UV70|PDP1_MOUSE	[Pyruvate dehydrogenase [acetyl-transferring]]-phosphatase 1, mitochondrial OS=Mus musculus GN=Pdp1 PE=2 SV=1	4	20.324	0.020	32.509
sp|P05784|K1C18_MOUSE	Keratin, type I cytoskeletal 18 OS=Mus musculus GN=Krt18 PE=1 SV=5	23	19.409	0.002	1.380
sp|P43276|H15_MOUSE	Histone H1.5 OS=Mus musculus GN=Hist1h1b PE=1 SV=2	13	19.231	0.002	1.786
sp|P43275|H11_MOUSE	Histone H1.1 OS=Mus musculus GN=Hist1h1a PE=1 SV=2	4	18.535	0.001	4.018
sp|P15864|H12_MOUSE	Histone H1.2 OS=Mus musculus GN=Hist1h1c PE=1 SV=2	12	17.539	0.015	1.837
sp|Q8CGB3|UACA_MOUSE	Uveal autoantigen with coiled-coil domains and ankyrin repeats OS=Mus musculus GN=Uaca PE=1 SV=2	9	16.904	0.020	19.231
sp|Q8K0E8|FIBB_MOUSE	Fibrinogen beta chain OS=Mus musculus GN=Fgb PE=2 SV=1	36	15.849	0.005	1.445
sp|Q8CG76|ARK72_MOUSE	Aflatoxin B1 aldehyde reductase member 2 OS=Mus musculus GN=Akr7a2 PE=1 SV=3	4	15.704	0.028	1.706
sp|Q9Z2D8|MBD3_MOUSE	Methyl-CpG-binding domain protein 3 OS=Mus musculus GN=Mbd3 PE=1 SV=1	2	15.560	0.036	32.211
sp|P11679|K2C8_MOUSE	Keratin, type II cytoskeletal 8 OS=Mus musculus GN=Krt8 PE=1 SV=4	33	13.932	0.001	1.343

sp|Q8BVQ5|PPME1_MOUSE	Protein phosphatase methylesterase 1 OS=Mus musculus GN=Ppme1 PE=1 SV=5	4	13.305	0.041	32.211
sp|Q61687|ATRX_MOUSE	Transcriptional regulator ATRX OS=Mus musculus GN=Atrx PE=1 SV=3	5	13.062	0.025	3.837
sp|Q6PAR5|GAPD1_MOUSE	GTPase-activating protein and VPS9 domain-containing protein 1 OS=Mus musculus GN=Gapvd1 PE=1 SV=2	3	12.823	0.036	32.211
sp|Q8K3H5|MYO3A_MOUSE	Myosin-IIIa OS=Mus musculus GN=Myo3a PE=2 SV=1	4	12.589	0.035	4.699
sp|Q6PDL0|DC1L2_MOUSE	Cytoplasmic dynein 1 light intermediate chain 2 OS=Mus musculus GN=Dync1li2 PE=1 SV=2	4	10.965	0.002	4.446
sp|P43025|TETN_MOUSE	Tetranectin OS=Mus musculus GN=Clec3b PE=1 SV=2	2	10.568	0.034	2.831
sp|Q80WJ7|LYRIC_MOUSE	Protein LYRIC OS=Mus musculus GN=Mtdh PE=1 SV=1	3	10.280	0.037	5.200
sp|Q99JI6|RAP1B_MOUSE	Ras-related protein Rap-1b OS=Mus musculus GN=Rap1b PE=2 SV=2	14	10.000	0.041	31.623
sp|G5E8K5|ANK3_MOUSE	Ankyrin-3 OS=Mus musculus GN=Ank3 PE=1 SV=1	10	9.638	0.001	3.311
sp|Q80W54|FACE1_MOUSE	CAAX prenyl protease 1 homolog OS=Mus musculus GN=Zmpste24 PE=1 SV=2	2	9.462	0.019	31.623
sp|P10605|CATB_MOUSE	Cathepsin B OS=Mus musculus GN=Ctsb PE=1 SV=2	8	8.790	0.046	1.995
sp|A4Q9F4|TTL11_MOUSE	Tubulin polyglutamylase TTLL11 OS=Mus musculus GN=Ttll11 PE=2 SV=1	2	8.790	0.041	33.113
sp|Q9D8S9|BOLA1_MOUSE	BolA-like protein 1 OS=Mus musculus GN=Bola1 PE=1 SV=1	2	8.790	0.002	4.487
sp|Q8R3B1|PLCD1_MOUSE	1-phosphatidylinositol 4,5-bisphosphate phosphodiesterase delta-1 OS=Mus musculus GN=Plcd1 PE=2 SV=2	5	8.472	0.043	31.623
sp|Q8VCM7|FIBG_MOUSE	Fibrinogen gamma chain OS=Mus musculus GN=Fgg PE=2 SV=1	28	8.166	0.006	1.380
sp|P57784|RU2A_MOUSE	U2 small nuclear ribonucleoprotein A' OS=Mus musculus GN=Snrpa1 PE=1 SV=2	3	8.091	0.038	31.333
sp|Q8R2G4|NAR3_MOUSE	Ecto-ADP-ribosyltransferase 3 OS=Mus musculus GN=Art3 PE=2 SV=2	4	8.091	0.001	4.487
sp|Q80U72|SCRIB_MOUSE	Protein scribble homolog OS=Mus musculus GN=Scrib PE=1 SV=2	2	7.516	0.039	4.487
sp|Q8K2C6|SIR5_MOUSE	NAD-dependent protein deacylase sirtuin-5, mitochondrial OS=Mus musculus GN=Sirt5 PE=1 SV=1	2	7.516	0.001	6.252
sp|B2RU80|PTPRB_MOUSE	Receptor-type tyrosine-protein phosphatase beta OS=Mus musculus GN=Ptprb PE=1 SV=1	2	7.447	0.001	3.597
sp|Q9EPS3|GLCE_MOUSE	D-glucuronyl C5-epimerase OS=Mus musculus GN=Glce PE=1 SV=2	2	7.244	0.003	4.446

sp|P07759|SPA3K_MOUSE	Serine protease inhibitor A3K OS=Mus musculus GN=Serpina3k PE=1 SV=2	19	7.178	0.015	1.419
sp|P28843|DPP4_MOUSE	Dipeptidyl peptidase 4 OS=Mus musculus GN=Dpp4 PE=1 SV=3	3	7.112	0.004	4.487
sp|Q6P1F6|2ABA_MOUSE	Serine/threonine-protein phosphatase 2A 55 kDa regulatory subunit B alpha isoform OS=Mus musculus GN=Ppp2r2a PE=1 SV=1	3	6.855	0.035	33.420
sp|Q61233|PLSL_MOUSE	Plastin-2 OS=Mus musculus GN=Lcp1 PE=1 SV=4	14	6.730	0.030	1.803
sp|Q9D8E6|RL4_MOUSE	60S ribosomal protein L4 OS=Mus musculus GN=Rpl4 PE=1 SV=3	10	6.607	0.041	1.500
sp|Q04857|CO6A1_MOUSE	Collagen alpha-1(VI) chain OS=Mus musculus GN=Col6a1 PE=2 SV=1	29	6.607	0.025	1.282
sp|P62806|H4_MOUSE	Histone H4 OS=Mus musculus GN=Hist1h4a PE=1 SV=2	37	6.081	0.010	1.445
sp|P17047|LAMP2_MOUSE	Lysosome-associated membrane glycoprotein 2 OS=Mus musculus GN=Lamp2 PE=2 SV=2	2	5.058	0.015	2.729
sp|Q9JLC8|SACS_MOUSE	Sacsin OS=Mus musculus GN=Sacs PE=1 SV=2	6	4.742	0.004	4.446
sp|Q9CQD1|RAB5A_MOUSE	Ras-related protein Rab-5A OS=Mus musculus GN=Rab5a PE=1 SV=1	5	4.742	0.003	3.664
sp|Q8BI84|MIA3_MOUSE	Melanoma inhibitory activity protein 3 OS=Mus musculus GN=Mia3 PE=1 SV=2	2	4.656	0.043	31.333
sp|Q9CQW2|ARL8B_MOUSE	ADP-ribosylation factor-like protein 8B OS=Mus musculus GN=Arl8b PE=2 SV=1	5	4.613	0.019	4.446
sp|Q9WVH9|FBLN5_MOUSE	Fibulin-5 OS=Mus musculus GN=Fbln5 PE=2 SV=1	13	4.571	0.035	1.406
sp|Q9CPY7|AMPL_MOUSE	Cytosol aminopeptidase OS=Mus musculus GN=Lap3 PE=1 SV=3	20	4.487	0.012	1.854
sp|Q9CSU0|RPR1B_MOUSE	Regulation of nuclear pre-mRNA domain-containing protein 1B OS=Mus musculus GN=Rprd1b PE=1 SV=2	2	4.406	0.002	4.529
sp|P97449|AMPN_MOUSE	Aminopeptidase N OS=Mus musculus GN=Anpep PE=1 SV=4	11	4.130	0.019	2.291
sp|P48678|LMNA_MOUSE	Prelamin-A/C OS=Mus musculus GN=Lmna PE=1 SV=2	47	4.130	0.004	1.225
sp|Q9DBH5|LMAN2_MOUSE	Vesicular integral-membrane protein VIP36 OS=Mus musculus GN=Lman2 PE=2 SV=2	5	4.093	0.003	2.188
sp|P61358|RL27_MOUSE	60S ribosomal protein L27 OS=Mus musculus GN=Rpl27 PE=2 SV=2	8	4.018	0.004	2.032
sp|P18242|CATD_MOUSE	Cathepsin D OS=Mus musculus GN=Ctsd PE=1 SV=1	18	3.981	0.003	1.570
sp|Q6R0H7|GNAS1_MOUSE	Guanine nucleotide-binding protein G(s) subunit alpha isoforms XLas OS=Mus musculus GN=Gnas PE=2 SV=1	7	3.908	0.041	2.965

sp|Q9D1X0|NOL3_MOUSE	Nucleolar protein 3 OS=Mus musculus GN=Nol3 PE=1 SV=1	6	3.733	0.052	4.487
sp|Q91YE8|SYNP2_MOUSE	Synaptopodin-2 OS=Mus musculus GN=Synpo2 PE=1 SV=2	8	3.733	0.007	2.780
sp|P45376|ALDR_MOUSE	Aldose reductase OS=Mus musculus GN=Akr1b1 PE=1 SV=3	24	3.664	0.000	1.169
sp|Q8BVZ1|PLIN5_MOUSE	Perilipin-5 OS=Mus musculus GN=Plin5 PE=1 SV=1	4	3.532	0.047	4.699
sp|Q3TJD7|PDLI7_MOUSE	PDZ and LIM domain protein 7 OS=Mus musculus GN=Pdlim7 PE=2 SV=1	2	3.436	0.019	2.704
sp|Q60770|STXB3_MOUSE	Syntaxin-binding protein 3 OS=Mus musculus GN=Stxbp3 PE=1 SV=1	3	3.311	0.031	14.191
sp|Q6PDQ2|CHD4_MOUSE	Chromodomain-helicase-DNA-binding protein 4 OS=Mus musculus GN=Chd4 PE=1 SV=1	8	3.281	0.019	4.406
sp|P17182|ENOA_MOUSE	Alpha-enolase OS=Mus musculus GN=Eno1 PE=1 SV=3	70	3.251	0.004	1.419
sp|Q8K1J6|TRNT1_MOUSE	CCA tRNA nucleotidyltransferase 1, mitochondrial OS=Mus musculus GN=Trnt1 PE=2 SV=1	2	3.048	0.046	4.446
sp|P37804|TAGL_MOUSE	Transgelin OS=Mus musculus GN=Tagln PE=1 SV=3	22	3.048	0.002	1.247
sp|Q8CHT0|AL4A1_MOUSE	Delta-1-pyrroline-5-carboxylate dehydrogenase, mitochondrial OS=Mus musculus GN=Aldh4a1 PE=1 SV=3	16	3.020	0.030	1.368
sp|O08677|KNG1_MOUSE	Kininogen-1 OS=Mus musculus GN=Kng1 PE=1 SV=1	26	2.992	0.044	1.330
sp|P10852|4F2_MOUSE	4F2 cell-surface antigen heavy chain OS=Mus musculus GN=Slc3a2 PE=1 SV=1	4	2.938	0.016	2.729
sp|P24452|CAPG_MOUSE	Macrophage-capping protein OS=Mus musculus GN=Capg PE=1 SV=2	3	2.911	0.038	28.314
sp|Q6PGC1|DHX29_MOUSE	ATP-dependent RNA helicase Dhx29 OS=Mus musculus GN=Dhx29 PE=2 SV=1	3	2.780	0.001	4.742
sp|P09671|SODM_MOUSE	Superoxide dismutase [Mn], mitochondrial OS=Mus musculus GN=Sod2 PE=1 SV=3	21	2.754	0.031	1.236
sp|Q60675|LAMA2_MOUSE	Laminin subunit alpha-2 OS=Mus musculus GN=Lama2 PE=1 SV=1	54	2.489	0.048	1.169
sp|P97478|COQ7_MOUSE	Ubiquinone biosynthesis protein COQ7 homolog OS=Mus musculus GN=Coq7 PE=2 SV=3	4	2.421	0.001	2.089
sp|Q9CWE0|FA54B_MOUSE	Protein FAM54B OS=Mus musculus GN=Fam54b PE=1 SV=1	3	2.399	0.004	2.729
sp|Q61292|LAMB2_MOUSE	Laminin subunit beta-2 OS=Mus musculus GN=Lamb2 PE=2 SV=2	30	2.377	0.005	1.888
sp|Q61554|FBN1_MOUSE	Fibrillin-1 OS=Mus musculus GN=Fbn1 PE=1 SV=1	28	2.355	0.048	1.236

sp|Q99KK2|NEUA_MOUSE	N-acylneuraminate cytidylyltransferase OS=Mus musculus GN=Cmas PE=1 SV=2	4	2.312	0.033	4.446
sp|Q9JK48|SHLB1_MOUSE	Endophilin-B1 OS=Mus musculus GN=Sh3glb1 PE=1 SV=1	4	2.291	0.002	2.421
sp|Q3TTY5|K22E_MOUSE	Keratin, type II cytoskeletal 2 epidermal OS=Mus musculus GN=Krt2 PE=1 SV=1	2	2.270	0.045	5.012
sp|Q91WK0|LRRF2_MOUSE	Leucine-rich repeat flightless-interacting protein 2 OS=Mus musculus GN=Lrrfip2 PE=1 SV=1	8	2.270	0.015	2.228
sp|P30681|HMGB2_MOUSE	High mobility group protein B2 OS=Mus musculus GN=Hmgb2 PE=1 SV=3	12	2.249	0.045	1.754
sp|P40142|TKT_MOUSE	Transketolase OS=Mus musculus GN=Tkt PE=1 SV=1	23	2.249	0.037	1.191
sp|P04444|HBBZ_MOUSE	Hemoglobin subunit beta-H1 OS=Mus musculus GN=Hbb-bh1 PE=2 SV=3	8	2.188	0.003	1.514
sp|Q9ESB3|HRG_MOUSE	Histidine-rich glycoprotein OS=Mus musculus GN=Hrg PE=1 SV=2	3	2.168	0.040	4.446
sp|Q5XKE0|MYPC2_MOUSE	Myosin-binding protein C, fast-type OS=Mus musculus GN=Mybpc2 PE=1 SV=1	3	2.148	0.007	3.281
sp|P05125|ANF_MOUSE	Natriuretic peptides A OS=Mus musculus GN=Nppa PE=1 SV=2	32	2.148	0.006	1.225
sp|Q811D0|DLG1_MOUSE	Disks large homolog 1 OS=Mus musculus GN=Dlg1 PE=1 SV=1	3	2.128	0.019	4.487
sp|Q9DCV7|K2C7_MOUSE	Keratin, type II cytoskeletal 7 OS=Mus musculus GN=Krt7 PE=1 SV=1	10	2.109	0.021	2.704
sp|P04919|B3AT_MOUSE	Band 3 anion transport protein OS=Mus musculus GN=Slc4a1 PE=1 SV=1	39	2.089	0.004	1.180
sp|Q9CQX2|CYB5B_MOUSE	Cytochrome b5 type B OS=Mus musculus GN=Cyb5b PE=1 SV=1	2	2.089	0.003	2.729
sp|Q9QWY8|ASAP1_MOUSE	Arf-GAP with SH3 domain, ANK repeat and PH domain-containing protein 1 OS=Mus musculus GN=Asap1 PE=1 SV=2	4	2.070	0.007	5.012
sp|Q9WVA3|BUB3_MOUSE	Mitotic checkpoint protein BUB3 OS=Mus musculus GN=Bub3 PE=2 SV=2	3	2.070	0.001	2.014
sp|P04370|MBP_MOUSE	Myelin basic protein OS=Mus musculus GN=Mbp PE=1 SV=2	4	2.032	0.034	2.965
sp|Q64152|BTF3_MOUSE	Transcription factor BTF3 OS=Mus musculus GN=Btf3 PE=2 SV=3	9	2.014	0.004	2.729
sp|P31428|DPEP1_MOUSE	Dipeptidase 1 OS=Mus musculus GN=Dpep1 PE=1 SV=2	7	1.995	0.039	1.514
sp|Q8K4G5|ABLM1_MOUSE	Actin-binding LIM protein 1 OS=Mus musculus GN=Ablim1 PE=1 SV=1	20	1.995	0.016	1.225
sp|Q9CRD2|EMC2_MOUSE	ER membrane protein complex subunit 2 OS=Mus musculus GN=Emc2 PE=2 SV=1	2	1.977	0.045	4.487
sp|Q99KN9|EPN4_MOUSE	Clathrin interactor 1 OS=Mus musculus GN=Clint1 PE=1 SV=2	6	1.977	0.024	2.729
sp|O70622|RTN2_MOUSE	Reticulon-2 OS=Mus musculus GN=Rtn2 PE=1 SV=1	6	1.941	0.004	3.802

sp|Q8C7H1|MMAA_MOUSE	Methylmalonic aciduria type A homolog, mitochondrial OS=Mus musculus GN=Mmaa PE=2 SV=1	2	1.923	0.037	2.729
sp|Q61234|SNTA1_MOUSE	Alpha-1-syntrophin OS=Mus musculus GN=Snta1 PE=1 SV=1	5	1.905	0.008	1.722
sp|Q9WUZ7|SH3BG_MOUSE	SH3 domain-binding glutamic acid-rich protein OS=Mus musculus GN=Sh3bgr PE=2 SV=1	5	1.888	0.034	1.259
sp|P62315|SMD1_MOUSE	Small nuclear ribonucleoprotein Sm D1 OS=Mus musculus GN=Snrpd1 PE=2 SV=1	2	1.854	0.043	4.446
sp|P07356|ANXA2_MOUSE	Annexin A2 OS=Mus musculus GN=Anxa2 PE=1 SV=2	44	1.854	0.001	1.191
sp|Q6DFW4|NOP58_MOUSE	Nucleolar protein 58 OS=Mus musculus GN=Nop58 PE=1 SV=1	6	1.820	0.043	4.571
sp|Q3UM45|PP1R7_MOUSE	Protein phosphatase 1 regulatory subunit 7 OS=Mus musculus GN=Ppp1r7 PE=1 SV=2	12	1.820	0.011	1.247
sp|Q9DAW9|CNN3_MOUSE	Calponin-3 OS=Mus musculus GN=Cnn3 PE=2 SV=1	6	1.820	0.001	2.399
sp|Q8BR92|PALM2_MOUSE	Paralemmin-2 OS=Mus musculus GN=Palm2 PE=1 SV=1	2	1.738	0.042	23.550
sp|Q921J2|RHEB_MOUSE	GTP-binding protein Rheb OS=Mus musculus GN=Rheb PE=1 SV=1	2	1.614	0.037	4.446
sp|P70336|ROCK2_MOUSE	Rho-associated protein kinase 2 OS=Mus musculus GN=Rock2 PE=1 SV=1	8	1.614	0.020	22.909
sp|Q9ER72|SYCC_MOUSE	Cysteine--tRNA ligase, cytoplasmic OS=Mus musculus GN=Cars PE=1 SV=2	6	1.614	0.018	1.923
sp|Q91WU5|AS3MT_MOUSE	Arsenite methyltransferase OS=Mus musculus GN=As3mt PE=2 SV=2	2	1.585	0.036	2.312
sp|P11276|FINC_MOUSE	Fibronectin OS=Mus musculus GN=Fn1 PE=1 SV=4	76	1.585	0.009	1.107
sp|Q9D7J9|ECHD3_MOUSE	Enoyl-CoA hydratase domain-containing protein 3, mitochondrial OS=Mus musculus GN=Echdc3 PE=2 SV=1	2	1.570	0.039	22.699
sp|Q99K85|SERC_MOUSE	Phosphoserine aminotransferase OS=Mus musculus GN=Psat1 PE=1 SV=1	2	1.570	0.010	4.529
sp|Q6A068|CDC5L_MOUSE	Cell division cycle 5-like protein OS=Mus musculus GN=Cdc5l PE=1 SV=2	4	1.542	0.006	2.858
sp|P08032|SPTA1_MOUSE	Spectrin alpha chain, erythrocytic 1 OS=Mus musculus GN=Spta1 PE=2 SV=3	95	1.514	0.023	1.259
sp|Q9WVA4|TAGL2_MOUSE	Transgelin-2 OS=Mus musculus GN=Tagln2 PE=1 SV=4	36	1.486	0.053	1.191
sp|Q9CPQ3|TOM22_MOUSE	Mitochondrial import receptor subunit TOM22 homolog OS=Mus musculus GN=Tomm22 PE=2 SV=3	6	1.472	0.002	3.105
sp|Q03958|PFD6_MOUSE	Prefoldin subunit 6 OS=Mus musculus GN=Pfdn6 PE=2 SV=1	2	1.459	0.038	4.446

sp|Q8BHC4|DCAKD_MOUSE	Dephospho-CoA kinase domain-containing protein OS=Mus musculus GN=Dcakd PE=2 SV=1	2	1.459	0.018	1.977
sp|Q8K4L3|SVIL_MOUSE	Supervillin OS=Mus musculus GN=Svil PE=1 SV=1	5	1.459	0.006	4.529
sp|Q8VE95|CH082_MOUSE	UPF0598 protein C8orf82 homolog OS=Mus musculus PE=2 SV=1	2	1.459	0.001	1.706
sp|P15508|SPTB1_MOUSE	Spectrin beta chain, erythrocytic OS=Mus musculus GN=Sptb PE=1 SV=4	87	1.445	0.012	1.213
sp|P97447|FHL1_MOUSE	Four and a half LIM domains protein 1 OS=Mus musculus GN=Fhl1 PE=2 SV=3	9	1.432	0.012	1.282
sp|O08582|GTPB1_MOUSE	GTP-binding protein 1 OS=Mus musculus GN=Gtpbp1 PE=1 SV=2	3	1.393	0.053	4.446
sp|Q9CX80|CYGB_MOUSE	Cytoglobin OS=Mus musculus GN=Cygb PE=2 SV=1	3	1.380	0.043	1.941
sp|Q8CC88|VWA8_MOUSE	von Willebrand factor A domain-containing protein 8 OS=Mus musculus GN=Vwa8 PE=2 SV=2	33	1.380	0.018	1.236
sp|P46412|GPX3_MOUSE	Glutathione peroxidase 3 OS=Mus musculus GN=Gpx3 PE=2 SV=2	7	1.380	0.012	1.259
sp|Q9QZE7|TSNAX_MOUSE	Translin-associated protein X OS=Mus musculus GN=Tsnax PE=1 SV=1	3	1.368	0.034	1.380
sp|Q9JM76|ARPC3_MOUSE	Actin-related protein 2/3 complex subunit 3 OS=Mus musculus GN=Arpc3 PE=1 SV=3	5	1.355	0.042	1.236
sp|Q9EPK7|XPO7_MOUSE	Exportin-7 OS=Mus musculus GN=Xpo7 PE=2 SV=3	5	1.343	0.032	2.208
sp|Q3TL44|NLRX1_MOUSE	NLR family member X1 OS=Mus musculus GN=Nlrx1 PE=2 SV=1	2	1.330	0.019	1.556
sp|P32233|DRG1_MOUSE	Developmentally-regulated GTP-binding protein 1 OS=Mus musculus GN=Drg1 PE=1 SV=1	3	1.318	0.050	1.343
sp|Q571C7|BDP1_MOUSE	Transcription factor TFIIIB component B'' homolog OS=Mus musculus GN=Bdp1 PE=2 SV=2	2	1.306	0.040	5.200
sp|P17710|HXK1_MOUSE	Hexokinase-1 OS=Mus musculus GN=Hk1 PE=1 SV=3	57	1.306	0.037	1.117
sp|Q9ES82|POPD2_MOUSE	Popeye domain-containing protein 2 OS=Mus musculus GN=Popdc2 PE=2 SV=1	2	1.282	0.002	1.148
DECREASED EXPRESSION					
sp|Q9Z126|PLF4_MOUSE	Platelet factor 4 OS=Mus musculus GN=Pf4 PE=2 SV=1	2	0.731	0.054	21.478
sp|Q9D7G0|PRPS1_MOUSE	Ribose-phosphate pyrophosphokinase 1 OS=Mus musculus GN=Prps1 PE=1 SV=4	4	0.711	0.054	1.738

sp|Q920A5|RISC_MOUSE	Retinoid-inducible serine carboxypeptidase OS=Mus musculus GN=Scpep1 PE=2 SV=2	4	0.705	0.006	1.786
sp|Q9WV80|SNX1_MOUSE	Sorting nexin-1 OS=Mus musculus GN=Snx1 PE=1 SV=1	6	0.692	0.017	2.729
sp|Q9D1M0|SEC13_MOUSE	Protein SEC13 homolog OS=Mus musculus GN=Sec13 PE=2 SV=3	3	0.667	0.039	1.888
sp|Q9JI46|NUDT3_MOUSE	Diphosphoinositol polyphosphate phosphohydrolase 1 OS=Mus musculus GN=Nudt3 PE=1 SV=1	2	0.661	0.049	2.051
sp|P60824|CIRBP_MOUSE	Cold-inducible RNA-binding protein OS=Mus musculus GN=Cirbp PE=1 SV=1	3	0.655	0.009	4.529
sp|Q9CQF3|CPSF5_MOUSE	Cleavage and polyadenylation specificity factor subunit 5 OS=Mus musculus GN=Nudt21 PE=2 SV=1	2	0.643	0.010	2.729
sp|Q9DBC7|KAP0_MOUSE	cAMP-dependent protein kinase type I-alpha regulatory subunit OS=Mus musculus GN=Prkar1a PE=1 SV=3	15	0.637	0.045	1.202
sp|Q9QXS1|PLEC_MOUSE	Plectin OS=Mus musculus GN=Plec PE=1 SV=2	150	0.637	0.043	1.076
sp|Q64213|SF01_MOUSE	Splicing factor 1 OS=Mus musculus GN=Sf1 PE=1 SV=6	5	0.631	0.038	1.786
sp|Q99L04|DHRS1_MOUSE	Dehydrogenase/reductase SDR family member 1 OS=Mus musculus GN=Dhrs1 PE=2 SV=1	2	0.625	0.031	2.729
sp|Q8BL66|EEA1_MOUSE	Early endosome antigen 1 OS=Mus musculus GN=Eea1 PE=2 SV=2	11	0.614	0.048	1.472
sp|Q91XQ0|DYH8_MOUSE	Dynein heavy chain 8, axonemal OS=Mus musculus GN=Dnahc8 PE=2 SV=2	7	0.614	0.025	1.614
sp|Q9D9V3|ECHD1_MOUSE	Ethylmalonyl-CoA decarboxylase OS=Mus musculus GN=Echdc1 PE=1 SV=2	3	0.608	0.011	1.528
sp|Q9R062|GLYG_MOUSE	Glycogenin-1 OS=Mus musculus GN=Gyg1 PE=2 SV=3	11	0.592	0.054	1.486
sp|Q9CQS4|S2546_MOUSE	Solute carrier family 25 member 46 OS=Mus musculus GN=Slc25a46 PE=1 SV=1	4	0.586	0.027	2.992
sp|Q9CQC9|SAR1B_MOUSE	GTP-binding protein SAR1b OS=Mus musculus GN=Sar1b PE=1 SV=1	9	0.586	0.025	1.459
sp|Q8VDD5|MYH9_MOUSE	Myosin-9 OS=Mus musculus GN=Myh9 PE=1 SV=4	145	0.581	0.019	1.096
sp|Q91YH5|ATLA3_MOUSE	Atlastin-3 OS=Mus musculus GN=Atl3 PE=2 SV=1	3	0.575	0.036	4.487
sp|Q91W50|CSDE1_MOUSE	Cold shock domain-containing protein E1 OS=Mus musculus GN=Csde1 PE=2 SV=1	3	0.570	0.052	1.837
sp|Q71LX4|TLN2_MOUSE	Talin-2 OS=Mus musculus GN=Tln2 PE=1 SV=3	65	0.570	0.029	1.368
sp|P09103|PDIA1_MOUSE	Protein disulfide-isomerase OS=Mus musculus GN=P4hb PE=1 SV=2	59	0.555	0.022	1.202

sp|Q9JI39|ABCBA_MOUSE	ATP-binding cassette sub-family B member 10, mitochondrial OS=Mus musculus GN=Abcb10 PE=2 SV=1	4	0.550	0.005	1.854
sp|Q1HFZ0|NSUN2_MOUSE	tRNA (cytosine(34)-C(5))-methyltransferase OS=Mus musculus GN=Nsun2 PE=1 SV=2	5	0.540	0.030	4.446
sp|P62259|1433E_MOUSE	14-3-3 protein epsilon OS=Mus musculus GN=Ywhae PE=1 SV=1	38	0.535	0.030	1.213
sp|P08113|ENPL_MOUSE	Endoplasmin OS=Mus musculus GN=Hsp90b1 PE=1 SV=2	50	0.530	0.041	1.202
sp|Q3B7Z2|OSBP1_MOUSE	Oxysterol-binding protein 1 OS=Mus musculus GN=Osbp PE=1 SV=2	4	0.525	0.028	1.459
sp|O35972|RM23_MOUSE	39S ribosomal protein L23, mitochondrial OS=Mus musculus GN=Mrpl23 PE=2 SV=1	2	0.525	0.011	1.600
sp|Q8BX02|KANK2_MOUSE	KN motif and ankyrin repeat domain-containing protein 2 OS=Mus musculus GN=Kank2 PE=1 SV=1	3	0.520	0.051	24.210
sp|Q61941|NNTM_MOUSE	NAD(P) transhydrogenase, mitochondrial OS=Mus musculus GN=Nnt PE=1 SV=2	42	0.520	0.000	1.127
sp|P63017|HSP7C_MOUSE	Heat shock cognate 71 kDa protein OS=Mus musculus GN=Hspa8 PE=1 SV=1	103	0.515	0.047	1.117
sp|P27773|PDIA3_MOUSE	Protein disulfide-isomerase A3 OS=Mus musculus GN=Pdia3 PE=1 SV=2	35	0.511	0.020	1.138
sp|P62192|PRS4_MOUSE	26S protease regulatory subunit 4 OS=Mus musculus GN=Psmc1 PE=1 SV=1	19	0.501	0.031	1.247
sp|Q9D0F9|PGM1_MOUSE	Phosphoglucomutase-1 OS=Mus musculus GN=Pgm1 PE=1 SV=4	50	0.497	0.044	1.294
sp|Q9JI91|ACTN2_MOUSE	Alpha-actinin-2 OS=Mus musculus GN=Actn2 PE=1 SV=2	191	0.497	0.003	1.086
sp|Q6ZQ38|CAND1_MOUSE	Cullin-associated NEDD8-dissociated protein 1 OS=Mus musculus GN=Cand1 PE=2 SV=2	29	0.492	0.015	1.191
sp|Q3UHX2|HAP28_MOUSE	28 kDa heat- and acid-stable phosphoprotein OS=Mus musculus GN=Pdap1 PE=1 SV=1	4	0.488	0.013	4.093
sp|O08807|PRDX4_MOUSE	Peroxiredoxin-4 OS=Mus musculus GN=Prdx4 PE=1 SV=1	7	0.483	0.013	4.487
sp|O35737|HNRH1_MOUSE	Heterogeneous nuclear ribonucleoprotein H OS=Mus musculus GN=Hnrnph1 PE=1 SV=3	22	0.479	0.013	2.109
sp|Q9DCF9|SSRG_MOUSE	Translocon-associated protein subunit gamma OS=Mus musculus GN=Ssr3 PE=1 SV=1	4	0.474	0.039	2.754
sp|Q921I1|TRFE_MOUSE	Serotransferrin OS=Mus musculus GN=Tf PE=1 SV=1	144	0.474	0.001	1.169
sp|P14211|CALR_MOUSE	Calreticulin OS=Mus musculus GN=Calr PE=1 SV=1	33	0.466	0.010	1.406

sp|Q99MR8|MCCA_MOUSE	Methylcrotonoyl-CoA carboxylase subunit alpha, mitochondrial OS=Mus musculus GN=Mccc1 PE=2 SV=2	4	0.461	0.053	4.446
sp|Q9D8N0|EF1G_MOUSE	Elongation factor 1-gamma OS=Mus musculus GN=Eef1g PE=1 SV=3	24	0.445	0.033	1.330
sp|P80314|TCPB_MOUSE	T-complex protein 1 subunit beta OS=Mus musculus GN=Cct2 PE=1 SV=4	38	0.445	0.004	1.202
sp|O35295|PURB_MOUSE	Transcriptional activator protein Pur-beta OS=Mus musculus GN=Purb PE=1 SV=3	7	0.441	0.019	2.831
sp|Q8BH59|CMC1_MOUSE	Calcium-binding mitochondrial carrier protein Aralar1 OS=Mus musculus GN=Slc25a12 PE=1 SV=1	42	0.437	0.025	1.169
sp|Q9DC77|SMPX_MOUSE	Small muscular protein OS=Mus musculus GN=Smpx PE=2 SV=2	4	0.433	0.005	1.472
sp|Q8BMJ3|IF1AX_MOUSE	Eukaryotic translation initiation factor 1A, X-chromosomal OS=Mus musculus GN=Eif1ax PE=2 SV=3	6	0.425	0.013	1.660
sp|Q99N92|RM27_MOUSE	39S ribosomal protein L27, mitochondrial OS=Mus musculus GN=Mrpl27 PE=2 SV=1	3	0.413	0.017	2.188
sp|P14824|ANXA6_MOUSE	Annexin A6 OS=Mus musculus GN=Anxa6 PE=1 SV=3	62	0.413	0.002	1.138
sp|P20029|GRP78_MOUSE	78 kDa glucose-regulated protein OS=Mus musculus GN=Hspa5 PE=1 SV=3	64	0.406	0.033	1.117
sp|P62843|RS15_MOUSE	40S ribosomal protein S15 OS=Mus musculus GN=Rps15 PE=2 SV=2	11	0.406	0.009	1.854
sp|Q9DB77|QCR2_MOUSE	Cytochrome b-c1 complex subunit 2, mitochondrial OS=Mus musculus GN=Uqcrc2 PE=1 SV=1	94	0.406	0.001	1.259
sp|Q61768|KINH_MOUSE	Kinesin-1 heavy chain OS=Mus musculus GN=Kif5b PE=1 SV=3	32	0.402	0.002	1.330
sp|P99024|TBB5_MOUSE	Tubulin beta-5 chain OS=Mus musculus GN=Tubb5 PE=1 SV=1	100	0.384	0.054	1.282
sp|P09411|PGK1_MOUSE	Phosphoglycerate kinase 1 OS=Mus musculus GN=Pgk1 PE=1 SV=4	74	0.373	0.036	1.213
sp|Q99KI0|ACON_MOUSE	Aconitate hydratase, mitochondrial OS=Mus musculus GN=Aco2 PE=1 SV=1	151	0.370	0.006	1.096
sp|Q9CY58|PAIRB_MOUSE	Plasminogen activator inhibitor 1 RNA-binding protein OS=Mus musculus GN=Serbp1 PE=1 SV=2	13	0.363	0.014	1.570
sp|P54731|FAF1_MOUSE	FAS-associated factor 1 OS=Mus musculus GN=Faf1 PE=1 SV=2	6	0.360	0.019	4.285
sp|P14152|MDHC_MOUSE	Malate dehydrogenase, cytoplasmic OS=Mus musculus GN=Mdh1 PE=1 SV=3	74	0.360	0.014	1.107
sp|P14869|RLA0_MOUSE	60S acidic ribosomal protein P0 OS=Mus musculus GN=Rplp0 PE=1 SV=3	17	0.356	0.030	1.368
sp|P38647|GRP75_MOUSE	Stress-70 protein, mitochondrial OS=Mus musculus GN=Hspa9 PE=1 SV=3	81	0.350	0.017	1.138

sp|Q9R0Y5|KAD1_MOUSE	Adenylate kinase isoenzyme 1 OS=Mus musculus GN=Ak1 PE=1 SV=1	21	0.347	0.009	1.472
sp|O55126|NIPS2_MOUSE	Protein NipSnap homolog 2 OS=Mus musculus GN=Gbas PE=2 SV=1	21	0.340	0.038	1.406
sp|P14131|RS16_MOUSE	40S ribosomal protein S16 OS=Mus musculus GN=Rps16 PE=2 SV=4	10	0.331	0.034	2.109
sp|Q5SYD0|MYO1D_MOUSE	Unconventional myosin-Id OS=Mus musculus GN=Myo1d PE=1 SV=1	4	0.331	0.018	2.704
sp|P15116|CADH2_MOUSE	Cadherin-2 OS=Mus musculus GN=Cdh2 PE=1 SV=2	24	0.331	0.015	1.514
sp|Q9WTQ5|AKA12_MOUSE	A-kinase anchor protein 12 OS=Mus musculus GN=Akap12 PE=1 SV=1	25	0.331	0.013	1.419
sp|P20152|VIME_MOUSE	Vimentin OS=Mus musculus GN=Vim PE=1 SV=3	103	0.328	0.003	1.318
sp|Q921F4|HNRLL_MOUSE	Heterogeneous nuclear ribonucleoprotein L-like OS=Mus musculus GN=Hnrpll PE=1 SV=3	5	0.322	0.053	2.729
sp|O35943|FRDA_MOUSE	Frataxin, mitochondrial OS=Mus musculus GN=Fxn PE=1 SV=1	6	0.322	0.034	1.837
sp|Q8BKC5|IPO5_MOUSE	Importin-5 OS=Mus musculus GN=Ipo5 PE=1 SV=3	21	0.322	0.001	1.486
sp|P02772|FETA_MOUSE	Alpha-fetoprotein OS=Mus musculus GN=Afp PE=2 SV=1	51	0.322	0.000	1.107
sp|Q91VH6|MEMO1_MOUSE	Protein MEMO1 OS=Mus musculus GN=Memo1 PE=1 SV=1	3	0.319	0.015	5.012
sp|Q8R086|SUOX_MOUSE	Sulfite oxidase, mitochondrial OS=Mus musculus GN=Suox PE=1 SV=2	4	0.313	0.046	2.704
sp|P31786|ACBP_MOUSE	Acyl-CoA-binding protein OS=Mus musculus GN=Dbi PE=1 SV=2	8	0.313	0.042	1.888
sp|P12815|PDCD6_MOUSE	Programmed cell death protein 6 OS=Mus musculus GN=Pdcd6 PE=1 SV=2	4	0.313	0.001	1.905
sp|P14142|GTR4_MOUSE	Solute carrier family 2, facilitated glucose transporter member 4 OS=Mus musculus GN=Slc2a4 PE=1 SV=3	4	0.310	0.005	2.355
sp|Q9Z1E4|GYS1_MOUSE	Glycogen [starch] synthase, muscle OS=Mus musculus GN=Gys1 PE=1 SV=2	11	0.310	0.000	1.722
sp|Q69ZR2|HECD1_MOUSE	E3 ubiquitin-protein ligase HECTD1 OS=Mus musculus GN=Hectd1 PE=1 SV=2	7	0.305	0.029	2.443
sp|Q91V61|SFXN3_MOUSE	Sideroflexin-3 OS=Mus musculus GN=Sfxn3 PE=1 SV=1	5	0.305	0.017	4.656
sp|P97807|FUMH_MOUSE	Fumarate hydratase, mitochondrial OS=Mus musculus GN=Fh PE=1 SV=3	82	0.296	0.022	1.542
sp|P35486|ODPA_MOUSE	Pyruvate dehydrogenase E1 component subunit alpha, somatic form, mitochondrial OS=Mus musculus GN=Pdha1 PE=1 SV=1	54	0.296	0.020	1.514
sp|Q9Z2I9|SUCB1_MOUSE	Succinyl-CoA ligase [ADP-forming] subunit beta, mitochondrial OS=Mus musculus GN=Sucla2 PE=1 SV=2	41	0.294	0.054	1.432

sp|P56480|ATPB_MOUSE	ATP synthase subunit beta, mitochondrial OS=Mus musculus GN=Atp5b PE=1 SV=2	296	0.291	0.013	1.086
sp|P62245|RS15A_MOUSE	40S ribosomal protein S15a OS=Mus musculus GN=Rps15a PE=2 SV=2	8	0.288	0.044	1.706
sp|Q3UZ39|LRRF1_MOUSE	Leucine-rich repeat flightless-interacting protein 1 OS=Mus musculus GN=Lrrfip1 PE=1 SV=2	6	0.283	0.017	4.487
sp|Q8JZQ2|AFG32_MOUSE	AFG3-like protein 2 OS=Mus musculus GN=Afg3l2 PE=1 SV=1	22	0.281	0.012	1.259
sp|Q8BMF4|ODP2_MOUSE	Dihydrolipoyllysine-residue acetyltransferase component of pyruvate dehydrogenase complex, mitochondrial OS=Mus musculus GN=Dlat PE=1 SV=2	32	0.275	0.047	1.355
sp|P70404|IDHG1_MOUSE	Isocitrate dehydrogenase [NAD] subunit gamma 1, mitochondrial OS=Mus musculus GN=Idh3g PE=1 SV=1	34	0.270	0.009	1.432
sp|Q60864|STIP1_MOUSE	Stress-induced-phosphoprotein 1 OS=Mus musculus GN=Stip1 PE=1 SV=1	30	0.265	0.034	1.355
sp|Q3TMH2|SCRN3_MOUSE	Secernin-3 OS=Mus musculus GN=Scrn3 PE=1 SV=1	2	0.265	0.023	2.729
sp|Q9D2R6|COA3_MOUSE	Cytochrome C oxidase assembly factor 3 homolog, mitochondrial OS=Mus musculus GN=Ccdc56 PE=2 SV=1	3	0.254	0.009	2.466
sp|Q07417|ACADS_MOUSE	Short-chain specific acyl-CoA dehydrogenase, mitochondrial OS=Mus musculus GN=Acads PE=2 SV=2	36	0.251	0.035	1.500
sp|Q9QXS6|DREB_MOUSE	Drebrin OS=Mus musculus GN=Dbn1 PE=1 SV=4	2	0.247	0.023	2.208
sp|P47857|K6PF_MOUSE	6-phosphofructokinase, muscle type OS=Mus musculus GN=Pfkm PE=1 SV=3	41	0.247	0.013	1.169
sp|P51174|ACADL_MOUSE	Long-chain specific acyl-CoA dehydrogenase, mitochondrial OS=Mus musculus GN=Acadl PE=2 SV=2	77	0.244	0.053	1.432
sp|Q9R1P0|PSA4_MOUSE	Proteasome subunit alpha type-4 OS=Mus musculus GN=Psma4 PE=1 SV=1	5	0.244	0.053	1.542
sp|P62717|RL18A_MOUSE	60S ribosomal protein L18a OS=Mus musculus GN=Rpl18a PE=1 SV=1	8	0.242	0.035	1.486
sp|P25444|RS2_MOUSE	40S ribosomal protein S2 OS=Mus musculus GN=Rps2 PE=1 SV=3	15	0.240	0.000	1.259
sp|Q8BVA5|CB043_MOUSE	UPF0554 protein C2orf43 homolog OS=Mus musculus PE=2 SV=1	3	0.238	0.042	2.805
sp|Q9WTP7|KAD3_MOUSE	GTP:AMP phosphotransferase, mitochondrial OS=Mus musculus GN=Ak3 PE=1 SV=3	15	0.238	0.023	1.820
sp|P05201|AATC_MOUSE	Aspartate aminotransferase, cytoplasmic OS=Mus musculus GN=Got1 PE=1 SV=3	58	0.238	0.021	1.236

sp|P99028|QCR6_MOUSE	Cytochrome b-c1 complex subunit 6, mitochondrial OS=Mus musculus GN=Uqcrh PE=1 SV=2	16	0.236	0.053	3.020
sp|P56392|CX7A1_MOUSE	Cytochrome c oxidase subunit 7A1, mitochondrial OS=Mus musculus GN=Cox7a1 PE=2 SV=1	5	0.236	0.034	1.556
sp|Q2TPA8|HSDL2_MOUSE	Hydroxysteroid dehydrogenase-like protein 2 OS=Mus musculus GN=Hsdl2 PE=2 SV=1	32	0.233	0.043	1.282
sp|Q8CI94|PYGB_MOUSE	Glycogen phosphorylase, brain form OS=Mus musculus GN=Pygb PE=1 SV=3	54	0.233	0.007	1.330
sp|P05202|AATM_MOUSE	Aspartate aminotransferase, mitochondrial OS=Mus musculus GN=Got2 PE=1 SV=1	76	0.229	0.004	1.247
sp|Q3UBX0|TM109_MOUSE	Transmembrane protein 109 OS=Mus musculus GN=Tmem109 PE=1 SV=2	3	0.227	0.035	1.941
sp|Q91VR2|ATPG_MOUSE	ATP synthase subunit gamma, mitochondrial OS=Mus musculus GN=Atp5c1 PE=1 SV=1	39	0.223	0.010	2.168
sp|P24369|PPIB_MOUSE	Peptidyl-prolyl cis-trans isomerase B OS=Mus musculus GN=Ppib PE=2 SV=2	13	0.219	0.039	1.406
sp|P08249|MDHM_MOUSE	Malate dehydrogenase, mitochondrial OS=Mus musculus GN=Mdh2 PE=1 SV=3	129	0.219	0.008	1.629
sp|Q8VEA4|MIA40_MOUSE	Mitochondrial intermembrane space import and assembly protein 40 OS=Mus musculus GN=Chchd4 PE=1 SV=1	3	0.217	0.048	5.248
sp|P52480|KPYM_MOUSE	Pyruvate kinase isozymes M1/M2 OS=Mus musculus GN=Pkm PE=1 SV=4	83	0.215	0.000	1.318
sp|Q0II04|NEBL_MOUSE	Nebulette OS=Mus musculus GN=Nebl PE=2 SV=1	25	0.209	0.003	1.236
sp|P23116|EIF3A_MOUSE	Eukaryotic translation initiation factor 3 subunit A OS=Mus musculus GN=Eif3a PE=1 SV=5	23	0.207	0.007	1.570
sp|Q8C5Q4|GRSF1_MOUSE	G-rich sequence factor 1 OS=Mus musculus GN=Grsf1 PE=1 SV=2	4	0.205	0.024	4.529
sp|Q9DCL9|PUR6_MOUSE	Multifunctional protein ADE2 OS=Mus musculus GN=Paics PE=1 SV=4	17	0.205	0.009	2.992
sp|Q9CZX8|RS19_MOUSE	40S ribosomal protein S19 OS=Mus musculus GN=Rps19 PE=1 SV=3	11	0.205	0.000	1.660
sp|P41216|ACSL1_MOUSE	Long-chain-fatty-acid--CoA ligase 1 OS=Mus musculus GN=Acsl1 PE=1 SV=2	48	0.203	0.012	1.306
sp|O70435|PSA3_MOUSE	Proteasome subunit alpha type-3 OS=Mus musculus GN=Psma3 PE=1 SV=3	9	0.198	0.003	1.368
sp|Q91YT0|NDUV1_MOUSE	NADH dehydrogenase [ubiquinone] flavoprotein 1, mitochondrial OS=Mus musculus GN=Ndufv1 PE=1 SV=1	34	0.196	0.028	1.770

sp|Q78PY7|SND1_MOUSE	Staphylococcal nuclease domain-containing protein 1 OS=Mus musculus GN=Snd1 PE=1 SV=1	19	0.196	0.022	1.247
sp|P62270|RS18_MOUSE	40S ribosomal protein S18 OS=Mus musculus GN=Rps18 PE=1 SV=3	12	0.196	0.002	2.109
sp|Q8K0D5|EFGM_MOUSE	Elongation factor G, mitochondrial OS=Mus musculus GN=Gfm1 PE=2 SV=1	17	0.194	0.012	1.419
sp|O35857|TIM44_MOUSE	Mitochondrial import inner membrane translocase subunit TIM44 OS=Mus musculus GN=Timm44 PE=2 SV=2	12	0.192	0.042	1.294
sp|Q8BTG7|NDRG4_MOUSE	Protein NDRG4 OS=Mus musculus GN=Ndrg4 PE=1 SV=1	2	0.192	0.011	3.436
sp|P62821|RAB1A_MOUSE	Ras-related protein Rab-1A OS=Mus musculus GN=Rab1A PE=1 SV=3	25	0.192	0.001	2.188
sp|Q8BMS1|ECHA_MOUSE	Trifunctional enzyme subunit alpha, mitochondrial OS=Mus musculus GN=Hadha PE=1 SV=1	202	0.187	0.018	1.706
sp|P54071|IDHP_MOUSE	Isocitrate dehydrogenase [NADP], mitochondrial OS=Mus musculus GN=Idh2 PE=1 SV=3	94	0.184	0.029	1.368
sp|P54822|PUR8_MOUSE	Adenylosuccinate lyase OS=Mus musculus GN=Adsl PE=2 SV=2	11	0.184	0.027	1.528
sp|P16125|LDHB_MOUSE	L-lactate dehydrogenase B chain OS=Mus musculus GN=Ldhb PE=1 SV=2	46	0.184	0.007	1.259
sp|Q9CZR8|EFTS_MOUSE	Elongation factor Ts, mitochondrial OS=Mus musculus GN=Tsfm PE=2 SV=1	10	0.182	0.012	2.089
sp|P18572|BASI_MOUSE	Basigin OS=Mus musculus GN=Bsg PE=1 SV=2	7	0.179	0.002	2.228
sp|Q60597|ODO1_MOUSE	2-oxoglutarate dehydrogenase, mitochondrial OS=Mus musculus GN=Ogdh PE=1 SV=3	103	0.179	0.000	1.259
sp|P46638|RB11B_MOUSE	Ras-related protein Rab-11B OS=Mus musculus GN=Rab11b PE=1 SV=3	18	0.177	0.008	1.556
sp|P63028|TCTP_MOUSE	Translationally-controlled tumor protein OS=Mus musculus GN=Tpt1 PE=1 SV=1	13	0.177	0.007	1.419
sp|P30416|FKBP4_MOUSE	Peptidyl-prolyl cis-trans isomerase FKBP4 OS=Mus musculus GN=Fkbp4 PE=1 SV=5	7	0.175	0.010	3.698
sp|Q9DC69|NDUA9_MOUSE	NADH dehydrogenase [ubiquinone] 1 alpha subcomplex subunit 9, mitochondrial OS=Mus musculus GN=Ndufa9 PE=1 SV=2	43	0.175	0.000	1.600
sp|Q9QYG0|NDRG2_MOUSE	Protein NDRG2 OS=Mus musculus GN=Ndrg2 PE=1 SV=1	28	0.174	0.008	1.445
sp|P04117|FABP4_MOUSE	Fatty acid-binding protein, adipocyte OS=Mus musculus GN=Fabp4 PE=1 SV=3	25	0.174	0.006	2.630
sp|Q9CQ62|DECR_MOUSE	2,4-dienoyl-CoA reductase, mitochondrial OS=Mus musculus GN=Decr1 PE=1 SV=1	34	0.169	0.021	2.489

sp|O08759|UBE3A_MOUSE	Ubiquitin-protein ligase E3A OS=Mus musculus GN=Ube3a PE=2 SV=1	5	0.167	0.029	4.529
sp|Q91VM9|IPYR2_MOUSE	Inorganic pyrophosphatase 2, mitochondrial OS=Mus musculus GN=Ppa2 PE=2 SV=1	12	0.167	0.001	1.803
sp|P11499|HS90B_MOUSE	Heat shock protein HSP 90-beta OS=Mus musculus GN=Hsp90ab1 PE=1 SV=3	74	0.166	0.023	1.294
sp|P97443|SMYD1_MOUSE	SET and MYND domain-containing protein 1 OS=Mus musculus GN=Smyd1 PE=1 SV=3	22	0.166	0.005	3.192
sp|Q9QYJ0|DNJA2_MOUSE	DnaJ homolog subfamily A member 2 OS=Mus musculus GN=Dnaja2 PE=1 SV=1	13	0.164	0.005	1.472
sp|Q91ZJ5|UGPA_MOUSE	UTP--glucose-1-phosphate uridylyltransferase OS=Mus musculus GN=Ugp2 PE=2 SV=3	27	0.164	0.000	1.500
sp|Q60676|PPP5_MOUSE	Serine/threonine-protein phosphatase 5 OS=Mus musculus GN=Ppp5c PE=2 SV=2	5	0.163	0.043	2.559
sp|P01867|IGG2B_MOUSE	Ig gamma-2B chain C region OS=Mus musculus GN=Igh-3 PE=1 SV=3	7	0.163	0.027	1.888
sp|P42125|ECI1_MOUSE	Enoyl-CoA delta isomerase 1, mitochondrial OS=Mus musculus GN=Eci1 PE=2 SV=2	29	0.161	0.000	1.318
sp|Q6GQT9|NOMO1_MOUSE	Nodal modulator 1 OS=Mus musculus GN=Nomo1 PE=1 SV=1	6	0.160	0.030	4.446
sp|Q91YP2|NEUL_MOUSE	Neurolysin, mitochondrial OS=Mus musculus GN=Nln PE=2 SV=1	4	0.158	0.035	2.858
sp|Q924X2|CPT1B_MOUSE	Carnitine O-palmitoyltransferase 1, muscle isoform OS=Mus musculus GN=Cpt1b PE=2 SV=1	49	0.158	0.002	1.432
sp|P50544|ACADV_MOUSE	Very long-chain specific acyl-CoA dehydrogenase, mitochondrial OS=Mus musculus GN=Acadvl PE=1 SV=3	110	0.157	0.002	1.445
sp|P70670|NACAM_MOUSE	Nascent polypeptide-associated complex subunit alpha, muscle-specific form OS=Mus musculus GN=Naca PE=1 SV=2	82	0.156	0.003	1.368
sp|O55143|AT2A2_MOUSE	Sarcoplasmic/endoplasmic reticulum calcium ATPase 2 OS=Mus musculus GN=Atp2a2 PE=1 SV=2	207	0.156	0.000	1.117
sp|P34928|APOC1_MOUSE	Apolipoprotein C-I OS=Mus musculus GN=Apoc1 PE=2 SV=1	5	0.150	0.041	1.995
sp|Q8QZT1|THIL_MOUSE	Acetyl-CoA acetyltransferase, mitochondrial OS=Mus musculus GN=Acat1 PE=1 SV=1	72	0.149	0.011	1.675
sp|P62852|RS25_MOUSE	40S ribosomal protein S25 OS=Mus musculus GN=Rps25 PE=2 SV=1	8	0.146	0.015	1.803

sp|Q8BGK2|ARHL1_MOUSE	[Protein ADP-ribosylarginine] hydrolase-like protein 1 OS=Mus musculus GN=Adprhl1 PE=2 SV=1	12	0.146	0.000	2.355
sp|Q01768|NDKB_MOUSE	Nucleoside diphosphate kinase B OS=Mus musculus GN=Nme2 PE=1 SV=1	32	0.145	0.014	1.614
sp|P31001|DESM_MOUSE	Desmin OS=Mus musculus GN=Des PE=1 SV=3	101	0.142	0.000	1.138
sp|O70325|GPX41_MOUSE	Phospholipid hydroperoxide glutathione peroxidase, mitochondrial OS=Mus musculus GN=Gpx4 PE=1 SV=4	5	0.141	0.008	4.406
sp|Q8CGK3|LONM_MOUSE	Lon protease homolog, mitochondrial OS=Mus musculus GN=Lonp1 PE=1 SV=2	38	0.139	0.037	1.247
sp|P34914|HYES_MOUSE	Bifunctional epoxide hydrolase 2 OS=Mus musculus GN=Ephx2 PE=1 SV=2	26	0.137	0.026	1.225
sp|Q00623|APOA1_MOUSE	Apolipoprotein A-I OS=Mus musculus GN=Apoa1 PE=1 SV=2	44	0.136	0.000	1.355
sp|P58252|EF2_MOUSE	Elongation factor 2 OS=Mus musculus GN=Eef2 PE=1 SV=2	79	0.132	0.000	1.318
sp|P61759|PFD3_MOUSE	Prefoldin subunit 3 OS=Mus musculus GN=Vbp1 PE=2 SV=2	6	0.131	0.042	2.070
sp|Q80YD1|SUV3_MOUSE	ATP-dependent RNA helicase SUPV3L1, mitochondrial OS=Mus musculus GN=Supv3l1 PE=2 SV=1	2	0.129	0.026	4.742
sp|P62301|RS13_MOUSE	40S ribosomal protein S13 OS=Mus musculus GN=Rps13 PE=1 SV=2	15	0.129	0.000	1.343
sp|P60867|RS20_MOUSE	40S ribosomal protein S20 OS=Mus musculus GN=Rps20 PE=1 SV=1	5	0.126	0.042	3.020
sp|Q9D173|TOM7_MOUSE	Mitochondrial import receptor subunit TOM7 homolog OS=Mus musculus GN=Tomm7 PE=2 SV=1	3	0.122	0.008	3.698
sp|Q9D1G3|HHATL_MOUSE	Protein-cysteine N-palmitoyltransferase HHAT-like protein OS=Mus musculus GN=Hhatl PE=1 SV=2	5	0.120	0.054	4.055
sp|P28650|PURA1_MOUSE	Adenylosuccinate synthetase isozyme 1 OS=Mus musculus GN=Adssl1 PE=1 SV=2	18	0.120	0.029	1.600
sp|P05064|ALDOA_MOUSE	Fructose-bisphosphate aldolase A OS=Mus musculus GN=Aldoa PE=1 SV=2	111	0.112	0.000	1.306
sp|P49717|MCM4_MOUSE	DNA replication licensing factor MCM4 OS=Mus musculus GN=Mcm4 PE=2 SV=1	2	0.101	0.026	5.649
sp|P11404|FABPH_MOUSE	Fatty acid-binding protein, heart OS=Mus musculus GN=Fabp3 PE=1 SV=5	50	0.096	0.005	1.923
sp|P14873|MAP1B_MOUSE	Microtubule-associated protein 1B OS=Mus musculus GN=Map1b PE=1 SV=2	4	0.095	0.044	3.192
sp|Q6ZWV3|RL10_MOUSE	60S ribosomal protein L10 OS=Mus musculus GN=Rpl10 PE=2 SV=3	16	0.095	0.000	1.355
sp|P62702|RS4X_MOUSE	40S ribosomal protein S4, X isoform OS=Mus musculus GN=Rps4x PE=2 SV=2	15	0.084	0.000	2.377

sp|Q9WUB3|PYGM_MOUSE	Glycogen phosphorylase, muscle form OS=Mus musculus GN=Pygm PE=1 SV=3	73	0.082	0.000	1.271
sp|P62631|EF1A2_MOUSE	Elongation factor 1-alpha 2 OS=Mus musculus GN=Eef1a2 PE=1 SV=1	38	0.082	0.026	1.660
sp|P01869|IGH1M_MOUSE	Ig gamma-1 chain C region, membrane-bound form OS=Mus musculus GN=Ighg1 PE=1 SV=2	8	0.082	0.001	1.472
sp|P07310|KCRM_MOUSE	Creatine kinase M-type OS=Mus musculus GN=Ckm PE=1 SV=1	112	0.077	0.002	1.247
sp|Q99KV1|DJB11_MOUSE	DnaJ homolog subfamily B member 11 OS=Mus musculus GN=Dnajb11 PE=1 SV=1	3	0.077	0.048	1.690
sp|P21550|ENOB_MOUSE	Beta-enolase OS=Mus musculus GN=Eno3 PE=1 SV=3	91	0.076	0.000	1.803
sp|Q921U8|SMTN_MOUSE	Smoothelin OS=Mus musculus GN=Smtn PE=2 SV=2	3	0.074	0.020	4.571
sp|P04247|MYG_MOUSE	Myoglobin OS=Mus musculus GN=Mb PE=1 SV=3	94	0.074	0.004	1.629
sp|P45591|COF2_MOUSE	Cofilin-2 OS=Mus musculus GN=Cfl2 PE=1 SV=1	14	0.073	0.022	1.690
sp|Q8R5A0|SMYD2_MOUSE	N-lysine methyltransferase SMYD2 OS=Mus musculus GN=Smyd2 PE=1 SV=1	2	0.065	0.022	2.333
sp|P70335|ROCK1_MOUSE	Rho-associated protein kinase 1 OS=Mus musculus GN=Rock1 PE=1 SV=1	5	0.065	0.006	2.938
sp|Q99MS7|EH1L1_MOUSE	EH domain-binding protein 1-like protein 1 OS=Mus musculus GN=Ehbp1l1 PE=2 SV=1	12	0.061	0.015	2.729
sp|O09110|MP2K3_MOUSE	Dual specificity mitogen-activated protein kinase kinase 3 OS=Mus musculus GN=Map2k3 PE=1 SV=2	3	0.060	0.010	8.630
sp|Q62446|FKBP3_MOUSE	Peptidyl-prolyl cis-trans isomerase FKBP3 OS=Mus musculus GN=Fkbp3 PE=1 SV=2	8	0.059	0.047	2.754
sp|Q9CU62|SMC1A_MOUSE	Structural maintenance of chromosomes protein 1A OS=Mus musculus GN=Smc1a PE=1 SV=4	6	0.057	0.021	8.166
sp|Q8BJS4|SUN2_MOUSE	SUN domain-containing protein 2 OS=Mus musculus GN=Sun2 PE=1 SV=3	5	0.054	0.027	4.831
sp|P82348|SGCG_MOUSE	Gamma-sarcoglycan OS=Mus musculus GN=Sgcg PE=1 SV=2	3	0.046	0.004	13.305
sp|Q80VP1|EPN1_MOUSE	Epsin-1 OS=Mus musculus GN=Epn1 PE=1 SV=3	5	0.045	0.037	2.754
sp|Q9QZ08|NAGK_MOUSE	N-acetyl-D-glucosamine kinase OS=Mus musculus GN=Nagk PE=2 SV=3	4	0.044	0.051	32.810
sp|P62073|TIM10_MOUSE	Mitochondrial import inner membrane translocase subunit Tim10 OS=Mus musculus GN=Timm10 PE=1 SV=1	2	0.033	0.007	2.858
sp|Q9Z2N8|ACL6A_MOUSE	Actin-like protein 6A OS=Mus musculus GN=Actl6a PE=1 SV=2	5	0.028	0.007	4.365

sp|Q8BU85|MSRB3_MOUSE	Methionine-R-sulfoxide reductase B3, mitochondrial OS=Mus musculus GN=Msrb3 PE=1 SV=2	2	0.024	0.004	2.148
sp|Q63810|CANB1_MOUSE	Calcineurin subunit B type 1 OS=Mus musculus GN=Ppp3r1 PE=1 SV=3	5	0.021	0.004	2.884

To be included here, proteins had to meet the following criteria: a protein threshold (Unused ProtScore (conf)) > 0.05, detected with 2 or more peptides and a statistically significant (i.e. p<0.05) fold change of >1.25 or <0.75. For each protein identified, the corresponding Swiss-Prot Accession number is shown, together with the protein name as it is given in the Swiss-Prot database, iTRAQ ratio (fold change), p value and the number of peptides used for the identification. iTRAQ ratios were bias and background corrected. p-values were generated by the ProteinPilot software.

Appendix 3. Gene ontology (GO) analysis of the proteins differentially expressed in the heart from SMA mice

ENRICHED TERMS	COUNT	P-VALUE	PROTEINS
UPREGULATED PROTEINS			
Biological process			
Protein transport	14	3.10E-03	Rab5a, Ap1s1, Btf3, Xpo5, Xpo7, Kpna3, Lman2, Mia3, Nup188, Ppt1, Rabep2, Stxbp3, Tomm22, Vps4b
Cell-cell adhesion	12	1.30E-06	Dhx29, Gapvd1, Cnn3, Capg, Cgn, Clint1, Eno1, Hist2h3c1, Ppme1, Scrib, Slc3a2, Tagln2
Nucleosome assembly	6	2.60E-03	Atrx, Hist1h1a, Hist1h1b, Hist1h1c, Hist1h4h, Hist2h3c1
Epithelial cell differentiation	5	3.30E-03	Cnn3, Ctsb, Tgfb1i1, Tagln2, Tagln
Extracellular matrix organization	5	2.10E-02	Dnajb6, Fn1, Fbln5, Lama2, Lamb2
Regulation of cell shape	5	3.90E-02	Dlg1, Fn1, Palm2, Palm, Spta1
Actin cytoskeleton organization	5	4.10E-02	Dnajb6, Pdlim7, Rock2, Rhog, Spta1
Fibrinolysis*	4	3.10E-04	Anxa2, Fgb, Fgg, Hrg
Negative regulation of extrinsic apoptotic signaling pathway via death domain receptors*	4	1.50E-03	Fgb, Fgg, Hmgb2, Nol3
Platelet aggregation*	4	5.00E-03	Gnas, Fgb, Fgg, Stxbp3
Hemostasis*	4	8.50E-03	Fgb, Fgg, Hrg, Kng1

Response to hydrogen peroxide*	4	1.60E-02	Bak1, Hp, Slc4a1, Sod2
Positive regulation of smooth muscle cell proliferation	4	3.70E-02	Rab5a, Akr1b3, Alox12, Mtor
Blood coagulation*	4	4.20E-02	Fgb, Fgg, Hrg, Kng1
Chromosome segregation	4	4.80E-02	Arl8a, Arl8b, Bub3, Ppp1r7
Establishment or maintenance of epithelial cell apical/basal polarity	3	8.00E-03	Dlg1, Mtcl1, Scrib
Plasma membrane organization*	3	9.10E-03	Ank3, Spta1, Sptb
Actin filament capping*	3	1.20E-02	Capg, Spta1, Sptb
Nuclear envelope organization	3	1.60E-02	Lemd2, Lmna, Zmpste24
Tumor necrosis factor-mediated signaling pathway*	3	2.20E-02	Krt18, Krt8, Plvap
Protein targeting to plasma membrane	3	2.30E-02	Ank3, Anxa2, Palm
Bicellular tight junction assembly	3	2.50E-02	Cgn, Dlg1, Mtdh
Positive regulation of exocytosis*	3	2.70E-02	Rab5a, Fgg, Fgb
Response to nutrient levels	3	4.00E-02	Mbd3, Sirt5, Sod2
Response to ischemia	3	4.30E-02	Camk2a, Hk1, Nol3
Neuromuscular junction development	3	4.70E-02	Ank3, Lamb2, Snta1
Platelet activation*	3	4.90E-02	Fgb, Fgg, Hrg
Negative regulation of muscle atrophy	2	1.80E-02	Mtor, Nlo3
Positive regulation of membrane tubulation	2	2.70E-02	Asap1, Sh3glb1
Age-dependent response to oxidative stress	2	2.70E-02	Coq7, Sod2
Membrane raft organization	2	4.50E-02	Dlg1, Ppt1
Cellular component			

Nucleus	71	4.30E-03	Bdp1, Bub3, Dhx29, Dnajb6, Emc2, Gnas, Lemd2, Nop58, Pdlim7, Rock2, Atrx, Anxa2, Arih2, Btf3, Camk2a, Capg, Cdc5l, Chd4, Cmas, Coq7, Dlg1, Dr1, Eno1, Xpo5, Xpo7, Fhl1, Hnrnph2, Hmga1, Hmgb2, Hist1h1a, Hist1h1b, Hist1h1c, Hist1h4h, Hist2h3c1, Kpna3, Krt18, Krt2, Krt7, Krt8, Lmna, Lap3, Mtor, Mtdh, Mbd3, Mcm6, Mbp, Nppa, Nup188, Ppt1, Palm, Plcd1, Pfdn6, Ppp1r7, Pcbd1, Rprd1b, Rpa2, Rpl27, Rpl4, Sirt5, Snrpd1, Snrpa1, Slc3a2, Svil, Synpo2, Sin3b, Tgfb1i1, Tkt, Tsnax, Uaca, Vps4b, Zmpste24
Exosome	69	3.30E-17	Arl8a, Arl8b, Art3, Clec3b, Gnas, Hddc2, Rab5a, Rap1b, Rheb, Sh3glb1, Arpc3, Ap1s1, Anpep, Akr1b3, Akr7a5, Anxa2, Alox12, Cpped1, Capg, Ctsb, Ctsd, Col6a1, Dpep1, Dpp4, Dlg1, Eno1, Fbn1, Fgb, Fgg, Fn1, Fbln5, Gusb, Gpx3, Hp, Hrg, Hist1h4h, Hist2h3c1, Krt18, Krt2, Krt7, Krt8, Kng1, Lama2, Lamb2, Lman2, Lap3, Lcp1, Lamp2, Ppt1, Plcd1, Psat1, Plvap, Ppp1r7, Pcbd1, Rhog, Rpl27, Rpl4, Scrib, Serpina3k, Slc3a2, Slc4a1, Sod2, Stxbp3, Trmt112, Tagln2, Tkt, Uaca, Vps4b, Zmpste24
Mitochondrion	35	6.70E-06	Abcb7, Bak1, Clpb, Dhx29, Emc2, Hddc2, Nlrx1, CH082, Sh3glb1, Aldh4a1, Akr7a5, As3mt, Bola1, Camk2a, Ctsb, Ctsd, Cyb5b, Coq7, Dcakd, Echdc3, Hk1, Lap3, Mtor, Mmaa, Mtfr1l, Nol3, Plin5, Pdpr, Pdp1, Sirt5, Sod2, Trnt1, Tomm22, Uaca, Vwa8
Extracellular space*	26	1.70E-03	Clec3b, Anpep, Akr1b3, Anxa2, Ctsb, Ctsd, Dpep1, Eno1, Fbn1, Fgb, Fgg, Fn1, Fbln5, Gusb, Gpx3, Hp, Hmgb2, Krt2, Kng1, Lman2, Lcp1, Lamp2, Mtcl1, Nppa, Ppt1, Serpina3k
Cytoskeleton	21	2.00E-03	Arl8b, Pdlim7, Rock2, Arpc3, Ablim1, Ank3, Chd4, Dynlrb1, Dync1li2, Lcp1, Mtcl1, Myo3a, Mybpc2, Sgcb, Spta1, Sptb, Svil, Snta1, Tgfb1i1, Ttll11, Uaca
Cell-cell adherens junction	17	2.30E-08	Asap1, Dhx29, Gapvd1, Sh3glb1, Anxa2, Cnn3, Capg, Cgn, Clint1, Dlg1, Eno1, Hist2h3c1, Krt18, Ppme1, Scrib, Slc3a2, Tagln2
Perinuclear region of cytoplasm	16	1.30E-03	Dnajb6, Gnas, Rab5a, Akr1b3, Anxa2, Ctsb, Cdc5l, Clint1, Dlg1, Hmgb2, Lmna, Mtdh, Nppa, Plvap, Tsnax, Uaca
Focal adhesion	14	4.70E-05	Pdlim7, Arpc3, Cnn3, Dpp4, Fhl1, Hmga1, Lap3, Lcp1, Rhog, Rpl27, Rpl4, Svil, Synpo2, Tgfb1i1
Protein complex	13	1.00E-02	Rab5a, Sh3glb1, Anxa2, Chd4, Col6a1, Hk1, Hmgb2, Hist1h4h, Hist2h3c1, Mbd3, Sptb, Snta1, Trmt112
Cell junction	13	2.60E-02	Rap1b, Ank3, Anxa2, Camk2a, Cgn, Dpp4, Dlg1, Lcp1, Mtdh, Scrib, Svil, Snta1, Tgfb1i1

Sarcolemma	11	9.70E-08	Gnas, Ank3, Anxa2, Alox12, Ctsb, Col6a1, Krt8, Lama2, Popdc2, Sgcb, Snta1
Membrane raft	10	5.60E-04	Gnas, Rab5a, Anxa2, Ctsd, Dpp4, Dlg1, Hk1, Lamp2, Ppt1, Plcd1
Extracellular matrix	10	1.30E-03	Ctsd, Col6a1, Fbn1, Fn1, Fbln5, Hist1h4h, Lmna, Lamb2, Rpl27, Tgfb1i1
Blood microparticle*	9	2.50E-05	Fgb, Fgg, Fn1, Hp, Hbb-bh1, Hrg, Kng1, Serpina3k, Slc4a1
Apical plasma membrane	9	9.00E-03	Ctsb, Dpep1, Dpp4, Fn1, Mtdh, Mtcl1, Scrib, Slc3a2, Stxbp3
Lysosome	9	9.40E-03	Arl8a, Arl8b, Ank3, Ctsb, Ctsd, Gusb, Lamp2, Mtor, Ppt1
Proteinaceous extracellular matrix	8	2.30E-02	Clec3b, Anxa2, Col6a1, Fbn1, Fn1, Fbln5, Lama2, Lamb2
Chromosome	8	3.40E-02	Bub3, Atrx, Hmgb2, Hist1h1a, Hist1h1b, Hist1h1c, Mbd3, Ppp1r7
Actin cytoskeleton	7	9.10E-03	Pdlim7, Rab5a, Ablim1, Cnn3, Lcp1, Svil, Synpo2
Basolateral plasma membrane	7	9.50E-03	Ank3, Anxa2, Dlg1, Palm, Scrib, Slc4a1, Stxbp3
Melanosome	6	2.00E-03	Rab5a, Anxa2, Capg, Ctsb, Ctsd, Slc3a2
Midbody	6	6.00E-03	Arl8a, Arl8b, Sh3glb1, Anxa2, Mtcl1, Svil
Late endosome membrane	5	7.80E-03	Arl8a, Arl8b, Anxa2, Lamp2, Vps4b
Ruffle	5	1.00E-02	Gnas, Pdlim7, Rab5a, Anxa2, Lcp1
Basement membrane	5	1.10E-02	Anxa2, Fbn1, Fn1, Lama2, Lamb2
Nucleosome	5	1.60E-02	Hist1h1a, Hist1h1b, Hist1h1c, Hist1h4h, Hist2h3c1
Intermediate filament*	5	2.00E-02	Krt18, Krt2, Krt7, Krt8, Lmna
Z disc	5	2.40E-02	Dnajb6, Ank3, Krt8, Slc4a1, Synpo2
Nuclear chromosome, telomeric region	5	2.60E-02	Atrx, Hist1h4h, Hist2h3c1, Mcm6, Rpa2
Stress fiber	4	2.20E-02	Pdlim7, Ablim1, Anxa2, Lcp1
Fibrinogen complex*	3	1.60E-03	Fgb, Fgg, Fn1
Platelet alpha granule*	3	7.60E-03	Fgb, Fgg, Stxbp3
Apicolateral plasma membrane	3	1.50E-02	Krt8, Mtcl1, Palm
Podosome	3	3.20E-02	Asap1, Lcp1, Svil
Spectrin*	2	4.30E-02	Spta1, Sptb
DOWNREGULATED PROTEINS			

Biological process			
Transport	36	8.40E-04	Atp5b, Atp5c1, Abcb10, Atp2a2, Ndufa9, Ndufv1, Rab11b, Rab1a, Sec13, Afp, Apoa1, Apoc1, Cpt1b, Chchd4, Dbi, Fabp3, Fabp4, Fxn, Got2, Ipo5, Mb, Naca, Osbp, Sar1b, Sfxn3, Slc2a4, Slc25a12, Slc25a46, Snx1, Trf, Timm10, Timm44, Tomm7, Tmem109, Uqcrc2, Uqcrh
Oxidation-reduction process	25	4.90E-07	Decr1, Ndufa9, Ndufv1, Acadl, Acads, Acadvl, Chchd4, Dhrs1, Fxn, Gpx4, Hadha, Hsdl2, Idh2, Idh3g, Ldhb, Mdh1, Mdh2, Msrb3, Nnt, Ogdh, Prdx4, Pdha1, Suox, Uqcrc2, Uqcrh
Translation	21	2.20E-08	Gfm1, Tsfm, Eef1a2, Eef1g, Eef2, Eif1ax, Eif3a, Mrpl23, Mrpl27, Rpl10, Rpl18a, Rps13, Rps15, Rps15a, Rps16, Rps18, Rps19, Rps2, Rps20, Rps4x, Slc25a12
Metabolic process	21	2.30E-07	Ugp2, Acat1, Aco2, Acsl1, Acadl, Acads, Acadvl, Pygb, Dlat, Echdc1, Eci1, Ephx2, Gys1, Hadha, Pygm, Ogdh, Pfkm, Paics, Pdha1, Pkm, Sucla2
Protein folding	15	1.50E-10	Dnaja2, Dnajb11, Fkbp3, Fkbp4, Calr, Cct2, Hspa8, Hspa9, Hsp90ab1, Hsp90b1, Ppib, P4hb, Pdia3, Tubb5, Vbp1
Lipid metabolic process	11	3.20E-02	Decr1, Atp5b, Acsl1, Acadl, Acads, Acadvl, Apoa1, Cpt1b, Eci1, Ephx2, Hadha
Tricarboxylic acid cycle	10	1.70E-11	Aco2, Dlat, Fh1, Idh2, Idh3g, Mdh1, Mdh2, Ogdh, Pdha1, Sucla2
Fatty acid metabolic process	9	3.50E-04	Decr1, Acsl1, Acadl, Acads, Acadvl, Cpt1b, Eci1, Fabp4, Hadha
Cell-cell adhesion	9	1.20E-03	Aldoa, Bsg, Eef1g, Lrrfip1, Paics, Plec, Rps2, Serbp1, Snd1
Carbohydrate metabolic process	9	2.10E-03	Pygb, Dlat, Ldhb, Mdh1, Mdh2, Pygm, Pgm2, Pgk1, Pdha1
Glycolytic process	6	4.50E-05	Aldoa, Eno3, Ogdh, Pfkm, Pgk1, Pkm
Protein homotetramerization	6	1.40E-03	Decr1, Actn2, Acadl, Acads, Aldoa, Pfkm
2-oxoglutarate metabolic process	5	3.90E-05	Got2, Got1, Idh2, Idh3g, Ogdh
ATP metabolic process	5	9.70E-04	Atp5b, Atp5c1, Ak1, Ak3, Hspa8
Proteolysis involved in cellular protein catabolic process	5	3.60E-03	Hspa5, Lonp1, Psma3, Psma4, Scpep1
Response to nutrient	5	8.70E-03	Acsl1, Adsl, Apoa1, Plec, Suox
Response to endoplasmic reticulum stress	5	1.00E-02	Atp2a2, Eef2, Hspa5, P4hb, Pdia3
NADH metabolic process	4	2.70E-04	Idh3g, Mdh1, Mdh2, Ogdh

Oxaloacetate metabolic process	4	4.40E-04	Got2, Got1, Mdh1, Mdh2
Ribosomal small subunit assembly	4	1.50E-03	Rps15, Rps19, Rps2, Rps25
Cellular response to interleukin-4	4	3.20E-03	Hspa5, Hsp90ab1, Rps2, Rplp0
Glycogen metabolic process	4	9.10E-03	Ugp2, Pygb, Gys1, Pygm
Aerobic respiration	4	9.10E-03	Ndufv1, Adsl, Fxn, Uqcrc2
Microtubule-based process	4	1.00E-02	Kif5b, Map1b, Tubb5, Vbp1
Positive regulation of phagocytosis	4	1.60E-02	Calr, Hspa8, Ighg1, Ighg2b
Receptor-mediated endocytosis	4	2.90E-02	Atp5b, Apoa1, Calr, Hsp90b1
Cellular response to oxidative stress	4	3.30E-02	Atp2a2, Nme2, Chchd4, Lonp1
Cholesterol homeostasis	4	3.30E-02	Apoa1, Ephx2, Fabp3, Fabp4
Glucose metabolic process	4	4.00E-02	Dlat, Pgm2, Pdha1, Pkm
AMP biosynthetic process	3	1.20E-03	Adsl, Adssl1, Prps1
Aspartate metabolic process	3	1.80E-03	Adssl1, Got2, Got1
Isocitrate metabolic process	3	1.80E-03	Aco2, Idh2, Idh3g
Malate metabolic process	3	3.30E-03	Fh1, Mdh1, Mdh2
Purine nucleotide metabolic process	3	3.30E-03	Nme2, Adsl, Adssl1
Muscle cell cellular homeostasis	3	1.70E-02	Aldoa, Cfl2, Pfkm
Ribosomal small subunit biogenesis	3	1.80E-02	Rps15, Rps16, Rps19
Skeletal muscle tissue regeneration	3	2.00E-02	Eno3, Naca, Pkm
Antigen processing and presentation of exogenous peptide antigen via MHC class I, tap-dependent	3	4.30E-02	Calr, Psma3, Psma4
Sarcomere organization	3	4.60E-02	Actn2, Cfl2, Prkar1a
Protein import into mitochondrial intermembrane space	2	3.30E-02	Afg3l2, Afg3l2

Regulation of postsynaptic density protein 95 clustering	2	4.40E-02	Cdh2, Dbn1
ADP biosynthetic process	2	4.40E-02	Ak1, Ak3
Cellular component			
Exosome	93	2.10E-28	Decr1, Atp5b, Atp5c1, Dnaja2, Fkbp4, Nagk, Ndrg2, Nme2, Rab11b, Rab1a, Sec13, Ugp2, Acat1, Actn2, Ak1, Aldoa, Anxa6, Apoa1, Apoc1, Bsg, Pygb, Cdh2, Calr, Cct2, Cfl2, Cand1, Des, Dbi, Eea1, Eno3, Echdc1, Eci1, Ephx2, Eef1g, Eef2, Fabp3, Fabp4, Fh1, Got2, Got1, Gpx4, Gyg, Hspa5, Hspa8, Hspa9, Hsp90ab1, Hsp90b1, Idh2, Ldhb, Mdh1, Mdh2, Pygm, Mb, Myo1d, Myh9, Naca, Nudt3, Ppib, Prdx4, Pfkm, Pgm2, Pgk1, Paics, Plec, Pdcd6, P4hb, Psma3, Psma4, Pdia3, Ppa2, Pkm, Rps13, Rps15a, Rps16, Rps18, Rps19, Rps2, Rps20, Rps25, Rps4x, Rplp0, Scpep1, Serbp1, Slc2a4, Snd1, Sucla2, Trf, Tmem109, Tubb5, Tpt1, Ywhae, Uqcrc2, Vim
Nucleus	84	1.20E-03	Decr1, Atp5b, Dnaja2, Dnajb11, Fkbp3, Fkbp4, Faf1, Hectd1, Ndrg2, Ndufa9, Nme2, Nsun2, Sec13, Smyd1, Smyd2, Sun2, Tsfm, Ugp2, Aco2, Actl6a, Acads, Acadvl, Aldoa, Anxa6, Apoa1, Calr, Cfl2, Cirbp, Cand1, Dbi, Epn1, Eef1a2, Eef1g, Eef2, Eif3a, Fabp4, Got1, Gpx4, Hspa5, Hspa8, Hspa9, Hsp90b1, Hnrnph1, Hnrnpll, Ipo5, Lrrfip1, Lonp1, Mdh2, Memo1, Mcm4, Myh9, Naca, Nudt21, Nudt3, Osbp, Ppib, Prdx4, Pdcd6, Psmc1, Psma3, Psma4, Pdia3, Ppp5c, Purb, Pdha1, Pkm, Rps13, Rps18, Rps2, Rps25, Rps4x, Rplp0, Serbp1, Smpx, Sf1, Snd1, Stip1, Smc1a, Supv3l1, Tmem109, Tubb5, Tpt1, Ube3a, Vbp1
Mitochondrion	76	8.90E-29	Decr1, Afg3l2, Atp5b, Atp5c1, Abcb10, Fkbp4, Gfm1, Grsf1, Kank2, Ndrg4, Ndufa9, Ndufv1, Nme2, Rab11b, Tsfm, Acat1, Aco2, Acsl1, Acadl, Acads, Acadvl, Ak3, Adsl, Aldoa, Anxa6, Bsg, Cpt1b, Chchd4, Coa3, Cox7a1, Dhrs1, Dbi, Dlat, Eci1, Fxn, Fh1, Gbas, Got2, Gpx4, Hspa5, Hspa9, Hsp90ab1, Hadha, Hsdl2, Idh2, Idh3g, Ldhb, Lonp1, Mdh1, Mdh2, Msrb3, Mccc1, Mrpl23, Mrpl27, Nln, Nnt, Ogdh, Prdx4, Pdia3, Ppa2, Pdha1, Pkm, Rps15a, Sfxn3, Slc25a12, Slc25a46, Snd1, Sucla2, Suox, Supv3l1, Timm10, Timm44, Tomm7, Ywhae, Uqcrc2, Uqcrh
Focal adhesion	26	3.60E-13	Akap12, Actn2, Anxa6, Bsg, Cdh2, Calr, Hspa5, Hspa8, Hspa9, Hsp90b1, Myh9, Ppib, Plec, P4hb, Pdia3, Rps13, Rps15, Rps16, Rps18, Rps19, Rps2, Rps4x, Rplp0, Tln2, Ywhae, Vim

Endoplasmic reticulum	26	2.50E-03	Atp2a2, Dnajb11, Rab1a, Sec13, Acsl1, Apoc1, Atl3, Calr, Dhrs1, Dbi, Eef1g, Hspa5, Hsp90b1, Hhatl, Ldah, Msrb3, Osbp, Ppib, Prdx4, Pdcd6, P4hb, Pdia3, Rpl10, Sar1b, Ssr3, Tmem109
Mitochondrial inner membrane	25	2.10E-12	Afg3l2, Atp5b, Atp5c1, Abcb10, Ndufa9, Ndufv1, Acat1, Acadvl, Csde1, Coa3, Cox7a1, Dhrs1, Eci1, Got2, Gpx4, Hadha, Idh2, Mdh2, Mccc1, Nnt, Slc25a12, Timm10, Timm44, Uqcrc2, Uqcrh
Myelin sheath	23	5.60E-17	Atp5b, Atp5c1, Nme2, Aco2, Aldoa, Cct2, Dlat, Eef1a2, Got2, Hspa5, Hspa8, Hspa9, Ldhb, Mdh1, Mdh2, Myo1d, Pdia3, Pdha1, Pkm, Slc25a12, Stip1, Sucla2, Uqcrc2
Extracellular matrix	22	3.80E-12	Atp5b, Calr, Cct2, Eef2, Hspa5, Hspa8, Hspa9, Hsp90b1, Hadha, Myh9, Plec, P4hb, Pkm, Rps13, Rps15a, Rps16, Rps18, Rps19, Rps20, Rps25, Tubb5, Vim
Cell-cell adherens junction	22	1.50E-11	Rab11b, Rab1a, Aldoa, Bsg, Cdh2, Dbn1, Eef1g, Eef2, Hspa5, Hspa8, Hsp90ab1, Kif5b, Lrrfip1, Myh9, Paics, Plec, Pkm, Rps2, Serbp1, Snx1, Snd1, Ywhae
Perinuclear region of cytoplasm	21	3.40E-05	Atp2a2, Fkbp4, Faf1, Ndrg2, Nme2, Ak1, Anxa6, Calr, Dbn1, Hspa8, Hsp90b1, Hhatl, Kif5b, Map1b, Osbp, Ppib, Plec, Serbp1, Slc2a4, Trf, Vim
Intracellular ribonucleoprotein complex	17	2.30E-07	Eef2, Hspa8, Hnrnph1, Hnrnpll, Mrpl23, Mrpl27, Rpl18a, Rps13, Rps15, Rps16, Rps18, Rps19, Rps2, Rps20, Rps25, Rps4x, Rplp0
Ribosome	15	9.90E-09	Mrpl23, Mrpl27, Rpl10, Rpl18a, Rps13, Rps15, Rps15a, Rps16, Rps18, Rps19, Rps2, Rps20, Rps25, Rps4x, Rplp0
Mitochondrial matrix	15	9.90E-09	Ndufa9, Tsfm, Acat1, Acadl, Acads, Ak3, Eci1, Got2, Lonp1, Mdh2, Mccc1, Ogdh, Pdha1, Supv3l1, Timm44
Melanosome	12	7.70E-09	Rab1a, Anxa6, Bsg, Hspa5, Hspa8, Hsp90ab1, Hsp90b1, Ppib, P4hb, Pdia3, Snd1, Ywhae
Mitochondrial nucleoid	7	7.50E-06	Atp5b, Grsf1, Acadvl, Hspa9, Hadha, Lonp1, Supv3l1
Mitochondrial membrane	7	6.30E-04	Atp5b, Ndufa9, Nme2, Acadl, Acads, Ogdh, Sfxn3
Sarcolemma	7	1.40E-03	Anxa6, Bsg, Des, Plec, Ppp3r1, Sgcg, Slc2a4
Z disc	6	9.30E-03	Actn2, Aldoa, Cfl2, Des, Pygm, Nebl
Polysome	5	9.90E-04	Calr, Eef2, Rps25, Rps4x, Vbp1
Mitochondrial intermembrane space	5	7.60E-03	Ak3, Chchd4, Nln, Pdia3, Suox
Peroxisome	5	4.70E-02	Acsl1, Ephx2, Hsdl2, Idh2, Vim

Blood microparticle	5	4.90E-02	Apoa1, Hspa8, Ighg1, Ighg2b, Trf
Contractile fiber	4	9.30E-04	Des, Dbi, Plec, Smpx
Sarcoplasmic reticulum	4	2.20E-02	Atp2a2, Calr, Pygm, Tmem109
Respiratory chain	4	2.20E-02	Ndufa9, Ndufv1, Uqcrc2, Uqcrh
Proteasome complex	4	3.10E-02	Psmc1, Psma3, Psma4, Ube3a
Plasma membrane raft	3	6.50E-03	Cdh2, Myo1d, Prkar1a
Fascia adherens	3	7.70E-03	Cdh2, Des, Tln2
Axonal growth cone	3	3.40E-02	Fkbp4, Dbn1, Kif5b
Cytoplasmic ribonucleoprotein granule	3	3.40E-02	Rps4x, Rplp0, Tubb5
Cop9 signalosome	3	4.50E-02	Hspa5, Hsp90ab1, Myh9
Tubulin complex	2	4.10E-02	Tubb5, Tpt1
Axonal spine	2	4.10E-02	Dbn1, Eea1

Enriched terms connected to biological process and cellular component are presented for upregulated and downregulated proteins, together with the p-value and the number of annotated proteins. Proteins are presented as gene symbols. *In the category of upregulated proteins, enriched terms that contained mostly blood-derived proteins and keratins were excluded from the analysis. These proteins were: haptoglobin (Hp), fibrinogen beta chain (Fgb), fibrinogen gamma chain (Fgg), kininogen 1 (Kng1), histidine-rich glycoprotein (Hrg), spectrin alpha, erythrocytic 1 (Spta1), spectrin beta, erythrocytic (Sptb), hemoglobin Z, beta-like embryonic chain (Hbb-bh1), keratin 2 (Krt2), keratin 7 (Krt7), keratin 8 (Krt8), keratin 18 (Krt18), serine (or cysteine) peptidase inhibitor, clade A, member 3K (Serpina3k), natriuretic peptide type A (Nppa), solute carrier family 4 (anion exchanger), member 1 (Slc4a1), cytoglobin (Cygb), glutathione peroxidase 3 (Gpx3), C-type lectin domain family 3, member b (Clec3b), dipeptidase 1 (renal) (Dpep1), lymphocyte cytosolic protein 1 (Lcp1).

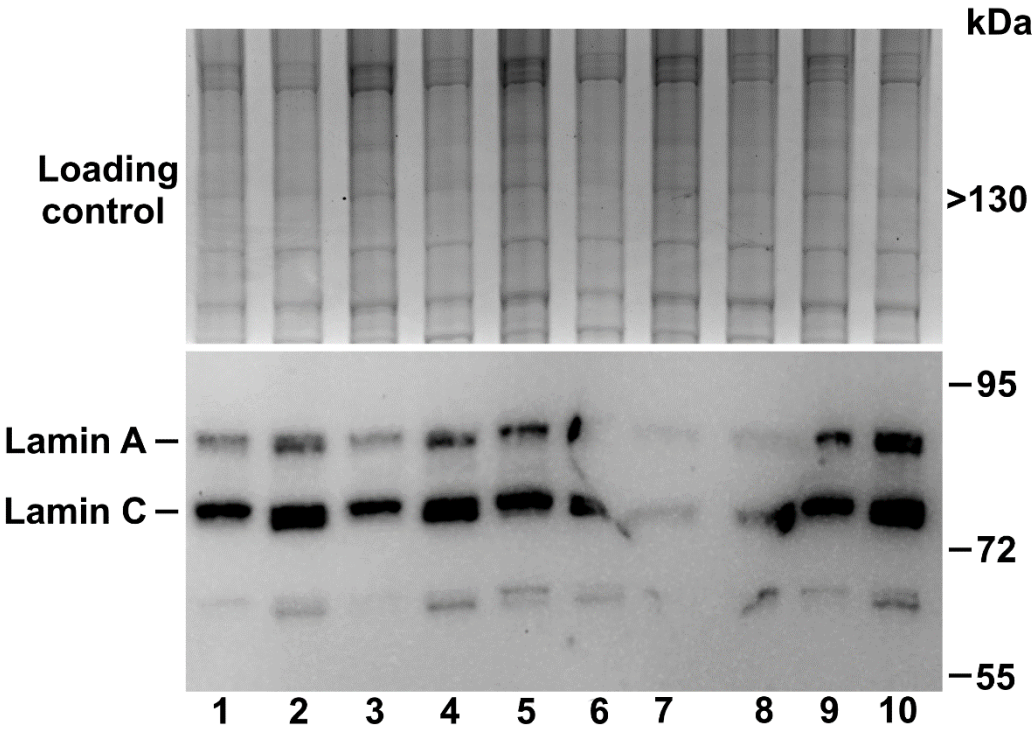

Appendix 4. Electrophoretic mobility of lamin A/C in the heart from late-symptomatic SMA mice (P8). Western blot showing lamin A and lamin C levels in the heart tissue extracts from SMA mice (n=5) and age-matched healthy controls (n=5). Coomassie stained gel was used as internal, total protein loading control. Odd numbers indicate control samples, and even numbers SMA samples.